Calcium Fluoride for Nucleophilic Fluorination

A thesis submitted to the Board of the Faculty of Physical Sciences, in partial fulfilment of the requirements for the degree of Doctor of Philosophy at the University of Oxford.

Calum Patel

Merton College

University of Oxford

Michaelmas Term 2024

Author's Declaration

The work presented in this thesis was conducted under the supervision of Professor Véronique Gouverneur at the Department of Chemistry, University of Oxford. All the work is my own and has not been submitted for any other degree at this or any other university. Work done in collaboration with, or with the assistance of others is indicated as such.

Calum Patel

10th October 2024

Contents

Abstract

Chapter 1 (Introduction) summarises the origin and role of fluorochemicals used in our everyday lives, including the production and use of hydrogen fluoride (HF). An account of the development of fluorine chemistry, including nucleophilic fluorination and CaF_2 chemistry, is also provided. This chapter concludes with an outline of the work disclosed in this thesis.

Chapter 2 (Fluorochemicals from Fluorspar via a Phosphate-Enabled Mechanochemical Process that Bypasses HF) begins with a brief introduction to mechanochemistry, mechanochemical fluorination and powder X-ray diffraction. The development of an inorganic fluorinating reagent (**Fmix**) via the solid-state (mechanochemical) activation of acid-grade fluorspar (>97% CaF_2) using K_2HPO_4 is disclosed. Applications of **Fmix** for S-F and C-F bond formation is described, followed by a mechanistic study on the composition of **Fmix** and the discovery of novel fluorinating reagents [$K_3(HPO_4)F$] and $K_{2-x}Ca_y(PO_3F)_a(PO_4)_b$.

Chapter 3 (Low-Temperature Activation of Fluorspar in Water via Brønsted and Lewis Acid Cooperativity) first provides an overview of the reported methods for CaF_2 activation using Brønsted acids, followed by a brief introduction to boron and silicon fluorides. The development of a method entailing activation of acid-grade fluorspar in water (solution-phase) using $B(OH)_3$ or SiO_2 in the presence of a Brønsted acid, optimally oxalic acid, is then disclosed. The application of this technology for preparing fluorinating reagents well-documented for aromatic fluorination is then presented. Finally, mechanistic studies for HF monitoring by ^{19}F NMR spectroscopy, and a study comparing the efficacy of oxalic acid versus H_2SO_4 are reported.

Chapter 4 (Experimental) contains experimental details for the work disclosed in Chapters 2 and 3, including procedures and characterisation for synthesised compounds and supplementary mechanistic data.

Acknowledgements

First, I would like to thank Professor Véronique Gouverneur for offering me the opportunity to come to Oxford and work in her group. Her unwavering support, guidance and advice were instrumental to bringing this work to fruition. Professor Gouverneur's passion, commitment and enthusiasm is truly inspiring. It has been a privilege to work under her supervision and alongside her team of remarkable scientists. This opportunity has changed my life and helped me grow in many ways. I am truly grateful for Véronique's willingness to take a risk and for her valuable time.

I am deeply indebted to the Synthesis of Biology and Medicine Centre for Doctoral Training, the European Research Council and FluoRok, which generously funded my continued studies and research at this esteemed institution.

I express my sincere appreciation to Professor Michael Hayward for his utmost scientific expertise and patience, which have been invaluable on numerous occasions. I extend my thanks to Dr. Xabier Martinez de Irujo-Labalde, for his generosity and support. My gratitude goes out to Professor Simon Aldridge for continued support throughout my DPhil studies and to Dr. Duncan Browne and Dr. Jamie Leitch for advice and discussions about mechanochemistry during the early days. I extend my appreciation to Prof. Robert Paton and Dr. Robert Syvret for their invaluable contributions.

Enormous thanks go to Dr. Emy André-Joyaux, it was a privilege to work with her during the start of my DPhil. I am grateful that we both shared a curiosity for calcium fluoride. I extend my gratitude to Dr. Gabriele Pupo, Dr. Francesco Ibba and Dr. Jeroen Sap whose advice and guidance helped shaped me into a better chemist during the start of my DPhil.

Thank you to the CaF_2 subgroup, especially Dr. Chris Goult for all of his support with solid-state analytical work, and Dr. Immo Klose and Dr. Anirban Mondal during the latter half of my DPhil. Many thanks to the analytical services and workshop team at Oxford, also.

A warm thanks goes to the members of the lab group, with a special mention to Claire, Joe, and Sebastiano. Our friendship and the memories made over the years are truly cherished. In Oxford, I have had the great privilege of meeting remarkable people who deeply influenced my life and stood by me consistently. A special thanks to Artemis, Ben, Marlene, Will, Alex, Hannah and Rob. This journey would not have been the same without you.

Finally, I extend my heartfelt thanks to my parents, my sister, my family and my many cousins, notably Akshay, Trusha, Selina, Aaron and Nytin for their unconditional support. Thank you for keeping me smiling and for keeping me going.

Abbreviations and Acronyms

Å	angstrom, 10^{-10} m
° C	degrees Celsius
15-crown-5	1,4,7,10,13-Pentaoxacyclopentadecane
18-crown-6	1,4,7,10,13,16-Hexaoxacyclooctadecane
A	absorption factor
Ac	acetyl
AGF	acid-grade fluorspar
Am	amyl
anh.	anhydrous
aq.	aqueous
Ar	aryl
b.p.	boiling point
Bn	benzyl
Boc	*tert*-butyloxycarbonyl
br	broad
Bu	butyl
cal	calorie
cbz	benzyloxycarbonyl
CFC	chlorofluorocarbon
CN	nitrile
COSY	correlation spectroscopy
CPMAS	cross polarisation magic angle spinning
d	doublet
d	interplanar d-spacing
DAST	diethylaminosulfur trifluoride
DAST	diethylaminosulfur trifluoride
DCB	dichlorobenzene
DCM	dichloromethane
DeoxoFluor	bis(2-methoxyethyl) aminosulfur trifluoride
ΔU_L	lattice energy
DIPEA	*N,N*-diisopropyl-ethylamine
DMA	dimethylacetamide
DMAP	4-dimethylaminopyridine
DMAP	4-dimethylaminopyridine
DMF	dimethylformamide
DMSO	dimethyl sulfoxide
DOI	digital object identifier
DPMAS	direct polarisation magic angle spinning
e^-	electron
E	energy
EDG	electron donating group
E_{diss}	dissociation energy
ee	enantiomeric excess
EI	electron ionisation

eq	equation
equiv	equivalent
ESF	ethene sulfonyl fluoride
ESI-MS	electrospray ionisation mass spectrometry
Et	ethyl
EtCN	propionitrile
eV	electron volt
EWG	electron withdrawing group
exp	exponential
F	structure factor
f	atomic scattering factor
FA	4-fluoroanisole
FCC	flash column chromatography
FCC	face-centred cubic
FDA	Food and Drug Administration
g	gram
G	Gibbs free energy
GC-MS	gas chromatography mass spectrometry
GST	glutathione S-transferases
h	hour
hept	heptet
HFC	hydrofluorocarbon
HMBC	Heteronuclear Multiple Bond Correlation
HPDEC	High-power decoupling
HPLC	high performance liquid chromatography
HRMS	high resolution mass spectrometry
HSQC	Heteronuclear Single Quantum Coherence
Hz	hertz
ICDD	International Centre for Diffraction Data
ICP-MS	inductively coupled plasma mass spectrometry
INEPT	refocused Insensitive Nuclei Enhanced Polarisation Transfer
I	intensity
iPr	isopropyl
IR	infrared spectroscopy
IUPAC	International Union of Pure and Applied Chemistry
J	joule
J	scalar coupling constant
k	kilo
K	Kelvin
K_{221}	Kryptofix 2.2.1 (4,7,13,16,21-Pentaoxa-1,10-diazabicyclo[8.8.5]tricosane)
K_{222}	Kryptofix 2.2.2 (4,7,13,16,21,24-Hexaoxa-1,10-diazabicyclo[8.8.8]hexacosane)
L	litre
L	Lorentz-polarisation function constant
LAG	liquid assisted grinding
LC	liquid chromatography
LED	light-emitting diode

LG	leaving group
M	mega
M	molar
m	milli
m	metre
m.p.	melting point
MAS	magic angle spinning
mCPBA	*meta*-chloroperoxybenzoic acid
Me	methyl
MeCN	acetonitrile
MeOH	methanol
mg	milligram
min	minute
MK2	mitogen-activated protein (MAP) kinase-activated protein kinase 2
mL	millilitre
µL	microlitre
mmol	millimole
mol	mole
MP	meting point
MS	mass spectrometry
Ms	mesyl
MTBE	methyl tert-butyl ether
n	neutron
n	number of experiments
N	number of scans
NBS	*N*-bromosuccinimide
NBSF	*p*-nitrobenzenesulfonyl fluoride
nBu	*n*-butyl
NCS	*N*-chlorosuccinimide
NFSI	*N*-fluorobenzenesulfonimide
NMR	nuclear magnetic resonance spectroscopy
OLED	organic light-emitting diodes
Ox	oxalate
p	pentet
PET	positron emission tomography
PFAS	per- and polyfluoroalkyl substances
PFCs	perfluorinated compounds
Ph	phenyl
Phth	phthalimide
pin	pinacol
PMSF	phenylmethanesulfonyl fluoride
ppm	parts per million
ppt.	precipitate
PTFE	Poly(tetrafluoroethylene)
PVDF	Poly(vinylidene difluoride)
PXRD	powder X-ray diffraction
py	pyridine
qd	quartet of doublets

qNMR	quantitative nuclear magnetic resonance
ref	reference
rt	room temperature
s	second
s	singlet
SARS-CoV-2	severe acute respiratory syndrome coronavirus 2
Selectfluor	1-chloromethyl-4-fluoro-1,4-diazoniabicyclo[2.2.2]octane bis(tetrafluoroborate)
SEM	scanning electron microscopy
Ser	serine
SET	single electron transfer
S_NAr	nucleophilic aromatic substitution
SPPS	Solid Phase Peptide Synthesis
SuFEx	sulfur fluorine exchange
t	triplet
tAm	tert-amyl
TBAF	tetrabutylammonium fluoride
tBu	tert-butyl
TEDA	triethylenediamine
TEDA	tetra ethylene diamine
TFA	trifluoroacetic acid
TFFH	fluoro-*N,N,N′,N′*-tetramethylformamidinium hexafluorophosphate
Tf	triflate
TGA	thermogravimetric analysis
THF	tetrahydrofuran
TLC	thin layer chromatography
TM	trademark
TMAF	tetramethylammonium fluoride
TMS	trimethylsilane
TREAT-HF	Triethylamine trihydrofluoride
TRIS	time resolved in situ
Ts	tosyl
TSE	twin screw extrusion
U_{iso}	isotropic thermal displacement factor
US	United States
USGS	United States Geological Survey
UV	ultraviolet
V	volt
w/w	weight per weight
δ	chemical shift (ppm)
θ	Incident angle
Δ	difference in
λ	wavelength
μ	micro
ν	wavenumber (cm^{-1})
χ	electronegativity

1.Introduction

1.1 The Fluorosphere

Fluorine is Earth's 13th most abundant element, found in significant quantities in oceans (2.2×10^6 Mt), the atmosphere (7.5 Mt) and the Earth's crust (1.4×10^{10} Mt).[1] It is relatively abundant for a halogen, with an estimated abundance almost three times greater than that of chlorine (0.065% for fluorine compared to 0.02% for chlorine).[2] The *fluorosphere*, which considers the flux and reservoirs of fluorine on Earth, is outlined in Figure 1.1. Anthropogenic factors do not influence the abundance of fluorine; however, the distribution of fluorochemicals is strongly affected by human activity.[3]

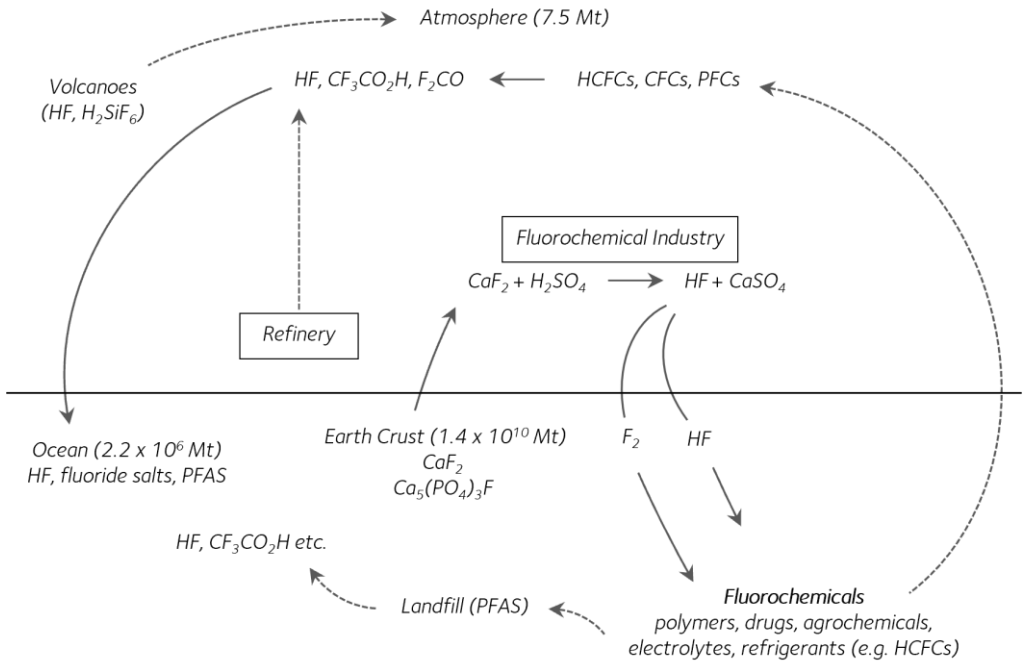

Figure 1.1. The fluorosphere with natural and anthropogenic fluorine reservoirs and flux.[1]

The origin of fluorine (^{19}F) in the universe is debated. Continued studies have pointed to its stellar formation, including the neutrino spallation of ^{20}Ne to afford ^{19}F through the ejection of a proton.[4] On Earth, all halogens, including fluorine, are suggested to have initially arrived at the planetary surface through geothermal processes and highly energetic events such as volcanic eruptions. Today, between 60,000 to 6 million tons of hydrogen fluoride

(HF) and fluorosilicates (e.g. H_2SiF_6) are estimated to be produced yearly by volcanic activity alone, depending on the number of eruptions. Since its discovery in 1886, the existence of elemental fluorine in nature was heavily debated. That was until scientists detected fluorine trapped in a radioactive variety of fluorite called antozonite, which releases F_2 gas upon crushing.[5] While fluoride is abundant in the Earth's crust, fluorinated natural products are scarce compared to other halogenated products, with only five uncontested examples reported.[6]

The three most important natural sources of fluoride (F^-) are fluorspar (fluorite, calcium fluoride, CaF_2), cryolite [$Na_3(AlF_6)$] and fluorapatite [$Ca_5(PO_4)_3F$]. Potassium fluoride (KF) and lithium fluoride (LiF) also exist as the rare minerals carobbiite and griceite, respectively. Between 2016 and 2020, global fluorspar production increased from approximately 5.4 to 6.5 million tons, with major sources coming from China, Mexico, South Africa, and Spain.[7] In 2023, the United States Geological Survey (USGS) estimated the global reserve of fluorspar to be 280 million tonnes.[8] While cryolite [$Na_3(AlF_6)$] reserves are now exhausted, phosphate rock containing fluorapatite [$Ca_5(PO_4)_3F$] is highly abundant, with the USGS estimating global reserves of more than 74 billion tons, containing about 5 billion tons of 100% fluorspar equivalent.[8,9] Global production of phosphoric acid (H_3PO_4) relies on this reserve; indeed, approximately 80 million tonnes of H_3PO_4 is manufactured from phosphate rock per year, ranking it the second most produced acid on the planet after sulfuric acid (H_2SO_4). Despite being the largest reserve of fluorine, fluorapatite is not directly exploited for its fluorine content. Instead, the contained fluorine is liberated as silicon tetrafluoride (SiF_4) and HF, forming hexafluorosilicic acid (H_2SiF_6). An estimated 40,000 tonnes of H_2SiF_6 were derived from processing phosphate rock in the United States in 2023. Phosphate rock derived H_2SiF_6 is converted into synthetic CaF_2 for HF and AlF_3 manufacture.[8] However,

because of differing physical properties, AlF_3 produced from synthetic CaF_2 is not readily substituted for AlF_3 produced from natural fluorspar.

About half of the fluorspar produced globally is metallurgical grade fluorspar (metspar, 60-90% CaF_2) used directly as flux to reduce melting points and increase the viscosity of metals in iron, aluminium and steel production.[10] The production of hydrogen fluoride (HF) accounts for the second largest consumption of fluorspar, with annual consumption of HF throughout the world reaching an estimated 1.1 million tonnes per year.[11] HF production demands fluorspar of acid-grade purity (acidspar, >97% CaF_2).

1.2 Historical Background

Georgius Agricola, the *father of minerology*, first described fluorspar (fluorite, CaF_2) as a fluoride containing salt in 1529, which was later named by Napione in 1797 from the Latin word, *fluere* or *to flow*.[12] The phenomenon of fluorescence is directly associated with fluorite and is especially prominent in fluorite specimens from specific locations due to certain impurities in the crystal. The chemistry linking naturally occurring fluorspar (CaF_2) to the entire fluorochemical industry is based on the isolation of two highly toxic, low boiling point gases, hydrogen fluoride (HF, b.p. 19.5 °C, m.p -83.4 °C) and fluorine gas (F_2, b.p. -188.1 °C, m.p. -219.6 °C). The history of fluorine is a tragic record, with many fluorine chemists of the early 18th and 19th century being described as "fluorine martyrs".[13] While F_2 is an extremely reactive and toxic gas at room temperature, exposure to HF can be lethal, causing deep chemical burns upon contact. In contrast, the native fluorspar (CaF_2) conveys no hint of aggressive chemical properties. Marggraf first prepared HF in 1764 by heating fluorspar with oil of vitriol [sulfuric acid (H_2SO_4)] in glassware, which became corroded by the product. Carl W. Scheele studied the reaction three years later and published his findings

in the seminal paper "*Undersökning om fluss-spat och dess syra*" (Investigation of fluorite and its acid) to the Royal Swedish Academy of Sciences in 1771 (Scheme 1.1).[14] Scheele confirmed the generation of HF by reacting "acid of fluor" with calcium hydroxide solution (CaOH, limewater) which resulted in the precipitation of synthetic CaF_2.[15]

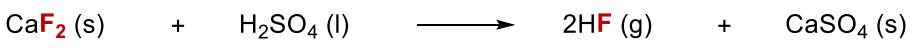

Scheme 1.1. Synthesis of HF from CaF_2 first reported by Scheele in 1771.

Progress isolating elemental fluorine (F_2) was slowed by the considerable dangers of generating and collecting F_2 and operational difficulties associated with the corrosiveness and reactivity of HF. After 74 years of efforts by many chemists, a breakthrough came in 1886 when French chemist Henri Moissan isolated F_2, through the electrolysis of a solution of potassium bifluoride (KHF_2) in liquid HF (Scheme 1.2).[13,16] KHF_2 was prepared by neutralising HF with potassium hydroxide (KOH), as initially reported by Edmond Frémy. Two months before his death, Moissan received the Nobel Prize in Chemistry for his achievements in 1906.

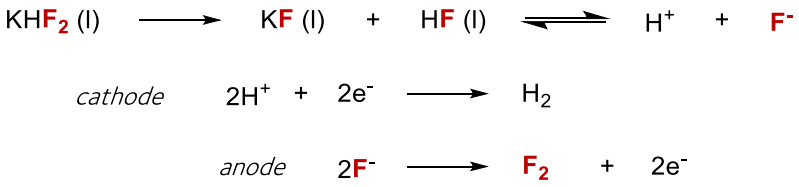

Scheme 1.2. Moissan's electrolysis of KHF_2 to prepare F_2 gas, reported in 1886.

1.3 Development of Fluorine Chemistry

Moissan's work isolation of fluorine gas marked a turning point in fluorine chemistry, which was pivotal in driving significant scientific and technological advances in the 20th century. Nevertheless, HF holds a position of utmost significance to the fluorochemical industry, serving as the starting point for the synthesis and preparation of all commercially available fluorinating reagents, including elemental fluorine (F_2). Organofluorine chemistry, the chemistry of organic compounds that contain a carbon–fluorine bond, remained relatively underdeveloped until the late 19th century. Halogen exchange of the respective organic halide with fluoride using HF or HF-derived metal fluorides, like antimony trifluoride (SbF_3), represents the simplest method to prepare an alkyl fluoride, as demonstrated by Swarts in 1892 when synthesising the first chlorofluorocarbon, CF_2Cl_2 (Freon-12) (Scheme 1.3).[17]

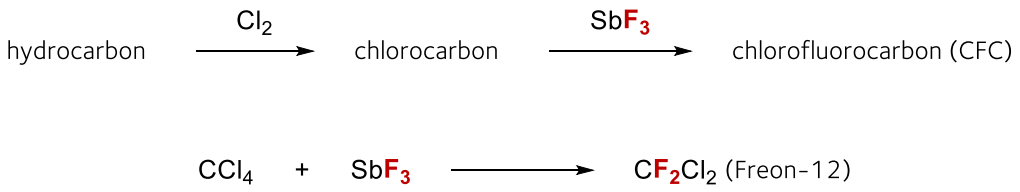

Scheme 1.3. Key "Swarts" process for conversion of chlorocarbons to chlorofluorocarbons.

From 1920 until the early 1940s, the DuPont company commercialised organofluorine compounds, specifically chlorofluorocarbons (CFCs), on large scale, including the production of Freon-12 for refrigerant applications.[18] In subsequent years, it was quickly realised that the photodissociation of CFCs in the stratosphere produced significant amounts of chlorine atoms.[19] This led to the destruction of atmospheric ozone and resulted in several worldwide measures (e.g. the Montreal Protocol in 1987) to ban CFCs and find immediate replacements, such as hydrofluorocarbons (HFCs), with less environmental impact. Another landmark finding was the invention of poly(tetrafluoroethylene) (PTFE) from

tetrafluoroethylene (C_2F_4), which was commercialised following its serendipitous discovery in 1938 (Scheme 1.4).[20]

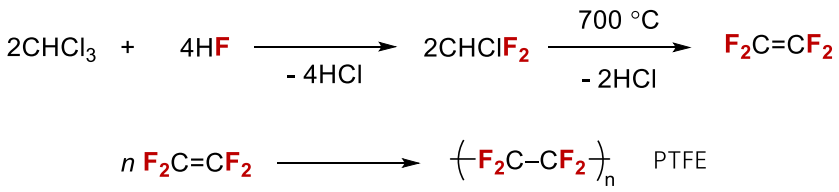

Scheme 1.4. Synthesis of PTFE from tetrafluoroethylene prepared via chloroform.

The first large-scale production of elemental fluorine (F_2) was carried out for the Manhattan Project atomic bomb during the Second World War.[21] Within the same decade, Simons disclosed the first electrochemical fluorination of C-H bonds relying on anhydrous HF and a nickel anode for the production of highly fluorinated compounds, such as trifluoromethanesulfonic acid (CF_3SO_3H, TfOH).[22,23] In 1927, Balz and Schiemann discovered an aromatic fluorination process wherein diazonium tetrafluoroborate salts (ArN_2BF_4, Ar = aryl) were first prepared from arylamines, then decomposed with heating to furnish fluorinated aromatic compounds containing C(sp^2)–F bonds (Scheme 1.5a).[24] Today the Balz-Schiemann reaction is considered to be one of the most important fluorination reactions, opening the field of aromatic fluorination to general study. Another popular aromatic fluorination process is the halogen exchange (halex) reaction, reported by Gottlieb in 1936 for the fluorination of 1-chloro-2,4-dinitrobenzene in nitrobenzene ($PhNO_2$) at 200 °C. This nucleophilic aromatic substitution reaction (S_NAr) entails the conversion of electron-deficient aromatic chlorides to the corresponding aromatic fluorides using KF as a fluorine source (Scheme 1.5b).[25] In this transformation, a fluoride anion selectively replaces a halogen leaving group on a carbon atom through a specific anionic Meisenheimer complex, which is stabilised mesomerically by electron-withdrawing substituents (e.g. NO_2) on the

aromatic scaffold. Release of the original *ipso* substituent, for example as KCl, then restores aromaticity and furnishes the fluoroarene product.

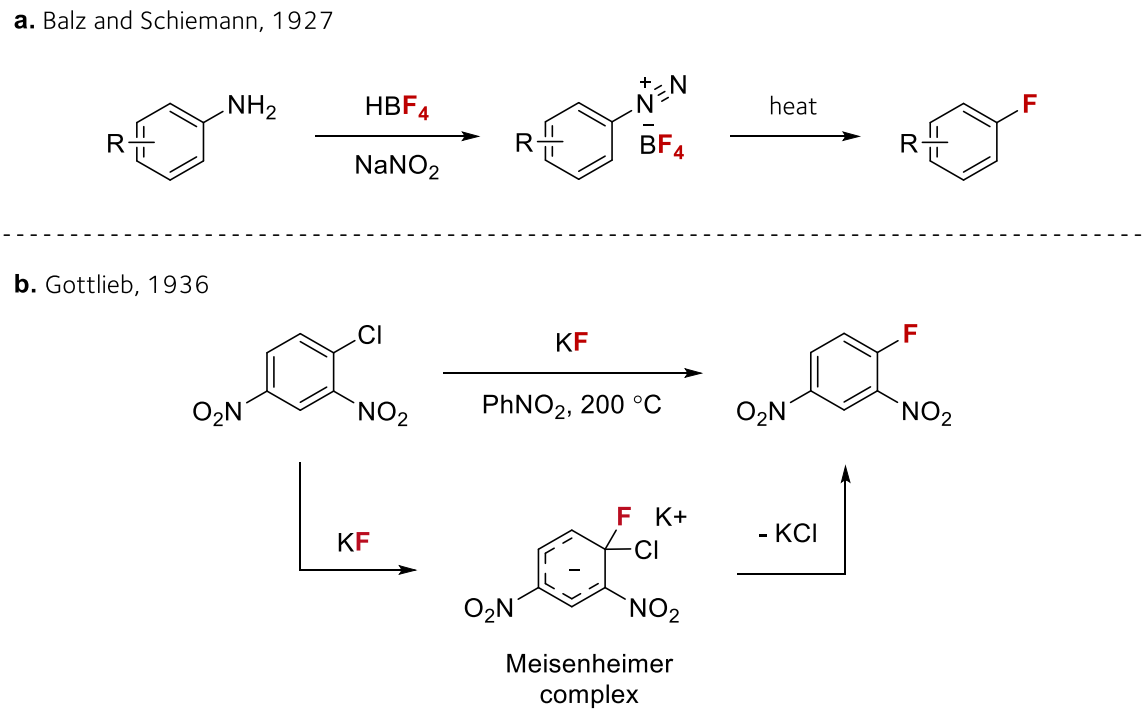

Scheme 1.5. Key examples of nucleophilic aromatic fluorination.

The emergence of milder fluorinating reagents did not occur until the second half of the 20th century. In 1957, the discovery of the first deoxyfluorination reagent, Yarovenko's reagent, revolutionised the field of aliphatic fluorination for the construction of C-F bonds from alkyl alcohols (Scheme 1.6a).[26] Deoxyfluorination gained notable attention following the development of diethylaminosulfur trifluoride (DAST) in 1975 (Scheme 1.6c),[27] which superseded the use of sulfur tetrafluoride (SF_4) (Scheme 1.6b) as a popular deoxyfluorinating reagent used in industry, and HF-complexes used in the fluorination of secondary and tertiary alcohols upon unimolecular nucleophilic substitution (S_N1).[28–30]

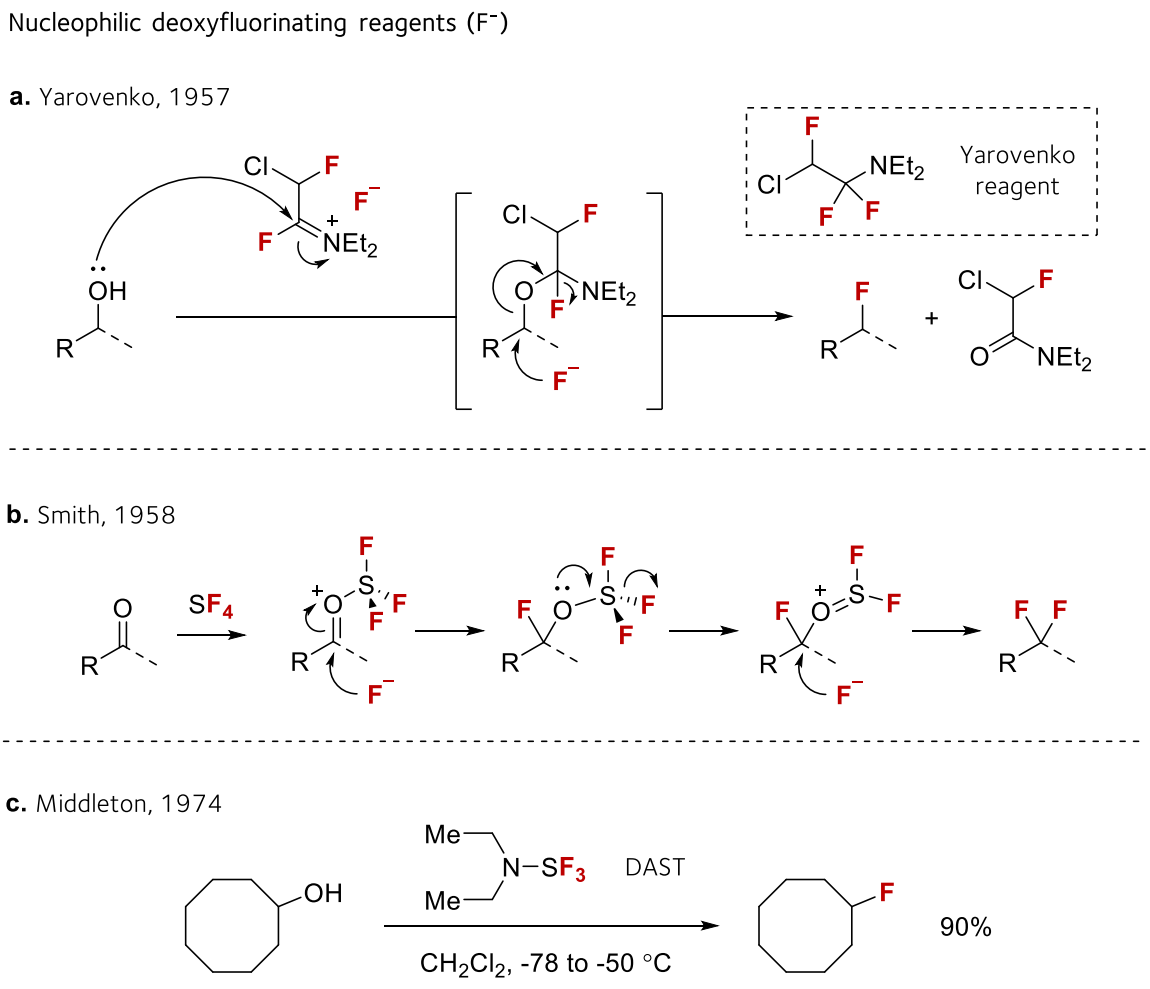

Scheme 1.6. Key developments in deoxyfluorination (DAST, diethylaminosulfur trifluoride).

Organofluorine chemistry took a significant step forward with the discovery of electrophilic (F^+) fluorinating reagents, which are prepared from F_2. Noteworthy examples include *N*-fluorobenzenesulfonimide (NFSI) and 1-chloromethyl-4-fluoro-1,4-diazoniabicyclo[2.2.2]octane bis(tetrafluoroborate) (Selectfluor™), which emerged successively between 1986 and 1992 and were quickly integrated as user-friendly reagents into a wide range of methodologies and enabled previously challenging transformations such as C–H fluorination and asymmetric fluorination.[31,32] Key to the success of these electrophilic N–F reagents is how closely their reduction potentials align with their fluorinating capabilities, aiding in the selection of suitable fluorinating agents for specific reactions (Scheme 1.7).[33,34]

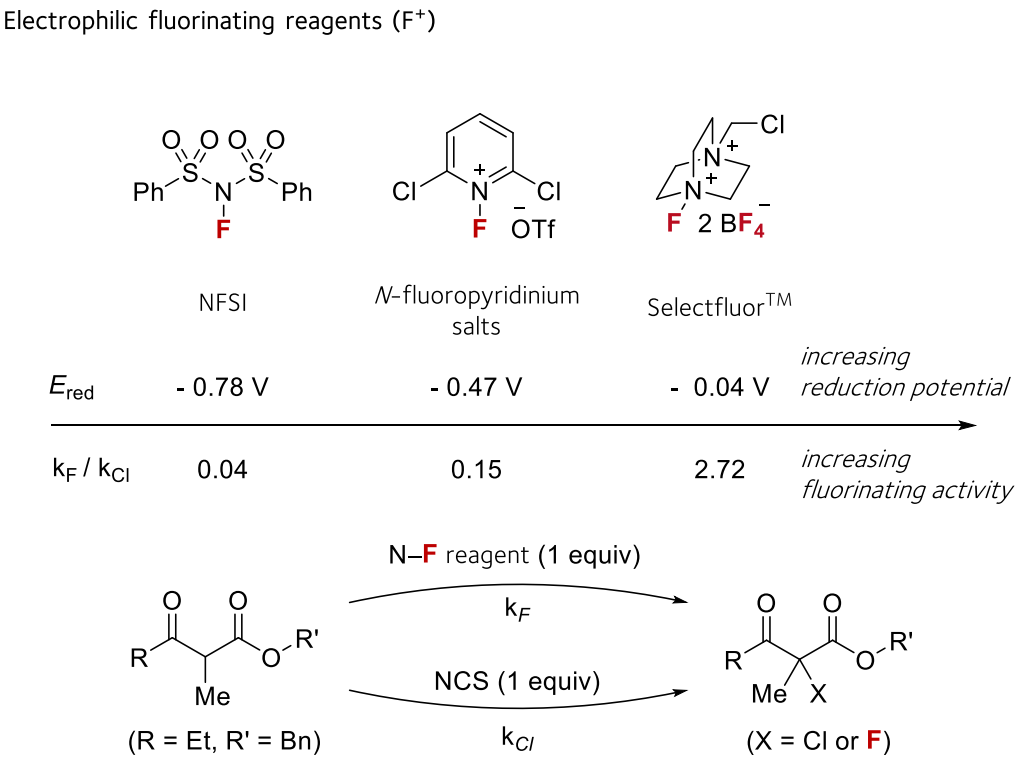

Scheme 1.7. Examples of electrophilic fluorinating reagents and competitive halogenation of a β-keto ester to determine relative rates of fluorination (Togni and co-workers).[34]

Remarkably, the first chemical synthesis of elemental fluorine was achieved by Karl O. Christie in 1986, exactly 100 years after the isolation of F_2 by Moissan, from dipotassium hexafluoromanganate (K_2MnF_6) and antimony pentafluoride (SbF_5).[35] Despite their usefulness, electrophilic fluorinating reagents are difficult and expensive to synthesise, relying on the production, handling and storage of F_2 gas. In contrast, nucleophilic sources of fluoride (F^-), specifically metal fluoride salts (MF, M = Li, Na, K, Cs), are considered cost-effective (e.g., KF £17/mol, Selectfluor® £1800/mol), safer and environmentally friendly fluorinating reagents. However, the use of these metal fluoride salts for fluorination is not trivial. The predominant challenge when considering these metal fluoride salts as reagents is their lack of solubility in organic solvents, rendering reactivity unattainable in most cases.

1.4 Fluorochemicals in Modern Society

Fluorochemicals are utilised in the manufacture of a whole host of items used daily. This class of molecules remains in increasing demand due to their critical role as pharmaceuticals to cure diseases, agrochemicals for food security, coolants for refrigeration, agents for non-invasive medical imaging (^{18}F), fluoropolymers in an abundance of materials and in the production of Li-ion batteries.[9,36,37] Since the Food and Drug Administration (FDA) approved the first fluorocorticosteroid (fludrocortisone) in 1956, over 191 FDA approved drugs (18% of total pharmaceuticals) have been developed that contain at least one fluorine atom. Several blockbuster pharmaceuticals owe their biological activities to the presence of fluorine within their structures (Figure 1.2a).[38] Globally, the use of medications such as favipiravir, an antiviral drug employed in the treatment of viral infections, such as severe acute respiratory syndrome coronavirus 2 (SARS-CoV-2), has resulted in saving numerous lives.[39] Registered fluoro-pharmaceuticals have significantly contributed to the decline in disease prevalence and the enhancement of health outcomes.[40] Amongst them is atorvastatin (Lipitor), a fluorine-containing cholesterol-lowering drug by Pfizer, which is registered as one the best-selling drugs worldwide and the most prescribed medication in the United States.

Fluorochemicals also encompass agrochemicals required to ensure the food security of a growing global population of just over 8 billion people (2024).[41] Fluorine atoms play a key role in addressing this global problem. It is estimated that 50% of agrochemicals registered in the past two decades contain a fluorine atom, including globally used herbicides, such as clodinafop and indaziflam, and fungicides such as tetraconazole (Figure 1.2b).[42]

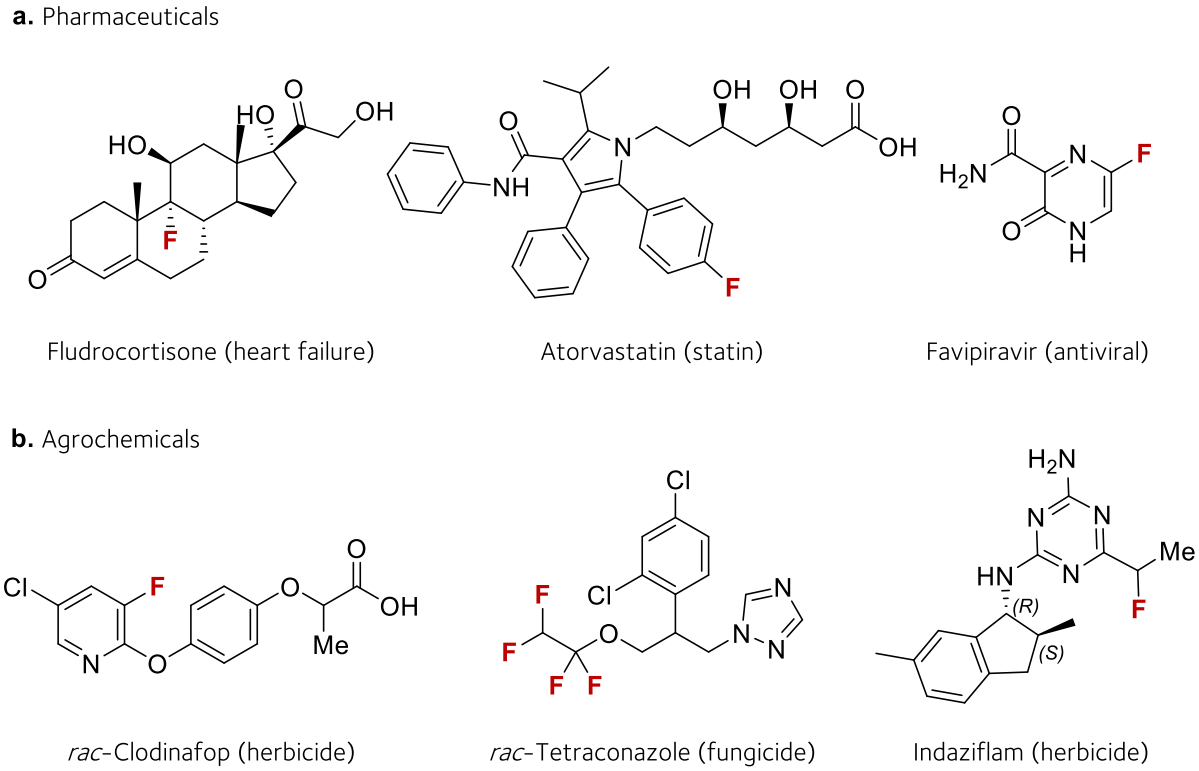

Figure 1.2. Examples of important fluorochemicals in modern society.

A vast number of organofluorine compounds are used for the preparation of fluoropolymers (Figure 1.2c). One of the most important fluoropolymers is undoubtably poly(tetrafluoroethylene) (m.p. 327 °C), a highly chemically resistant, hydrophobic, and low-friction material which has a variety of applications, from non-stick coating (Teflon®) and lubricants to functional textiles such as waterproof jackets (GORE-TEX).[43] When fluorine atoms satisfy all valences of a carbon chain, the zig-zag-shaped carbon skeleton is twisted out of its plane in the form of a helix, and the carbon skeleton is entirely enveloped by fluorine, shielding it from chemical attack.[44] Poly(vinylidene difluoride) (PVDF), a highly non-

reactive thermoplastic fluoropolymer (m.p. 177 °C), is also produced in high quantities for use in applications as films in semiconductors and Li-ion batteries.[45] In addition to polymers, organofluorine compounds are commonly found in liquid crystals for electronic displays and organic light-emitting diodes (OLEDs).[46]

Population growth and a higher standard of living will demand sufficient cheap energy. Fluorine chemistry is poised to be a key player in the future of energy, specifically in the transition towards electrification to substitute fossil fuel-based processes, assisting in achieving net zero emissions and carbon neutrality targets by 2050 or earlier.[47] Renewable energy sources, including solar cells, rely on fluoropolymer backing components, and new-generation hydrogen fuel cells operate on perfluorinated sulfonic acid membranes such as Nafion®.[48,49] Importantly, electrolytes require lithium hexafluorophosphate ($LiPF_6$) as a major component for lithium-ion transport in next-generation batteries for smartphones and electric cars.[50]

1.5 Fluorine Chemistry

Fluorine's small size (van der Waals radius: 1.47 Å; ionic radius 1.33 Å), along with its electron configuration ($1s^2$, $2s^2$, $2p^5$), renders it the most electronegative of all the elements (Pauling electronegativity χ = 3.98) which translates in low-energy atomic orbitals ($2s$(F) = -40.1 eV, $2p$(F) = -18.9 eV).[51,52] As a consequence, fluorine forms highly polarised bonds with marked electrostatic/ionic character that are amongst the strongest covalent bonds known (Table 1.1). For instance, carbon and fluorine valence atomic orbitals have similar energies ($2s$(C) = -19.4 eV vs. $2p$(F) = -18.9 eV) which ensure optimal orbital overlap; the corresponding C–F bond is therefore the strongest known carbon single bond [C(sp^3)–F 460 kJ/mol].

Table 1.1. Mean bond lengths and bond dissociation energies of covalent fluorine bonds.[53]

Bond	Mean bond length (Å)	Dissociation Energy (kJ/mol)	Bond	Mean bond length (Å)	Dissociation Energy (kJ/mol)
F–F	1.44 (F_2)	158.7	C(sp^2)–F	1.34 (C_6H_5F)	532.0
S–F	1.53 (SF_4)	343.5	H–F	0.92 (HF)	569.7
P–F	1.58 (PF_6^-)	405.0	Si–F	1.69 (SiF_6^{2-})	576.4
C(sp^3)–F	1.39 (CH_3F)	460.2	B–F	1.37 (BF_4^-)	732.0

Introducing fluorine into a biologically active compound is a very effective means for modulating its physicochemical and biological properties, such as metabolic stability, lipophilicity, acidity (pK_a) and reactivity.[36] Because of fluorine's similar size to hydrogen, the C–F bond is only slightly longer than the C–H bond [C(sp^3)–F bond 1.39 Å versus C(sp^3)–H 1.09 Å], enabling the substitution of hydrogen for fluorine as a bioisosteric replacement without drastically changing the structure and steric profile of the compound.[53,54] However, unlike hydrogen, the high electronegativity of fluorine (χ = 3.98) relative to carbon (χ = 2.55) imparts a strong dipole moment to the C–F bond through a negative inductive effect. Consequently, fluorine substituents often engage in hydrogen-bonding and dipole-dipole interactions with adjacent functional groups on the bioactive molecule itself or with the biological target of interest.[55] Such interactions have been extensively characterised through NMR spectroscopy and X-ray crystallographic studies for applications in medicinal chemistry and catalysis.[56,57]

The low-lying, antibonding orbital (σ^*) of the C–F bond enables it to participate in hyperconjugation interactions, resulting in subtle stereoelectronic effects, such as the gauche effect, which can influence the conformation of fluorinated molecules.[58] The introduction of fluorine can also alter the pK_a of neighbouring functionalities and increase the

stability of adjacent bonds. For example, the C–F bond energy increases from approximately 460 kJ/mol in CH_3F to 550 kJ/mol in CF_4 (CH_3–F 1.39 Å versus CF_3-F 1.32 Å).[59]

Fluorine is a monoisotopic element, and its only naturally existing nuclide is ^{19}F. This characteristic is beneficial for analytical uses as ^{19}F possesses a nuclear spin of I = ½, which can be likened to a proton in terms of sensitivity. The gyromagnetic ratio of ^{19}F amounts to 94% of that of ^{1}H (^{1}H γ 26.75 versus ^{19}F γ 25.18 10^7 rad T^{-1} s^{-1}). Thus, it is very convenient to use ^{19}F NMR spectroscopy (solution-phase or solid-state) as an analytical technique for monitoring reaction progress and to gain information about a fluorinated compound's structure, aggregation and conformation.[60,61] Typical chemical shifts for selected fluorinated compounds, which in practice depends on solvent and temperature, are listed in Figure 1.3. Coupling constant (*J*) values provide valuable information for characterisation and vary significantly, such as 100-200 Hz for a ^{19}F–^{13}C one-bond coupling and 500-1500 Hz for ^{19}F–^{31}P couplings.[62]

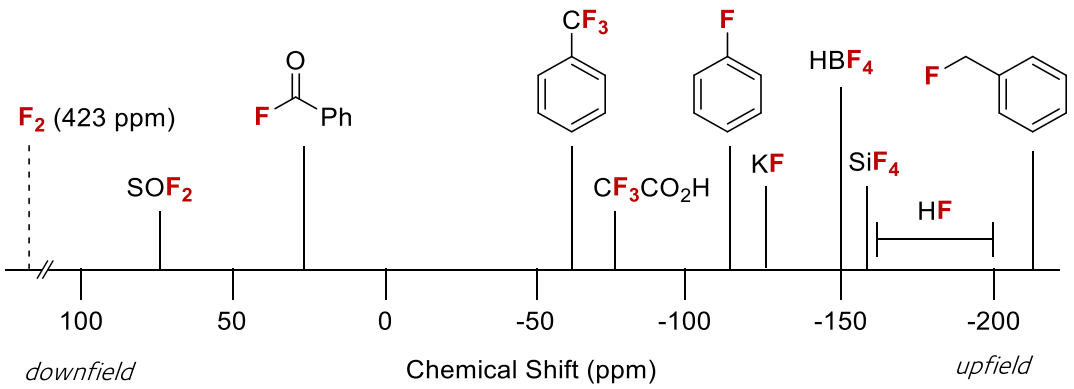

Figure 1.3. Chemical shifts of selected fluorochemicals in $CDCl_3$ ($CFCl_3$ ref δ=0.65 ppm).

The other widely recognised isotope is ^{18}F, an important positron-emitting radioisotope produced for applications in positron emission tomography (PET) medical imaging.[63,64]

1.6 The Fluorochemical Industry

Hydrogen fluoride (HF) sits at the apex of the entire fluorochemical industry. Current industrial production of HF involves feeding a slurry of acid-grade fluorspar [AGF, >97% CaF_2, main impurities SiO_2 (1%), $CaCO_3$ (1%), Al_2O_3 and Fe_2O_3 (1%)] and concentrated sulfuric acid (H_2SO_4) into a rotary kiln at approximately 285 °C.[65] The process is highly endothermic and generates HF as gas and calcium sulfate ($CaSO_4$) as a solid by-product, which serves as feedstock for synthetic gypsum used in the construction industry.[66,67] The gaseous products are cooled, scrubbed, and condensed to afford anhydrous HF (98 to 99% grade), which is purified by distillation to 99.5% purity by assay, the principal impurities being SiF_4, H_2SO_4, H_2O and FSO_3H.[68] HF is primarily manufactured in the United States and Europe, relying on fluorspar imported from China, Spain and Mexico by boat, rail or barge (approximately 600,000 tonnes of AGF is consumed by the United States alone annually). The HF produced is stored as a liquefied gas (b.p. - 19.5 °C), or diluted in water to produce aqueous hydrofluoric acid solutions [b.p. 112 °C, 38% w/w (H_2O)], serving as the chemical feedstock for all fluorochemicals (Figure 1.4).[69]

Approximately 80% of HF is consumed in (1) the manufacture of fluorocarbons [CFCs, HFCs, HCFCs (hydrochlorofluorocarbons)], (2) the manufacture of synthetic cryolite [$Na_3(AlF_6)$] and (3) petroleum alkylation.[9,10] The remaining 20% encompasses the manufacture of fluorinating reagents, including metal fluoride salts, SF_4 and F_2 gas for the downstream production of fluorochemicals.[44]

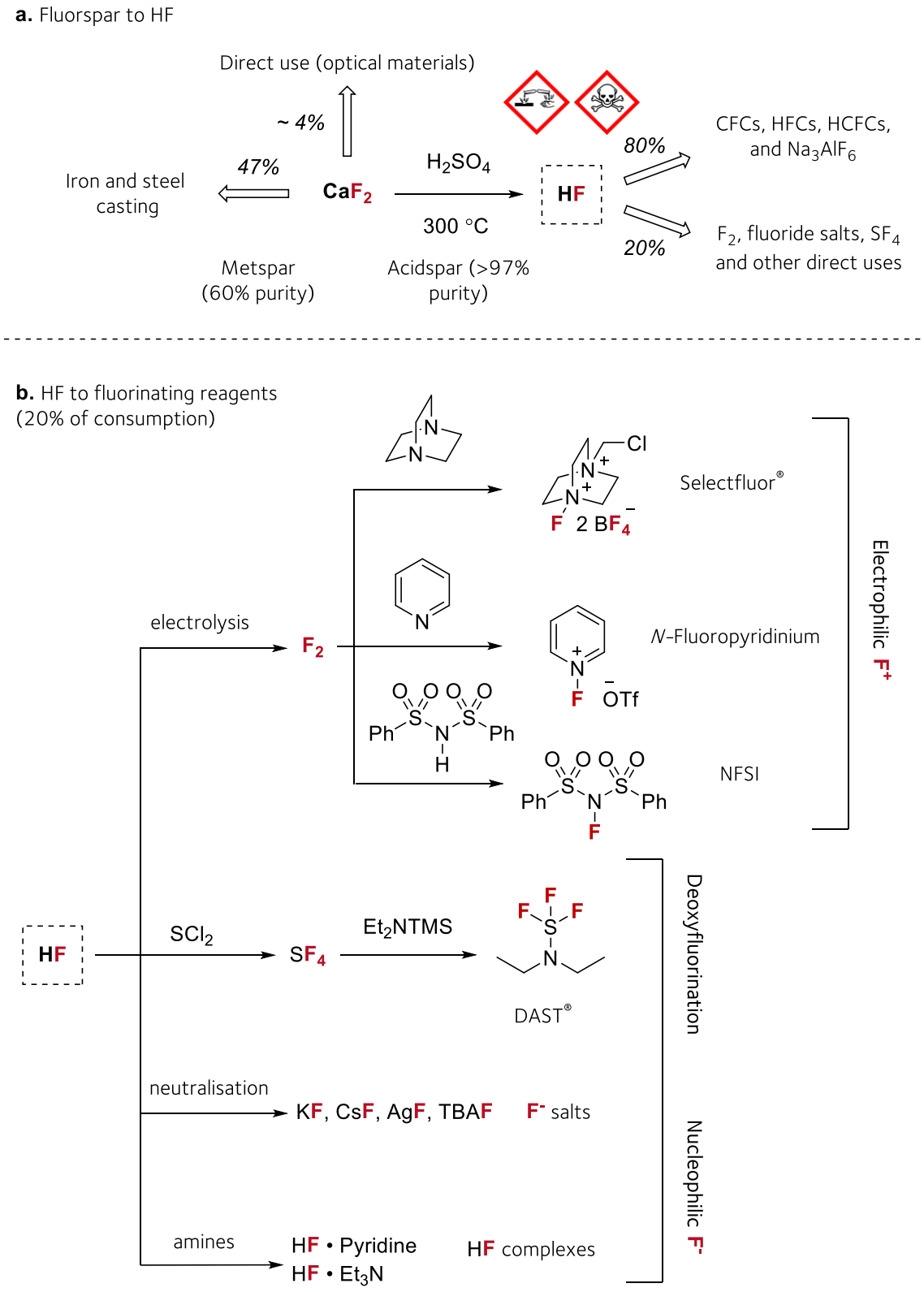

Figure 1.4. Industrial fluorochemical chain supply toward fluorinating reagents used to prepare fluorochemicals.

HF is not a process-friendly reagent in a typical laboratory setting, as it can dissolve glass by reacting with silicon. In diluted, aqueous systems, HF is only a weak acid (pK_a 3.19) forming acidic $[H_3O]^+F^-$ pairs instead of fully dissociated hydronium ions (H_3O^+) due to high H-F affinity.[69] Many laboratories in the pharmaceutical industry continue to use aqueous HF in solid-phase peptide synthesis (SPPS) to remove side chain protecting groups, such as *tert*-butyloxycarbonyl (Boc) or benzyl (Bn), from peptides and release them from the solid support resin. All electrophilic fluorinating reagents are derived from F_2 gas, which in turn is prepared by electrolysis of HF in a perfected version of Moissan's process. Furthermore, HF is used directly in the synthesis of many fluorocarbons, notably CCl_2F_2, $CClF_3$ and tetrafluoroethylene, and fluoropolymers (section 1.3 Development of Fluorine Chemistry).

Apart from synthesis, HF is used in the glass, semiconductor and nanotechnology industries as etching and polishing agents.[70] This leads to the generation of aqueous waste that contains substantial amounts of HF, which can be treated via coagulation using calcium hydroxide [$Ca(OH)_2$] or calcium chloride ($CaCl_2$) to afford synthetic CaF_2.[71] The fate of most of this synthetic CaF_2 is landfill. HF is also commonly used as a solvent for inorganic salts, for pickling of stainless steel, and as a catalyst in alkylation reactions in petroleum refineries.[72] The process of producing gasoline through HF-based alkylation instils the highest fear among refinery workers and safety specialists, and this concern is justified.[73] HF is a highly dangerous acid that requires specialised equipment, storage and constant vigilance to prevent a release. Due to its corrosive nature, it must be handled carefully since it can penetrate the skin, causing severe burns and toxicity as the fluoride ion reacts with calcium in the body.[73]

Despite stringent safety guidelines, HF spills have occurred, some with fatal accidents and detrimental environmental impacts. For example, a leak of approximately 2,500 litres of HF in a South Korean factory in 2012 caused widespread environmental damage, sickening thousands of workers with long-lasting health effects and leaving a disaster zone in its

wake.[74,75] In 2019, a fire and multiple explosions occurred at a Philadelphia refinery due to HF corroding through a pipe, releasing over 3000 kg of HF and ultimately resulting in the plant's bankruptcy.[76]

Today, industrial fluorinations still heavily rely on the use of dangerous reagents such as HF (nucleophilic fluorination), F_2 (electrophilic fluorination), or SF_4 (deoxyfluorination), which often result in violent, sometimes explosive reactions.[77,78] The principal methods for the preparation of organic fluorine compounds include substitution of hydrogen in hydrocarbon feedstocks for fluorine, halogen-fluorine exchange (Swarts-type chemistry or nucleophilic aromatic fluorination), building block approaches using reactive fluorinated synthons or the addition of fluorine to unsaturated bonds.[44,79]

1.6 Nucleophilic Fluorination

Nucleophilic fluorination strategies provide an effective method for the installation of fluorine through polar mechanisms, such as bimolecular (S_N2) or unimolecular (S_N1) nucleophilic substitution reactions leveraging a diverse range of pre-installed or native functional groups (Figure 1.5).[80] However, fluoride's limited reactivity as a nucleophile and strong basic properties present a considerable synthetic challenge for achieving nucleophilic fluorination through substitution reactions.

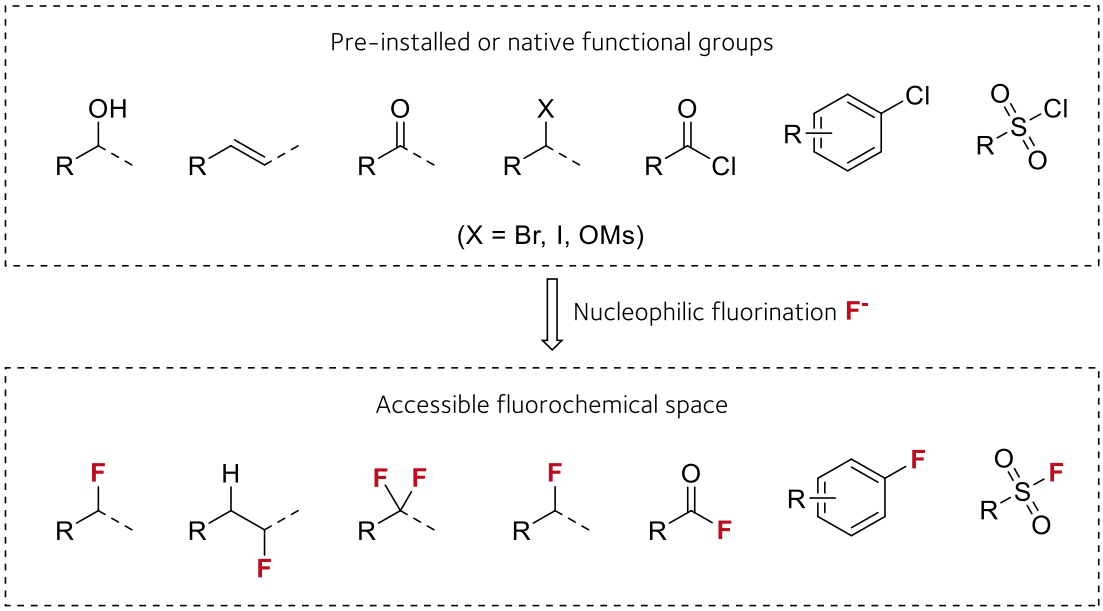

Figure 1.5. Strategies to leverage functional groups for nucleophilic fluorination.[80]

The simplest and cheapest source of nucleophilic fluoride is CaF_2, followed by HF. Since HF is only a weak acid in an aqueous solution, fluorination reactions are often carried out using anhydrous HF as both reagent and solvent, typically in the form of anionic $[(HF)_nF^-]$ species or as HF-complexes. The most prominent are triethylamine (TREAT-HF, $Et_3N.3HF$) and pyridine adducts (Olah's reagent), which are commercially available.[81] However, HF-based reagents require specialised handling and strict safety precautions.

Alkali metal fluorides are popular nucleophilic fluorinating reagents as they are easy to handle and safer than HF-based reagents. Lithium fluoride (LiF), sodium fluoride (NaF), potassium fluoride (KF), rubidium fluoride (RbF) and cesium fluoride (CsF) are all formed upon treatment of aqueous HF with the respective metal hydroxide or carbonate. Given its high charge density, fluoride anion forms extremely strong ionic bonds with alkali metal cations to form ionic solids with high lattice energy (ΔU_L).[53,82] The lattice energy of the alkali metal fluoride decreases with increasing ionic radius of the cation (Table 1.2).

Table 1.2. Physical properties of metal fluorides.

Metal Fluoride	Cation radius (Å)	ΔU_L (kJ/mol)	Solubility (g/100 mL H_2O, 25 °C)	m.p. (°C)
CsF	1.67 (Cs^+)	744	573	703
KF	1.52 (K^+)	808	102	858
NaF	1.16 (Na^+)	910	3.97	995
LiF	0.90 (Li^+)	1030	-	848
CaF_2	1.14 (Ca^{2+})	2640	0.0016	1420

The dense negative charge of fluoride anions causes them to be stabilised and deactivated in most chemical environments by strong electrostatic attractions with their countercations or by hydrogen bonding with other molecules such as water, alcohols or amides. The crystal structures of the two deliquescent hydrates of KF ($KF{\cdot}2H_2O$ and $KF{\cdot}4H_2O$) have been determined and unveiled hydrogen bonding between fluoride ions and water molecules.[83] In the presence of water, fluoride forms tight hydration shells (ΔG_{hydr} = -436 kJ/mol).[84] As a consequence, alkali metal fluoride salts are hygroscopic, a property which increases with cation size (CsF is highly hygroscopic, whereas LiF is non-hygroscopic). The relationship between solubility in water and lattice energy is such that CsF has the weakest crystalline lattice and thus highest solubility in water. Although alkali metal fluorides are poorly soluble in organic solvents, CsF is fully soluble in methanol at room temperature (191 g/100 mL of methanol). On the other hand, KF is extremely soluble in glacial acetic acid (27.7 g/100 mL).[85] However, the nucleophilicity of the fluoride ions is significantly reduced due to strong hydrogen bonding.

Considerable attention has been dedicated to investigating sources of highly reactive "naked" fluoride anions which are soluble in organic solvents. To obtain reasonable solubility of alkali metal fluoride salts in organic solvents, crown ethers or cryptands that can

encapsulate the metal cation liberating "naked" fluoride are commonly used (Figure 1.6).[86,87] Of these, 18-crown-6 is highly effective at increasing metal fluoride solubility in organic solvent, especially when the cation ion size matches the cavity of the crown ether.

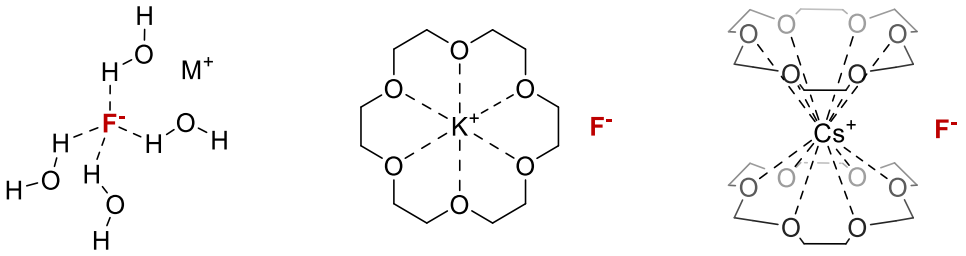

F^- ionic radius 1.33 Å
ΔG_{hydr} = -436 kJ/mol

18-crown-6 KF complex
K^+ ionic radius 1.52 Å

18-crown-6 CsF sandwich
Cs^+ ionic radius 1.67 Å

Figure 1.6. Hydrated fluoride with H-bonding and 18-crown-6 fluoride complexes.

An alternative, closely related approach to overcome the low solubility of metal fluorides is to instead use fluoride salts with large organic cations. [88] Of these, tetraalkylammonium salts TMAF (Me_4NF) and TBAF (n-Bu_4NF) are by far the most commonly used nucleophilic fluorinating reagents (Figure 1.7). However, given their high hygroscopicity, they are often prepared as hydrates and then subsequently dried to their anhydrous form, which can cause stability issues. This is the case for TBAF which bears β-hydrogens that are prone to Hofmann elimination even at 25 °C.[89]

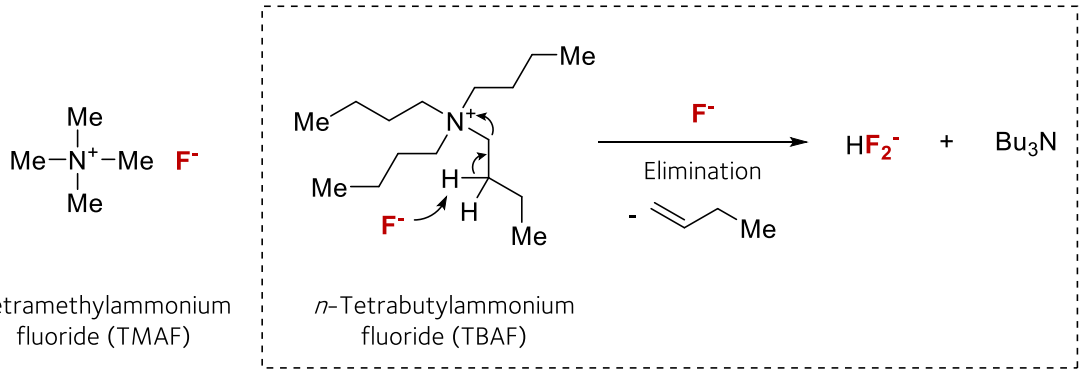

Tetramethylammonium fluoride (TMAF)

n-Tetrabutylammonium fluoride (TBAF)

Figure 1.7. Archetypal tetraalkylammonium fluoride salts, tetramethylammonium fluoride (TMAF) and tetrabutylammonium fluoride (TBAF), which is prone to Hofmann elimination.

A caveat of these approaches is that although encapsulation or separation of the cation allows for the release of "naked" fluoride, thus increasing its nucleophilicity, the basicity of fluoride is also enhanced.[90] In some cases, this can lead to unwanted side reactions such as cleavage of base-labile groups or elimination. Basic fluoride reacts readily with weak hydrogen bond donors to form HF, which can react further with fluoride to afford bifluoride (HF_2^-), a stable anion with the strongest known hydrogen bond (~ 212 kJ/mol).[91–93]

Strategies to solubilise and control fluoride reactivity, favouring nucleophilicity over basicity by harnessing the power of H-bonding interactions, have also been developed. A 1994 study by Yonezawa and co-workers assessing the reactivity of a series of alcohol TBAF adducts in a model S_N2 reaction with benzyl bromide revealed that the reaction rate positively correlated with the steric bulk of the hydrogen bond donor (*t*-BuOH ≫ *i*-PrOH > *n*-BuOH > H_2O).[94] Kim and co-workers reported that performing fluorinations in bulky aliphatic alcohol solvents, such as *tert*-amyl alcohol (*t*-AmOH) and *tert*-butanol (*t*-BuOH), greatly enhanced the rate and selectivity in S_N2 fluorination with CsF through alcohol-fluoride hydrogen bonding interactions.[95] Building on detailed reactivity and characterisation studies of urea-fluoride and alcohol-fluoride complexes as fluorinating reagents, in 2018, the Gouverneur group disclosed a chiral *N*-alkyl *bis*-urea hydrogen bonded fluoride complex for solid-liquid phase transfer to enable catalytic enantioselective nucleophilic fluorination of *β*-bromosulfides with CsF (Figure 1.8). [96–99] Whilst this was the first example using an alkali metal fluoride salt for enantioselective fluorination, it also marked significant progress in the field by using hydrogen bonding interactions within an organocatalytic system to surmount challenges associated with the insolubility of metal fluoride salts in organic solvents.[100] This strategy, coined Hydrogen Bonding Phase Transfer Catalysis (HB-PTC) has since advanced to enable enantioselective fluorinations of azetidinium (using CsF) and aziridinium substrates (using KF).[101,102] In a more complex setting, hydrogen bonding strategies could be synergised

with calcium cation (Ca^{2+} ionic radius 1.14 Å) complexation to solubilise CaF_2 for fluorination; however, this represents a challenging endeavour.

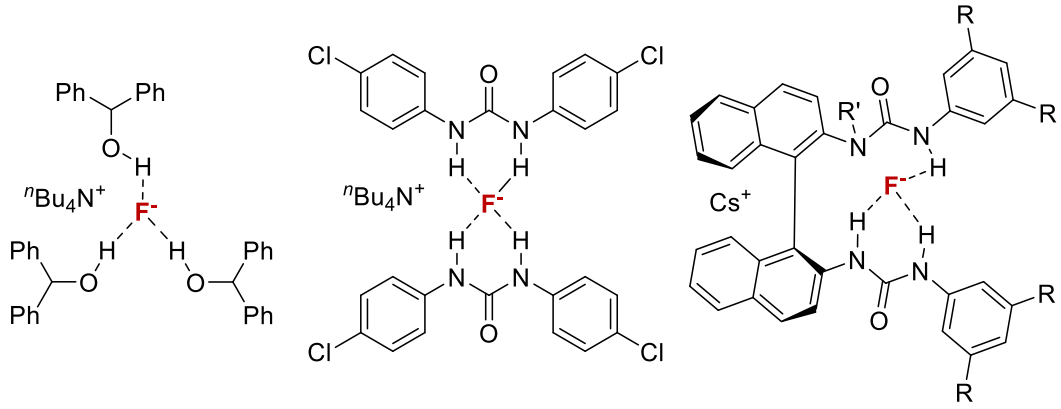

Diphenylmethanol TBAF complex (3:1)

Urea TBAF complex (2:1)

Chiral *N*-alkyl bis-urea CsF complex

Figure 1.8. Coordination diversity in hydrogen-bonded fluoride-alcohol and urea complexes synthesised and characterised by the Gouverneur Group (R = CF_3, R' = *i*-Pr).

1.7 Calcium Fluoride Chemistry

The prospect of directly employing CaF_2 as a fluorinating reagent was first conceptualised by Bruce Smart at the 17th American Winter Fluorine Conference, stating, "There are no direct processes that use fluorspar, except to make HF".[103] This goal is well recognised in the field of fluorine chemistry and many research groups in academia and industry have tried to formulate solutions, unsuccessfully. Access to essential fluorochemicals directly from fluorspar (CaF_2), thereby avoiding the production, storage and transportation of HF, decreasing energy requirements, and streamlining the current high-maintenance supply chain would represent a paradigm shift. Reducing step count signals a shift toward sustainable fluorochemical production by reducing or eliminating the generation of waste otherwise produced in the current "state-of-the-art" process.[104] Furthermore, fluorspar is the cheapest source of fluoride (£1.50 per mol CaF_2).

Fluorination chemistry using CaF_2 directly is viewed as inaccessible because of its high lattice energy (ΔU_L 2640 kJ/mol, or 1320 kJ·mol^{-1} for each mole of fluoride generated) and its almost complete insolubility in any solvent, including water (0.016 mg/mL, 18 °C).[53] Under ambient conditions, CaF_2 (m.p. 1420 °C) crystallises in the well-recognised face-centred cubic (FCC) fluorite structure (space group $Fm\bar{3}m$) wherein Ca^{2+} ions are cubically coordinated to eight nearest-neighbour F^- ions (Figure 1.9).

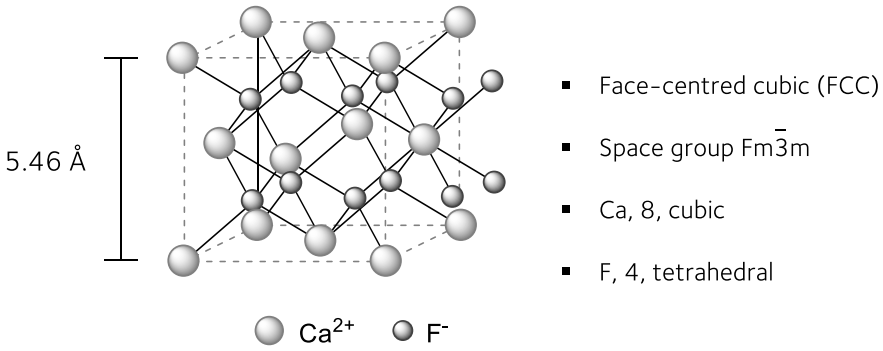

Figure 1.9. Unit cell of CaF_2, known as fluorite structure, with crystallographic parameters.

The use of porous high surface area CaF_2, prepared from soda lime (~80% CaOH) and HF, has been used in combination with KF for the halex reaction of α-chloro ethers.[105] However, few methods to prepare fluorochemicals from CaF_2 have been developed. Rare examples rely on harsh reaction conditions such as elevated pressures and high temperatures (> 200 °C) and highly corrosive chemicals, such as sulfur trioxide (SO_3), necessitating specialised equipment and glassware. In 1941, Frary and co-workers reported the synthesis of phosphorus fluorine-containing compounds from CaF_2 (Scheme 1.8).[106]

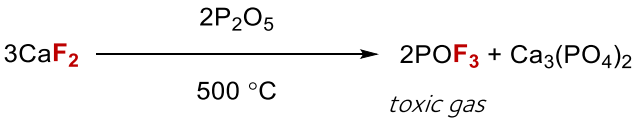

Scheme 1.8. Reaction of P_2O_5 with CaF_2 by Frary and co-workers (1941).

When heated to 500 °C, mixtures of CaF_2 and phosphorus pentoxide (P_2O_5) in an iron vessel afforded volatile phosphorus oxyfluoride (POF_3, -39.7 °C), a highly toxic gas. No yield for POF_3 was reported. The production of phosphorus pentafluoride (PF_5, b.p. -84.6 °C) gas directly from CaF_2 has also been described in a patent (Scheme 1.9).[107] A rotating autoclave containing iron balls, CaF_2 (3 equiv) and P_2O_5 (1 equiv) was heated to 300 °C with the addition of of sulfur trioxide (SO_3, 4 equiv) gas to yield PF_5. Replacement of P_2O_5 for boron trioxide (B_2O_3) or arsenic trioxide (As_2O_3) afforded boron trifluoride (BF_3) or arsenic trifluoride (AsF_3) as gaseous products, respectively.

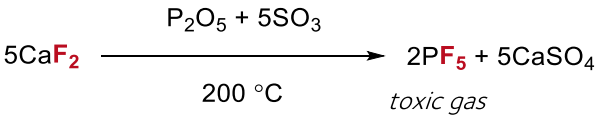

Scheme 1.9. Reaction of P_2O_5 and SO_3 with CaF_2 (1932).

Muetterties and Coffman demonstrated that the reaction of CaF_2 and 2 moles of SO_3 at 200 °C occurred slowly to give calcium fluorosulfonate [$Ca(SO_3F)_2$].[108] It was noted that $Ca(SO_3F)_2$ converted into CaF_2 and SO_3 at temperatures >500 °C. Alternatively, the reaction of CaF_2 with excess SO_3 (3 equiv) at 300 °C for 24 h, followed by the addition of H_2O, afforded pyrosulfuryl fluoride ($S_2O_5F_2$), with $CaSO_4$ as a by-product (Scheme 1.10).

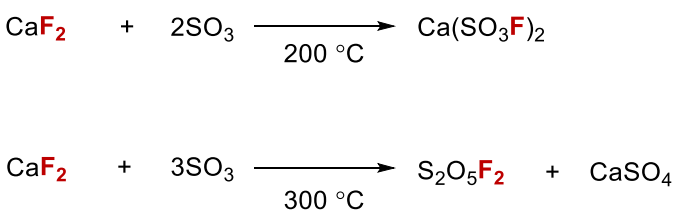

Scheme 1.10. Calcium fluorosulfonate [$Ca(SO_3F)_2$] and pyrosulfuryl fluoride ($S_2O_5F_2$) from the reaction of SO_3 with CaF_2.

Pyrosulfuryl fluoride ($S_2O_5F_2$, b.p. 51 °C) has been employed in the synthesis of fluorosulfates, however, the high toxicity and operational challenges associated with this reagent has impeded adoption in organic chemistry.[109,110] By contrast, the chemistry of $Ca(SO_3F)_2$ is unexplored.[111] A patent filed in 1975 reported the observed formation of difluoromethylated compounds upon passing gaseous carbonyl precursors over $Ca(SO_3F)_2$ heated to 200-300 °C. For example, the employment of carbon monoxide (CO) gas generated tetrafluoroethylene, exclusively.[112]

In 2020, Togni and co-workers disclosed a deoxygenative fluorination reaction in which phosphine oxides were converted to organophosphorus(V) fluorides compounds using KF and oxalyl chloride [$(COCl)_2$].[113] In the presence of excess KF (6 equiv) and $(COCl)_2$ (3 equiv), triphenylphosphine oxide underwent quantitative conversion to difluorotriphenyl-λ^5-phosphorane (Ph_3PF_2) at room temperature in acetonitrile (MeCN). In a supporting information, the authors reported that the replacement of KF for CaF_2 (12 equiv) led to the formation of Ph_3PF_2 in 48% yield (as measured by ^{19}F NMR spectroscopy). The authors propose that the fluorination reaction proceeds through putative generation of oxalyl fluoride *in situ*, halex exchange or direct fluorination of phosphorus.

Lithium hexafluorophosphate ($LiPF_6$) is the main commercial electrolyte for Li-ion batteries at present. In industry, $LiPF_6$ is prepared via the reaction of LiF and PF_5. For the process, PF_5 is obtained via the fluorination of PCl_5 with HF. In addition to the high toxicity of HF, the method suffers from the generation of corrosive HCl waste which is oversupplied in the market and requires careful waste management. A method to address these drawbacks was disclosed by Yu and co-workers in 2019, who demonstrated a HF-free route to PF_5 via the reaction of CaF_2 (>99%, 1 tonne) and PCl_5 (1 tonne) at 350°C.[114] In this case, $CaCl_2$ is generated as a by-product. Introduction of the generated PF_5 to a suspension of LiF in

butyronitrile (C_3H_7CN) enabled the generation of $LiPF_6$ on kilogram scale (97% yield) (Scheme 1.12).

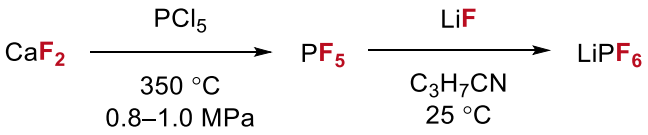

Scheme 1.12. Synthetic route of $LiPF_6$ developed by Yu and co-workers (2019).

Methods to prepare C-F bonds using CaF_2 directly are practically non-existent. An early example, disclosed in 1933 by E. I. DuPont de Nemours and Co, includes the preparation of CF_2Cl_2 and CF_3Cl by passing vapourised CCl_4 over heated CaF_2 (500 °C).[115] It is unclear whether HCl or HF are generated or involved at any stage of the process. In 1978, the Allied Chemical Corporation patented a method to prepare acetyl fluoride via halex exchange at 70-130 °C using CaF_2 in the presence of a crown ether. Although the patent describes product yield in up to 65%, yields of fluorinated products were estimated based on the relative amounts of unreacted starting material found.[116]

In 1949, Dow Chemical Company disclosed the formation of alkali metal fluorides and calcium hydroxide [$Ca(OH)_2$] by activating ground fluorspar with an alkali metal hydroxide at high temperatures.[117] Heating fluorspar (1 equiv) and KOH (2 equiv) to 250 °C for 2 h formed a dry solid composed of KF and $Ca(OH)_2$, in addition to small proportions of the perovskite potassium calcium fluoride ($KCaF_3$), as evidenced by powder X-ray diffraction (PXRD) analysis. Heating the solid to 800 °C resulted in a final material containing KF (50%), CaO (40%) and $KCaF_3$ (10%). Grinding the material and adding it to ethyl chloroacetate or benzoyl chloride in a steel autoclave with heating (up to 243 °C) afforded ethyl fluoroacetate and benzoyl fluoride, in 50% and 45% yield, respectively. Hydroxides of sodium, lithium, barium and strontium were also investigated, and corresponding binary

metal fluorides were formed (evidenced by PXRD) in all cases. In the presence of moisture, or when added to water, the solid products formed upon heating ground fluorspar with the alkali metal hydroxide revert almost instantly to CaF_2 and the initial alkaline hydroxide, restoring the thermodynamically stable states at standard conditions.

In inorganic chemistry, few examples of well-defined calcium fluoride complexes are reported, ranging from inorganic clusters to main group complexes (Figure 1.10). Despite their complex structure, these cluster complexes usually feature interconnected cages with bridging Ca–F bonds and multidentate ligands at calcium. Independently reported β-diketiminate complexes by Roesky and by Barrett and Hill, marked the introduction of the first distinct dimeric Ca–F complexes that displayed solubility in organic solvents (C_6D_6). However, neither system was directly synthesised from CaF_2 nor demonstrated the delivery of nucleophilic fluoride anions. The groups of Aldridge and Gouverneur recently published findings on the synthesis and reactivity of 4,5-bis(2,6-diisopropylanilido)-2,7-di-*tert*-butyl-9,9-dimethylxanthene (NON) and 1,4,7-triazacyclononane (TACN) stabilised Ca-F complexes prepared using trimethyl tin fluoride (Me_3SnF) and tetramethylammonium fluoride (Me_4NF), respectively.[118,119] The reported anionic complexes are unique in being able to deliver fluoride to electrophilic substrates, such as triphenylsilyl chloride (Ph_3SiCl). These discoveries will guide future endeavours in formulating soluble molecular Ca–F complexes, thereby enhancing the foundational knowledge of the nucleophilic nature of the Ca–F bond.

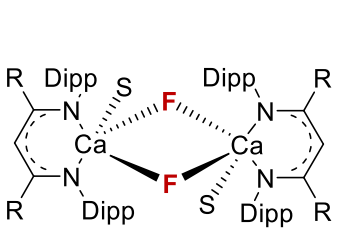

Roesky (R = Me) 2007
Barrett & Hill (R = CF_3) 2007

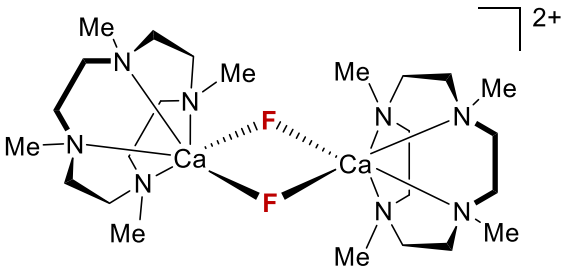

Okuda 2020

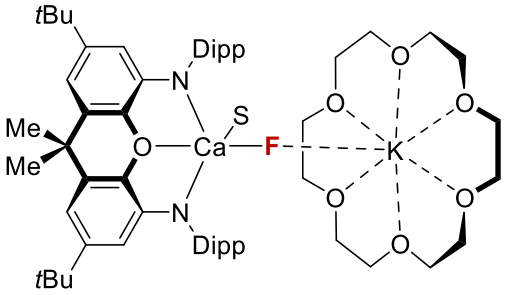

[K(18-crown-6)FCa(THF)(DippNON)]

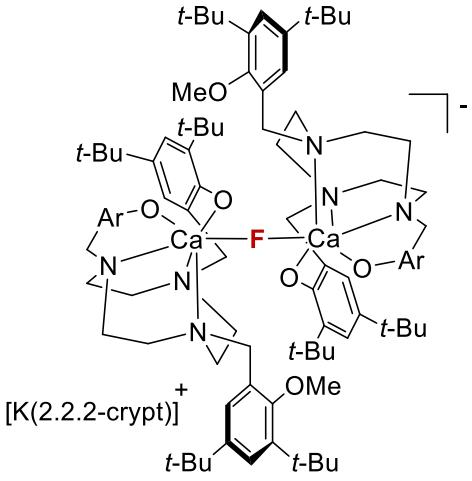

[K(2.2.2-crypt){(*t*-BuTACN-Me)Ca}$_2$(μ-F)]

Aldridge and Gouverneur 2024

Figure 1.10. Selected examples of calcium fluoride complexes [S = THF, Dipp = 2,6-*i*-$Pr_2C_6H_3$, NON = 4,5-bis(2,6-diisopropylanilido)-2,7-di-*tert*-butyl-9,9-dimethylxanthene, 2.2.2-crypt = 4,7,13,16,21,24-hexaoxa-1,10-diazabicyclo(8.8.8)hexacosane, TACN = 1,4,7-triazacyclononane].

1.8 Overview of Thesis

Fluorine chemistry has progressed significantly since Scheele's synthesis of HF and Moissan's discovery of elemental fluorine and has played a vital role in modern advances of the 21st century. Despite early demonstrations of the potential of CaF_2 as a fluoride source, albeit under harsh conditions often relying on hazardous chemicals, the use of fluorspar as a fluorinating reagent remained relatively underexplored. Today, current manufacturing of all

fluorochemicals still relies on the centuries-old process of reacting acid-grade fluorspar with concentrated H_2SO_4 at 285 °C to give HF - one of the most dangerous acids used on scale in manufacturing plants. Accessing fluorochemicals directly from fluorspar would represent an attractive alternative, however, the challenge at hand is considerable, given the high insolubility of CaF_2.

This thesis focuses on the development of methodologies that convert fluorspar into essential fluorochemicals applying operationally simple, non-hazardous and energy-efficient methods that bypass the production of HF. Thinking beyond traditional solution-phase chemistry, the first method discussed in **Chapter 2** examines the mechanochemical (solid-state) activation of fluorspar using a basic phosphate salt. Distinct from the current Brønsted acid (H_2SO_4) based activation, this method involves ball milling acid-grade fluorspar (>97% CaF_2) with a potassium phosphate salt to create a new inorganic fluorinating reagent capable of forging S-F and C-F bonds, bypassing HF entirely. Also discussed are mechanistic studies on the solid-state reaction between CaF_2 and K_2HPO_4 using powder X-ray diffraction, solution-phase and solid-state nuclear magnetic resonance (NMR) spectroscopy, which ultimately led to the discovery of two novel fluorine containing species which possess fluorinating ability.

The mechanochemical activation of fluorspar stands out because it bypasses the production, storage and complex transport chain of HF. However, a significant limitation encountered was its broad application to the synthesis of fluoroarenes commonly used for the production of pharmaceuticals and agrochemicals. Also, mechanochemical reactions require specialised equipment available in only few laboratories. Not bound to solid-state chemistry induced by mechanical force, **Chapter 3** explores the solution-phase activation of fluorspar in water under mild acidic conditions using a Brønsted acid, optimally oxalic acid at

50 °C, in the presence of a Lewis acid such as silicon dioxide (SiO_2) or boric acid [$B(OH)_3$] as a fluoride scavenger to afford silicon fluoride (H_2SiF_6) and boron fluoride (HBF_4) based reagents. These reagents were successfully converted into other fluorochemicals, including fluoroarenes and inorganic fluorinating reagents, expanding the scope of fluorochemicals from fluorspar not within reach using the first-generation solid-state method. Application of this process to lower purity grade metspar (80-90% CaF_2), an untapped fluoride reserve for fluorochemical production, is also examined. Finally, **Chapter 3** compares oxalic acid and H_2SO_4 activation of fluorspar at room temperature and the potential viability of such technology for sustainable fluorochemical manufacturing in a possible future.

Detailed experimental procedures for the work described herein, including chemical synthesis, mechanistic studies, purity analysis and the full characterisation of novel compounds is given in **Chapter 4**.

1.9 References

1. Tavener, S. J. & Clark, J. H. Chapter 5 Fluorine: Friend or Foe? A Green Chemist's Perspective. in *Advances in Fluorine Science* (ed. Tressaud, A.) vol. 2 177–202 (Elsevier, 2006).
2. Haupt, A. *Organic and Inorganic Fluorine Chemistry: Methods and Applications*. (De Gruyter, 2021).
3. Evich, M. G. *et al.* Per- and polyfluoroalkyl substances in the environment. *Science* **375**, eabg9065 (2022).
4. Mathew, T., Munoz, S. B., Forni, O., Tressaud, A. & Prakash, G. K. S. Advances in pursuit of fluorine in the interstellar medium and beyond: relevance to its terrestrial chemistry. *J. Fluor. Chem.* **269**, 110149 (2023).
5. Schmedt auf der Günne, J., Mangstl, M. & Kraus, F. Occurrence of Difluorine F_2 in Nature—In Situ Proof and Quantification by NMR Spectroscopy. *Angew. Chem. Int. Ed.* **51**, 7847–7849 (2012).
6. O'Hagan, D. & B. Harper, D. Fluorine-containing natural products. *Journal of Fluorine Chemistry* **100**, 127–133 (1999).
7. Idoine, N. E. *et al.* World Mineral Production 2016-2020. *British Geographical Survey* (2022).
8. E. McRae, M. Fluorspar, Mineral Commodity Summaries 2024. *U.S. Geological Survey* (2024).
9. Harsanyi, A. & Sandford, G. Organofluorine chemistry: applications, sources and sustainability. *Green Chem.* **17**, 2081–2086 (2015).
10. Villalba, G., Ayres, R. U. & Schroder, H. Accounting for Fluorine: Production, Use, and Loss. *J. Ind. Ecol.* **11**, 85–101 (2007).
11. Dreveton, A. Overview of the Fluorochemicals Industrial Sectors. *Procedia Eng.* **138**, 240–247 (2016).
12. Agricola, G. *Bermannuns, Sive De Re Metallica*. (Basel, 1530).
13. Weeks, M. E. The discovery of the elements. XVII. The halogen family. *J. Chem. Educ.* **9**, 1915 (1932).
14. Scheele, C. W. Undersökning om fluss-spat och dess syra (Investigation of fluoride and its acid). in *Kongl. Vetenskaps Academiens Handlingar (Transactions of the Royal Swedish Academy of Sciences)* 120–138 (1771).

15. Lennartson, A. The Chemical Works of Carl Wilhelm Scheele. in *The Chemical Works of Carl Wilhelm Scheele* (ed. Lennartson, A.) 19–103 (Springer International Publishing, Cham, 2017).
16. Moissan, H. Action d'un courant électrique sur l'acide fluorhydrique anhydre. *Comptes rendus hebdomadaires des séances de l'Académie des sciences* 1543–1544 (1886).
17. Okazoe, T. Overview on the history of organofluorine chemistry from the viewpoint of material industry. *Proc Jpn Acad Ser B Phys Biol Sci* **85**, 276–289 (2009).
18. Dolbier, W. R. Fluorine chemistry at the millennium. *J. Fluor. Chem.* **126**, 157–163 (2005).
19. Molina, M. J. & Rowland, F. S. Stratospheric sink for chlorofluoromethanes: chlorine atom-catalysed destruction of ozone. *Nature* **249**, 810–812 (1974).
20. Plunkett, R. J. Tetrafluoroethylene polymers. (1941).
21. Goldwhite, H. The Manhattan Project. *J. Fluor. Chem.* **33**, 109–132 (1986).
22. Simons, J. H. Production of Fluorocarbons: I. The Generalized Procedure and its Use with Nitrogen Compounds. *J. Electrochem. Soc.* **95**, 47 (1949).
23. Howells, R. D. & Mc Cown, J. D. Trifluoromethanesulfonic acid and derivatives. *Chem. Rev.* **77**, 69–92 (1977).
24. Balz, G. & Schiemann, G. Über aromatische Fluorverbindungen, I.: Ein neues Verfahren zu ihrer Darstellung. *Berichte der deutschen chemischen Gesellschaft (A and B Series)* **60**, 1186–1190 (1927).
25. Gottlieb, H. B. The Replacement of Chlorine by Fluorine in Organic Compounds. *J. Am. Chem. Soc.* **58**, 532–533 (1936).
26. Takaoka, A., Iwamoto, K., Kitazume, T. & Ishikawa, N. Preparation of benzoheterocycles containing a chlorofluoromethyl group using the 'Yarovenko reagent'. *J. Fluor. Chem.* **14**, 421–428 (1979).
27. Middleton, W. J. New fluorinating reagents. Dialkylaminosulfur fluorides. *J. Org. Chem.* **40**, 574–578 (1975).
28. Smith, W. C. *et al.* Fluorination Reactions of Sulfur Tetrafluoride. *J. Am. Chem. Soc.* **81**, 3165–3166 (1959).
29. Olah, G. A. *et al.* Synthetic methods and reactions. 63. Pyridinium poly(hydrogen fluoride) (30% pyridine-70% hydrogen fluoride): a convenient reagent for organic fluorination reactions. *J. Org. Chem.* **44**, 3872–3881 (1979).
30. Ferreira, S. B. Diethylaminosulfur Trifluoride (DAST). *Synlett* **2006**, 1130–1131 (2006).

31. Lal, G. S., Pez, G. P. & Syvret, R. G. Electrophilic NF Fluorinating Agents. *Chem Rev* **96**, 1737–1756 (1996).
32. Szpera, R., Moseley, D. F. J., Smith, L. B., Sterling, A. J. & Gouverneur, V. The Fluorination of C–H Bonds: Developments and Perspectives. *Angew. Chem. Int. Ed.* **58**, 14824–14848 (2019).
33. Gilicinski, A. G., Pez, G. P., Syvret, R. G. & Lal, G. S. On the relative power of electrophilic fluorinating reagents of the N-F class. *J. Fluor. Chem.* **59**, 157–162 (1992).
34. Toullec, P. Y., Devillers, I., Frantz, R. & Togni, A. Relative Electrophilic Fluorinating Power as Assayed by Competitive Catalytic Halogenation Reactions. *Helvetica Chimica Acta* **87**, 2706–2711 (2004).
35. Christe, K. O. Chemical synthesis of elemental fluorine. *Inorg. Chem.* **25**, 3721–3722 (1986).
36. Purser, S., Moore, P. R., Swallow, S. & Gouverneur, V. Fluorine in medicinal chemistry. *Chem. Soc. Rev.* **37**, 320–330 (2008).
37. Haupt, A. Fluoroorganic compounds – unusual properties and versatile applications. in *Organic and Inorganic Fluorine Chemistry: Methods and Applications* 283–300 (De Gruyter, 2021).
38. Inoue, M., Sumii, Y. & Shibata, N. Contribution of Organofluorine Compounds to Pharmaceuticals. *ACS Omega* **5**, 10633–10640 (2020).
39. Zhang, C. Fluorine in Medicinal Chemistry: In Perspective to COVID-19. *ACS Omega* **7**, 18206–18212 (2022).
40. Wang, J. *et al.* Fluorine in Pharmaceutical Industry: Fluorine-Containing Drugs Introduced to the Market in the Last Decade (2001–2011). *Chem. Rev.* **114**, 2432–2506 (2014).
41. Adam, D. How far will global population rise? Researchers can't agree. *Nature* **597**, 462–465 (2021).
42. Ogawa, Y., Tokunaga, E., Kobayashi, O., Hirai, K. & Shibata, N. Current Contributions of Organofluorine Compounds to the Agrochemical Industry. *iScience* **23**, 101467 (2020).
43. Teflon™ Fluoropolymers for Medical Uses. https://www.teflon.com/en/industries-and-solutions/industries/medical.
44. Siegemund, G. *et al.* Fluorine Compounds, Organic. in *Ullmann's Encyclopedia of Industrial Chemistry* 1–56 (Wiley, Weinheim, Germany, 2016).
45. Holmes-Siedle, A. G., Wilson, P. D. & Verrall, A. P. PVdF: An electronically-active polymer for industry. *Materials & Design* **4**, 910–918 (1983).

46. Kirsch, P. Fluorine in liquid crystal design for display applications. *J. Fluor. Chem.* **177**, 29–36 (2015).
47. Vogt, E. T. C. & Weckhuysen, B. M. The refinery of the future. *Nature* **629**, 295–306 (2024).
48. Mauritz, K. A. & Moore, R. B. State of Understanding of Nafion. *Chem. Rev.* **104**, 4535–4586 (2004).
49. Powering Fuel Cells with Nafion™ Membranes and Dispersions. https://www.nafion.com/en/applications/fuel-cells.
50. Blois, M. Electrolyte makers chase opportunities in US battery industry. *Chemical & Engineering News*.
51. Fleming, I. *Molecular Orbitals and Organic Chemical Reactions*. (Wiley, a John Wiley and Sons, Limited, Publications, 2010).
52. Kirsch, P. *Modern Fluoroorganic Chemistry: Synthesis, Reactivity, Applications*. (John Wiley & Sons, 2013).
53. Haynes, W. M. *CRC Handbook of Chemistry and Physics, 95th Edition*. (CRC Press, Hoboken, 2014).
54. Meanwell, N. A. Fluorine and Fluorinated Motifs in the Design and Application of Bioisosteres for Drug Design. *J. Med. Chem.* **61**, 5822–5880 (2018).
55. Champagne, P. A., Desroches, J. & Paquin, J.-F. Organic Fluorine as a Hydrogen-Bond Acceptor: Recent Examples and Applications. *Synthesis* **47**, 306–322 (2014).
56. Takemura, H., Ueda, R. & Iwanaga, T. C–F···HO hydrogen bond in 8-fluoro-4-methyl-1-naphthol. *Journal of Fluorine Chemistry* **130**, 684–688 (2009).
57. Ibba, F. *et al.* Impact of Multiple Hydrogen Bonds with Fluoride on Catalysis: Insight from NMR Spectroscopy. *J. Am. Chem. Soc.* **142**, 19731–19744 (2020).
58. Aufiero, M. & Gilmour, R. Informing Molecular Design by Stereoelectronic Theory: The Fluorine Gauche Effect in Catalysis. *Acc. Chem. Res.* **51**, 1701–1710 (2018).
59. Lemal, D. M. Perspective on Fluorocarbon Chemistry. *J. Org. Chem.* **69**, 1–11 (2004).
60. Pettinari, C. & Rafaiani, G. NMR Applications, Solution state ^{19}F. in *Encyclopedia of Spectroscopy and Spectrometry (Third Edition)* (eds. Lindon, J. C., Tranter, G. E. & Koppenaal, D. W.) 117–124 (Academic Press, Oxford, 2017).
61. Miller, J. M. Fluorine-19 magic-angle spinning NMR. *Prog. Nucl. Magn. Reson. Spectrosc.* **28**, 255–281 (1996).

62. Haupt, A. 19F-NMR – an important analytical tool for fluorine chemists. in *Organic and Inorganic Fluorine Chemistry: Methods and Applications* 43–50 (De Gruyter, 2021).
63. Ametamey, S. M., Honer, M. & Schubiger, P. A. Molecular Imaging with PET. *Chem. Rev.* **108**, 1501–1516 (2008).
64. Ajenjo, J., Destro, G., Cornelissen, B. & Gouverneur, V. Closing the gap between ^{19}F and ^{18}F chemistry. *EJNMMI Radiopharm Chem* **6**, 33 (2021).
65. Aigueperse, J. *et al.* Fluorine Compounds, Inorganic. in *Ullmann's Encyclopedia of Industrial Chemistry* (ed. Wiley-VCH Verlag GmbH & Co. KGaA) 11–307 (Wiley-VCH, Weinheim, Germany, 2000).
66. Bowden, R. D. The industrial process: A computer simulation of the fluorspar/sulphuric acid reaction. *J. Fluor. Chem.* **45**, 203 (1989).
67. Singh, N. B. & Middendorf, B. Calcium sulphate hemihydrate hydration leading to gypsum crystallization. *Progress in Crystal Growth and Characterization of Materials* **53**, 57–77 (2007).
68. Du Boisson, R. A. The Fluorochemical Industry. in *Organofluorine Chemistry: Principles and Commercial Applications* (eds. Banks, R. E., Smart, B. E. & Tatlow, J. C.) 579–593 (Springer US, Boston, MA, 1994).
69. Haupt, A. Hydrogen fluoride. in *Organic and Inorganic Fluorine Chemistry: Methods and Applications* 15–22 (De Gruyter, 2021).
70. Knotter, D. M. Etching Mechanism of Vitreous Silicon Dioxide in HF-Based Solutions. *J. Am. Chem. Soc.* **122**, 4345–4351 (2000).
71. Lin, M.-F. *et al.* Recycle of synthetic calcium fluoride and waste sulfuric acid to produce electronic grade hydrofluoric acid. *Environ. Sci. Pollut. Res. Int.* **28**, 40633–40639 (2021).
72. Robinson, P. R. Petroleum Processing Overview. in *Practical Advances in Petroleum Processing* (eds. Hsu, C. S. & Robinson, P. R.) 1–78 (Springer, New York, NY, 2006).
73. Horowitz, D. Opinion | This Chemical Kills. Why Aren't Regulators Banning It? *The New York Times* (2019).
74. Yoo, S.-H. *et al.* Psychological effects of a disastrous hydrogen fluoride spillage on the local community. *Ann of Occup and Environ Med* **29**, 40 (2017).
75. Park, S. B. Alert over South Korea toxic leaks. *Nature* **494**, 15–16 (2013).
76. Failure to replace corroded pipe led to 2019 explosion in Philadelphia. *Chemical & Engineering News*.

77. Znidar, D., Dallinger, D. & Kappe, C. O. Practical Guidelines for the Safe Use of Fluorine Gas Employing Continuous Flow Technology. *ACS Chem. Health Saf.* **29**, 165–174 (2022).
78. Harris, J., Minor, P., Chawla, N. & Singh, S. Development and Implementation of a Hydrofluoric Acid Safety Program in an Academic Institution. *ACS Chem. Health Saf.* **27**, 183–189 (2020).
79. Petrov, V. A. & Thrasher, J. S. From alternate routes to fluorspar (CaF_2) or anhydrous HF (aHF) to conversion of fluorspar into a nucleophilic fluorinating agent. *J. Fluor. Chem.* **275**, 110274 (2024).
80. Leibler, I. N.-M., Gandhi, S. S., Tekle-Smith, M. A. & Doyle, A. G. Strategies for Nucleophilic C(sp^3)–(Radio)Fluorination. *J. Am. Chem. Soc.* **145**, 9928–9950 (2023).
81. Yoneda, N. The combination of hydrogen fluoride with organic bases as fluorination agents. *Tetrahedron* **47**, 5329–5365 (1991).
82. Haupt, A. Main group element fluorides. in *Organic and Inorganic Fluorine Chemistry: Methods and Applications* 55–160 (De Gruyter, 2021).
83. Beurskens, G. & Jeffrey, G. A. Crystal Structure of Potassium Fluoride Tetrahydrate. *J. Chem. Phys.* **41**, 917–923 (1964).
84. Zhan, C.-G. & Dixon, D. A. Hydration of the Fluoride Anion: Structures and Absolute Hydration Free Energy from First-Principles Electronic Structure Calculations. *J. Phys. Chem. A* **108**, 2020–2029 (2004).
85. Emsley, J. Solutions of potassium fluoride in glacial acetic acid. *J. Chem. Soc. A* 2702–2708 (1971).
86. Wynn, D. A., Roth, M. M. & Pollard, B. D. The solubility of alkali-metal fluorides in non-aqueous solvents with and without crown ethers, as determined by flame emission spectrometry. *Talanta* **31**, 1036–1040 (1984).
87. Liotta, C. L. & Harris, H. P. Chemistry of naked anions. I. Reactions of the 18-crown-6 complex of potassium fluoride with organic substrates in aprotic organic solvents. *J. Am. Chem. Soc.* **96**, 2250–2252 (1974).
88. Pozzi, G., Quici, S. & Fish, R. H. Fluorous phase transfer catalysts: From onium salts to crown ethers. *Journal of Fluorine Chemistry* **129**, 920–929 (2008).
89. Iashin, V., Wirtanen, T. & Perea-Buceta, J. E. Tetramethylammonium Fluoride: Fundamental Properties and Applications in C-F Bond-Forming Reactions and as a Base. *Catalysts* **12**, 233 (2022).

90. Clark, J. H. Fluoride ion as a base in organic synthesis. *Chem. Rev.* **80**, 429–452 (1980).
91. Grabowski, S. J. $[FHF]^-$—The Strongest Hydrogen Bond under the Influence of External Interactions. *Crystals* **6**, 3 (2016).
92. Kang, S. O., Powell, D., Day, V. W. & Bowman-James, K. Trapped Bifluoride. *Angew. Chem. Int. Ed.* **45**, 1921–1925 (2006).
93. Emsley, J. Very strong hydrogen bonding. *Chem. Soc. Rev.* **9**, 91 (1980).
94. Yonezawa, T., Sakamoto, Y. & Nogawa, N. Preparation of Tetrabutylammonium Fluoride–Alcohol Adducts as Fluorination Agents. *Jpn. Kokai Tokkyo Koho* JP 06316551 A (1994).
95. Kim, D. W. *et al.* Facile Nucleophilic Fluorination Reactions Using *tert*-Alcohols as a Reaction Medium: Significantly Enhanced Reactivity of Alkali Metal Fluorides and Improved Selectivity. *J. Org. Chem.* **73**, 957–962 (2008).
96. Engle, K. M. *et al.* Coordination diversity in hydrogen-bonded homoleptic fluoride–alcohol complexes modulates reactivity. *Chem. Sci.* **6**, 5293–5302 (2015).
97. Pfeifer, L. *et al.* Hydrogen-Bonded Homoleptic Fluoride–Diarylurea Complexes: Structure, Reactivity, and Coordinating Power. *J. Am. Chem. Soc.* **138**, 13314–13325 (2016).
98. Kim, D. W., Jeong, H.-J., Lim, S. T. & Sohn, M.-H. Tetrabutylammonium Tetra(*tert*-Butyl Alcohol)-Coordinated Fluoride as a Facile Fluoride Source. *Angew. Chem. Int. Ed.* **47**, 8404–8406 (2008).
99. Pupo, G. *et al.* Asymmetric nucleophilic fluorination under hydrogen bonding phase-transfer catalysis. *Science* **360**, 638–642 (2018).
100. Pupo, G. & Gouverneur, V. Hydrogen Bonding Phase-Transfer Catalysis with Alkali Metal Fluorides and Beyond. *J. Am. Chem. Soc.* **144**, 5200–5213 (2022).
101. Pupo, G. *et al.* Hydrogen Bonding Phase-Transfer Catalysis with Potassium Fluoride: Enantioselective Synthesis of β-Fluoroamines. *J. Am. Chem. Soc.* **141**, 2878–2883 (2019).
102. Roagna, G. *et al.* Hydrogen Bonding Phase-Transfer Catalysis with Ionic Reactants: Enantioselective Synthesis of γ-Fluoroamines. *J. Am. Chem. Soc.* **142**, 14045–14051 (2020).
103. Fluorine Chemistry's Uncharted Territory. *Chemical & Engineering News*.
104. Flerlage, H. & Slootweg, J. C. Modern chemistry is rubbish. *Nat Rev Chem* **7**, 593–594 (2023).

105. Quan, H.-D., Tamura, M., Gao, R.-X. & Sekiya, A. Preparation and application of porous calcium fluoride—a novel fluorinating reagent and support of catalyst. *J. Fluor. Chem.* **116**, 65–69 (2002).

106. Tarbutton, G., Egan, E. P. & Frary, S. G. Phosphorus-Halogen Compounds from Phosphorus Pentoxide and Halides. Properties of Phosphorus Trifluoride and Phosphorus Oxyfluoride. *J. Am. Chem. Soc.* **63**, 1782–1789 (1941).

107. Michael, O. & Leopold, B. 'Production of volatile fluorides' US1865204A. (1932).

108. Muetterties, E. L. & Coffman, D. D. Chemistry of Some Sulfur Oxyfluorides. *J. Am. Chem. Soc.* **80**, 5914–5918 (1958).

109. Boudakian, M. M., Hyde, G. A. & Kongpricha, S. Reactions of pyrosulfuryl fluoride. *J. Org. Chem.* **36**, 940–942 (1971).

110. Ball, N. D. Properties and Applications of Sulfur(VI) Fluorides. in *Emerging Fluorinated Motifs* 621–674 (John Wiley & Sons, Ltd, 2020).

111. Jache, A. W. Fluorosulfuric Acid, Its Salts, and Derivatives. in *Advances in Inorganic Chemistry and Radiochemistry* (eds. Emeléus, H. J. & Sharpe, A. G.) vol. 16 177–200 (Academic Press, 1974).

112. Jordan, R. K. 'Carbonyl Fluorination Process' US4087475. (1975).

113. Bornemann, D. *et al.* Deoxygenative Fluorination of Phosphine Oxides: A General Route to Fluorinated Organophosphorus(V) Compounds and Beyond. *Angew. Chem. Int. Ed.* **59**, 22790–22795 (2020).

114. Liu, J. *et al.* Synthesis of $LiPF_6$ Using CaF_2 as the Fluorinating Agent Directly: An Advanced Industrial Production Process Fully Harmonious to the Environments. *Ind. Eng. Chem. Res.* **58**, 20491–20494 (2019).

115. Du Pont. 'Improvements in process of producing carbon halides' GB390191A. (1933).

116. Evans, F. E., Berenbaum, M. B., Eibeck, R. E. & Robinson, M. A. 'Preparation of fluoroorganic compounds with calcium fluoride' US4174349A. (1979).

117. Anderson, R. J. 'Method of producing a fluoride-containing composition' US127770A. (1954).

118. Struijs, J. J. C., Ellwanger, M. A., Crumpton, A. E., Gouverneur, V. & Aldridge, S. Enabling nucleophilic reactivity in molecular calcium fluoride complexes. *Nat. Chem.* 1–8 (2024).

119. Apolinar, O., Struijs, J. J. C., Sarkar, D., Gouverneur, V. & Aldridge, S. Nucleophilic Fluoride Anion Delivery from Triazacyclononane-Supported Molecular Ca–F Complexes. *Angew. Chem. Int. Ed.* e202414790 (2024).

2.Fluorochemicals from Fluorspar via a Phosphate-Enabled Mechanochemical Process that Bypasses HF

The work described in this chapter was carried out in collaboration with a team of scientists. Preliminary experiments and early optimisation work were performed with Dr. Emy André-Joyaux, Dr. Gabriele Pupo and Dr. Jamie Leitch. Job Struijs completed the development of reaction conditions for benzylic fluorination and assisted in the synthesis of benzylic fluorides (**30** to **34**) and α-fluoro carbonyls (**37**, **39** and **42**) after initial optimisation work by Dr. Emy André-Joyaux. Dr. Xabier Martínez de Irujo-Labalde and Prof. Michael Hayward conducted all Rietveld refinement work for crystal structure simulation. Dr. Christopher Goult and Job Struijs assisted in acquiring and analysing solid-state NMR data. SEM images were also acquired by Dr. Christopher Goult.

The results of this chapter have been partially described, see:

C. Patel, E. André-Joyaux, J. A. Leitch, X. M. de Irujo-Labalde, F. Ibba, J. Struijs, M. A. Ellwanger, R. Paton, D. L. Browne, G. Pupo, S. Aldridge, M. A. Hayward, V. Gouverneur, Fluorochemicals from fluorspar via a phosphate-enabled mechanochemical process that bypasses HF. *Science* **381**, 302–306 (2023).

2.1 Introduction

2.1.1 Mechanochemistry

The low solubility, high melting point and inert nature of CaF_2 limits its applicability to conventional synthetic methods, including solution-phase chemistry and traditional solid-state chemistry (furnaces). Thinking beyond solution-phase chemistry, mechanochemistry enables transformations independent of reactant solubility.[1] In contrast to usual methods of chemical activation, namely using heat, irradiation and electrochemistry, mechanochemical reactions are far less studied. Mechanistically they may be defined as a "chemical transformation" that is promoted by the absorption of mechanical energy, via compression, shear, or friction. In natural environments, mechanochemical reactions are frequently induced by physical processes such as earthquakes or glacier movement.[2–4] Notably, inconspicuous mechanochemical processes with accompanying chemical changes take place everyday in milder and low energy environments, such as grinding and milling used extensively to process grains, building materials (concrete) and pharmaceuticals.[5]

The first examples of mechanochemical reactions were recorded by early scholars including Theophrastus who described the reduction of mercury sulfide (HgS) using a copper pestle and mortar (4th century BC) and Faraday, in 1820, who reported the reduction of silver chloride (AgCl) by grinding with zinc in a mortar.[6,7] Seminal contributions to the early developments of mechanochemistry were made by Spring and Carey Lea. In 1885, Spring disclosed an ion exchange between barium sulfate ($BaSO_4$) and sodium carbonate (Na_2CO_3) using compression and pulverization to afford barium carbonate ($BaCO_3$) and sodium sulfate (Na_2SO_4).[8] Notably, this reaction is challenging to achieve in aqueous solution owing to the poor solubility of $BaSO_4$ (0.002 mg/mL H_2O, 20 °C).[9] Carey Lea established distinct

reactivity differences between the thermochemical and mechanochemical treatment of mercury chloride ($HgCl_2$) and silver chloride (AgCl) salts.[10] Chemistry Nobel prize winner Wilhelm Ostwald first coined the term "mechanochemistry" at the end of the 19th century. The field progressed relatively slowly during the first half of the 20th century compared to closely related disciplines such as metal alloying and tribology - the study of friction, lubrication and rubbing of solids.[11] The development of milling devices during the 1960s facilitated the adoption of mechanochemistry, widening the scope of reactions induced by mechanical force. Mechanochemical reactions are typically carried out in ball mill or a planetary mill (Figure 2.1).[12]

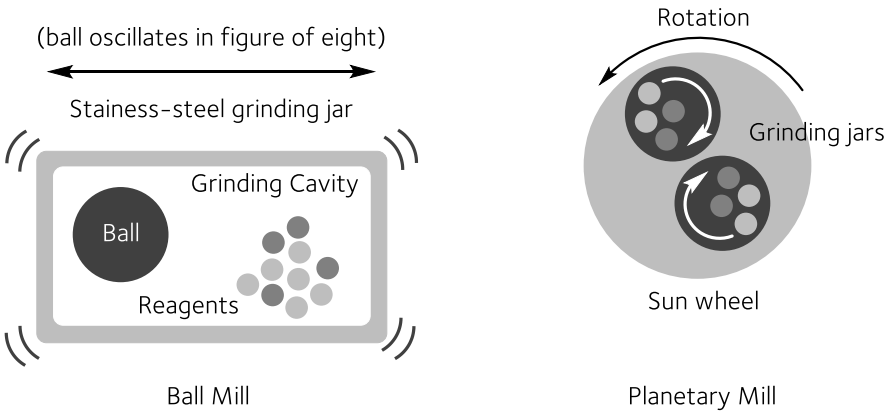

Figure 2.1. Schematics of equipment used for laboratory scale mechanochemical reactions.

Ball milling is a representative mechanochemical strategy that uses the mechanical agitation-induced effects to activate substrates. Automated laboratory ball mills (shaker mills) are a popular tool for mechanochemical reactions. In this system, reagents and one or more ball bearings are enclosed in a jar (reaction vessel) which oscillates back and forth at a desired frequency (up to 35 Hz) causing the enclosed ball bearing(s) to grind the reagents together via impact forces (collision). The addition of sub-stoichiometric amounts of liquids (liquid-assisted grinding, LAG) may enhance the reactivity of reagents in a mechanochemical reaction. The planetary mill is the other most commonly used milling device. Instead of a

shaking motion, one or more jars are mounted onto a spinning disc that spins counter-directionally to the balls enclosed in the jars. This results in an applied shearing force (attrition) where speeds can reach up to 800 rotations per minute (rpm). Milling jars (vessels) and ball bearings are typically composed of stainless steel, zirconia or poly(tetrafluoroethylene) (PTFE). The main optimisable parameters are oscillation frequency, hardness of the milling material, jar volume, and the quantity and weight of milling media (ball bearings and reagents).[13] For large-scale mechanochemical processes twin-screw extrusion can be used (Figure 2.2).[14] Metal-organic frameworks (MOFs) have been prepared on kilogram scale using extruders that continuously force material through confined spaces within minutes and apply shear and compression forces.[15] Alternatively, tumbling (drum) mills, which are commonly used to prepare concrete, may be used to process large quantities of materials, typically hundreds of kilograms (Figure 2.2).[16]

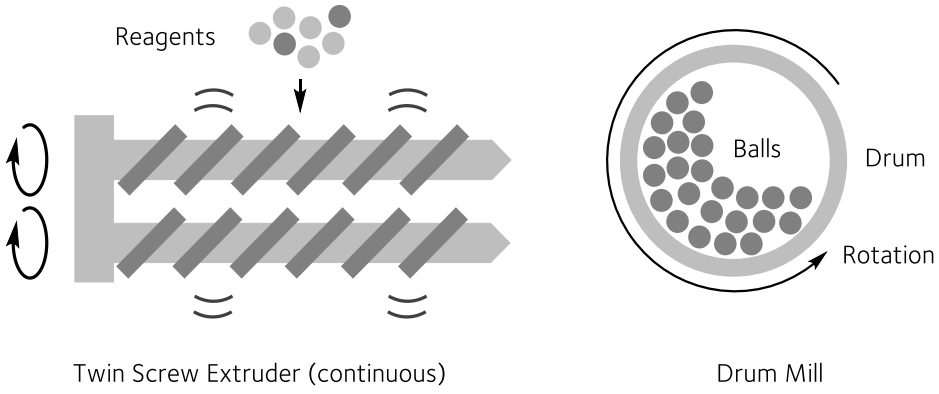

Figure 2.2. Schematics of equipment typically used for scale-up (kg) mechanochemistry.

Mechanochemistry offers unique reactivity benefits in terms of reaction outcome, selectivity and reduced reaction time. Indeed, mechanochemical methods have been shown to provide products and, in some cases, follow reaction pathways that may not be accessible by conventional thermal methods.[17] If substrate solubility is no longer a factor in reaction design, the list of possible reactants and products accessible is greatly increased.[13] In the

absence of bulk solvents, the product achieved through solid-state mechanochemical methods is a result of high concentration and mechanical force causing the system to deviate away from equilibrium into an energetically activated "steady state", thereby affording products governed mostly by kinetic factors (Figure 2.3).[18,19] Moreover, mechanical treatment of solids can promote a reduction in particle size, generation of reactive fracture sites and changes in the morphology and amorphization of the material.[20]

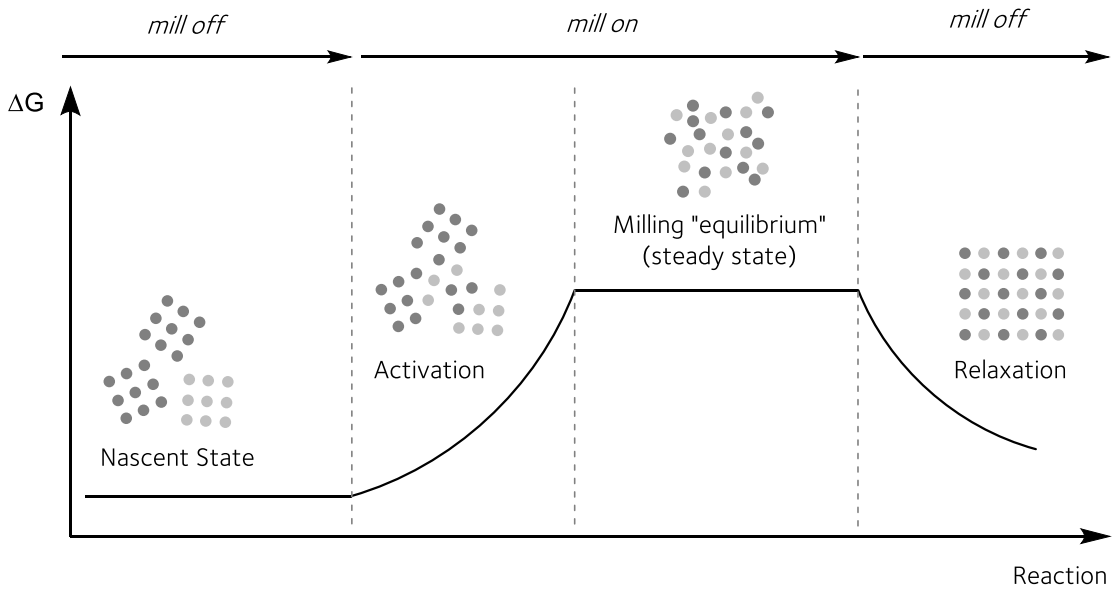

Figure 2.3. Influence of mechanical force on the energetics of solids adapted from Michalchuk and Emmerling (G, Gibbs free energy).[19]

Determining fundamental reaction parameters such as the applied force (F), time of reactant under force (t), and conversion at various time points is a challenging task for the majority of mechanochemical processes. Tuning the milling frequency is a facile way to control the energy input into a reaction. By increasing the milling frequency, the acceleration and in turn the impact energy of the milling balls is increased, resulting in both better dispersion and transfer of energy to reagents through reactive collisions at high velocity. Reactant structure, temperature (T), particle size, ball mass and vessel loading are also known to effect reaction rate. Given that all of these factors work in combination, specifying

how mechanical forces influence the potential energy surface of a system and alter the reaction trajectory of reactants to products is challenging. The "hotspot" model proposes that when ball bearings collide with surfaces and each other, it leads to localised short-lived heating, hypothesised to reach over 1000 K over a millisecond period, due to the release of kinetic energy.[21] Although local heating can be observed upon milling, several experimental studies have questioned whether these temperature increases provide enough energy to overcome reaction activation barriers.[22] Fluctuations in temperature within the reaction mixture due to localised endothermic or exothermic reactions, may influence the advancement of a mechanochemical reaction, yet they are usually outside the experimenter's control and cannot be reliably relied on to govern reactivity.[23]

A comprehensive understanding of mechanochemical reactions involves observing and describing both chemical (formation and reactivity of chemical species) and physical (mixing state and rheology) transformations occurring in the reacting sample. Mechanistic studies typically involve a stepwise approach in which milling is periodically interrupted and samples of the bulk reaction mixture are characterised *ex situ* using techniques such as powder X-ray diffraction (PXRD), solid-state NMR spectroscopy, infrared or Raman spectroscopy (Table 2.1).[24] PXRD plays a crucial role in acquiring structural details like phases, purity levels, and sizes of crystallites, while solid-state NMR is beneficial in examining crystalline to amorphous phase transitions. Despite the widespread use of *ex situ* methods in various research studies, a main caveat is the possibility of obtaining misleading results as a consequence of the sample either relaxing to its nascent state or reacting with the surrounding atmosphere during preparation for analysis.

Table 2.1. Brief summary of non-destructive solid-state analytical techniques.

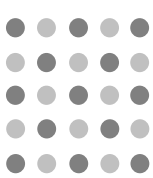

Long range order
Crystalline (e.g. CaF_2)

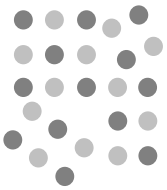

Intermediate order
Nanocrystalline

Complete disorder
Amorphous (e.g. SiO_2)

Technique	Detection	Application	Sensitivity
PXRD	Intensities and scattering angle of X-ray photons	Crystal unit cell and structure, particle size, phase determination, quantitative	Crystalline, co-crystals, polymorphs, nanocrystalline
Solid-state NMR	Response of nuclei with spin ≠ 0 in magnetic field	Structure determination, quantitative, distinction of polymorphs	Crystalline, polymorphs, amorphous
IR	Change in dipole moment (light absorption)	Structure determination	Crystalline, amorphous
Raman	Change in polarizability (light scattering)	Structure determination	Crystalline, amorphous

Considerable progress in understanding mechanochemical reactions came with the first real time *in situ* analysis of the mechanochemical synthesis of zeolitic-imidazolate based metal-organic frameworks (MOFs) using synchrotron PXRD by Friscic and co-workers, enabling the direct observation of the crystalline phase evolution over the entire milling period.[25] Importantly, this study permitted the continuous characterisation and monitoring of crystalline solids without interfering with the milling process, thus enabling the detection of multiple crystalline intermediates before the final product was obtained. Time resolved *in situ* (TRIS) methods have since opened the door to exceptional detail regarding mechanochemical transformations, for example in the study of ion exchange reactions and, more recently, phase transitions in solids.[26–28] Implementation of real time monitoring techniques for ball milling using Raman spectroscopy and solid-state NMR spectroscopy offer insight to molecular structural changes rather than just crystallinity, enabling *in situ*

studies of organic reactions that may traverse through amorphous intermediates, and other short-lived metastable phases.[29,30] TRIS monitoring of isotope-labelled solids has provided compelling evidence for dynamic exchange of atoms and molecules between crystallites during ball milling via continuous particle comminution and growth.[31] As our analytical capabilities advance, combined with improved sampling and data collection strategies, the development of techniques encompassing multivariable factors (microscopic and macroscopic) and consistently incorporating new experimental observations are anticipated to enable better physical models and therefore predictions of mechanochemical reactions.[32]

The substantial advancements in understanding mechanochemical reactivity are shaping mechanochemistry as a key synthetic tool for present-day chemists. Over the past two decades, the chemical sciences have seen exponential growth in publications appearing under the term "mechanochemical", resulting in a highly active interdisciplinary area of research.[33] This newly available reaction space has opened new possibilities in chemistry including catalysis (mechanocatalysis), polymer science (mechanoradical), and redox chemistry through the employment of piezoelectric materials (mechanoredox).[13,34–37] Recent research endeavours have even coupled mechanochemistry with energy inputs from heat, light, electrical impulses and sound (sono-mechanochemistry).[23] The synthesis of gaseous products, such as ammonia (the second most produced chemical worldwide), has also been achieved using mechanochemistry through the development of modified mechanochemical reactor vessels adapted with gas valves.[38,39] Undeniably, mechanochemistry offers new opportunities to provide disruptive, sustainable solutions for challenges in chemical manufacturing, if the processes developed are competitive in terms of cost, energy and scalability. As an inherently solvent-free concept, mechanochemistry also has the potential to be more sustainable than solvothermal counterparts, proceeding with lower relative energy demand and without toxic solvents. Accounting for approximately

80-90% of the total mass of an organic reaction, solvents are widely recognised to be of great environmental concern and a significant contributor to all chemical manufacturing waste (>60%).[40] Indeed, mechanochemistry has been dubbed one of the "top 10 emerging technologies in chemistry" that can change our world by the International Union of Pure and Applied Chemistry (IUPAC).[41]

2.1.2 Mechanochemical Fluorination

Mechanochemical fluorination presents the advantage of avoiding challenges associated with solubilising alkali metal fluoride salts, which can in principle, simplify synthetic strategies. Despite this, the area has generally been dominated by the use of electrophilic fluorinating reagents, such as Selectfluor™, for mono and polyfluorination reactions.[42–45] Only a few mechanochemical fluorinations using nucleophilic fluoride sources have been reported.

A rare example of solid-state nucleophilic fluorination of alkyl substrates bearing halides and pseudohalide leaving groups was achieved using a heated screw conveyer and a cellulose *n*-$Bu_4NF{\cdot}3H_2O$ complex (Scheme 2.1).[46] Primary alkyl fluorides were furnished in up to 96% yield within residence times of 20 seconds. Nucleophilic substitution of alcohols with fluoride *via* reactive isouronium salts was demonstrated under mechanochemical conditions by the Kananovich group.[47] In a single deoxyfluorination example using 1-naphthalene methanol, fluorination occurred in 40% yield using CsF and fluoro-*N,N,N',N'*-tetramethylformamidinium hexafluorophosphate (TFFH). The authors observed no fluorination upon replacing CsF for KF (ΔU_L CsF 744 kJ/mol versus KF 808 kJ/mol).

Dastager, 2020

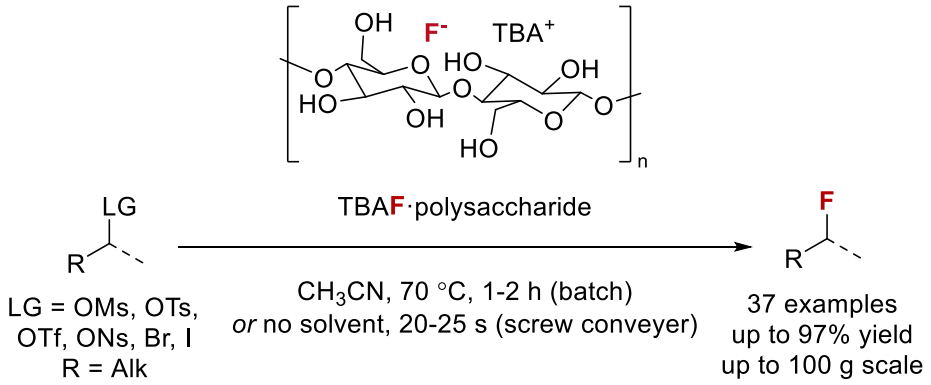

Kananovich, 2022

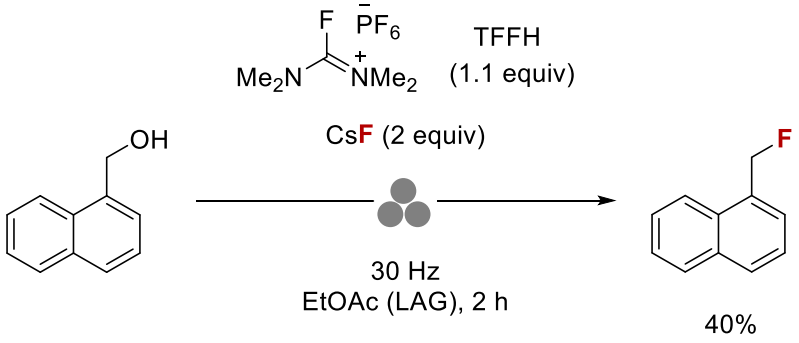

Bolm, 2023

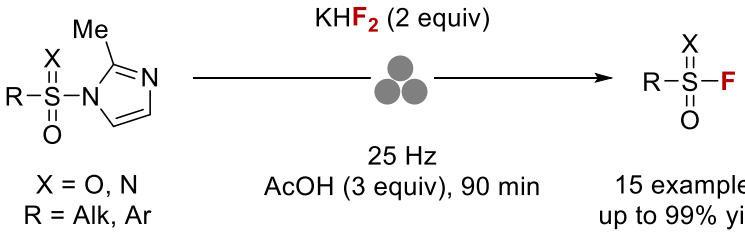

Scheme 2.1. Examples of mechanochemical nucleophilic fluorination of organic substrates.

In 2023, Bolm and co-workers reported the nucleophilic fluorination of sulfonyl 2-methylimidazoles under ball milling conditions, using potassium bifluoride (KHF_2) in the presence of acetic acid (AcOH) to afford sulfonyl fluorides.[48] Under tuned experimental conditions, sulfonimidoyl and sulfoxyl fluorides were also accessed. The ball milling of *p*-bromobenzyl bromide using alkali metal fluoride salts has also been reported.[49]

Beyond organofluorine compounds, mechanochemistry has been used to synthesise fluoride salts, including alkaline earth metal fluorides, aluminium fluoride salts and apatites.[50] Substitution of hydroxide in hydroxyapatite [$Ca_5(PO_4)_3(OH)$] for fluoride affords fluorapatite [$Ca_5(PO_4)_2F$], a highly stable compound (ΔU_L 17046 kJ/mol; 3409 kJ/mol per Ca^{2+} ion) which has the highest hardness (Mohs scale 5) and lowest solubility among all calcium phosphates.[51] As key components of tooth enamel, synthetic $Ca_5(PO_4)_3(OH)$ and $Ca_5(PO_4)_3F$ are highly demanded in dentistry as materials used for bone tissue restoration, which has motivated research into their mechanochemical synthesis.[52] Nikcevic *et al.* demonstrated that fluorapatite can be obtained after 9 h of milling a mixture of $Ca(OH)_2$, P_2O_5 and CaF_2 in a planetary mill.[53] Alternatively, Lyakhov and co-workers demonstrated that a powdered mixture of anhydrous $CaHPO_4$, CaO and CaF_2 could be readily converted into fluorapatite with varying degrees of hydroxyl group substitution upon ball milling (Scheme 2.2).[54]

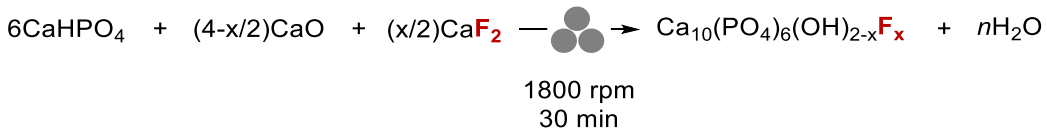

Scheme 2.2. Mechanochemical synthesis of fluorapatite by planetary ball milling by Lyakhov and co-workers (hydroxyl group substitution for fluorine from x = 0 to 2).

The influence of ball milling on crystalline CaF_2 has been studied using planetary ball milling with analysis by PXRD and ^{19}F solid-state NMR spectroscopy.[55] In addition to the broadening of the X-ray reflections and ^{19}F resonances, the variance in relaxation time (T_1) of the ^{19}F nuclei (91.2 s for crystalline CaF_2 and 3.9 s CaF_2 after 4 h of ball milling) highlighted a distinct impact of the mechanical force on particle size. Moreover, CaF_2 nanomaterials containing surface defects, synthesised using high-energy ball milling, exhibit increased ionic conductivities which may be beneficial for electrolyte applications.[56]

2.1.3 Powder X-ray Diffraction

Three-dimensional structural information of a crystalline solid can be obtained from a one-dimensional powder X-ray diffraction (PXRD) pattern (diffractogram). A PXRD experiment involves exposing a region of a powder sample with a monochromatic incident X-ray beam and measuring the intensity as a function of the angle between the incident beam and detector.[57] Scattering intensities leave the sample in cones of uniform intensity (Deybe-Scherrer cones) (Figure 2.4a). A crystal contains planes described by Miller indices (hkl) and Braggs law gives the angle of constructively scattered intensity, where λ is the radiation wavelength, d_{hkl} the interplanar spacing, and 2θ is the diffraction angle (Equation 1).[57] For constructive interference, the path difference should be an integral multiple of the wavelength of the incident radiation. The possible angles of diffracted intensity (2θ) in a diffraction pattern depend solely on the size and shape of the unit cell. For any crystal system, d_{hkl} can be related to the unit-cell parameters (*a*, *b*, *c*, α, β, γ) by trigonometry (Figure 2.4b).

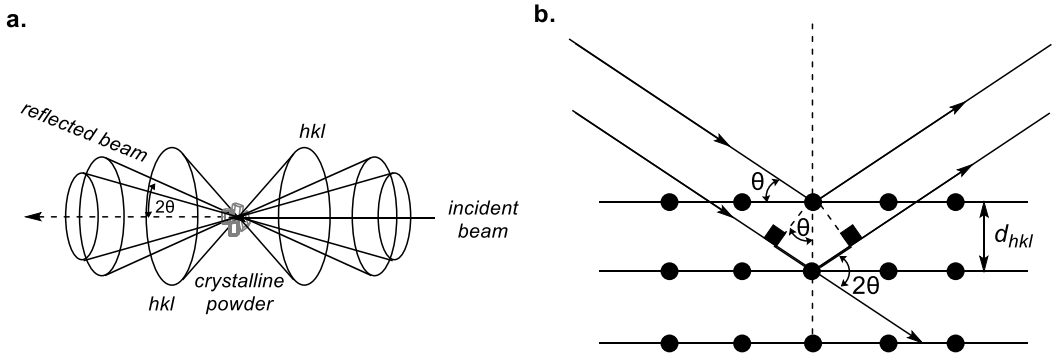

Figure 2.4. Scattered beams (X-rays) originating from a crystalline powder (Debye-Scherrer cones are drawn in reciprocal space). Adapted from Nature Primers.[57]

$$n\lambda = 2d_{hkl}sin\theta$$

Equation 1. Bragg equation, *n* is the order of diffraction, λ is the wavelength of the probe, d_{hkl} is the spacing between a well-defined set of crystal planes and the diffraction angle is 2θ. In Bragg's law *n* is an integer, referred to as the order of diffraction, and is often unity.

The intensity I_{hkl} of reflected radiations (reflection) observed in a diffractogram (Equation 2) is determined by the identity and positions of the atoms inside the unit cell via the structure factor, F_{hkl} (Equation 3).

$$I_{hkl} \propto LmA|F_{hkl}|^2$$

Equation 2. I_{hkl} of each hkl reflection, where L is the Lorentz-polarisation function constant, m is the reflection multiplicity, A is the absorption factor and F_{hkl} is the structure factor.

$$F_{hkl} = \Sigma_n f_n(\theta)\exp\left[2\pi i(hx_n + ky_n + lz_n)\right]\exp\left[\frac{-8\pi^2 U_{iso_n} sin^2\theta_{hkl}}{\lambda^2}\right]$$

Equation 3. Structure factor F_{hkl}, where f_n is the atomic scattering factor, (x,y,z) are the fractional coordinates of the atoms in the unit cell and, U_{iso} is the isotropic thermal displacement factor.

Indexing methods aim to computationally reconstruct the 3D crystal lattice from the 1D distribution of d_{hkl} values determined from the powder pattern. Structural information in the powder pattern is extracted using modelling methods based on regression. The methodology involves using a whole-pattern fitting process that includes a structural model, peak shape descriptions, and background parameters to calculate a powder pattern. The calculated intensity (y_{calc}), at each step in 2θ, is then compared to the observed intensity (y_{obs}), and the difference between the two is minimised by changing specific parameters of the model. By comparing the computed powder pattern with the measured one, the model's parameters are refined using a regression algorithm (least-squares refinement) that minimises the difference between the calculated and measured data through iterative refinement cycles. The R-factor is a measure of the agreement between the two datasets.

Structural parameters, including unit-cell dimensions, fractional atomic coordinates (Wyckoff position), atomic occupancies, and atomic displacement parameters, are typically

refined during data fitting, along with instrument calibration parameters and parameters describing any 2θ-dependent intensity corrections (e.g. due to absorption).[58] The process of using crystallographic models to refine crystal structures using powder diffraction data is called Rietveld refinement.[59] Experimentally determined PXRD data and PXRD data of a suitable starting model are required to perform a Rietveld refinement analysis, which is carried out using computational software such as TOPAS.[60] Rietveld refinement also provides a standardless approach to quantitative PXRD, relying solely on crystal structure information for the solids analysed.[61]

2.2 Aims

The aim of this study was to develop a fluorination method employing CaF_2 as the nucleophilic fluoride source. From a thermodynamic viewpoint, the viability of nucleophilic fluorination involving alkali metal or alkaline earth metal fluorides hinges on the specific bonds that are broken and formed during the fluorination reaction, as well as the lattice energy (ΔU_L) of the metal fluoride salt. For instance, with KF, the formation of a strong C–F bond (CH_3F, 460 kJ/mol) in place of a weaker C-Br bond (CH_3Br, 294 kJ/mol) compensates for the loss incurred from its high lattice energy with respect to KBr (ΔU_L KF, 808 kJ/mol; ΔU_L KBr, 671 kJ/mol); this scenario is however far from sufficient for fluorinations with CaF_2. For direct fluorination with CaF_2, we considered the formation of a calcium by-product with a lattice energy greater than CaF_2 (ΔU_L 2640 kJ/mol) as a powerful thermodynamic sink, such as $Ca_3(PO_4)_2$ (ΔU_L 10602 kJ/mol; 3534 kJ/mol per Ca^{2+} ion). The innate insolubility of CaF_2 prompted us to consider mechanochemistry as an attractive solution to harness its potential as a fluorination reagent, a strategy aligned with the growing demand for sustainable processes, and new technologies that overcome otherwise prohibitively slow solid-state diffusion rate.

2.3 Results and Discussion

2.3.1 Reaction Development

2.3.1.1 Solution Phase Fluorination

The fluorination of sulfonyl chlorides using CaF_2 (reagent grade, >97%) was first investigated. Sulfur(VI) fluoride exchange (SuFEx) is a powerful click reaction with applications in chemical biology and material science.[62] Moreover, sulfonyl fluorides are commonly used as deoxyfluorinating reagents for the synthesis of C-F bonds.[63] The bond dissociation energy of the S–F bond in SO_2F_2 (379 kJ/mol) is far larger than the S–Cl bond in SO_2Cl_2 (192 kJ/mol), thereby offering a modest compensation for the energetic penalty incurred upon CaF_2 dissociation.[9]

As initially reported by Davies and Dick in 1931, a classic approach for sulfonyl fluoride synthesis is chloride–fluoride exchange on a sulfonyl chloride substrate.[64] Over eighty years ago, the fluoride salts of potassium, sodium, ammonium, and zinc were introduced as the initial reagents for converting sulfonyl chloride to fluoride, and typical reaction conditions involved refluxing the metal fluoride with sulfonyl chloride in water-organic biphasic mixtures.[65] The use of KF, 18-crown-6 and acetonitrile became widely adopted conditions, largely because of the increased nucleophilicity of fluoride.[66] Alternatively, the Sharpless group advocated the use of potassium bifluoride (KHF_2) which exhibited excellent reactivity when used "on water"-that is, in reactions performed with a vigorously stirred or agitated water-organic interface, representing a robust and reliable method of sulfonyl fluoride synthesis.[67]

The reaction of 4-toluene sulfonyl chloride (TsCl) with CaF_2 (4 equiv) in acetonitrile for 3 h at 100 °C did not afford 4-toluene sulfonyl fluoride (TsF, **1**) (Table 2.2). Fluorination

was not observed upon addition of 18-crown-6 (1 equiv) or Schreiner's catalyst (1 equiv), a well precedented urea hydrogen bond donor for fluoride (Table 2.2 entries 2 and 3).

Table 2.2. Preliminary fluorination experiments of TsCl in solution.

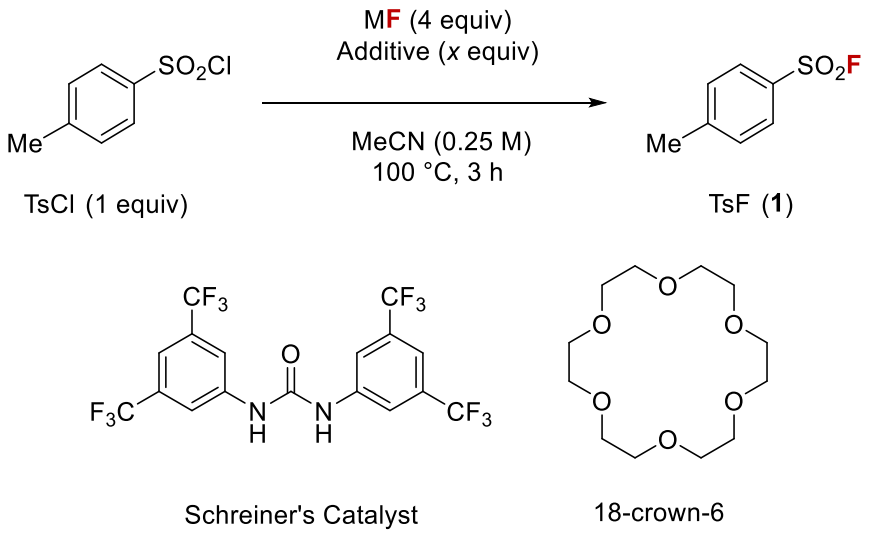

Entry	MF	Additive	Additive equiv	TsCl (%)	TsF (**1**) (%)
1	CaF_2	-	-	100	0
2	CaF_2	18-crown-6	1	93	0
3	CaF_2	Schreiner's Cat.	1	100	0
4	CaF_2	K_3PO_4	1	23	3
5	CaF_2	K_3PO_4 : Schreiner's Cat.	1 : 1	29	2
6	KF	-	-	0	99

Reagent grade CaF_2 (≥ 97%, Alfa Aesar) and KF (99%, Alfa Aesar) was used. Yields determined by quantitative ^{19}F and ^{1}H NMR spectroscopy using 4-fluoroanisole (FA) as internal standard (10 µL).

In the aim of producing a calcium phosphate by-product as a thermodynamic sink, a combination of CaF_2 and anhydrous tripotassium phosphate (K_3PO_4) was tested. In this case, a singlet corresponding to the formation of **1** (δ_F = 66.3 ppm) was observed in the crude reaction mixture by ^{19}F NMR spectroscopy ($CDCl_3$), evidencing fluorination of TsCl in 3% [quantified using an internal standard of 4-fluoroanisole (FA)] (Table 2.2, entry 4).

Replacement of CaF_2 for KF (4 equiv) resulted in quantitative yield of **1** (Table 2.2, entry 6). The observed increased nucleophilic reactivity of fluoride anion in KF when compared to CaF_2 is associated with the lower lattice energy of KF (808 kJ/mol for KF versus 2640 kJ/mol for CaF_2). These preliminary experiments demonstrated that solution-phase chemistry had a poor outlook for improvement, prompting a transition to solid-state chemistry.

2.3.1.2 Mechanochemical Activation

Nucleophilic fluorination using CaF_2 in a ball mill (mixer mill) was first examined. The fluorination of TsCl (1.0 mmol) was investigated using reagent grade CaF_2 (5 equiv) under ball milling conditions (30 Hz) using a stainless steel jar (15 mL) and a stainless steel ball (4 g) (Scheme 2.3). No conversion to TsF (**1**) was observed using CaF_2 after 3 h of ball milling (full starting material recovery), however, a control experiment replacing CaF_2 for KF (1 equiv) gave full conversion (>95%) to TsF (**1**) (determined by ^{19}F NMR spectroscopy).

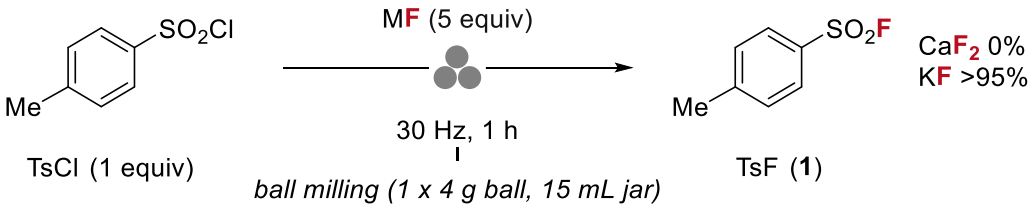

Scheme 2.3. Preliminary mechanochemical experiments of TsCl (solid-state). Yields determined by ^{19}F NMR spectroscopy using FA as internal standard (10 µL).

CaF_2 crystalises in a simple cubic motif (fluorite structure) with a distinct set of diffraction peaks at 2θ = 28.3, 47.0, 55.8 and 68.7° corresponding to the (111), (220), (311) and (400) *hk*/reflections, respectively (Figure 2.5). Powder X-ray diffraction patterns of un-milled reagent grade CaF_2 (≥ 97.0%, Alfa Aesar) and ball milled CaF_2 (3 h at 30 Hz) revealed that diffraction peaks become broader with a decrease in intensity, indicative of a

reduction in particle size as a consequence of non-uniform strain induced by mechanical force (Figure 2.5). CaF_2 particles are highly uniform (mean grain size 332 nm, CaF_2 sourced from Sigma Aldrich). Even after ball milling CaF_2 for 16 h at 30 Hz, complete amorphization is not observed. Although physical changes are observed upon ball milling CaF_2 (by PXRD), these alone are not sufficient for nucleophilic fluorination to ensue.

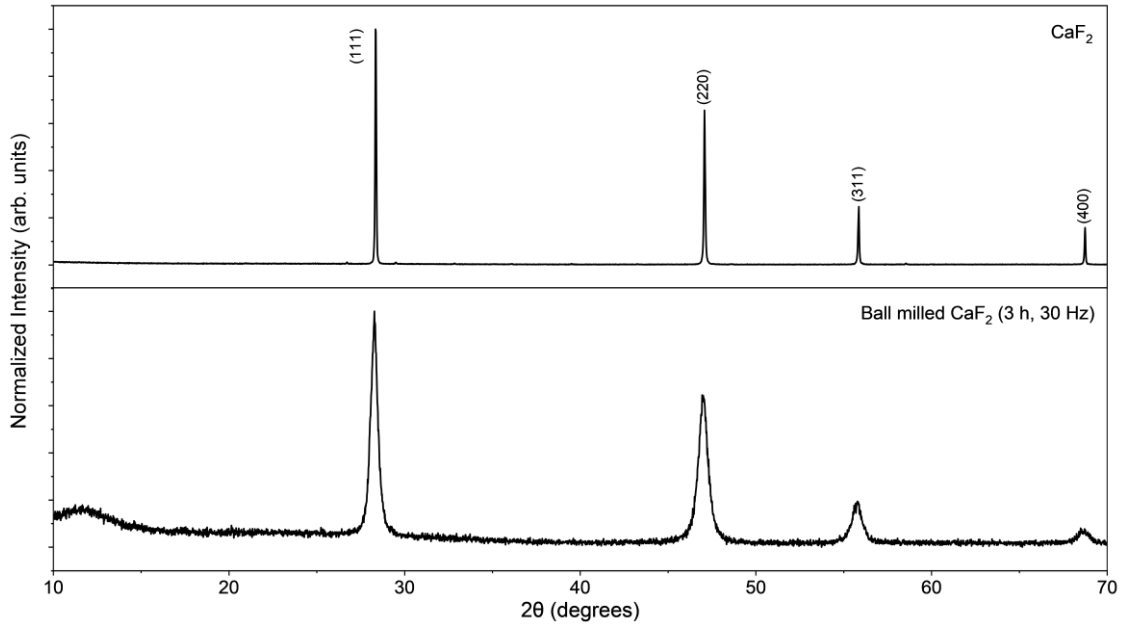

Figure 2.5. PXRD data of CaF_2 (≥97% Alfa Aesar) and ball milled CaF_2 (3 h, 30 Hz). Each reflection (peak) is labelled with the corresponding Miller planes.

2.3.1.3 Phosphate-enabled Activation

Next, the reactivity of CaF_2 in the presence of an inorganic phosphate salt under mechanochemical conditions was probed. In this scenario, a calcium phosphate by-product of lattice energy greater than that of CaF_2, such as $Ca_3(PO_4)_2$ (ΔU_L = 3534 kJ/mol per Ca ion) would serve as a thermodynamic driving force. Sodium and potassium orthophosphates with the chemical formula $M_xH_{3-x}PO_4$ were investigated (Table 2.3).

Table 2.3. Preliminary study of phosphate activation of CaF_2

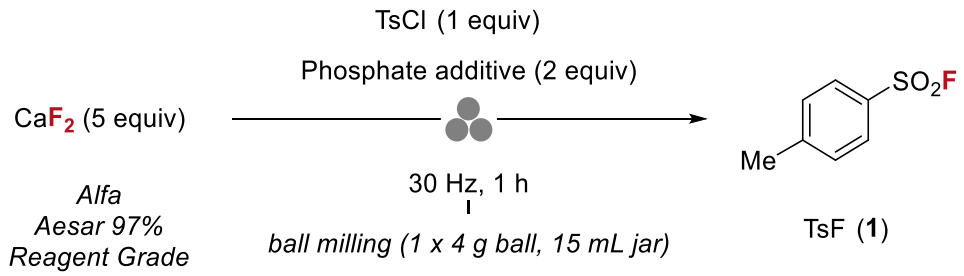

Entry	Phosphate additive	TsCl (%)	TsF (**1**) (%)	Mass balance (%)
1	K_3PO_4	7	7	14
2	**K_2HPO_4**	**56**	**17**	**73**
3	KH_2PO_4	95	0	95
4	Na_3PO_4	64	4	68
5	Na_2HPO_4	86	2	88
6	NaH_2PO_4	90	0	90

Yields determined by quantitative ^{19}F and ^{1}H NMR spectroscopy using FA as internal standard.

Gratifyingly, ball milling TsCl (1.0 mmol, 1 equiv), CaF_2 (5 equiv) and anhydrous K_3PO_4 (2 equiv) at 30 Hz using a stainless steel jar (15 mL) and stainless steel ball (4 g) led to the formation of TsF (**1**) in 7% yield (determined by ^{19}F NMR spectroscopy) (Table 2.3, entry 1). Only 7% of the TsCl starting material remained, as judged by the quantitative ^{1}H NMR spectra of the reaction mixture. This initial discovery uncovered a previously unseen reactivity of CaF_2 which was unlocked through mechanochemical activation in the presence of a phosphate salt. This proof of concept was further elaborated through an assessment of different inorganic phosphates. Dipotassium phosphate (K_2HPO_4) was found to be a highly effective activator, affording **1** in 17% yield (with 56% starting material recovered) (entry 2). TsCl underwent fluorination using CaF_2 and dibasic and tribasic sodium phosphate salts, albeit in lower yield compared to potassium phosphates (entries 4 and 5). Anhydrous

dihydrogen phosphate salts of potassium (KH_2PO_4) or sodium (NaH_2PO_4) were ineffective, resulting in complete starting material recovery only (entries 3 and 6).

For greater impact force and reactivity in ball milling, it is recommended to minimise the number of balls and increase their weight, either by using larger balls or those with higher density.[68] Whilst retaining the volume of the stainless steel jar (15 mL) and total mass of solid reagents, the effect of changing stainless steel ball size in the range of 2 g (8 mm) to 7 g (12 mm) was investigated. A product yield of 30% was achieved using one 7 g stainless steel ball. A substantial decrease in the available path for movement and acceleration, along with weaker impact forces, can result from increasing the number of balls or their size. Indeed, lower yields for the fluorination of TsCl were observed using stainless steel balls of lower mass, even in cases where more than one ball was employed (Table 2.4).

Table 2.4. Optimisation of stainless steel ball size for mechanochemical fluorination.

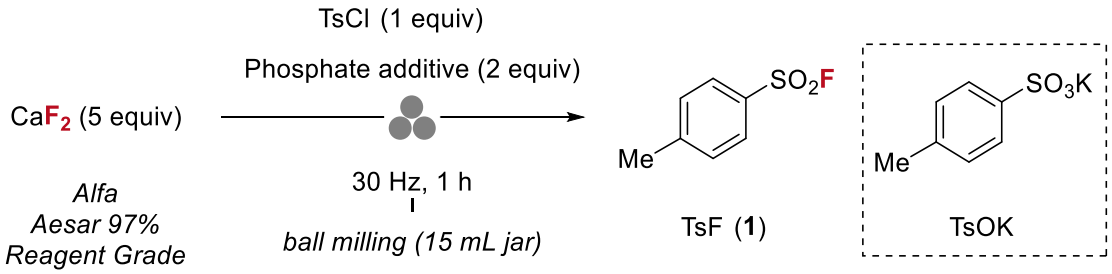

Entry	Ball size (g)	Ball diameter (mm)	Number of balls	TsCl (%)	TsF (**1**) (%)	TsOK (%)	Mass balance (%)
2	3	9	1	55	23	0	78
3	4	10	1	56	17	0	73
4	**7**	**12**	**1**	**9**	**30**	**2**	**41**
5	3	15	2	46	19	0	65

Yields determined by quantitative ^{19}F and ^{1}H NMR spectroscopy using FA as internal standard.

A yield of 31% of TsF (**1**) could be achieved upon lowering the amount of CaF_2 from 5 to 4 equivalents with 3 h of milling (Table 2.5, entry 1). Ball milling CaF_2 (4 equiv) and K_2HPO_4 (2 equiv) prior to addition of TsCl was next examined. The reaction mixture was then milled for an additional time period (1-3 h). Mechanochemical activation (pre-milling) of CaF_2 with K_2HPO_4 was found to be beneficial to the solid-state fluorination reaction. Milling CaF_2 (4 equiv) and K_2HPO_4 (2 equiv) for 3 h prior to addition of TsCl, and further milling of this mixture for 3 hours gave 66% (entry 4) of the corresponding sulfonyl fluoride **1** with no recovery of starting material. The fate of the remaining substrate was subsequently investigated through a series of control experiments testing the stability of TsCl and TsF (**1**) under mechanochemical conditions.

Table 2.5. Preliminary investigation into pre-milling CaF_2 with K_2HPO_4 prior to fluorination.

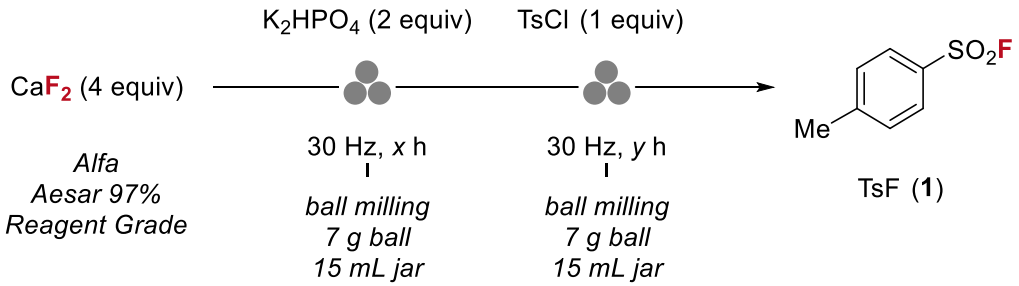

Entry	Pre-milling (*x* h)	Fluorination (*y* h)	TsCl (%)	TsF (**1**) (%)	Mass balance
1	0	3	4	31	35
2	1	1	47	29	76
3	2	1	22	41	63
4	**3**	**3**	**0**	**66**	**66**

Yields determined by quantitative ^{19}F and ^{1}H NMR spectroscopy using FA as internal standard.

2.3.1.4 Substrate Stability

Partial degradation of TsCl and TsF (**1**) in the presence of K_2HPO_4 to the corresponding potassium sulfonate salt (TsOK) was observed under mechanochemical conditions (stainless steel jar and balls, 30 Hz, 1 h) (Table 2.6). Analysis of the reaction mixtures formed in these ball milling experiments by quantitative ^{1}H NMR spectroscopy ($CDCl_3$) enabled the determination of remaining TsCl or TsF (**1**) present. The addition of water to the reaction samples and analysis of the aqueous component by ^{1}H NMR spectroscopy (D_2O) revealed two distorted doublets at δ_H = 7.65 ppm and δ_H = 7.32 ppm (pair of aromatic CH), and a singlet at δ_H = 2.35 ppm (CH_3) in all cases, consistent with the formation of potassium tosylate (TsOK) (Scheme 2.4).[69] Ball milling TsF (**1**) in the presence of K_2HPO_4 without CaF_2 resulted in the formation of TsOK and KF, as evidenced by ^{19}F NMR spectroscopy (D_2O) (singlet, δ_F = -122 ppm) (Table 2.6, entry 2 and Scheme 2.4). Full NMR spectroscopy data is included in Chapter **4**.

Table 2.6. Stability of TsCl and TsF (1) under mechanochemical conditions.

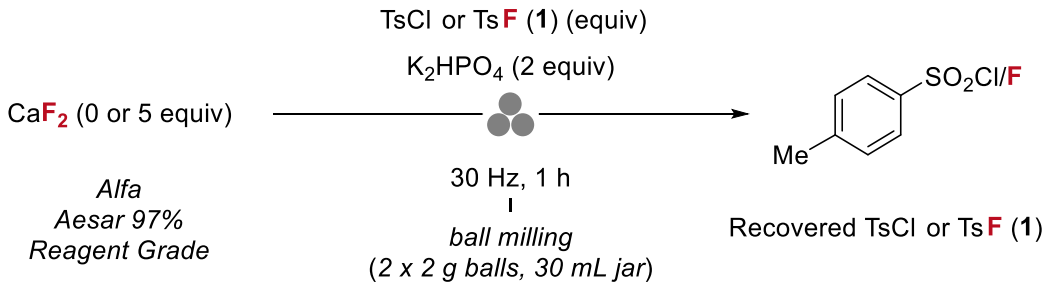

Entry	Substrate	CaF_2 (equiv)	K_2HPO_4 (equiv)	Recovered Substrate (%)
1	TsF (**1**)	5	2	81
2	TsF (**1**)	0	2	89
3	TsCl	0	2	78

Yields determined by quantitative ^{19}F and ^{1}H NMR spectroscopy using FA as internal standard.

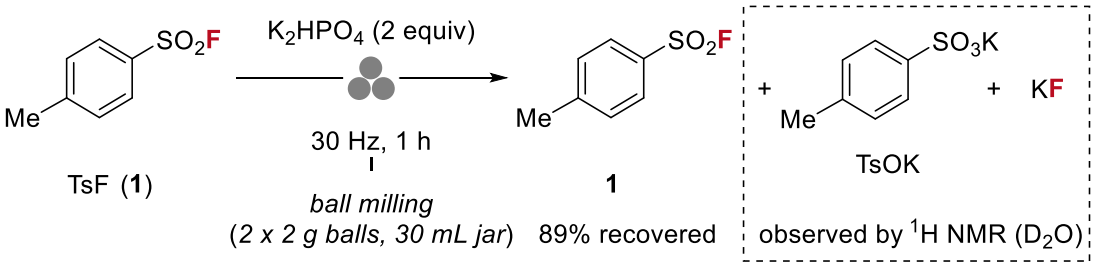

Scheme 2.4. Ball milling TsF (1) with K_2HPO_4 stability control experiment ().

The finding that partial degradation of both TsCl and TsF took place under mechanochemical conditions led to a refined protocol involving pre-milling CaF_2 with K_2HPO_4 and using the resultant powder for the fluorination of TsCl in solution.

2.3.1.5 Two-step Protocol Development

A two-step protocol involving milling CaF_2 (4 equiv) with K_2HPO_4 (2 equiv), followed by using the resulting powder in solution (MeCN, 0.25 M) at 100 °C in the presence of TsCl (0.25 mmol) was examined (Table 2.7). This protocol led to **1** in 62% yield (determined by ^{19}F NMR spectroscopy, entry 1), which could be improved by adding 18-crown-6 (70%) or a combination of 18-crown-6 and Schreiner's urea (79%) (entries 2 and 3). These additives are well documented for their ability to activate KF, that we postulated, may form upon milling CaF_2 with K_2HPO_4. Complexes of K^+ and Ca^{2+} with Kryptofix 2.2.1 (2.2.1-crypt) exhibit high stability constants, particularly $[Ca(2.2.1\text{-crypt})]^{2+}$ which is considered to be one of the most stable calcium complexes.[70] For this reason, Kryptofix 2.2.1 was also investigated as an additive, however, this led to 52% TsF (**1**) and 48% of a tosylate species [$(TsO)_xM$, where M could be K^+ or Ca^{2+}, x = 1 or 2] (entry 5).

Table 2.7. Investigation into mechanochemical activation of CaF_2 with K_2HPO_4 followed by fluorination in solution using additives.

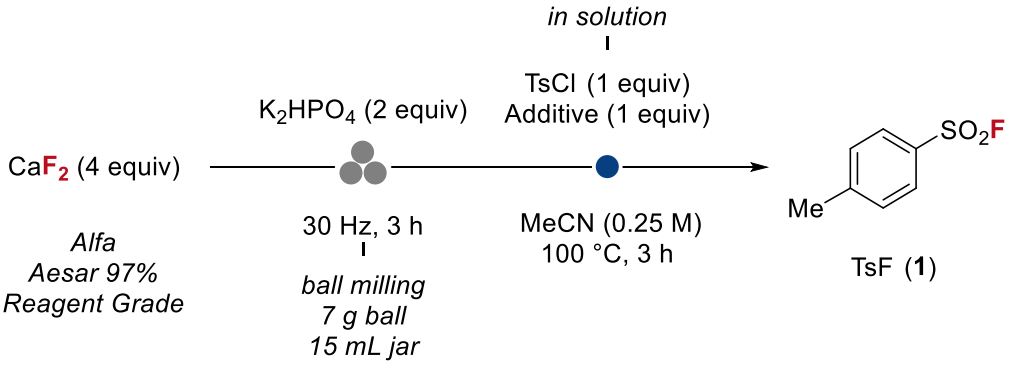

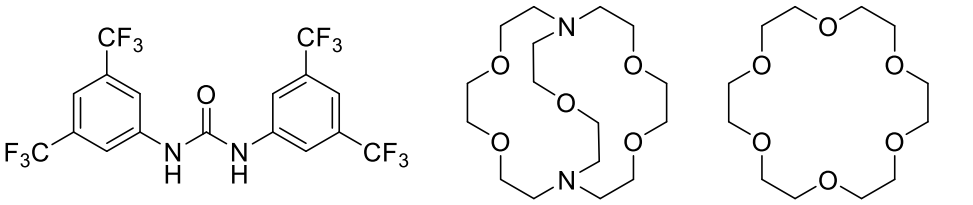

Schreiner's Urea | Kryptofix 2.2.1 | 18-crown-6

Entry	Additive (in solution)	TsCl (%)	TsF (**1**) (%)	TsOK (%)
1	-	15	62	0
2	18-crown-6	0	70	0
3	Schreiner's Urea	8	64	0
4	**Schreiner's Urea & 18-crown-6**	**0**	**79**	**20**
5	Kryptofix 2.2.1	0	52	48

Yields determined by quantitative ^{19}F and ^{1}H NMR spectroscopy using FA as internal standard.

Notably, pre-milling an equimolar amount of CaF_2 (1 mmol, 4 equiv) with K_2HPO_4 (1 mmol, 4 equiv) and using the resultant powder in the fluorination of TsCl (0.25 mmol, 1 equiv) in MeCN enabled 76% yield of **1** without the use of any additives (Table 2.8, entry 2). The starting material was fully consumed under these conditions. Increasing the amount of K_2HPO_4 further (up to 16 equivalents) resulted in reduced yields (Table 2.8, entries 5 and 6).

In each entry of Table 2.8, the quantities of CaF_2 and K_2HPO_4 were calculated to give approximately 1 g of material for ball milling (experimental details are included in Chapter **4**).

Table 2.8. Effect of changing the equivalents of CaF_2 to K_2HPO_4 in the solid-state step.

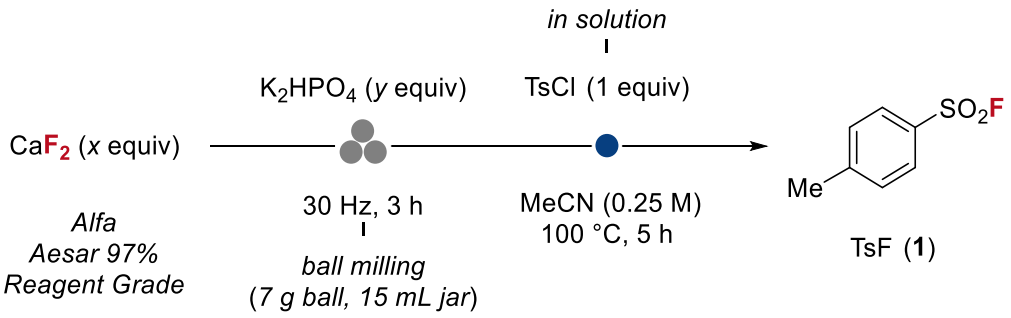

Entry	CaF_2 (*x* equiv)	K_2HPO_4 (*y* equiv)	TsCl (%)	TsF (**1**) (%)	Mass balance (%)
1	4	2	15	62	77
2	**4**	**4**	**0**	**76**	**76**
3	8	2	10	51	61
4	16	2	0	78	78
5	4	6	0	69	69
6	2	16	0	30	30

Equivalents of CaF_2 and K_2HPO_4 respect to TsCl (0.25 mmol, 1 equiv). Yields determined by quantitative ^{19}F and ^{1}H NMR spectroscopy using FA as internal standard.

2.3.1.6 Development of Solution Phase Fluorination Step

Although fluorination of TsCl was achieved in 76% yield using the pre-milled CaF_2-K_2HPO_4 powder (Table 2.9, entry 1), a control experiment unveiled that exposure of TsCl to K_2HPO_4 (2 equiv) in solution (MeCN, 0.25 M) at 100 °C for 3 h resulted in degradation to TsOK (observed by ^{1}H NMR spectroscopy), accounting for the loss of starting material. Conducting the fluorination of TsCl (0.25 mmol, 1 equiv) in MeCN at 25 °C using the pre-milled equimolar amount of CaF_2 (1 mmol, 4 equiv) with K_2HPO_4 (1 mmol, 4 equiv)

for 12 h led to improved mass percentage recovery, albeit with reduced conversion of TsCl to **1** (entry 2), even at increased solvent concentration (MeCN, 0.5 M) (entry 3).

Table 2.9. Optimisation of solution phase fluorination.

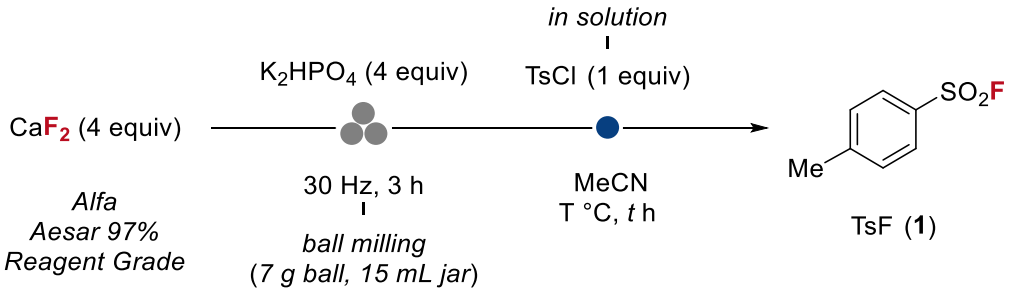

Entry	Temp. (° C)	Time (h)	Concentration (M)	TsCl (%)	TsF (**1**) (%)	Mass balance (%)
1	100	5	0.25	0	76	76
2	25	12	0.25	48	51	99
3	25	12	0.5	30	68	98

Yields determined by quantitative ^{19}F and ^{1}H NMR spectroscopy using FA as internal standard.

The impact of solvent on the fluorination of TsCl (0.25 mmol) using pre-milled equimolar amount of CaF_2 (1 mmol) with K_2HPO_4 (1 mmol) (at 30 Hz, 3 h) was studied next. This screening campaign included solvents that bind metal cations, such as dimethylformamide (DMF) and dimethyl sulfoxide (DMSO), and hydrogen-bond-donating solvents that can stabilise fluoride anion, like tert-butanol (*tert*-BuOH). Collectively, the data in Figure 2.6 show that the fluorination can be achieved in high yield (80% or greater determined by ^{19}F NMR spectroscopy) using propionitrile (EtCN), chlorobenzene (PhCl), 1,2-dichlorobenzene (1,2-DCB) or *tert*-BuOH as anhydrous solvents. Although a clear trend between solvent dielectric constant and fluorination yield is not observed, fluorination was permitted in a wide range of solvents, diverse in polarity and binding ability. Overall, best results in terms of reactivity were achieved using *tert*-BuOH (81%), EtCN (80%) and

chlorinated aromatics, 1,2-DCB (84%) and PhCl (92%). As *tert*-BuOH can be easily removed *in vacuo* during reaction work-up, this solvent was selected for subsequent optimisation studies.

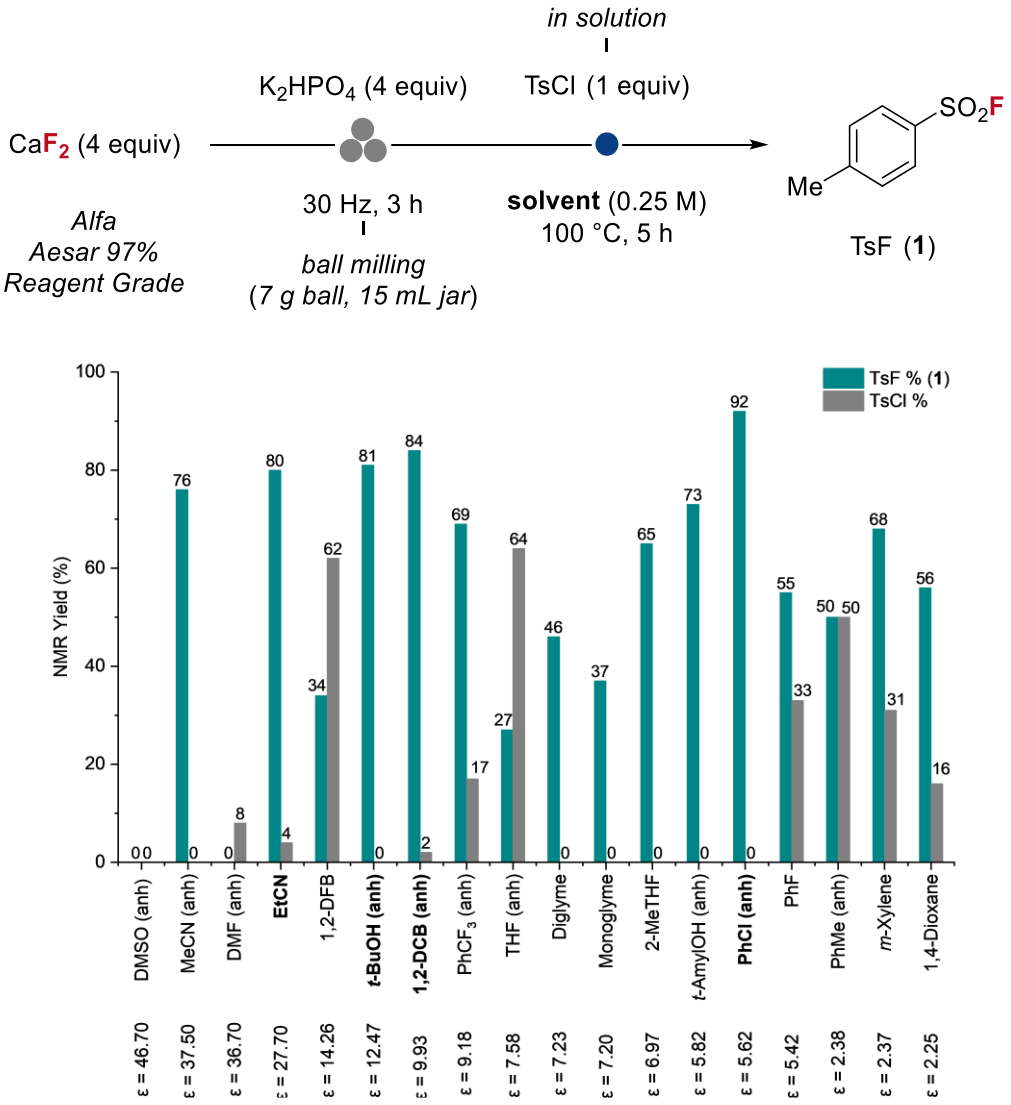

Figure 2.6. Optimisation of solvent for fluorination step (with dielectric constants, ε), yields determined by ^{19}F and ^{1}H NMR spectroscopy using FA as internal standard.

2.3.1.7 Fluorspar Activation and Reassessment of Phosphate Salts

Gratifyingly, replacement of synthetic reagent-grade calcium fluoride with acid-grade fluorspar (AGF, >97% CaF_2) was equally effective, affording **1** in 78% yield (Table 2.10). Having developed a 2-step reaction protocol, the phosphate additives in the initial solid-state step were re-examined to assess any variations in reactivity during the subsequent fluorination step in solution. This screening campaign was extended to Ca-phosphates, and K- and Na-polyphosphates. However, K_2HPO_4 was still found to be optimal, followed by K-pyrophosphate ($K_4P_2O_7$) (54%) and Na_2HPO_4 (38%).

Table 2.10. Re-evaluation of phosphate additives using acid grade fluorspar.

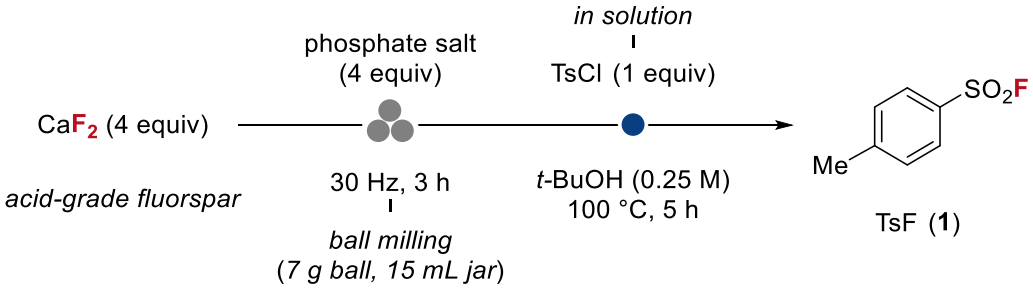

Entry	Phosphate additive	TsCl (%)	TsF (**1**) (%)	Mass balance (%)
1	K_3PO_4	0	1	1
2	**K_2HPO_4**	**0**	**78**	**78**
3	KH_2PO_4	95	4	99
4	$K_4P_2O_7$	0	54	54
5	$K_5P_3O_{10}$	19	23	42
6	Na_3PO_4	90	10	100
7	Na_2HPO_4	16	38	54
8	NaH_2PO_4	95	3	98
9	$Na_4P_2O_7$	0	33	33

10	$Na_5P_3O_{10}$	91	7	98
11	$CaHPO_4$	36	0	36
12	α-$Ca_3(PO_4)_2$	90	0	90

Yields determined by quantitative ^{19}F and ^{1}H NMR spectroscopy using FA as internal standard.

2.3.1.8 Development of Mechanochemical Activation Step

The energy input on the reactants in mechanochemistry is directly affected by the milling frequency, with faster reactions typically resulting from higher frequencies that enhance dispersion, surface abrasion and reactive collisions.[12] At higher frequencies, the acceleration and in turn the impact energy of the milling balls is greater than for lower speeds. In reality, the accumulation and subsequent relaxation of energy is highly complex, involving microscopic (electronic and vibrational) effects, defect generation, and temperature development.[13]

The effect of milling frequency on the solid-state activation step was examined (Figure 2.7). Ball milling an equimolar quantity of AGF with K_2HPO_4 at 35 Hz for 3 h led to a powder (**A**) which possessed greater fluorinating ability compared to the powder produced at 30 Hz. Using 4 equivalents of powder **A** prepared at 35 Hz in the fluorination of TsCl (0.125 mmol) proved to be optimal, affording TsF (**1**) in 93% NMR yield with no recovery of starting material (compared to 78% of **1** afforded using the same powder produced at 30 Hz). Using 1 equivalent of powder **A** prepared at 35 Hz yielded 46% of TsF (**1**) with 43% recovered starting material.

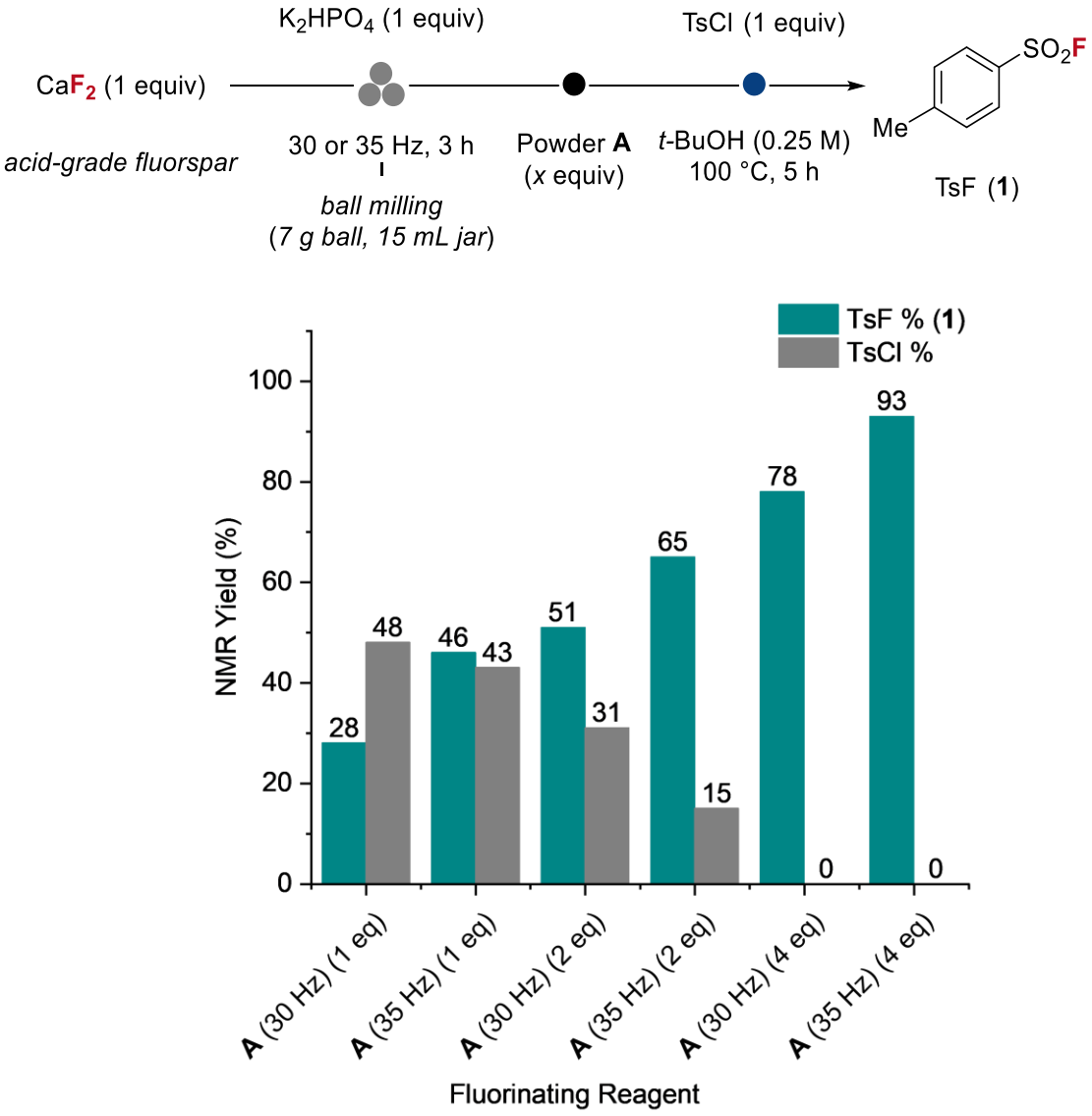

Figure 2.7. Comparison of reactivity of powder A prepared at 30 Hz versus 35 Hz; yields determined by ^{19}F and ^{1}H NMR spectroscopy using 4-FA as internal standard.

The use of 4 equivalents of powder **A** involves 8 equivalents of fluoride to forge a single S-F bond, which is suboptimal in terms of reaction stoichiometry. In the aim of achieving comparable reactivity with a lower loading of powder **A**, ideally 0.5 equivalents, systematic optimisation of the solid-state reaction accompanied by powder X-ray diffraction analysis was undertaken.

Powder X-ray diffraction (PXRD) is a fast and non-destructive method for characterising crystalline materials, i.e. those which have a degree of long-range periodic

order to their structure. Comparing measured diffraction peaks to a database of known patterns allows for the identification of phase(s) within the sample. Provided that a single crystal X-ray diffraction structure is available, the percentage and relative distribution of a phase can be determined. This approach requires adding a known amount of internal standard where the crystal structure is known, such as nickel oxide (NiO). A quantitative Rietveld phase analysis can be used to provide the weight fraction of the crystalline component (Figure 2.8). Assuming that the percentage of crystalline CaF_2 is 100% prior to ball milling, it was found that 60.5% of crystalline CaF_2 was present in the sample after ball milling with an equimolar quantity of K_2HPO_4 (powder **A**) at 35 Hz for 3 h (Table 2.11, entry 2). Increasing the milling time to 6 h did not significantly increase the amount of crystalline CaF_2 consumed (48.7% crystalline CaF_2 remaining after 6 h of ball milling with K_2HPO_4). Furthermore, prolonged milling of the powder did not greatly improve its fluorinating ability (Table 2.12).

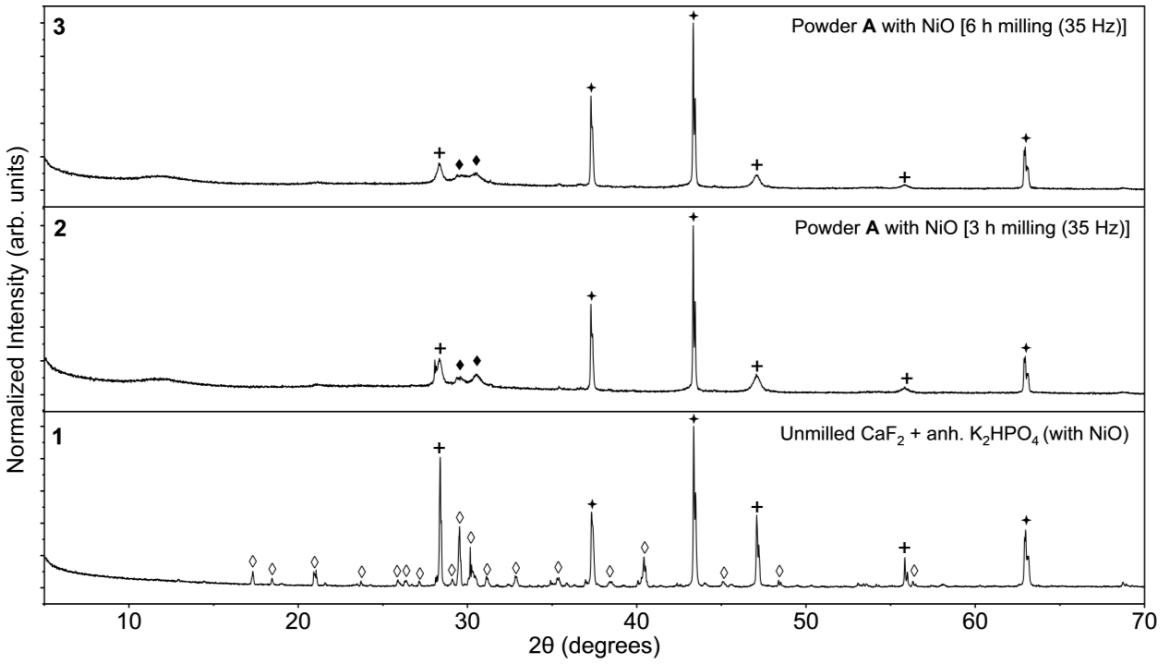

Figure 2.8. Evolution of PXRD data of un-milled CaF_2 and K_2HPO_4 (1:1) (1), ball milled CaF_2 and K_2HPO_4 (1:1) for 3 h (powder A) (2), ball milled CaF_2 and K_2HPO_4 (1:1) for 6 h (3) (◊ = anhydrous K_2HPO_4, + = CaF_2, ✦ = NiO, ♦ = new crystalline phase).

Table 2.11. Table of extracted mass ratio of CaF_2 to NiO values from Rietveld refinement.

Trace	Ball milling (h)	Mass ratio NiO : CaF_2	Ratio NiO : CaF_2	Crystalline CaF_2 (%)
1	0	44.7 (1.6) : 55.2 (1.6)	1: 1.23	100
2	3	57.3 (1.2) : 42.7 (1.2)	1:0.745	60.5
3	6	62.5 (1.3) : 37.5 (1.3)	1:0.60	48.7

Mass ratio of CaF_2 determined using NiO (99.99%, Sigma Aldrich) as crystalline internal standard.

Table 2.12.Reactivity of AGF milled with K_2HPO_4 (1:1) over time at 35 Hz.

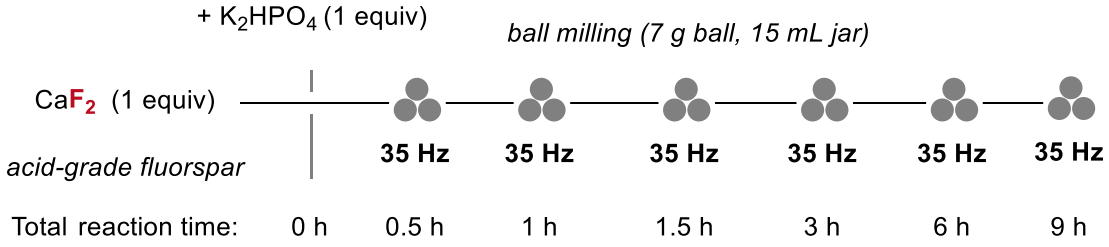

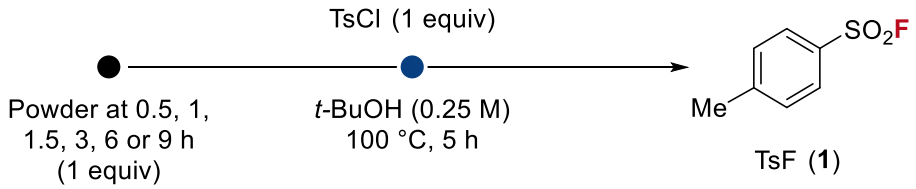

Entry	Total milling time (h)	TsCl (%)	TsF (**1**) (%)	Mass balance (%)
1	0 h	100	0	100
2	0.5 h	64	9	73
3	1 h	60	19	79
4	1.5 h	62	21	83
5	3 h	43	46	89
6	6 h	34	58	92
7	9 h	23	55	78

Yields determined by quantitative ^{19}F and ^{1}H NMR spectroscopy using FA as internal standard.

2.3.1.8 Final Reaction Conditions

Taken together, the data in Table 2.11 indicate that the fluorinating ability of **A** (prepared by ball milling an equimolar quantity of AGF with K_2HPO_4) is limited by the consumption of crystalline CaF_2 in the solid-state reaction. An increased consumption of the crystalline CaF_2 was achieved by successively spiking powder **A** with additional K_2HPO_4 and milling for additional 3 h periods (powder **A** to **C**). Reaction monitoring by PXRD revealed that as the amount of K_2HPO_4 added to the reaction increased, the intensity of peaks corresponding to crystalline CaF_2 diminished with concomitant formation of new crystalline species (Figure 2.9). Peaks corresponding to the new species displayed the greatest intensity in powder **C** (prepared by adding a total of 2.5 equivalents of K_2HPO_4 in three portions to 1 equivalent of AGF over a total milling time of 9 h).

The reactivity of powders **A** to **C** in the fluorination of TsCl in *tert*-BuOH (0.25 M, 100 °C) was subsequently investigated (Figure 2.10). A yield of 67% of TsF (**1**) was achieved using just 1 equivalent of powder **C** (containing 1 equivalent of fluorspar, CaF_2) in solution. Although, the beneficial effect of water in fluoride exchange reactions of sulfonyl chlorides has been documented, the strong hydrogen-bond donating ability of water is typically detrimental for fluoride nucleophilicity.[71] The addition of water to the fluorination reaction was assessed. Interestingly, the introduction of 2 equivalents of water to the solution-phase fluorination reaction improved the yield of TsF (**1**) to 93% (from 67%) without starting material recovery (Figure 2.11). Greater loadings of water were detrimental to the yield of **1**, with TsOK formation observed by ^{1}H NMR spectroscopy ($CDCl_3$) in the reaction mixture when 6 equivalents of water were added to the reaction.

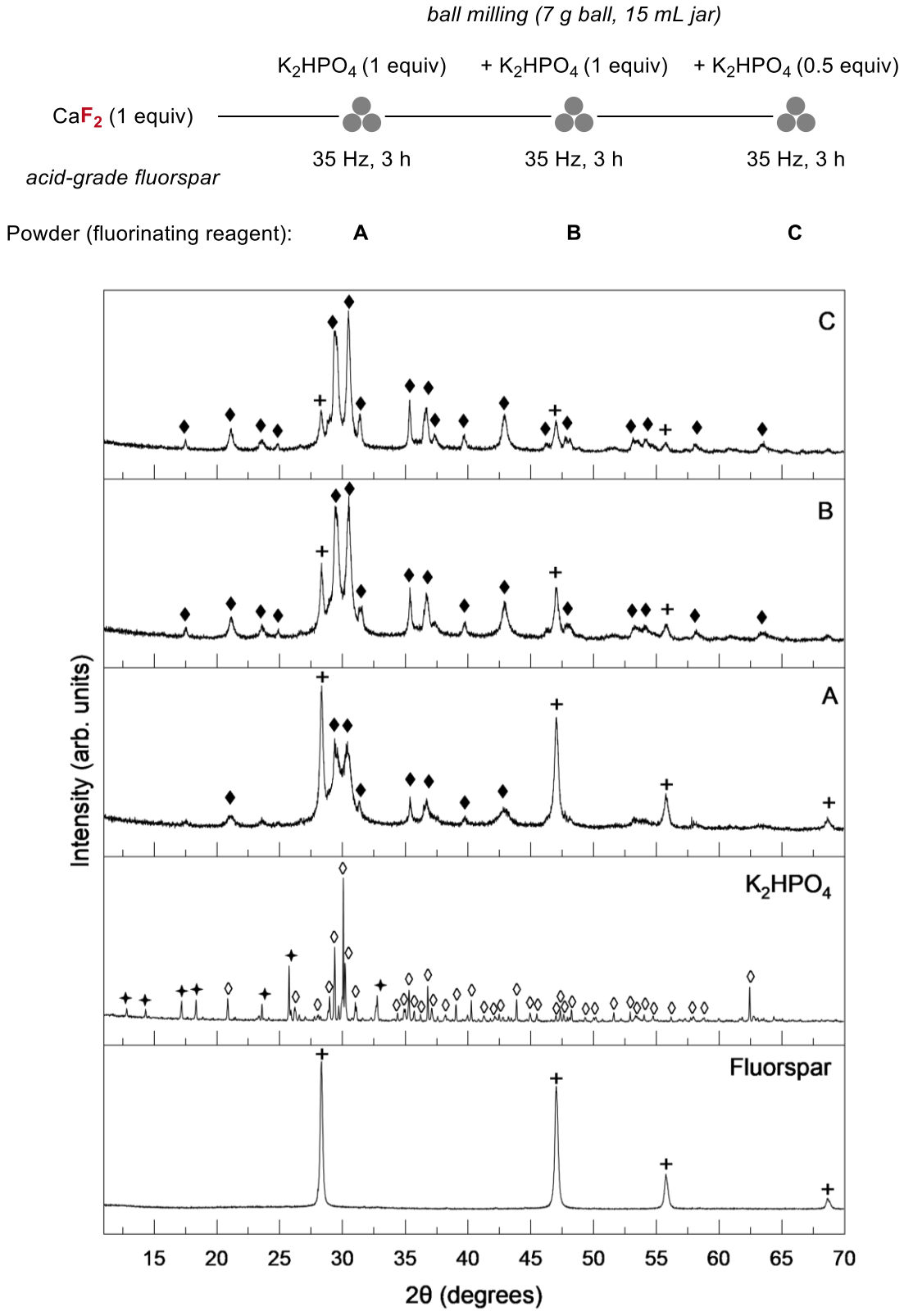

Figure 2.9. The evolution of the PXRD patterns of acid-grade fluorspar milled with K_2HPO_4 added in portions at 3 h intervals (total ball milling time of 9 h) at 35 Hz. [+ = CaF_2, ◊ = anhydrous K_2HPO_4, ✦ = $K_2HPO_4{\cdot}3H_2O$, ♦ = new crystalline phase][72].

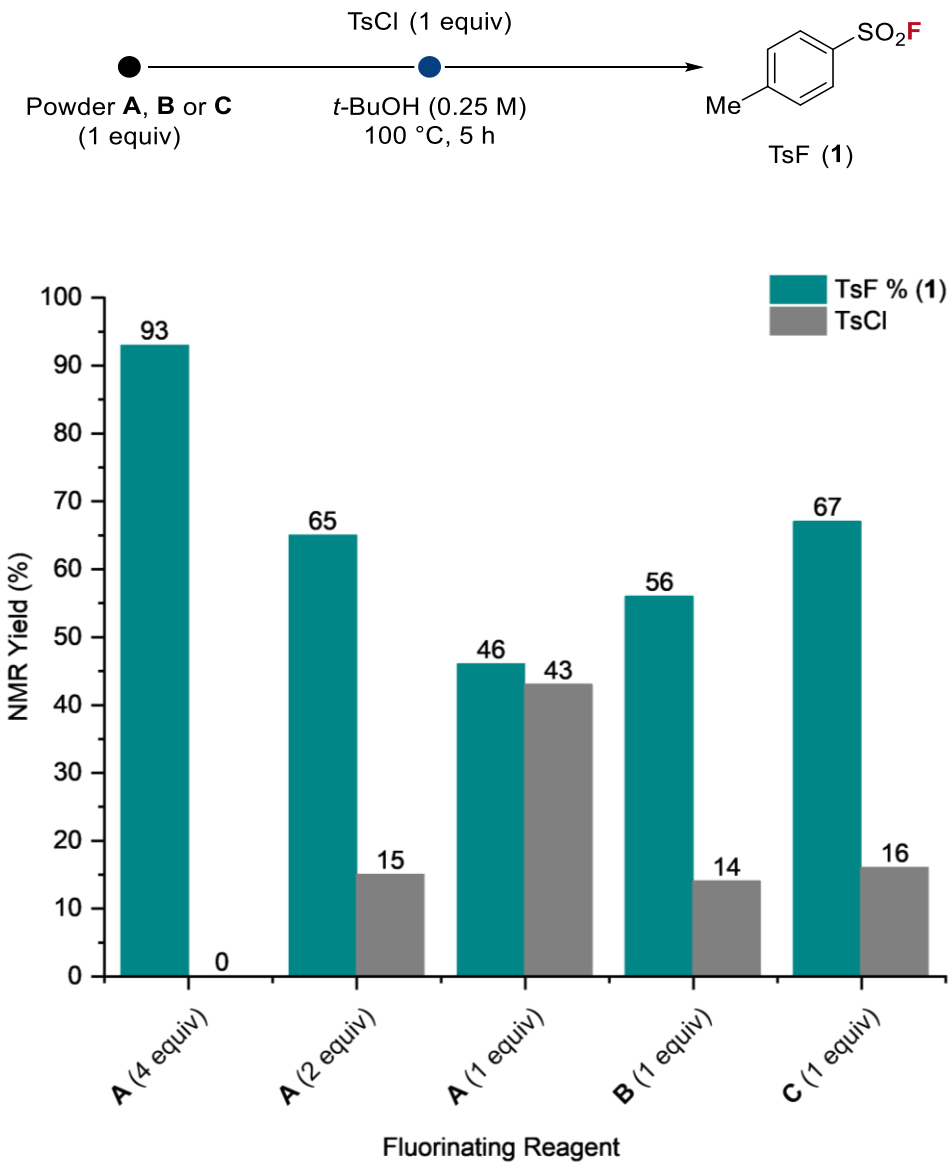

Figure 2.10. Reactivity of powders **A**, **B** and **C** prepared at 35 Hz (1 to 4 equiv); yields determined by ^{19}F and ^{1}H NMR spectroscopy using FA as internal standard.

The high reactivity achieved using power **C** (referred to as **Fmix**) in *tert*-BuOH with 2 equivalents of water provided a set of optimised conditions that was applied to a scope of sulfonyl chlorides (section 2.3.2). The procedure for the synthesis of **Fmix** is outlined in Scheme 2.5 (full experimental details can be found in Chapter **4**).

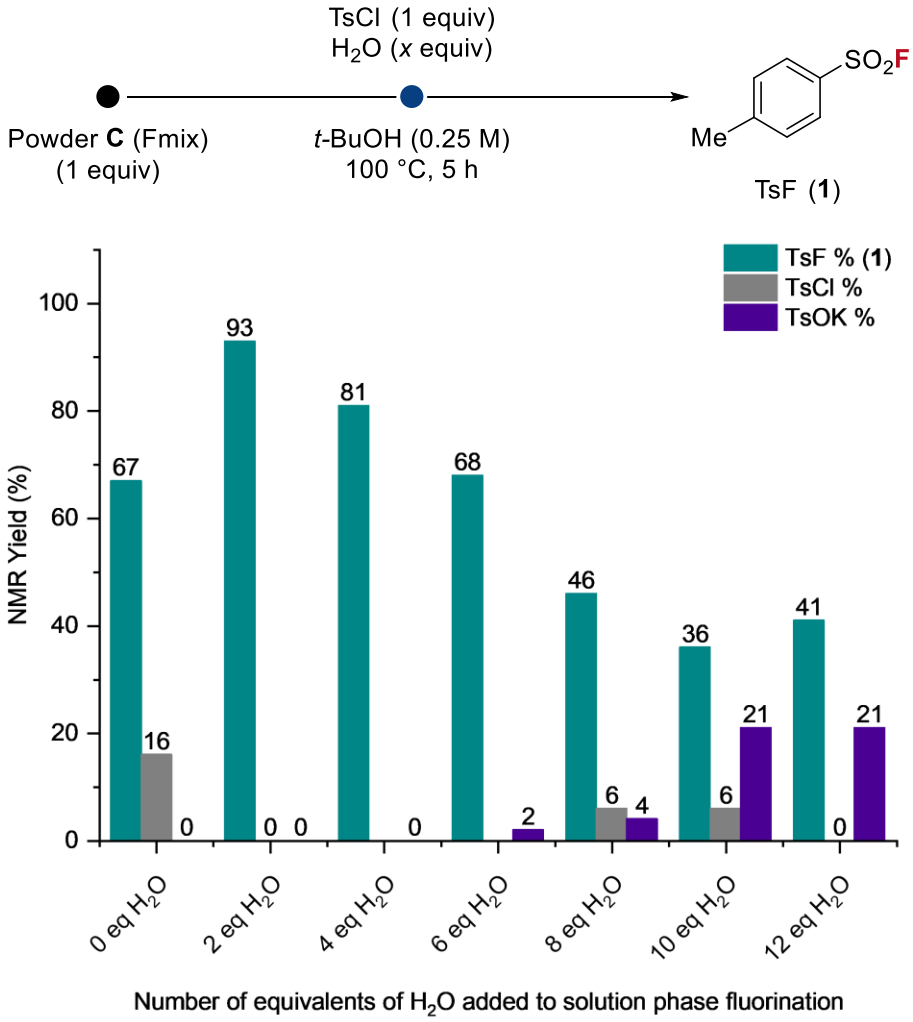

Figure 2.11. Effect of H_2O in the fluorination of TsCl using powder **C** (1 equiv prepared at 35 Hz); yields determined by ^{19}F and ^{1}H NMR spectroscopy using FA as internal standard.

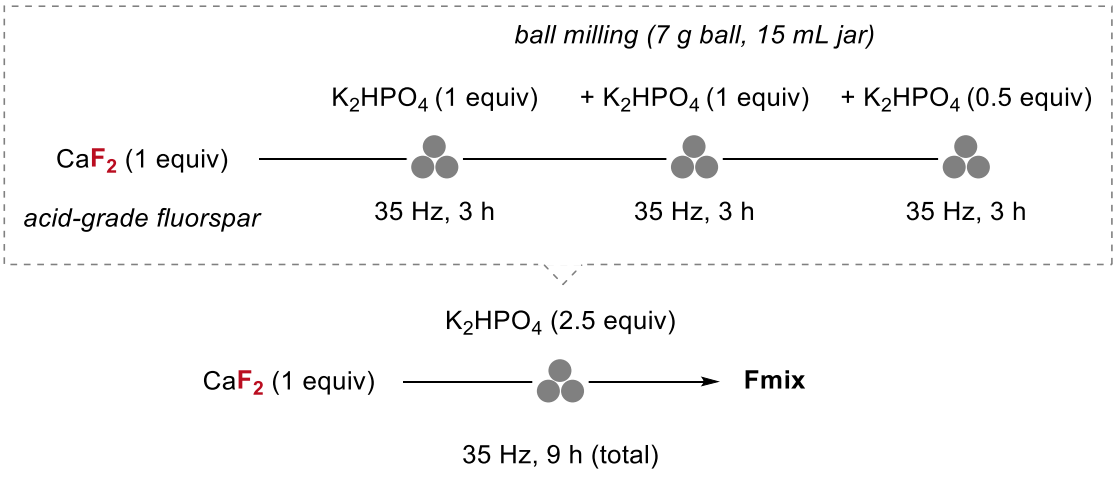

Scheme 2.5. General procedure for the synthesis of **Fmix**.

2.3.1.9 Using 0.5 equivalents of Fmix

With respect to stoichiometry, the optimal approach is to employ 0.5 mmol of CaF_2 for the fluorination of 1 mmol of TsCl. However, a reduction in **Fmix** equivalents to 0.5 equivalents led to incomplete fluorination (58% TsF **1**) (Figure 2.12). The fluorination yield did not improve with additional water or extended reaction time, indicating that the reactivity was likely hindered by the insufficient supply of 'reactive' fluoride in 0.5 equivalents of **Fmix**.

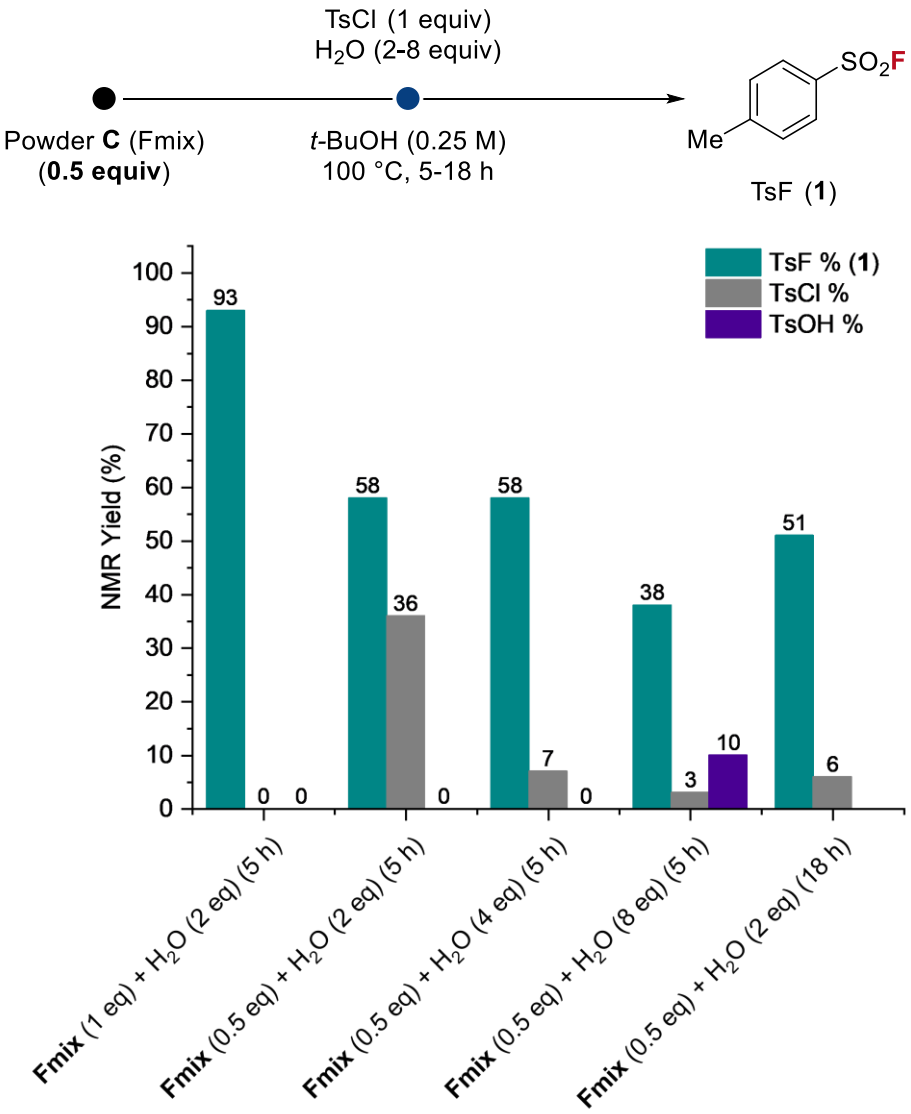

Figure 2.12. Investigated the use of 0.5 equivalents of **Fmix** in the fluorination of TsCl.

2.3.2 Sulfur Fluorine Bond Formation

The scope of the fluorination of sulfonyl chlorides was investigated using **Fmix** (1 equiv) and water (2 equiv) in *tert*-BuOH as solvent within a temperature range of 25 °C to 100 °C (Figure 2.13). This optimised protocol afforded various sulfonyl fluorides of importance in medicinal chemistry, chemical biology, and material science. Full details of the conditions used to synthesise each substrate (and corresponding starting materials) are available in the experimental section of this thesis (Chapter **4**). Aromatic sulfonyl chlorides, including those featuring electron-donating and electron-withdrawing substituents in the *meta* and *para* positions, reacted to give the corresponding sulfonyl fluorides (compounds **2**-**8**) in modest to high yield (up to 98%).

Unlike sulfonyl fluorides, which are particularly resistant in aqueous environments, sulfonyl chlorides, especially those bearing electron-withdrawing substituents, are reported to undergo hydrolysis under mild conditions.[62] Substituting *tert*-BuOH for propionitrile (EtCN), a solvent previously shown to be effective for the fluorination process, improved the fluorination of sulfonyl chlorides with electron-withdrawing substituents (compounds **3**, **6**-**8**). Alternatively, the use of 2 equiv of **Fmix** could be employed, as demonstrated in the fluorination of 2-nitrobenzene sulfonyl chloride to afford antibiotic pharmacophore 2-nitrobenzene sulfonyl fluoride (NBSF, **10**) in 50% yield.[73] Low molecular weight sulfonyl fluorides were also prepared, including the multi-purpose chemical ethene sulfonyl fluoride (ESF, **19**, b.p. 119 °C) in 72% yield (determined by ^{19}F NMR spectroscopy), a commonly used intermediate in SuFEx click chemistry[74]. In a one pot fashion, **19** was treated with freshly prepared farnesyl-thiol **S7** to afford molecule L-28 (**20**), a documented lipoprotein lipase inhibitor in 40% (over 2 steps).[75]

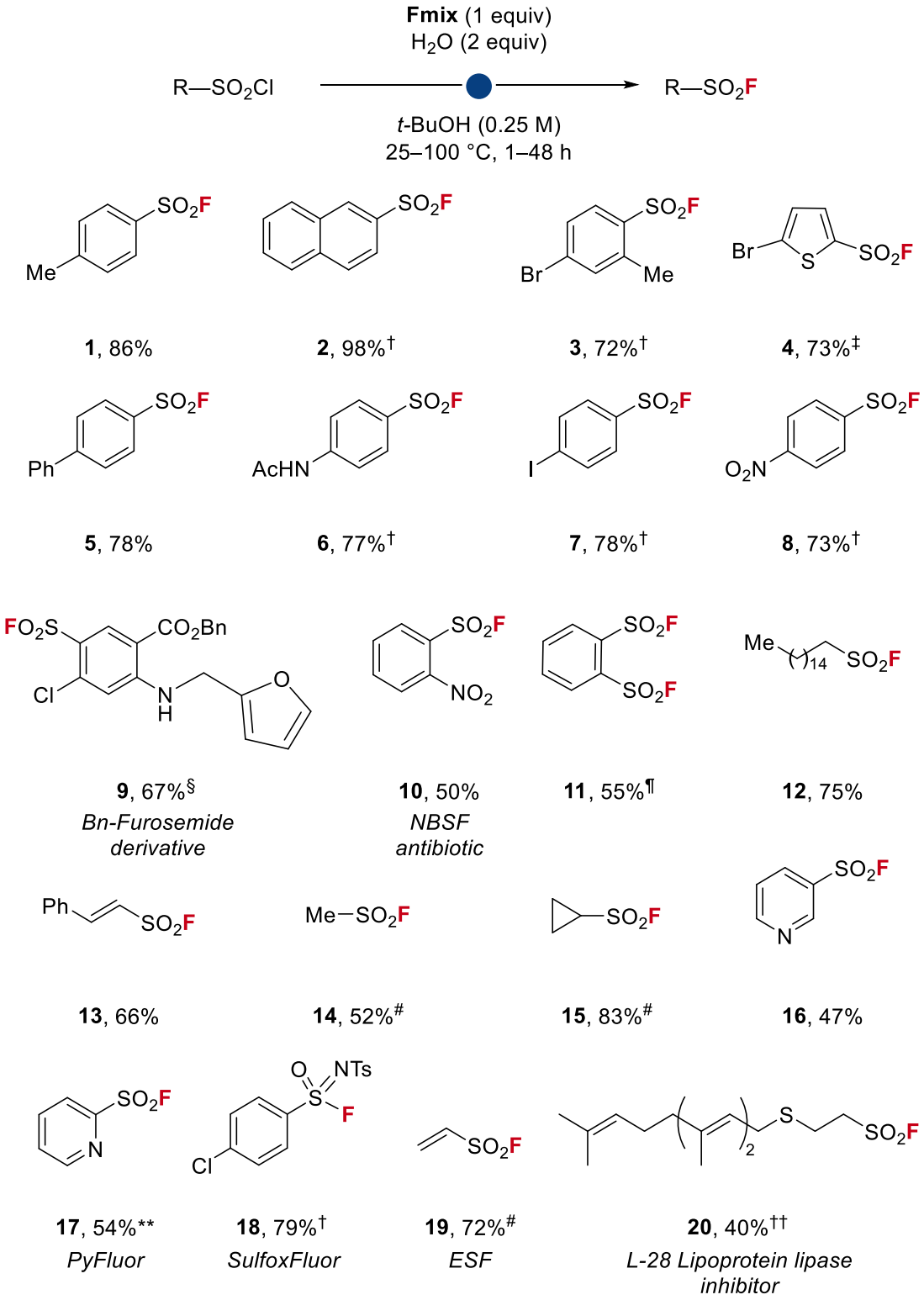

Figure 2.13. Scope of S-F bond containing fluorochemicals using **Fmix**. All yields are for isolated products (0.5 mmol scale unless otherwise stated). †EtCN as solvent; ‡Using 1.2 equiv of **Fmix**; §0.25 mmol scale; ¶Using 2.2 equiv of **Fmix** #^{19}F NMR yields using FA as internal standard; **1,2-DCB as solvent; ††Yield over two steps, prepared by addition of *trans,trans*-farnesyl mercaptan (S7) to ESF (19). Full experimental in Chapter **4**.

Fluorination of 2-pyridine sulfonyl chloride **S3**, which was prepared via oxidative chlorination of 2-mercaptopyridine using bleach (aqueous NaOCl), afforded PyFluor (**17**) in 54% isolated yield, a highly reactive deoxyfluorinating reagent developed by Doyle and co-workers.[76] Alternatively, the deoxychlorination of sodium 4-chlorobenzene sulfinate, followed by fluorination using **Fmix** (1 equiv) in propionitrile afforded SulfoxFluor (**18**), an example of a sulfonimidoyl fluoride deoxyfluorination reagent.[77]

Bioactive sulfonyl fluorides could also be prepared using **Fmix** (Figure 2.14). The chlorination and fluorination of a benzyloxycarbonyl (Cbz) protected L-leucinol with *N*-chlorosuccinimide (NCS) and **Fmix** (1 equiv), respectively, lead to the formation of a L-leucine sulfonyl fluoride **23** (45%), an intermediate used in the development of analogues of bortezomib and carfilzomib, documented protease inhibitors.[78] Sulfonyl fluorides which contain acidic protons in the α-position leading to the formation of sulfene-type intermediates, such as phenylmethanesulfonyl fluoride (PMSF, **24**) and hexadecanesulfonyl fluoride (**12**), could also be prepared using **Fmix**, resulting in yields of 26% and 75%, respectively. Substrates bearing carboxylic acids, such as 4-(chlorosulfonyl)benzoic acid, were not suitable for fluorination using **Fmix**. However, methyl 4-(chlorosulfonyl)benzoate underwent fluorination to give methyl 4-(fluorosulfonyl)benzoate (**25**) a reported glutathione S-transferase inhibitor in 50% yield (Figure 2.14).

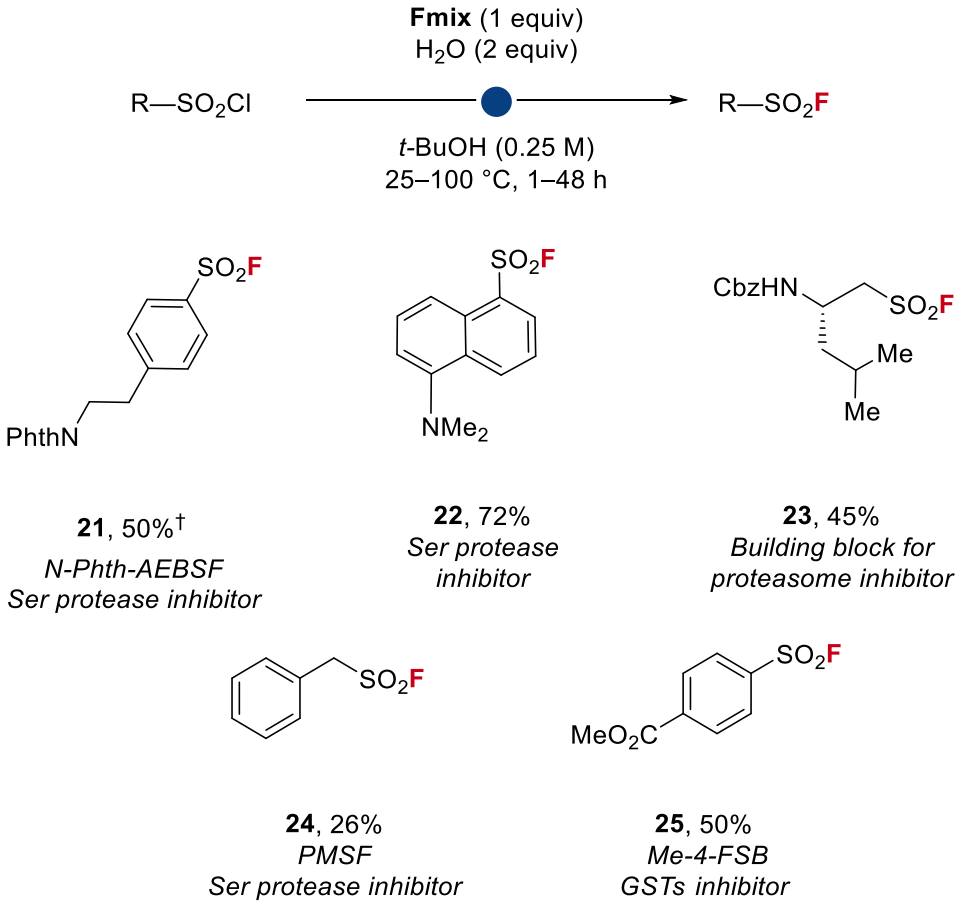

Figure 2.14. Extended scope of S-F bond containing bioactive fluorochemicals using **Fmix**. All yields are for isolated products (0.5 mmol scale unless otherwise stated). †EtCN as solvent. GSTs glutathione S-transferases; Phth, phthalimide; PMSF, phenylmethanesulfonyl fluoride; Ser, serine.

2.3.3 Carbon (sp^3) Fluorine Bond Formation

Advancements in C(sp^3)–F bond formation methods are highly sought after in medicinal and biological chemistry due to the presence of organofluorine compounds in agrochemicals and pharmaceuticals.[79] The possibility of C(sp^3)–F bond formation using **Fmix** was examined, starting with benzylic fluorination as a model reaction. Methods for benzylic fluorination using nucleophilic fluoride include deoxyfluorination,[76,80] photoredox induced fluorination,[81,82] and oxidative C-H mono fluorination, pioneered by Groves and co-workers.[83,84] Nucleophilic fluorination of organohalide precursors, such as benzylic bromides,

can also be used, but in case of incomplete consumption of the starting material, similar polarity of the fluorinated product and its precursor often give rise to purifications issues. Despite the fluorination of TsCl proceeding smoothly in *tert*-BuOH using **Fmix**, the reaction of 4-bromobenzyl bromide (**26**) under similar conditions was ineffective, resulting in starting material recovery (82%) and the formation of benzyl *tert*-butyl ether **27** (13%) (Table 2.13, entry 1). The addition of water did not lead to any improvement (entry 2).

Table 2.13. Optimisation of benzylic fluorination using **Fmix**.

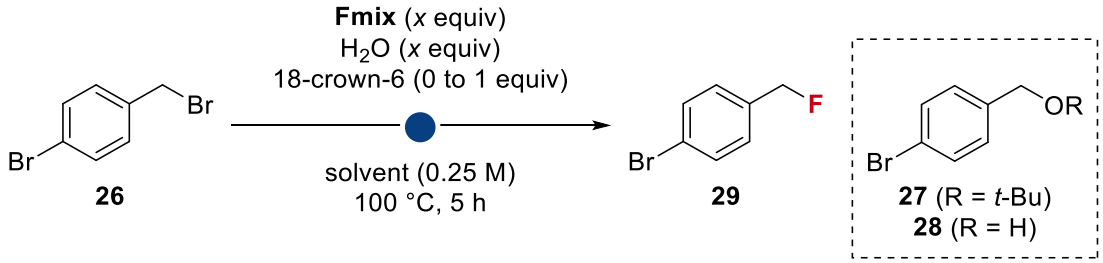

Entry	Solvent	**Fmix** (equiv)	H_2O (equiv)	18-crown-6 (equiv)	**26** (%)	**29** (%)	**27** (%)	**28** (%)
1	*t*-BuOH	1	0	0	82	0	13	0
2	*t*-BuOH	1	2	0	71	0	18	8
3	*t*-BuOH	1	0	1	8	56	23	0
4	PhCl	2	0	1	81	4	-	2
5	*t*-BuOH	2	0	1	0	57	22	7
6	*t*-BuOH	2	2	1	4	70	17	6
7	***t*-BuOH**	**2**	**5**	**1**	**0**	**73**	**11**	**8**
8	*t*-BuOMe	2	**5**	1	99	0	0	0

0.125 mmol scale. Yields determined by quantitative ^{19}F and ^{1}H NMR spectroscopy using FA as internal standard.

Fluorination was, however, observed upon the addition of 18-crown-6 (1 equiv), affording the desired 4-bromobenzyl fluoride (**29**) in 56% yield (Table 2.13, entry 3). The formation of ether **27** (23%) was observed under these conditions, which was challenging

to separate from the desired benzyl fluoride using flash column chromatography (SiO_2) due to the similar polarity of the fluorinated product and the ether. To avoid the formation of the ether **27** alternative reaction solvents were considered. Although fluorination of TsCl using **Fmix** was achieved in high yield using PhCl as solvent (refer to Figure 2.6), this solvent was less effective than *tert*-BuOH for benzylic fluorination (entry 4). Complete conversion of the starting benzyl bromide (**26**) was achieved using 2 equivalents of **Fmix** and 18-crown-6 (1 equiv) to afford the desired benzyl fluoride (**29**) in a yield of 57% (Table 2.13, entry 4). Using 5 equivalents of water enabled full consumption of the starting benzylic bromide with fluorinated product obtained in 73% with accompanying formation of *tert*-butyl ether **27** (11%) (entry 7). The replacement of *tert*-BuOH for methyl *tert*-butyl ether (MTBE) was hypothesised to prevent the formation of ether **27** (entry 8). However, under these conditions, fluorination did not proceed. This pronounced result underscores the importance of alcohol-hydrogen bonding interactions in affecting fluoride reactivity. With an optimised set of conditions for C(sp^3)–F bond formation established, the scope of this transformation was studied (Figure 2.15). The fluorination of various benzylic bromides across a range of electron rich and electron poor scaffolds were carried out using **Fmix** (2 equiv), H_2O (5 equiv) and 18-crown-6 (1 equiv) in *tert*-BuOH at 100 °C (**30** to **34**). As shown in Figure 2.15, α-bromo benzyl esters and amides underwent halogen exchange to afford desired fluorinated products **35** (41%) and **36** (78%). The scope of C(sp^3)–F fluorochemicals could be broadened to α-fluoro carbonyl and amide compounds (**37** to **44**), synthesised from the corresponding bromides (see Chapter **4** for experimental details). Methyl 2-fluoropropanoate (**39**), a precursor to the globally used agrochemical Indaziflam,[85] and an analogue of androstane steroid fluasterone (**42**) [diastereomeric mixture (1:2 α:β)] could be prepared in 53% and 24% yield, respectively.[86] The developed fluorination protocol also

worked for primary alkyl halide (**45** to **47**), propargylic (**48**) and allylic (**49**) substrates using **Fmix** (2 to 2.5 equiv).

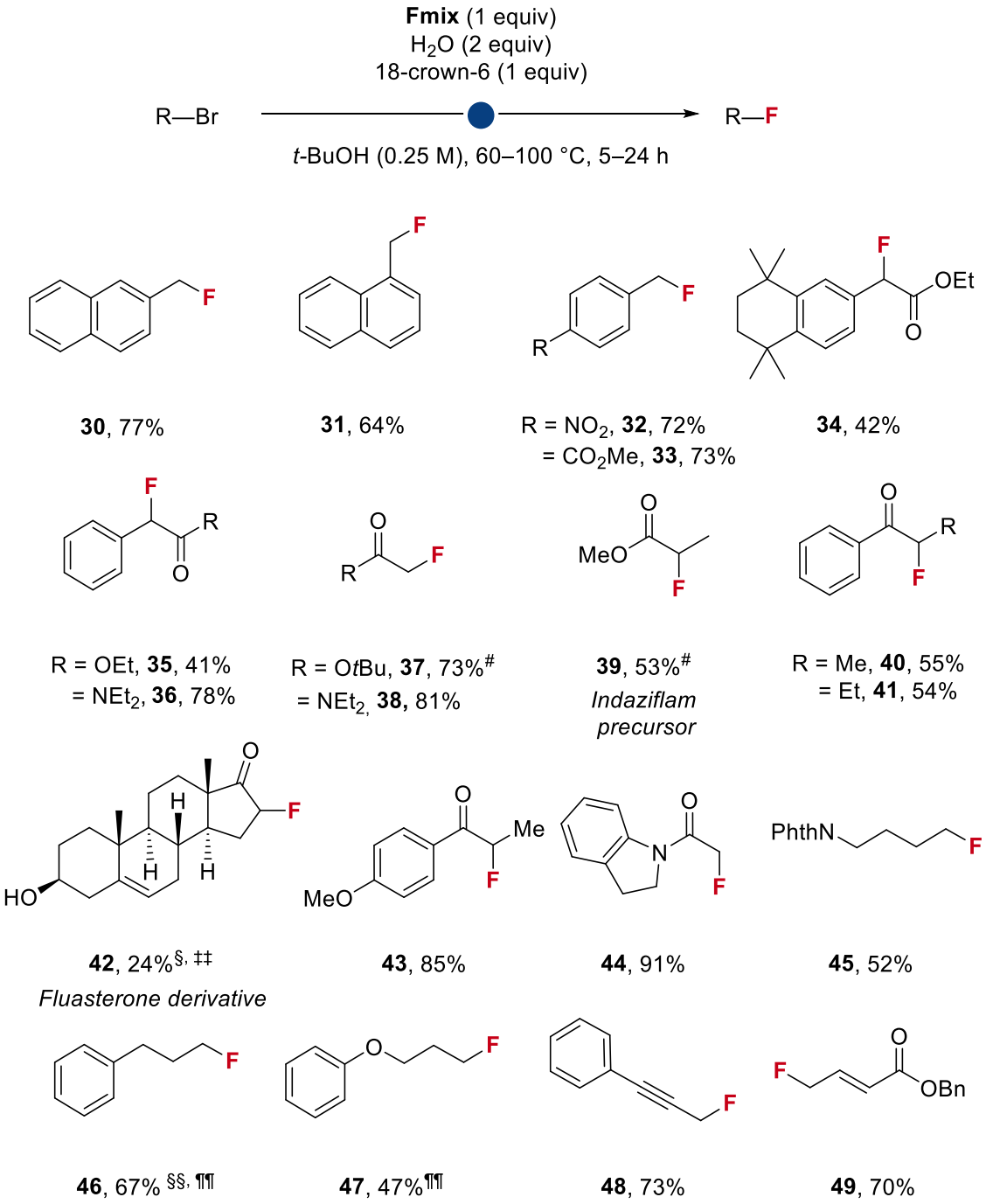

Figure 2.15. Scope of C(sp^3)–F bond containing fluorochemicals using **Fmix**. All yields are for isolated products (0.5 mmol scale unless otherwise stated). #^{19}F NMR yields using FA as internal standard; ‡‡Isolated as a diastereomeric mixture (1:2 *α*:*β*); §§From R–I; ¶¶ using 2.5 equiv of **Fmix**. Full experimental in Chapter **4**.

2.3.4 Carbon (sp^2) Fluorine Bond Formation

2.3.4.1 Aryl fluorides

Aryl and heteroaryl fluorides are ubiquitous motifs in agrochemicals, functionalised materials, and globally marketed pharmaceuticals (approximately 10%).[87] Nucleophilic methods to prepare (hetero)aryl fluorides include transition-metal catalysed cross couplings, the decomposition of aryl diazonium salts (Balz-Schiemann reaction) or the exchange of a chloride (halex reaction) or nitro group for fluoride in electron-poor (hetero)arenes via nucleophilic aromatic substitution (S_NAr).[88,89] As a case study for (hetero)aromatic C(sp^2)–F bond formation, 3,4-dichloronitrobenzene (**50**) was selected as a model substrate, featuring an electron withdrawing nitro (NO_2) group in the *para* position to the chloride leaving group [σ_{para} (NO_2) = 0.78 vs σ_{para} (Cl) = 0.23, where σ_{para} is the Hammett constant], for S_NAr fluorination.[90] Alcoholic solvents, such as *tert*-BuOH, which can potentially act as competing nucleophiles toward the fluoroarene product, were avoided. Studies were initiated by examining the reaction of aryl chloride **50** and **Fmix** (2 equiv) in anhydrous DMSO (0.5 M, 130 °C) for 3 h (Table 2.14, entry 1). Analysis of the crude reaction mixture by ^{19}F NMR spectroscopy ($CDCl_3$) revealed trace amounts (5%) of the desired aryl fluoride **51** (m, δ_F = -103.9 ppm) (95% starting material recovered). The addition of a phase transfer additive was hypothesised to improve the solubility and thus reactivity of the fluoride source in **Fmix**. Phase transfer additives such as tetramethylammonium chloride (Me_4NCl) are known to undergo equilibrium ion exchange with fluoride sources, such as KF, leading to the formation of Me_4NF in low concentrations. The S_NAr reaction of **50** with **Fmix** (2 equiv) in the presence of Me_4NCl (1 equiv) resulted in 21% yield of the desired aryl fluoride (79% starting material) (entry 2).

Table 2.14. Preliminary studies for nucleophilic aromatic fluorination using **Fmix**

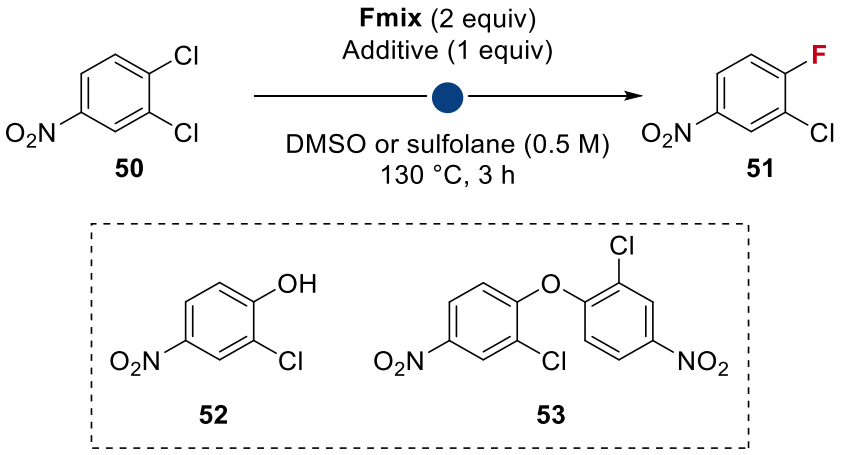

Entry	Solvent	Temperature (°C)	Additive	**50** (%)	**51** (%)	**52** (%)	**53** (%)
1	DMSO	130	-	95	5	0	0
2	DMSO	130	Me_4NCl	79	21	0	0
3	DMSO	130	Me_4NCl + 18-crown-6	65	34	0	0
4	Sulfolane	130	Me_4NCl	68	32	0	0
5	Sulfolane	130	Ph_4PCl	59	23	8	0
6	Sulfolane	130	Bu_4NCl	42	42	16	0
7	Sulfolane	150	Me_4NCl	44	44	12	0
8	DMSO	150	Me_4NCl	35	58	0	7
9	DMSO*	150	Me_4NCl	33	58	9	5

0.25 mmol scale. Yields determined by quantitative ^{19}F and ^{1}H NMR spectroscopy using FA as internal standard. *Concentration 0.25 M using 0.25 mmol aryl chloride.

A moderate improvement of yield (34%) was observed upon the addition of 18-crown-6 (1 equiv) (entry 3). Replacement of anhydrous DMSO for sulfolane, a commonly used solvent for high temperature halex reactions (sulfolane b.p. 287 °C versus DMSO b.p. 189 °C), afforded the desired aryl fluoride **51** in 32% yield (68% starting material recovery) (entry 4).[91] Examining different phase transfer additives demonstrated that an improved yield of 42% of the aryl fluoride **51** could be achieved using

n-tetrabutylammonium chloride (*n*-Bu_4NCl), albeit with formation of phenol **52** (16%) (entry 6). Subsequent temperature screening studies prioritised Me_4NCl over *n*-Bu_4NCl, as *n*-Bu_4NX salts can decompose through Hofmann elimination.[92] Me_4NF with a very high thermal stability, only starts to slowly decompose into trimethylamine and fluoromethane at temperatures >180 °C. At 150 °C, using DMSO as solvent and Me_4NCl (1 equiv), aryl fluoride **51** was produced in 58% (entry 9). The stoichiometry of the phase transfer additive Me_4NCl could be reduced to sub-stoichiometric amounts (0.5 equivalents), allowing fluorination with **Fmix** (2 equiv) at 150 °C (3 h) to give the desired aryl fluoride **51** in 51% yield (Figure 2.16).

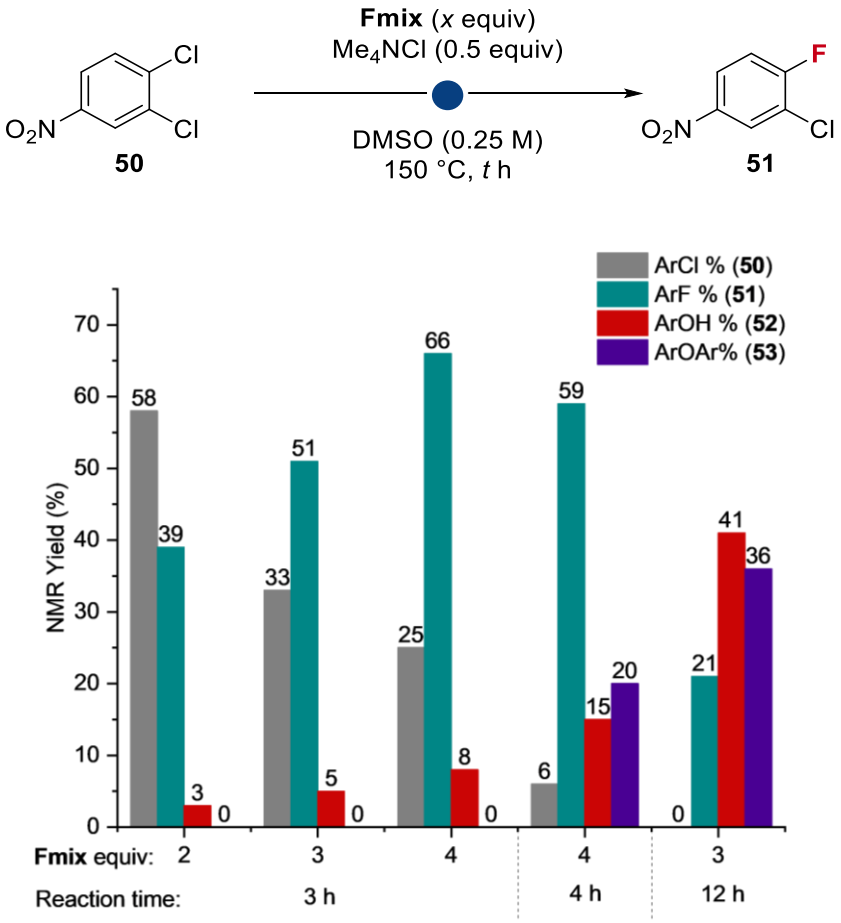

Figure 2.16. Optimisation of **Fmix** loading (2 to 4 equiv) and reaction time (3 to 12 h) of S_NAr fluorination of 3,4-dichloronitrobenzene (**50**) (0.5 mmol scale). Yields determined by ^{19}F NMR spectroscopy using FA as internal standard.

The yield of **51** was improved to 66% yield using 4 equivalents of **Fmix** (as measured by ^{19}F NMR spectroscopy), albeit with undesired phenol (**52**) formation (8%). Allowing the reaction to proceed for 12 hours resulted in a complex mixture of aryl fluoride **51** (21%), phenol **52** (41%) and aryl ether **53** (36%).

Nonetheless, under the developed reaction conditions (150 °C, 4 h), aryl fluoride **51** could be prepared and isolated in 48% yield after purification by flash column chromatography. Aryl ether **53** was also isolated as a side product (16%) and characterised by ^{1}H NMR spectroscopy (further details in Chapter **4**).

With these conditions in hand a scope of (hetero)aryl fluorides was prepared from the corresponding chlorides (Figure 2.17). 2-Chloropyridines underwent fluorination using 3 equivalents of **Fmix** at 150 °C in under 2 hours to afford 2-fluoropyridines **54** and **55** in 61% and 58% yield as isolated products. Pyridazine, imidazopyridazine and quinoline chlorides also reacted to afford (hetero)aromatic fluoride products **56** to **58**. While the feasibility of aromatic fluorination using **Fmix** was demonstrated, the S_NAr chemistry developed in this chapter is limited to electron-deficient substrates, and phenolic and aryl ether side-products were formed in almost all cases. Less electron deficient chloroarenes 4-nitrochlorobenzene and 2-nitrochlorobenzene afforded fluoroarenes **59** and **60** in <10% yield. In order to enhance the reactivity of these chloroarenes, it may be necessary to raise the reaction temperatures above 160 °C; however, temperatures above 180 °C were avoided due to DMSO's thermal instability (decomposition reported at 189 °C). Owing to its greater thermal stability, sulfolane may serve as an alternative appropriate solvent. The complete conversion of 2,4-dinitrochlorobenzene, which serves as a precursor for fluoride **62**, into phenol occurred when exposed to **Fmix** at 100 °C. Structurally varied heteroaromatic scaffolds, such as 5-chloropyrazine-2-carbonitrile (precursor to **63**) and 2-

chloro-5-nitropyridine (precursor to **64**), experienced total degradation under the reaction conditions.

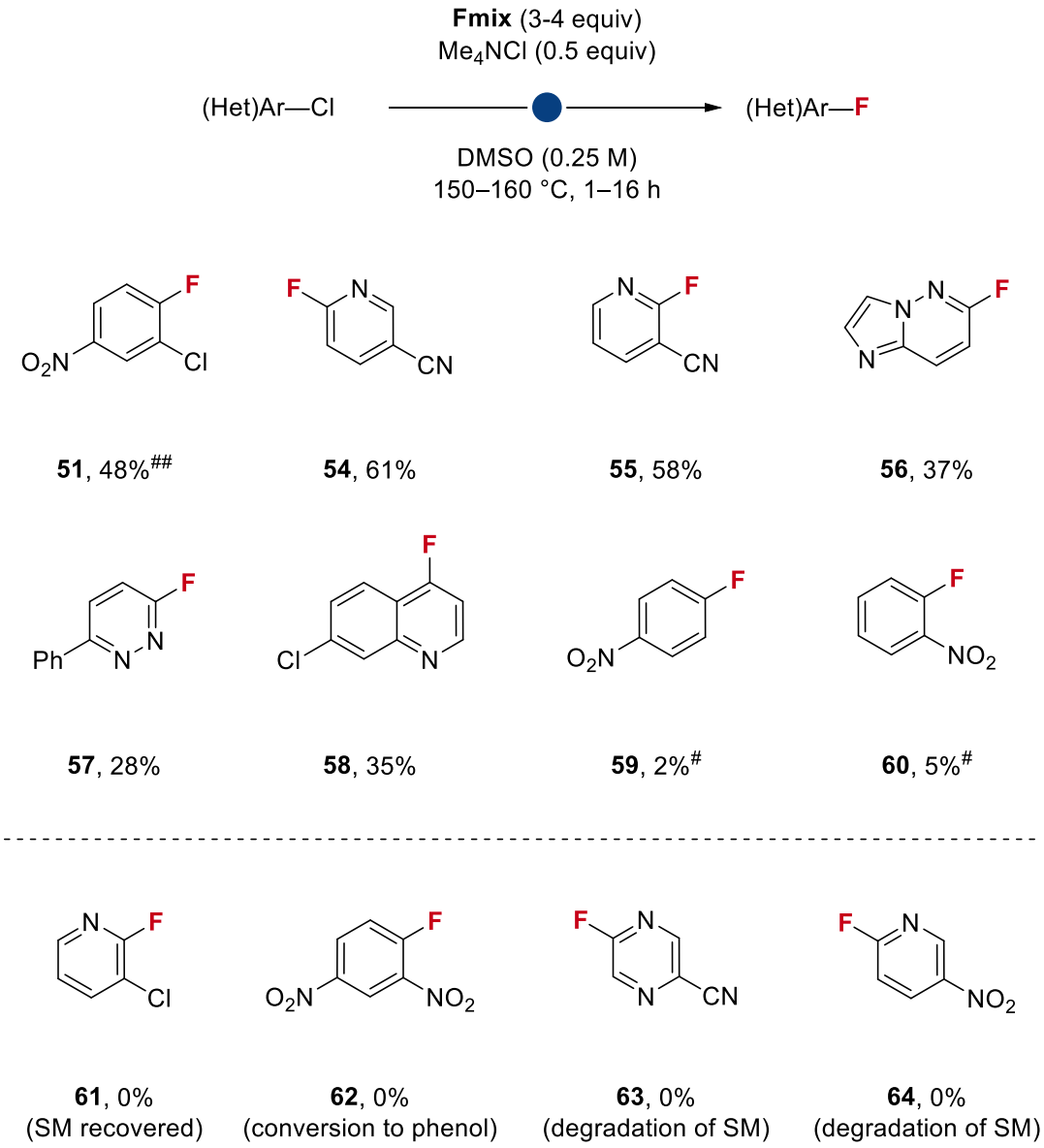

Figure 2.17. Scope of C(sp^2)-F bond containing fluorochemicals using Fmix. All yields are for isolated products (0.5 mmol scale unless otherwise stated). #^{19}F NMR yields using FA as internal standard, ##using 4 equiv of **Fmix**.

A stability study demonstrated that aryl fluoride **51** converts to phenol **52** (29%) and aryl ether **53** (11%) when exposed to K_2HPO_4 (2 equiv) and Me_4NCl (0.5 equiv) at 150 °C in

DMSO (as observed in the reaction mixture by ^{1}H NMR spectroscopy). In contrast, reacting the starting aryl chloride substrate **50** with K_2HPO_4 (2 equiv) under identical reaction conditions led to starting material recovery (Scheme 2.6).

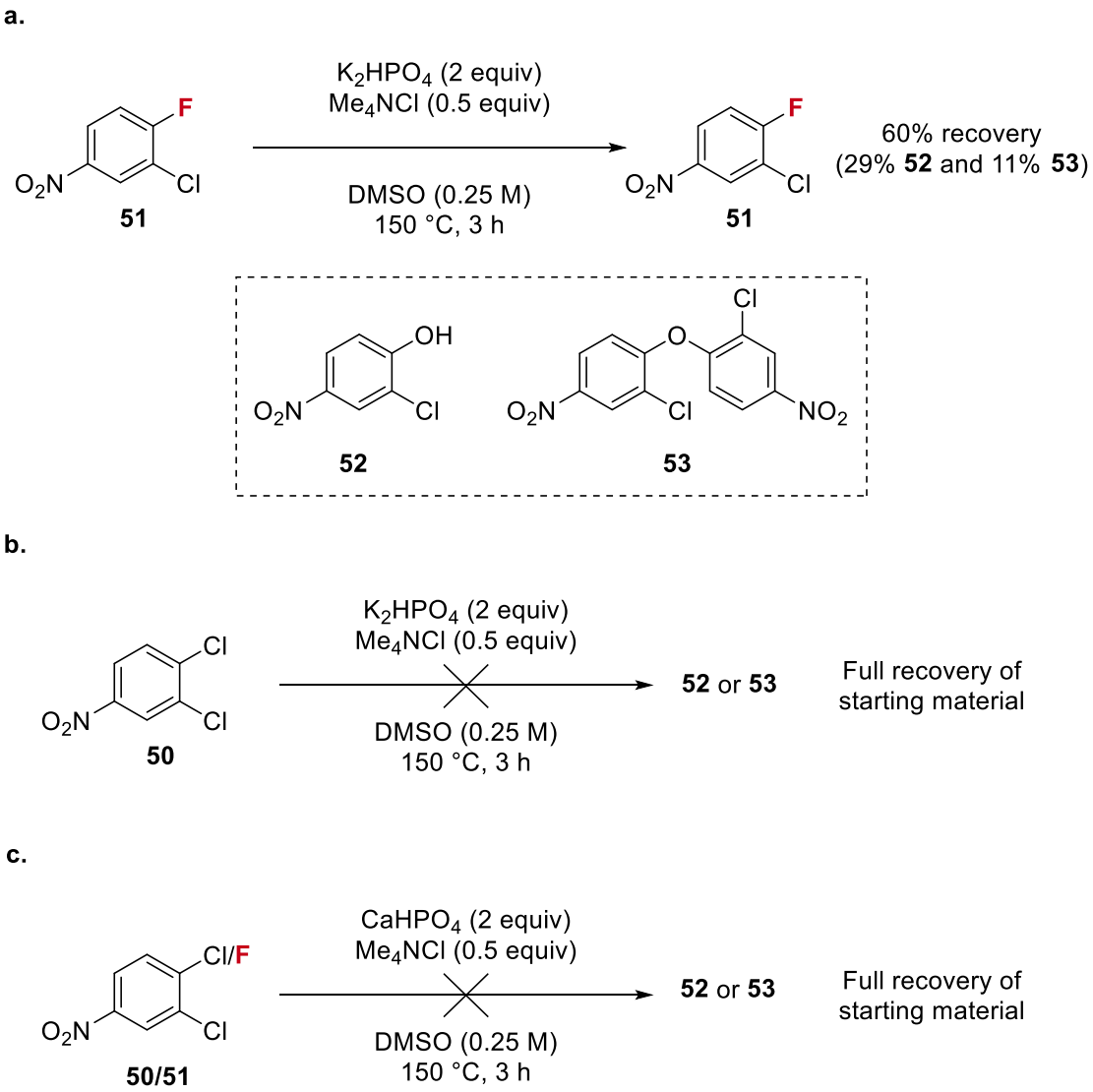

Scheme 2.6. Stability experiments of aryl fluoride **51** in the presence of K_2HPO_4 and Me_4NCl at 150 °C in anhydrous DMSO (**a**); aryl chloride **50** under identical conditions (**b**) and **50** or **51** in the presence of $CaHPO_4$ and Me_4NCl (**c**).

The observed reactivity of the aryl fluoride compared to the aryl chloride toward K_2HPO_4 correlates with the increased electrophilicity of the former and greater propensity of fluoride as a leaving group compared to chloride. In the presence of $CaHPO_4$, no conversion of the starting aryl chloride **50** or fluoride **51** was observed in DMSO (150 °C, 3 h). Control experiments using KF (4 equiv) or a mixture of KF and K_2HPO_4 (4 equiv of each) for the fluorination of **50** yielded the aryl fluoride product **51** in 98% and 80% yield, respectively (Table 2.15). In the latter case, ether **53** was observed in 16%. Taken together, these data indicate that the low yields of aryl fluoride **51** can be attributed to the sensitivity of the product towards phosphate containing species (or derivative thereof) found in **Fmix**.

Table 2.15. Control fluorination experiments of **50** using **Fmix**, KF and KF/K_2HPO_4.

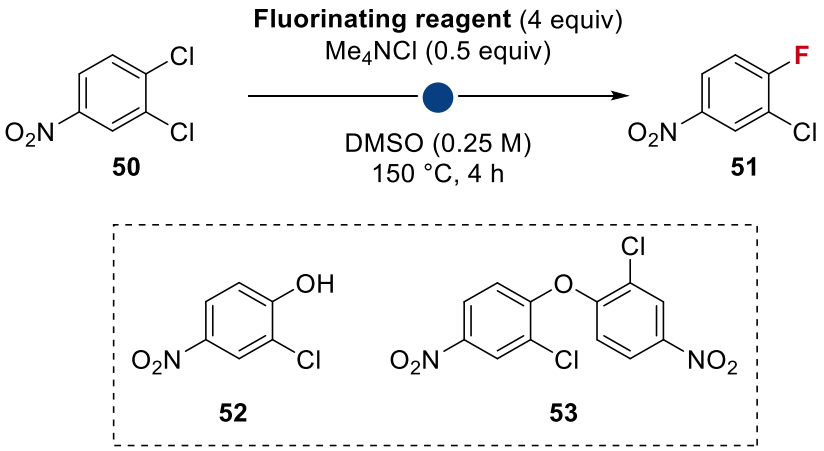

Entry	Fluorinating reagent	**50** (%)	**51** (%)	**52** (%)	**53** (%)
1	**Fmix** (4 equiv)	6	59	15	20
2	KF (4 equiv)	0	98	0	2
3	KF/K_2HPO_4 (4 equiv of each)	0	80	4	16

Yields determined by quantitative ^{19}F and ^{1}H NMR spectroscopy using FA as internal standard. * Concentration 0.25 M using 0.125 mmol aryl chloride.

2.3.4.2 Acyl fluorides

Often utilised as electrophiles in acyl transfer reactions, acyl fluorides are valuable intermediates in organic synthesis. They find diverse application as flexible coupling partners in a range of transition-metal-catalysed cross-couplings, peptide couplings and can even act as anhydrous fluoride sources for nucleophilic fluorination reactions.[93,94] Traditional synthesis of acyl fluorides focused on fluorine-chlorine exchange of acyl chlorides using metal fluoride salts (NaF, KF and KHF_2), however, these methods suffer from drawbacks such as time-consuming drying of the fluoride salt, extended high-temperature reactions, and the requirement for distillation to isolate the desired products.[95–97] Recently, considerable efforts have been made to develop mild and easy-to-handle deoxyfluorinating reagents designed to convert carboxylic acids and alcohols to acyl fluorides.[98]

As a case study, the fluorination of 4-methoxybenzoyl chloride (**65**, 0.25 mmol, 1 equiv) using **Fmix** was investigated. Conversion of acyl chloride **65** to the corresponding acyl fluoride **66** occurred in 27% in *tert*-BuOH as solvent at 40 °C (24 h) [as determined by ^{19}F NMR spectroscopy ($CDCl_3$), singlet, $\delta_F = 15.86$ ppm] (Table 2.16, entry 1). Analysis of a reaction mixture by quantitative ^1H NMR spectroscopy revealed the presence of 4-methoxybenzoic acid (**67**) and 4-methoxybenzoic anhydride (**68**) in 29% and 37% yield, respectively. When 4-methoxybenzoyl chloride (**65**) was treated with KF (2 equivalents) in PhCl in a control experiment, 4-methyoxybenzoyl fluoride (**66**) was formed in 97% yield (entry 6). Combining acyl chloride **65** with **Fmix** (2 equiv) in anhydrous PhCl for 24 h (40 °C), fluorination proceeded to give acyl fluoride **66** in 18% yield and the formation of acid **67** and anhydride **68** was completely suppressed (entry 2). However, allowing the reaction to proceed for 72 h, resulted in formation of carboxylic acid **67** only (entry 3).

Fluorination proceeded in 45% yield after 24 h (40 °C) upon the addition of Me_4NCl (1 equiv) (entry 4).

Table 2.16. Preliminary studies for acyl chloride fluorination using **Fmix**

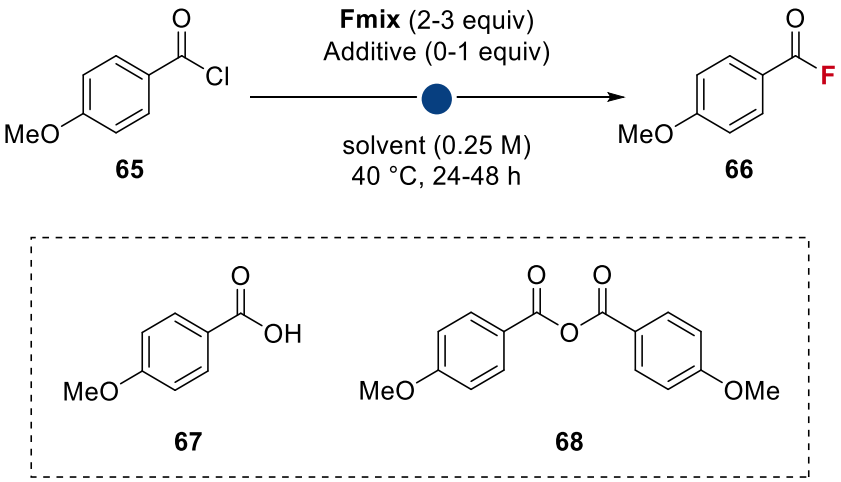

Entry	Solvent	**Fmix** equiv	Reaction time (h)	Additive (1 equiv)	**65** (%)	**66** (%)	**67** (%)	**68** (%)
1	*t*-BuOH	2	24	-	0	27	29	37
2	PhCl	2	24	-	82	18	0	0
3	PhCl	2	72	-	0	0	98	0
4	PhCl	2	24	Me_4NCl	55	45	0	0
5	PhCl	2	24	18-crown-6	0	0	0	99
6*	PhCl	-	24	-	3	97	0	0

*Using KF (2 equiv) as fluorinating reagent

In the presence of 18-crown-6 (1 equiv) only formation of the anhydride product **68** was observed (Table 2.16, entry 5). Analysis of a reaction mixture by ^{19}F NMR spectroscopy displayed a doublet (δ_F = -81.44 ppm, J = 955.6 Hz) in the ^{19}F NMR spectrum (Figure 2.18). This doublet was assigned to difluorophosphate ($F_2PO_2^{2-}$). A triplet in the ^{31}P NMR spectrum (δ_P =-14.17 ppm, J = 955.6 Hz) was also observed and consistent with difluorophosphate ($F_2PO_2^{2-}$), which has been previously characterised in $CDCl_3$.[99]

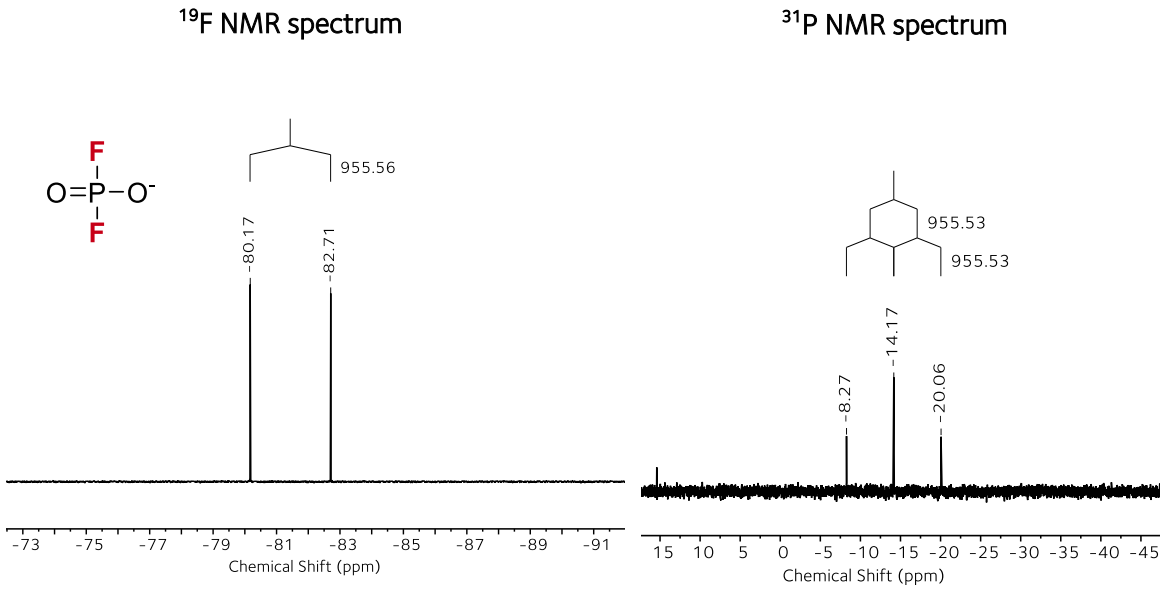

Figure 2.18. ^{31}P NMR and ^{19}F NMR spectra of reaction mixture (entry 5, Table 2.16) evidencing difluorophosphate ($F_2PO_2^{2-}$). $^{1}J_{P-F}$ = 956 Hz observed.

Mechanistic studies on the composition of **Fmix** (sections 2.4.1 Insights from Solution NMR Spectroscopy and 2.4.2 Monofluorophosphate Investigation) revealed that **Fmix** contains HPO_4^{2-} and monofluorophosphate (PO_3F^{2-}) as the sole P-F containing species. When **Fmix** was heated to 150 °C for 3 h in PhCl the formation of difluorophosphate was not observed, even after the addition of 18-crown-6, indicating that, in the presence of 18-crown-6 the formation of difluorophosphate may involve a reaction between PO_3F^{2-} and acyl fluoride **66**. Such a process would be detrimental to the yield of **66**. Overall, the observed sensitivity of the acyl substrates toward acid and anhydride formation, and possible formation of a difluorophosphate side product, demonstrate the difficulties associated with the development of acyl chloride fluorination using **Fmix**. Further investigations to access this fluorochemical class were not undertaken.

2.4 Preliminary Mechanistic Insights

Ball milling CaF_2 and K_2HPO_4 was hypothesised to afford calcium hydrogen phosphate ($CaHPO_4$) and potassium fluoride (KF), or derivatives thereof, via ion exchange (Scheme 2.7).

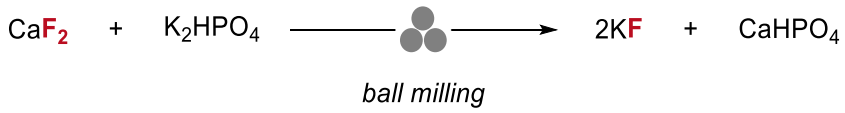

Scheme 2.7. Hypothesised mechanochemical ion exchange between CaF_2 with K_2HPO_4.

Mechanistic studies were employed to provide insight on the ion exchange pathways of CaF_2 and K_2HPO_4, the composition of **Fmix** and how it serves as a fluorinating reagent.

2.4.1 Insights from Solution NMR Spectroscopy

AGF (>97% CaF_2) was ball milled for a total of 9 h at 35 Hz in the presence of anhydrous K_2HPO_4 (2.5 equiv total). A sample of the resultant solid (**Fmix**) was stirred in D_2O. Analysis of the supernatant by ^{19}F NMR (D_2O) spectroscopy showed a singlet (δ_F = -121.4 ppm) assigned to fluoride (Figure 2.19).[100] A second ^{19}F peak was observed and assigned as monofluorophosphate (FPO_3^{2-}, doublet, δ_F = -73.8 ppm, $^1J_{P-F}$ = 862 Hz). A signal at δ_P = 2.7 ppm identified as orthophosphate (PO_4^{3-}/HPO_4^{2-}), and a doublet at δ_P = 1.1 ppm ($^1J_{P-F}$ = 862 Hz) arising from the coupling of ^{31}P to ^{19}F in the PO_3F^{2-} ion was observed by ^{31}P NMR (D_2O) (Figure 2.20).[101] Using quantitative ^{19}F NMR spectroscopy (D_2O), the amount of water soluble fluoride and monofluorophosphate released from the sequential ball milling of AGF with K_2HPO_4 was measured (powder **A** to **Fmix**) (Figure 2.21).

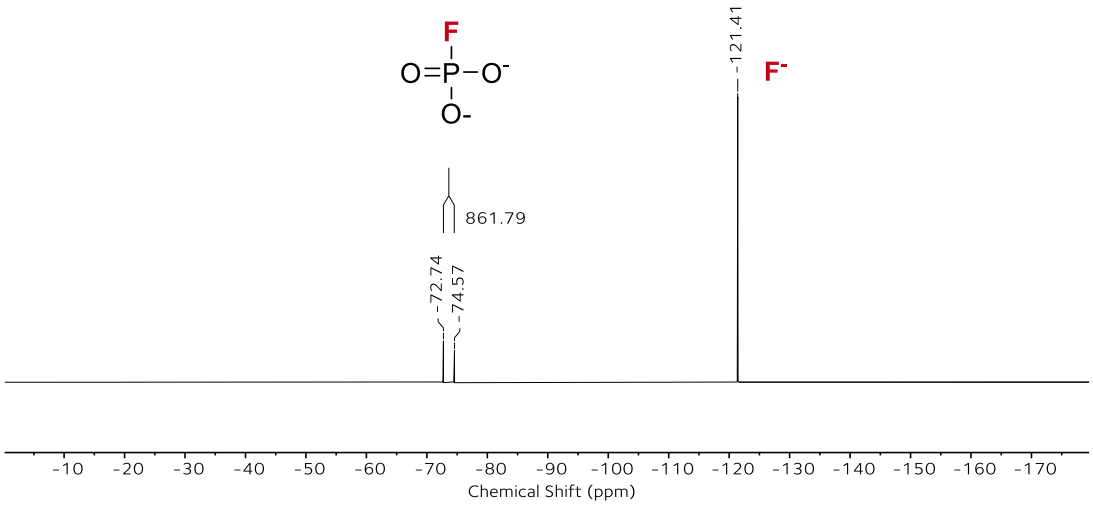

Figure 2.19. ^{19}F NMR (D_2O) spectra of **Fmix** (PO_3F^{2-},d ,δ = -73.83 ppm, J= 862 Hz and F^-,s , δ = -121.41 ppm).

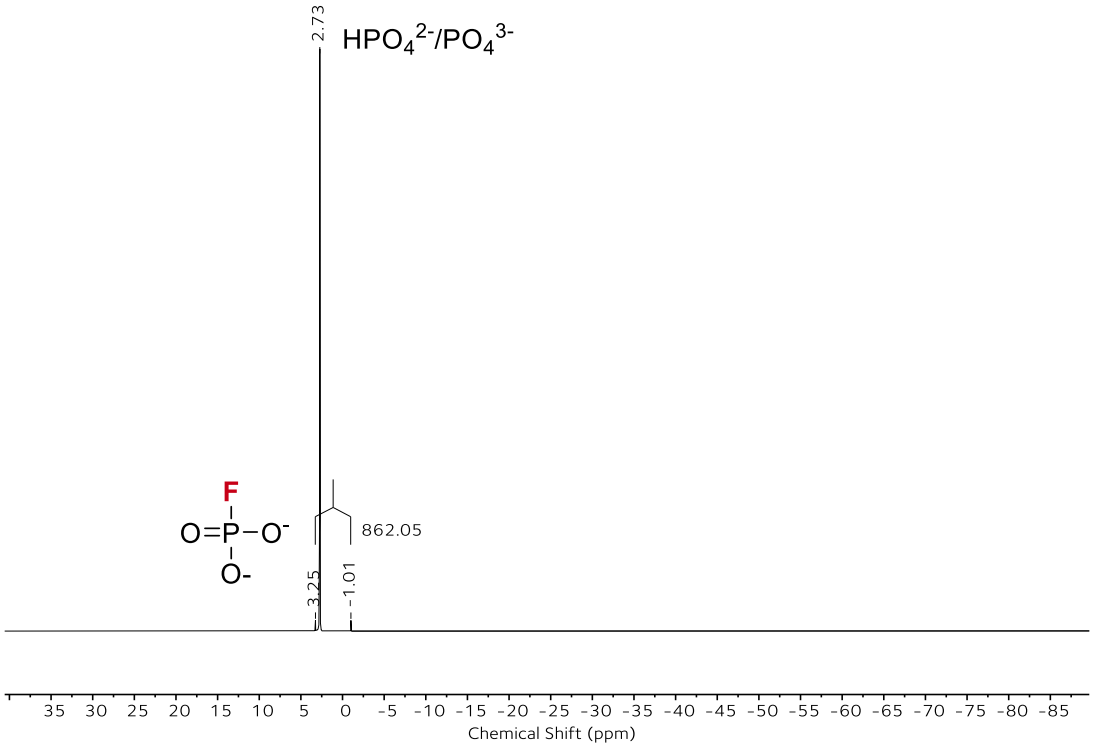

Figure 2.20. ^{31}P NMR (D_2O) spectra of **Fmix** (PO_3F^{2-}, d, δ =1.10 ppm, J = 862 Hz, HPO_4^{2-}/PO_4^{3-}, s, δ =2.73 ppm).

Measurements were repeated in triplicate from three different batches of each powder and the relaxation time constant (T_1) was determined by an inversion recovery experiment to ensure all NMR signals could be accurately quantified (full experimental details and NMR

parameters can be found in Chapter **4**). As shown in Figure 2.21 , the concentration of both F^- and PO_3F^{2-} increases over the course of the ball milling process, however, the concentration of the PO_3F^{2-} is consistently an order of magnitude lower than fluoride.

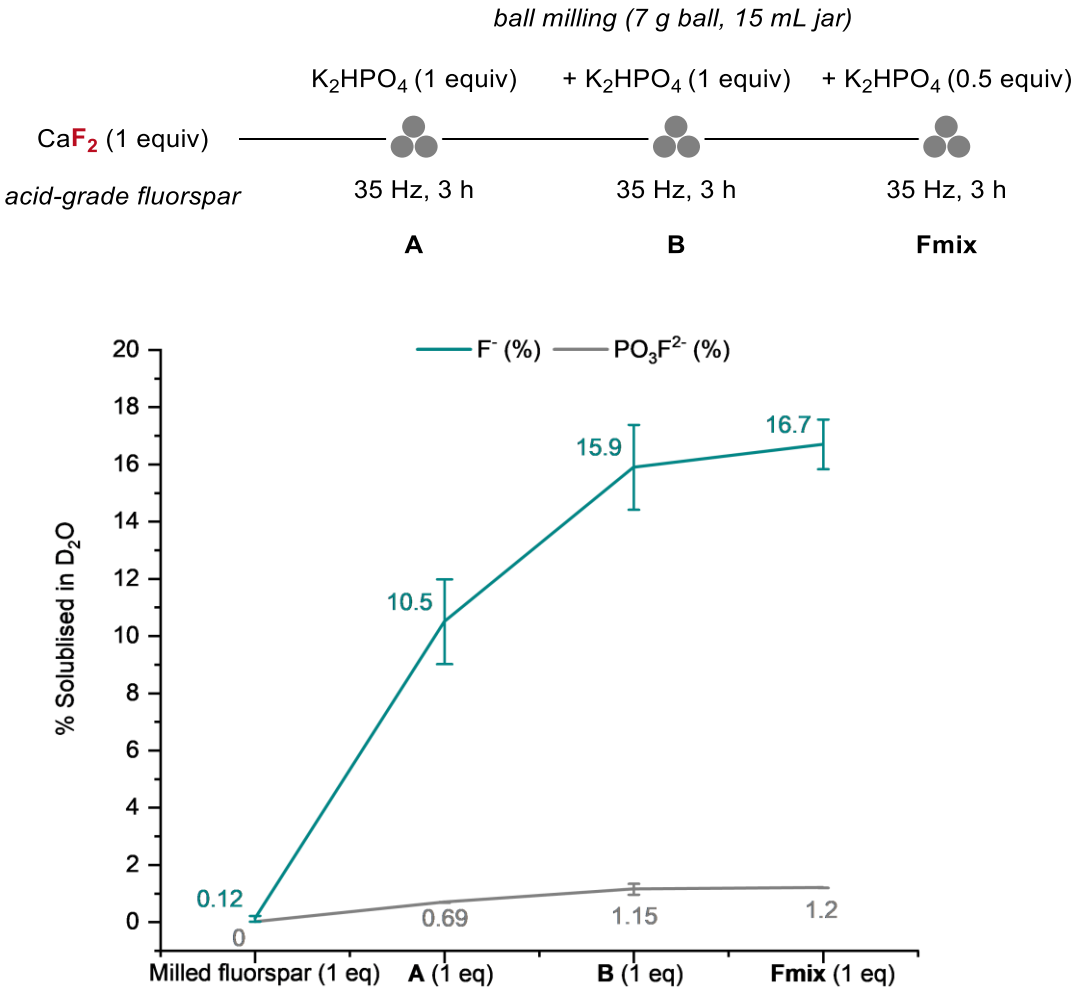

Figure 2.21. Investigation of the amount of water-soluble fluoride generated at each milling stage between AGF and K_2HPO_4. The legend denotes the quantity of F^- and PO_3F^{2-} measured as a mean percentage of the maximum amount of fluoride released from 0.25 mmol CaF_2 (quantified by ^{19}F NMR spectroscopy using NaOTf as internal standard). Reported quantities of F^- and PO_3F^{2-} are the average of 3 runs, with error bars representing the standard error.

Evaluation of the water-soluble fluoride content (% F^-) and reactivity of each powder demonstrates that while reactivity increases from powder **A** to **Fmix**, the level of water soluble fluoride is consistently lower than the TsF (**1**) yield and reaches a maximum of

approximately 17% (calculated from the theoretical amount of fluoride available from 0.25 mmol of CaF_2). The discrepancy may arise due to the differences in solvents used in each case as the amount of soluble fluoride in D_2O does not correlate with the amount of "reactive" fluoride available for fluorination in *tert*-BuOH.

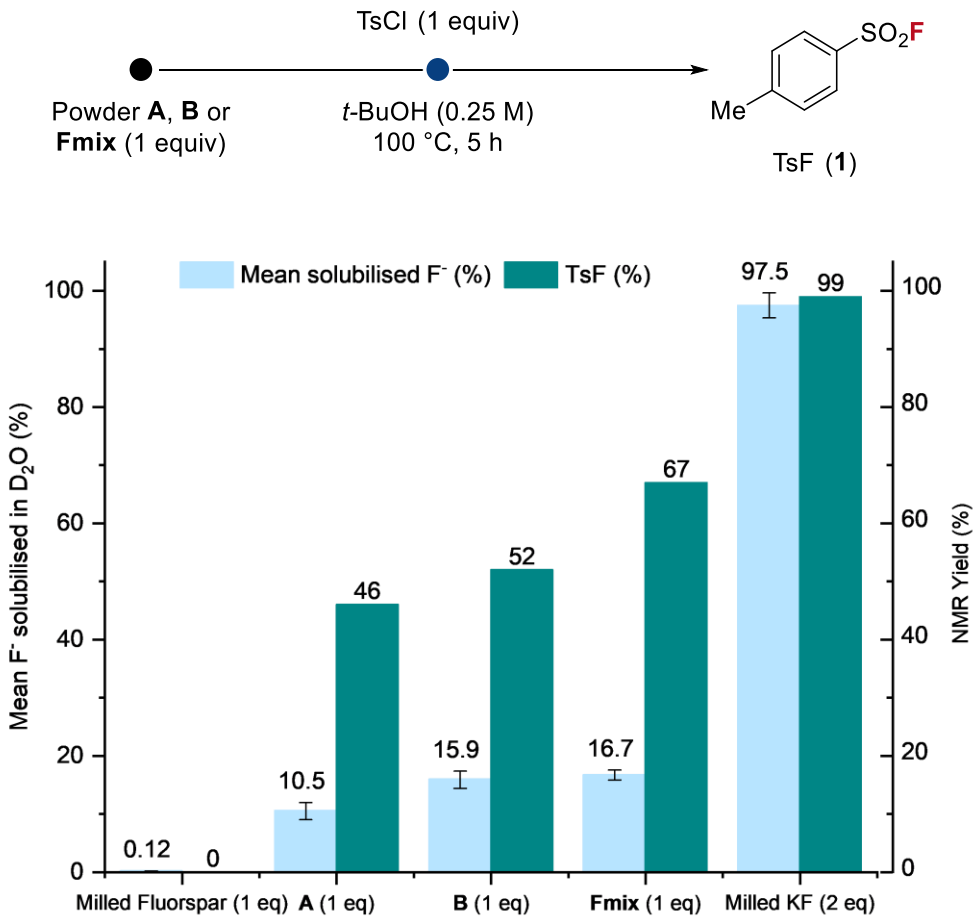

Figure 2.22. Comparison between the mean percentage of water-soluble fluoride (D_2O) and fluorinating ability of milled fluorspar (3 h, 35 Hz), powders **A**, **B** and **Fmix** and milled KF (3 h, 35 Hz). Fluorination reactions were conducted on 0.125 mmol scale and yields of TsF (**1**) were quantified by ^{19}F NMR spectroscopy using FA as internal standard.

Interestingly, stirring a sample of **Fmix** in *tert*-BuOH-d_{10} at 25 °C and analysing the supernatant by ^{19}F NMR spectroscopy (30 to 60 °C using variable temperature experiments) showed no trace of fluoride in solution, indicating that fluorination in

tert-BuOH may be operating under heterogenous conditions. A singlet corresponding to fluoride (δ_F = -111 ppm) was observed when KF was dissolved in *tert*-BuOH-d_{10}. Alternatively, dissolution of **Fmix** in D_2O may lead to the formation (or reformation) of an insoluble fluoride salt such as CaF_2 or with lower solubility than CaF_2, such as fluorapatite [$Ca_5(PO_4)_3F$]. Further details delineating the stability of **Fmix** in water can be found in Section 2.4.10.

2.4.2 Monofluorophosphate Investigation

Initial mechanistic investigations focused on elucidating the monofluorophosphate species (PO_3F^{2-}) observed in **Fmix** by ^{19}F and ^{31}P NMR spectroscopy (D_2O). Inorganic monofluorophosphates, first introduced by Lange in 1929, are well known for their application in toothpastes and insecticides.[102] In contrast, organic monofluorophosphates can be highly toxic and have been used as chemical warfare agents. The monofluorophosphate species in **Fmix** was tentatively assigned to either calcium monofluorophosphate ($CaPO_3F$), which commonly exists as a dihydrate ($CaPO_3F{\cdot}2H_2O$), or potassium monofluorophosphate (K_2PO_3F). The reaction between commercially available sodium monofluorophosphate (Na_2PO_3F) and calcium chloride ($CaCl_2$) in water resulted in the precipitation of $CaPO_3F{\cdot}2H_2O$ (Scheme 2.8). Alternatively, ball milling equimolar quantities of KF and potassium metaphosphate (KPO_3) resulted in complete conversion to K_2PO_3F. Whilst K_2PO_3F is highly soluble in water, $CaPO_3F{\cdot}2H_2O$ is only sparingly soluble in water [4.17 mg/mL (H_2O, 27 °C)].[103] The samples of $CaPO_3F{\cdot}2H_2O$ and K_2PO_3F were characterised by PXRD (Figure 2.23) (see Chapter **4** for experimental details).

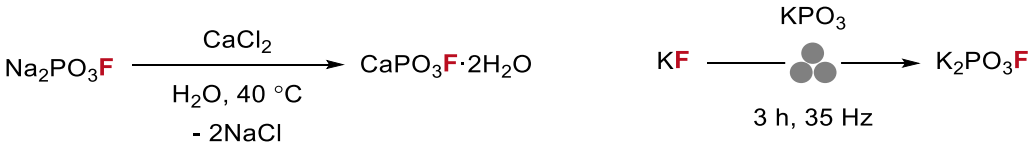

Scheme 2.8. Synthesis of $CaPO_3F{\cdot}H_2O$ and mechanochemical synthesis of K_2PO_3F.

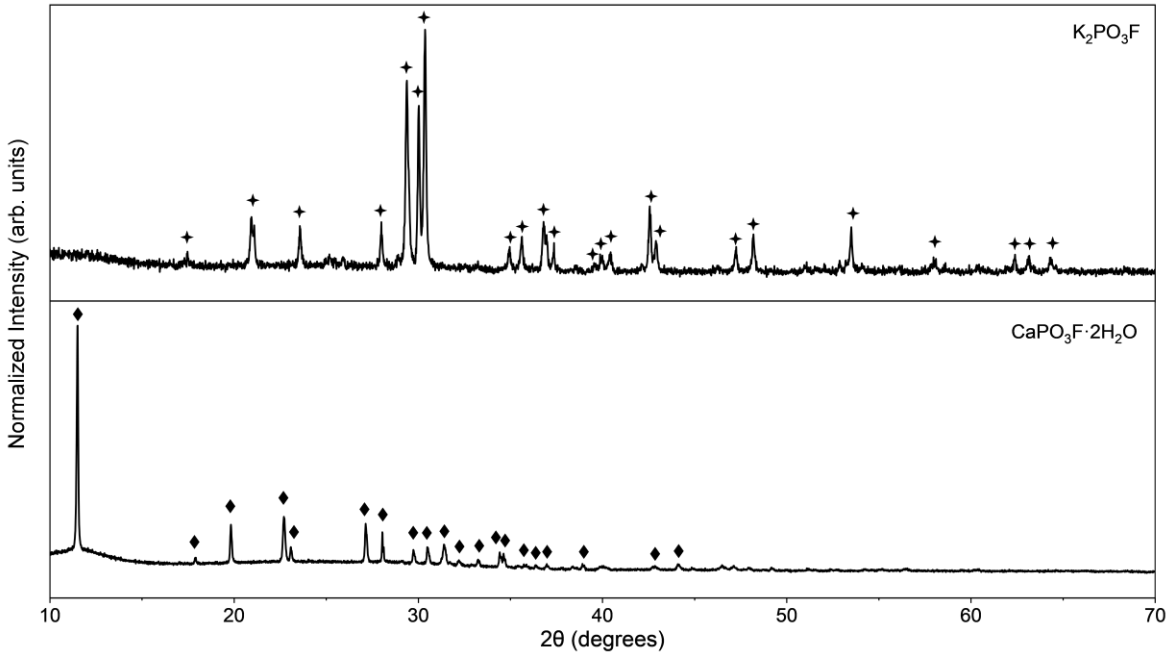

Figure 2.23. PXRD data of prepared $CaPO_3F{\cdot}H_2O$ and K_2PO_3F. Peaks are labelled according to the ICDD database [♦ = $CaPO_3F{\cdot}H_2O$ (00-029-0323), ✦ = K_2PO_3F (00-050-0379)].[104]

A systematic study on the fluorinating ability of the $CaPO_3F{\cdot}2H_2O$ and K_2PO_3F was conducted using TsCl as a model substrate (Figure 2.24). Fluorination was not observed when $CaPO_3F{\cdot}2H_2O$ (4 equiv) was used as a fluorinating reagent, however, TsF (**1**) formed in 32% yield (as measured by ^{19}F NMR spectroscopy) using K_2PO_3F (4 equiv). The addition of K_2HPO_4 (4 equiv) to the solution-phase fluorination led to a TsF (**1**) yield of 54%. Cummins and co-workers recently investigated the cleavage of monofluorophosphate P-F bonds under mechanochemical conditions (30 Hz).[101] Their findings revealed that milling sodium monofluorophosphate (Na_2PO_3F) on its own leads to the production of sodium fluoride and fluoropyrophosphate ($Na_3P_2O_6F$). Pre-milling K_2PO_3F with KH_2PO_4 and using the subsequent

powder as a fluorinating reagent enabled with the formation of TsF (**1**) in 61% yield. A substantial increase in fluorination yield was observed when using a pre-milled mixture of K_2PO_3F and K_2HPO_4 (3 h, 35 Hz) in an equimolar ratio (98% TsF **1**). Analysis of the ball milled mixture of K_2PO_3F and K_2HPO_4 by ^{19}F NMR spectroscopy in D_2O revealed the presence of PO_3F^{2-} and F^- in a 6:1 ratio (Figure 2.25). A ball milled mixture of K_2PO_3F and anhydrous $CaHPO_4$ was also found to be an effective fluorinating reagent (80% TsF **1**). A sample of this mixture was analysed by ^{19}F NMR spectroscopy in D_2O and revealed the presence of water soluble PO_3F^{2-} and fluoride in approximately a 2:1 ratio.

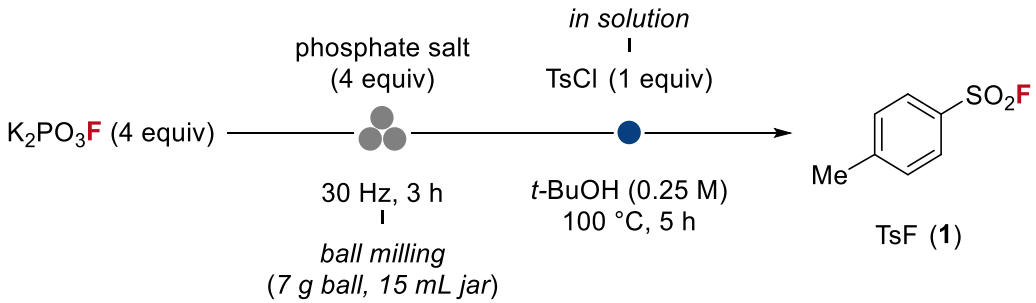

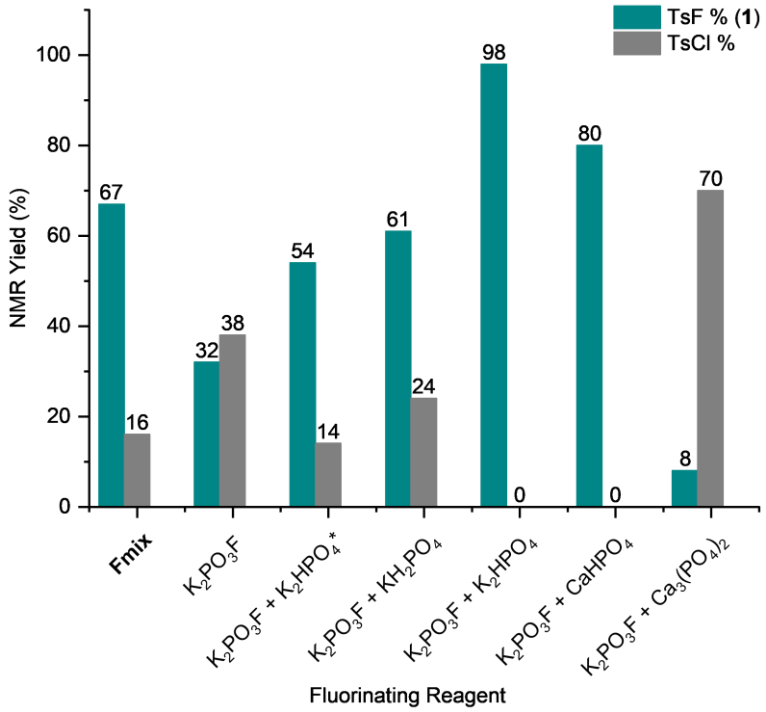

Figure 2.24. Fluorinating ability (0.125 mmol scale) of K_2PO_3F and mixtures of K_2PO_3F ball milled with phosphate salts. *K_2HPO_4 added to K_2PO_3F in solution instead of ball milling.

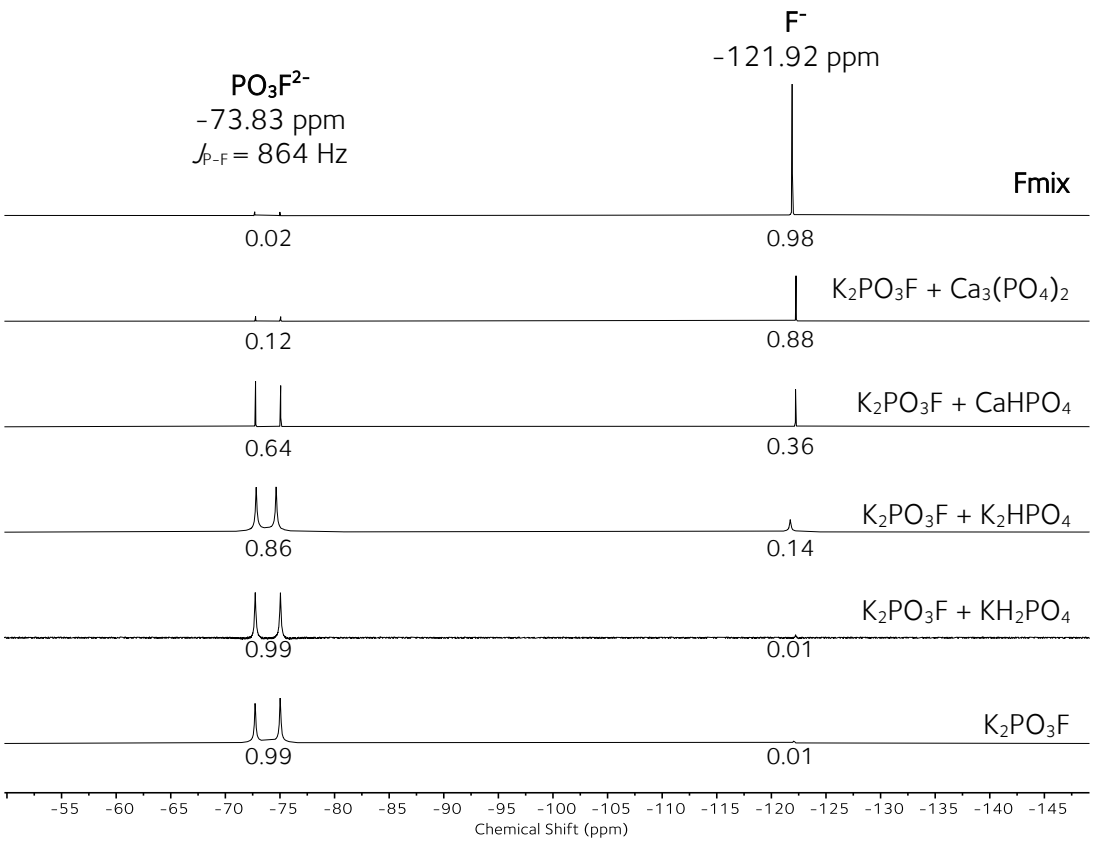

Figure 2.25. ^{19}F NMR (D_2O) spectra of **Fmix**, K_2PO_3F and K_2PO_3F ball milled with phosphate salts in an equimolar ratio. Monofluorophosphate (PO_3F^{2-},d ,δ = -73.83 ppm, J = 864.6 Hz) to fluoride (F^-,s , δ = -121.92 ppm) ratios are provided as nuclei integrals.

The ^{31}P NMR spectrum (D_2O) of the ball milled mixture of K_2PO_3F and $CaHPO_4$ displayed a signal characteristic of pyrophosphate ($P_2O_7^{4-}$, singlet, δ_P = -8.63 ppm), which was not observed in **Fmix** (Figure 2.26).[101] Tripolyphosphate ($P_3O_{10}^{5-}$) was observed in the ^{31}P NMR spectrum (D_2O) of the ball milled K_2PO_3F and $Ca_3(PO_4)_2$ mixture [doublet, δ_P = -5.37 ppm, $^2J_{P-P}$ = 18.2 Hz (terminal phosphates) and triplet, δ_P = -18.88 ppm, $^2J_{P-P}$ = 18.2 (bridging phosphate)]. Although these results demonstrate that K_2PO_3F can act as a competent fluorinating reagent, possibly serving as a pro-nucleophile, the X-ray diffractogram of K_2PO_3F argued against the presence of this salt in **Fmix** (Figure 2.27).

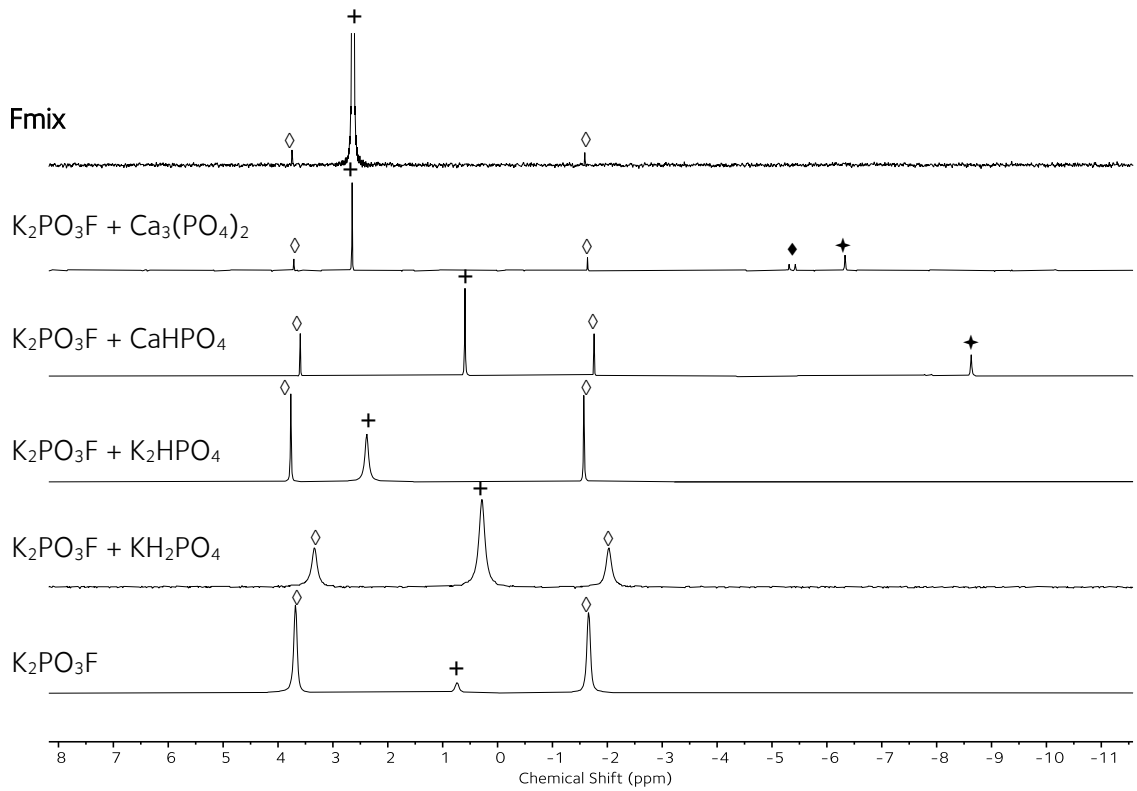

Figure 2.26. ^{31}P NMR (D_2O) spectra of **Fmix**, K_2PO_3F and K_2PO_3F ball-milled with phosphate salts in an equimolar ratio. [◊ = PO_3F^{2-} (doublet, δ =1.10 ppm, J = 864.6 Hz), + = $H_2PO_4^-$ /HPO_4^{2-}/PO_4^{3-} (s, δ =2.38 ppm), ✦ = $P_2O_4^{4-}$ (s, δ =-8.63 ppm), ♦ = $P_3O_{10}^{5-}$ (doublet, δ =-5.37 ppm, J = 18.2 Hz and weak triplet, δ =-18.88 ppm, J = 18.2 Hz)].

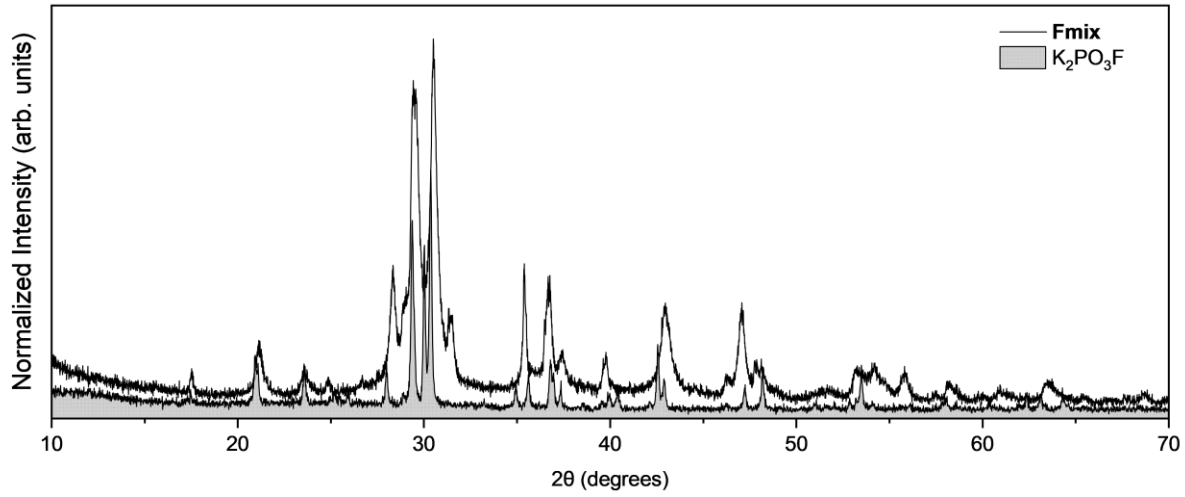

Figure 2.27. Comparison between PXRD data of **Fmix** and K_2PO_3F.

2.4.3 Insights from Powder X-ray Diffraction

The improvement in reactivity observed by sequentially ball milling AGF (>97% CaF_2) with anhydrous K_2HPO_4 correlates with the evolution of crystalline structures formed during the mechanochemical process. Figure 2.28 shows the time evolution of PXRD patterns of AGF (1 equiv) ball milled with K_2HPO_4 (1 equiv) from 0 to 9 h at 35 Hz. The time evolution of the PXRD patterns shows the clear appearance of new crystalline phases, indicating that under mechanochemical conditions K_2HPO_4 reacts with CaF_2 within just 1 h of ball milling. Peaks (reflections) corresponding to crystalline CaF_2 are observed over the entire milling period with peak broadening, indicative of amorphization and a reduction in CaF_2 particle size. Peaks corresponding to K_2HPO_4 and $K_2HPO_4{\cdot}3H_2O$ steadily decrease in intensity and are not observed after 1.5 h of milling. Multiple reflection peaks appear at 2θ = 21.1, 29.6, 30.5, 31.5, 35.3, 36.7 and 42.9 ° after 1.5 h of milling, which broaden upon further ball milling. The intensity of the peaks corresponding to CaF_2 does not significantly decrease after 3 h. The reactivity of the powders prepared at each time point was previously examined in the fluorination of TsCl under optimised reaction conditions. No significant improvements in the fluorination yield were observed using the powders milled for a total reaction time >3 h as fluorinating reagents (refer to Table 2.12).

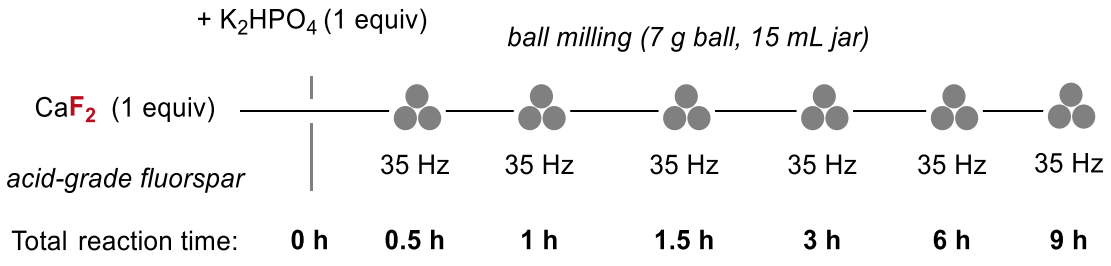

Scheme 2.9. Ball milling AGF with an equimolar amount of K_2HPO_4 over a period of 9 h (35 Hz).

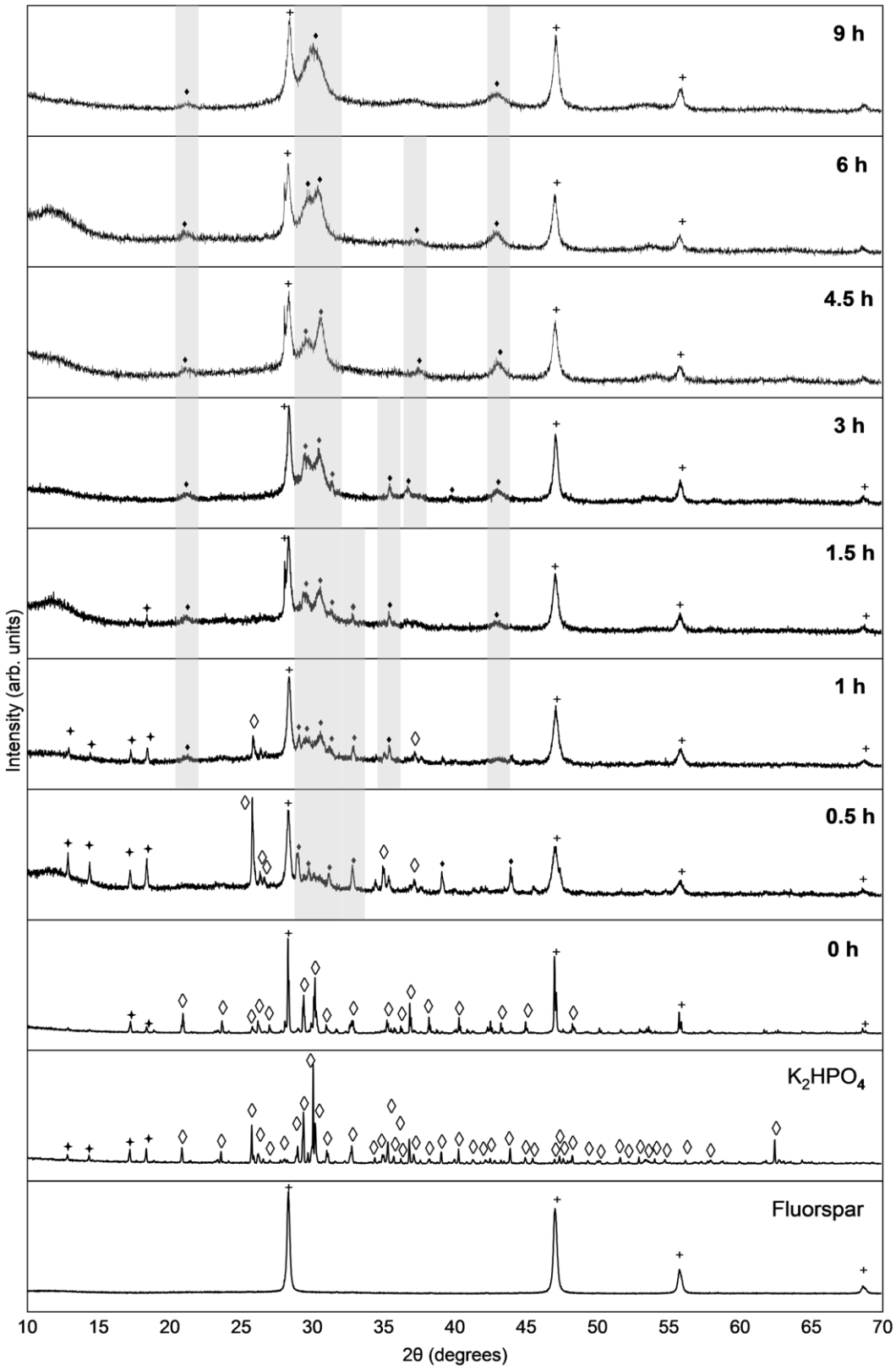

Figure 2.28. The time evolution of the X-ray powder diffraction patterns of acid grade fluorspar milled with K_2HPO_4 from 0 to 9 h (35 Hz). [+ = CaF_2, ◊ = anhydrous K_2HPO_4, ✦ = $K_2HPO_4 \cdot 3H_2O$, ♦ = new crystalline phase (shaded)].

These findings indicate that the availability of fluoride for fluorination is restricted by the consumption of crystalline CaF_2 during the solid-state ball milling process. As prolonged ball milling did not increase the consumption of CaF_2, additional equivalents of anhydrous K_2HPO_4 were milled with AGF in a portion-wise manner at 35 Hz [powders **A** to **C** (**Fmix**)]. Monitoring the solid-state reaction by PXRD (*ex situ*) revealed that as the amount of K_2HPO_4 added to the reaction increased, the intensity of peaks corresponding to crystalline CaF_2 [diagnostic reflections at 2θ = 28.3, 47.0, 55.8 and 68.7° corresponding to the (111), (220), (311) and (400) planes] diminished with concomitant formation of new crystalline phases. Peaks corresponding to the new species displayed the greatest intensity in **Fmix** (prepared by adding a total of 2.5 equivalents of K_2HPO_4 in three portions to 1 equivalent of AGF over a total milling time of 9 h).

In considering the structures of these new inorganic species, an ion exchange between CaF_2 and K_2HPO_4 was considered. In this scenario, potassium fluoride (KF) and calcium hydrogen phosphate ($CaHPO_4$) were hypothesised to form. Comparing measured diffraction peaks to a database of known patterns allows for the identification of phase(s) within the sample. Neither the anhydrous form or dihydrate of KF was observed in the diffractogram of **Fmix** (Figure 2.30).

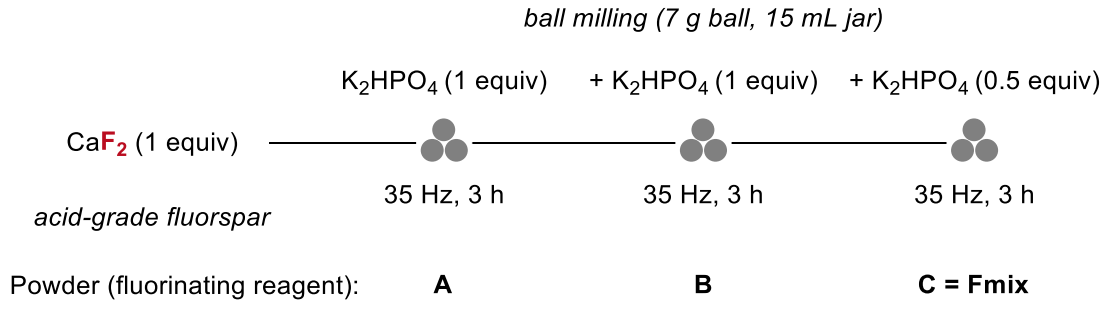

Scheme 2.10. Ball milling acid-grade fluorspar portion-wise addition of K_2HPO_4 (2.5 equiv in total) over a period of 9 h (35 Hz).

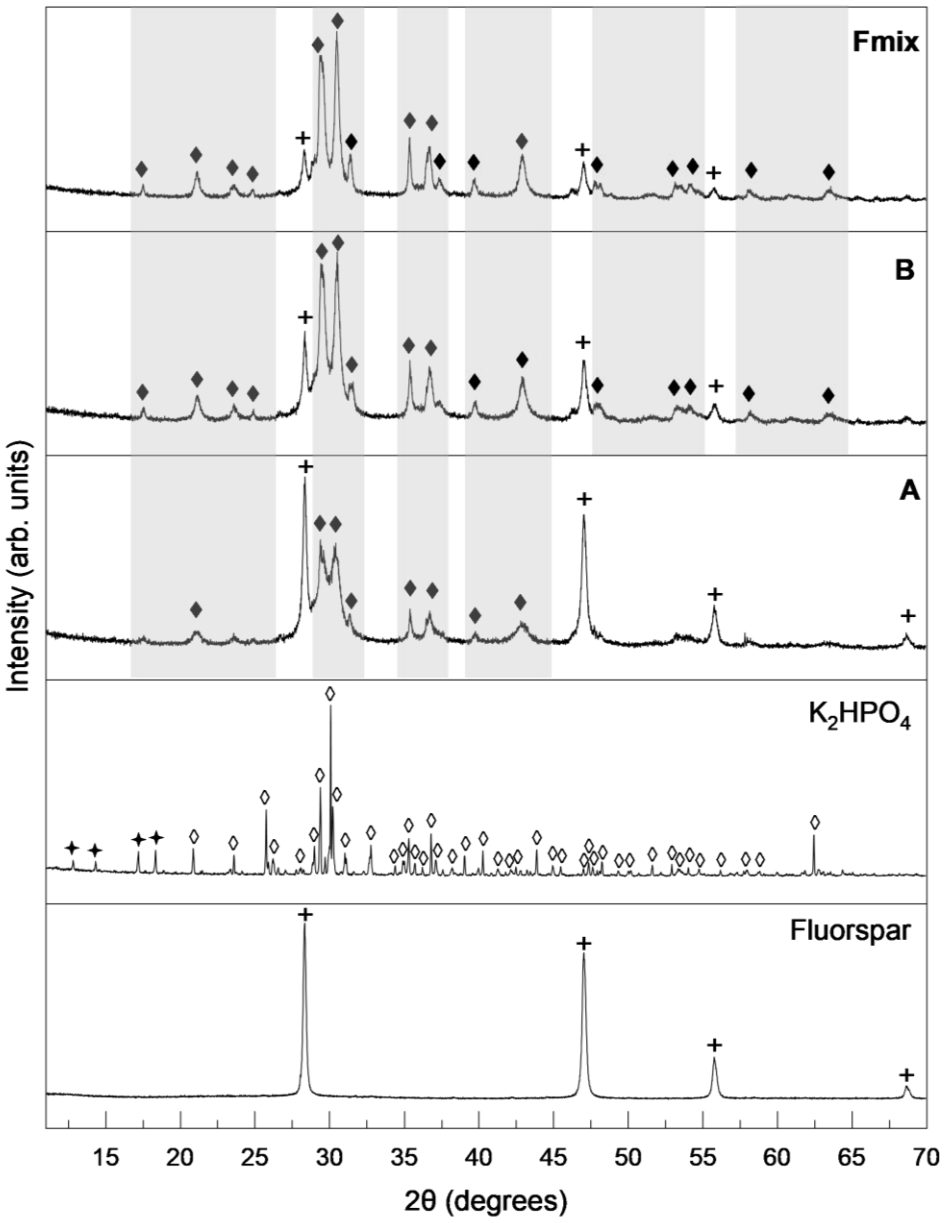

Figure 2.29. The evolution of the power X-ray diffraction patterns of acid grade fluorspar milled with K_2HPO_4 added in portions at 3 h intervals (total ball milling time of 9 h) at 35 Hz [+ = CaF_2, ◊ = anhydrous K_2HPO_4, ✦ = $K_2HPO_4 \cdot 3H_2O$, ♦ = new crystalline phase (shaded)].

There are three crystalline forms of $CaHPO_4$ known; monohydrate ($CaHPO_4 \cdot H_2O$), dihydrate ($CaHPO_4 \cdot 2H_2O$) and anhydrous. Amorphous calcium hydrogen phosphates, which lack long-range, periodic atomic-scale order, have also been reported.[105] No crystalline

forms of $CaHPO_4$ were observed in the diffractogram of **Fmix**. Additionally, no fluorapatite [$Ca_5(PO_4)_3F$] or hydroxyapatite [$Ca_5(PO_4)_3OH$] was detected by PXRD (Figure 2.30).

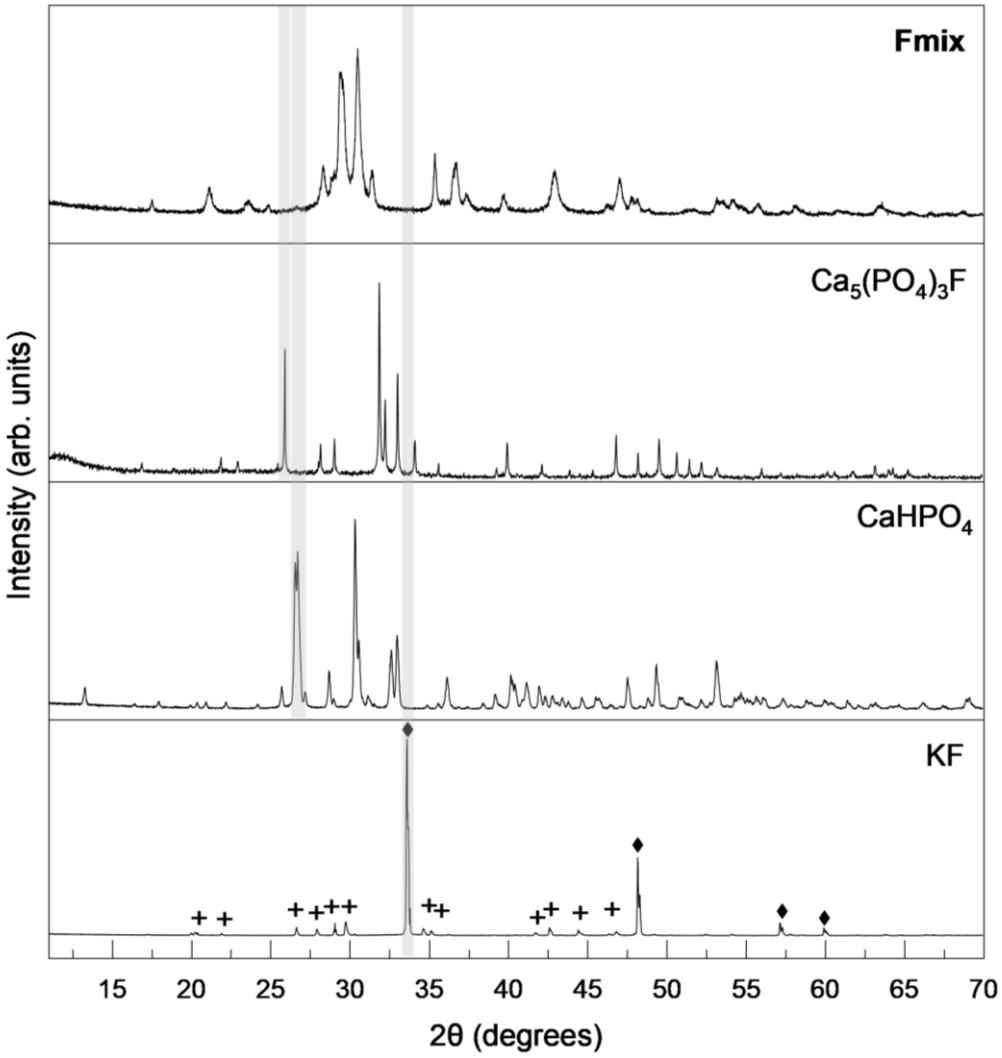

Figure 2.30. Powder X-ray diffraction pattern of **Fmix** (top trace) and commercial fluorapatite [$Ca_5(PO_4)_3F$], anhydrous calcium hydrogen phosphate ($CaHPO_4$) and potassium fluoride (KF) [♦ = anhydrous KF and + = KF dihydrate]. Reflections (shaded) diagnostic of anhydrous KF (33.6 °), anhydrous $CaHPO_4$ (26.7 °) and $Ca_5(PO_4)_3F$ (25.9 °) not observed in the diffraction pattern of **Fmix**.

2.4.4 Discovery of X [$K_3(HPO_4)F$]

It is plausible that one equivalent of CaF_2 could react with one equivalent of K_2HPO_4 to afford two equivalents of KF and one equivalent of $CaHPO_4$ (Scheme 2.11), without consideration of H_2O and the possibility of hydrated salts or hydroxides. The finding that more than one equivalent of K_2HPO_4 was required to maximise the consumption of CaF_2 under mechanochemical conditions, suggested that K_2HPO_4 was reacting with a species other than CaF_2. Alternatively, the reaction may be operating under a reversible equilibrium (see Section 2.4.11). For example, any KF formed could be reacting with CaF_2. To determine the feasibility of these reaction pathways, mechanistic experiments were conducted systematically. Ball milling CaF_2 (1 equiv) with anhydrous KF (1 equiv) led to the formation of perovskite potassium calcium trifluoride ($KCaF_3$) [diagnostic reflections at (2θ = 28.4°, 41.5°, 47.1°, 51.0 and 55.8) (Figure 2.31). A sample of $KCaF_3$ was independently prepared by a high-temperature solid-state reaction between KF and CaF_2 at 520 °C (1 h).

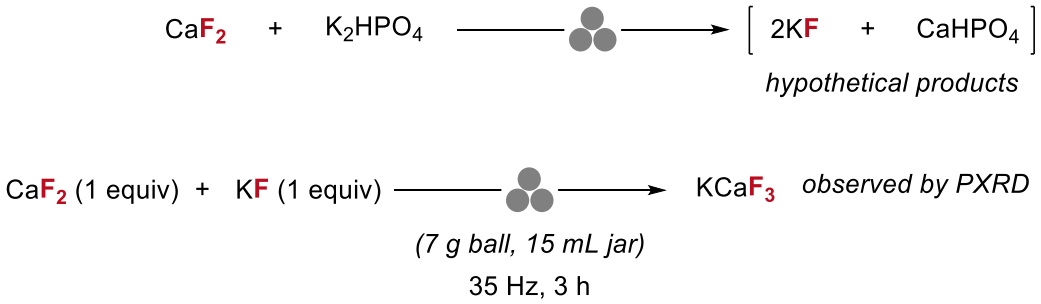

Scheme 2.11. Hypothesised mechanochemical ion exchange between CaF_2 with K_2HPO_4 and observed formation of $KCaF_3$ through ball milling CaF_2 with KF.

The perovskite crystal structure is defined as any ABX_3 compound with a network of corner-sharing BX_6 octahedra surrounding a larger A-site cation (e.g. K^+), where X is typically a halogen or chalcogen.[106] Although the crystal structure and thermal properties of $KCaF_3$

have been examined, its fluorination ability has not been widely studied.[107] Importantly, the fingerprint PXRD pattern of $KCaF_3$ did not match with any of the peaks observed in the diffractogram of **Fmix** (Figure 2.32).

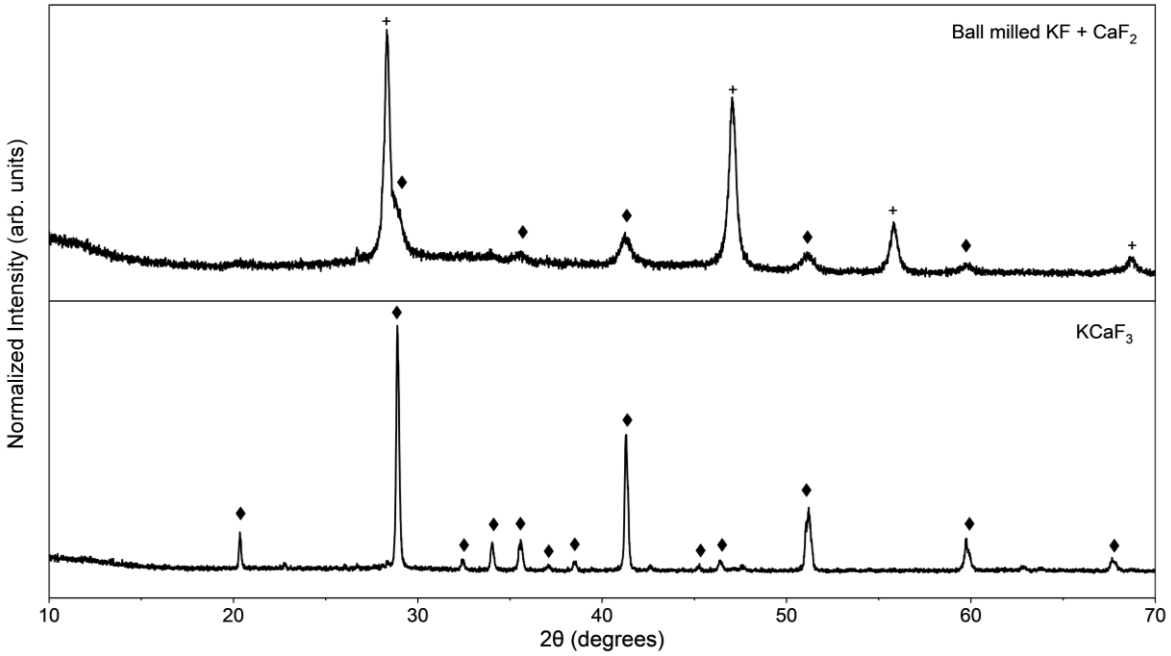

Figure 2.31. PXRD data of ball milled equimolar amount of KF and CaF_2 (3 h, 35 Hz) and $KCaF_3$. [♦ = $KCaF_3$, + = CaF_2]. $KCaF_3$ matches reported pattern (ICDD 01-080-4365).[107]

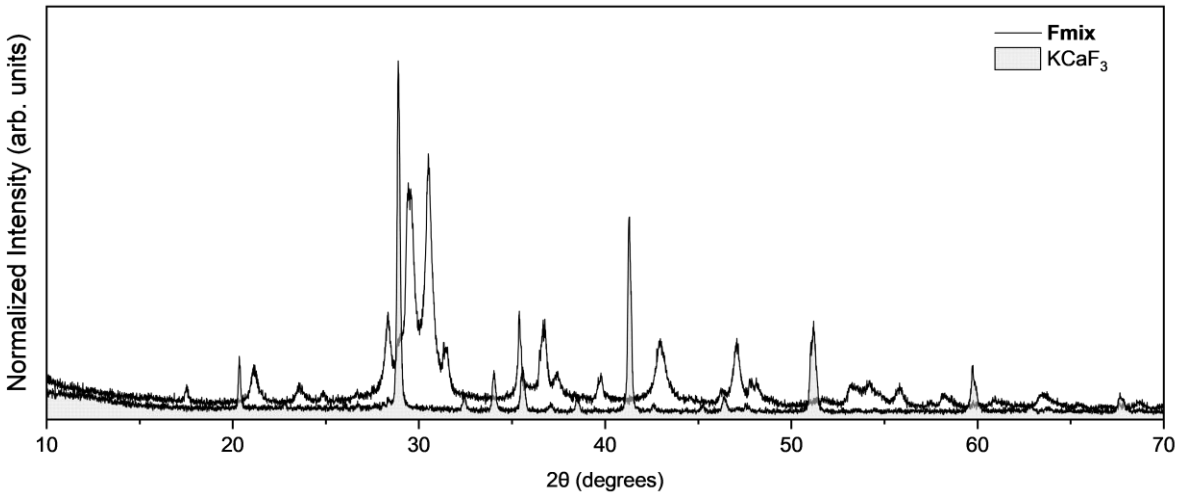

Figure 2.32. Comparison between PXRD data of **Fmix** and $KCaF_3$.

In a next set of mechanistic experiments, K_2HPO_4 was ball milled with KF (Scheme 2.12). A new crystalline phase (**X**) was formed upon ball milling an equimolar quantity of anhydrous K_2HPO_4 and KF.

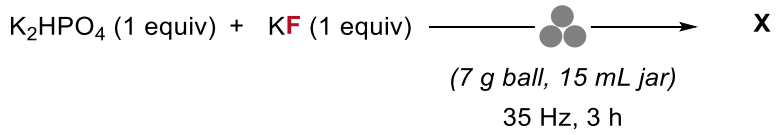

Scheme 2.12. Mechanochemical synthesis of **X** via ball milling K_2HPO_4 and KF.

Figure 2.33 shows the diffractogram of **X**. Neither K_2HPO_4 or KF (anhydrous or hydrate salts) are observed in the diffractogram of **X**. Although the crystal structure of **X** was unknown at this stage, the diffractogram contained reflections with positions and intensities consistent to those observed in the diffractogram of **Fmix**.

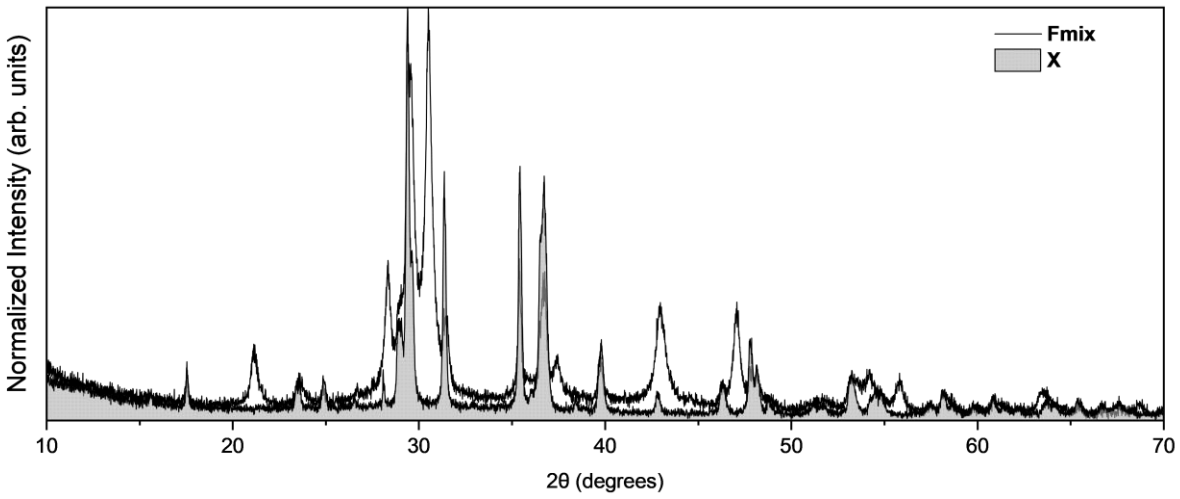

Figure 2.33. Comparison between PXRD data of **Fmix** and **X**.

Using experimental powder X-ray diffraction data of **X** and tripotassium fluoride fluorophosphate [$K_3(PO_3F)F$] as a starting model, replacing the PO_3F^{2-} units with HPO_4^{2-} the structure of **X** was deduced as tripotassium hydrogen phosphate fluoride [$K_3(HPO_4)F$].[108]

These models were refined against the experimental data to achieve a good fit. $K_3(HPO_4)F$ crystallises in a monoclinic lattice [*a* = 7.1684(8) Å, *b* = 7.1989(8) Å, *c* = 11.438(1) Å, β = 90.586(3) °] and is isostructural to $K_3(PO_3F)F$, which is reported to crystallise in a tetragonal lattice.[108,109] The Rietveld refinement analysis of **X** was conducted by Prof. Michael Hayward (University of Oxford) (Figure 2.34). Refined structural parameters of **X** including unit-cell parameters, space group, atom positions and isotropic thermal parameters (B_{iso}) of all the atoms are tabulated in Chapter **4**.

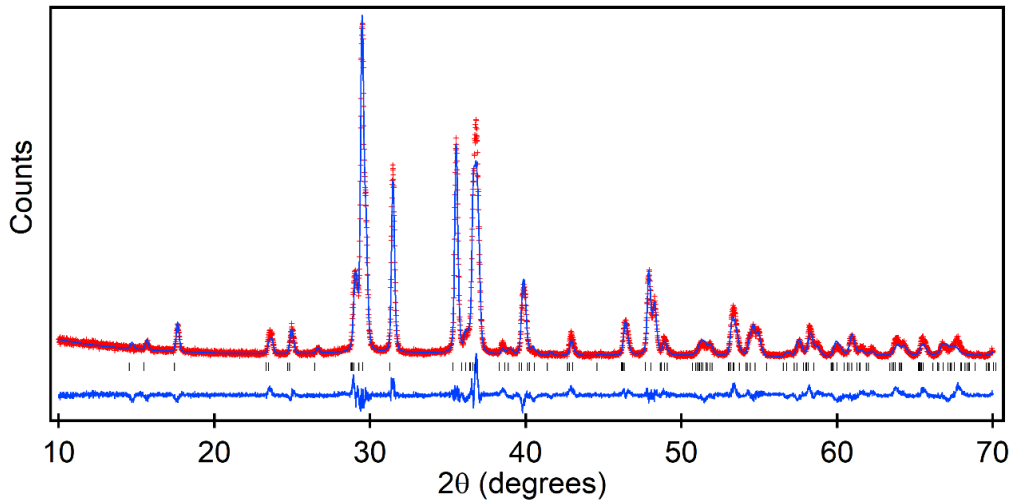

Figure 2.34. Observed (red), calculated (blue) and difference plots from the structural refinement of phase **X** against X-ray powder diffraction data collected at room temperature.

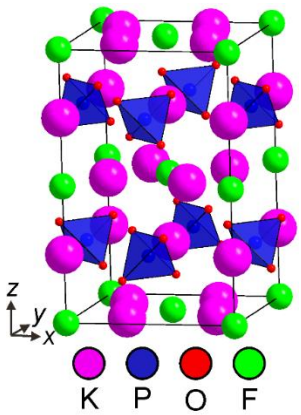

Figure 2.35. Proposed structure of phase **X** [$K_3(HPO_4)F$].

Phase **X** is solely crystalline $K_3(HPO_4)F$. A sample of **X** was dissolved in D_2O and analysed by NMR spectroscopy. In agreement with the spectroscopic data for **Fmix** in D_2O, the ^{19}F NMR spectrum of **X** revealed a singlet attributed to fluoride at a chemical shift of δ_F = -121.98 ppm. By ^{31}P NMR spectroscopy, a singlet corresponding to HPO_4^{2-} was also observed (δ_P = 2.71 ppm). However, in line with the structure proposed from the diffraction data of **X** [$K_3(HPO_4)F$], no signals characteristic of a PO_3F^{2-} species were found, implying that a different species alongside **X** existed in **Fmix**.

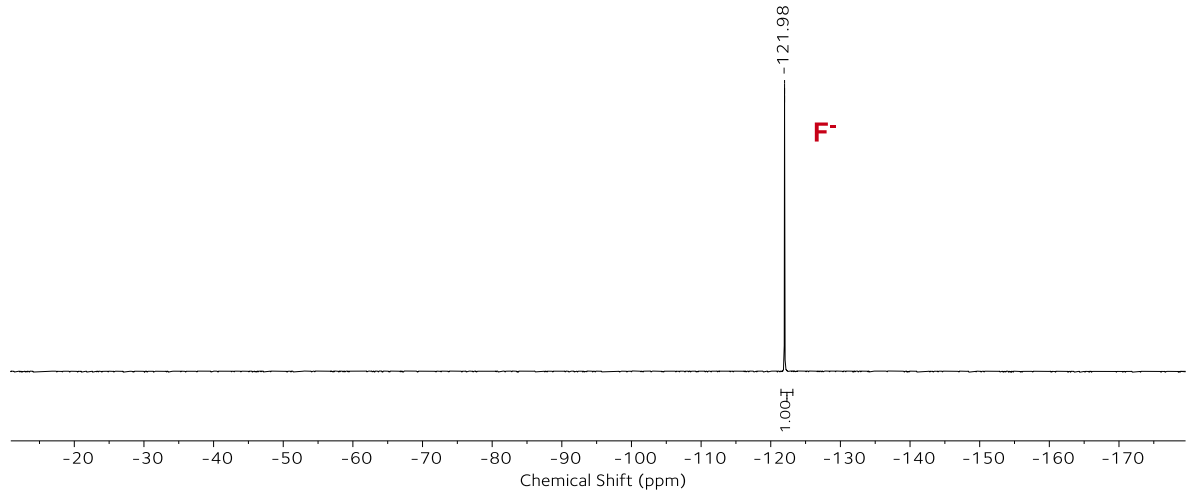

Figure 2.36. ^{19}F NMR (D_2O) spectra of **X** (F^-,s , δ = -121.92 ppm).

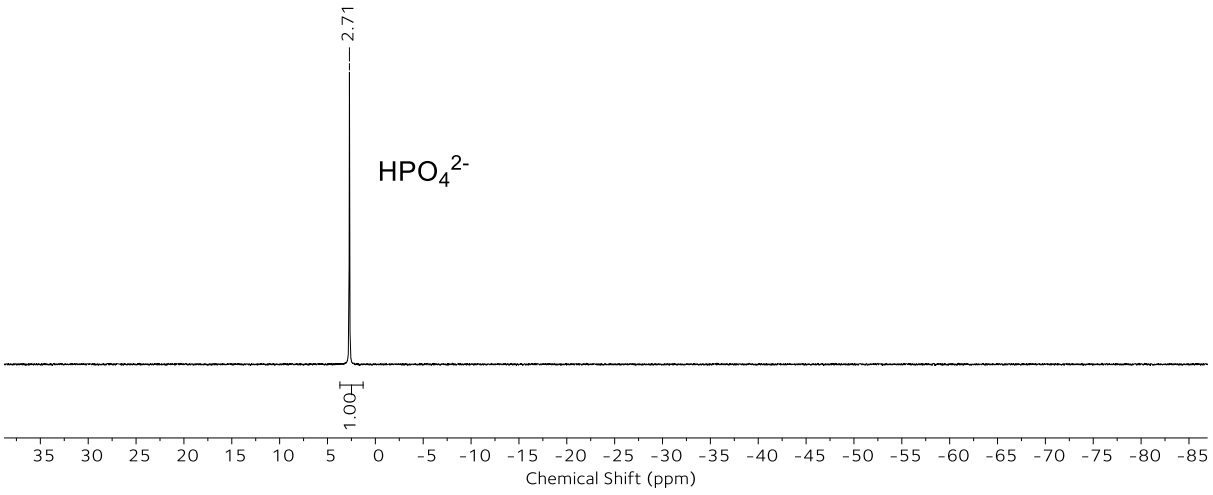

Figure 2.37. ^{31}P NMR (D_2O) spectra of **X** (HPO_4^{2-},s , δ = 2.71 ppm).

Magic-angle spinning (MAS) solid-state NMR (SS NMR) spectroscopy can probe a broad range of structural and dynamic features of diverse materials such as crystallites and amorphous materials.[110] Solid-state NMR spectroscopy was applied as a complementary technique to analyse the structure of **X** (Figure 2.38 to Figure 2.40).

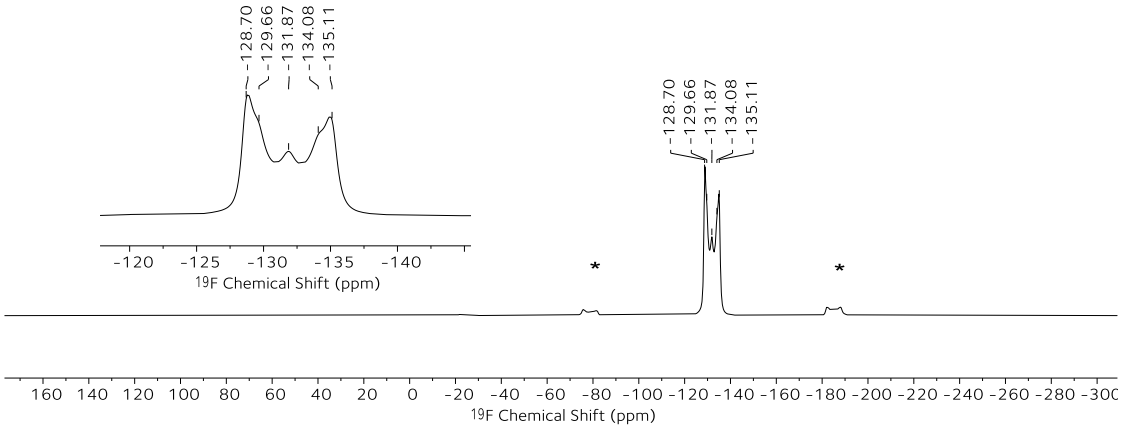

Figure 2.38. ^{19}F DPMAS solid-state NMR spectrum of **X** with zoomed region. Five fluorine environments (-128.7, -129.7, -132.0, -134.1, -135.1 ppm) with spinning sidebands (marked by *) ^{19}F DPMAS ν_{rot} = 20 kHz.

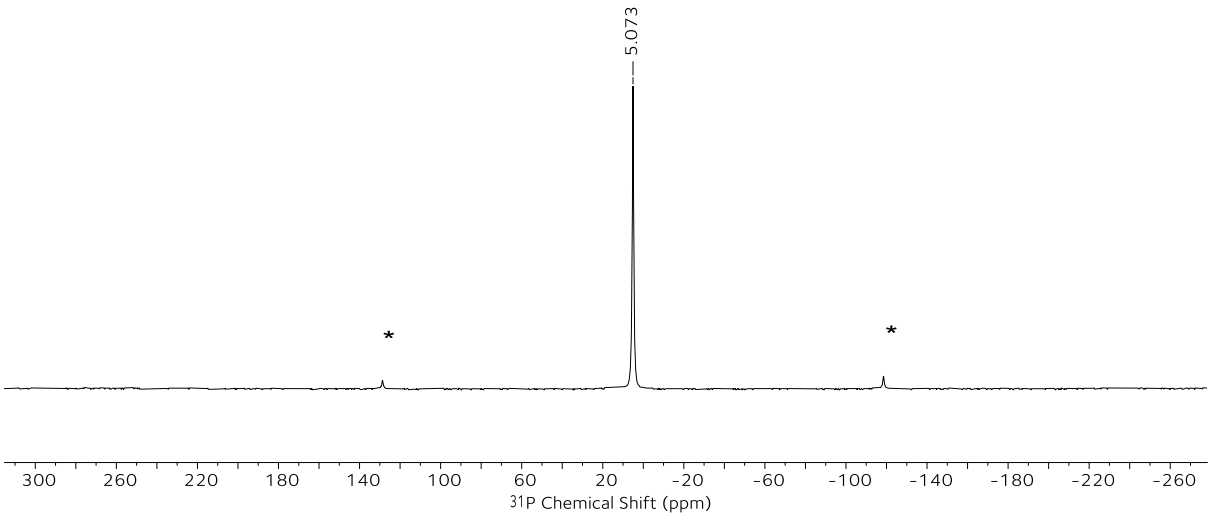

Figure 2.39. ^{31}P DPMAS solid-state NMR spectrum of **X**. Single phosphorus environment (-5.07 ppm) with spinning sidebands (marked by *) ν_{rot} = 20 kHz.

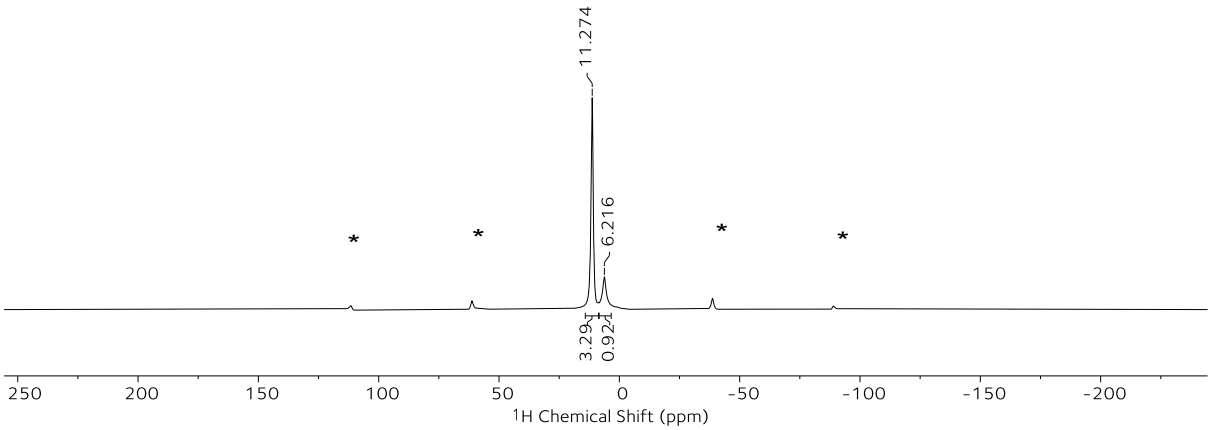

Figure 2.40. ^{1}H DPMAS solid-state NMR spectrum of **X**. Major proton environment (11.3 ppm) and H_2O (6.2 ppm) with spinning sidebands (marked by *) ν_{rot} = 20 kHz.

The ^{19}F solid-state NMR of **X** displays a complex set of signals that are assigned to five fluorine environments (δ_F = -128.7, -129.7, -132.0, -134.1, -135.1 ppm) with spinning side bands. The resonances of **X** lie within a chemical shift region that is expected for KF (δ_F = -133.3 ppm).[111] The ^{31}P solid-state NMR of **X** displays one signal, corresponding to one phosphorus environment for HPO_4^{2-} unit (δ_P = 5.07 ppm) (Figure 2.39). The ^{1}H solid-state NMR of **X** shows two signals, δ_H = 11.3 ppm ascribed to the proton of the HPO_4^{2-} unit and δ_H = 6.22 ppm which is assigned to either structural or surface adsorbed H_2O (Figure 2.40). Crystalline disordered phosphate compounds are well known for their proton conductivity; hence it is possible that the protons in **X** are dynamic.[103] For example, in metal phosphates such as $CaHPO_4 \cdot 2H_2O$, proton transfer involves not only movement of H^+ but also free rotation of the phosphate groups. If the 5 peaks are caused by the surrounding protons as hypothesised, a dynamic exchange between the fluorine resonances would be expected. Further studies into the characterisation of **X** are ongoing in our laboratories.

Compound **X** [$K_3(HPO_4)F$] was found to completely dissolve in water at room temperature. Drying an aqueous solution of **X** to completeness and remeasuring the PXRD of the corresponding solid demonstrated that **X** [$K_3(HPO_4)F$] is a water stable solid.

Furthermore, stirring an equimolar amount of KF and K_2HPO_4 in water, followed by evaporation to dryness [50 °C (13 mbar)] also results in the formation of **X**.

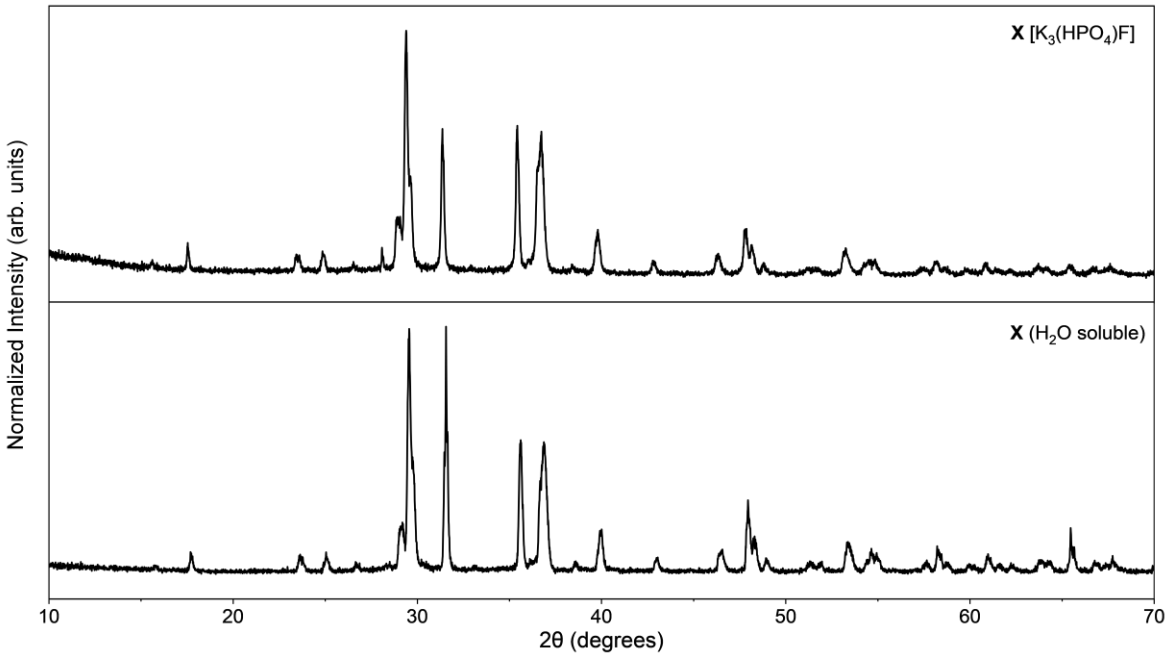

Figure 2.41. PXRD data of **X** and the solid obtained after evaporation of an aqueous solution of **X** (water soluble).

2.4.5 Discovery of Y [$K_{2-x}Ca_y(PO_3F)_a(PO_4)_b$]

The discovery of **X** [$K_3(HPO_4)F$] represented only one part of the composition of **Fmix**, which encouraged further studies to decipher the origin of the PO_3F^{2-} species observed by solution-phase NMR in D_2O (Scheme 2.13). Studies outlined in Section 2.4.2 Monofluorophosphate Investigation), indicated that K_2PO_3F and $CaPO_3F$ were unlikely candidates for the PO_3F^{2-} species in **Fmix**. The fate of the Ca^{2+} in **Fmix** was also unknown. A plausible product of the reaction between CaF_2 and K_2HPO_4 is $CaHPO_4$ (Scheme 2.13).

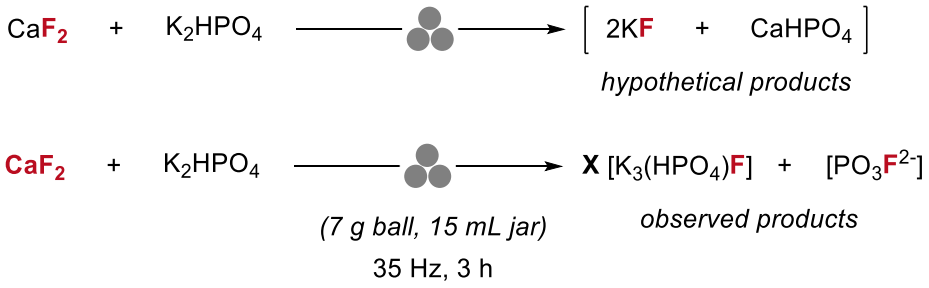

Scheme 2.13. Hypothesised mechanochemical ion exchange between CaF_2 with K_2HPO_4 and observed products (**X** and a monofluorophosphate containing species).

Whilst ball milling a mixture of CaF_2 and $CaHPO_4$ led to the formation of water insoluble solid, revealed to be a mixture of an apatite-type structure and CaF_2 by PXRD (see section 2.4.10), ball milling an equimolar quantity of **X** with anhydrous $CaHPO_4$ for 3 h at 35 Hz provided a new phase (**Y**) (Scheme 2.14). The PXRD pattern of **Y** contained broad peaks, typical of a substance with limited crystallinity and consistent with reported alkaline earth metal fluorophosphate salts, such as $CaPO_3F$, indicating that **Y** contains both crystalline and amorphous phases.[112] Superimposing the diffraction pattern of **Y** onto the diffraction pattern of **Fmix** clearly shows that the crystalline phase of **Y** is present in **Fmix** (Figure 2.42).

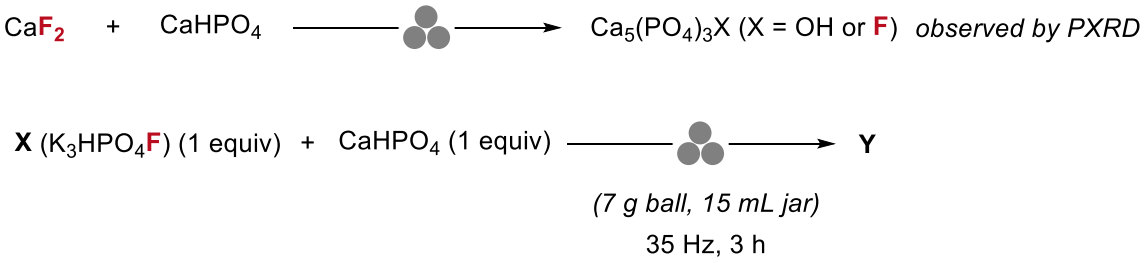

Scheme 2.14. Ball milling anhydrous $CaHPO_4$ with CaF_2 or **X** (K_3HPO_4F).

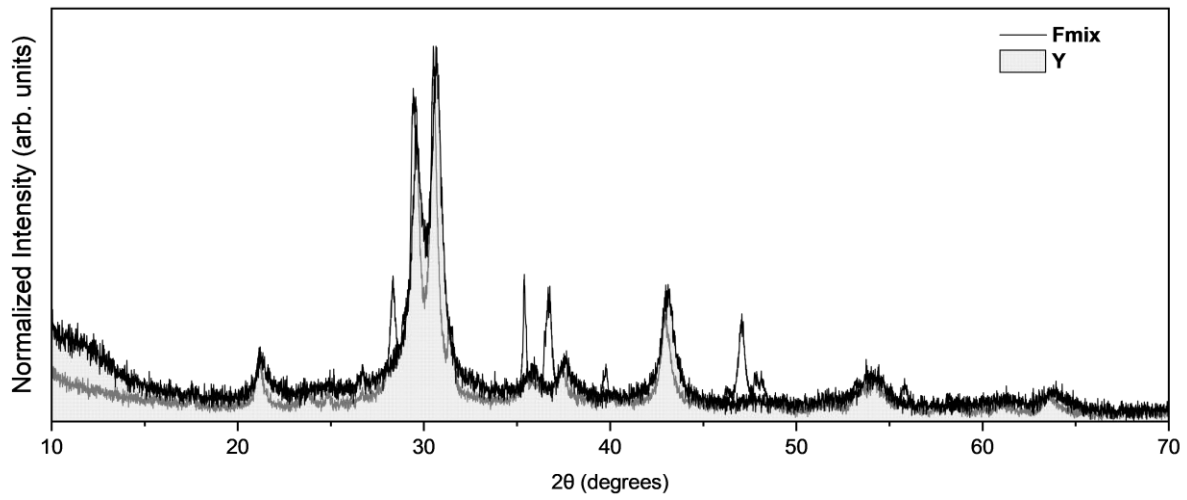

Figure 2.42. Comparison between PXRD data of **Fmix** and **Y**.

A sample of **Y** was stirred in D_2O. Centrifugation followed by ^{19}F NMR spectroscopic analysis of the supernatant showed resonance diagnostic of PO_3F^{2-} (doublet at $\delta_F = -73.91$ ppm with coupling constant $^1J_{P-F} = 865$ Hz) and a singlet at $\delta_F = -122.1$ ppm, ascribed to aqueous fluoride.

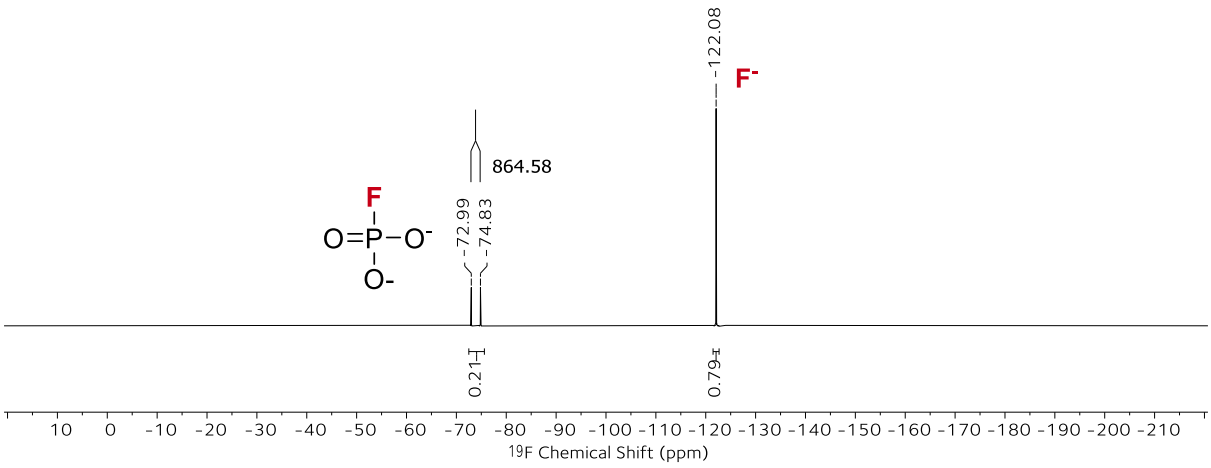

Figure 2.43. ^{19}F NMR (D_2O) spectra of **Y** (PO_3F^{2-},doublet ,$\delta = -73.91$, $J = 865$ Hz and F^-, singlet , $\delta = -121.92$ ppm).

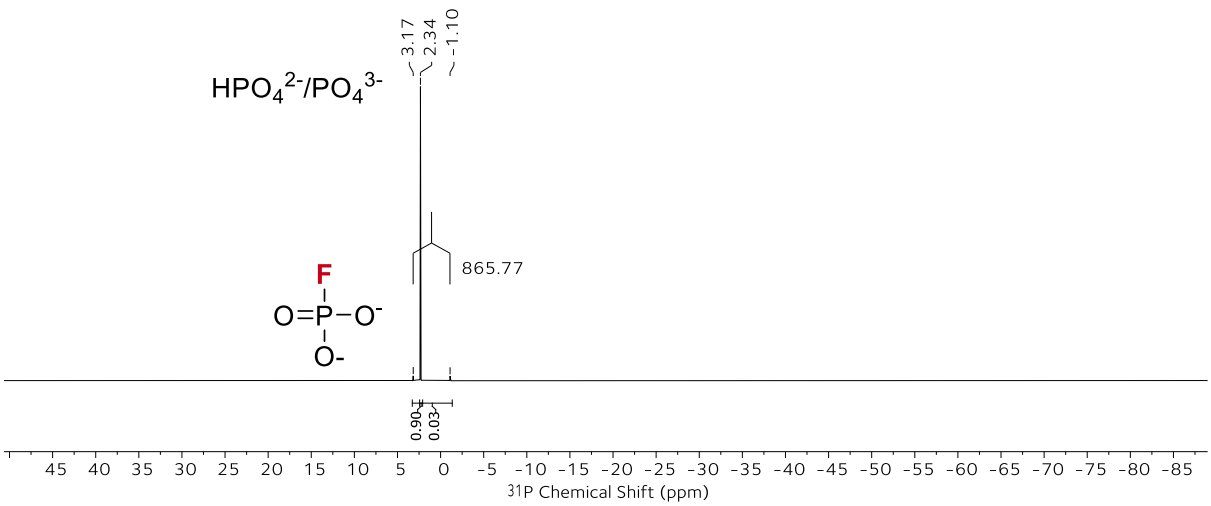

Figure 2.44. ^{31}P NMR (D_2O) spectra of **Y** (PO_3F^{2-}, doublet, δ =1.04 ppm, J= 866 Hz, PO_4^{3-}, singlet, δ =2.34 ppm).

There is no report of the phase **Y** documented in the literature. There are reported structures for $CaK(PO_4)$ and $K_2Ca(PO_4)F$, but the diffraction data clearly show that phase **Y** is neither of these.[113] Tripotassium sodium dichromate [$K_3Na(CrO_4)_2$] was used as a starting model for the refinement against the PXRD data collected for **Y** (Figure 2.45).

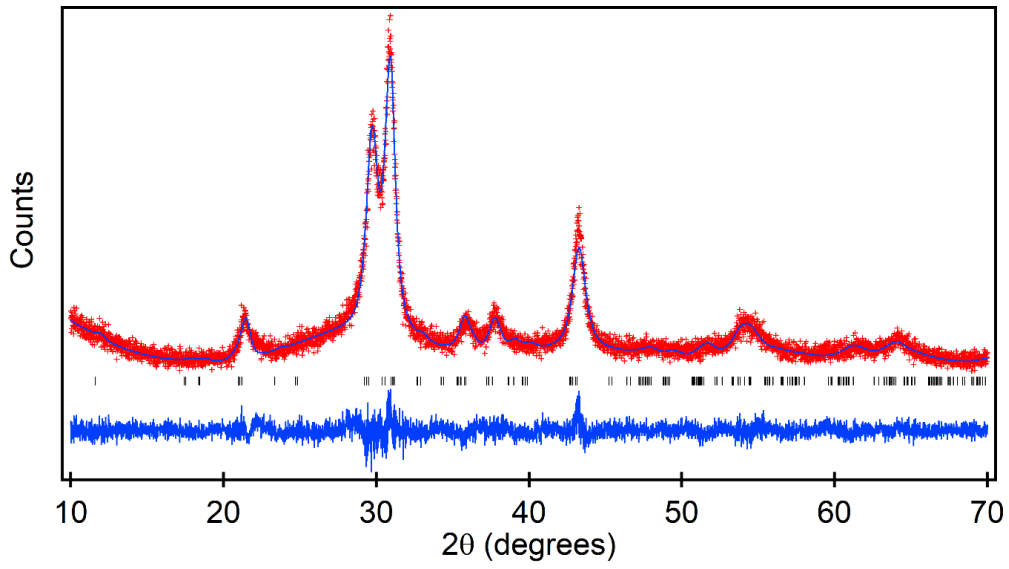

Figure 2.45. Observed (red), calculated (blue) and difference plots from the structural refinement of phase **Y** against X-ray powder diffraction data collected at room temperature.

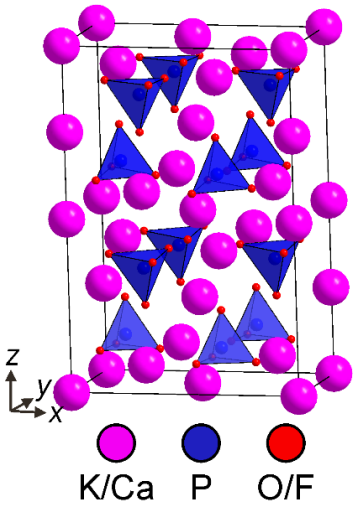

Figure 2.46. Proposed structure of the crystalline phase of **Y** [$K_{2-x}Ca_y(PO_3F)_a(PO_4)_b$].

Replacing the K/Na positions with K/Ca and CrO_4^{2-} with $P(O/F)_4$, the crystalline phase of **Y** has the proposed composition $K_{2-x}Ca_y(PO_3F)_a(PO_4)_b$ [a = 10.105(9) Å, b = 5.851(3) Å, c = 15.155(3) Å, β = 90.155(3) °]. Structural parameters from the refinement of **Y** can be found in Chapter **4**. The proposed crystal structure of **Y** [$K_{2-x}Ca_y(PO_3F)_a(PO_4)_b$] is isostructural with $M_2(POX_4)$ and not $M_2(PX_4)F$, i.e. an additional fluoride is not tolerated in the lattice. This suggests that the fluoride observed in the ^{19}F NMR spectrum (D_2O) of **Y** is contained in an amorphous phase or released from the PO_3F^{2-} unit via P–F bond cleavage. It is plausible that **Y** [$K_{2-x}Ca_y(PO_3F)_a(PO_4)_b$] is produced through the reaction of **X** [$K_3(HPO_4)F$] and anhydrous $CaHPO_4$ with the release of H_2O, as outlined in Scheme 2.15.

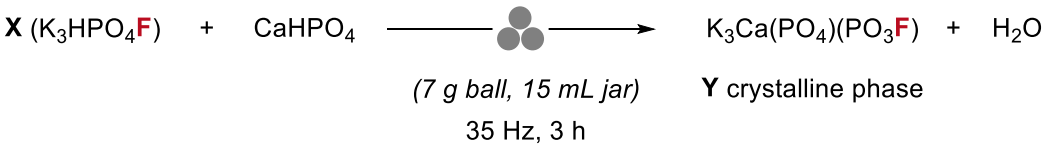

Scheme 2.15. Formation of the crystalline phase of **Y** [$K_{2-x}Ca_y(PO_3F)_a(PO_4)_b$ with x = 0.5, y = 0.5, a = 0.5, b = 0.5] with accompanying release of water.

The crystalline phase of **Y** [$K_{2-x}Ca_y(PO_3F)_a(PO_4)_b$] is a mixed anion compound with a variable composition where the K/Ca and $(PO_3F)/(PO_4)$ ratio can change upon anionic or cationic substitution into the lattice.[114] For instance, $K_3Ca(PO_3F)(PO_4)$ would correspond to $K_{2-x}Ca_y(PO_3F)_a(PO_4)_b$ (with x = 0.5, y = 0.5, a = 0.5, b = 0.5), a structure type closely related to the reported structure of calcium potassium phosphate [$K_3CaH(PO_4)_2$], which features a bridging Ca^{2+} between two phosphate units.[115]

The crystalline phase of **Y** is also observed in the solid formed upon ball milling KF (1 equiv) with K_2HPO_4 (1 or 2 equiv) and $CaHPO_4$ (1 equiv) in one-pot (Scheme 2.16).

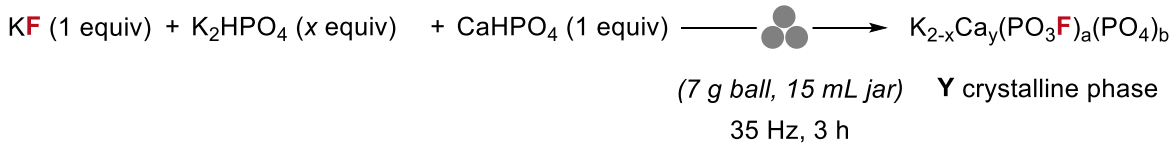

Scheme 2.16. Alternative routes to phase **Y** involving ball milling KF, K_2HPO_4 and $CaHPO_4$ (all anhydrous) in a one-pot fashion. The amount of K_2HPO_4 is varied (x = 1 or 2).

The PXRD patterns of the solids (Figure 2.47a-c) formed in the reactions outlined in Schemes 2.15 and 2.16 all contain peaks that correspond to the proposed structure $K_{2-x}Ca_y(PO_3F)_a(PO_4)_b$. The unchanged 2θ values suggest no volumetric differences between these solids, despite the differing amount of K_2HPO_4 content used during their formation. However, differences in *hkl* intensities of $K_{2-x}Ca_y(PO_3F)_a(PO_4)_b$ were noted, where the solid formed upon ball milling equimolar quantities of KF, K_2HPO_4 and $CaHPO_4$ lacks sharp Bragg peaks and is poorly crystalline (Figure 2.47c). This is in contrast to the $K_{2-x}Ca_y(PO_3F)_a(PO_4)_b$ phase observed in Figure 2.47b [prepared by ball milling KF (1 equiv) , K_2HPO_4 (2 equiv) and $CaHPO_4$ (1 equiv)].

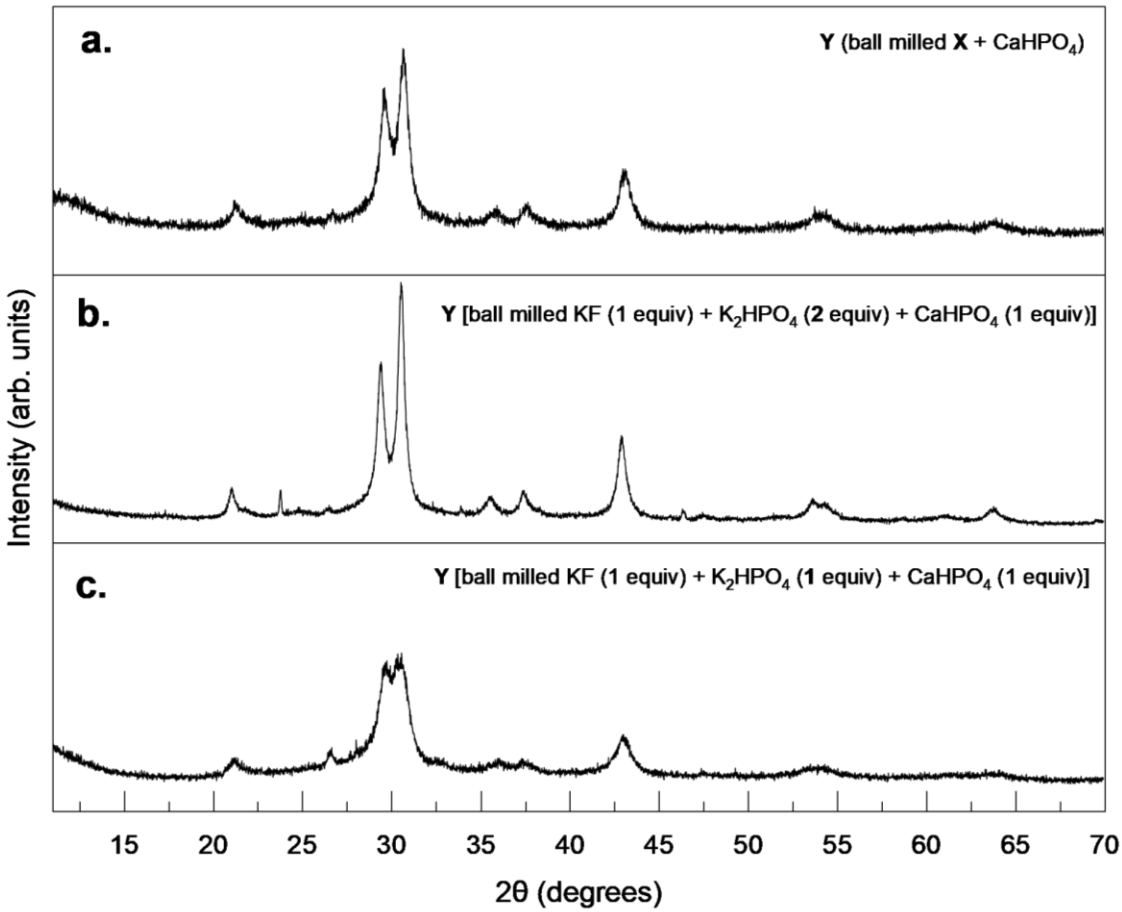

Figure 2.47. PXRD data of **Y**, prepared via **X** (top trace) or ball milling KF, K_2HPO_4 and $CaHPO_4$ in one-pot (35 Hz, 3 h) in varying ratios (middle and bottom trace).

Solid-state NMR spectroscopy revealed that the powder prepared from ball milling KF (1 equiv), K_2HPO_4 (2 equiv) and $CaHPO_4$ (1 equiv) (PXRD pattern in Figure 2.47b), which is representative of **Y**, contains a significant contribution of a PXRD silent (amorphous) fluoride (F^-) (Figure 2.48). In addition to two identifiable fluorine resonances at $\delta_F \approx -131.7$ and -72.0 ppm accounting for KF and PO_3F^{2-}, respectively, a broad resonance centred at $\delta_F = -115.5$ ppm is also observed. This broad resonance can be attributed to F^- present in the sample.

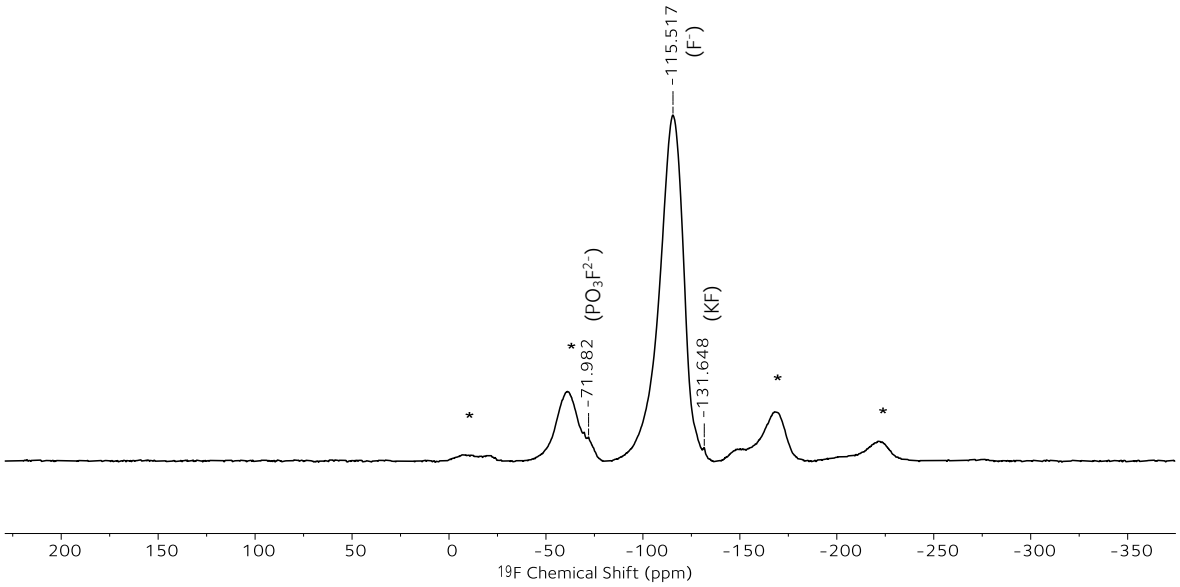

Figure 2.48. ^{19}F DPMAS solid-state NMR spectra of **Y** [prepared by ball milling KF (1 equiv), K_2HPO_4 (2 equiv) and $CaHPO_4$ (1 equiv)] with resonances at -72 ppm (PO_3F^{2-}), -115.5 ppm (F^-) and -131.7 ppm (KF) with spinning sidebands (marked by *) ν_{rot} = 20 kHz.

In a related study, a powder containing $K_3CaH(PO_4)_2$ was produced by grinding K_2HPO_4 together with anhydrous $CaHPO_4$ (Scheme 2.17). Further ball milling of this powder with KF, resulted in the formation of KH_2PO_4 (Figure 2.49).

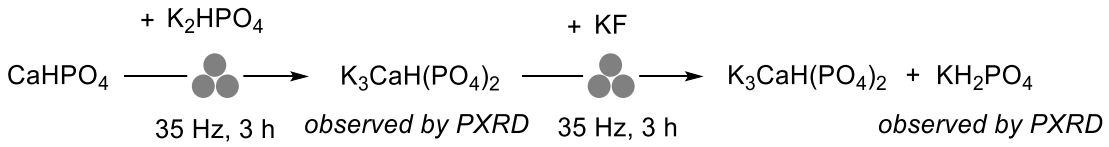

Scheme 2.17. Ball milling anhydrous $CaHPO_4$ (1 equiv) and K_2HPO_4 (1 equiv) followed by KF (1 equiv).

The fate of the fluoride anion is this system is unknown. The involvement of $K_3CaH(PO_4)_2$ in the proposed mechanism of **Fmix** formation was disregarded because there is no indication of KH_2PO_4 formation.

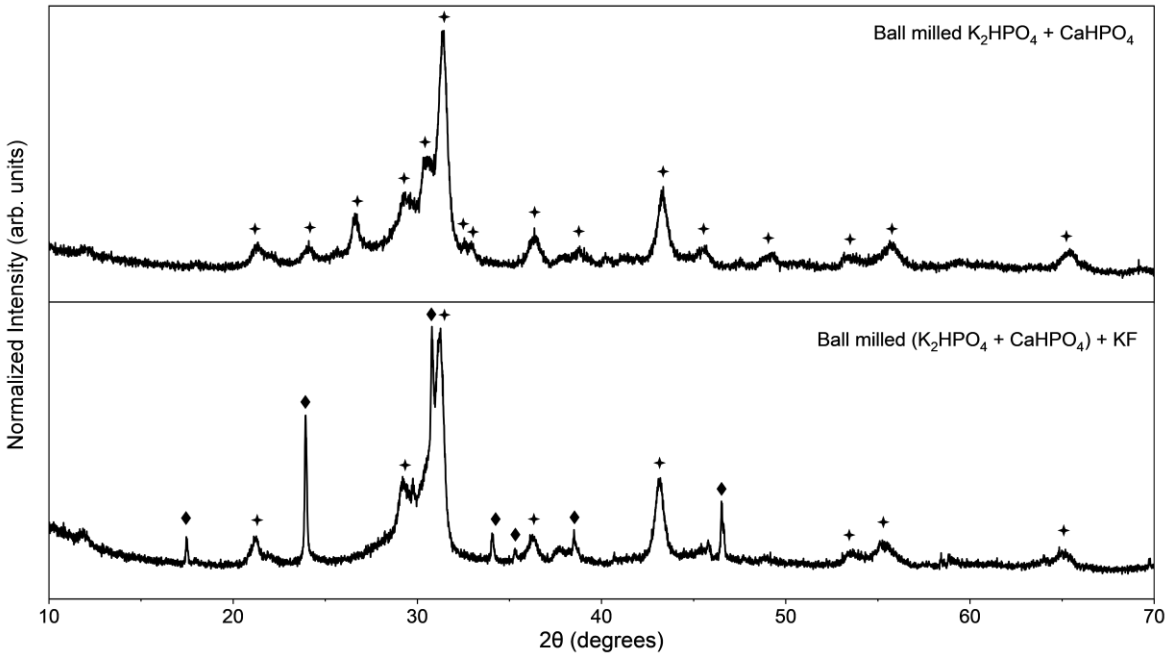

Figure 2.49. PXRD data of ball milled equimolar amount of K_2HPO_4 and $CaHPO_4$ (3 h, 35 Hz) (top), followed by subsequent milling with an equimolar amount of KF (bottom). [♦ = KH_2PO_4 (ICDD 01-079-0585), ✦ = $K_3CaH(PO_4)_2$ (ICDD 01-076-1248)].[115,116]

2.4.6 Discovery of Z

The solid matter (**Z**), produced from ball milling an equimolar amount of anhydrous KF and anhydrous $CaHPO_4$, is amorphous (Figure 2.50).

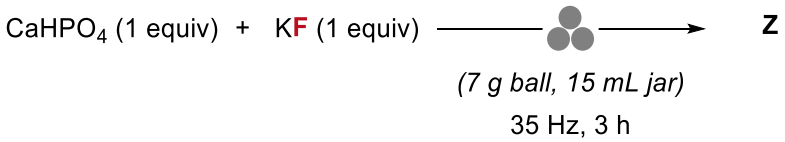

Scheme 2.18. Mechanochemical synthesis of **Z** via ball milling anhydrous $CaHPO_4$ and KF.

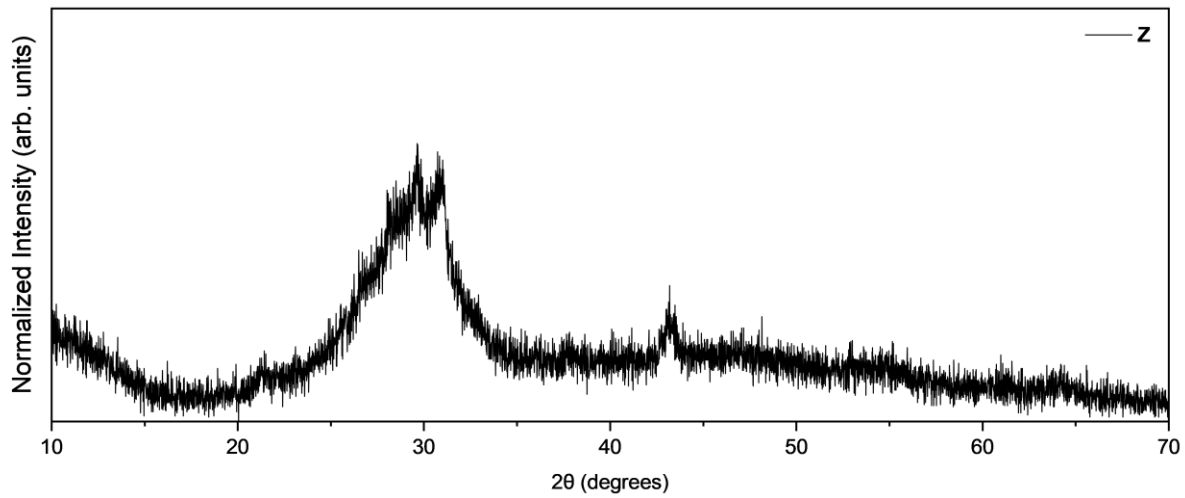

Figure 2.50. Powder X-ray diffraction pattern of **Z** (ball milled anhydrous $CaHPO_4$ and KF).

In the ^{19}F solid-state NMR spectrum of **Z** (Figure 2.51) a single major resonance was identified at $\delta_F \approx -105.6$ ppm. An additional contribution at $\delta_F \approx -132.1$ ppm is ascribed to residual KF in the sample.[111] The chemical shift of this resonance is centred between the chemical shift of calcium fluoride [CaF_2 ($\delta_F \approx -107.7$ ppm] and fluorapatite [$Ca_5(PO_4)_3F$, $\delta_F \approx -103.8$ ppm]. A single broad resonance is observed in the ^{31}P solid-state NMR spectrum of **Z**, centred at $\delta_P \approx 1.3$ ppm. The ^{1}H solid-state NMR spectrum of **Z** shows a broad resonance within the region of δ_H 0 to 18 ppm which is ascribed to HPO_4^{2-} and H_2O ($\delta_H = 6.84$ ppm). No reflections are observed in the diffractogram of **Z** (amorphous) (Figure 2.50).

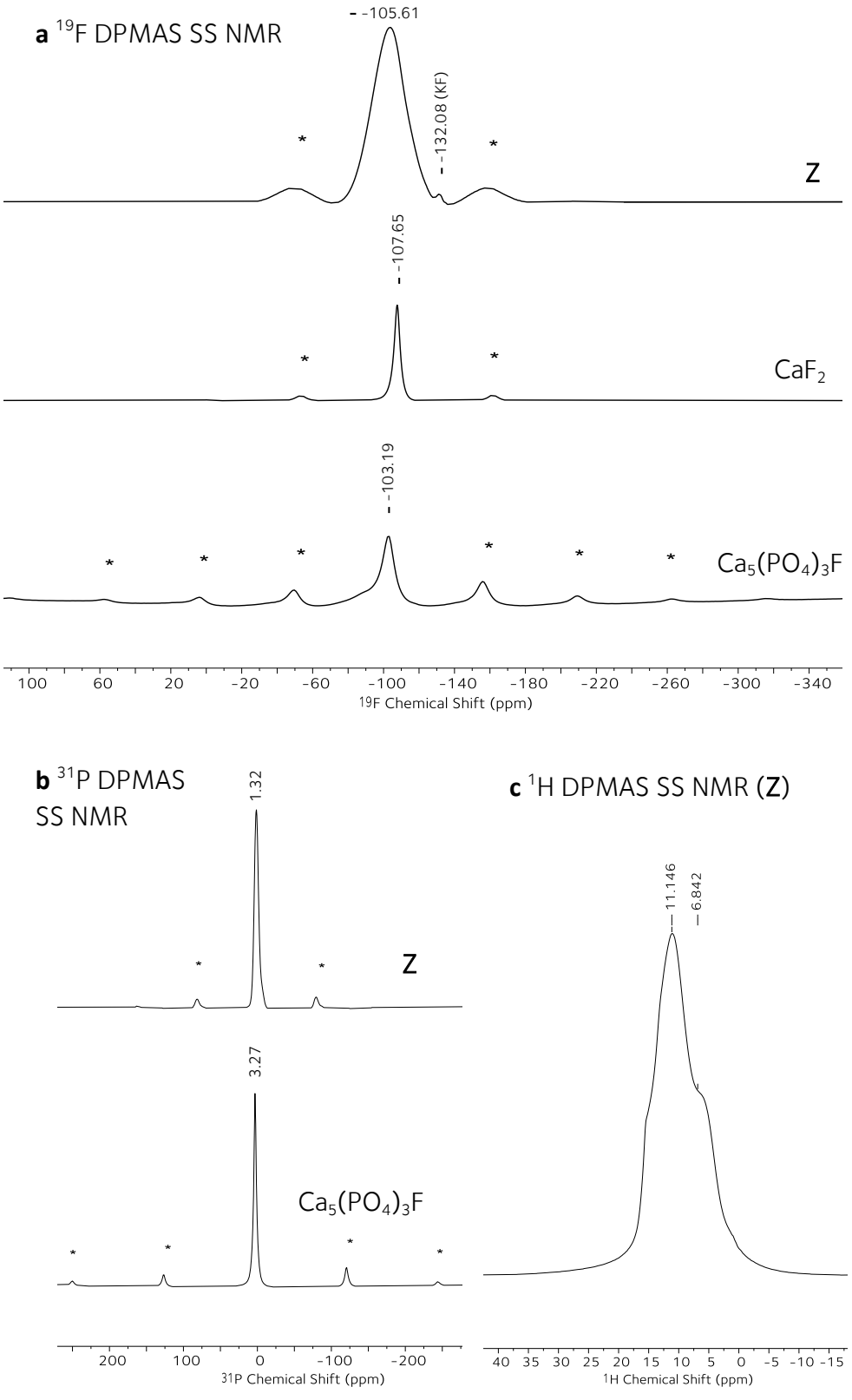

Figure 2.51. **a**)^{19}F DPMAS SS NMR spectra of **Z** (top) -105.6 and -132.1 ppm (KF), CaF_2 (middle), $Ca_5(PO_4)_3F$ (bottom), with spinning sidebands (marked by *) ν_{rot} = 20 kHz; **b**) ^{31}P DPMAS SS NMR spectra of **Z** and $Ca_5(PO_4)_3F$ with spinning sidebands (marked by *) ν_{rot} = 14 kHz (top), 20 kHz (bottom); **c**) ^{1}H SS MMR of **Z** ν_{rot} = 20 kHz. (SS = solid-state).

2.4.7 Discovery of Z'

Further ball milling of **Z** with anhydrous K_2HPO_4 (1 equiv) afforded **Z'** which was found to contain the crystalline phase $K_{2-x}Ca_y(PO_3F)_a(PO_4)_b$ (observed in **Y**) as evidenced by PXRD (Figure 2.52). This data suggests that $K_{2-x}Ca_y(PO_3F)_a(PO_4)_b$ can form via **X** [$K_3(HPO_4)F$] or **Z** (amorphous).

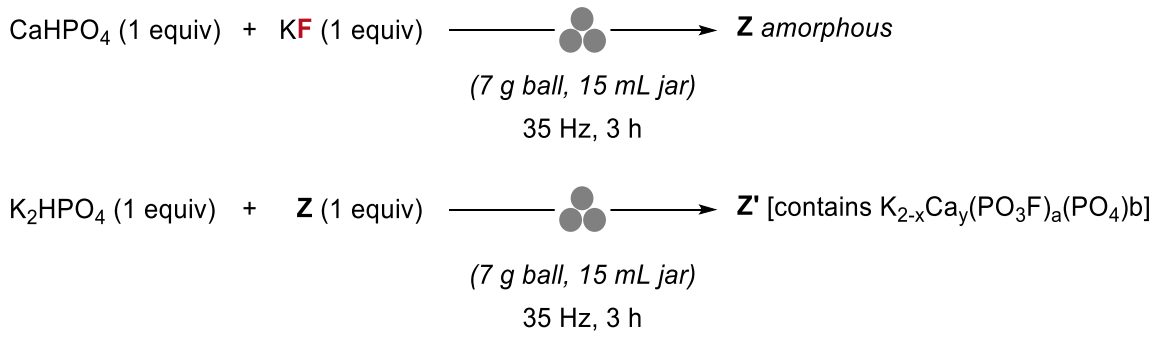

Scheme 2.19. Ball milling **Z** with K_2HPO_4 (1 equiv) affords **Z'** [contains the crystalline phase observed in **Y** ($K_{2-x}Ca_y(PO_3F)_a(PO_4)_b$)].

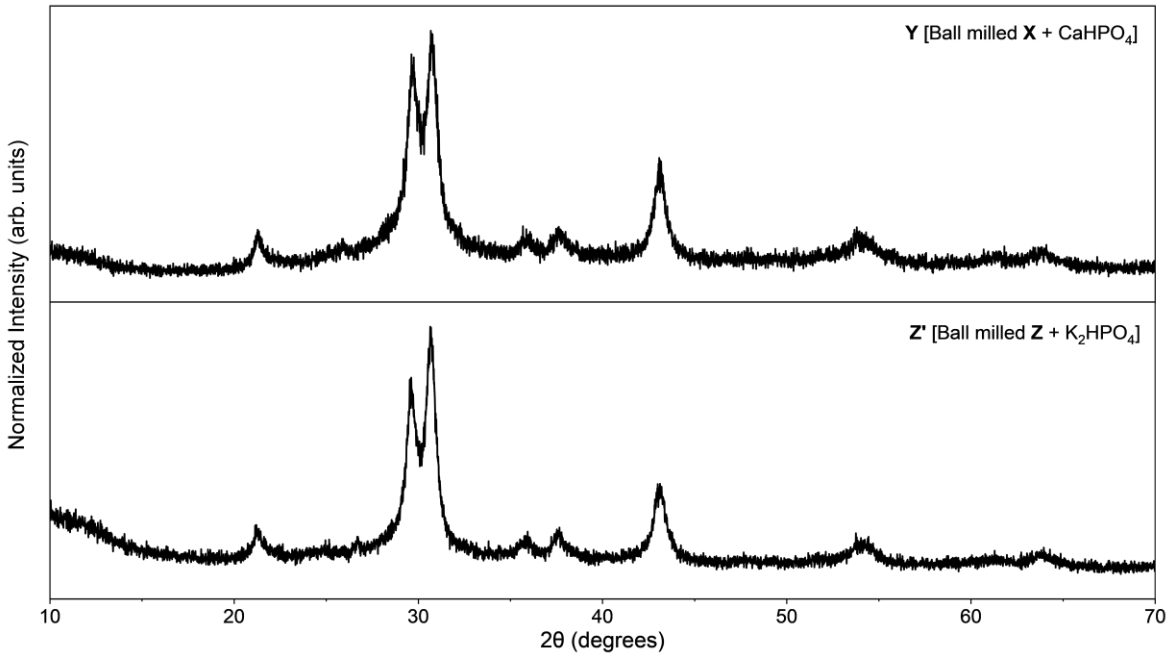

Figure 2.52. PXRD data of ball milled equimolar amount of **X** [$K_3(HPO_4)F$] and $CaHPO_4$ (3 h, 35 Hz) (top), ball milled **Z** with an equimolar amount of K_2HPO_4 (bottom) (3h, 35 Hz).

Ball milling **Z** with K_2HPO_4 has significant effects on its structure, as observed by solid-state NMR spectroscopy. Unlike the ^{19}F solid-state NMR spectrum of **Z** which displays a single resonance at $\delta_F \approx -105.6$ ppm, the ^{19}F solid-state NMR spectrum of **Z'** (Figure 2.53) reveals three identifiable fluorine resonances at $\delta_F \approx -131.4$, -116.6, and -72.5 ppm. The resonance at $\delta_F \approx -72.5$ ppm is assigned to PO_3F^{2-} anion, which is consistent with the $K_{2-x}Ca_y(PO_3F)_a(PO_4)_b$ crystalline phase observed in **Z'**. The minor resonance at $\delta_F \approx -131.4$ ppm is attributed to KF.[111] Notably, the ^{19}F solid-state NMR spectrum of **Z'** is dominated by the major resonance at $\delta_F \approx -116.6$ ppm. The resonance shift of the fluoride anion from $\delta_F \approx -105.6$ ppm (**Z**) to $\delta_F \approx -116.6$ ppm (**Z'**) from a Ca^{2+} rich phase to a K^+ enriched phase is consistent with a dynamic solid with ranging calcium to potassium ratio. Based on these data, it is possible that **Y** and **Z'** contain a phase (or phases), in addition to crystalline $K_{2-x}Ca_y(PO_3F)_a(PO_4)_b$, that lacks long-range order. The ^{19}P and ^1H solid-state NMR spectra of **Z'** show single resonances at centred at $\delta_P \approx 0$ ppm and $\delta_H \approx 10.98$ ppm, respectively.

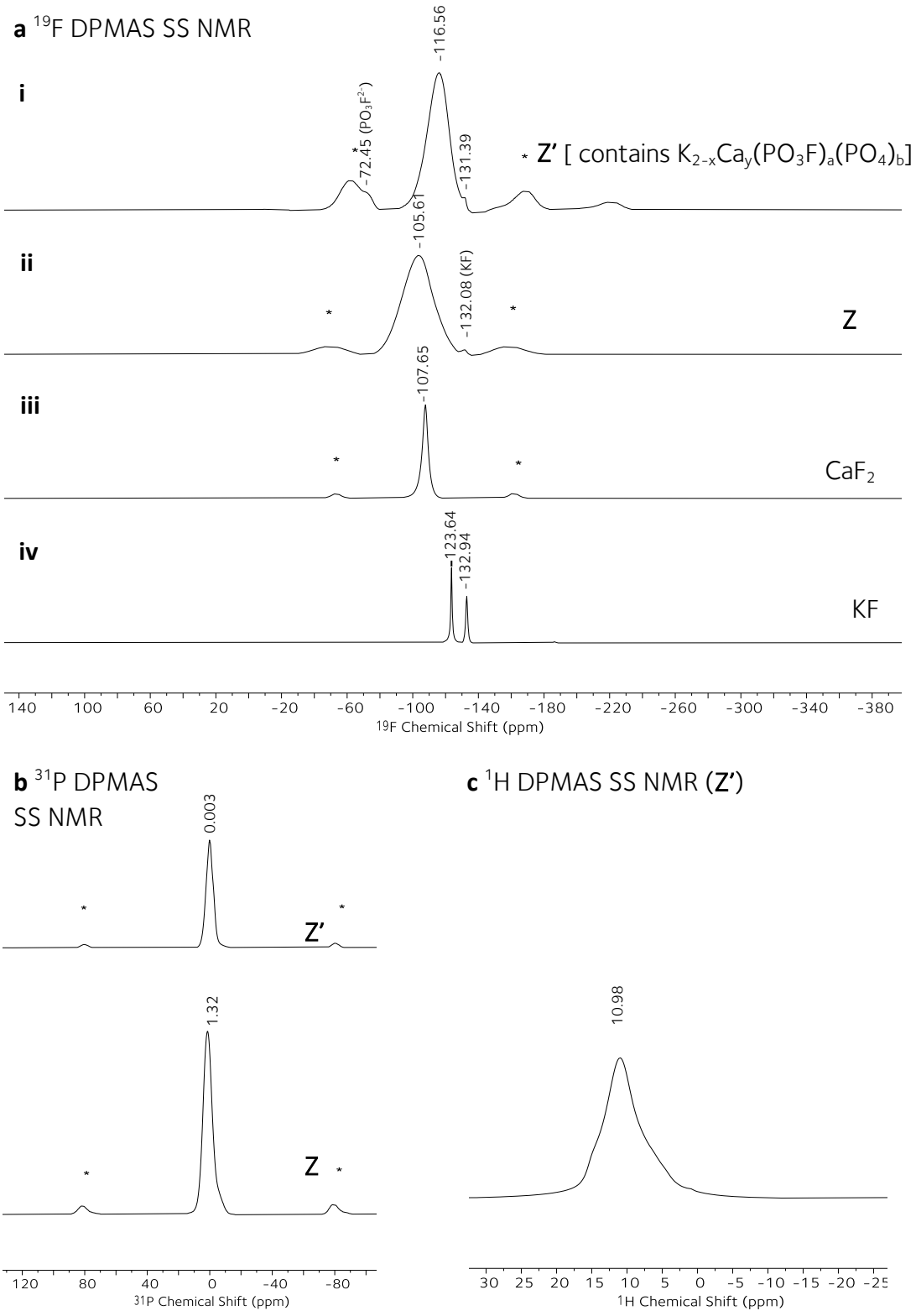

Figure 2.53. **a)** ^{19}F DPMAS SS NMR spectra of **i) Z'** -72.5 (PO_3F^{2-}) -116.6 and -131.4 ppm (KF), **ii) Z** -105.6 and -132.1 ppm (KF), **iii)** CaF_2 and **iv)** KF -123.64 (KF) and -132.94 ($KF{\cdot}2H_2O$) ppm with spinning sidebands (marked by *) ν_{rot} = 20 kHz. **b)** ^{31}P DPMAS SS NMR spectra of **Z'** (top) and **Z** (bottom), with spinning sidebands (marked by *) ν_{rot} = 20 kHz (top), 20 kHz (bottom); **c)** ^{1}H SS MMR of **Z'** ν_{rot} = 20 kHz (SS = solid-state).

2.4.8 Solid-State NMR of Fmix

The ^{19}F solid-state NMR spectrum of **Fmix** displays a resonance centred at δ_F = -132 ppm ascribed to **X** [$K_3(HPO_4)F$]. An additional peak centred at δ_F = -108.1 ppm, consists of contributions from CaF_2 ($\delta_F \approx$ -107.7 ppm) and **Y** ($\delta_F \approx$ -115.5 ppm) or **Z'** ($\delta_F \approx$ -116.6 ppm). A peak at δ_F = -71.6 ppm was assigned to PO_3F^{2-}.

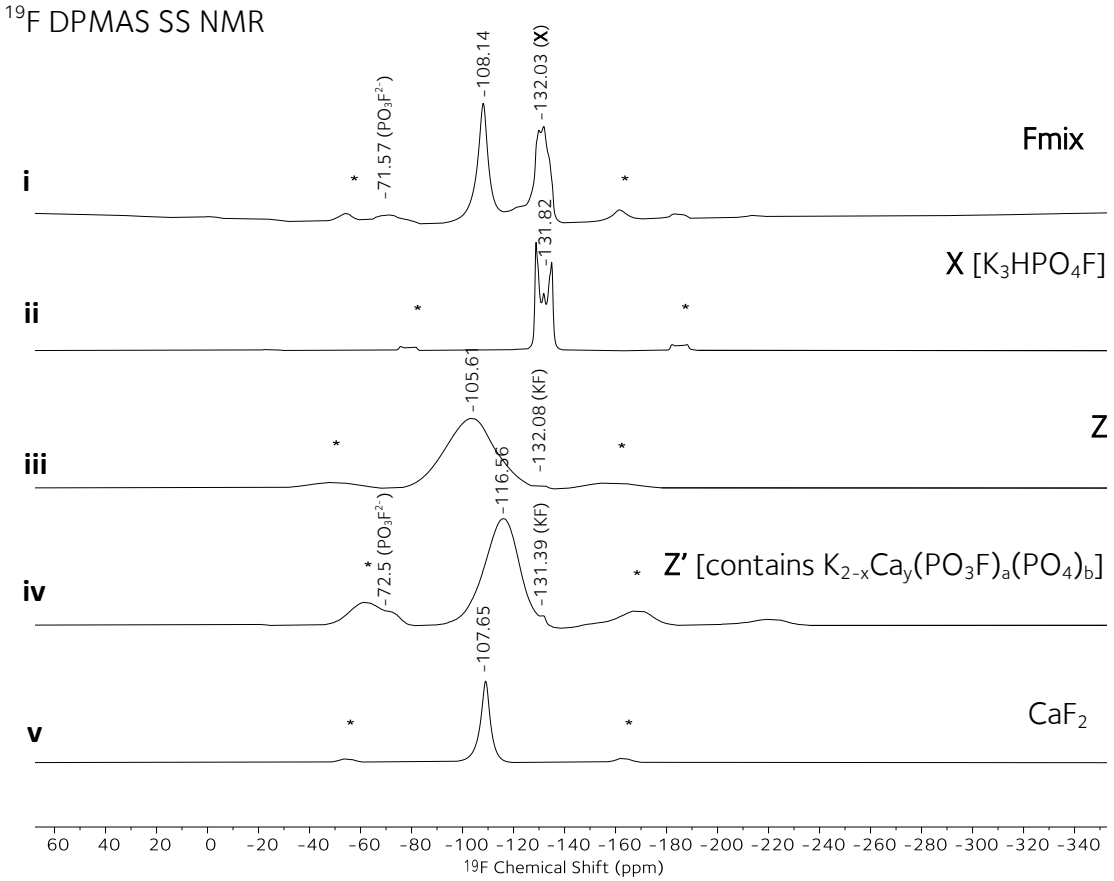

Figure 2.54. ^{19}F DPMAS SS NMR spectra of **i) Fmix** -71.6 (PO_3F^{2-}) -108.1 and -132 ppm (**X**), **ii) X** five resonances centred at -131.8 ppm, **iii) Z** -105.6 and -132.1 ppm (KF), **iv) Z'** -72.5 (PO_3F^{2-}) -116.6 and -131.4 ppm (KF), **iii)** CaF_2 with spinning sidebands (marked by *) ν_{rot} = 20 kH (SS = solid-state).

The ^{31}P solid-state NMR spectrum of **Fmix** (Figure 2.55) displays one broad resonance between the chemical shift range of δ_P = -5 to 10 ppm. The line shape of the

broad resonance suggests that several orthophosphate and fluorophosphate environments (PO_4^{3-}, HPO_4^{2-} and PO_3F^{2-}) may be present in **Fmix**.[117–119] Monofluorophosphates typically give rise to resonances within this region (K_2PO_3F δ_P = 7.61 ppm).[120] The ^{1}H solid-state NMR spectrum (Figure 2.56) shows a similar broad resonance assigned to the HPO_4^{2-} anion.

.

^{31}P SS NMR

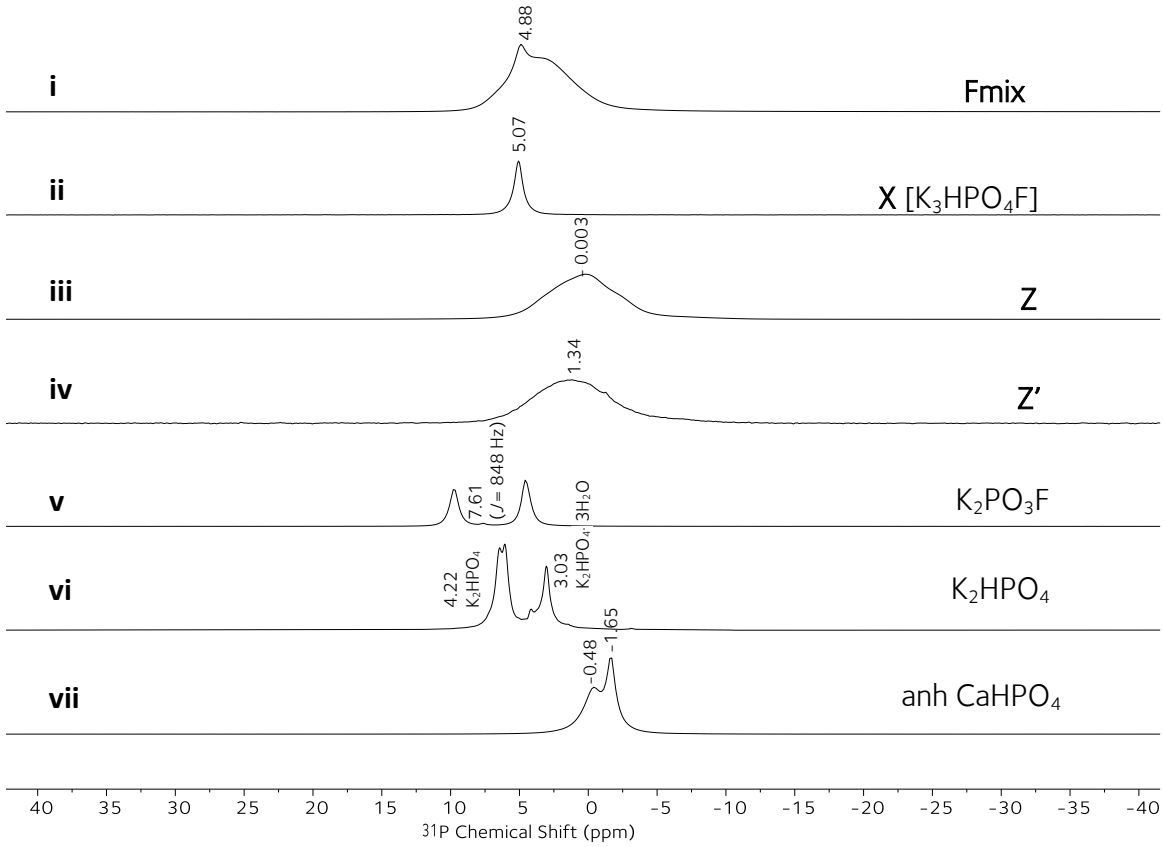

Figure 2.55. ^{31}P SS NMR spectra of **i**) ^{31}P DPMAS SS NMR of **Fmix** broad resonance between 10 – -5 ppm **ii**) ^{31}P DPMAS SS NMR of **X** centered at 5.07 ppm, **iii**) ^{31}P DPMAS SS NMR of **Z** broad resonance centered at 0 ppm, **iv**) ^{31}P DMPAS SS NMR of **Z'** broad resonance centered at 1.34 ppm **v**) ^{31}P DPMAS SS NMR of K_2PO_3F 7.61ppm (d, J = 848 Hz), **vi**) ^{31}P HPDEC SS NMR of K_2HPO_4 (ref[118]) and **vii**) ^{31}P DPMAS SS NMR of anhydrous $CaHPO_4$ shows two peaks at -0.48 ppm and -1.65 ppm due to disordered hydrogen-bonding in the $CaHPO_4$ structure giving rise to two inequivalent tetrahedra of phosphorus (ref[121,122]). Spinning sidebands (marked by *) ν_{rot} = 20 kHz (SS = solid-state).

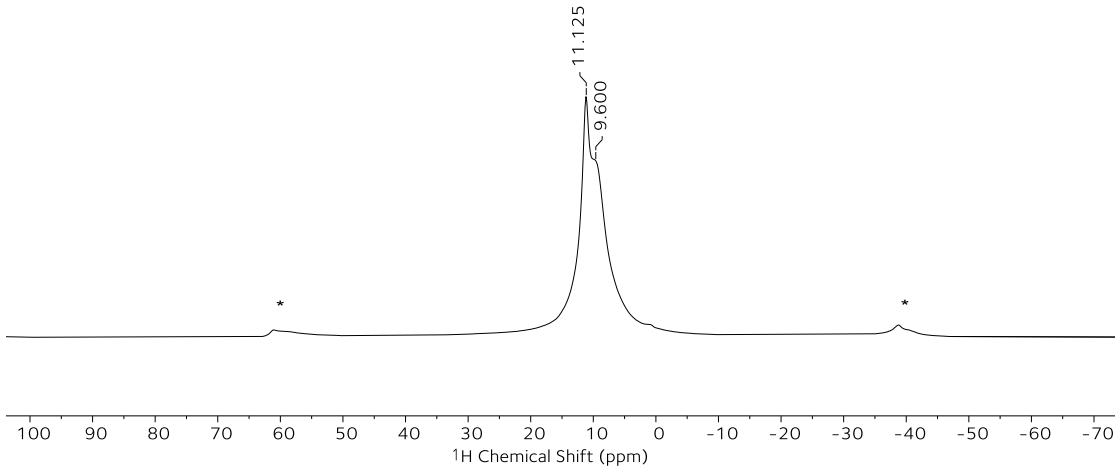

Figure 2.56. ^{1}H SS NMR spectrum of **Fmix**. Major proton environment (11.1 ppm) and shoulder at 9.60 ppm with spinning sidebands (marked by *) ν_{rot} = 20 kHz.

A summary of the crystalline and amorphous phases in **Fmix**, **X**, **Y**, **Z** and **Z'** observed, by PXRD and solid-state NMR spectroscopy is provided in Table 2.17.

Table 2.17. Summary of the crystalline and amorphous phases in **Fmix**, **X**, **Y**, **Z** and **Z'**.

Solid Product	Description	Crystalline phases (PXRD)	Amorphous F^- phase (SS NMR)
Fmix	crystalline, amorphous	CaF_2, K_3HPO_4F, $K_{2-x}Ca_y(PO_3F)_a(PO_4)_b$	Fluoride containing (δ_F -108.1 ppm)
X	crystalline	K_3HPO_4F	-
Y	crystalline, amorphous	$K_{2-x}Ca_y(PO_3F)_a(PO_4)_b$	Fluoride containing (δ_F -115.5 ppm)
Z	amorphous	-	Fluoride containing (δ_F -105.6 ppm)
Z'	crystalline, amorphous	$K_{2-x}Ca_y(PO_3F)_a(PO_4)_b$	Fluoride containing (δ_F -116.6 ppm)

SS = solid-state

2.4.9 Reactivity of X, Y and Z

The reactivity of **X**, **Y**, **Z** and KF was tested in the fluorination of TsCl in solution under optimised conditions and compared against the reactivity of **Fmix** (Figure 2.58). A ^{19}F NMR yield of 90% for the fluorination of TsCl using **X** demonstrates that **X** is an effective fluorinating reagent. As a fluorinating reagent, **Y** shows a level of performance markedly lower than **Fmix** (44%). Powder **Z**, prepared through ball milling an equimolar amount of KF and anhydrous $CaHPO_4$ (Scheme 2.20), afforded only 8% TsF (**1**). Portion-wise addition of anhydrous K_2HPO_4 to **Y** and **Z** afforded **Y'** and **Z'**, respectively. The diffractograms of **Y**, **Y'**, **Z'** are provided in Figure 2.57. Powders **Y'** and **Z'** showed improved reactivity compare to their precursors. For instance, whilst 8% of TsF (**1**) was observed using **Z**, fluorination proceeded in 40% using **Z'**. Further ball milling of **Z'** with one equivalent of K_2HPO_4 provided **Z''**, which enabled up to 81% fluorination (Figure 2.58). By PXRD, $K_{2-x}Ca_y(PO_3F)_a(PO_4)_b$ is observed in both **Z'** and **Z''**, however, no changes to 2θ values were detected between solids, despite the additional amount of K^+ and HPO_4^{2-} ions in **Z''**.

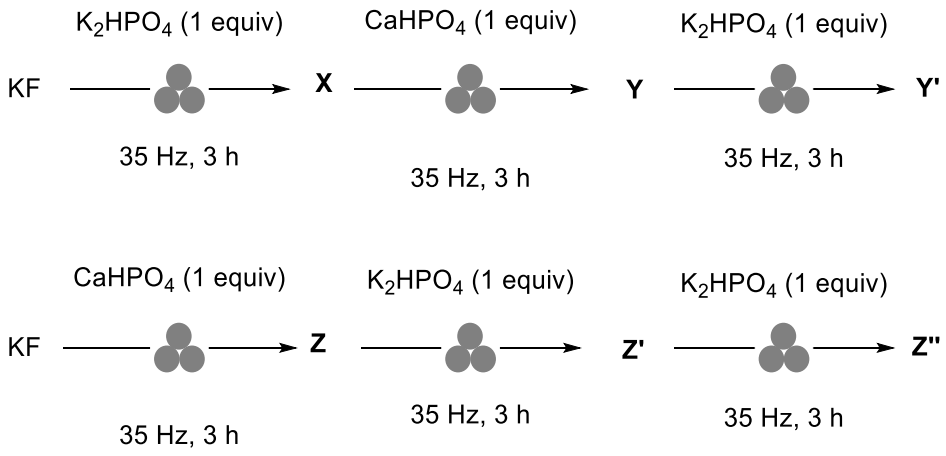

Scheme 2.20. Synthesis of **X** [crystalline phase $K_3(HPO_4)F$], **Y**, **Y'**, **Z**, **Z'** and **Z''**. All products are powders. Powders **Y**, **Y'**, **Z'** and **Z''** all contain the crystalline phase $K_{2-x}Ca_y(PO_3F)_a(PO_4)_b$ and amorphous phases.

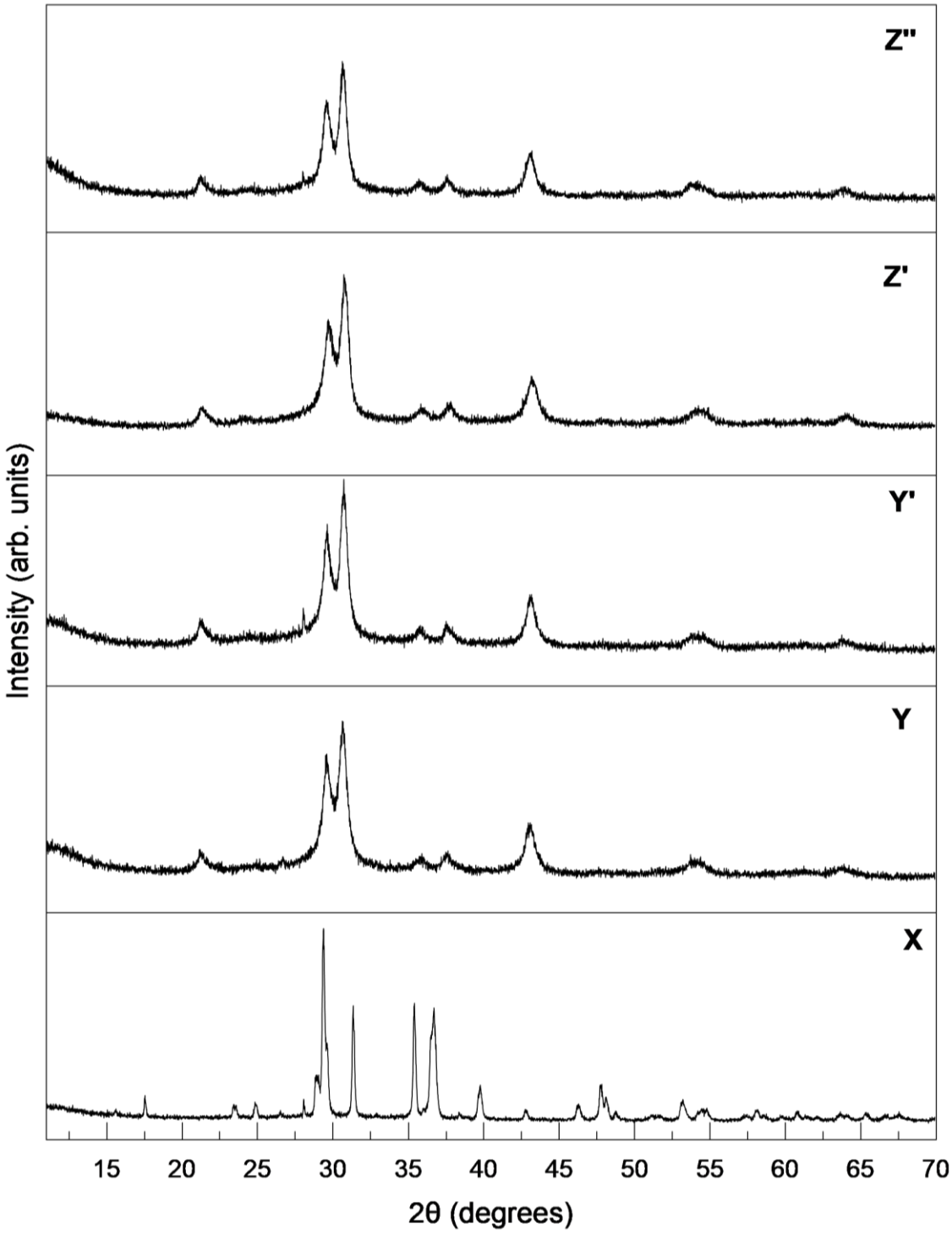

Figure 2.57. Powder X-ray diffraction patterns of **X**, **Y**, **Y'**, **Z'** and **Z''**. Crystalline phases of **X** is solely $K_3(HPO_4)F$, whilst $K_{2-x}Ca_y(PO_3F)_a(PO_4)_b$ is observed in phases **Y**, **Y'**, **Z'** and **Z''**. No significant shifts in 2θ are detected in phases **Y**, **Y'**, **Z'** and **Z''**. Diffraction peaks in **Y**, **Y'**, **Z'** and **Z''** are broad which is indicative of a material lacking crystallinity.

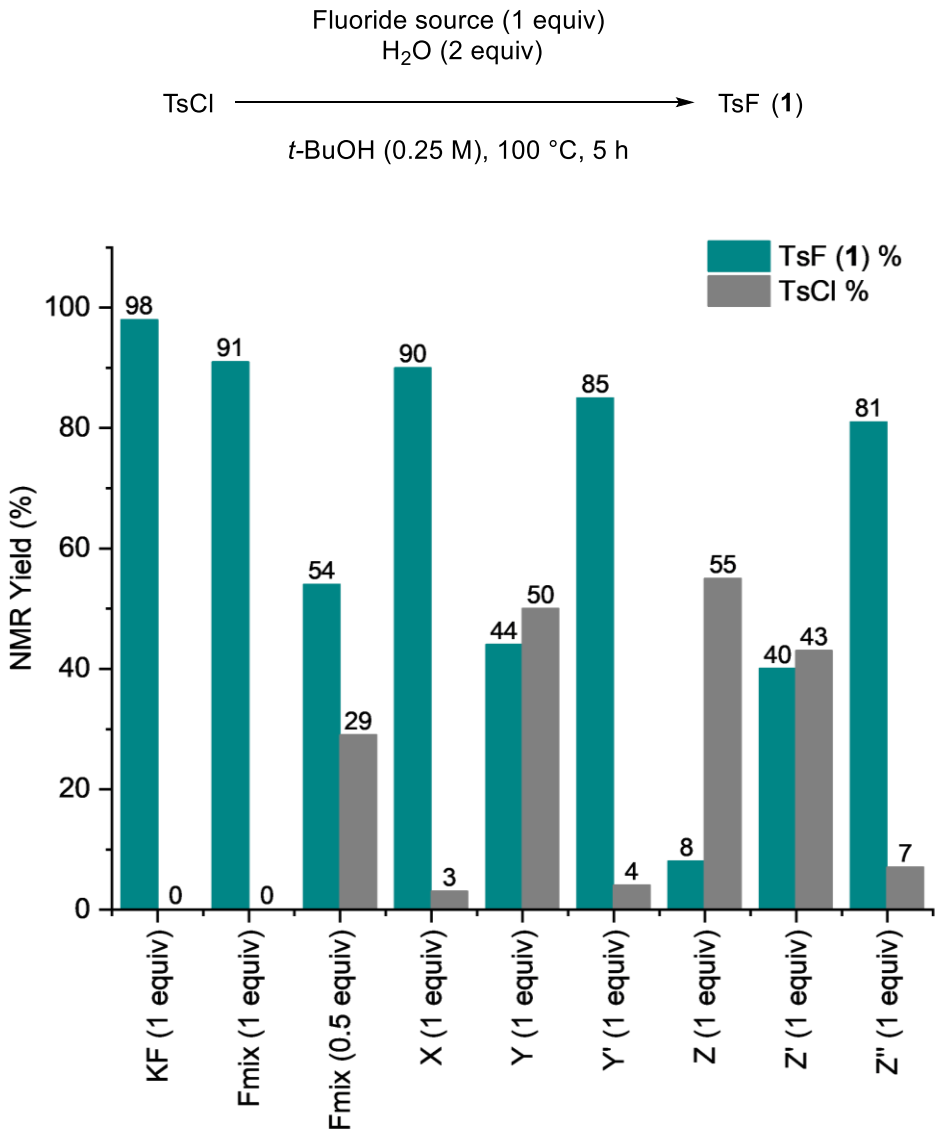

Figure 2.58. Fluorinating ability of **X**, **Y**, **Y'**, **Z**, **Z'**, **Z''** compared to **Fmix** and **KF** in the fluorination of TsCl, (0.125 mmol scale). Reactions using KF, **Fmix**, **X** and **Y** were run in triplicate and the reported NMR yields in this figure are an average of three repeats.

Collectively, these results indicate that the portion-wise addition of K_2HPO_4 to the salts **Y** and **Z** with subsequent ball milling improves their fluorinating ability. This finding parallels the increased reactivity observed through the portion-wise addition of K_2HPO_4 to AGF.

2.4.10 Observation of Apatite

A sample of **Fmix** was stirred in H_2O at room temperature and the resulting suspension was centrifuged. The supernatant was collected and evaporated to dryness to provide a highly hygroscopic crystalline powder [**Fmix**$_{(soluble)}$].

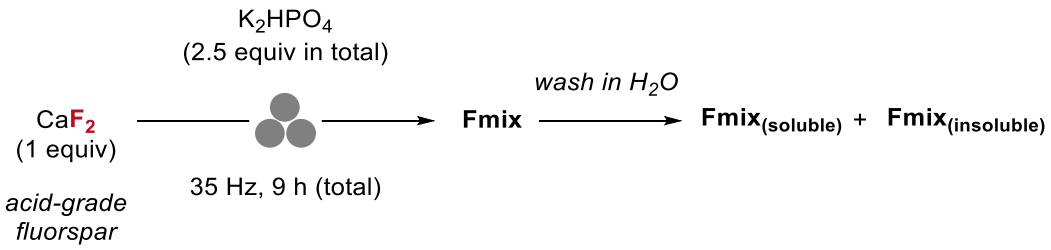

Scheme 2.21. Isolation of water soluble and insoluble components of **Fmix**.

The water insoluble component **Fmix**$_{(insoluble)}$ was also collected and allowed to dry to completeness at 25 °C. A diffractogram of **Fmix**$_{(insoluble)}$ indicated that the solid is comprised of crystalline CaF_2 and a phase consistent with an apatite-type structure $Ca_5(PO_4)_3X$ [or $Ca_{10}(PO_4)_3X_2$], where X=F or OH (Figure 2.59).

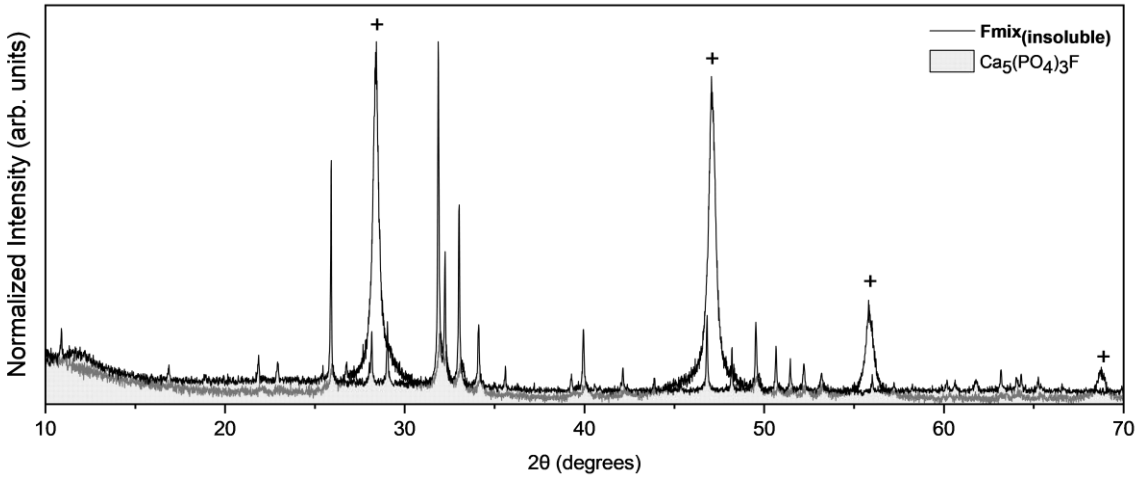

Figure 2.59. PXRD data of water insoluble component of **Fmix** and $Ca_5(PO_4)_3F$. Water insoluble component of **Fmix** contains CaF_2 [+] and an apatite phase (overlay).[123]

The apatite crystal structure is able to accommodate cations and anions of broadly different sizes.[124] Hydroxyapatite has a similar atomic structure and belongs to the same space group (hexagonal, $P6_3/m$) as fluorapatite, differing only in the substitution of hydroxide (OH^-) for fluoride (F^-). Since fluoride ions are smaller, this results in a more compact lattice of $Ca_5(PO_4)_3F$ than $Ca_5(PO_4)_3OH$, where a contraction is reported to occur in the *a*-axis (by approximately 0.0496 Å), but not in the *c*-axis dimension.[125] Analysis of the PXRD patterns of $Ca_5(PO_4)_3F$ and $Ca_5(PO_4)_3OH$ reveal that the main diffraction peak located between 2θ=31.86° and 32.05° is slightly shifted towards higher 2θ values for $Ca_5(PO_4)_3F$ (Figure 2.60).[126] Solid solutions of hydroxyfluorapatite with the composition $Ca_{10}(PO_4)_6F_x(OH)_{2-x}$ (where 0<x<2) are also reported.[127]

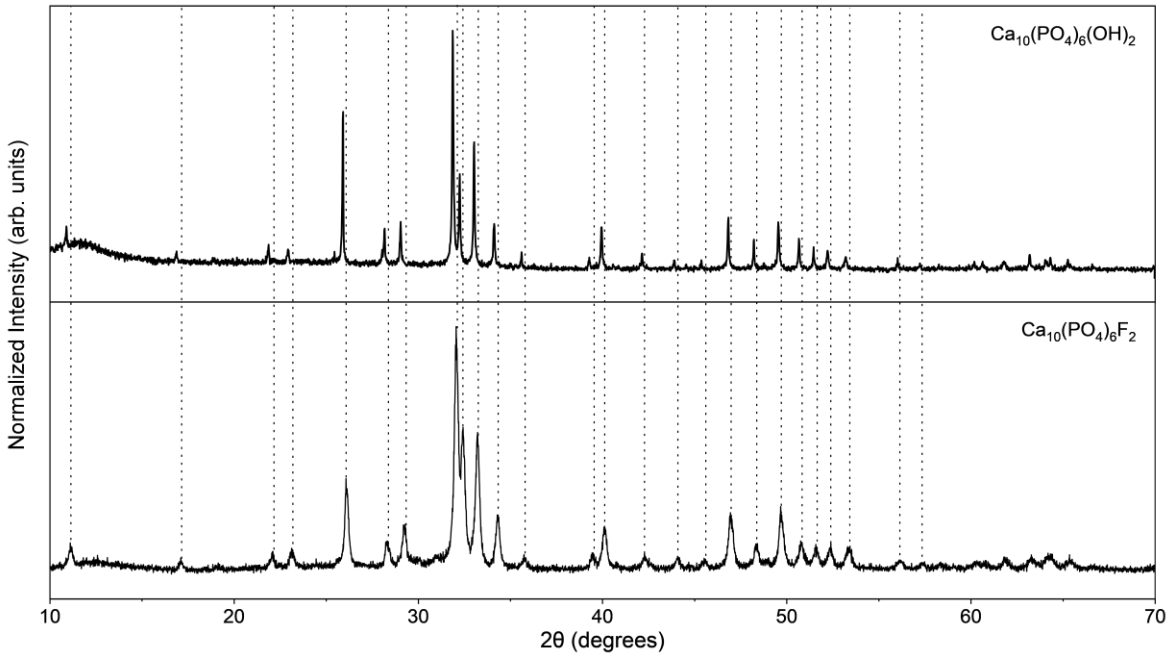

Figure 2.60. PXRD data of water insoluble component of commercially available $Ca_5(PO_4)_3(OH)_2$ and $Ca_5(PO_4)_3F$.

At this stage, it is unclear if the apatite phase forms during the mechanochemical activation of AGF with K_2HPO_4 or is consequently formed upon exposure of **Fmix** to water. The possibility of $Ca_5(PO_4)_3X$ generation during the formation of **Fmix** should not be ruled

out. Indeed, ball milling an equimolar quantity of CaF_2 with anhydrous $CaHPO_4$ (Scheme 2.22) results in the formation of a water insoluble solid, consistent with an apatite [$Ca_5(PO_4)_3X$] structure (Figure 2.61). This pathway may be operating during the formation of **Fmix**.

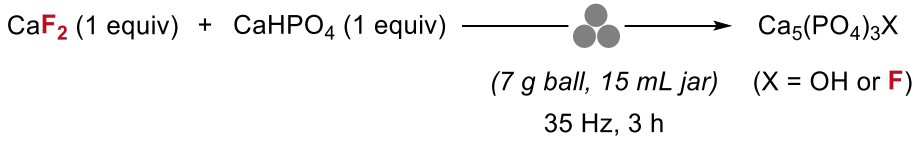

Scheme 2.22. Ball milling CaF_2 and $CaHPO_4$ results in the formation of an apatite structure.

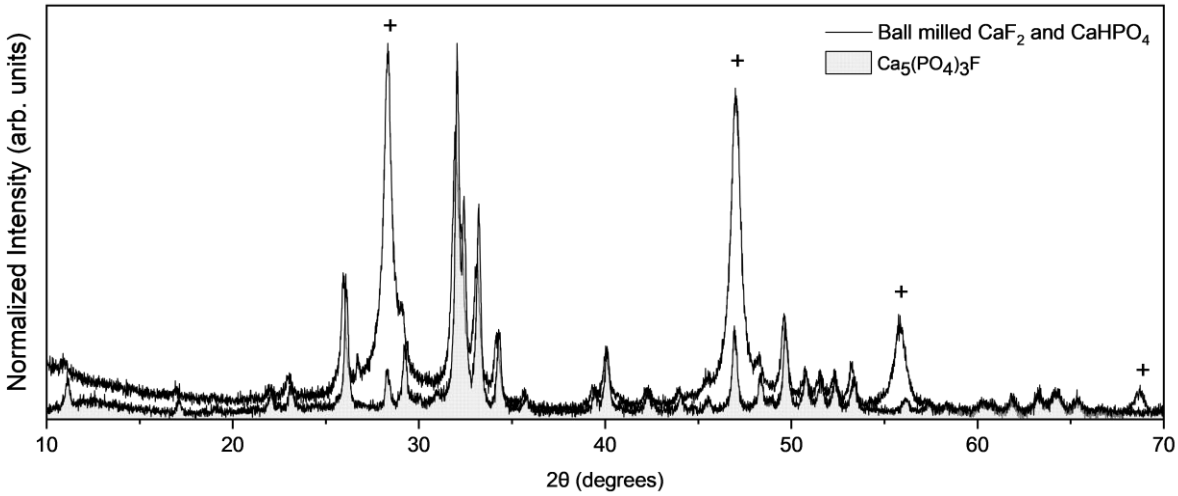

Figure 2.61. PXRD data of solid formed from ball milling CaF_2 and $CaHPO_4$, and $Ca_5(PO_4)_3F$. Water insoluble component of **Fmix** contains CaF_2 [+] and an apatite phase (overlay).

Currently, it is not established whether the apatite phase present in **Fmix**$_{(insoluble)}$ represents a distinct apatite phase [e.g. pure $Ca_5(PO_4)_3F$] or a solid solution. Further analysis employing infrared (IR) spectroscopy, to distinguish main vibrational bonds, and solid-state NMR spectroscopy is warranted. Moreover, the water-soluble component of **Fmix** was also isolated, however, the solid was highly hygroscopic and not suitable for powder X-ray diffraction (under ambient conditions).

2.4.11 Reaction between $CaHPO_4$ and KF

As previously described, an amorphous phase **Z** is formed upon ball milling anhydrous $CaHPO_4$ (1 equiv) with KF (1 equiv). The mechanochemical reaction between 1 equivalent of anhydrous $CaHPO_4$ and 2 equivalents of KF was also explored (Scheme 2.23). Increasing the number equivalents of KF to two, led to structural changes in the solid formed, including the formation of CaF_2 and an unidentified crystalline phase (Figure 2.62).

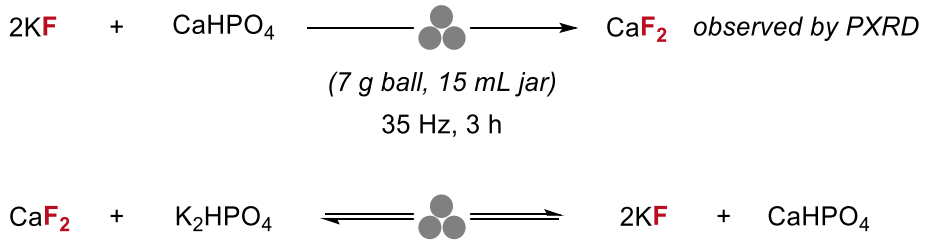

Scheme 2.23. Ball milling KF (2 equiv) and anhydrous $CaHPO_4$ (1 equiv) affords CaF_2 indicating that the mechanochemical activation of CaF_2 with K_2HPO_4 is reversible.

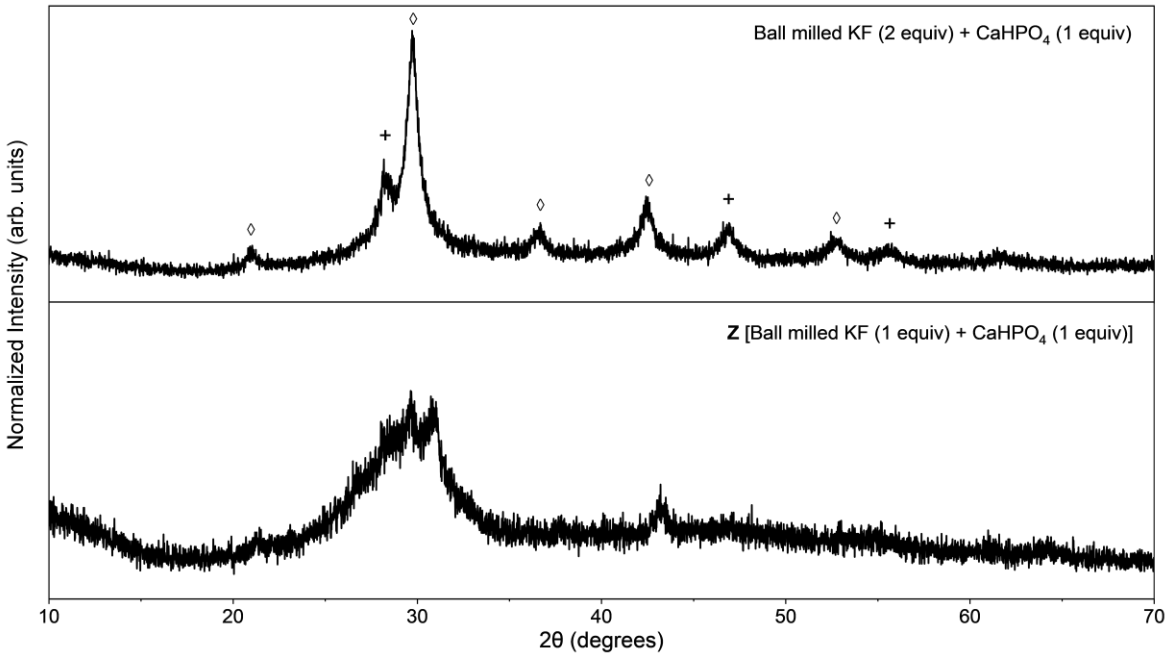

Figure 2.62. PXRD data of solid derived from ball milling $CaHPO_4$ (1 equiv) with KF (2 equiv), and CaF_2 (1 equiv) with KF (1 equiv) (**Z**) (+ = CaF_2, ◊ = new crystalline phase).

These findings indicate that under mechanochemical conditions, CaF_2 is kinetically accessible from the more thermodynamically stable $CaHPO_4$ in presence of at least 2 equivalents of KF. Notably, this result implies that the ball milling of CaF_2 with K_2HPO_4 is reversible under mechanochemical conditions (Scheme 2.23), and there is a potential for the equilibrium to shift upon the addition of excess K_2HPO_4.

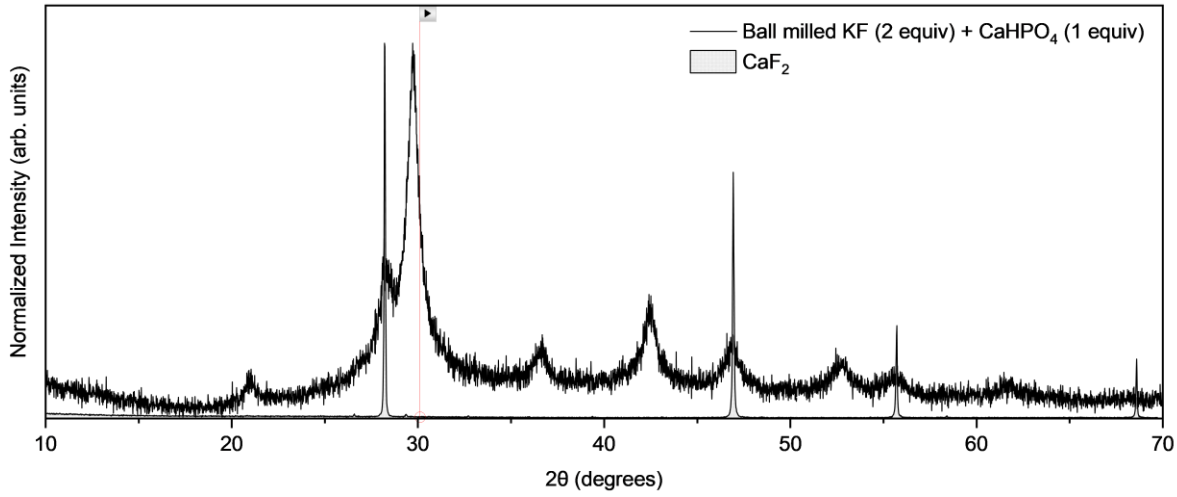

Figure 2.63. PXRD data of data of solid derived from ball milling $CaHPO_4$ (1 equiv) with KF (2 equiv) compared with PXRD of CaF_2.

2.4.12 Microstructure Analysis and Stability

Scanning electron microscopy (SEM) was employed to monitor the microstructural evolution in the powders prepared during the milling of AGF with K_2HPO_4. Complementing the structural analysis acquired by PXRD and solid-state NMR spectroscopy, SEM allows for the tracking of morphological changes such as particle size distribution. SEM images of AGF (>97% CaF_2) revealed a polycrystalline powder of size < 50 μm, with particles surrounded by abrasive edges (Figure 2.64). Ball milling AGF with K_2HPO_4 (1 equiv) for 3 h at 35 Hz led to the formation of a polydisperse sample with a range of particle sizes (diameter ranging from 2 – 220 nm) (Figure 2.65).

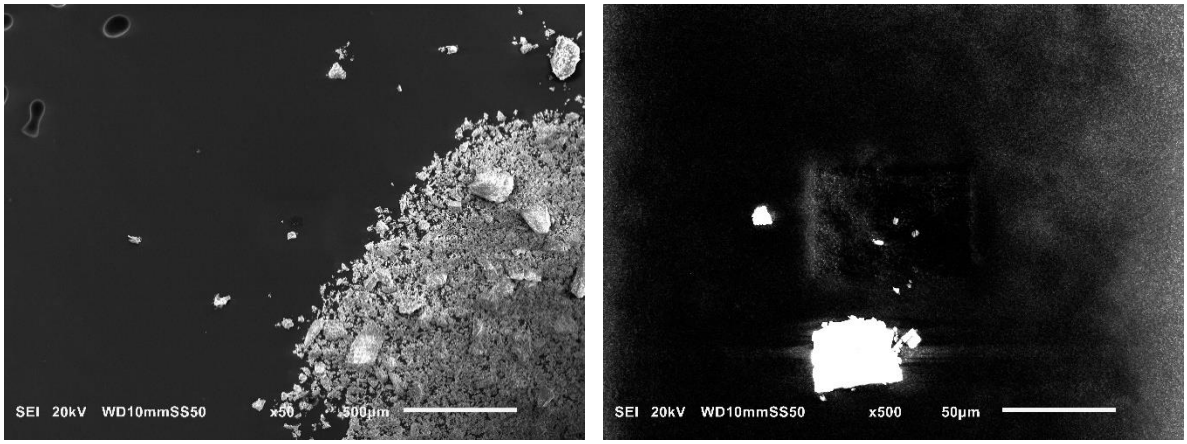

Figure 2.64. SEM images of AGF, images shown at x50 and x500 magnification.

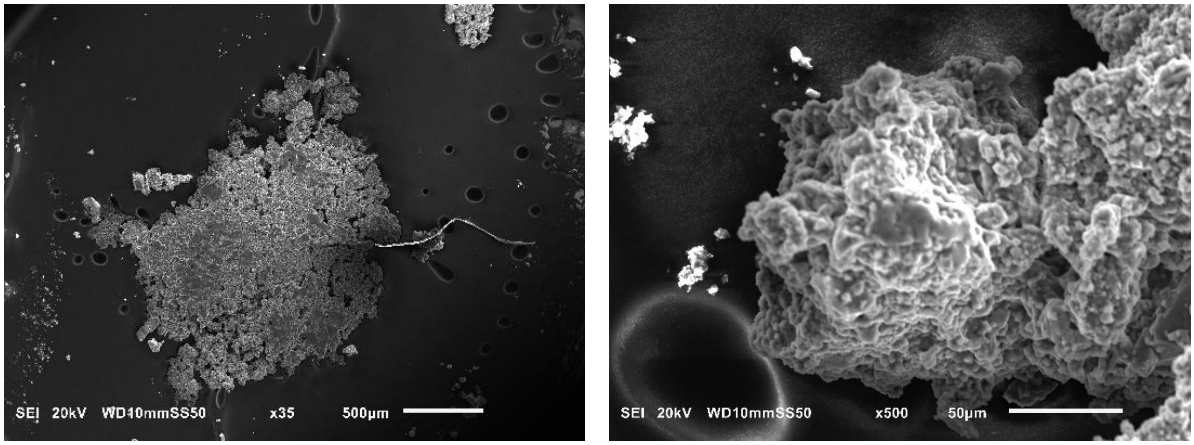

Figure 2.65. SEM images of AGF ball milled with K_2HPO_4 (1 equiv, 3 h, 35 Hz), images shown at x50 and x500 magnification.

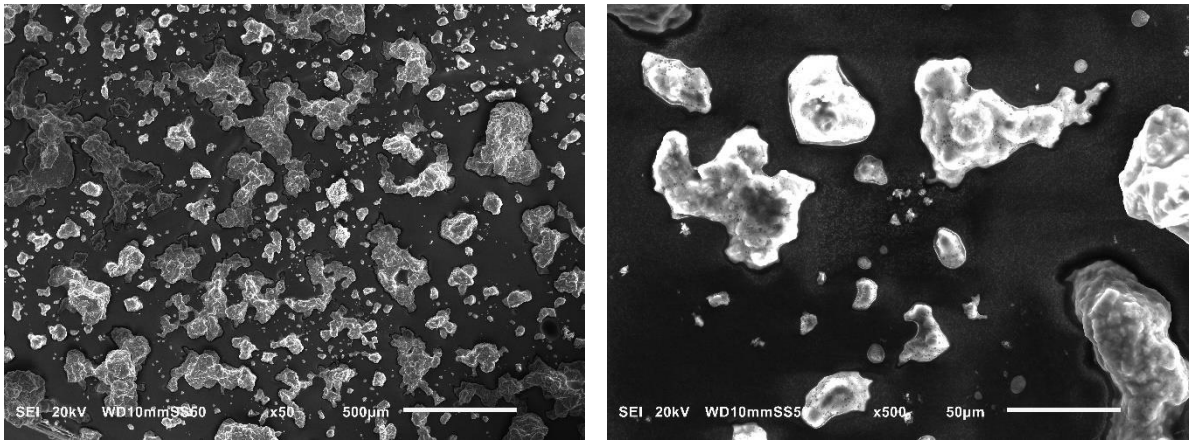

Figure 2.66. SEM images of **Fmix** [AGF ball milled with K_2HPO_4 (2.5 equiv in total, 9 h in total, 35 Hz), images shown at x50 and x500 magnification.

The proportion of large particles reduces with additional K_2HPO_4 addition and extended milling time (Figure 2.66). Sintering of the particles into highly irregular shaped agglomerated particles (~100 μm) is observed in **Fmix**. The size of the single particles is mostly comprised between 5–10 μm, with few being as small as 1 μm.

The performance of **Fmix** (stored in a sealed borosilicate glass vial) was investigated over a 9-month period (Figure 2.67).

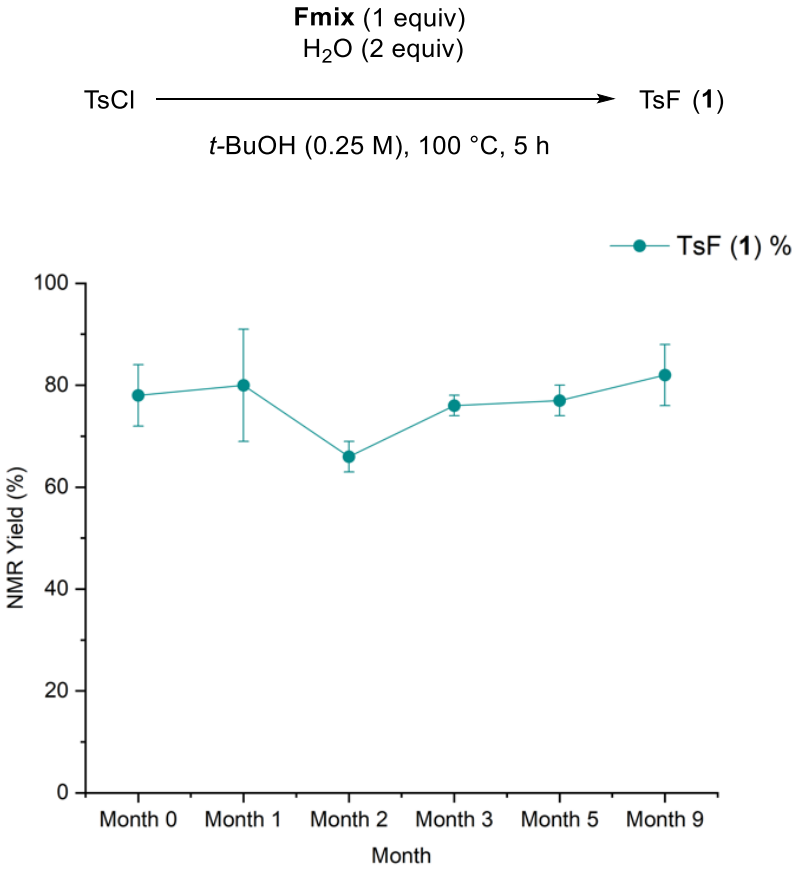

Figure 2.67. Reactivity of **Fmix** (stored over a 9-month period) in the fluorination of TsCl under optimised conditions at monthly intervals. NMR yields (determined by ^{19}F and ^{1}H NMR spectroscopy) are an average of 3 runs (with S.E. bars).

The reactivity of the **Fmix** sample was tested at monthly intervals using the fluorination of TsCl as a model substrate under optimised reaction conditions. The TsF (**1**) yield (determined

by ^{19}F NMR spectroscopy) ranged between 66% to 82%, with no significant loss in yield over 9 months. No observable differences were observed in the PXRD patterns of **Fmix** measured after 9 months of storage in a sealed borosilicate glass vial (see Chapter **4** for more details).

Thermogravimetric analysis (TGA) profiles of AGF, anhydrous K_2HPO_4 and **Fmix** with different exposure times to air were recorded (Figure 2.68). Similar to KF, **Fmix** is hygroscopic. Upon increasing the exposure time, an increasing weight loss (<100 °C) is observed which is ascribed to loss of adsorbed water. It was found that **Fmix** presented high thermal stability until approximately 400 °C, where a degradation event corresponding to phosphate dehydration is observed.[128]

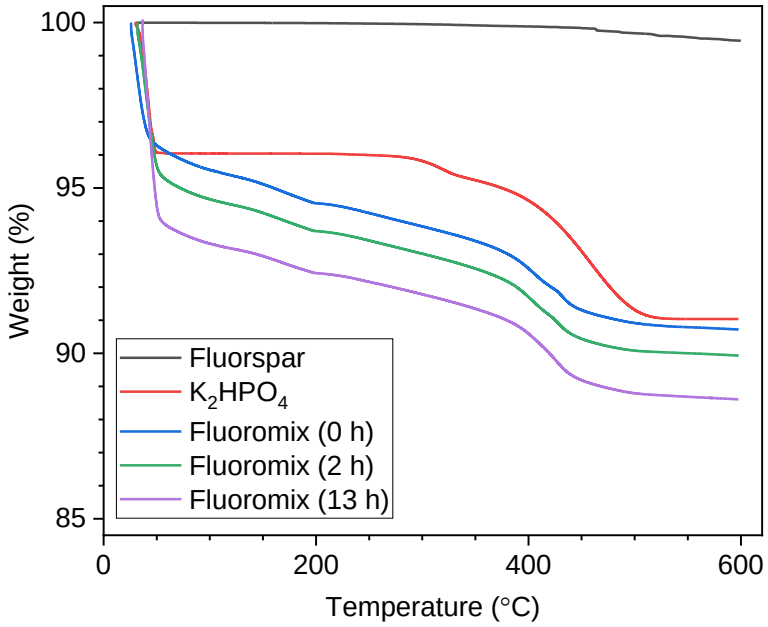

Figure 2.68. TGA of Fmix with different exposure times to air, acid grade fluorspar, and K_2HPO_4.

2.4.13 Thermal Activation of Fluorspar

In a typical solid-state synthesis, a heterogenous mixture of precursor powders evolves into a product phase through solid-solid interfacial reactions, traversing through a variety of intermediates along the way.[129,130] Solid reactants are ground in a mortar and pestle to reduce particle size, thereby increasing the surface area, before being heated in a vessel such as a ceramic crucible, to high temperature. This high temperature process aims to obtain the most thermodynamically stable phase. To enhance inter-grain contact, the pre-heated sample can undergo regrinding before further heating, until a pure phase is achieved.

Given the significant difference in reaction environment between mechanochemical and thermal solid-state methods, it is reasonable to expect significant differences in reaction outcome. As a case study, an equimolar ratio of AGF (>97% CaF_2) and anhydrous K_2HPO_4 were weighed, ground and heated in air at 200 °C for 1 h. The powder was collected, then reground and heated to 500 °C for 1 h (Figure 2.69). Analysis of the powder by PXRD revealed the presence of CaF_2 and potassium pyrophosphate ($K_4P_2O_7$), formed via the dehydration of K_2HPO_4 (>400 °C) (Figure 2.70).[128] During the thermal treatment, no new crystalline phases were observed after heating CaF_2 with K_2HPO_4 for 1 h at 200 °C. This is in contrast to the mechanochemical treatment where new crystalline phases [$K_3(HPO_4)F$ or $K_{2-x}Ca_y(PO_3F)_a(PO_4)_b$] form after just 1 h of ball milling at 35 Hz. Notably, $K_4P_2O_7$ was not observed during the mechanochemical reaction between CaF_2 and K_2HPO_4.

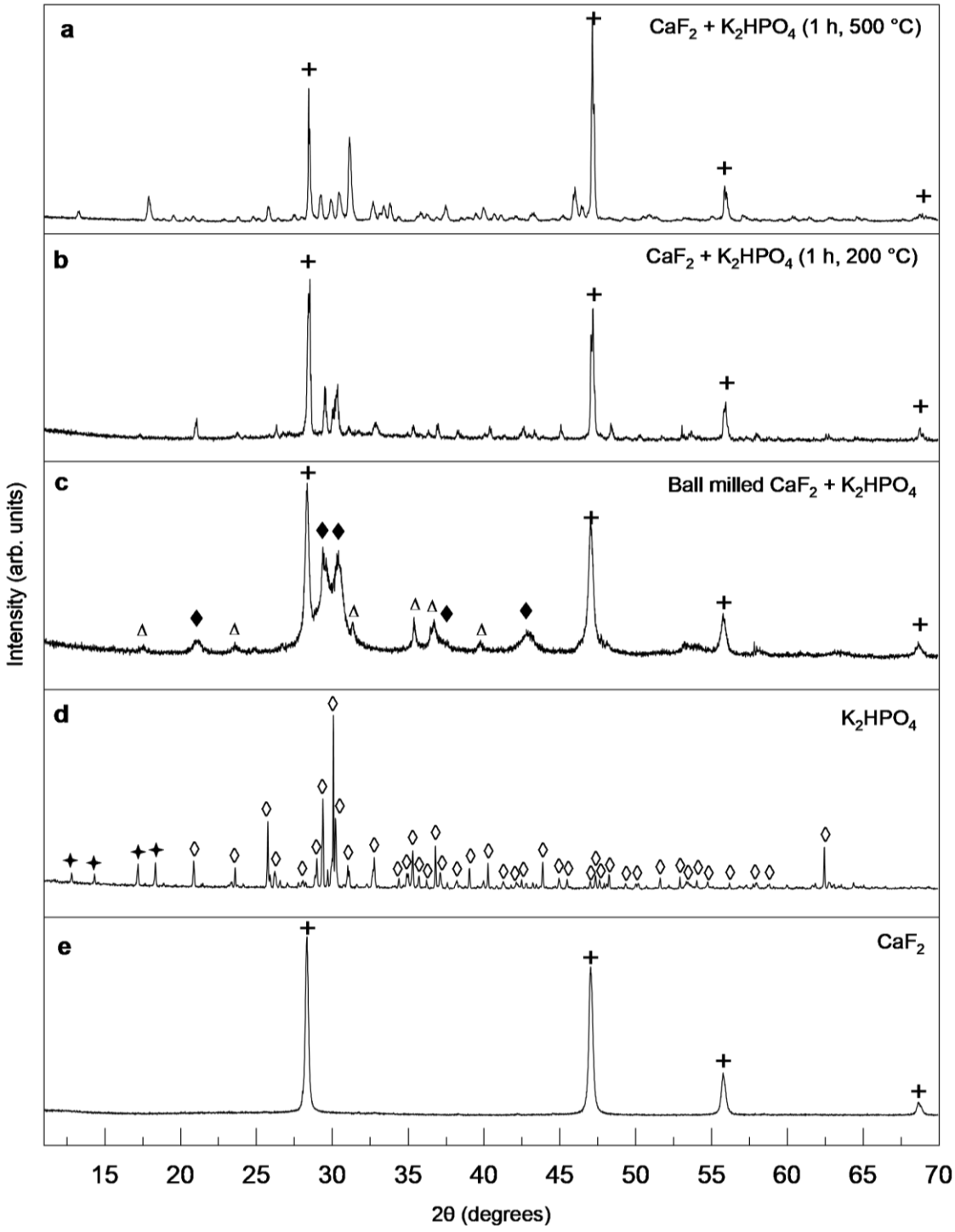

Figure 2.69. PXRD pattern of **a**) thermally treated equimolar CaF_2 and K_2HPO_4 for 1 h, at 500 °C, **b**)1 h at 200 °C, **c**) ball milled equimolar CaF_2 and K_2HPO_4 (3 h, 35 Hz) [Δ = K_3HPO_4F, ♦= $K_{2-x}Ca_y(PO_3F)_a(PO_4)_b$], **d**) K_2HPO_4 (◊ = anhydrous K_2HPO_4, ✦ = $K_2HPO_4{\cdot}3H_2O$) and **e**) CaF_2 (+).

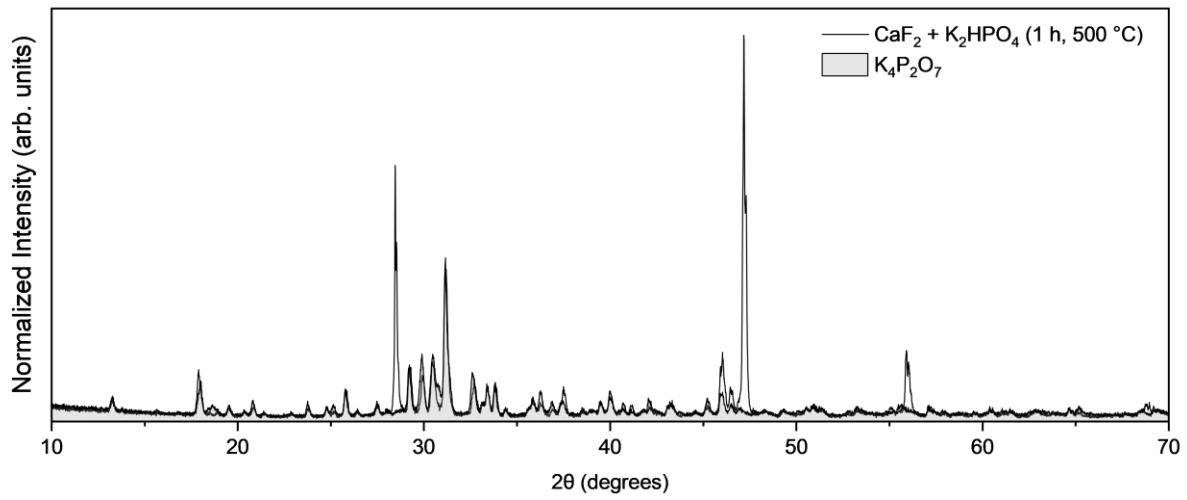

Figure 2.70. PXRD pattern of thermally treated equimolar CaF_2 and K_2HPO_4 for 1 h, at 500 °C compared to PXRD pattern of commercial potassium pyrophosphate ($K_4P_2O_7$).

Differences between the outcomes of the mechanochemical treatment and thermal treatment of CaF_2 with K_2HPO_4 suggest that conditions induced by mechanical force are critical for CaF_2 activation and its subsequent use for nucleophilic fluorination. Cutting-edge *in situ* approaches incorporating X-ray diffraction and Raman spectroscopy, in addition to thermography, offer a means to investigate spatial temperature profiles in mechanochemical reactions. [22] Tracking structural changes together with a temperature profile could offer valuable new insights on the reaction mechanism of K_2HPO_4-enabled CaF_2 activation.

2.5 Scalability

Scaling-up in mechanochemistry is the subject of various accounts acknowledging that translation from "batch" ball milling to "continuous" methods is paramount for broad usage. Twin-Screw extrusion is the leading technology for wide adoption of mechanochemistry in industry.[14] Considerable optimisation is required to formulate a scale-up protocol of impeccable reproducibility. Portion-wise addition of K_2HPO_4 to AGF using 35 mL stainless steel jars each loaded with a 16 g stainless steel ball and 6 g of material for milling afforded 21.5 g of **Fmix** (Scheme 2.24). This **Fmix** was used in the fluorination of naphthalene-2-sulfonyl chloride (5 g, 22 mmol) and gave the desired sulfonyl fluoride (**2**) in 41% yield [compared to 98% of **2** using **Fmix** prepared on 1 g scale (15 mL jar, 7 g ball)].

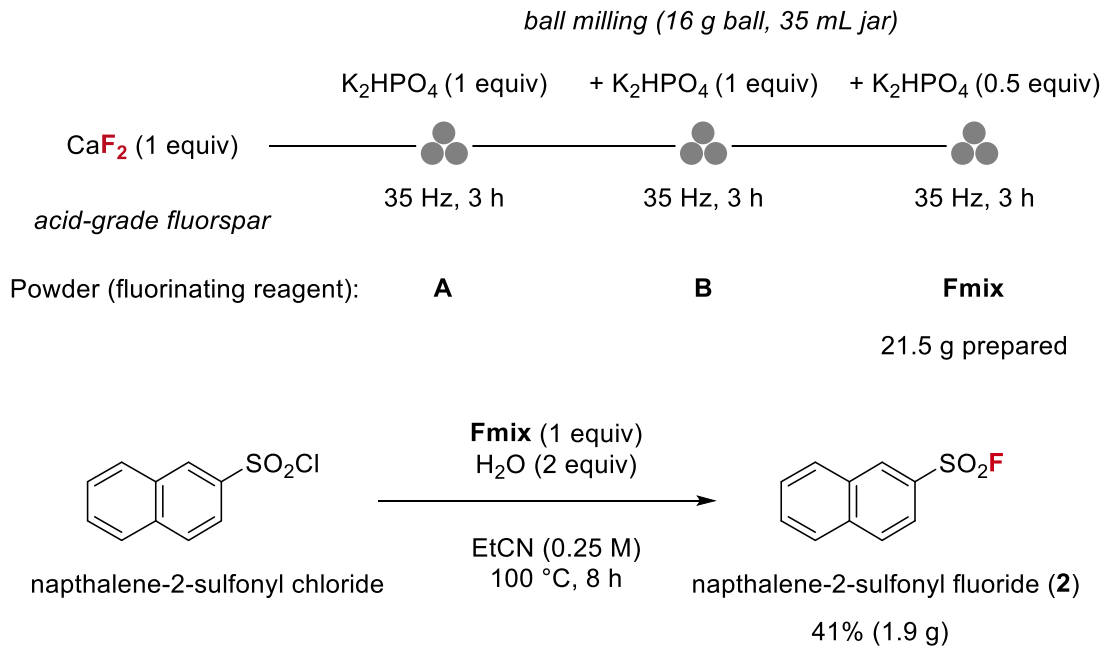

Scheme 2.24. Synthesis of **Fmix** on 4 x 6 g scale with scale-up fluorination of naphthalene-2-sulfonyl chloride on 5 g scale.

Differences in the reactivity of **Fmix** prepared on 6 g scale versus 1 g scale can be attributed to an incomplete mechanochemical reaction, as evidenced by unreacted K_2HPO_4 observed in the PXRD of **Fmix** produced on 6 g scale (see Chapter **4** for supplementary PXRD data).

The preparation of **Fmix** requires a total of 9 h of milling with portion-wise addition of K_2HPO_4 (2.5 equiv total) to AGF (1 equiv). With the view of developing a process more amenable to scale-up, alternative milling routes to prepare **Fmix** were pursued (Scheme 2.25). The reactivity of **Fmix I**, **Fmix II** and **Fmix III** was investigated in the fluorination of TsCl (0.125 mmol scale). Reaction yield was determined by quantitative ^{1}H and ^{19}F NMR spectroscopy (Table 2.18). A yield of 86% is observed using **Fmix II** yet a significant drop is observed using **Fmix III** (58%). Future work should focus on optimising **Fmix III**, where increased milling time may ameliorate the reduced reactivity observed.

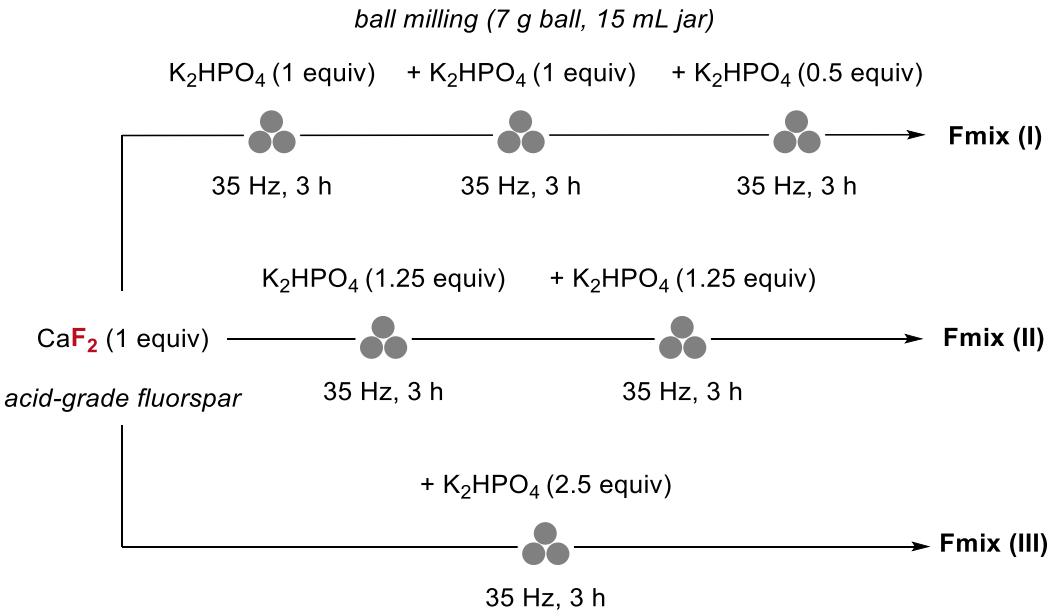

Scheme 2.25. Alternative mechanochemical routes to **Fmix**.

Table 2.18. Reactivity of **Fmix I** to **III** (prepared via different mechanochemical routes) in the fluorination of TsCl.

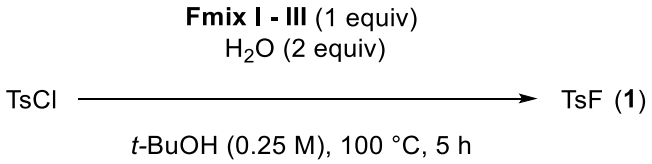

Entry	Fmix	Total milling time (h)	TsCl (%)	TsF (**1**) (%)
1	I	9	0	93
2	II	6	6	86
3	III	3	5	58

0.125 mmol scale. Yields determined by quantitative ^{19}F and ^{1}H NMR spectroscopy using FA as internal standard.

2.6 Conclusion

This work reports the mechanochemical activation of AGF (>97% CaF_2) using K_2HPO_4, to produce a new fluorine containing salts which enable nucleophilic fluorination in solution to forge S-F and C-F bonds. This study is both relevant for our fundamental understanding of fluorspar reactivity and for the design of next-generation materials that can further expand the range of fluorochemicals directly within reach from fluorspar and other untapped fluoride sources. Further mechanistic experiments are required to improve our understanding of both the composition of **Fmix** and all of the species (phases) discovered in this thesis (**X**, **Y**, **Z**, and **Z'**). Quantifying of each phase over time would be beneficial to advance our understanding of the kinetics of **Fmix** evolution and may offer insight into the pathways connecting crystalline and amorphous phases. Research along these lines might also pave the way for the development of more reactive forms of **Fmix** by maximising the formation of **X** [$K_3(HPO_4)F$] over less reactive phases **Y**, **Z**, and **Z'**.

2.7 References

1. Gomes, C. *et al.* Advanced Mechanochemistry Device for Sustainable Synthetic Processes. *ACS Omega* **5**, 10868–10877 (2020).
2. Kita, I., Matsuo, S. & Wakita, H. H_2 generation by reaction between H_2O and crushed rock: An experimental study on H_2 degassing from the active fault zone. *J. Geophys. Res.* **87**, 10789–10795 (1982).
3. Telling, J. *et al.* Rock comminution as a source of hydrogen for subglacial ecosystems. *Nature Geosci* **8**, 851–855 (2015).
4. Stone, J., Edgar, J. O., Gould, J. A. & Telling, J. Tectonically-driven oxidant production in the hot biosphere. *Nat Commun* **13**, 4529 (2022).
5. Takacs, L. The historical development of mechanochemistry. *Chem. Soc. Rev.* **42**, 7649–7659 (2013).
6. Boldyreva, E. Mechanochemistry of inorganic and organic systems: what is similar, what is different? *Chem. Soc. Rev.* **42**, 7719 (2013).
7. Takacs, L. Quicksilver from cinnabar: The first documented mechanochemical reaction? *JOM* **52**, 12–13 (2000).
8. Tan, D. & García, F. Main group mechanochemistry: from curiosity to established protocols. *Chem. Soc. Rev.* **48**, 2274–2292 (2019).
9. Haynes, W. M. *CRC Handbook of Chemistry and Physics, 95th Edition*. (CRC Press, Hoboken, 2014).
10. Takacs, L. M. Carey Lea, the first mechanochemist. *J. Mater. Sci.* **39**, 4987–4993 (2004).
11. Michalchuk, A. A. L., Boldyreva, E. V., Belenguer, A. M., Emmerling, F. & Boldyrev, V. V. Tribochemistry, Mechanical Alloying, Mechanochemistry: What is in a Name? *Frontiers in Chemistry* **9**, (2021).
12. Howard, J. L., Cao, Q. & Browne, D. L. Mechanochemistry as an emerging tool for molecular synthesis: what can it offer? *Chem. Sci.* **9**, 3080–3094 (2018).
13. Hwang, S., Grätz, S. & Borchardt, L. A guide to direct mechanocatalysis. *Chem. Commun.* **58**, 1661–1671 (2022).
14. Bolt, R. R. A., Leitch, J. A., Jones, A. C., Nicholson, W. I. & Browne, D. L. Continuous flow mechanochemistry: reactive extrusion as an enabling technology in organic synthesis. *Chem. Soc. Rev.* **51**, 4243–4260 (2022).

15. Crawford, D. E., Miskimmin, C. K. G., Albadarin, A. B., Walker, G. & James, S. L. Organic synthesis by Twin Screw Extrusion (TSE): continuous, scalable and solvent-free. *Green Chem.* **19**, 1507–1518 (2017).
16. Reichle, S. & Felderhoff, M. On the Theory and Recent Developments in "Batch Mechanochemical Synthesis – Scale-Up". in *Mechanochemistry and Emerging Technologies for Sustainable Chemical Manufacturing* (CRC Press, 2023).
17. Jones, A. C., Leitch, J. A., Raby-Buck, S. E. & Browne, D. L. Mechanochemical techniques for the activation and use of zero-valent metals in synthesis. *Nat. Synth* **1**, 763–775 (2022).
18. Linberg, K., Sander, P. C., Emmerling, F. & Michalchuk, A. A. L. In situ investigation of controlled polymorphism in mechanochemistry at elevated temperature. *RSC Mechanochem.* **1**, 43–49 (2024).
19. Michalchuk, A. A. L. & Emmerling, F. Time-Resolved In Situ Monitoring of Mechanochemical Reactions. *Angew. Chem. Int. Ed.* **61**, e202117270 (2022).
20. Bolm, C. & Hernández, J. G. Mechanochemistry of Gaseous Reactants. *Angew. Chem. Int. Ed.* **58**, 3285–3299 (2019).
21. Tricker, A. W., Samaras, G., Hebisch, K. L., Realff, M. J. & Sievers, C. Hot spot generation, reactivity, and decay in mechanochemical reactors. *Chem. Eng. J.* **382**, 122954 (2020).
22. Kulla, H. *et al.* Warming up for mechanosynthesis – temperature development in ball mills during synthesis. *Chem. Commun.* **53**, 1664–1667 (2017).
23. Martinez, V., Stolar, T., Karadeniz, B., Brekalo, I. & Užarević, K. Advancing mechanochemical synthesis by combining milling with different energy sources. *Nat Rev Chem* **7**, 51–65 (2023).
24. Silva, I. d'Anciães A., Bartalucci, E., Bolm, C. & Wiegand, T. Opportunities and Challenges in Applying Solid-State NMR Spectroscopy in Organic Mechanochemistry. *Adv. Mater.* **35**, 2304092 (2023).
25. Friščić, T. *et al.* Real-time and in situ monitoring of mechanochemical milling reactions. *Nature Chem* **5**, 66–73 (2013).
26. Lampronti, G. I. *et al.* Changing the game of time resolved X-ray diffraction on the mechanochemistry playground by downsizing. *Nat Commun* **12**, 6134 (2021).
27. Julien, P. A. & Friščić, T. Methods for Monitoring Milling Reactions and Mechanistic Studies of Mechanochemistry: A Primer. *Cryst. Growth Des.* **22**, 5726–5754 (2022).

28. Amrute, A. P., Łodziana, Z., Schreyer, H., Weidenthaler, C. & Schüth, F. High-surface-area corundum by mechanochemically induced phase transformation of boehmite. *Science* **366**, 485–489 (2019).
29. Lukin, S., Užarević, K. & Halasz, I. Raman spectroscopy for real-time and in situ monitoring of mechanochemical milling reactions. *Nat Protoc* **16**, 3492–3521 (2021).
30. Julien, P. A., Malvestiti, I. & Friščić, T. The effect of milling frequency on a mechanochemical organic reaction monitored by in situ Raman spectroscopy. *Beilstein J Org Chem* **13**, 2160–2168 (2017).
31. Lukin, S. *et al.* Isotope Labeling Reveals Fast Atomic and Molecular Exchange in Mechanochemical Milling Reactions. *J. Am. Chem. Soc.* **141**, 1212–1216 (2019).
32. Zholdassov, Y. S. *et al.* Acceleration of Diels-Alder reactions by mechanical distortion. *Science* **380**, 1053–1058 (2023).
33. Cuccu, F. *et al.* Mechanochemistry: New Tools to Navigate the Uncharted Territory of "Impossible" Reactions. *ChemSusChem* **15**, e202200362 (2022).
34. Mohapatra, H., Kleiman, M. & Esser-Kahn, A. P. Mechanically controlled radical polymerization initiated by ultrasound. *Nature Chem* **9**, 135–139 (2017).
35. Krusenbaum, A., Grätz, S., Tigineh, G. T., Borchardt, L. & Kim, J. G. The mechanochemical synthesis of polymers. *Chem. Soc. Rev.* **51**, 2873–2905 (2022).
36. Leitch, J. A. & Browne, D. L. Mechanoredox Chemistry as an Emerging Strategy in Synthesis. *Chem. Eur. J.* **27**, 9721–9726 (2021).
37. Kubota, K., Pang, Y., Miura, A. & Ito, H. Redox reactions of small organic molecules using ball milling and piezoelectric materials. *Science* **366**, 1500–1504 (2019).
38. Reichle, S., Felderhoff, M. & Schüth, F. Mechanocatalytic Room-Temperature Synthesis of Ammonia from Its Elements Down to Atmospheric Pressure. *Angew. Chem. Int. Ed.* **60**, 26385–26389 (2021).
39. Han, G.-F. *et al.* Mechanochemistry for ammonia synthesis under mild conditions. *Nat. Nanotechnol.* **16**, 325–330 (2021).
40. Henderson, R. K. *et al.* Expanding GSK's solvent selection guide – embedding sustainability into solvent selection starting at medicinal chemistry. *Green Chem.* **13**, 854 (2011).
41. Gomollón-Bel, F. Ten Chemical Innovations That Will Change Our World: IUPAC identifies emerging technologies in Chemistry with potential to make our planet more sustainable. *Chemistry International* **41**, 12–17 (2019).

42. Borodkin, G. I., Elanov, I. R. & Shubin, V. G. Mechanochemical Fluorination of Naproxen and Its Salts with F–TEDA–BF4. *Russ J Org Chem* **59**, 1858–1866 (2023).
43. Howard, J. L., Sagatov, Y., Repusseau, L., Schotten, C. & Browne, D. L. Controlling reactivity through liquid assisted grinding: the curious case of mechanochemical fluorination. *Green Chem.* **19**, 2798–2802 (2017).
44. Riley, W., Jones, A. C., Singh, K., Browne, D. L. & Stuart, A. M. Accessing novel fluorinated heterocycles with the hypervalent fluoroiodane reagent by solution and mechanochemical synthesis. *Chem. Commun.* **57**, 7406–7409 (2021).
45. Wang, X. *et al.* Mechanochemical Synthesis of Aryl Fluorides by Using Ball Milling and a Piezoelectric Material as the Redox Catalyst. *Angew. Chem. Int. Ed.* **62**, e202307054 (2023).
46. Said, M. S. *et al.* A New TBAF Complex, Highly Stable, Facile and Selective Source for Nucleophilic Fluorination: Applications in Batch and Flow Chemistry. *Asian Journal of Organic Chemistry* **9**, 1022–1026 (2020).
47. Dalidovich, T., Nallaparaju, J. V., Shalima, T., Aav, R. & Kananovich, D. G. Mechanochemical Nucleophilic Substitution of Alcohols via Isouronium Intermediates. *ChemSusChem* **15**, e202102286 (2022).
48. Passia, M. T., Amer, M. M., Demaerel, J. & Bolm, C. Synthesis of Sulfonyl, Sulfonimidoyl, and Sulfoxyl Fluorides under Solvent-Free Mechanochemical Conditions in a Mixer Mill by Imidazole-to-Fluorine Exchange. *ACS Sustainable Chem. Eng.* **11**, 6838–6843 (2023).
49. Vogel, P., Figueira, S., Muthukrishnan, S. & Mack, J. Environmentally benign nucleophilic substitution reactions. *Tetrahedron Lett.* **50**, 55–56 (2009).
50. Scholz, G. Mechanochemistry of fluoride solids: from mechanical activation to mechanically stimulated synthesis. *ChemTexts* **7**, 16 (2021).
51. Flora, N. J., Yoder, C. H. & Jenkins, H. D. B. Lattice Energies of Apatites and the Estimation of $\Delta H_f°(PO_4^{3-},g)$. *Inorg. Chem.* **43**, 2340–2345 (2004).
52. Dorozhkin, S. V. Calcium orthophosphates in dentistry. *J Mater Sci: Mater Med* **24**, 1335–1363 (2013).
53. Nikčević, I. *et al.* Mechanochemical synthesis of nanostructured fluorapatite/fluorhydroxyapatite and carbonated fluorapatite/fluorhydroxyapatite. *J. Solid State Chem.* **177**, 2565–2574 (2004).

54. Bulina, N. V., Makarova, S. V., Prosanov, I. Yu., Vinokurova, O. B. & Lyakhov, N. Z. Structure and thermal stability of fluorhydroxyapatite and fluorapatite obtained by mechanochemical method. *J. Solid State Chem.* **282**, 121076 (2020).
55. Scholz, G., Dörfel, I., Heidemann, D., Feist, M. & Stösser, R. Nanocrystalline CaF2 particles obtained by high-energy ball milling. *J. Solid State Chem.* **179**, 1119–1128 (2006).
56. Molaiyan, P. & Witter, R. Surface defect-enhanced conductivity of calcium fluoride for electrochemical applications. *Mater. Des. Process. Commun.* **1**, e44 (2019).
57. Kaduk, J. A. *et al.* Powder diffraction. *Nat Rev Methods Primers* **1**, 1–22 (2021).
58. Evans, J. S. O. & Evans, I. R. Structure Analysis from Powder Diffraction Data: Rietveld Refinement in Excel. *J. Chem. Educ.* **98**, 495–505 (2021).
59. Rietveld, H. M. Line profiles of neutron powder-diffraction peaks for structure refinement. *Acta Cryst* **22**, 151–152 (1967).
60. Coelho, A. A. TOPAS and TOPAS-Academic: an optimization program integrating computer algebra and crystallographic objects written in C++. *J Appl Cryst* **51**, 210–218 (2018).
61. Mandile, A. J. & Hutton, A. C. Quantitative X-ray diffraction analysis of mineral and organic phases in organic-rich rocks. *Int. J. Coal Geol.* **28**, 51–69 (1995).
62. Lou, T. S.-B. & Willis, M. C. Sulfonyl fluorides as targets and substrates in the development of new synthetic methods. *Nat Rev Chem* **6**, 146–162 (2022).
63. Nielsen, M. K., Ahneman, D. T., Riera, O. & Doyle, A. G. Deoxyfluorination with Sulfonyl Fluorides: Navigating Reaction Space with Machine Learning. *J. Am. Chem. Soc.* **140**, 5004–5008 (2018).
64. Davies, W. & Henry Dick, J. CCLXXXVI Aromatic sulphonyl fluorides. A convenient method of preparation. *J. Chem. Soc. (Resumed)* **0**, 2104–2109 (1931).
65. Davies, W. & Dick, J. H. Aliphatic sulphonyl fluorides. *J. Chem. Soc.* 483 (1932) doi:10.1039/jr9320000483.
66. Bianchi, T. A. & Cate, L. A. Phase transfer catalysis. Preparation of aliphatic and aromatic sulfonyl fluorides. *J. Org. Chem.* **42**, 2031–2032 (1977).
67. Dong, J., Krasnova, L., Finn, M. G. & Sharpless, K. B. Sulfur(VI) Fluoride Exchange (SuFEx): Another Good Reaction for Click Chemistry. *Angew. Chem. Int. Ed.* **53**, 9430–9448 (2014).
68. Halasz, I. *et al.* In situ and real-time monitoring of mechanochemical milling reactions using synchrotron X-ray diffraction. *Nat Protoc* **8**, 1718–1729 (2013).

69. Wernik, M., Poechlauer, P., Schmoelzer, C., Dallinger, D. & Kappe, C. O. Design and Optimization of a Continuous Stirred Tank Reactor Cascade for Membrane-Based Diazomethane Production: Synthesis of α-Chloroketones. *Org. Process Res. Dev.* **23**, 1359–1368 (2019).
70. Trautnitz, M. F. K., Haas, T., Schubert, H. & Seitz, M. Unexpected discovery of calcium cryptates with exceptional stability. *Chem. Commun.* **56**, 9874–9877 (2020).
71. Bare, G. A. L. Synthesis of Sulfonyl Fluorides Using Direct Chloride/Fluoride Exchange in Potassium Fluoride and Water/Acetone. *J. Org. Chem.* **88**, 4761–4764 (2023).
72. Lis, T. Isomorphous crystals: K_2HPO_4 and $K_5Na(HPO_4)_3$. *Acta Cryst C* **50**, 484–487 (1994).
73. Sadlowski, C. *et al.* Nitro sulfonyl fluorides are a new pharmacophore for the development of antibiotics. *Mol. Syst. Des. Eng.* **3**, 599–603 (2018).
74. Zheng, Q., Dong, J. & Sharpless, K. B. Ethenesulfonyl Fluoride (ESF): An On-Water Procedure for the Kilogram-Scale Preparation. *J. Org. Chem.* **81**, 11360–11362 (2016).
75. Aguilar, B., Amissah, F., Duverna, R. & Lamango, N. S. Polyisoprenylation Potentiates the Inhibition of Polyisoprenylated Methylated Protein Methyl Esterase and the Cell Degenerative Effects of Sulfonyl Fluorides. *Curr Cancer Drug Targets* **11**, 752–762 (2011).
76. Nielsen, M. K., Ugaz, C. R., Li, W. & Doyle, A. G. PyFluor: A Low-Cost, Stable, and Selective Deoxyfluorination Reagent. *J. Am. Chem. Soc.* **137**, 9571–9574 (2015).
77. Guo, J. *et al.* Rapid Deoxyfluorination of Alcohols with *N* -Tosyl-4-chlorobenzenesulfonimidoyl Fluoride (SulfoxFluor) at Room Temperature. *Chem. Eur. J.* **25**, 7259–7264 (2019).
78. Brouwer, A. J. *et al.* Peptido Sulfonyl Fluorides as New Powerful Proteasome Inhibitors. *J. Med. Chem.* **55**, 10995–11003 (2012).
79. *Modern Synthesis Processes and Reactivity of Fluorinated Compounds: Progress in Fluorine Science*. (Elsevier, Amsterdam ; Boston, 2016).
80. Goldberg, N. W., Shen, X., Li, J. & Ritter, T. AlkylFluor: Deoxyfluorination of Alcohols. *Org. Lett.* **18**, 6102–6104 (2016).
81. Ortalli, S., Ford, J., Trabanco, A. A., Tredwell, M. & Gouverneur, V. Photoredox Nucleophilic (Radio)fluorination of Alkoxyamines. *J. Am. Chem. Soc.* **146**, 11599–11604 (2024).

82. Webb, E. W. *et al.* Nucleophilic (Radio)Fluorination of Redox-Active Esters via Radical-Polar Crossover Enabled by Photoredox Catalysis. *J. Am. Chem. Soc.* **142**, 9493–9500 (2020).
83. Liu, W., Huang, X. & Groves, J. T. Oxidative aliphatic C-H fluorination with manganese catalysts and fluoride ion. *Nat Protoc* **8**, 2348–2354 (2013).
84. Huang, X., Liu, W., Hooker, J. M. & Groves, J. T. Targeted Fluorination with the Fluoride Ion by Manganese-Catalyzed Decarboxylation. *Angew. Chem. Int. Ed.* **54**, 5241–5245 (2015).
85. Brabham, C. *et al.* Focus on Weed Control: Indaziflam Herbicidal Action: A Potent Cellulose Biosynthesis Inhibitor. *Plant Physiology* **166**, 1177 (2014).
86. Burgess, J. P. *et al.* Identification of [^{14}C]Fluasterone Metabolites in Urine and Feces Collected from Dogs after Subcutaneous and Oral Administration of [^{14}C]Fluasterone. *Drug Metab Dispos* **37**, 1089–1097 (2009).
87. de la Torre, B. G. & Albericio, F. The Pharmaceutical Industry in 2020. An Analysis of FDA Drug Approvals from the Perspective of Molecules. *Molecules* **26**, 627 (2021).
88. Campbell, M. G. & Ritter, T. Modern Carbon–Fluorine Bond Forming Reactions for Aryl Fluoride Synthesis. *Chem. Rev.* **115**, 612–633 (2015).
89. Britton, R. *et al.* Contemporary synthetic strategies in organofluorine chemistry. *Nat Rev Methods Primers* **1**, 47 (2021).
90. Hansch, C. & Leo, A. *Substituent Constants for Correlation Analysis in Chemistry and Biology*. (Wiley, 1979).
91. Tilstam, U. Sulfolane: A Versatile Dipolar Aprotic Solvent. *Org. Process Res. Dev.* **16**, 1273–1278 (2012).
92. Iashin, V., Wirtanen, T. & Perea-Buceta, J. E. Tetramethylammonium Fluoride: Fundamental Properties and Applications in C-F Bond-Forming Reactions and as a Base. *Catalysts* **12**, 233 (2022).
93. Gonay, M., Batisse, C. & Paquin, J.-F. Recent Advances in the Synthesis of Acyl Fluorides. *Synthesis* **53**, 653–665 (2020).
94. Ryan, S. J., Schimler, S. D., Bland, D. C. & Sanford, M. S. Acyl Azolium Fluorides for Room Temperature Nucleophilic Aromatic Fluorination of Chloro- and Nitroarenes. *Org. Lett.* **17**, 1866–1869 (2015).
95. Tullock, C. W. & Coffman, D. D. Synthesis of Fluorides by Metathesis with Sodium Fluoride. *J. Org. Chem.* **25**, 2016–2019 (1960).

96. Oláh, G., Kuhn, S. & Beke, S. Darstellung und Untersuchung organischer Fluorverbindungen XX. Darstellung von Säurefluoriden. *Chemische Berichte* **89**, 862–864 (1956).
97. Tryniszewski, M. & Barbasiewicz, M. Gram-Scale Preparation of Acyl Fluorides and Their Reactions with Hindered Nucleophiles. *Synthesis* **54**, 1446–1460 (2021).
98. Bonnefoy, C. *et al.* Unlocking the Power of Acyl Fluorides: A Comprehensive Guide to Synthesis and Properties. *Eur. J. Org. Chem.* **27**, e202400142 (2024).
99. Brunner, H. *et al.* Tuning the Dissociation of the Fe–PPh_2(OR) Bond in Chiral-at-Metal Complexes [CpFe(Prophos)PPh_2(OR)]PF_6 (R = Me, Et, iPr, *t*Bu). The Preparative Trick of $N2_2$ Bubbling. *Organometallics* **32**, 4904–4911 (2013).
100. Hudlicky, M. Chemical shifts of fluorine in hydrogen fluoride and fluoride ion. *J. Fluor. Chem.* **28**, 461–472 (1985).
101. Zhai, F., Xin, T., Geeson, M. B. & Cummins, C. C. Sustainable Production of Reduced Phosphorus Compounds: Mechanochemical Hydride Phosphorylation Using Condensed Phosphates as a Route to Phosphite. *ACS Cent. Sci.* **8**, 332–339 (2022).
102. New Baby in the Fluorine Family. *Ind. Eng. Chem.* **40**, 7A-24A (1948).
103. Rowley, H. H. & Stuckey, J. E. Preparation and Properties of Calcium Monofluorophosphate Dihydrate. *J. Am. Chem. Soc.* **78**, 4262–4263 (1956).
104. Payen, J.-L., Durand, J., Cot, L. & Galigne, J.-L. Etude structurale du monofluorophosphate de potassium K_2PO_3F. *Can. J. Chem.* **57**, 886–889 (1979).
105. Lu, B.-Q. *et al.* Short-Range Structure of Amorphous Calcium Hydrogen Phosphate. *Crystal Growth & Design* **19**, 3030–3038 (2019).
106. Bartel, C. J. *et al.* New tolerance factor to predict the stability of perovskite oxides and halides. *Sci. Adv.* **5**, eaav0693 (2019).
107. Ratuszna, A., Rousseau, M. & Daniel, P. Crystal structure of $KCaF_3$ determined by the Rietveld profile method. *Powder Diffr.* **12**, 70–75 (1997).
108. Grimmer, A.-R., Jost, K.-H., Müller, D. & Neels, J. Kristallographische und hochauflusende festkurper-NMR-untersuchungen an $K_3F(PO_3F)$. *J. Fluor. Chem.* **34**, 347–360 (1987).
109. Skakle, J. M. S., Fletcher, J. G. & West, A. R. The crystal structures of the potassium oxyfluorides, K_3SeO_4F and $K_3PO_3F_2$. *Anales de Quimica* **92**, 358–361 (1996).
110. Reif, B., Ashbrook, S. E., Emsley, L. & Hong, M. Solid-state NMR spectroscopy. *Nat Rev Methods Primers* **1**, 1–23 (2021).

111. Miller, J. M. Fluorine-19 magic-angle spinning NMR. *Prog. Nucl. Magn. Reson. Spectrosc.* **28**, 255–281 (1996).

112. Bollmeyer, M. M. & Yoder, C. H. Incorporation of fluorophosphate in apatite. *Polyhedron* **145**, 176–181 (2018).

113. Chai, K., Cheng, S., Li, H. & Dai, B. Modulation of perovskite-related frameworks induced by alkaline earth metals in phosphate fluorides A_2MPO_4F (A = K, Rb; M = Ba, Ca). *New J. Chem.* **43**, 7839–7845 (2019).

114. Kageyama, H. *et al.* Expanding frontiers in materials chemistry and physics with multiple anions. *Nat Commun* **9**, 772 (2018).

115. Frazier, A. W., Smith, J. P., Lehr, J. R. & Brown, W. E. Crystallography of the Calcium Potassium Phosphate $CaK_3H(PO_4)_2$. *Inorg. Chem.* **1**, 949–951 (1962).

116. Endo, S., Chino, T., Tsuboi, S. & Koto, K. Pressure-induced transition of the hydrogen bond in the ferroelectric compounds KH_2PO_4 and KD_2PO_4. *Nature* **340**, 452–455 (1989).

117. Yu, P., Marshall, J. W., Sadek, P. & Walton, J. H. Speciation of Phosphorus in Pet Foods by Solid-State ^{31}P-MAS-NMR Spectroscopy. *J Agric Food Chem* **71**, 8602–8612 (2023).

118. Turner, G. L., Smith, K. A., Kirkpatrick, R. J. & Oldfieldt, E. Structure and cation effects on phosphorus-31 NMR chemical shifts and chemical-shift anisotropies of orthophosphates. *J. Magn. Reson.* **70**, 408–415 (1986).

119. Hayashi, S. & Hayamizu, K. High-Resolution Solid-State ^{31}P NMR of Alkali Phosphates. *Bull. Chem. Soc. Jpn.* **62**, 3061–3068 (1989).

120. Haubenreisser, U., Sternberg, U. & Grimmer, A.-R. High-field ^{31}P N.M.R. investigations of the chemical shielding and indirect dipolar coupling of polycrystalline fluorophosphates. *Mol. Phys.* **60**, 151–163 (1987).

121. Yu, Y. *et al.* Advanced solid-state ^{1}H/^{31}P NMR characterization of pyrophosphate-doped calcium phosphate cements for biomedical applications: The structural role of pyrophosphate. *Ceram. Int.* **45**, 20642–20655 (2019).

122. Louati, B., Hlel, F., Guidara, K. & Gargouri, M. Analysis of the effects of thermal treatments on CaHPO4 by ^{31}P NMR spectroscopy. *J. Alloys Compd.* **394**, 13–18 (2005).

123. Rodríguez-Lorenzo, L. M., Hart, J. N. & Gross, K. A. Influence of fluorine in the synthesis of apatites. Synthesis of solid solutions of hydroxy-fluorapatite. *Biomaterials* **24**, 3777–3785 (2003).

124. Vaughn, J. S., Lindsley, D. H., Nekvasil, H., Hughes, J. M. & Phillips, B. L. Complex F,Cl Apatite Solid Solution Investigated Using Multinuclear Solid-State NMR Methods. *J. Phys. Chem. C* **122**, 530–539 (2018).

125. Wei, M., Evans, J. H., Bostrom, T. & Grøndahl, L. Synthesis and characterization of hydroxyapatite, fluoride-substituted hydroxyapatite and fluorapatite. *J. Mater. Sci.: Mater. Med.* **14**, 311–320 (2003).

126. Vandeginste, V., Cowan, C., Gomes, R. L., Hassan, T. & Titman, J. Natural fluorapatite dissolution kinetics and Mn^{2+} and Cr^{3+} metal removal from sulfate fluids at 35 °C. *J. Hazard. Mater.* **389**, 122150 (2020).

127. Rodríguez-Lorenzo, L. M., Hart, J. N. & Gross, K. A. Structural and Chemical Analysis of Well-Crystallized Hydroxyfluorapatites. *J. Phys. Chem. B* **107**, 8316–8320 (2003).

128. Frazier, A. W., Scheib, R. M. & Lehr, J. R. System potassium oxide-pyrophosphoric acid-water at 0 and 25 deg. *J. Agric. Food Chem.* **20**, 146–150 (1972).

129. Moore, E. A. & Smart, L. E. *Solid State Chemistry: An Introduction*. (CRC Press, 2012).

130. Vartanian, A. Breaking down ceramic synthesis. *Nat Rev Mater* **6**, 464–464 (2021).

3. Low-Temperature Activation of Fluorspar in Water via Brønsted and Lewis Acid Cooperativity

The work described in this chapter was carried out in collaboration with Dr. Immo Klose and Dr. Anirban Mondal. The proof of concept and preliminary experimental work was performed by Dr. Immo Klose. Dr. Anirban Mondal completed the development of reaction conditions for the synthesis of tetrafluoroboric acid (from acid-grade fluorspar and metspar) and conducted all Balz-Schiemann fluorination chemistry to prepare fluoroarenes **69** to **81**. Dr. Coral Mycroft (NMR facility at the University of Oxford) assisted in conducting $^{19}F-^{29}Si$ rINEPT NMR experiments.

The results of this chapter have been partially described, see:

I. Klose, C. Patel, A. Mondal, A. Schwarz, G. Pupo, V. Gouverneur, Fluorspar to fluorochemicals upon low-temperature activation in water. *Nature* (accepted 2024).

3.1 Introduction

3.1.1 Fluorspar Activation using Brønsted Acid

For decades, alternative routes to HF beyond the traditional H_2SO_4-dependant pathway have been sought, all featuring inorganic Brønsted acids and requiring harsh reaction conditions. An early example was disclosed by Furcht and Scholz in 1980 demonstrating that CaF_2 in the presence of HCl ($pK_a = -6.2$) could be converted to anhydrous HF at temperatures above 300 °C (Scheme 3.1).[1] In this heterogenous gas-solid phase reaction, the full consumption of CaF_2 is hindered by the formation of solid $CaCl_2$ on the core of unreacted solid CaF_2, a phenomenon described as the shrinking core model.[2] Temperatures as high as 600 °C are required for quantitative conversion of CaF_2 to HF. At room temperature, the formation of CaF_2 (ΔU_L 2640 kJ/mol) from gaseous HF and solid $CaCl_2$ (ΔU_L 2268 kJ/mol) is thermodynamically favoured.[1]

$$CaF_2\,(s) + 2HCl\,(g) \xrightarrow[600\ °C]{} CaCl_2\,(s) + 2HF\,(g)$$

Scheme 3.1. Synthesis of HF from CaF_2 using HCl.

The reaction of CaF_2 with H_2SO_4 ($pK_a = -2.8$, 2.0) has also been studied using synthetic CaF_2 sludge from waste streams and silica-containing fluorite tailings produced as waste from the mining industry.[3] A study by Epov and co-workers, which examined the reaction of fluorite ore (92% CaF_2) combined with 2.45 % α-quartz (SiO_2) and concentrated H_2SO_4, highlighted the beneficial effect of SiO_2 on the breakdown of fluorite (Scheme 3.2).[4] A fluoride ion recovery of 77% in the form of hexafluorosilicic acid (H_2SiF_6) at 120 °C was

reported. The *in situ* generation of HF from solid CaF_2 with H_2SO_4 in organic solvents has also been disclosed by Sasson and co-workers.[5] In their study, dropwise addition of 98% H_2SO_4 to a slurry of CaF_2 in dichloromethane stirred using a mechanical stirrer is reported to give an organic solution of HF.

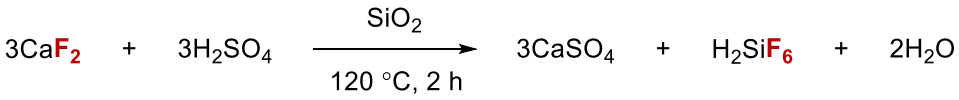

Scheme 3.2. Reaction of fluorite (92% CaF_2) with H_2SO_4 in the presence of α-quartz (SiO_2).[4]

Almost 125 years ago, the reactions of metallic fluorides with naturally occurring organic acids, namely oxalic acid ($C_2H_2O_4$, m.p. 189 °C–191 °C) and tartaric acid ($C_4H_6O_6$, m.p. 170 - 172 °C), was studied by Paternó and Alvisi.[6] When added to heated solutions of oxalic acid or tartaric acid, the researchers observed the complete consumption of powdered fluorspar. While these initial outcomes indicated the potential for fluorspar activation using an organic acid, the research did not progress further. In recent times, reactions between organic acids and metal fluorides were directed towards KHF_2 and KF for the construction of B–F bonds from fluorophilic boron precursors serving as Lewis acids.

The utility of potassium organotrifluoroborate (RBF_3K) salts in synthesis became widely popularised due to their role as robust alternatives to boronic acids in metal catalysed cross-coupling chemistry.[7] Potassium bifluoride (KHF_2) was proven by Vedejs *et al.* in 1995 to be a highly efficient fluorinating agent for the synthesis of organodifluoroboranes from organoboronic acids.[8] The reaction involves KHF_2 as a fluoride source that can activate the boronic acid through ligand exchange at boron, operating under weakly acidic conditions, to liberate the corresponding RBF_3K salt and HF. Despite the utility of this reaction, KHF_2 is

corrosive to glassware, resulting in etching and often necessitating the use of PTFE or plastic vessels. An alternative general "non-etching" approach employing KF and L-(+)-tartaric acid (pK_a 3.0, 4.3) as a Brønsted acid for the preparation of RBF_3K salts was reported by Lloyd-Jones and Lennox in 2012 (Scheme 3.3).[9]

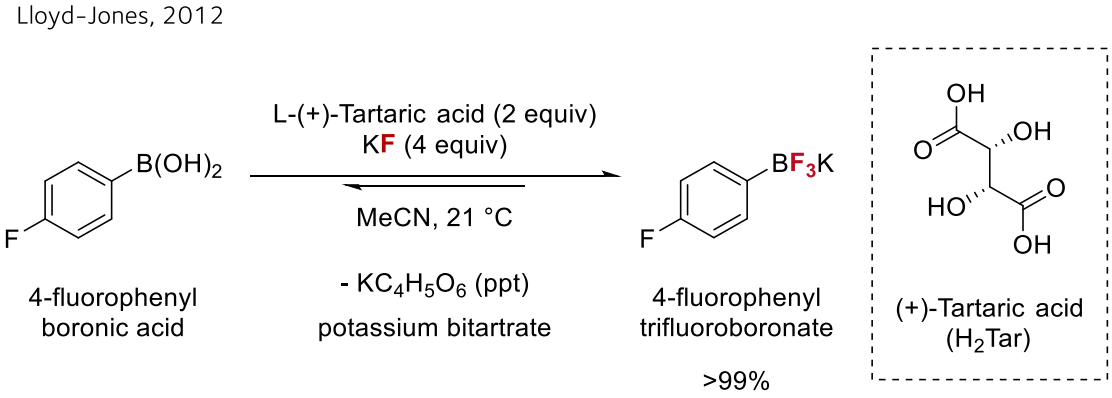

Scheme 3.3. Conversion of 4-fluorophenyl boronic acid to potassium 4-fluorophenyltrifluoroboronate using KF in the presence of L-(+)-tartaric acid.

L-(+)-Tartaric acid ($C_4H_6O_6$) is a cheap and readily handled solid, and the monopotassium salt (potassium bitartrate, "cream of tartar") exhibits low solubility in most organic solvents (insoluble in ethanol). By adding L-(+)-tartaric acid to a mixture of boronic acid and KF in acetonitrile, the equilibrium between aryl boronic acid, potassium fluoride and potassium trifluoroborate salt is driven toward the product through precipitation of potassium bitartrate ($KC_4H_5O_6$) (Scheme 3.4). Recently, a similar protocol was applied to bis-(pinacolato)diboron (B_2pin_2) to yield cesium and potassium trifluoroboronate products (PinB-BF_3M, M = K or Cs) using CsF and KF, respectively.[10]

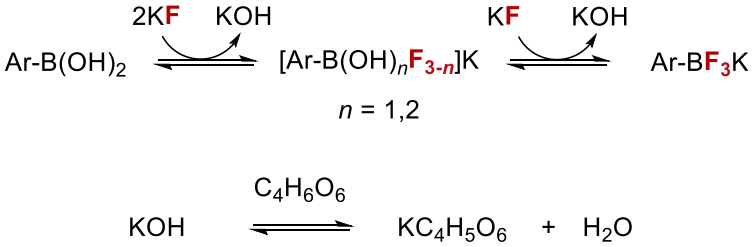

Scheme 3.4. Equilibrium between aryl boronic acid [$ArB(OH)_3$] and KF with mixed species, the second equation shows the potential for L-(+)-tartaric acid to drive the generation of the aryl trifluoroboronate product [$ArBF_3K$] through precipitation of $KC_4H_5O_6$.

In contrast to other metal fluorides, the activation of fluorspar using an organic Brønsted acid (with or without a Lewis acid) has received less attention. The synergistic use of a Brønsted acid and an appropriate fluorophilic Lewis acid to activate CaF_2, with calcium sequestration as an insoluble salt and simultaneous HF capture in a form appropriate for subsequent fluorination, could open a new pathway to fluorochemicals from fluorspar. Among the Lewis acids, boron and silicon stand out owing to the exceptional bond strengths of the B-F (732 kJ/mol) and Si-F (576 kJ/mol) bonds and the corresponding inorganic fluoride's (e.g. BF_4^-) unique reactivity, which makes them well-suited for downstream fluorochemical synthesis. The following part of this chapter briefly introduces the chemistry and synthesis of boron fluorides and silicon fluorides.

3.1.2 Boron Fluorides

In its neutral form, boron's outer shell bonding electrons ($2s^2$, $3p^1$) can participate in three sp^2 hybridised bonds, resulting in a trigonal planar configuration with an unoccupied *p*-orbital perpendicular to the plane. The unoccupied *p*-orbital in sp^2 boron compounds play a crucial role in determining their reactivity and physical traits, as they are open to electron donation from Lewis bases such as fluoride. Upon coordination, an anionic tetrahedral "ate" complex forms. The tetrafluoroborate anion (BF_4^-) stands out as one of the simplest complexes, recognised for its small size, non-nucleophilic behaviour, resistance to coordination (functioning as a weakly coordinating anion), and overall stability. Owing to these attributes, BF_4^- finds widespread use across organic chemistry. Tetrafluoroborate is commonly used in ionic liquids, as a spectator for chelates of catalytic transition metals and as a counter-ion to highly reactive cations (e.g., nitrosonium, nitronium, pyrylium and aryldiazonium).[11]

Tetrafluoroboric acid (HBF_4) is a colourless and toxic acid that does not exist in pure form, however, HBF_4 hydrates are well-characterised.[12,13] HBF_4 can be prepared from boron trifluoride (BF_3), which in turn is manufactured on technical scale by the reaction of either boron(III) oxide (B_2O_3) or boric acid [$B(OH)_3$] with HF (Scheme 3.5).[14]

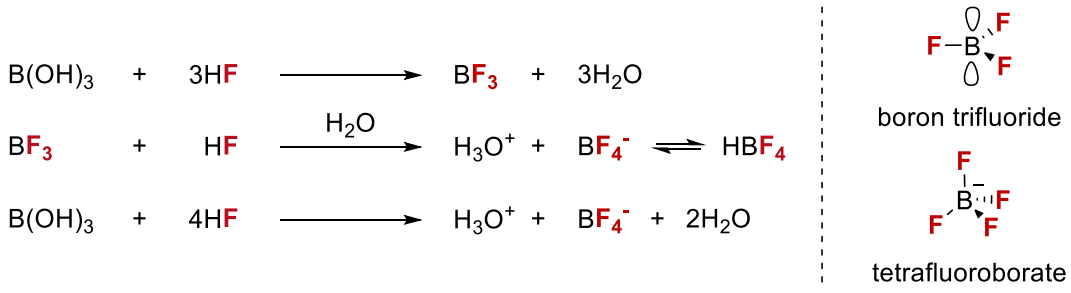

Scheme 3.5. Preparation of tetrafluoroboric acid via boric acid [$B(OH)_3$] and HF.

Metal tetrafluoroborate salts are synthesised from aq. HBF_4 and metal hydroxides or carbonates.[14] In aqueous solution, HBF_4 exists in equilibrium with a hydrolysis intermediate HBF_3OH and to a lesser extent, $HBF_2(OH)_2$ and HBF_3OH which have been characterised by ^{11}B and ^{19}F NMR spectroscopy (Scheme 3.6).[13] The acidity of each hydrolysed species decreases with each fluoride displacement, as unveiled by kinetic studies by Wamser on the reaction of HF with boric acid in water.[15]

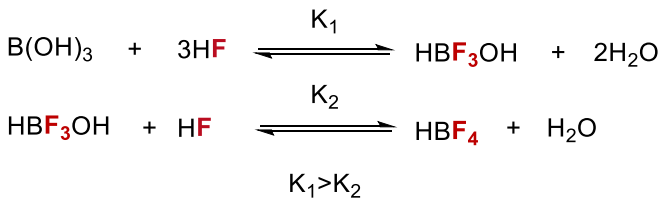

Scheme 3.6. Equilibrium between $B(OH)_3$, HF, HBF_3OH and HBF_4, where the reaction between $B(OH)_3$ and HF results in immediate formation of HBF_3OH, followed by a slower reaction with HF to afford HBF_4.

As a fluorinating reagent, tetrafluoroborates have wide synthetic potential in a host of nucleophilic fluorination reactions reliant on fluoride transfer from the BF_4^- anion.[11] Among these reactions, the Balz-Schiemann reaction is considered one of the most important fluorination reactions. It entails the thermal decomposition of aniline-derived diazonium tetrafluoroborate salts into fluoroarenes with excellent regioselectivity. Mechanistic studies support an S_N1-type heterolytic dediazotization mechanism, which involves the generation of an aryl cation with loss of nitrogen (N_2) followed by nucleophilic attack of fluoride directly transferred from the BF_4^- anion (Scheme 3.7).

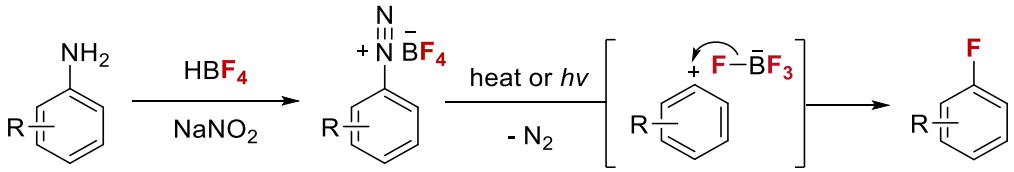

Scheme 3.7. Diazotization of an aniline followed by fluorination of the corresponding aryl diazonium salt (Balz–Schiemann reaction).

Since this key discovery, alternative approaches to fluorodediazoniation have been developed, including photochemical variants.[16,17] Industrially, fluorodediazoniation is one of the most commonly used methods for the production of (hetero)aryl fluorides that are inaccessible by S_NAr fluorination, for example, commercial 3-fluoropyridine is prepared by diazotization of 3-aminopyridine in anhydrous HF.[18] Importantly, unlike S_NAr fluorination, activated electron-poor arenes are not required for fluorodediazoniation, thus expanding the substrate scope to electron-rich and -neutral (hetero)fluoroarenes. However, the instability of the aryl diazonium tetrafluoroborate salt can lead to premature loss of N_2, resulting in sudden pressure build-ups and, in some cases, explosions.[19,20] To avoid the isolation of the diazonium salt, methodologies relying on *in situ* diazonium salt formation or operating under flow conditions that are amenable to large-scale processes (>1 kg) have been reported.[21]

3.1.3 Silicon Fluorides

The outer shell bonding electrons in neutral silicon ($1s^2$, $2s^2$, $2p^6$, $3s^2$, $3p^2$) allows it to engage in four sp^3 hybrid orbitals, resulting in a tetrahedral geometry, where the central silicon atom shares an electron pair with each of the four atoms bonded to it. The availability of vacant *d*-orbitals on silicon means that five- or six-coordinate intermediates or transition states are readily accessible.[22] The larger size of silicon also means that incoming reagents

are less sterically encumbered during attack at the silicon centre, compared to carbon analogues. However, although silicon has five 3*d* orbitals, its covalency does not rise above six. A well-documented example of the excitation of the silicon valency shell from 3sp^3 hybridization to 3sp^3d^2 hybridization is observed in the fluorosilicate anion (SiF_6^{2-}), which has an octahedral arrangement of fluorine around silicon. Silicon tetrafluoride (SiF_4, b.p. −90.3 °C) is a colourless gas that is unreactive in strictly anhydrous conditions, yet reacts rapidly in presence of moisture to form hexafluorosilicic acid (H_2SiF_6). SiF_4 forms via the reaction of SiO_2 with HF under anhydrous conditions, a process which may be realized by treatment of fluorspar and SiO_2 with concentrated H_2SO_4. H_2SiF_6 is formed if the SiF_4 is passed through steam.

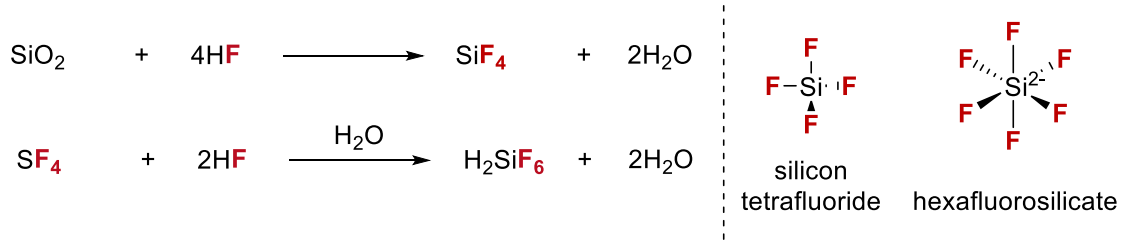

Scheme 3.8. Preparation of hexafluorosilicic acid (H_2SiF_6) via silicon dioxide [SiO_2] and HF.

Hexafluorosilicic acid has some technical relevance as it is also generated as a side product in the "wet" phosphoric acid process through the reaction of fluorapatite [$Ca_5(PO_4)_3F$] containing phosphate rock with concentrated H_2SO_4, where silica impurities react with HF to generate H_2SiF_6.[23] Pure H_2SiF_6 cannot be isolated from aqueous solutions, however, metal hexafluorosilicates (M_2SiF_6) are accessible through the neutralisation of H_2SiF_6 with metal hydroxides. Most hexafluorosilicate salts, such as potassium hexafluorosilicate (K_2SiF_6), are only sparingly soluble in water (K_2SiF_6 0.0012 mg/mL at 20 °C).[24] The corresponding metal fluoride (MF) and orthosilicic acid [$Si(OH)_4$] is formed upon alkaline hydrolysis of the metal fluorosilicate salt under aqueous conditions. $Si(OH)_4$ is

an unstable intermediate which readily oligomerizes to SiO_2.[25] The exact pathway for hydrolysis of hexafluorosilicate anion (SiF_6^{2-}) is complex, and several possibilities have been proposed (Scheme 3.9).[26,27]

neutral hydrolysis

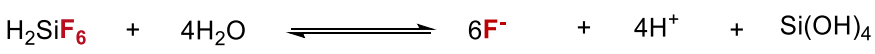

alkaline hydrolysis

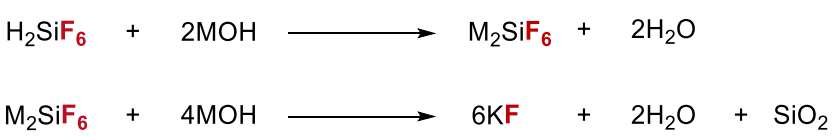

Scheme 3.9. Plausible hydrolysis pathways of hexafluorosilicic acid under neutral and basic (alkaline) conditions.

In aqueous solution, H_2SiF_6 exists in equilibrium with the intermediate $H_2SiF_5(OH)$ or $H_2SiF_5(OH_2)$.[26] The dissociation of H_2SiF_6 in water has been investigated by several research groups using ^{19}F NMR spectroscopy, predominantly for research purposes in water fluoridation. A clear pH dependency on the speciation of H_2SiF_6 in water is observed, with a diagnostic signal for $H_2SiF_5(OH)$ reported at δ_F =–129.5 ppm (below pH 3 in water).[26] At low temperature, two fluorine NMR peaks corresponding to the axial and equatorial fluorides of the SiF_5^- species are reported.[26,28] It is proposed that pentafluoro-silicate (SiF_5^-) undergoes intramolecular exchange that is catalysed by water. The mechanism can be interpreted as a rapid pre-equilibrium in which water coordinates to the central silicon of SiF_5^-, resulting in rapid interconversion between five and six coordinate geometries (Scheme 3.10).[28] While HF remains undetectable through ^{19}F NMR spectroscopy (at room temperature), the reaction in may also involve the coordination of water to the central silicon, followed by the release of HF (Scheme 3.11).

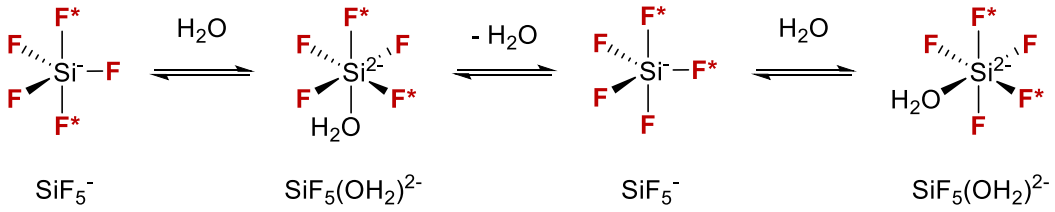

Scheme 3.10. Intramolecular fluorine exchange of SiF_5^- catalysed by water. Adapted from ref[28].

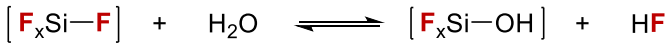

Scheme 3.11. Intermolecular fluorine exchange at silicon [x = 4 (SiF_5^-) or 5 (SiF_6^{2-})]. Adapted from ref[28].

3.2 Aims

The finding that acid-grade fluorspar (AGF) can be activated under mechanochemical conditions (solid-state) using a basic phosphate salt for fluorination chemistry has been described in Chapter **2**. This mechanochemical reaction stands out because it bypasses the production, storage and complex transport chain of HF. Still, a challenge encountered in this work was the widespread use of this approach in the synthesis of fluoroarenes that are highly coveted in pharmaceutical and agrochemical production and development. Also, mechanochemical equipment and setups are not accessible in all laboratories. This state of play encouraged the development of an alternative strategy for preparing fluorochemicals directly from fluorspar by applying mild conditions for its activation. We hypothesised that activating fluorspar in water could represent an attractive strategy compared to relying solely on mechanical energy for CaF_2 activation.

In search for a suitable manifold to activate CaF_2 in water, we considered mild acidic conditions that provide access to commonly used fluorinating reagents other than HF. We

hypothesized that the synergistic use of a Brønsted acid and a fluorophilic Lewis acid, would activate CaF_2, with Ca^{2+}sequestered as an insoluble salt, and simultaneous HF capture in a form suitable for subsequent fluorination chemistry (Scheme 3.12). Such technology could enable access to fluorinating reagents beyond the scope of the first solid-state activation method.

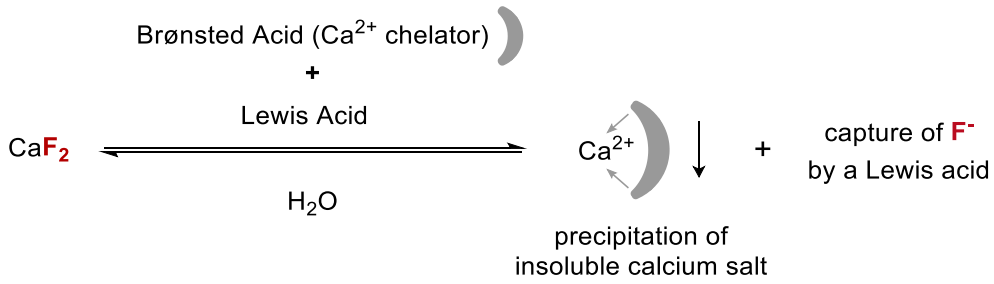

Scheme 3.12. Cooperative activation of fluorspar using both a Brønsted acid and a fluorophilic Lewis acid.

3.3 Results and Discussion

The synergetic activation described under Section **3.2** offers opportunities to convert AGF into various fluorinating reagents, through selection of Lewis acid, for fluoroarene synthesis. Whilst $B(OH)_3$ would enable the preparation of HBF_4 for the conversion of anilines to fluoroarenes (Balz-Schiemann reaction), the aqueous solution of fluorosilicic acid (H_2SiF_6) resulting from activation using SiO_2 can be treated with KOH to give KF for S_NAr fluorination. The reaction design is outlined in Scheme 3.13.

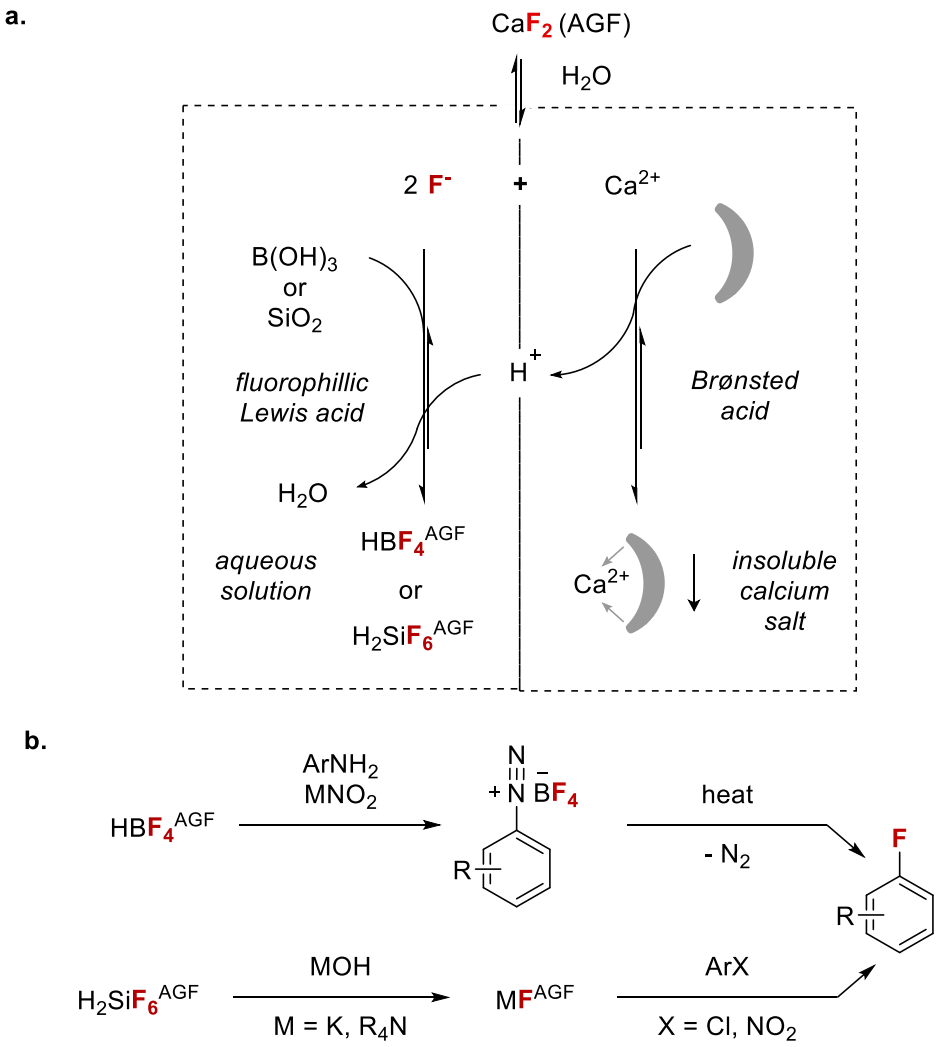

Scheme 3.13. Cooperative activation of acid-grade fluorspar (AGF) using a Brønsted acid and a fluorophilic Lewis acid [$B(OH)_3$ or SiO_2] (**a**) to afford HBF_4 or H_2SiF_6 which can be used directly or converted into fluorinating reagents for nucleophilic aromatic fluorination (**b**).

3.3.1 Reaction Development for Boron Fluorides

We surmised that the dissolution of CaF_2 in water with Brønsted acid in the presence of fluorophilic boric acid [$B(OH)_3$] may be driven by precipitation of an insoluble calcium salt and immediate capture of HF as a strong B–F bond (732 kJ mol^{-1}) in the form of tetrafluoroboric acid (HBF_4) with water as by-product. Our studies were initiated by the investigation of AGF activation (1.1 equiv CaF_2) at 50 °C with a range of Brønsted acids (1 to 2 equiv) in the presence of $B(OH)_3$ (0.5 equiv). In total 54 acids were screened, offering key insight on the interplay between acidity, denticity and solubility of the Ca^{2+} salt by-product. Fluoride capture was achieved in the form of [B-F] bond containing products HBF_4 and HBF_3OH (evidenced by ^{19}F NMR spectroscopy, see Section **3.2.3**).

Amongst the monoacids screened, a clear correlation was observed between the acidity of the activator and the fluoride release in the pK_a value range between 5 to –0.5, with HCl (2 equiv versus CaF_2) enabling 60% fluoride capture in the form of [B-F] products (40% HBF_4 and 20% HBF_3OH) (Figure 3.1). The process was also effective after 15 h at 50 °C, using concentrated H_2SO_4 (69%). The data suggest that lattice energy of Ca^{2+} salts alone is not sufficient for the prediction of activator performance, as exemplified with phosphoric acid (4%). Organic activators with more than one acidic functionality (1 equiv versus CaF_2) performed better than expected from pK_a values alone. Organic acids leading to five-membered Ca^{2+} chelates stood out with H_2Ox (pK_a= 1.3 and 4.1) being the most effective activator [total B-F 96% (HBF_4 76%, HBF_3OH 20%, $HOxBF_2$ <1%)] followed by croconic acid (pK_a = 0.8 and 2.2) and squaric acid (pK_a = 1.5 and 3.4).

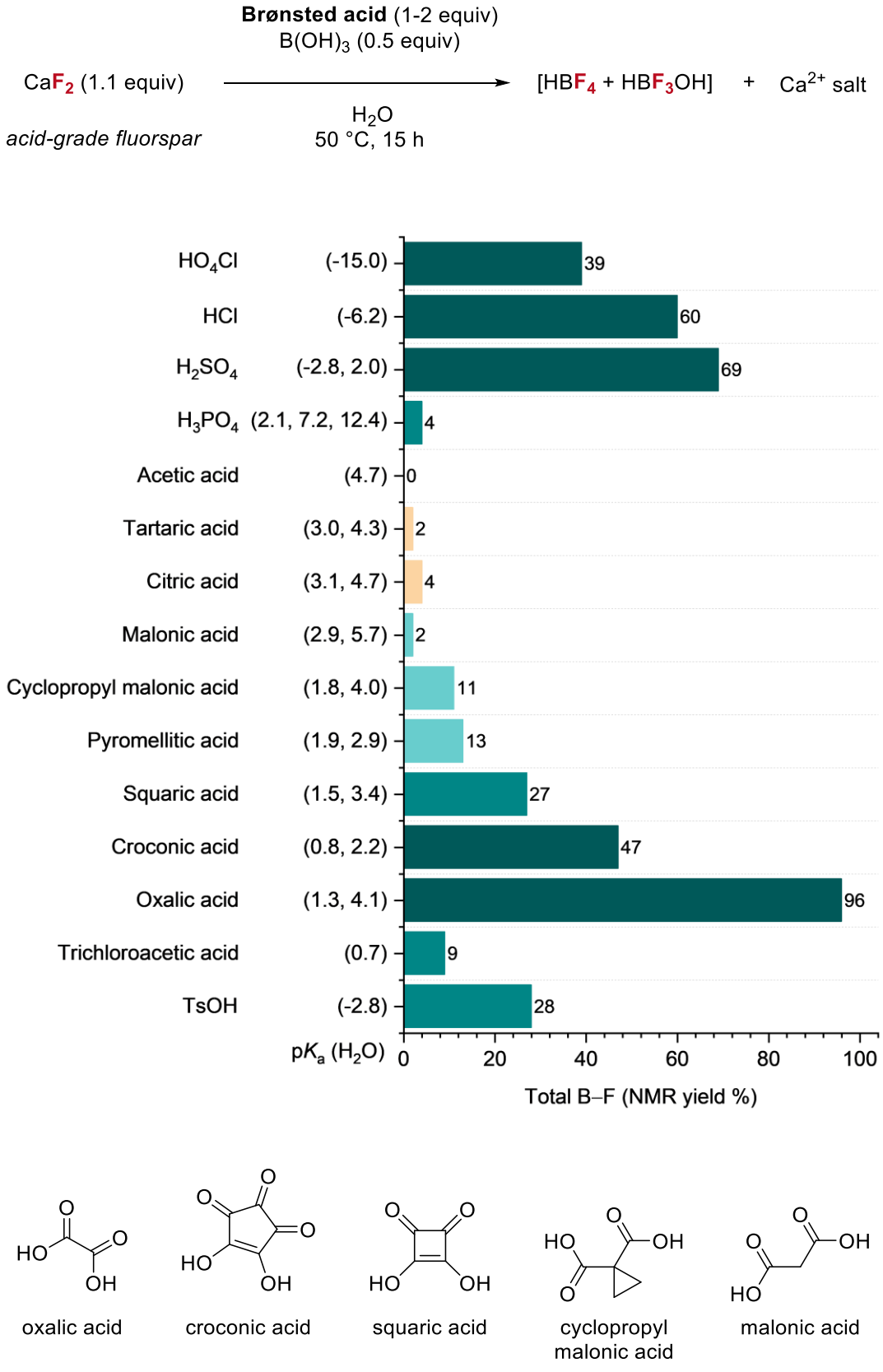

Figure 3.1. Screening of Brønsted acids for AGF activation with $B(OH)_3$ (2.0 mmol) at 50 °C; % HBF_4 and HBF_3OH determined by ^{19}F NMR spectroscopy (NaOTf as internal standard).

Key to the success of this approach is the formation of highly insoluble calcium oxalate (CaOx), one of the most thermodynamically stable complexes of calcium (and oxalic acid). Indeed, CaOx exhibits a lower solubility than $CaSO_4$ in water (solubility product constant, CaOx K_{sp} 2.32×10^{-9} versus $CaSO_4$ K_{sp} 4.93×10^{-5}) and is poorly soluble in water [0.0061 mg/mL (H_2O, 20 °C)].[29] Many species of plant accumulate crystals of CaOx in defence against herbivores and for cellular ion balance.[30]

Oxalic acid dihydrate ($H_2Ox{\cdot}2H_2O$) which is more cost-effective than anhydrous H_2Ox (£8/mol versus anhydrous oxalic acid £46/mol) gave the [B–F] products HBF_4 and HBF_3OH with efficacy similar to H_2Ox (total yield of 98%). Further optimisation of the reaction was conducted by Dr. Anirban Mondal. A concentration of $H_2Ox{\cdot}2H_2O$ in the range of 3-4 M was found to be optimal. Under optimised conditions, the reaction was performed at >20 g scale using AGF to afford an aqueous solution of tetrafluoroboric acid $[HBF_4]^{AGF}$ in 75% yield [total yield of B–F products 91%, including HBF_3OH 16% and HBF_2Ox (trace)] (Scheme 3.14). The solution of [B–F] was stored in a polypropylene container for up to 3 months at room temperature with no observable change in HBF_4 concentration (~ 4.80 M). The insoluble by-product of this reaction was unambiguously characterized as $CaOx{\cdot}H_2O$ by powder X-ray diffraction (PXRD) (Figure 3.2).

Notably, the reaction between AGF (1 equiv) with potassium oxalate monohydrate ($K_2Ox{\cdot}H_2O$, 1 equiv) did not lead to the release of KF (or calcium oxalate) in H_2O at 70 °C, highlighting the importance of Brønsted acid as a proton donor (Scheme 3.15). In a related experiment, stirring $CaOx{\cdot}H_2O$ (1 equiv) with KF (2 equiv) in H_2O led to the consumption of KF (42% remaining after stirring at 70 °C for 3 h), presumably to form CaF_2.

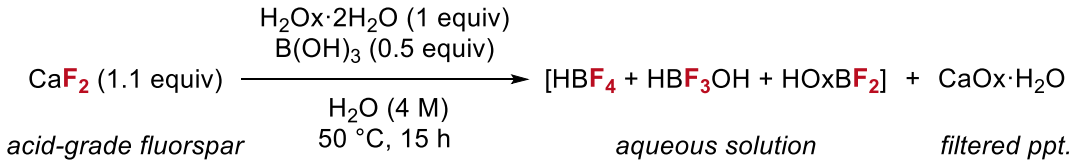

Scheme 3.14. Activation of AGF (27.8 g) using oxalic acid dihydrate and boric acid to give [B-F] products as an aqueous solution [HBF_4 (75%), HBF_3OH (16%) and HBF_2Ox (<1%)] and an insoluble precipitate (ppt).

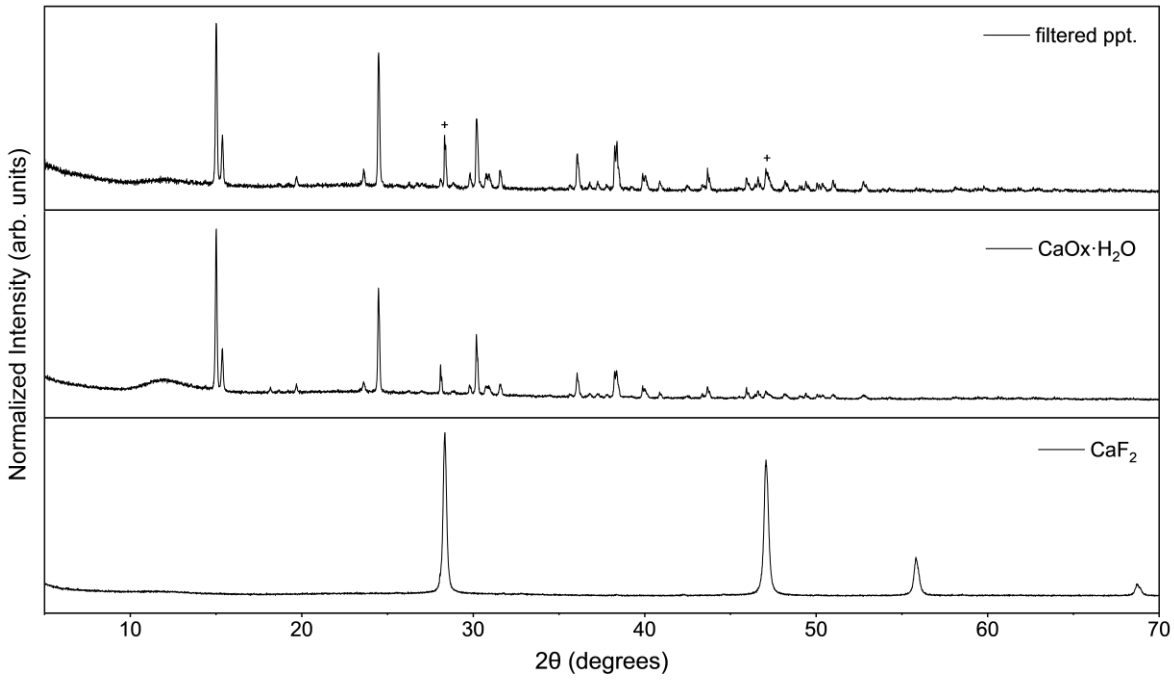

Figure 3.2. PXRD data of insoluble ppt. formed from the reaction between AGF, $H_2Ox{\cdot}2H_2O$ and $B(OH)_3$ [+ = CaF_2], calcium oxalate monohydrate (99%, Thermo Fisher Scientific) and calcium fluoride (≥97.0%, Alfa Aesar).

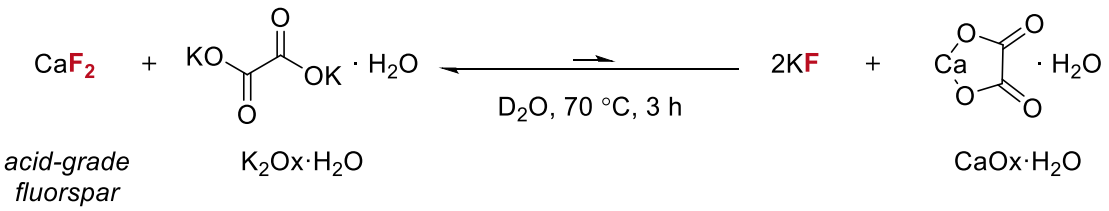

Scheme 3.15. Equilibrium between CaF_2, $K_2Ox{\cdot}H_2O$, $CaOx{\cdot}H_2O$ and KF. Control experiments using ^{19}F NMR spectroscopy suggest the equilibrium lies toward CaF_2 and $K_2Ox{\cdot}H_2O$.

3.3.2 Reaction Development for Silicon Fluorides

Oxalic acid was also found to be a suitable activator for AGF when combined with silica (SiO_2) in water at 50 °C for 15 h. In this reaction, a suspension containing CaOx is formed, with fluoride release as [Si–F] products (Si–F bond 577 kJ mol^{-1}) (Scheme 3.16). With the aim of accessing commonly used fluorinating reagents from these [Si–F] products, the resulting [Si-F] containing solution was treated with potassium hydroxide (KOH).

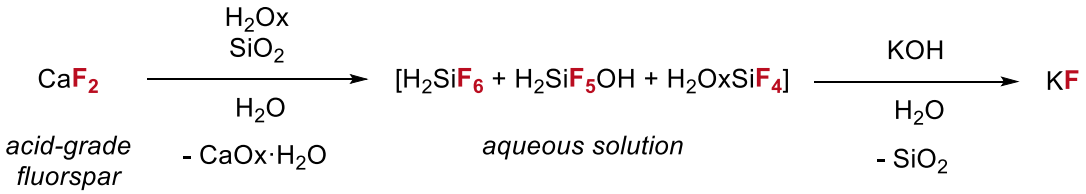

Scheme 3.16. Activation of AGF using oxalic acid and silica gel to give [Si–F] products as an aqueous solution [H_2SiF_6, H_2SiF_5OH and H_2OxSiF_4] and an insoluble precipitate.

Complete hydrolysis of all [Si-F] species in solution (evidenced by ^{19}F NMR spectroscopy) using 6 equivalents of KOH afforded an aqueous solution of KF, which was subsequently filtered from insoluble silica by-products and evaporated to dryness to afford solid KF. The amorphous silica by-product is most likely SiO_2. To assess the quantity of KF in the solid product, a sample of the solid product and NaOTf (>98 %) as an internal standard was dissolved in D_2O. The purity of KF in the solid was assessed by quantitative ^{19}F NMR spectroscopy (further details can be found in Chapter **4**). To calculate the KF yield, the solid KF mass yield was multiplied by the KF purity. This two-step protocol was optimised for reaction time, temperature and concentration. Using a reaction temperature of 50 °C for the CaF_2 activation step (step 1) and 70 °C (or above) for basic hydrolysis step (step 2), KF was isolated in 86% yield (87% purity) (Table 3.1). A reaction time of 15 h for the CaF_2

activation step and 1 h (or above) for basic hydrolysis step proved to be optimal for KF yield (up to 92%) (Table 3.2).

Table 3.1. Optimisation of reaction temperature for KF preparation (KF yields given in table with purity in parentheses). Reactions conducted using 3 M concentration of H_2Ox.

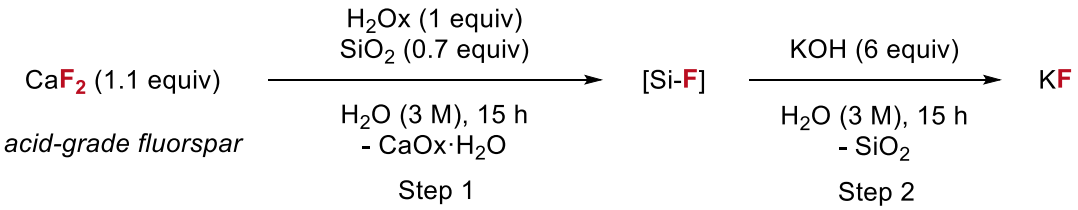

Step 1 \ Step 2	Temperature (°C)	25	50	70
	25	/	24% (24%)	33% (33%)
	50	40% (46%)	71% (81%)	86% (87%)
	70	26% (28%)	72% (77%)	73% (76%)

Using 8.0 mmol AGF. Yields determined by ^{19}F NMR spectroscopy using NaOTf as internal standard.

Table 3.2. Optimisation of reaction time for KF preparation (KF yields given in table with purity in parentheses). Reactions conducted using 3 M concentration of H_2Ox.

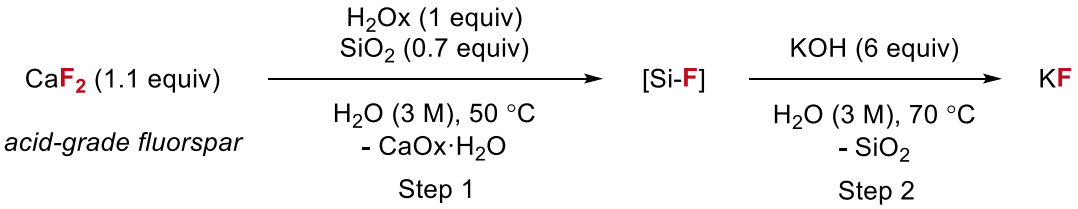

Step 1 \ Step 2	Reaction time (h)	1	3	15
	1	54% (54%)	/	45% (46%)
	3	53% (52%)	/	38% (38%)
	15	81% (80%)	92% (89%)	87% (86%)

Using 8.0 mmol AGF. Yields determined by ^{19}F NMR spectroscopy using NaOTf as internal standard.

Reducing the oxalic acid concentration from 3 M to 0.5 M was found be optimal for KF yield (91%, purity 96%), these conditions also ensured complete dissolution of oxalic acid in water. In theory, only 0.33 equivalents of SiO_2 are required to capture the maximum amount of HF that can be generated from AGF in the first activation step. Although high KF yields (95% KF, 97% purity) were retained using 0.33 equivalents of SiO_2, for the final reaction conditions 0.4 equivalents of SiO_2 was chosen (82% KF, 84% purity) to ensure complete HF consumption by the Lewis acid. Finally, oxalic acid dihydrate ($H_2Ox{\cdot}2H_2O$) was also found to be a suitable activator for AGF (1.1 equiv) when combined with SiO_2 (0.4 equiv) in water at 50 °C for 15 h, with fluoride release as [Si–F] products in 97% total yield (determined by quantitative ^{19}F NMR spectroscopy). The aqueous solution of [Si–F] was treated with KOH (6 equiv) to afford KF in 85% yield (87% purity).

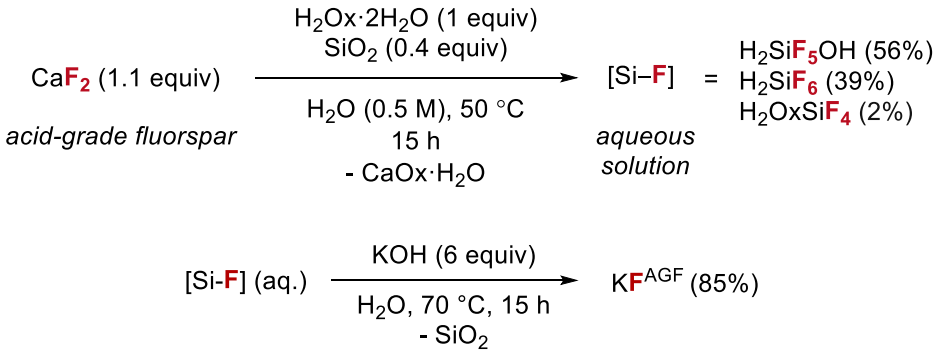

Scheme 3.17. Activation of AGF using oxalic acid dihydrate ($H_2Ox{\cdot}2H_2O$) and silica gel (SiO_2) to give [Si-F] products (total 97%) as an aqueous solution (under optimised conditions) followed alkaline hydrolysis of the aqueous [Si-F] solution using KOH.

3.3.3 Insights from NMR Spectroscopy

NMR spectroscopy was used to provide insight into the speciation of [B–F] and [Si–F] products formed upon dissolution of AGF in an aqueous solution of H_2Ox in the presence of $B(OH)_3$ and SiO_2. A detailed spectroscopic study is presented, with full characterisation of the [B–F] and [Si–F] species.

The reaction between AGF with anhydrous oxalic acid (H_2Ox) and $B(OH)_3$ in D_2O was monitored at 50 °C. All spectra were collected at 25 °C. The [B–F] products were identified by ^{19}F and ^{11}B NMR spectroscopy in D_2O (Figure 3.3 and Figure 3.4). By ^{19}F NMR spectroscopy, HBF_4 (quartet, $\delta_F = -150.3$ ppm, $^1J_{B-F} = 1.1$ Hz) and HBF_3OH (quartet, $\delta_F = -145.3$ ppm, $^1J_{B-F} = 10.7$ Hz) were identified as major products.[13] Coupling between ^{19}F and ^{11}B leads to a quintet of peaks in the ^{11}B NMR spectrum for the BF_4^- ion at $\delta_B = 1.46$ ppm, which cannot be resolved, and a quartet for the HBF_3OH at $\delta_B = 0.03$ ppm. Additionally, a broad singlet ($\delta_F = -152.3$ ppm) characteristic of difluoro(oxalate)borate species $HOxBF_2$ was observed in trace amount (<1%) in the ^{19}F NMR spectrum.[31] The peak at $\delta_B = -2.84$ ppm in the ^{11}B NMR spectrum of the reaction mixture was assigned to $HOxBF_2$.

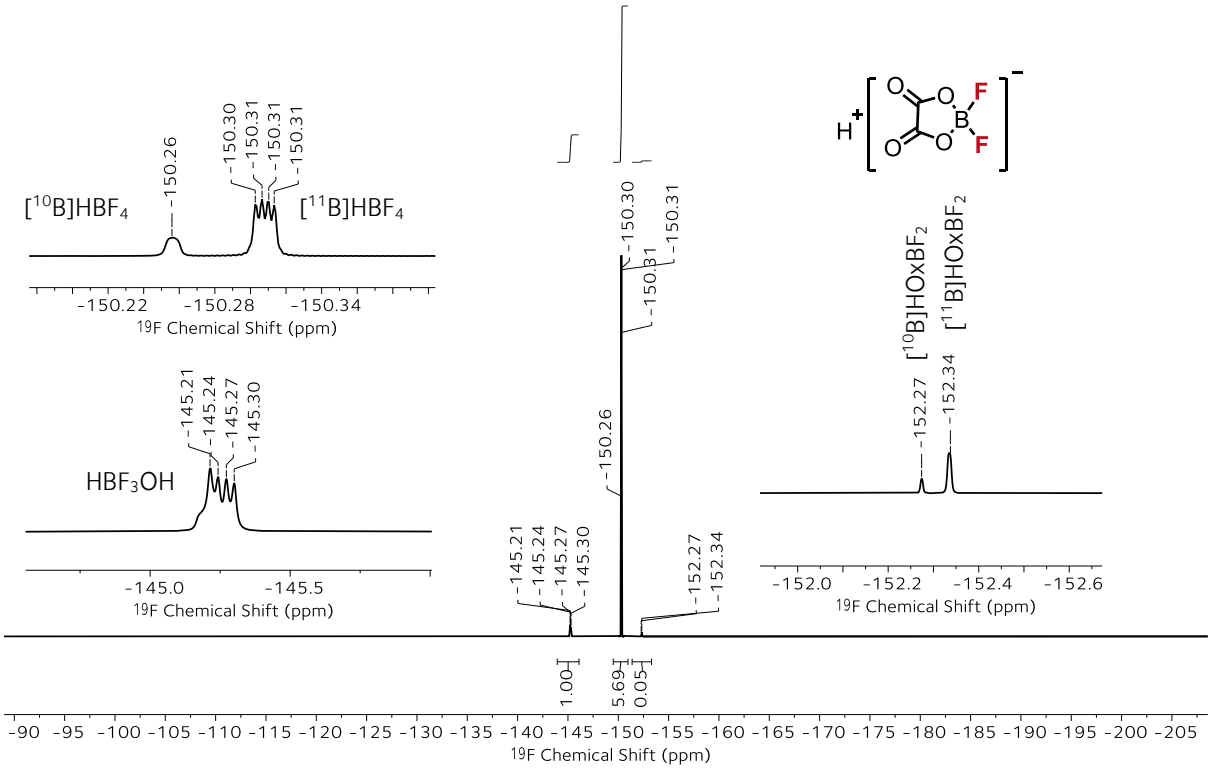

Figure 3.3. ^{19}F NMR (D_2O) of reaction between acid grade fluorspar (CaF_2), H_2Ox and $B(OH)_3$ at 50 °C (15 h). The species observed are HBF_4 at -150.3 ppm, HBF_3OH at -145.3 ppm and $HOxBF_2$ at -152.3 ppm. $^{11}B/^{10}B$ isotopes observed.

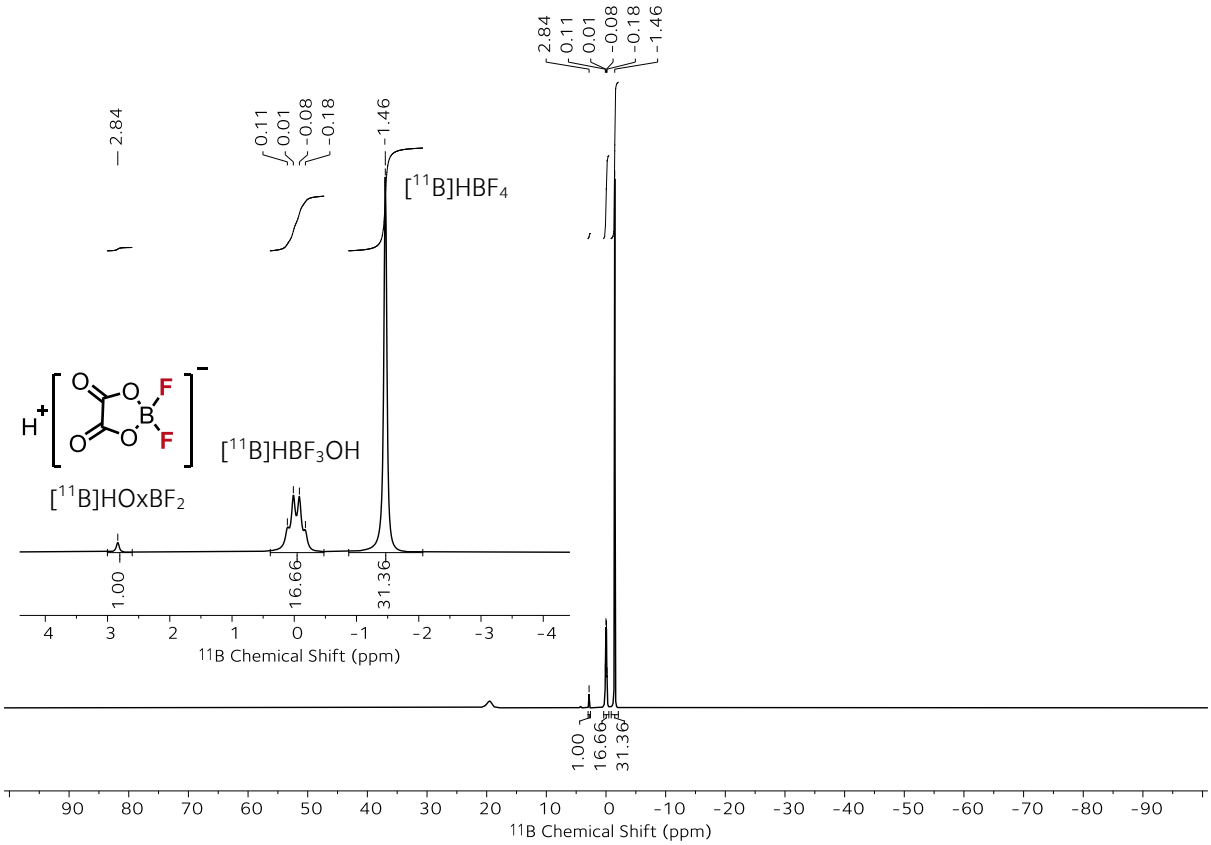

Figure 3.4 ^{11}B NMR (D_2O) of reaction between acid grade fluorspar (CaF_2), H_2Ox and $B(OH)_3$ at 50 °C (15 h). The species observed are HBF_4 at -1.46 ppm, HBF_3OH at -0.03 ppm and $HOxBF_2$ at 2.84 ppm.

The reaction between AGF (CaF_2, > 97.0%) with anhydrous oxalic acid and SiO_2 in D_2O next studied. The formation of H_2SiF_6 was observed after 5 min by ^{19}F NMR, in addition to two fluorine resonances (triplets) at δ_F = -124.9 ppm and δ_F = -136.2 ppm with $^2J_{F-F}$ coupling values of 8.9 Hz (Figure 3.5). These resonances were assigned to the oxalate fluorosilicate species H_2OxSiF_4, which has been previously characterised by Dean and Evans (Figure 3.6).[32] After 15 h, a second broad singlet was observed in the ^{19}F NMR spectrum of the reaction mixture at δ_F = -128.9 ppm which was assigned to the hydrolysis intermediate H_2SiF_5OH. The broad singlet at δ_F = -129.6 ppm was assigned to H_2SiF_6. Peaks corresponding to H_2SiF_6 and H_2SiF_5OH are broad and overlap due to fast fluoride exchange.[26]

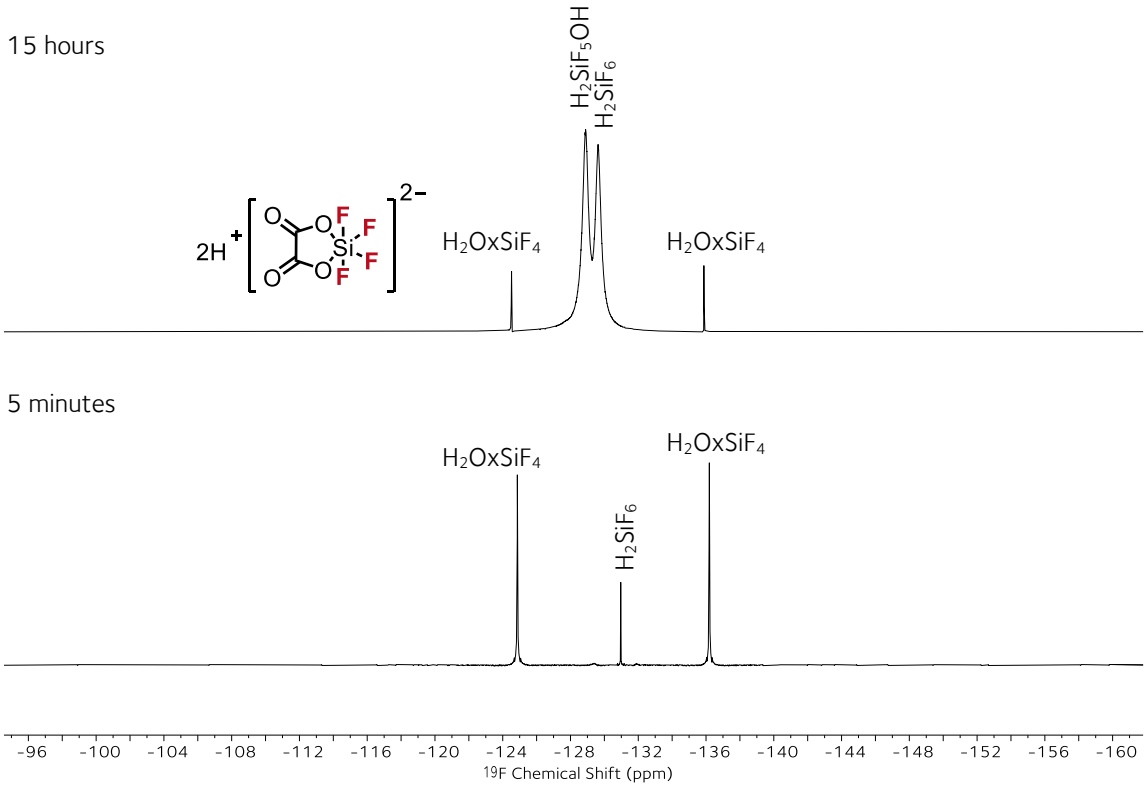

Figure 3.5. ^{19}F NMR (D_2O) of reaction between acid grade fluorspar (CaF_2), H_2Ox and SiO_2 at 50 °C. Reaction after 5 min (bottom); reaction after 15 h (top).

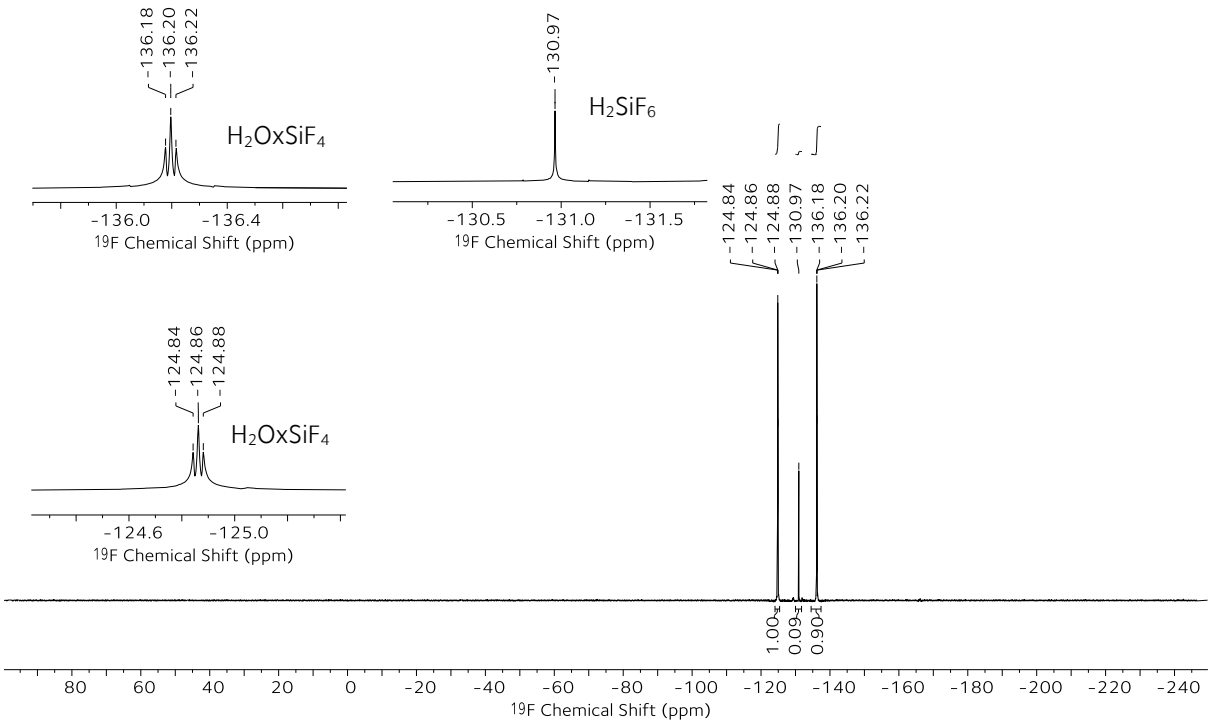

Figure 3.6. ^{19}F NMR (D_2O) of reaction between acid grade fluorspar (CaF_2), H_2Ox and SiO_2 (5 min, 50 °C). Aqueous species H_2SiF_6 (s, -131.0 ppm) and H_2OxSiF_4 (triplets at -124.9 ppm and -136.2 ppm with $^2J_{F-F}$ = 8.9 Hz) observed.

Next, experiments using ^{29}Si NMR spectroscopy (^{29}Si nuclear spin of I = ½) were undertaken to validate the proposed [Si–F] species. Fluorosilicates can be particularly challenging to characterise using ^{29}Si NMR spectroscopy because of ^{29}Si nuclide's low natural abundance (4.7%) and low gyromagnetic ratio (^{1}H γ 26.75 versus ^{29}Si γ -5.31 10^{7} rad T^{-1} s^{-1}), necessitating exceptionally long relaxation times which can hamper the direct detection of the ^{29}Si NMR signal of such compounds.[33] A method used to overcome these drawbacks and to improve the signal strength is the use of pulse sequences like refocused Insensitive Nuclei Enhanced Polarisation Transfer (rINEPT), typically used in ^{1}H to ^{13}C polarisation transfer in Heteronuclear Single Quantum Coherence (HSQC) NMR experiments. Direct (^{1}J) polarisation transfer from ^{19}F to ^{29}Si can significantly enhance the signal of the low sensitivity nuclei. Analysis of the reaction mixture after 5 min by ^{29}Si{^{19}F} NMR spectroscopy using the ^{29}Si-^{19}F rINEPT method displayed 2 signals at δ_{Si} = -178.2 ppm and δ_{Si} = -182.8 ppm, corresponding to H_2SiF_6 and H_2OxSiF_4, respectively (Figure 3.7).

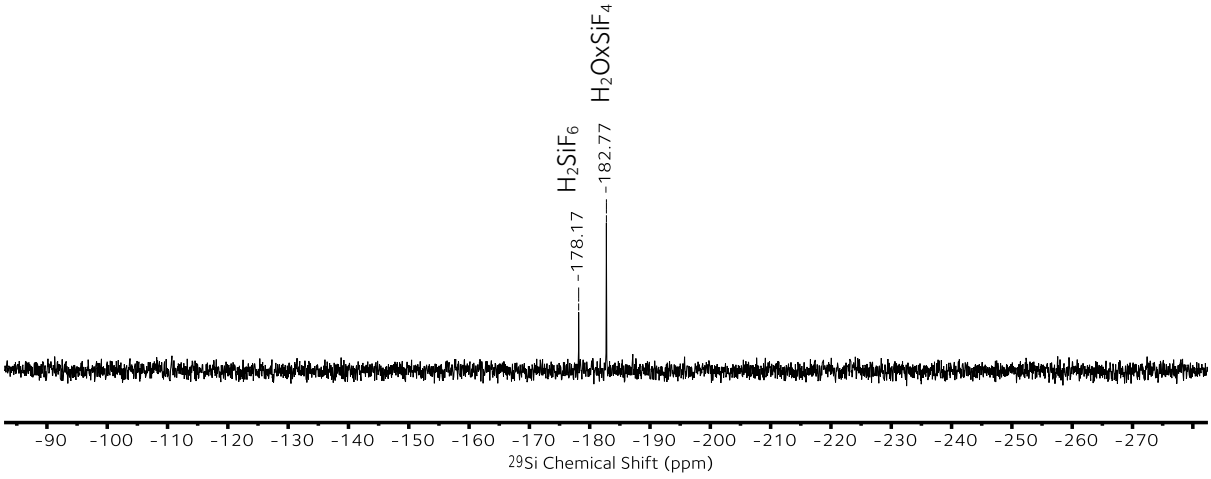

Figure 3.7. ^{29}Si{^{19}F} NMR (D_2O) of reaction between acid grade fluorspar (CaF_2), H_2Ox and SiO_2 (5 min, 50 °C). Aqueous species H_2SiF_6 (-178.2 ppm) and H_2OxSiF_4 (-182.8 ppm) observed. ^{29}Si{^{19}F} NMR spectra was acquired using ^{29}Si-^{19}F rINEPT NMR method.

The ^{19}F–^{29}Si bond of H_2SiF_6 and H_2OxSiF_4 was confirmed by a ^{19}F–^{29}Si Heteronuclear Multiple Bond Correlation (HMBC experiment optimised for a short-range coupling) (Figure 3.8). Finally, an ^{19}F to ^{29}Si rINEPT experiment was used to confirm $^{1}J_{Si-F}$ couplings (Figure 3.9). The aqueous species H_2SiF_6 (d, δ_F = -131.2 ppm with $^{1}J_{Si-F}$ = 139.4 Hz) and H_2OxSiF_4 (two dt at δ_F = 124.9 ppm with $^{1}J_{Si-F}$ = 135.2 Hz and $^{2}J_{F-F}$ = 8.9 Hz and at δ_F = 136.2 ppm with $^{1}J_{Si-F}$ = 113.8 Hz and $^{2}J_{F-F}$ = 8.9 Hz) were observed.

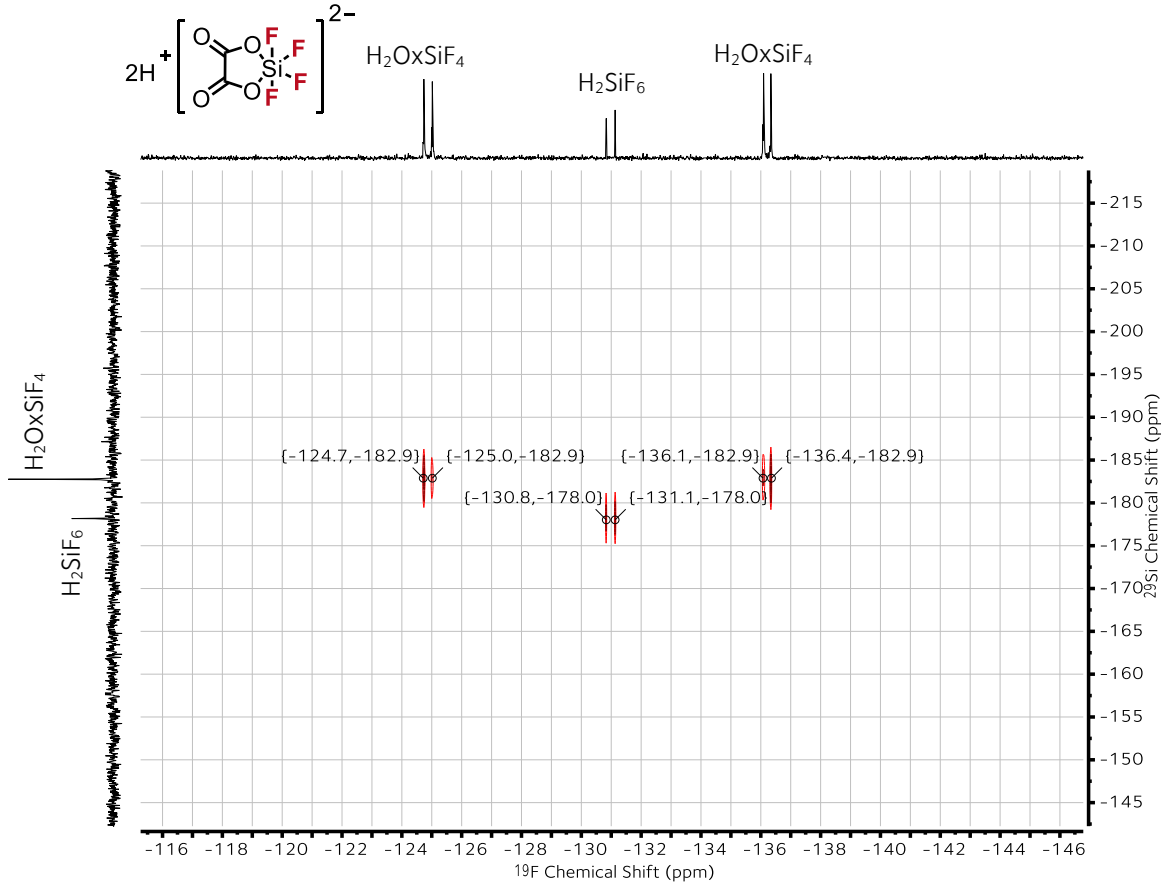

Figure 3.8. ^{29}Si–^{19}F HMBC NMR experiment (D_2O) of reaction between acid grade fluorspar (CaF_2), H_2Ox and SiO_2 (5 min, 50 °C) confirming ^{19}F–^{29}Si bonds and $^{1}J_{Si-F}$ couplings. The top trace is ^{19}F NMR spectrum (internal projection). Left trace is $^{29}Si\{^{19}F\}$ NMR spectrum (external projection).

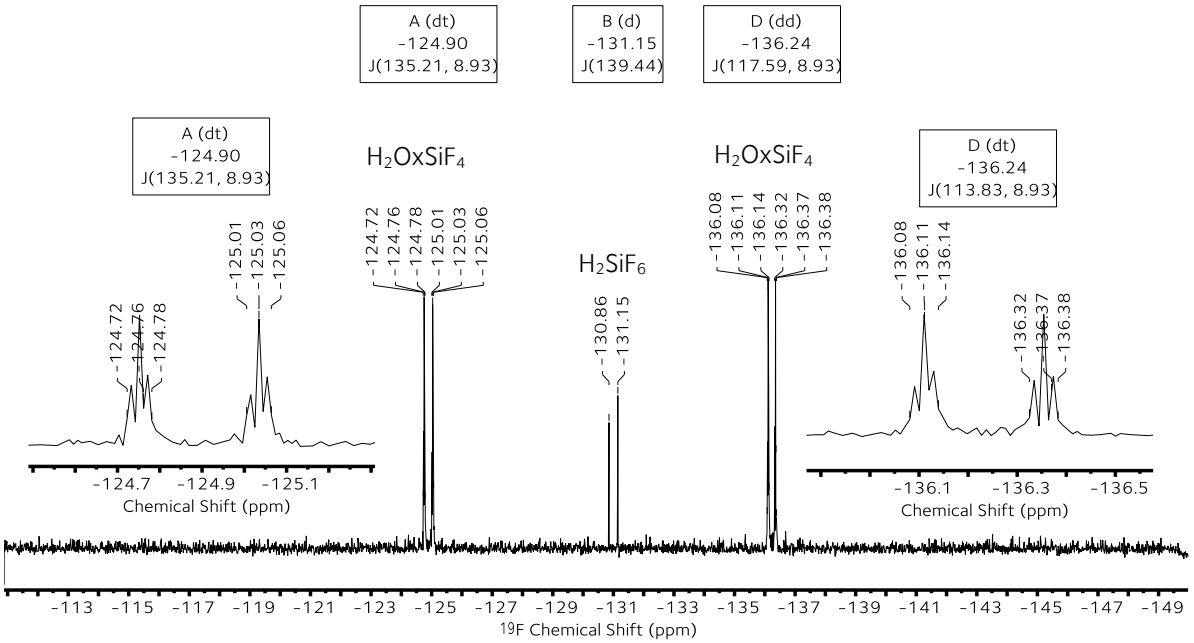

Figure 3.9. ^{19}F NMR (D_2O) of reaction between acid grade fluorspar (CaF_2), H_2Ox and SiO_2 (5 min, 50 °C), acquired using ^{29}Si-^{19}F rINEPT NMR method. Aqueous species H_2SiF_6 (d, -131.2 ppm with $^1J_{Si-F}$ = 139.4 Hz) and H_2OxSiF_4 (two dt at -124.9 ppm with $^1J_{Si-F}$ = 135.2 Hz and $^2J_{F-F}$ = 8.9 Hz and at -136.2 ppm with $^1J_{Si-F}$ = 113.8 Hz and $^2J_{F-F}$ = 8.9 Hz) were observed.

The composition of the [Si-F] solution (ratio between H_2SiF_6, H_2SiF_5OH and H_2OxSiF_4) was monitored by ^{19}F NMR spectroscopy and indicated that the aqueous solutions of $[Si-F]^{AGF}$ does not decompose over time (Table 3.3).

Table 3.3. Stability studies on $[Si-F]^{AGF}$ solution (stored at 25 °C in polypropylene tube).

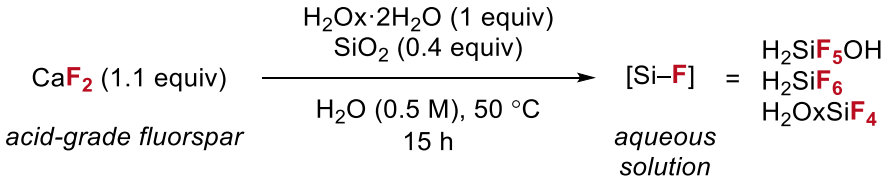

Entry	Time since initial preparation	H_2SiF_6 (%)	H_2SiF_5OH (%)	H_2OxSiF_4 (%)	Total [Si-F] (%)
1	0	39	56	2	97
2	4	54	38	3	95

Using 8.0 mmol AGF. Yields quantified by ^{19}F NMR spectroscopy using NaOTf as internal standard.

3.3.4 Synthesis of Nucleophilic Fluorinating Reagents

Subsequent studies focused on the synthesis of commonly used fluorinating reagents from the aqueous solution containing the [Si-F] products. Under optimised conditions, AGF (1.1 equiv) was reacted with $H_2Ox{\cdot}2H_2O$ (1 equiv) and SiO_2 (0.4 equiv) in water at 50 °C for 15 h (Scheme 3.18). This reaction was performed using 6.44 g (80 mmol) of AGF (>97% CaF_2) which was added portion-wise with SiO_2 to a solution of $H_2Ox{\cdot}2H_2O$ (0.5 M).

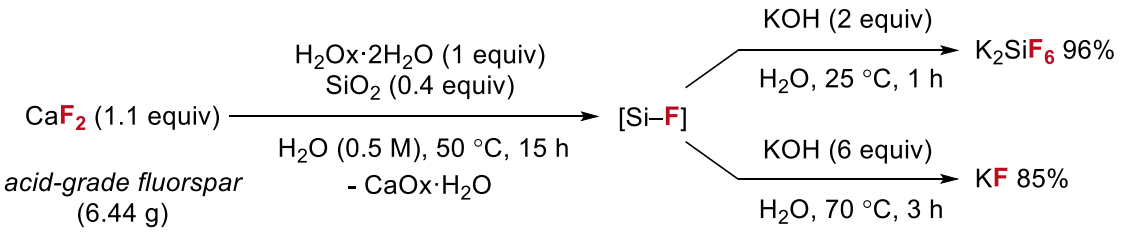

Scheme 3.18. Synthesis of $K_2SiF_6^{AGF}$ and KF^{AGF} from AGF via cooperative activation using $H_2Ox{\cdot}2H_2O$ and SiO_2 in water (50 °C, 15 h) (80 mmol scale CaF_2).

The reaction mixture was filtered and treated with KOH, the insoluble by-product of this filtration was unambiguously characterised as $CaOx{\cdot}H_2O$ (by PXRD). Neutralisation with KOH (2 equiv) led to the formation of potassium hexafluorosilicate (K_2SiF_6) in 96% yield (5.08 g), whilst treatment with excess KOH (6 equiv) afforded $[KF]^{AGF}$ in 85% yield (7.84 g). Both of these products were crystalline solids and were characterised by PXRD (Figure 3.10 and Figure 3.11). Purity of KF^{AGF} was determined by quantitative ^{19}F NMR spectroscopy (using NaOTf as an internal standard) and was calculated to be 90%. Elemental analysis by Inductively Coupled Plasma Optical Emission Spectroscopy (ICP-OES) revealed the composition of KF^{AGF} as 23.76% F, 56.27% K and 0.4% Si [the composition of commercial KF (Thermo Scientific) was found to be 29.88% F, 61.71% K]. KF^{AGF} exists as anhydrous KF and $KF{\cdot}2H_2O$. Replacing KOH for NaOH or $CsOH{\cdot}H_2O$ in the reaction outlined in Scheme 3.18

enabled access to NaF^{AGF} (85% yield, 94% purity) and CsF^{AGF} (89% yield, 96% purity), respectively (Scheme 3.19). Full purity analysis of these alkali metal fluorides and experimental details can be found in Chapter **4**.

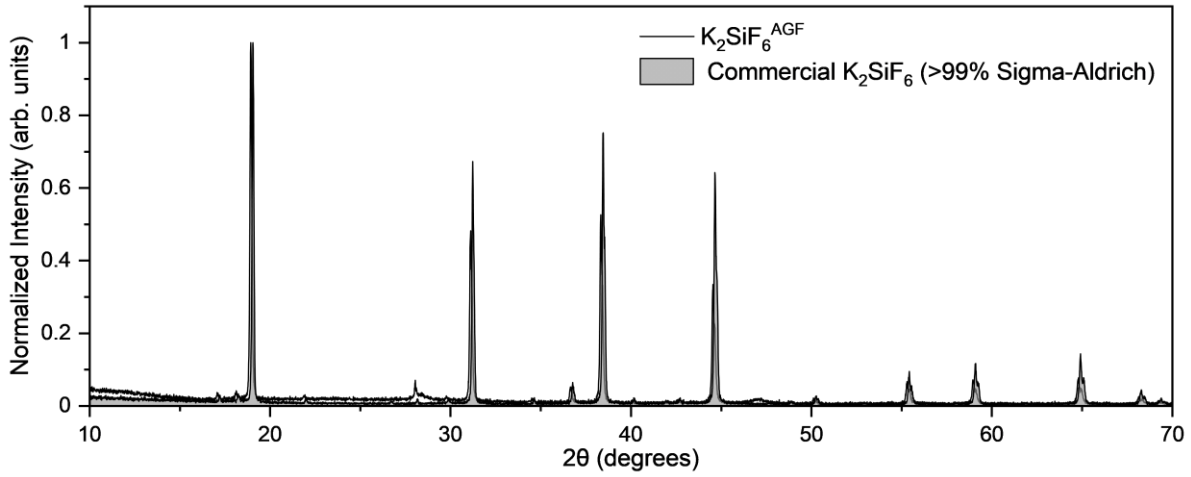

Figure 3.10. PXRD patterns of K_2SiF_6 prepared via AGF and commercial K_2SiF_6 (shaded).

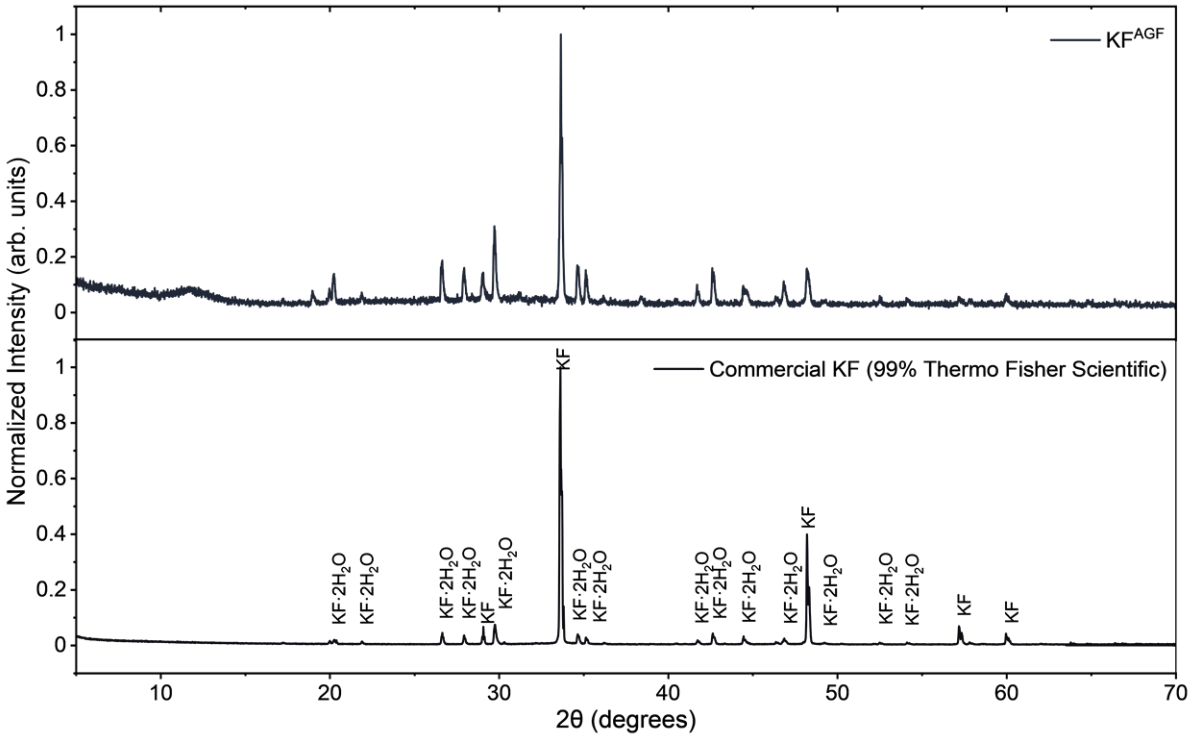

Figure 3.11. PXRD pattern of KF^{AGF} (top trace) and commercial KF (bottom trace) collected at room temperature. KF^{AGF} is comprised of crystalline anhydrous KF and KF dihydrate.

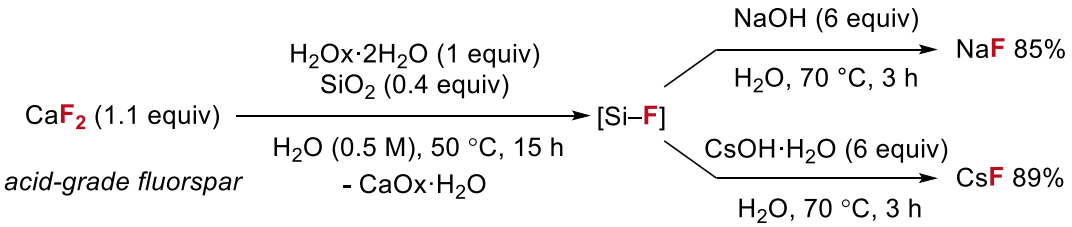

Scheme 3.19. Synthesis of NaF^{AGF} and CsF^{AGF} from AGF via cooperative activation using $H_2Ox{\cdot}2H_2O$ and SiO_2 in water (50 °C, 15 h) (8 mmol scale CaF_2).

Alternatively, tetramethylammonium fluoride hydrate [$Me_4NF{\cdot}(H_2O)_x$] was prepared from the filtered reaction mixture through treatment with aqueous tetramethylammonium hydroxide (Me_4NOH, 6 equiv). Subsequently, tetramethylammonium alcohol fluoride ($Me_4NF{\cdot}t$-AmOH)^{AGF} was prepared from the crude [$Me_4NF{\cdot}(H_2O)_x$]^{AGF} in 88% yield (Scheme 3.20). The *tert*-amyl alcohol complex of Me_4NF is a well-documented reagent for nucleophilic aromatic fluorination (S_NAr) reported by the Sanford group.[34] In another approach, treatment with six equivalents of tetrabutylammonium hydroxide (n-Bu_4NOH) gave tetrabutylammonium fluoride hydrate [n-$Bu_4NF{\cdot}(H_2O)_x$], which was transformed into the bench stable nucleophilic fluorinating reagent tetrabutylammonium tetra(*tert*-butyl alcohol) fluoride complex [$Bu_4NF{\cdot}(t$-$BuOH)_4$]^{AGF} (71% yield) upon recrystallisation in hexanes and *tert*-BuOH.

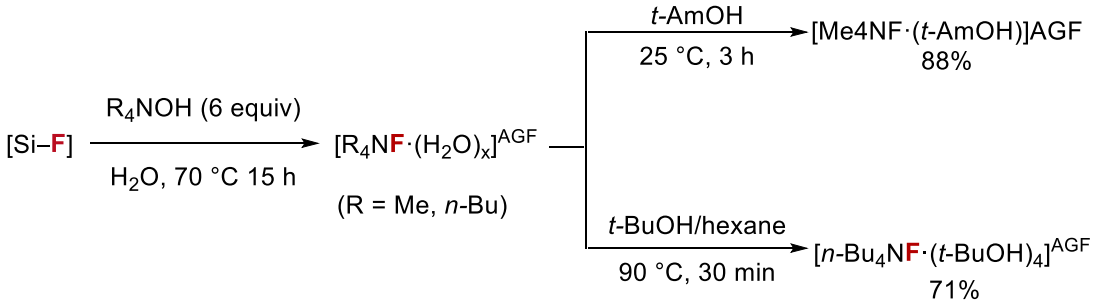

Scheme 3.20. Preparation of Me_4NF and *n*-Bu_4NF from [Si-F]^{AGF}(H_2SiF_6, H_2SiF_5OH and H_2OxSiF_4) and conversion into *tert*-alcohol complexes (Me_4NF·*t*-AmOH)^{AGF} and [Bu_4NF·(*t*BuOH)$_4$]^{AGF}.

Next, we turned to demonstrating that these AGF derived fluorinating reagents react as expected with the synthesis of industrially valuable fluoroarenes by Balz-Schiemann and S_NAr chemistry. A solution of [HBF_4]^{AGF} was prepared using 27.8 g AGF, to afford an aqueous solution of tetrafluoroboric acid [HBF_4]^{AGF} in 75% yield [total yield of B-F products 91% including HBF_3OH 16% and HBF_2Ox (trace)], which was subsequently stored in a polypropylene container (Scheme 3.21).

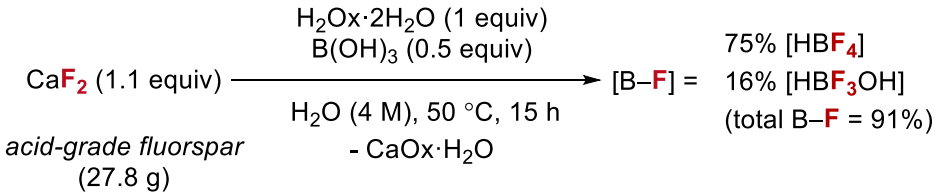

Scheme 3.21. Preparation of HBF_4 from AGF, $B(OH)_3$ and $H_2Ox·2H_2O$. Aqueous solution of [B-F] produced with products HBF_4, HBF_3OH and $HOxBF_2$ (<1%).

Dr. Anirban Mondal executed the Balz-Schiemann chemistry which entailed a two-step procedure. First, addition of *tert*-butyl nitrite (*t*-BuONO) to a solution of arylamine ($ArNH_2$) and aqueous [HBF_4]^{AGF} led to the precipitation of the corresponding aryl diazonium tetrafluoroborate salt (ArN_2BF_4), which was isolated and subsequently heated to liberate the desired fluoroarene (Scheme 3.22). This chemistry was subsequently applied to prepare multiple electron rich and electron deficient fluoroarenes commonly used as building blocks

in the synthesis of various organo-fluorine containing drugs, including **69** (98%) used to prepare the antidepressant Citalopram and **80** (72%) used in the synthesis of cholesterol lowering drug Lipitor.[35] The methodology also enabled the preparation of fluoropyridines (**72**, **76** and **81**) that are building blocks for mitogen-activated protein kinase 2 (MK2) inhibitors (inflammatory diseases), Vericiguat (heart failure), and agrochemicals such as Clodinafop.[36–38] In total, 13 electronically and structurally diverse fluoroarenes were prepared using $[HBF_4]^{AGF}$.

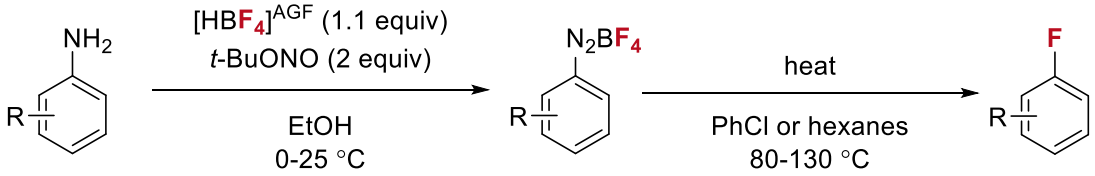

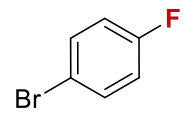

69, (93%/98%)[#]

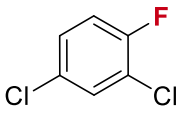

70, (84%/73%)

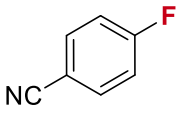

71, (87%/78%)

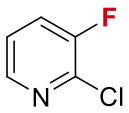

72, (93%/63%)

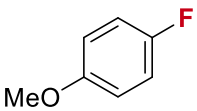

73, (93%/63%)

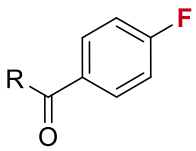

74,R = Me (89%/66%)
75, R = OMe (95%/85%)

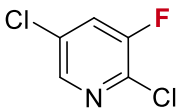

76, (62%/75%)

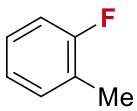

77, (75%/89%)[#]

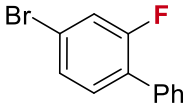

78, (71%/83%)

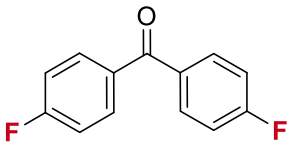

79, (95%/69%)

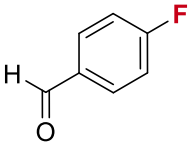

80, (86%/72%)

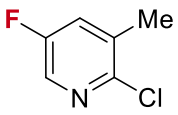

81, (73%/82%)

Scheme 3.22. Diazotization of an aniline using $[HBF_4]^{AGF}$ followed by dediazotization of the corresponding aryl diazonium salt (Balz–Schiemann reaction). Yield of diazotization/fluorodediazoniation). Diazotization reactions were carried out with 5.0 mmol of arylamine, excluding compounds **71**, **72**, **74**, **76**, **77** and **79** which were carried out on 1.0 mmol. Dediazoniation reactions were carried out on 1.0 mmol scale unless otherwise

stated. All yields are for isolated products (unless otherwise stated). #^{19}F NMR yields using FA as internal standard. Full experimental details can be found in Chapter **4**.

S_NAr fluorination reactions of chloroarenes and nitroarenes using DMSO as solvent was also studied. KF^{AGF} (90% purity) was found to achieve high-yielding fluorination of chloroarene substrates using catalytic Me_4NCl (5 mol%) to provide fluoroarenes **62**, **51**, **82** and **83**. KF^{AGF} performed comparably to commercial KF (99% purity, Sigma-Aldrich) (Scheme 3.23 and Scheme 3.24). Fluoroarenes **59**, **84** and **85** were prepared in high yield (up to 88%) via aromatic fluorodenitration (30-80 °C) using AGF derived $[Me_4NF{\cdot}t\text{-AmOH}]^{AGF}$.

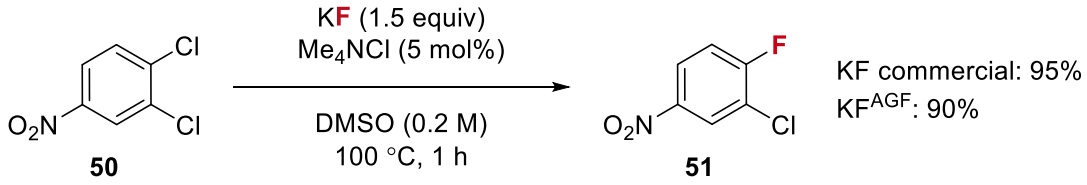

Scheme 3.23. S_NAr fluorination of **50** using KF (99% Sigma Aldrich) vs. KF^{AGF} (0.125 mmol scale, yields calculated by ^{19}F NMR spectroscopy using FA as internal standard).

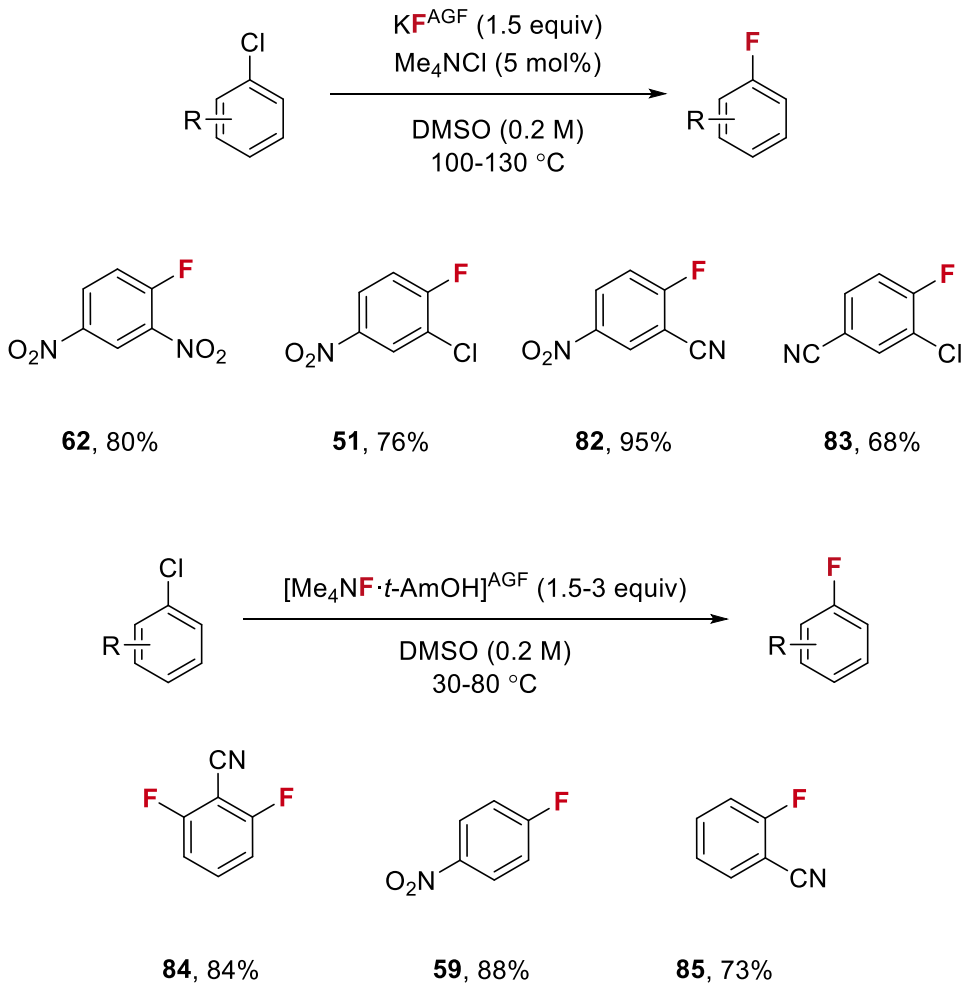

Scheme 3.24. Fluoroarenes prepared via halex exchange (S_NAr) of chloroarenes using AGF-derived KF $[KF]^{AGF}$ or fluorodenitration reactions of nitroarenes using AGF-derived $Me_4NF{\cdot}t$-AmOH. All yields are for isolated products (1.0 mmol scale unless otherwise stated).

3.3.5 Monitoring of Hydrogen Fluoride

Investigations utilising ^{19}F NMR spectroscopy in D_2O aimed to establish the generation of HF following the dissolution of CaF_2 with H_2Ox. Reactions were conducted in Teflon NMR tubes to enable the characterisation and quantification of HF (full experimental details can be found in Chapter **4**). In the absence of fluorophilic Lewis acid [$B(OH)_3$ or SiO_2], HF is observed (singlet, δ_F = -166.0 ppm), and an equilibrium is established with the amount of HF plateauing after 3 h at approximately 10% (Figure 3.12).

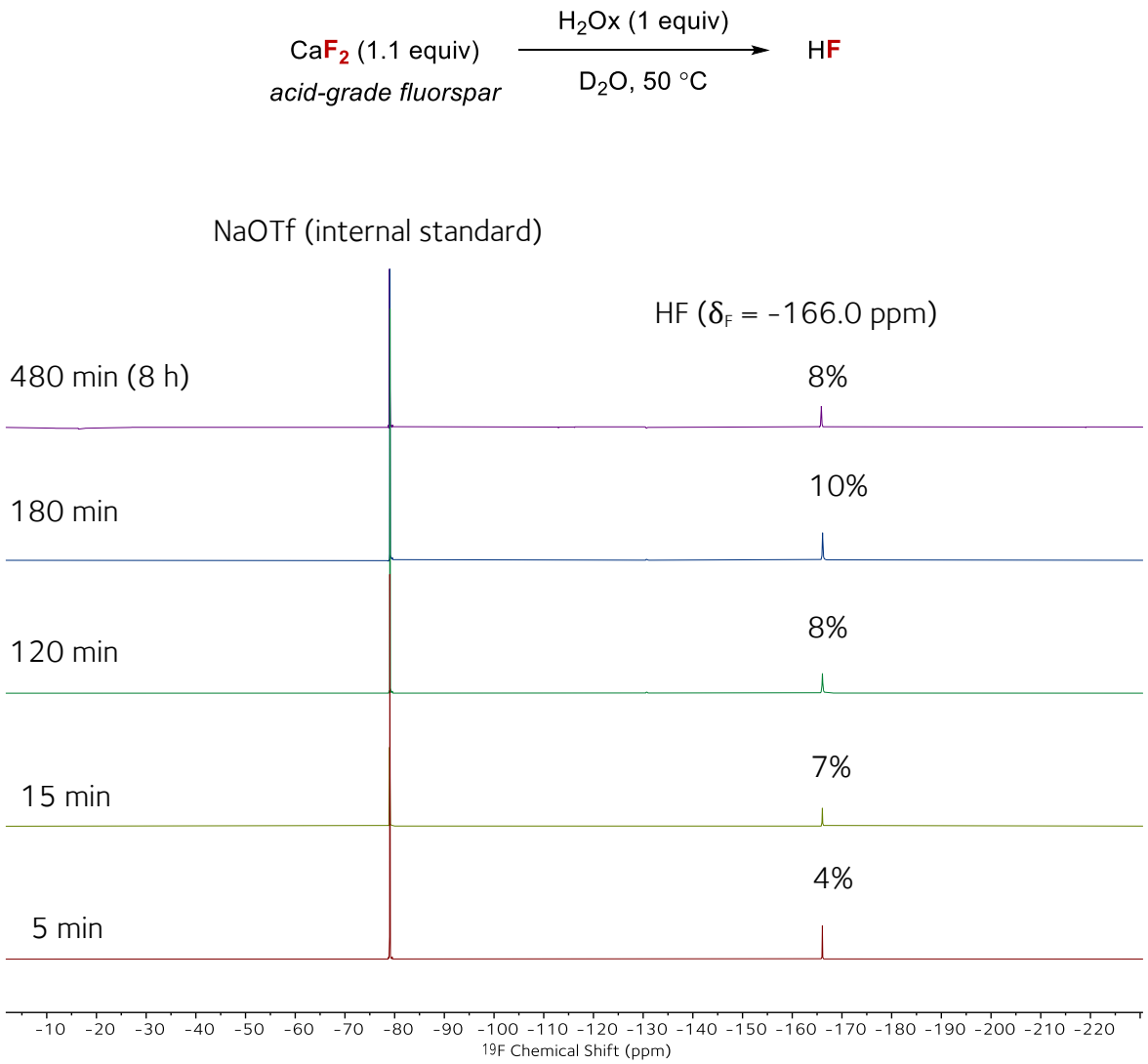

Figure 3.12. Reaction of AGF with H_2Ox in D_2O at 50 °C monitored by ^{19}F NMR. Singlet diagnostic of HF observed at -166.0 ppm. Sodium triflate internal standard at -78.0 ppm.

The reverse reaction of aqueous HF (48%) with calcium oxalate monohydrate ($CaOx{\cdot}H_2O$) was also monitored with 76% HF consumed after 6 h with accompanying CaF_2 formation.

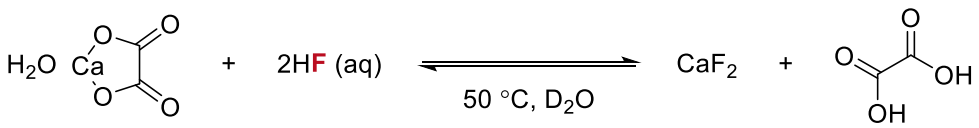

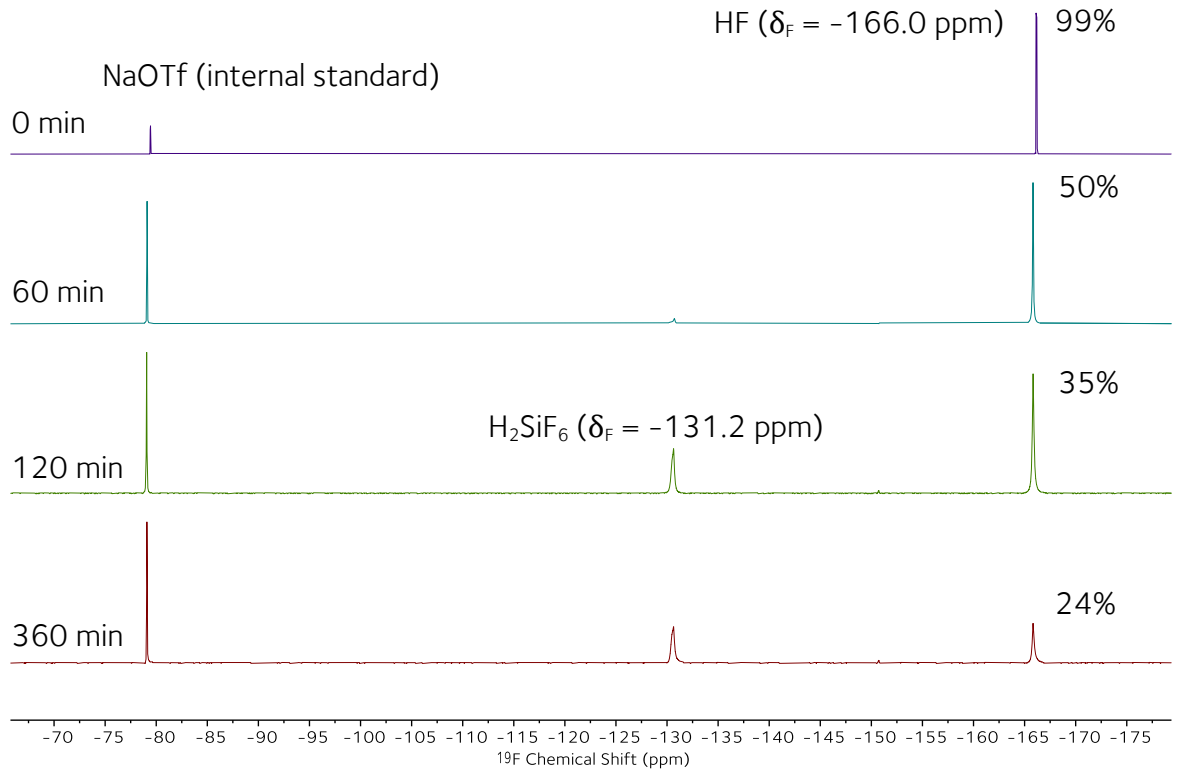

Figure 3.13. Reaction of calcium oxalate monohydrate (99%, Sigma Aldrich) with 2 equivalents of HF (48% aq. solution) in D_2O at 50 °C monitored by ^{19}F NMR spectroscopy. Singlet diagnostic of HF observed at -166.0 ppm. NaOTf internal standard at -78.0 ppm. H_2SiF_6 observed at -131.2 ppm (after 2 h reaction) due to silica impurity in calcium oxalate.

In the presence of either $B(OH)_3$ or SiO_2, the equilibrium is displaced via the precipitation of highly insoluble CaOx and immediate HF capture by the Lewis acid. Under these conditions, the singlet diagnostic of HF was not detected by ^{19}F NMR spectroscopy during the entire course of the reaction (Figure 3.14 and Figure 3.15). As anticipated, the reaction of AGF with fluorophilic Lewis acid in the absence of H_2Ox resulted in no fluoride release. These data highlight how Brønsted and Lewis acid cooperativity allows for fluorspar activation under mild conditions and prevents HF from accumulating.

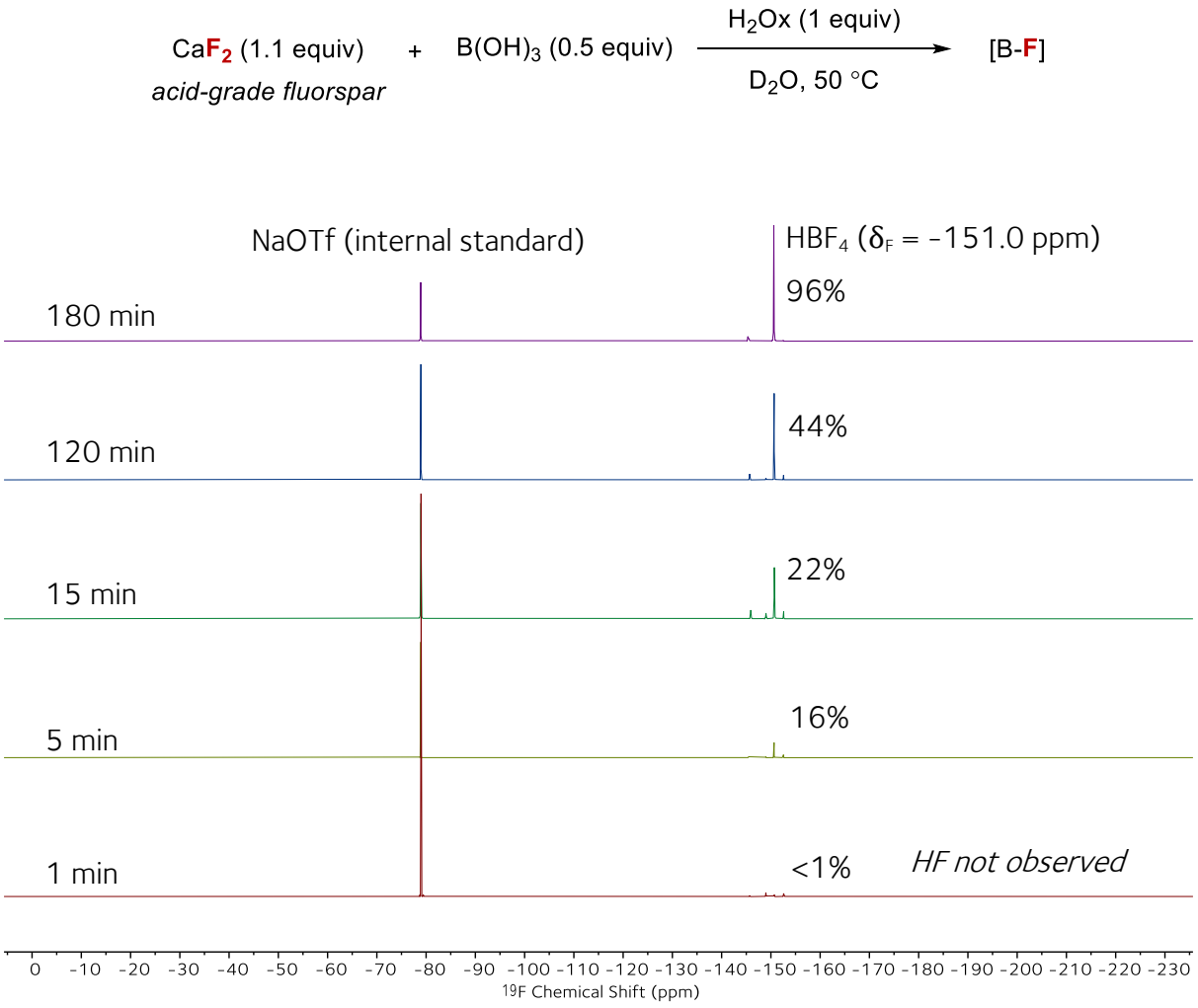

Figure 3.14. Reaction of AGF with H_2Ox and $B(OH)_3$ in D_2O at 50 °C monitored by ^{19}F NMR spectroscopy (D_2O). HBF_4 at -151.0 ppm. Sodium triflate internal standard at -78.0 ppm.

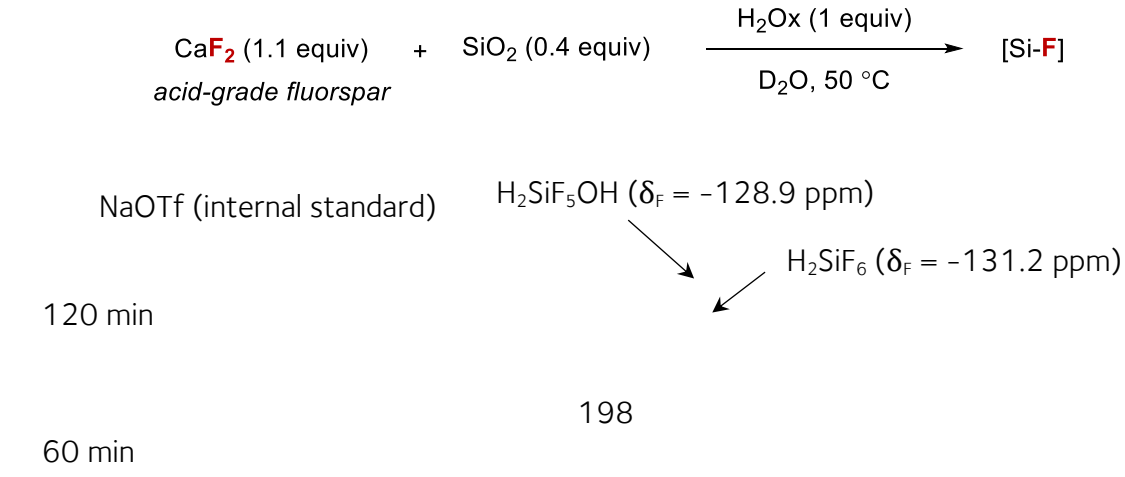

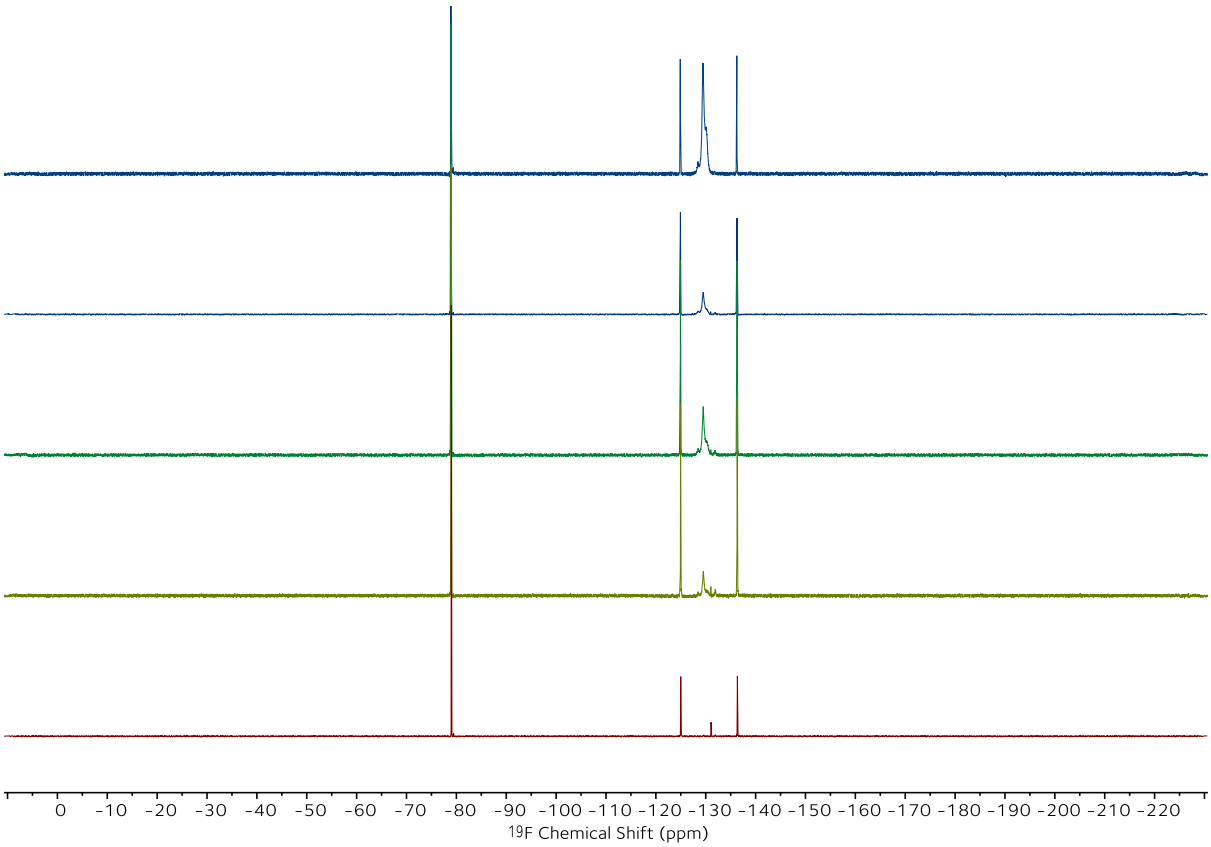

Figure 3.15. Reaction of AGF with H_2Ox and SiO_2 in D_2O at 50 °C monitored by ^{19}F NMR spectroscopy (D_2O). H_2SiF_6 at -131.2 ppm, H_2SiF_5OH at -128.9 ppm (broadening of signals due to fast intramolecular fluoride exchange) and H_2OxSiF_4 resonances at -124.5 ppm and -135.9 ppm. Sodium triflate standard at -78.0 ppm.

3.3.6 Comparison with Inorganic Acids

To better analyse this approach compared to the current H_2SO_4-dependent CaF_2 activation method, a detailed study comparing $H_2Ox{\cdot}2H_2O$ and H_2SO_4 for AGF activation in the presence of $B(OH)_3$ or SiO_2 was undertaken at two temperatures (25 °C and 50 °C). The initial acid screening (refer to Figure 3.1) established conditions for high-yielding fluoride release from AGF at 50 °C (15 h), where $H_2Ox{\cdot}2H_2O$ outperformed H_2SO_4 when $B(OH)_3$ was employed as a Lewis acid (96% using H_2Ox versus 69% yield using H_2SO_4 after 15 h). However, at 50°C, the combination of AGF, concentrated H_2SO_4 (95-97%), and

$B(OH)_3$ increased the yield of [B–F] products to 97% yield when the reaction time was extended to 24 h (Table 3.4, entry 3). This reaction was also effective at 25 °C offering [B–F] products in 94% yield [average of two runs (entries 5 and 6)] after a reaction time of 48 h. For comparison, $H_2Ox{\cdot}2H_2O$ afforded [B-F] products in 98% under these conditions (25 °C, 48 h) (entry 4).

Table 3.4. Yields of [B-F] products from reaction between acid-grade fluorspar and $B(OH)_3$ in the presence of H_2SO_4 or $H_2Ox{\cdot}2H_2O$ at 25 °C and 50 °C.

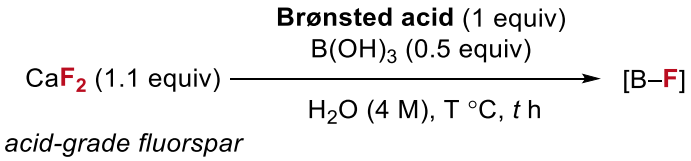

Entry	Acid	Temperature (°C)	Time (h)	HBF_4 (%)	HBF_3OH (%)	Total [B-F] (%)
1	$H_2Ox{\cdot}2H_2O$	50	15	76	20	96
2	conc. H_2SO_4	50	15	49	20	69
3	conc. H_2SO_4	50	24	84	13	97
4	$H_2Ox{\cdot}2H_2O$	25	48	82	16	98
5	conc. H_2SO_4	25	48	86	13	99
6*	conc. H_2SO_4	25	48	75	14	89

Using 8.0 mmol AGF. Yields determined by ^{19}F NMR spectroscopy using NaOTf as internal standard. *Repeat of entry 5. $HOxBF_2$ observed in <1% in reactions using $H_2Ox{\cdot}2H_2O$.

When SiO_2 served as the fluorophilic Lewis acid, activation of AGF with $H_2Ox{\cdot}2H_2O$ was also effective at 25 °C, albeit requiring a prolonged reaction time of 72 h. After neutralisation with KOH, KF was isolated in 74% yield (Table 3.5, entry 3). Replacement of oxalic acid for H_2SO_4 did not give satisfactory results. At 50 °C for 24 h, the reaction of AGF, concentrated H_2SO_4, and SiO_2 gave only partial fluoride release as H_2SiF_6 and H_2SiF_5OH, with a total [Si-F] product yield of 48% (quantified by ^{19}F NMR spectroscopy). At 25 °C with a 72 h reaction

time, the total [Si-F] product yield was reduced to 29%. Notably, the treatment of these [Si-F] solutions with KOH afforded a solid material containing both KF and K_2SO_4 [46% KF (50 °C) and 36% KF (25 °C)] as evidenced by PXRD analysis (Figure 3.16), two salts which are challenging to separate [KF, 1020 mg/mL; K_2SO_4 120 mg/mL (H_2O, 25 °C)]. The formation of K_2SO_4 is indicative of the incomplete reaction amongst AGF, H_2SO_4 and SiO_2. The overall superior reactivity of $H_2Ox.2H_2O$ compared to H_2SO_4 correlates with the solubility of the calcium by-product formed upon AGF activation [$CaOx.H_2O$, 0.0061 mg/mL versus $CaSO_4.2H_2O$, 2.1 mg/mL (H_2O, 20 °C)].

Table 3.5. Yields of KF from reaction between AGF and SiO_2 in the presence of H_2SO_4 or $H_2Ox{\cdot}2H_2O$ at 25 °C and 50 °C.

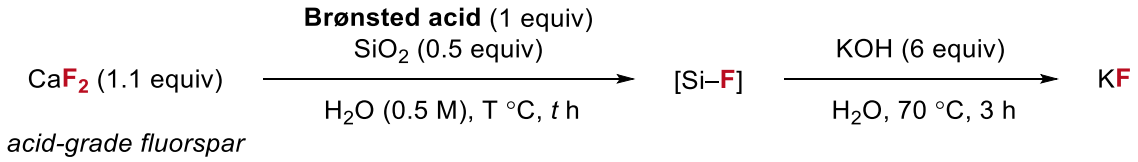

Entry	Acid	Temperature (°C)	Time (h)	KF yield (%)
1	$H_2Ox{\cdot}2H_2O$	50	15	85
2	conc. H_2SO_4	50	24	46
3	$H_2Ox{\cdot}2H_2O$	25	72	74
4	conc. H_2SO_4	25	72	36

Using 8.0 mmol AGF. Yields determined by ^{19}F NMR (D_2O) spectroscopy using NaOTf as internal standard.

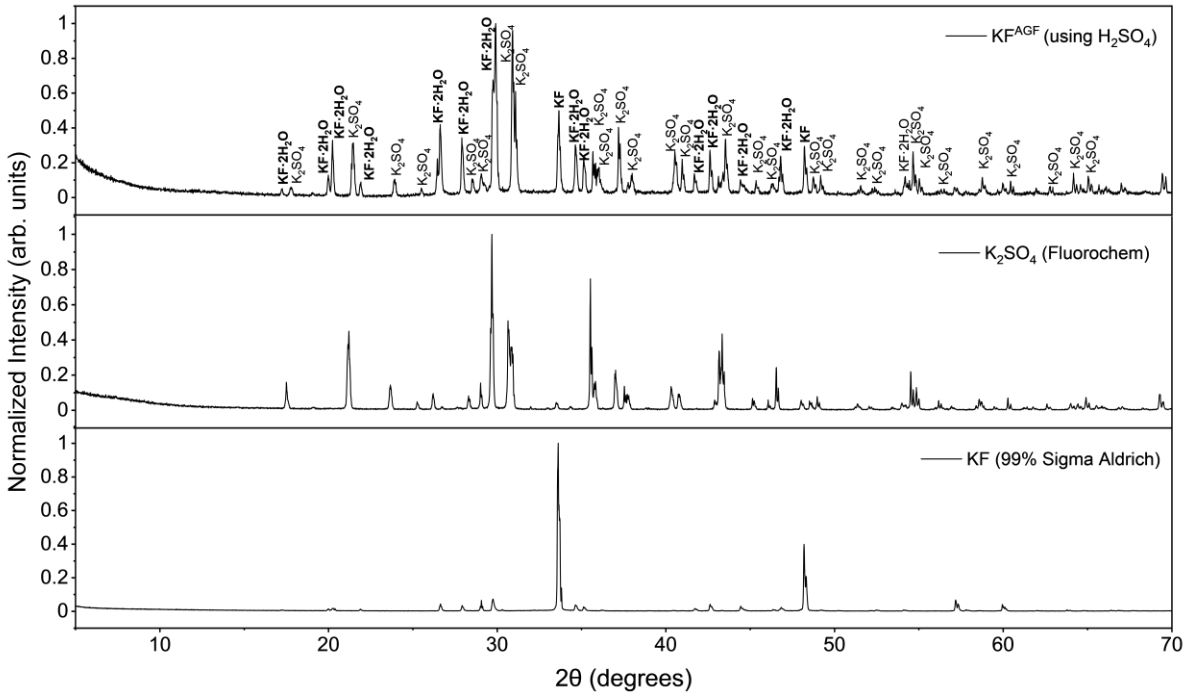

Figure 3.16. Powder X-ray diffraction patterns of the solid product formed in the reaction of acid-grade fluorspar (CaF_2) with H_2SO_4 and SiO_2 after 24 h at 50 °C (top), K_2SO_4 (middle) and KF (bottom).

In the initial acid screening (15 h, 50 °C, refer to Figure 3.1), HCl (2 equiv) was also observed to enable high-yielding fluoride release from AGF when $B(OH)_3$ was used as a Lewis acid (60% of [B-F] products). However, under identical reaction conditions no [Si-F] products were observed using SiO_2. In line with this observation, subsequent neutralisation of the reaction mixture resulted in the formation of KCl only, indicative of no reaction between AGF, HCl and SiO_2 (Scheme 3.25).

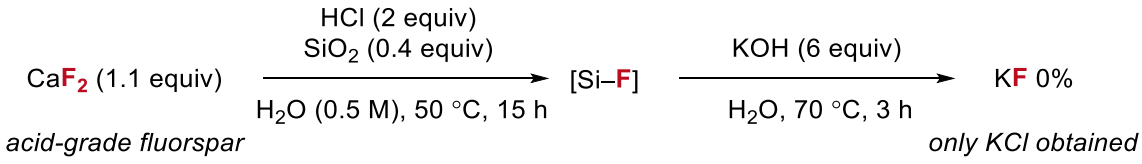

Scheme 3.25. Activation of AGF using HCl and silica gel to give [Si-F] which upon alkaline hydrolysis affords KCl only, indicative of no reaction between AGF, HCl and SiO_2.

3.3.7 Metspar derived KF

The successful cooperative activation of AGF in water and its application to the synthesis of fluoroarenes encouraged an investigation on the reactivity of lower-grade metallurgical fluorspar (metspar), a fluoride reservoir that has not been exploited for the synthesis of fluorochemicals to the best of our knowledge. These studies were performed with metspar sourced from China [Metspar I CaF_2 (85%), SiO_2 (10%), $CaCO_3$ (<5%), S (0.12%), P (0.1%)], and Mexico [Metspar II from CaF_2 (88.98%), SiO_2 (5.43%), $CaCO_3$ (4.02%), Al_2O_3 (0.41%), Fe_2O_3 (0.24%), S (0.011%), P (0.023%), Pb (<0.001%)] (Scheme 3.26). The reaction of metspar (1.1 equiv) with $H_2Ox{\cdot}2H_2O$ (1.04 - 1.09 equiv) and SiO_2 (0.4 equiv) enabled the preparation of over half a gram of metspar-derived KF (KF^M) [53% ($KF^{M(I)}$) and 63% ($KF^{M(II)}$) yield, calculated from metspar I or II, respectively], which performed comparably to commercial KF and KF^{AGF}. Due to the reduced purity of metspar compared to AGF, K_2SiF_6 was first prepared and isolated prior to basic hydrolysis (Scheme 3.26).

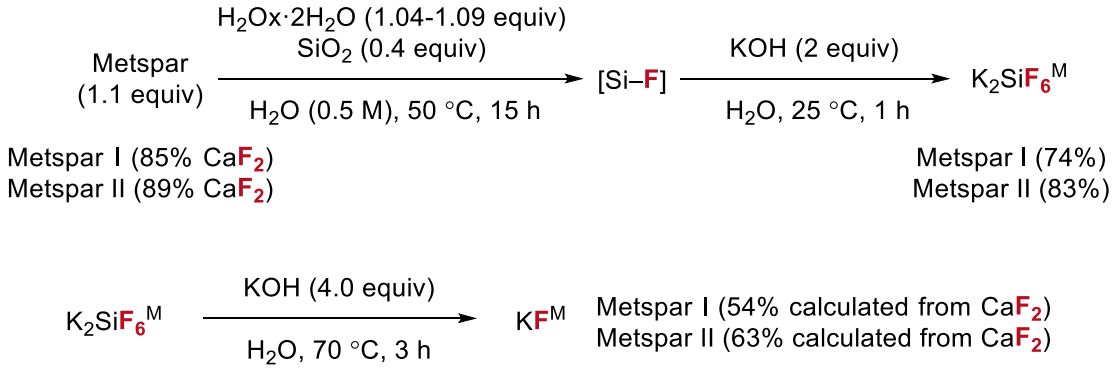

Scheme 3.26. Synthesis of KF^M via alkaline hydrolysis of $K_2SiF_6{}^M$ prepared from reacting metspar (85% CaF_2 or 89% CaF_2), $H_2Ox{\cdot}2H_2O$ and SiO_2 (50 °C, 15 h).

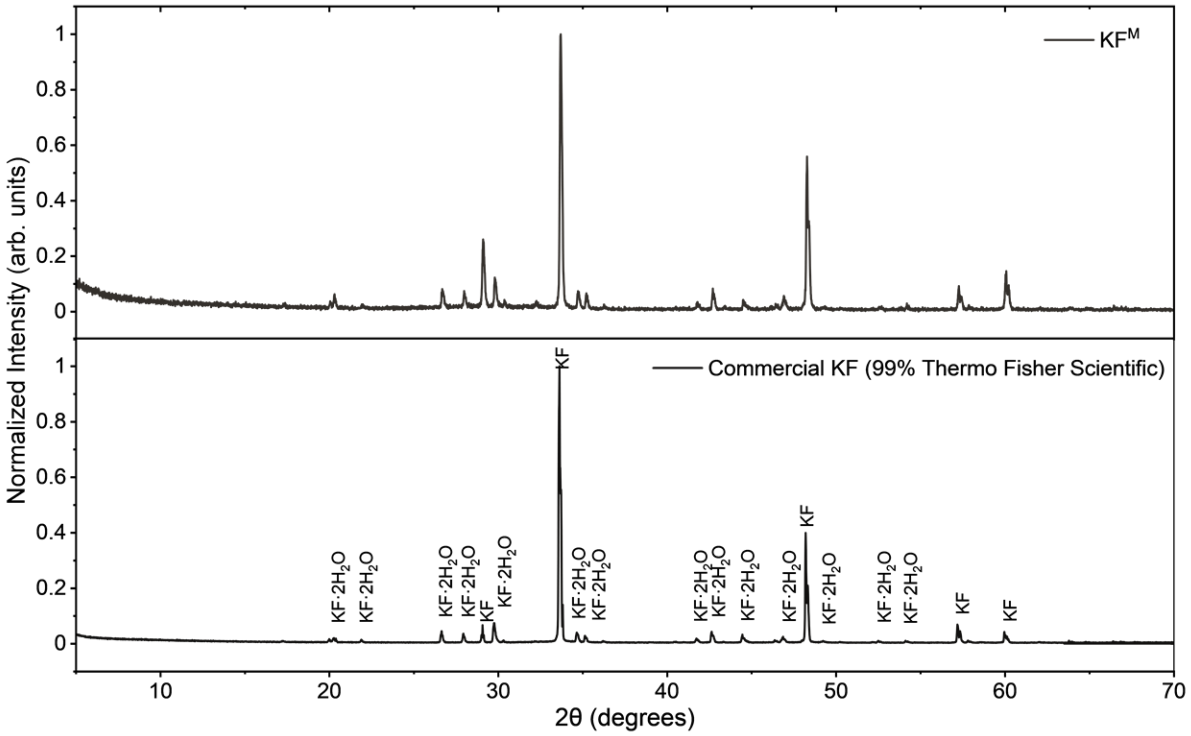

Figure 3.17. Powder X-ray diffraction pattern of $KF^{M(I)}$ (top trace) and commercial KF (bottom trace). $KF^{M(I)}$ is comprised of crystalline anhydrous KF and KF dihydrate.

3.4 Conclusion

The method developed in this chapter unlocks the reactivity of acid-grade fluorspar (AGF) in water using a Brønsted acid, optimally oxalic acid, in combination with a fluorophilic Lewis acid [$B(OH)_3$ or SiO_2] for immediate HF capture. For comparison, sulfuric acid (H_2SO_4) is effective when combined with $B(OH)_3$, but underperformed using SiO_2. Overall, oxalic acid is therefore superior to H_2SO_4 in terms of reactivity, releasing more fluoride from AGF under otherwise similar reaction conditions. The method stands out for proceeding under remarkably mild conditions (< 50 °C), being operationally simple and applicable to lower purity grade metspar. This approach offers the possibility of decentralised manufacturing, an attractive model for the fluorochemical industry that can save storage and transportation costs, as well as mitigate HF handling. With the renewed interest in innovative methods to

synthesise oxalic acid via CO_2 capture and biomass, and the challenges posed by our dependence on fossil fuels for sulfur and therefore H_2SO_4 supply, this technology may represent a novel departure toward a sustainable fluorochemical industry.[39–41] In the future, adaptation of this method to accommodate other Lewis acidic main group metals, such as aluminium, may offer access to a broader range of fluorochemicals.

3.5 References

1. Petrov, V. A. & Thrasher, J. S. From alternate routes to fluorspar (CaF_2) or anhydrous HF (aHF) to conversion of fluorspar into a nucleophilic fluorinating agent. *J. Fluor. Chem.* **275**, 110274 (2024).
2. Fogler, H. S. *Elements of Chemical Reaction Engineering*. (Prentice Hall PTR, 2006).
3. Lin, M.-F. *et al.* Recycle of synthetic calcium fluoride and waste sulfuric acid to produce electronic grade hydrofluoric acid. *Environ. Sci. Pollut. Res. Int.* **28**, 40633–40639 (2021).
4. Krysenko, G. F., Gordienko, P. S. & Epov, D. G. Sulfuric acid breakdown of fluorite in the presence of silica. *Russ. J. Inorg. Chem.* **54**, 1876–1879 (2009).
5. Rothenberg, G., Royz, M., Arrad, O. & Sasson, Y. In situ generation and synthetic applications of anhydrous hydrogen fluoride in a solid-liquid biphasic system. *J. Chem. Soc., Perkin Trans. 1* 1491–1494 (1999).
6. Paterno, E. & Alvisi, U. Inorganic chemistry Reactions of Metallic Fluorides. *J. Chem. Soc., Abstracts* **76**, B17–B34 (1899).
7. Lennox, A. J. J. Organotrifluoroborate Preparation. in *Organotrifluoroborate Preparation, Coupling and Hydrolysis* (ed. Lennox, A. J. J.) 11–36 (Springer International Publishing, Cham, 2013).
8. Vedejs, E., Chapman, R. W., Fields, S. C., Lin, S. & Schrimpf, M. R. Conversion of Arylboronic Acids into Potassium Aryltrifluoroborates: Convenient Precursors of Arylboron Difluoride Lewis Acids. *J. Org. Chem.* **60**, 3020–3027 (1995).

9. Lennox, A. J. J. & Lloyd-Jones, G. C. Preparation of Organotrifluoroborate Salts: Precipitation-Driven Equilibrium under Non-Etching Conditions. *Angew. Chem. Int. Ed.* **51**, 9385–9388 (2012).
10. Eghbarieh, N. & Masarwa, A. Desymmetrization of Diboron(4) by a Trifluorination B-Masking Strategy: Practical Synthesis of Unsymmetrical Diboron Species. *J. Org. Chem.* **89**, 11753–11760 (2024).
11. Cresswell, A. J., Davies, S. G., Roberts, P. M. & Thomson, J. E. Beyond the Balz–Schiemann Reaction: The Utility of Tetrafluoroborates and Boron Trifluoride as Nucleophilic Fluoride Sources. *Chem. Rev.* **115**, 566–611 (2015).
12. Mootz, D. & Steffen, M. Kristallstrukturen von Säurehydraten und Oxoniumsalzen. XX. Die Oxoniumtetrafluoroborate H_3OBF_4, $[H_5O_2]BF_4$ und $[H(CH_3OH)_2]BF_4$. *Z anorg allg chem* **482**, 193–200 (1981).
13. Ochoa, G., Pilgrim, C. D., Kerr, J., Augustine, M. P. & Casey, W. H. Aqueous geochemistry at gigapascal pressures: NMR spectroscopy of fluoroborate solutions. *Geochim. Cosmochim. Acta* **244**, 173–181 (2019).
14. Aigueperse, J. *et al.* Fluorine Compounds, Inorganic. in *Ullmann's Encyclopedia of Industrial Chemistry* (ed. Wiley-VCH Verlag GmbH & Co. KGaA) 11–307 (Wiley-VCH, Weinheim, Germany, 2000).
15. Wamser, C. A. Hydrolysis of Fluoboric Acid in Aqueous Solution. *J. Am. Chem. Soc.* **70**, 1209–1215 (1948).
16. Simon, K. *et al.* Generation of 1,2-Difluorobenzene via a Photochemical Fluorodediazoniation Step in a Continuous Flow Mode. *Org. Process Res. Dev.* **27**, 322–330 (2023).
17. Yang, L. & Zhang, C.-P. Revisiting the Balz–Schiemann Reaction of Aryldiazonium Tetrafluoroborate in Different Solvents under Catalyst- and Additive-Free Conditions. *ACS Omega* **6**, 21595–21603 (2021).
18. Siegemund, G. *et al.* Fluorine Compounds, Organic. in *Ullmann's Encyclopedia of Industrial Chemistry* 1–56 (Wiley, Weinheim, Germany, 2016).
19. Park, N. H., Senter, T. J. & Buchwald, S. L. Rapid Synthesis of Aryl Fluorides in Continuous Flow through the Balz–Schiemann Reaction. *Angew. Chem.* **128**, 12086–12090 (2016).

20. Firth, J. D. & Fairlamb, I. J. S. A Need for Caution in the Preparation and Application of Synthetically Versatile Aryl Diazonium Tetrafluoroborate Salts. *Org. Lett.* **22**, 7057–7059 (2020).
21. Yu, Z., Lv, Y. & Yu, C. A Continuous Kilogram-Scale Process for the Manufacture of o-Difluorobenzene. *Org. Process Res. Dev.* **16**, 1669–1672 (2012).
22. Lickiss, P. D. Silicon: Inorganic Chemistry. in *Encyclopedia of Inorganic and Bioinorganic Chemistry* (John Wiley & Sons, Ltd, 2011).
23. Yang, H. *et al.* Production of anhydrous hydrogen fluoride from fluorosilicic acid: a review. *Front. Chem.* **12**, (2024).
24. Zhao, H. *et al.* Solubility Measurement and Correlation of Potassium Hexafluorosilicate (K_2SiF_6) in H_2O, HCl, and H_3PO_4 Solutions at a Temperature Range of 5–70 °C. *J. Chem. Eng. Data* **68**, 2449–2459 (2023).
25. Igarashi, M. *et al.* Non-aqueous selective synthesis of orthosilicic acid and its oligomers. *Nat Commun* **8**, 140 (2017).
26. Finney, W. F., Wilson, E., Callender, A., Morris, M. D. & Beck, L. W. Reexamination of Hexafluorosilicate Hydrolysis by ^{19}F NMR and pH Measurement. *Environ. Sci. Technol.* **40**, 2572–2577 (2006).
27. Urbansky, E. T. Fate of Fluorosilicate Drinking Water Additives. *Chem. Rev.* **102**, 2837–2854 (2002).
28. Gibson, J. A., Ibbott, D. G. & Janzen, A. F. Fluorine N.M.R. Spectra of Sulfur, Phosphorus, and Silicon Fluorides: Hydrolysis and Intra- and Intermolecular Mechanisms of Fluorine Exchange. *Can. J. Chem.* **51**, 3203–3210 (1973).
29. Haynes, W. M. *CRC Handbook of Chemistry and Physics, 95th Edition*. (CRC Press, Hoboken, 2014).
30. He, H., Bleby, T. M., Veneklaas, E. J., Lambers, H. & Kuo, J. Morphologies and elemental compositions of calcium crystals in phyllodes and branchlets of Acacia robeorum (Leguminosae: Mimosoideae). *Ann Bot* **109**, 887–896 (2012).
31. Xu, Z. *et al.* Enhanced Performance of a Lithium–Sulfur Battery Using a Carbonate-Based Electrolyte. *Angew. Chem. Int. Ed.* **55**, 10372–10375 (2016).
32. W. Dean, P. A. & F. Evans, D. Spectroscopic studies of inorganic fluoro-complexes. Part III. Fluorine-19 nuclear magnetic resonance studies of silicon(IV), germanium(IV), and titanium(IV) fluoro-complexes. *J. Chem. Soc. A* **0**, 2569–2574 (1970).

33. Pietschnig, R. Improved ^{29}Si NMR detection of sterically protected fluorosilanes using the ^{29}Si(^{19}F)-INEPT technique. *Journal of Fluorine Chemistry* **128**, 150–152 (2007).
34. Kim, D. W. *et al.* Facile Nucleophilic Fluorination Reactions Using *tert*-Alcohols as a Reaction Medium: Significantly Enhanced Reactivity of Alkali Metal Fluorides and Improved Selectivity. *J. Org. Chem.* **73**, 957–962 (2008).
35. Vedantham, R., Vetukuri, V. P. R., Boini, A., Khagga, M. & Bandichhor, R. Improved One-Pot Synthesis of Citalopram Diol and Its Conversion to Citalopram. *Org. Process Res. Dev.* **17**, 798–805 (2013).
36. Velcicky, J. *et al.* Modulating ADME Properties by Fluorination: MK2 Inhibitors with Improved Oral Exposure. *ACS Med. Chem. Lett.* **9**, 392–396 (2018).
37. Hirth-Dietrich, C. *et al.* 'The use of sGC stimulators, sGC activators, alone and combinations with PDE5 inhibitors for the treatment of systemic sclerosis (SSc)' WO Patent WO2011147810A1. (2011).
38. Z. C. 'Preparation method of clodinafop propargyl', CN105418494A CN Patent. (2016).
39. Schuler, E., Demetriou, M., Shiju, N. R. & Gruter, G.-J. M. Towards Sustainable Oxalic Acid from CO_2 and Biomass. *ChemSusChem* **14**, 3636–3664 (2021).
40. Maslin, M., Van Heerde, L. & Day, S. Sulfur: A potential resource crisis that could stifle green technology and threaten food security as the world decarbonises. *Geogr. J.* **188**, 498–505 (2022).
41. Day, S., Alexander, P. & Maslin, M. Energy decarbonization threatens food security by reducing the availability of cheap sulfur. *Nat Food* **4**, 442–444 (2023).

4.Experimental

Unless otherwise stated, the work described in this chapter was completed by C. Patel.

4.1 Materials and Methods

Unless otherwise stated, all reagents were purchased from commercial suppliers, used without further purification and stored under ambient conditions unless otherwise stated. Solvents were purchased from commercial suppliers and used as provided without further purification. 18-Crown-6 ($C_{12}H_{24}O_6$, ≥ 99.0%, Sigma Aldrich, CAS 17455-13-9) was recrystallised from MeCN and stored in a desiccator. Tetramethylammonium chloride ($C_4H_{12}NCl$, ≥ 99.0%, Sigma Aldrich, 75-57-0) was also stored in a desiccator. Reagent grade calcium fluoride (CaF_2, ≥ 97.0%, Alfa Aesar, CAS 7789-75-5), anhydrous potassium phosphate (K_3PO_4, ≥98%, Acros Organics, CAS 7778-53-2), anhydrous dipotassium hydrogen phosphate (K_2HPO_4, ≥ 98.0%, Fisher Scientific, CAS 7758-11-4), anhydrous potassium dihydrogen phosphate (KH_2PO_4, ≥ 99.0%, Fisher Scientific, CAS 7778-77-0), anhydrous oxalic acid ($C_2H_2O_4$, Sigma Aldrich, CAS 144-62-7), oxalic acid dihydrate ($C_2H_6O_6$, Sigma Aldrich, CAS 6153-56-6), boric acid (H_3BO_3, ≥ 99.5%, Sigma Aldrich, CAS 10043-35-3), silica gel (SiO_2, silica gel 60 particle size 0.040-0.063 mm, Merck, CAS 7631-86-9) was used in this work.

Fluorspar (acid grade) was purchased from Mistral Industrial Chemicals (UK), sourced from Minersa group (Asturias region, Spain) and contains CaF_2 (> 97%), total carbonates (< 1.50%), SiO_2 (<1.00%), $BaSO_4$ (<0.50 %), Pb (< 0.10%), Fe_2O_3 (< 0.10%), S (< 0.15%), H_2O (< 1.0%).

Metspar was sourced from China (Luoyang Aurora Minechem. Co. Ltd, gifted by FluoRok) [Metspar^{I} CaF_2 (85%), SiO_2 (10%), $CaCO_3$ (<5%), S (0.12%), P (0.1%)], and Mexico (Mexichem Fluor S.A de C.V., gifted by Glencore UK) [Metspar^{II} from CaF_2 (88.98%), SiO_2 (5.43%), $CaCO_3$ (4.02%), Al_2O_3 (0.41%), Fe_2O_3 (0.24%), S (0.011%), P (0.023%), Pb (<0.001%)].

Deuterated solvents were purchased from VWR Chemicals or Sigma Aldrich and used as received.

Thin layer chromatography (TLC) was carried out on silica gel pre-coated aluminum sheets (Merck Kieselgel 60 F254 plates) and visualized using ultraviolet light of wavelength 254 nm or potassium permanganate stain. Flash column chromatography (FFC) was performed on Merck silica gel (60, particle size 0.040-0.063 mm).

Ball milling was carried out using either a Retsch MM 400 mixer mill (30 Hz experiments), Retsch MM 500 Vario mixer mill (35 Hz experiments) or an Insolido IST636 mixer mill (35 Hz experiments). Unless otherwise stated, mechanochemical reactions were carried out in 15 mL or 30 mL FormTech Scientific (FTS) stainless steel (316) jars with stainless steel (316) balls (2 g (8 mm), 3 g (9 mm), 4 g (10 mm), 7 g (12 mm), 9 g (13 mm), 16 g (15 mm)). O-ring inserts (15 mL stainless steel jars) supplied by FTS are made of EPDM (ethylene propylene diene monomer) rubber. Scale-up mechanochemical reactions were

carried out in a 35 mL Retsch stainless steel (316) jar. No precaution was taken to exclude air and moisture.

Reactions using fluorspar and Brønsted acids were performed in polypropylene (PP) vessels sealed with a low-density polyethylene cap or poly(tetrafluoroethylene) (PTFE) round bottom flask (RBF) under an atmosphere of air, unless otherwise stated. Reported concentrations refer to solution volumes at room temperature.

Fluorination reactions using **Fmix**, KF, $Me_4NF{\cdot}^tAmOH$ or HBF_4 were stirred at 1000 rpm using an IKA heating plate, aluminum block and borosilicate glass vials.
^{1}H NMR, ^{13}C NMR, ^{19}F NMR, ^{11}B NMR and ^{29}Si NMR spectra were recorded on Bruker AVIIIHD 400, AVIIIHD 500, AVII 500 or AV NEO 600. ^{1}H NMR spectra were recorded at 400 or 500 MHz. ^{13}C NMR spectra were recorded at 101 or 126 MHz with ^{1}H decoupling, ^{19}F NMR spectra were recorded at 377 or 471 MHz, ^{11}B NMR spectra were recorded at 128 MHz, ^{29}Si NMR spectra were recorded at 99 MHz. ^{1}H NMR, ^{13}C NMR,^{19}F NMR, ^{11}B NMR and ^{29}Si NMR spectral data are reported as chemical shifts (δ) in parts per million (ppm) relative to the solvent peak using the Bruker internal referencing procedure (edlock). Coupling constants, *J*, are reported in Hz to the nearest 0.1 Hz. Unless otherwise stated, ^{13}C spectra are ^{1}H decoupled and reported coupling constants for ^{13}C spectra correspond to ^{19}F–^{13}C heteronuclear coupling. Data are reported as follows: chemical shift, multiplicity (s = singlet, d = doublet, t = triplet, q = quartet, pent = pentet, hept = heptet, br = broad, m = multiplet), coupling constants (Hz) and integration. NMR (nuclear magnetic resonance) spectra were processed with MestReNova 14.1.2. Quantitative NMR analysis was determined using 4-fluoroanisole or sodium triflate (NaOTf) as an internal standard. The standard was added to the crude reaction mixture and an aliquot was taken to be analysed by quantitative ^{19}F NMR and ^{1}H NMR.

Solid state NMR spectra were recorded on a Bruker AVIII 400 spectrometer (Operating frequencies; ^{1}H 400.130 MHz, ^{19}F 376.498 MHz, ^{31}P 161.976 MHz) equipped with a HFXY 3.2 mm probe. Spectra were collected at 298 K and samples were acquired spinning at the magic angle $\theta = 54.7356^\circ$. Values of magic-angle spinning, MAS, speeds, ν_{rot}, range between 13 – 20 kHz. Powdered samples were loaded into 3.2 mm ZrO_2 rotors fitted with a Kel-F drive cap. Spectra are reported in chemical shift, δ, in parts per million (ppm) referenced against a secondary external standard ^{1}H adamantane ($\delta_H = 1.85$),[1] ^{19}F PTFE ($\delta_F = -122.7$)[2], ^{31}P the downfield resonance of ADP ($\delta_P = 10.2$)[3].

High resolution mass spectra (HRMS) were determined on a Thermo Exactive High-Resolution Orbitrap FTMS mass spectrometer (ESI+ or ESI-). Agilent 5977B was used for GC-MS (EI+). Some compounds were found to be unstable under a variety of MS ionization methods (CI, EI, ESI, GC-MS) and therefore no HRMS could be obtained for them.

X-ray powder diffraction (PXRD) data was collected at room temperature using a Bruker D8 Advance X-ray diffractometer (Bragg–Brentano geometry); the radiations Cu Kα1,2 were used.

Elemental analyses were carried out by London Metropolitan University. Elemental analysis Found values for carbon, hydrogen, nitrogen and sulfur are within 0.26%, 0.08%, 0.11% and 0,08% within the Calcd values for the proposed formula, respectively.

Inductively Coupled Plasma Optical Emission spectroscopy (ICP-OES) for metal analyses (Fe, Cr, Ni, Mn, Mo) was carried out by Dr. Nigel Howard at the University of Cambridge microanalysis facilities or MEDAC Ltd (KF^{AGF}, KF^{M}, CsF^{AGF} and NaF^{AGF}).

Reaction progress and initial structural characterisation (solid-state reactions) was performed using X-ray powder diffraction (PXRD) data collected using a Bruker D8 Advance X-ray diffractometer (Bragg–Brentano geometry); the radiations Cu Kα1,2 were used. Profile-matching refinements were performed on the XRD patterns for cell parameters determination, using the Rietveld refinement method with the TOPAS V.7 software.

Infrared spectra (IR) were recorded as the neat compound (neat) or as an evaporated solution (thin layer film) using a Bruker Tensor 27 FTIR spectrometer. Absorptions are reported in wavenumber (cm^{-1}).

Melting points of solids were measured on a Griffin apparatus and are uncorrected.

Thermogravimetric Analysis (TGA) was performed on a TA Discovery TGA 5500 instrument. Powder samples were loaded on a platinum high temperature pan and, if indicated, left to stand in air for 2 h. If indicated, the sample was then kept at room temperature (25 °C) under a nitrogen flow (25 mL min^{-1}, 5 h). The samples were heated from 30 to 200 °C at a rate of 2 °C min^{-1} and then from 200 to 600 °C at a rate of 5 °C min^{-1} under N_2 flow (25 mL min^{-1}).

Scanning Electron Microscope (SEM) images were recorded on a Jeol JSM6010 SEM.

Teflon NMR thin wall (5 mm) liner for reaction monitoring experiments was purchased from NEW ERA.

4.2 Fluorochemicals from Fluorspar via a Phosphate-Enabled Mechanochemical Process that bypasses HF

The experimental section for this work has been partially disclosed in Supplementary Materials for: C. Patel, E. André-Joyaux, J. A. Leitch, X. M. de Irujo-Labalde, F. Ibba, J. Struijs, M. A. Ellwanger, R. Paton, D. L. Browne, G. Pupo, S. Aldridge, M. A. Hayward, V. Gouverneur, Fluorochemicals from fluorspar via a phosphate-enabled mechanochemical process that bypasses HF. *Science* **381**, 302–306 (2023).

4.2.1 Reaction development

For preliminary optimisation experiments in Chapter **2**, the yield of products and by-products were determined by ^{1}H NMR and ^{19}F NMR spectroscopy with 4-fluoroanisole as internal standard unless otherwise stated. The CaF_2 (reagent grade or acid grade fluorspar) used is stated for each optimisation experiment.

Mass balance accounts for the % of unreacted 4-toluenesulfonyl chloride (TsCl), 4-toluenesulfonyl fluoride (TsF, **1**) and undesired by-product derived from TsCl (4-toluenesulfonic acid or its salt). A mass balance of less than 100% indicates that TsCl was converted into 4-toluenesulfonic acid (or its salt), which was not recovered.

4.2.1.1 Fluorination reactions carried out in solution

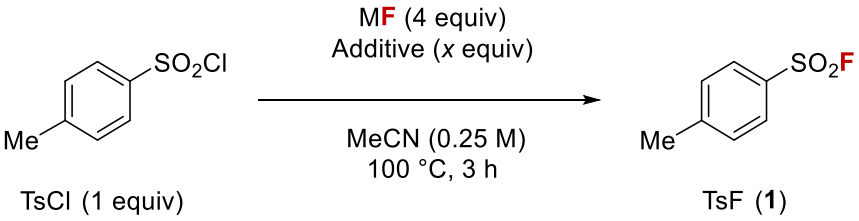

4-toluenesulfonyl chloride (47.7 mg, 0.25 mmol, 1 equiv), CaF_2 (78.1 mg, 1.0 mmol, 4 equiv) and additive (*x* equiv) [18-crown-6 or Schreiner's Urea] in MeCN (1 mL) was stirred for 3 h at 100 °C. After 3 h, the crude reaction mixture was concentrated *in vacuo*, and 4-fluoroanisole (10 µL, 11.1 mg, 88.3 µmol) was added as an internal standard. An aliquot was then diluted in deuterated chloroform. Reaction yield/conversion was determined by quantitative ^{1}H and ^{19}F NMR spectroscopy.

Data can be found in Table 2.2.

4.2.1.2 Preliminary solid-state fluorination experiments (one pot)

Fluorination of 4-toluenesulfonyl chloride was investigated at 1.0 mmol using reagent grade CaF_2 (≥ 97.0%, Alfa Aesar) and a phosphate additive under mechanochemical conditions (ball milling).

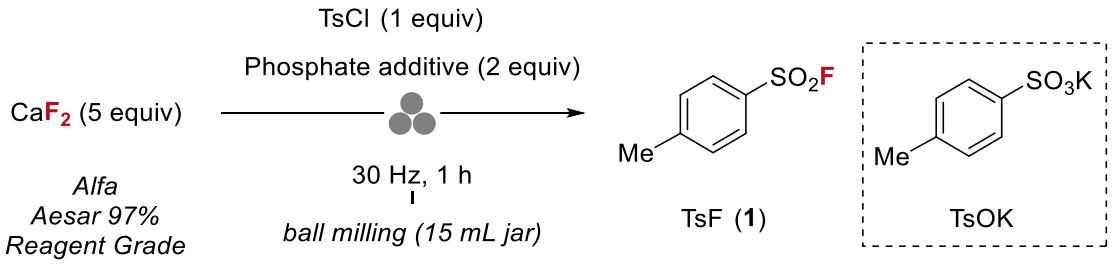

To a 15 mL stainless steel milling jar was added a stainless steel ball (4 g), 4-toluenesulfonyl chloride (191 mg, 1.0 mmol, 1 equiv), KF (1.1 to 5.0 equiv) or CaF_2 (390 mg, 5.0 mmol, 5 equiv). The jar was closed and securely fitted to the mill which was set for indicated time at 30 Hz. Upon completion, the jar was opened and rinsed with EtOAc (~ 5 mL). The crude reaction mixture was passed through a plug of silica eluting with EtOAc, concentrated *in vacuo*, and 4-fluoroanisole (10 µL, 11.1 mg, 88.3 µmol) was added as an internal standard.

An aliquot was then diluted in deuterated chloroform. Reaction yield/conversion was determined by quantitative ^{1}H and ^{19}F NMR spectroscopy.

Data can be found in Table 2.3.

4.2.1.3 Preliminary solid-state fluorination experiments (two-step protocol)

Fluorination of 4-toluenesulfonyl chloride was investigated at 1.0 mmol using reagent grade CaF_2 (≥ 97.0%, Alfa Aesar) and K_2HPO_4 (≥ 98.0%, Alfa Aesar) under mechanochemical conditions (ball milling). In this experiment, CaF_2 was first ball milled with K_2HPO_4 for *x* h before adding 4-toluenesulfonyl chloride in one portion and ball milling for a further *y* h.

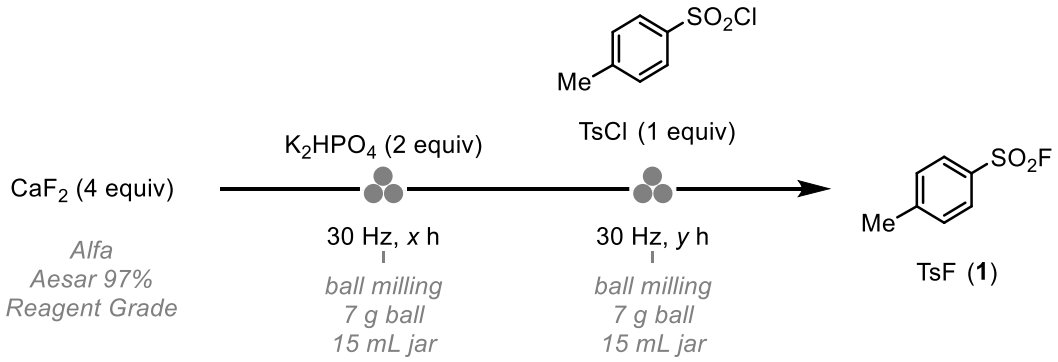

To a 15 mL stainless steel milling jar was added a stainless steel ball (7 g), CaF_2 (312 mg, 4.0 mmol, 4 equiv) and K_2HPO_4 (348 mg, 2.0 mmol, 2 equiv). The jar was closed and securely fitted to the mill which was set for the indicated pre-milling time (*x* h) at 30 Hz. After *x* h, the jar was opened and 4-toluenesulfonyl chloride (191 mg, 1.0 mmol, 1 equiv) was added. The jar was then closed and securely fitted to the mill which was set for the indicated milling time (*y* h) at 30 Hz. Upon completion, the jar was opened and rinsed with EtOAc (~ 5 mL). The crude reaction mixture was passed through a plug of silica eluting with EtOAc, concentrated in vacuo, and 4-fluoroanisole (10 µL, 11.1 mg, 88.3 µmol) was added as an internal standard. An aliquot was then diluted in deuterated chloroform. Reaction yield/conversion was determined by quantitative ^{1}H and ^{19}F NMR spectroscopy.

Data can be found in Table 2.5.

4.2.1.3 Stability of TsCl and TsF (1) under mechanochemical conditions

4-Toluenesulfonyl chloride (191 mg, 1.0 mmol, 1 equiv) or 4-toluenesulfonyl fluoride (**1**, 174 mg, 1.0 mmol, 1 equiv) was added to a 30 mL stainless steel milling jar with K_2HPO_4 (348 mg, 2.0 mmol, 2 equiv) and optional CaF_2 (390 mg, 5.0 mmol, 5 equiv). Two 2 g stainless steel balls were added to the jar. The jar was closed and securely fitted to the mill which was set for 1 h at the frequency of 30 Hz. Upon completion, the jar was opened and

rinsed with EtOAc (~ 5 mL). The crude reaction mixture was passed through a plug of silica eluting with EtOAc, concentrated *in vacuo*, and 4-fluoroanisole (10 µL, 11.1 mg, 88.3 µmol) was added as an internal standard. An aliquot was then diluted in deuterated chloroform. Reaction yield/conversion was determined by quantitative ^{1}H and ^{19}F NMR spectroscopy.

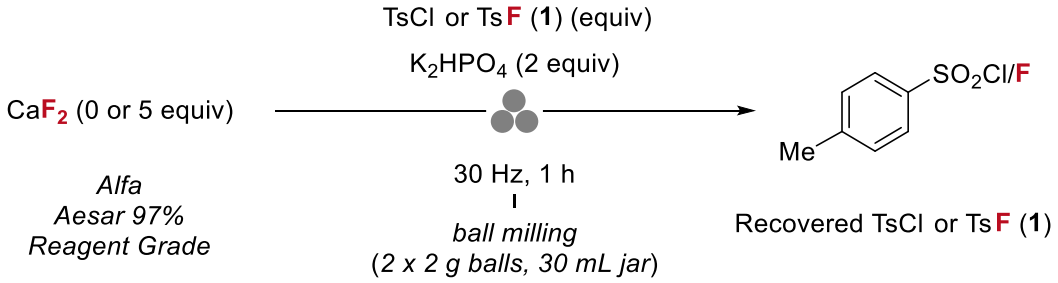

Entry	Substrate	CaF_2 (equiv)	K_2HPO_4 (equiv)	Recovered Substrate (%)
1	TsF (**1**)	5	2	81
2*	TsF (**1**)	0	2	89
3	TsCl	0	2	78

*The insoluble by-product was washed in D_2O (1 mL) and the suspension was transferred to a 1 mL centrifuge tube. After centrifugation with an acceleration time of 120 seconds (13,500 rpm) at 25 °C, the supernatant was analysed by NMR spectroscopy. Aqueous F^- (-121.70 ppm) and potassium tosylate were observed by ^{19}F NMR (D_2O).

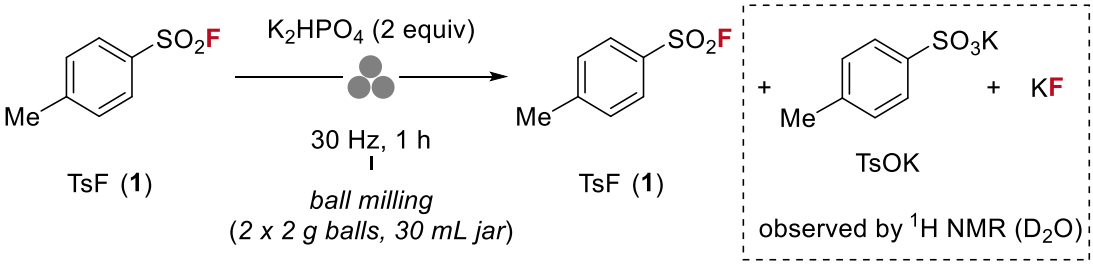

^{19}F NMR (D_2O) of supernatant - contains signal for KF (-121.70 ppm).

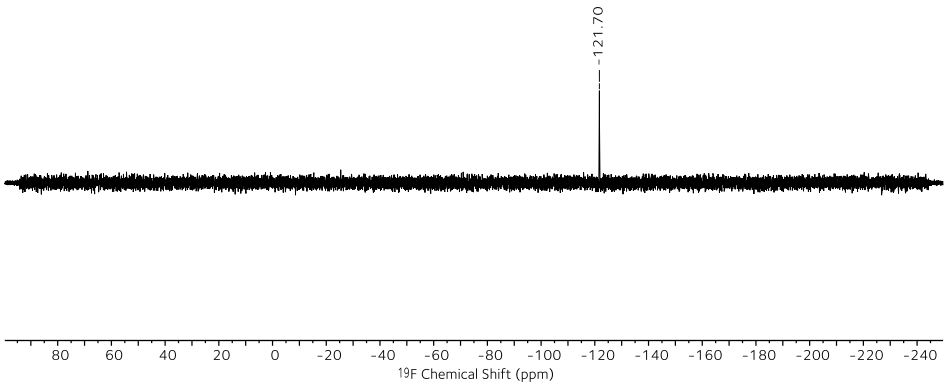

The ^{1}H NMR (D_2O) of the supernatant (**a**) from all of these control reactions displayed two doublets at 7.65 ppm and 7.32 ppm and a singlet at 2.35 ppm. This is consistent with the formation of potassium tosylate.[4]

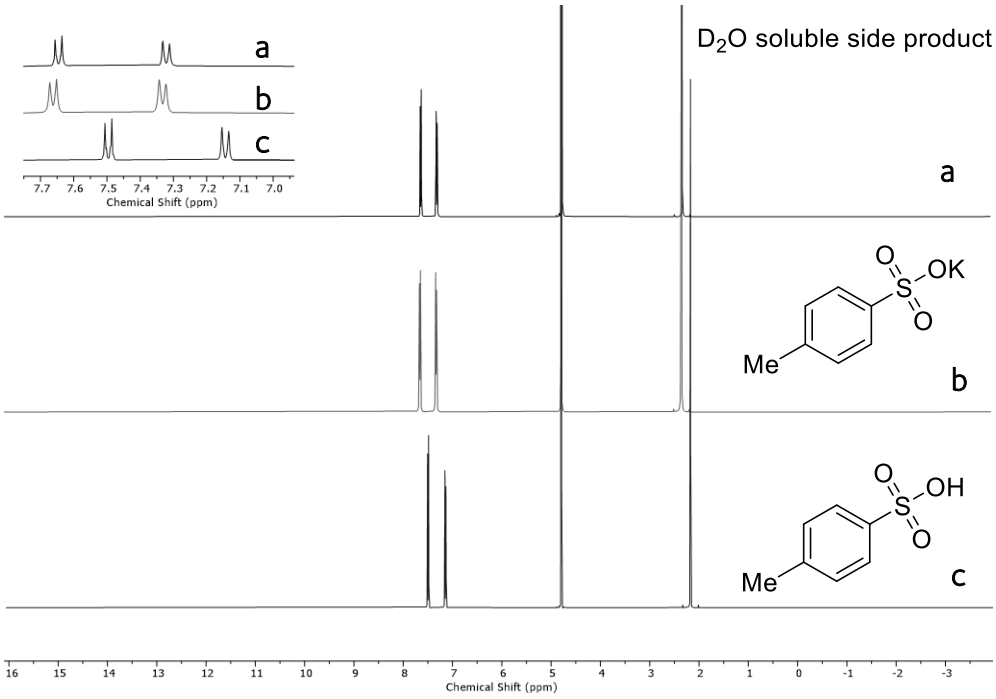

The observation that partial degradation of 4-toluenesulfonyl chloride and 4-toluenesulfonyl fluoride (**1**) occurs under mechanochemical conditions encouraged us to pre-mill CaF_2 with K_2HPO_4 (solid-state reaction) and use the resulting powder as a fluorinating reagent in solution.

4.2.1.4 Two-step Protocol Development (solid-state and solution-phase)

Optimisation of CaF_2 to K_2HPO_4 ratio

Reagent grade CaF_2 (≥ 97.0%, Alfa Aesar) was reacted with K_2HPO_4 (≥ 98.0%, Alfa Aesar) in different ratios under mechanochemical conditions (ball milling). The resultant solid powder was used in the fluorination of TsCl at 0.25 mmol scale in solution.

To a 15 mL stainless steel milling jar was added a stainless steel ball (7 g), CaF_2 and K_2HPO_4 to give approximately 1 g of milling material overall. For example, CaF_2 (309 mg, 3.96 mmol) and K_2HPO_4 (690 mg, 3.96 mmol) gives approximately 1 g of material where 1 equiv of CaF_2 is milled with 1 equiv of K_2HPO_4. In the subsequent reaction in solution, 252 mg of this powder is used for the fluorination (theoretically containing 1.0 mmol CaF_2 and 1.0 mmol K_2HPO_4 (4 equiv CaF_2 and 4 equiv K_2HPO_4 respect to substrate), example in entry 2). The jar was closed and securely fitted to the mill which was set for 3 h at the frequency of 30 Hz. Upon completion, the jar was opened, and the white powder was collected and stored in a borosilicate glass vial in a desiccator. To a glass reaction vessel was added the white powder (containing *x* equiv CaF_2 and *y* equiv K_2HPO_4 respect to 4-toluenesulfonyl chloride), 4-toluenesulfonyl chloride (47.7 mg, 0.25 mmol, 1 equiv), additive (0.25 mmol, 1 equiv) and MeCN (1 mL). After stirring at 100 °C for 5 h, the resulting suspension was cooled to room temperature, the crude reaction mixture was passed through a plug of silica eluting with EtOAc, concentrated *in vacuo*, and 4-fluoroanisole (10 µL, 11.1 mg, 88.3 µmol) was added as an internal standard. An aliquot was then diluted in deuterated chloroform. Reaction yield/conversion was determined by quantitative ^1H and ^{19}F NMR spectroscopy.

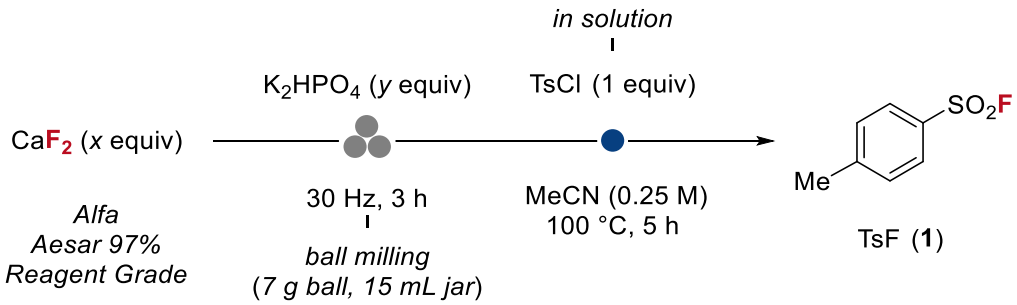

Entry	CaF_2 (*x* equiv)	K_2HPO_4 (*y* equiv)	TsCl (%)	TsF (**1**) (%)	Mass balance (%)
1	4	2	15	62	77
2	4	4	0	76	76
3	8	2	10	51	61
4	16	2	0	78	78
5	4	6	0	69	69
6	2	16	0	30	30

Quantities of CaF_2 to K_2HPO_4 used in the ball milling reactions are outlined below:

Entry	CaF_2 (equiv)	K_2HPO_4 (equiv)	CaF_2 (mg)	CaF_2 (mmol)	K_2HPO_4 (mg)	K_2HPO_4 (mmol)
1	1	1	309	3.96	690	3.96
2	1	0.5	472	6.05	527	3.02
3	1.5	1	402	5.15	598	3.43
4	4	1	642	8.22	358	2.06
5	8	1	782	10.02	218	1.25
6	1	8	53	0.68	948	5.44
7	1	1.5	230	2.95	770	4.42

Optimisation of solvent

Reagent grade CaF_2 (≥ 97.0%, Alfa Aesar) was reacted with K_2HPO_4 (≥ 98.0%, Alfa Aesar) in a 1:1 ratio under mechanochemical conditions (ball milling) for 3 h at 30 Hz. The resultant solid powder was used in the fluorination of 4-toluenesulfonyl chloride at 0.25 mmol scale.

To a 15 mL stainless steel milling jar was added a stainless steel ball (7 g), CaF_2 (309 mg, 3.96 mmol) and K_2HPO_4 (690 mg, 3.96 mmol) to give approximately 1 g of material for milling. The jar was closed and securely fitted to the mill which was set for 3 h at the frequency of 30 Hz. Upon completion, the jar was opened, and the white powder was collected and stored in a borosilicate glass vial in a desiccator. To a glass reaction vessel was added the white powder (252 mg, 1.0 mmol respect to CaF_2 and 1.0 mmol respect to K_2HPO_4, 4 equiv CaF_2 and 4 equiv K_2HPO_4), 4-toluenesulfonyl chloride (47.7 mg, 0.25 mmol, 1 equiv) and the solvent indicated (1 mL). After stirring for the 5 h at 100 °C, the resulting suspension was cooled to room temperature, the crude reaction mixture was passed through a plug of silica eluting with EtOAc, concentrated *in vacuo*, and 4-fluoroanisole (10 µL, 11.1 mg, 88.3 µmol) was added as an internal standard. An aliquot was then diluted in deuterated chloroform. Reaction yield/conversion was determined by quantitative ^{1}H and ^{19}F NMR spectroscopy.

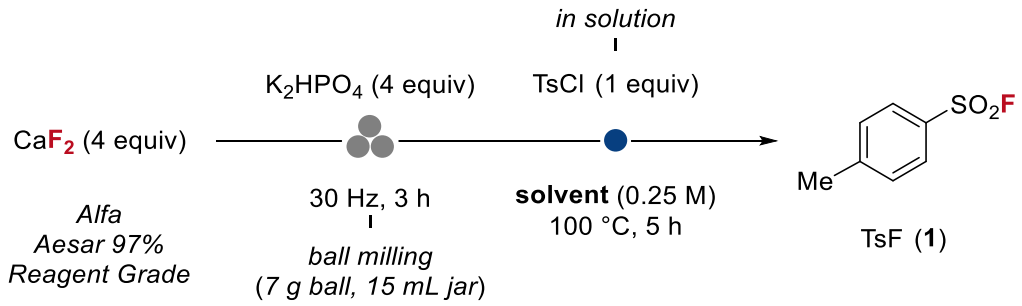

Entry	Solvent	TsCl (%)	TsF (**1**) (%)	Mass balance (%)
1	DMF (anh.)	8	0	8
2	DMA (anh.)	43	0	43
3	DMSO (anh.)	0	0	0
4	THF (anh.)	64	27	91
5	2-MeTHF	0	65	65
6	1,4-Dioxane	16	56	72
7	Diglyme	0	46	46
8	Monoglyme	0	37	37
9	MeCN (anh.)	0	76	76
10	EtCN	4	80	84
11	*t*BuCN	31	57	88
12	*t*AmylOH (anh.)	0	73	73
13	*t*BuOH (anh.)	0	81	81
14	PhMe (anh.)	50	50	100
15	*m*Xylene	31	68	99
16	$PhCF_3$ (anh.)	17	69	86
17	1,2-Difluorobenzene	62	34	96
18	1,2-Dichlorobenzene (anh.)	2	84	86
19	1,3-Dichlorobenzene	47	52	99
20	Fluorobenzene	33	55	88
21	Chlorobenzene (anh.)	0	92	92

anh. = anhydrous

Comparison of reagent grade CaF_2 to acid-grade fluorspar (>97% CaF_2)

To a 15 mL stainless steel milling jar was added a stainless steel ball (7 g), CaF_2 or acid grade fluorspar (309 mg, 3.96 mmol) and K_2HPO_4 (690 mg, 3.96 mmol) to give approximately 1 g of material for milling. The jar was closed and securely fitted to the mill which was set for 3 h at the frequency of 30 Hz. Upon completion, the jar was opened and the white powder was collected and stored in a borosilicate glass vial in a desiccator. To a glass reaction vessel was added the white powder (252 mg, 1.0 mmol respect to CaF_2 and 1.0 mmol respect to K_2HPO_4, 4 equiv CaF_2 and 4 equiv K_2HPO_4), 4-toluenesulfonyl chloride (47.7 mg, 0.25 mmol, 1 equiv) and *t*BuOH (1 mL). After stirring for 5 h at the 100 °C, the resulting suspension

was cooled to room temperature, the crude reaction mixture was passed through a plug of silica eluting with EtOAc, concentrated *in vacuo*, and 4-fluoroanisole (10 µL, 11.1 mg, 88.3 µmol) was added as an internal standard. An aliquot was then diluted in deuterated chloroform. Reaction yield/conversion was determined by quantitative ^{1}H and ^{19}F NMR spectroscopy.

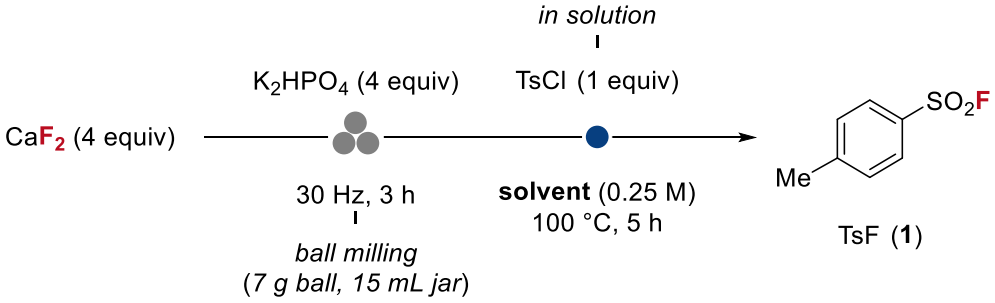

Entry	CaF_2 grade	TsCl (%)	TsF (**1**) (%)	Mass balance (%)
1	Reagent	0	81	81
2	Acid grade fluorspar	0	78	78

Reassessment of phosphate salts using acid-grade fluorspar

Acid grade fluorspar (CaF_2, > 97.0%, Minersa Group) was reacted with a phosphate additive in a 1:1 ratio under mechanochemical conditions (ball milling) for 3 h at 30 Hz. The resultant solid powder was used in the fluorination of 4-toluenesulfonyl chloride at 0.25 mmol scale.

To a 15 mL stainless steel milling jar was added a stainless steel ball (7 g), acid grade fluorspar (309 mg, 3.96 mmol, 1 equiv) and the indicated phosphate additive (1 equiv) to give approximately 1 g of material for milling. The jar was closed and securely fitted to the mill which was set for 3 h at the frequency of 30 Hz. Upon completion, the jar was opened and the white powder was collected and stored in a borosilicate glass vial in a desiccator. To a glass reaction vessel was added the white powder (1.0 mmol respect to CaF_2 and 1.0 mmol respect to phosphate additive, 4 equiv CaF_2 and 4 equiv phosphate additive), 4-toluenesulfonyl chloride (47.7 mg, 0.25 mmol, 1 equiv) and *t*BuOH (1 mL). After stirring for 5 h at the 100 °C, the resulting suspension was cooled to room temperature, the crude reaction mixture was passed through a plug of silica eluting with EtOAc, concentrated *in vacuo,* and 4-fluoroanisole (10 µL, 11.1 mg, 88.3 µmol) was added as an internal standard. An aliquot was then diluted in deuterated chloroform. Reaction yield/conversion was determined by quantitative ^{1}H and ^{19}F NMR spectroscopy.

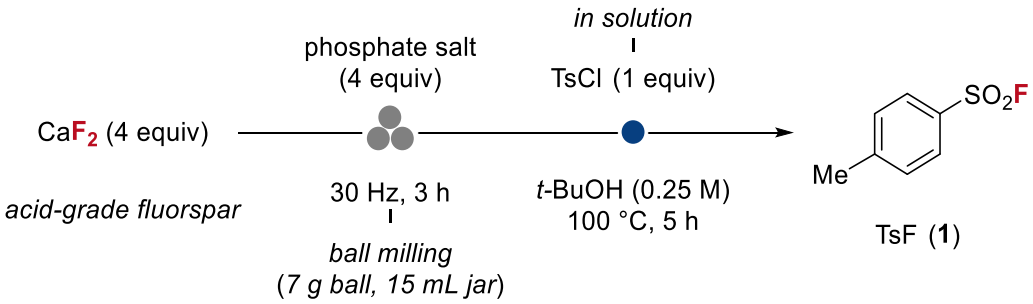

Entry	Phosphate additive	TsCl (%)	TsF (**1**) (%)	Mass balance (%)
1	K_3PO_4	0	1	1
2	K_2HPO_4	0	78	78
3	KH_2PO_4	95	4	99
4	$K_4P_2O_7$	0	54	54
5	$K_5P_3O_{10}$	19	23	42
6	Na_3PO_4	90	10	100
7	Na_2HPO_4	16	38	54
8	NaH_2PO_4	95	3	98
9	$Na_4P_2O_7$	0	33	33
10	$Na_5P_3O_{10}$	91	7	98
11	$CaHPO_4$	36	0	36
12	α-$Ca_3(PO_4)_2$	90	0	90

4.2.1.5 Optimisation studies of the solid-state step using acid-grade fluorspar

Milling frequency

Acid grade fluorspar (CaF_2, > 97.0%, Minersa Group) was reacted with K_2HPO_4 (≥ 98.0%, Alfa Aesar) in a 1:1 ratio under mechanochemical conditions (ball milling) for 3 h at 30 or 35 Hz. The resultant solid powder was used in the fluorination of 4-toluenesulfonyl chloride at 0.125 mmol scale.

To prepare powder **A** (1:1 ratio of fluorspar:K_2HPO_4), to a 15 mL stainless steel milling jar was added a stainless steel ball (7 g), acid grade fluorspar (309 mg, 3.96 mmol) and K_2HPO_4 (690 mg, 3.96 mmol) to give approximately 1 g of material for milling. The jar was then closed and securely fitted to the mill which was set for 3 h at the frequency of 30 or 35 Hz. Upon completion, the jar was opened and the white powder **A** was collected and stored in a borosilicate glass vial in a desiccator.

Fluorination of 4-toluenesulfonyl chloride investigated at 0.125 mmol using 1 equiv of powder **A** (contains 0.125 mmol of CaF_2). NMR yields of 4-toluenesulfonyl fluoride (**1**) and 4-toluenesulfonyl chloride achieved using powder **A** in different stoichiometries prepared at 30 Hz or 35 Hz were calculated.

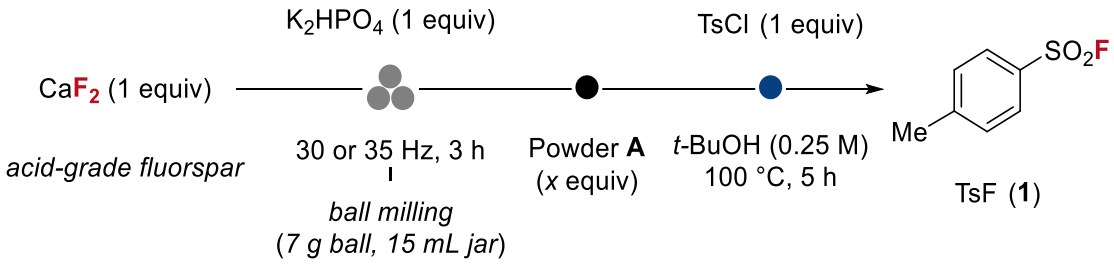

Entry	Milling frequency (Hz)	**A** equiv	CaF_2 equiv	K_2HPO_4 equiv	TsCl (%)	TsF (**1**) (%)	Mass balance (%)
1	30	1	1	1	48	28	76
2	35	1	1	1	43	46	89
3	30	2	2	2	31	51	82
4	35	2	2	2	15	65	80
5	30	4	4	4	0	78	78
6	35	4	4	4	0	93	93

Prolonged Milling Time Studies (35 Hz)

Acid grade fluorspar (CaF_2, > 97.0%, Minersa Group) was reacted with K_2HPO_4 (≥ 98.0%, Alfa Aesar) in a 1:1 ratio under mechanochemical conditions (ball milling) for *x* h at 35 Hz. The resultant solid powder was used in the fluorination of 4-toluenesulfonyl chloride at 0.125 mmol scale.

To a 15 mL stainless steel milling jar was added a stainless steel ball (7 g), acid grade fluorspar (309 mg, 3.96 mmol) and K_2HPO_4 (690 mg, 3.96 mmol) to give approximately 1 g of material for milling. The jar was then closed and securely fitted to the mill which was set for *x* h at the frequency of 35 Hz. Upon completion, the jar was opened and the white powder was collected and stored in a borosilicate glass vial in a desiccator. NMR yields of 4-toluenesulfonyl fluoride (**1**) and 4-toluenesulfonyl chloride achieved using the powder prepared by milling for different time periods at 35 Hz, were calculated.

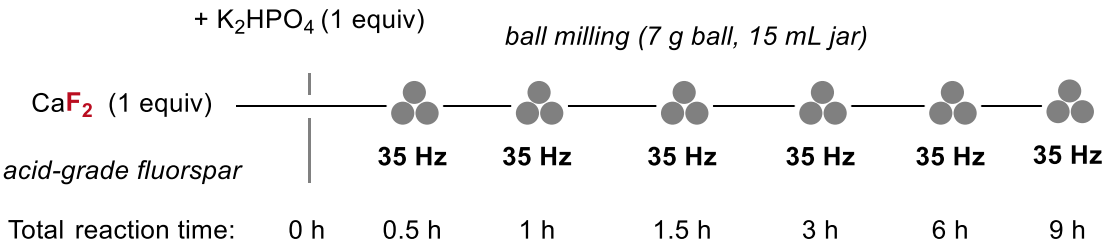

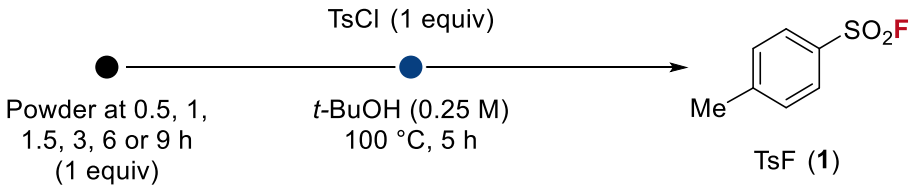

4.2.1.6 CaF_2 quantification experiments using NiO (PXRD)

Samples were prepared by C.Patel. PXRD data was recorded by C.Patel and analysed by Prof. M. Hayward. A quantitative Rietveld phase analysis can be used to provide the weight fraction of the crystalline component.

To a 15 mL stainless steel milling jar was added a stainless steel ball (7 g), acid grade fluorspar (309 mg, 3.96 mmol) and K_2HPO_4 (690 mg, 3.96 mmol) to give approximately 1 g of material for milling. The jar was then closed and securely fitted to the mill which was set for 0 to 6 h at the frequency of 35 Hz. To the resultant solid powder (at 0 h, 3 h and 6 h) was added nickel (II) oxide (99.99%, Sigma-Aldrich, 1313-99-1), to give a 40:60 molar ratio of CaF_2:NiO in each sample.

PXRD data for each sample were measured using a Bruker D8 Advance X-ray diffractometer.

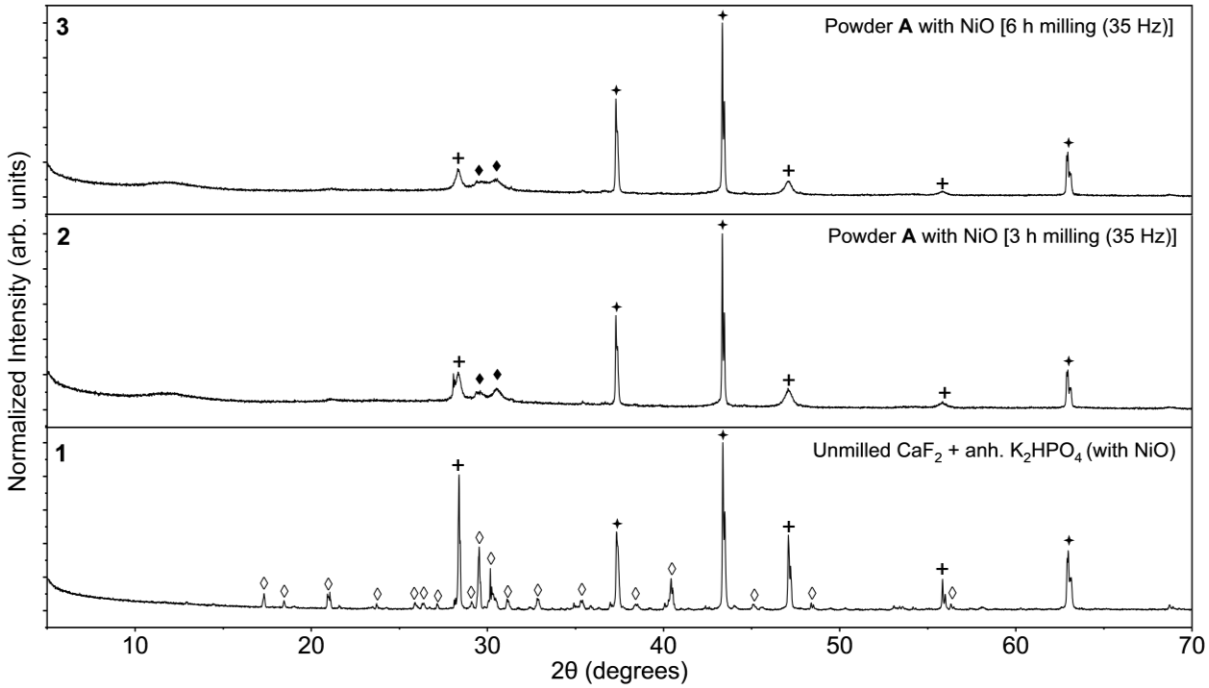

The mass ratio of CaF_2 : NiO_2 could be quantified from the PXRD patterns following Rietveld refinement:

Trace	Ball milling (h)	Mass ratio NiO : CaF_2	Ratio NiO : CaF_2	Crystalline CaF_2 (%)
1	0	44.7 (1.6) : 55.2 (1.6)	1: 1.23	100
2	3	57.3 (1.2) : 42.7 (1.2)	1:0.745	60.5
3	6	62.5 (1.3) : 37.5 (1.3)	1:0.60	48.7

4.2.1.7 Final optimisation studies for the fluorination reaction.

Portion-wise addition of K_2HPO_4 to acid-grade fluorspar at 35 Hz

In order to find the optimal ratio between acid grade fluorspar (CaF_2) and K_2HPO_4 in the final fluorinating reagent, such that fluorination could be achieved using fewer equivalents of CaF_2, the amount of K_2HPO_4 was increased through portion-wise addition every 3 h with additional milling time. At each stage, the powder is collected and stored in a borosilicate glass vial in a desiccator for usage in the next milling stage. Each powder is used within a week of storage.

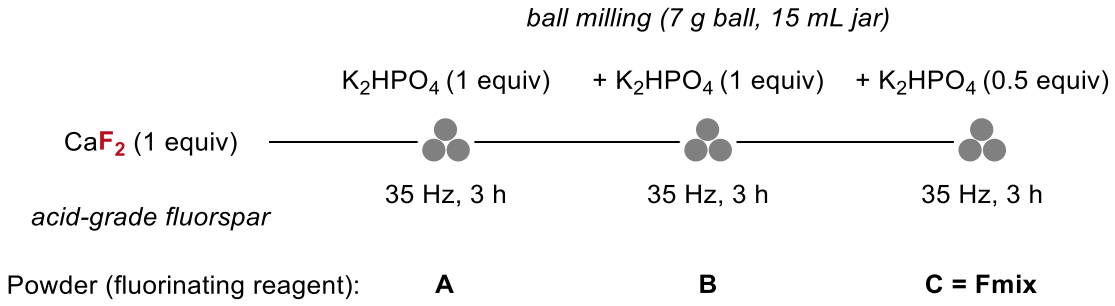

To prepare powder **A** (1:1 ratio of fluorspar:K_2HPO_4), to a 15 mL stainless steel milling jar was added a stainless steel ball (7 g), acid grade fluorspar (309 mg, 3.96 mmol) and K_2HPO_4 (690 mg, 3.96 mmol) to give approximately 1 g of material for milling. The jar was then closed and securely fitted to the mill which was set for 3 h at the frequency of 35 Hz. Upon completion, the jar was opened and the white powder **A** was collected.

To prepare powder **B** (1:2 ratio of fluorspar:K_2HPO_4), to a 15 mL stainless steel milling jar was added a stainless steel ball (7 g), **A** (592 mg, contains 2.34 mmol acid grade fluorspar and 2.34 mmol K_2HPO_4) and K_2HPO_4 (408 mg, 2.34 mmol) to give approximately 1 g of material for milling. The jar was then closed and securely fitted to the mill which was set for 3 h at the frequency of 35 Hz. Upon completion, the jar was opened and the white powder **B** was collected.

To prepare powder **C** (1:2.5 ratio of fluorspar:K_2HPO_4), to a 15 mL stainless steel milling jar was added a stainless steel ball (7 g), **B** (830 mg, contains 1.95 mmol acid grade fluorspar and 3.89 mmol K_2HPO_4) and K_2HPO_4 (170 mg, 0.98 mmol) to give approximately 1 g of material for milling. The jar was then closed and securely fitted to the mill which was set for 3 h at the frequency of 35 Hz. Upon completion, the jar was opened and the white powder **C** was collected.

The reactivity of powders **A**, **B** or **C** in the fluorination of 4-toluenesulfonyl chloride using our 2-step protocol was investigated at 0.25 mmol scale:

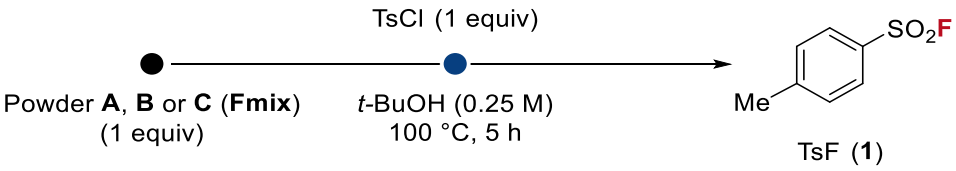

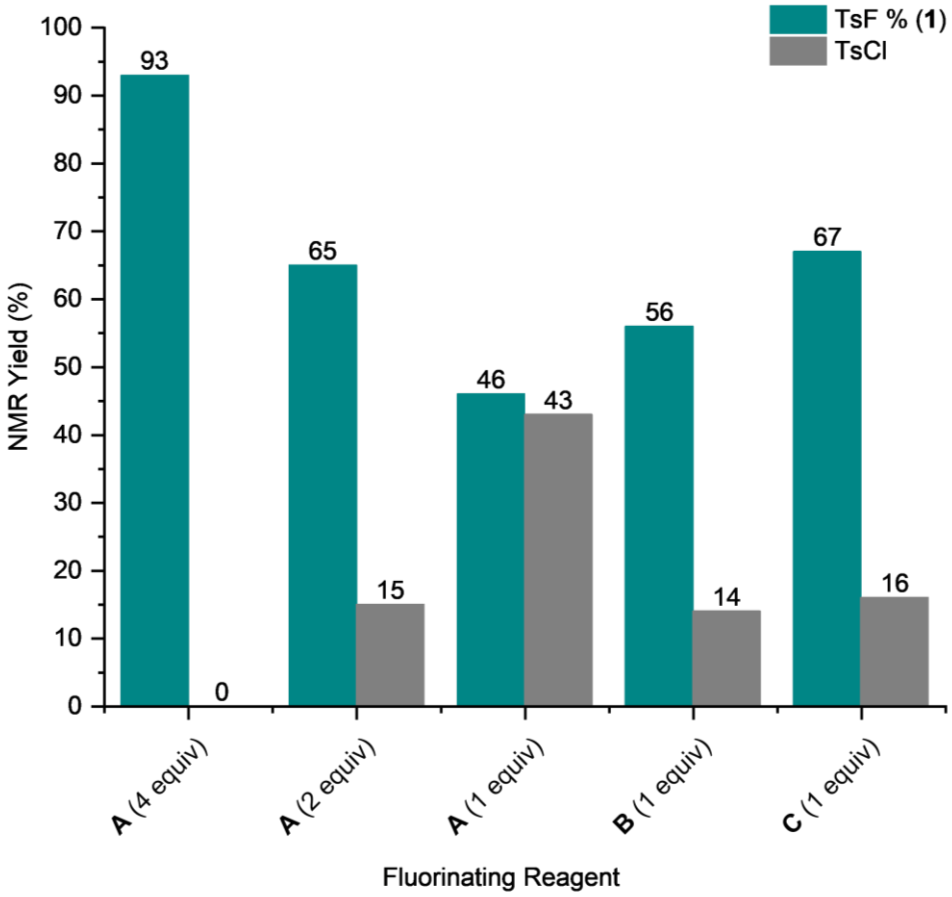

Final solution phase conditions

The effect of H_2O in the fluorination of 4-toluenesulfonyl chloride in solution using 1 equivalent of powder **C** (**Fmix**) prepared at 35 Hz was investigated.

To a glass reaction vessel was added powder **C** (**Fmix**) (64.2 mg, 0.125 mmol relative to CaF_2, 1.0 equiv), 4-toluenesulfonyl chloride (23.8 mg, 0.125 mmol, 1.0 equiv) and anhydrous *t*BuOH (0.25 M). H_2O (1 to 10 equiv) was added to the reaction mixture. After stirring for 5 h at the 100 °C, the resulting suspension was cooled to room temperature, the crude reaction mixture was passed through a plug of silica eluting with EtOAc, concentrated *in vacuo*, and 4-fluoroanisole (10 µL, 11.1 mg, 88.3 µmol) was added as an internal standard. An aliquot was then diluted in deuterated chloroform. Reaction yield/conversion was determined by quantitative ^{1}H and ^{19}F NMR spectroscopy. Potassium tosylate (TsOK) was observed as a side product in some reactions.

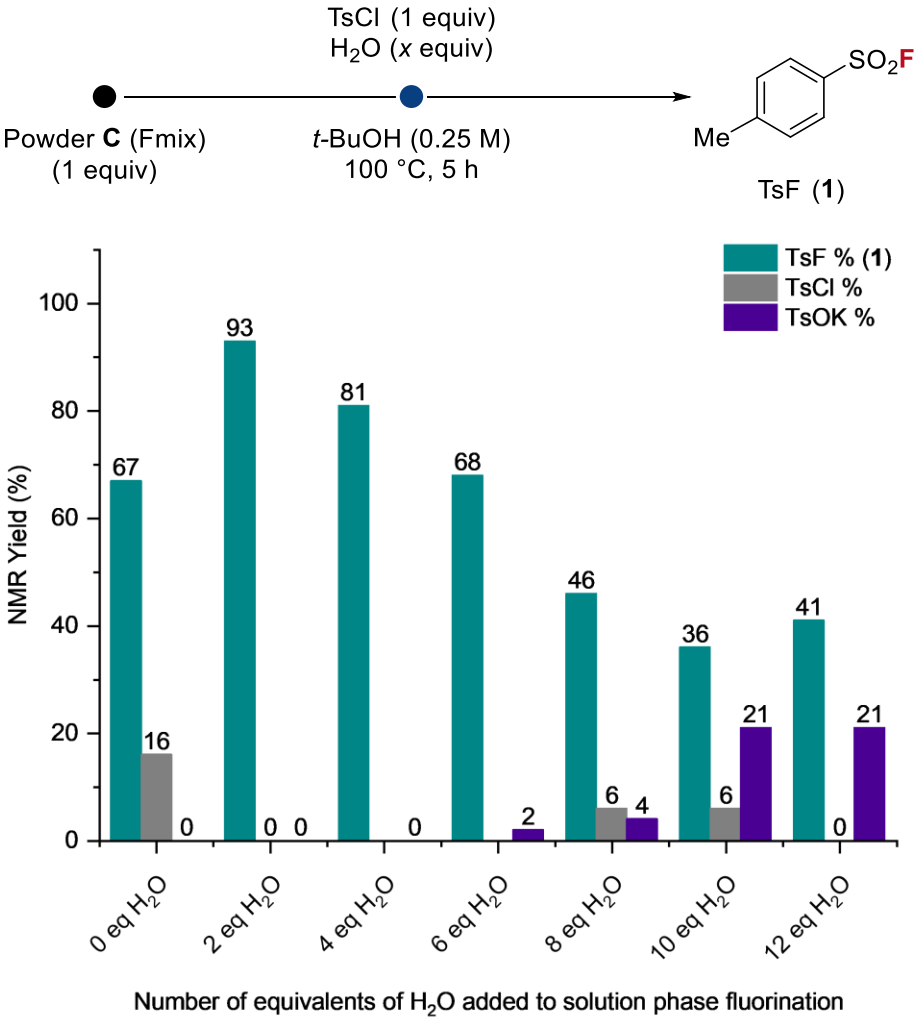

Reactions using 0.5 equivalents of Fmix

The effect of H_2O in the fluorination of 4-toluenesulfonyl chloride in solution using 0.5 equivalent of powder **C** (**Fmix**) prepared at 35 Hz was investigated using the same protocol outlined in **Final solution phase conditions**.

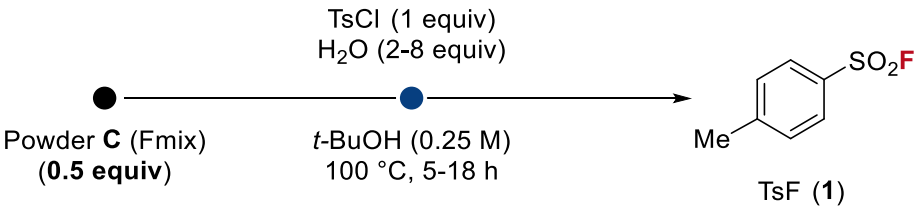

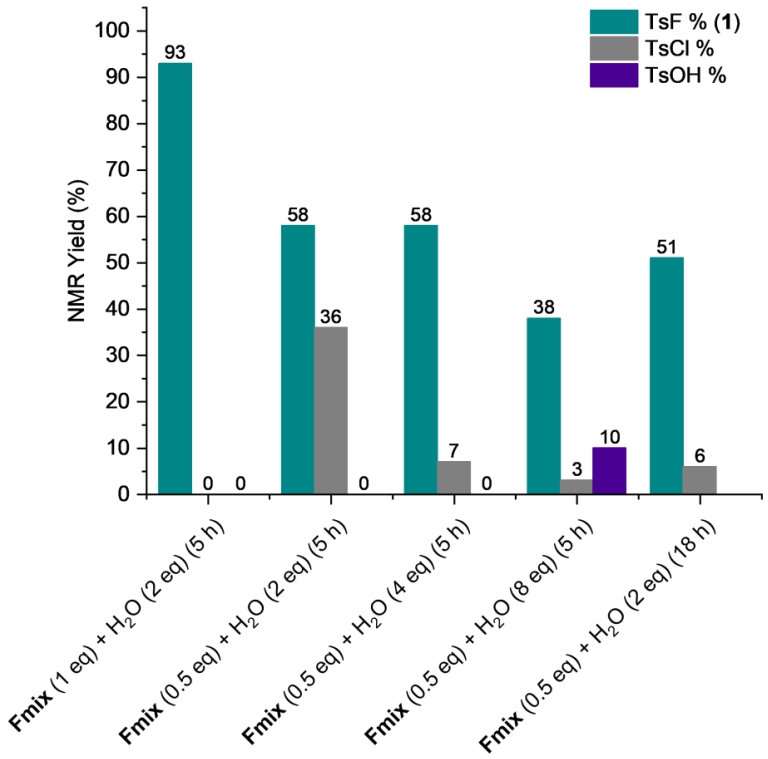

4.2.2 Photographic guide for experimental setup (ball milling)

Mixer Mills: Mechanochemical reactions were conducted using a Retsch MM400 mixer mill, Retsch MM500 Vario mixer mill and an IST636 high-energy mixer mill at the frequency denoted where relevant (see www.retsch.com and www.insolidotech.org for more details)

Solid reagents added to stainless steel 15 mL milling jar and one 7 g stainless steel ball added. The jar is closed and placed on mixer mill. Ball milling is initiated at 30 Hz (or 35 Hz) for 3 h. The reaction material (solid powder) is scraped from milling jar using a spatula and stored in borosilicate glass vial in a desiccator at room temperature until further usage (either solution phase chemistry or to prepare **Fmix**).

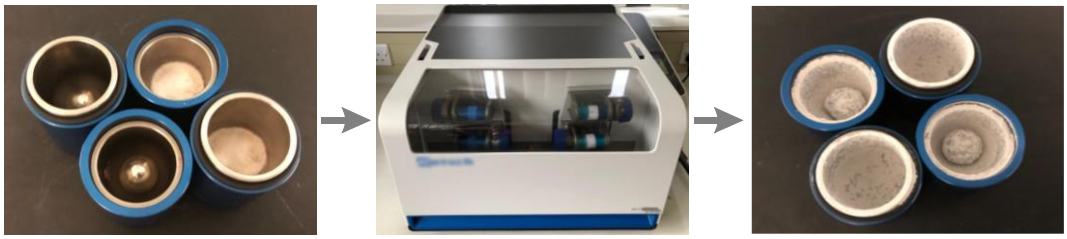

Solid reagents are placed in jar

Ball milling at 35 Hz

Powdered solid fluorinating reagent

4.2.3 Preparation, shelf life and performance of Fmix

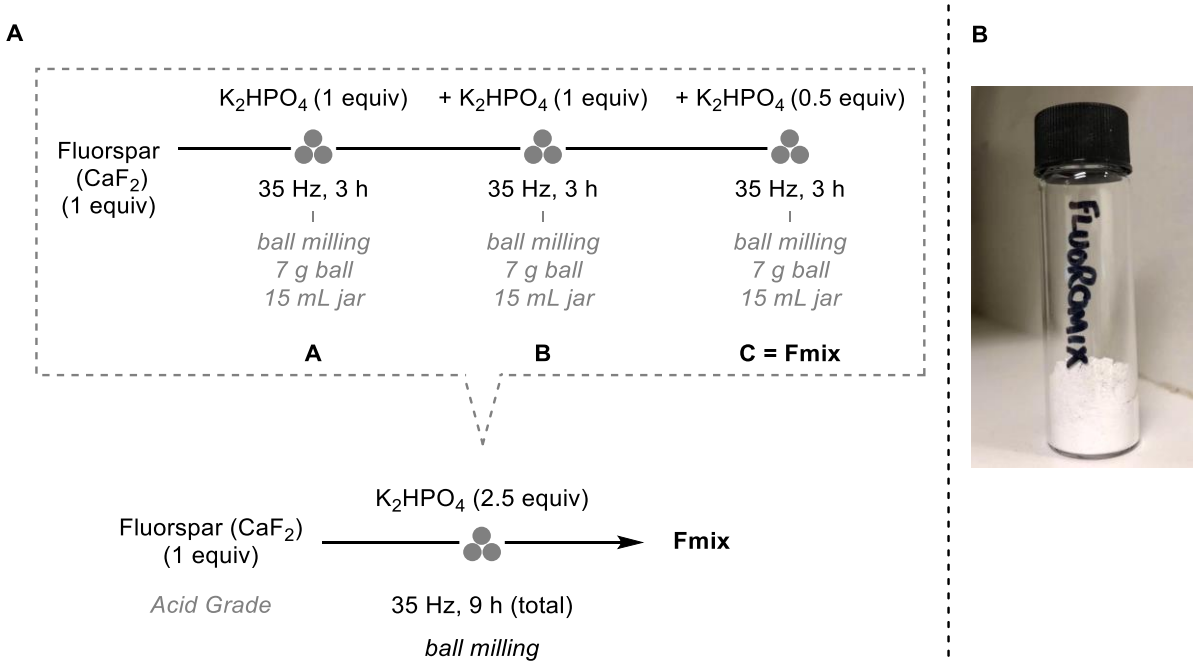

To prepare powder **A** (1:1 ratio of fluorspar:K_2HPO_4), to a 15 mL stainless steel-milling jar was added a stainless steel ball (7 g), acid grade fluorspar (309 mg, 3.96 mmol) and anhydrous K_2HPO_4 (690 mg, 3.96 mmol) to give approximately 1 g of material for milling. The jar was then closed and securely fitted to the mill which was set for 3 h at the frequency of 35 Hz. Upon completion, the jar was opened and the white powder **A** was collected.

To prepare powder **B** (1:2 ratio of fluorspar:K_2HPO_4), to a 15 mL stainless steel milling jar was added a stainless steel ball (7 g), **A** (592 mg, contains 2.34 mmol acid grade fluorspar and 2.34 mmol K_2HPO_4) and anhydrous K_2HPO_4 (408 mg, 2.34 mmol) to give approximately 1 g of material for milling. The jar was then closed and securely fitted to the mill which was set for 3 h at the frequency of 35 Hz. Upon completion, the jar was opened and the white powder **B** was collected.

To prepare powder **C** (1:2.5 ratio of fluorspar:K_2HPO_4), to a 15 mL stainless steel milling jar was added a stainless steel ball (7 g), **B** (830 mg, contains 1.95 mmol acid grade fluorspar and 3.89 mmol K_2HPO_4) and anhydrous K_2HPO_4 (170 mg, 0.98 mmol) to give approximately 1 g of material for milling. The jar was then closed and securely fitted to the mill which was set for 3 h at the frequency of 35 Hz. Upon completion, the jar was opened and the white powder **C** was collected. **C** will henceforth be referred to as **Fmix.**

The shelf life and performance of **Fmix** was investigated over a 9-month period. **Fmix** was stored in a sealed borosilicate glass vial under ambient conditions during the study and tested in the fluorination of 4-toluenesulfonyl chloride in solution (using 1 equivalent of **Fmix**). Reactions were conducted in triplicate and repeated at monthly intervals using the identical batch of **Fmix**, *t*BuOH and 4-toluenesulfonyl chloride.

To a glass reaction vessel was added **Fmix** (64.2 mg, 0.125 mmol relative to CaF_2, 1.0 equiv), 4-toluenesulfonyl chloride (23.8 mg, 0.125 mmol, 1.0 equiv) and anhydrous *t*BuOH (0.25 M). H_2O (4.5 µL, 0.25 mmol, 2.0 equiv) was added to the reaction mixture. After stirring for 5 h at the 100 °C, the resulting suspension was cooled to room temperature, the crude reaction mixture was passed through a plug of silica eluting with EtOAc, concentrated *in vacuo,* and 4-fluoroanisole (10 µL, 11.1 mg, 88.3 µmol) was added as an internal standard. An aliquot was then diluted in deuterated chloroform. Reaction yield/conversion was determined by quantitative ^{1}H and ^{19}F NMR spectroscopy.

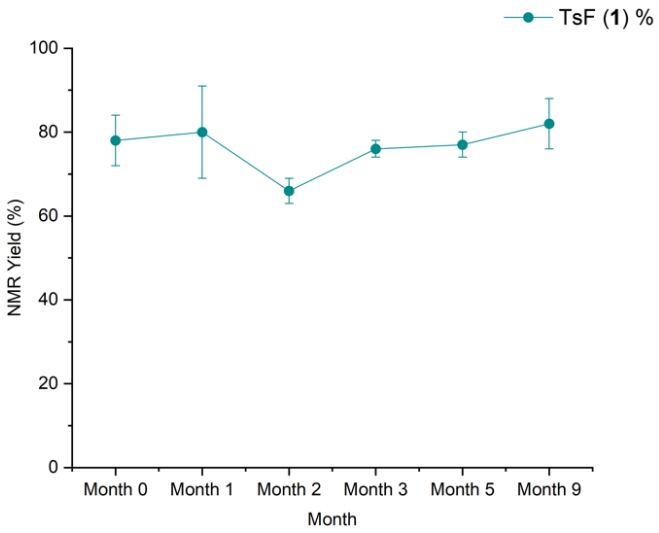

The mean 4-toluenesulfonyl fluoride (**1**) NMR yield ranged between 66% to 82%, with no significant loss in yield over 9 months.

PXRD of Fmix:

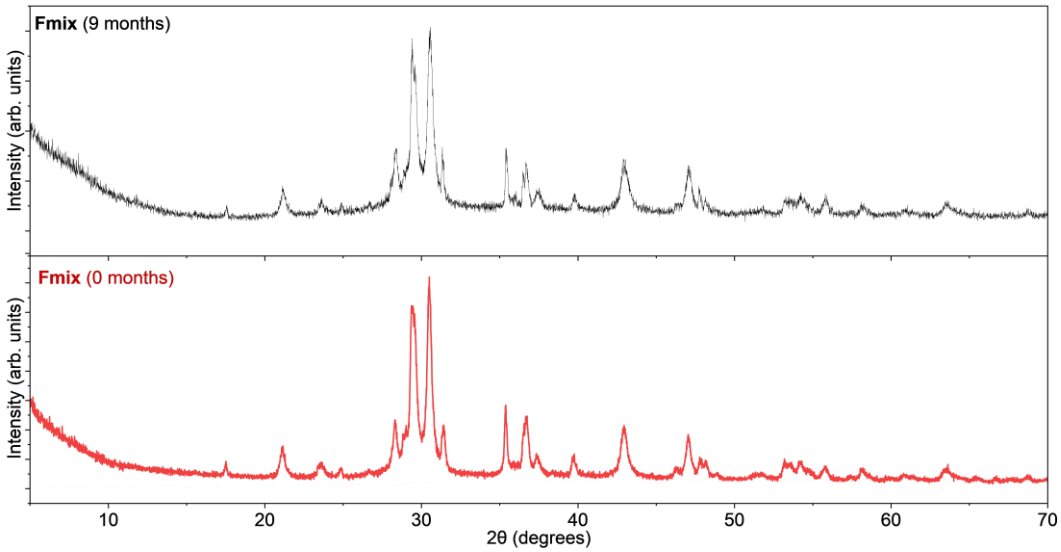

4.2.4 Application of Fmix to C(sp^2)–F bond formation

Aryl fluorides

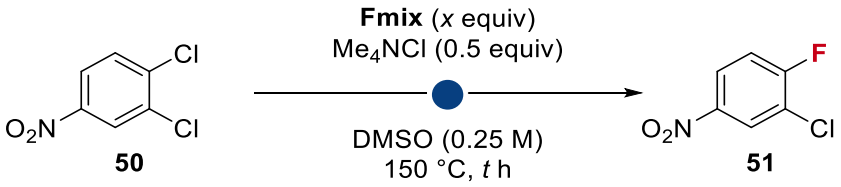

To a glass reaction vessel was added **Fmix** (2–4 equiv, e.g. 2 equiv weighs 128 mg and contains 2 equiv CaF_2 and 5 equiv K_2HPO_4), aryl chloride **50** (0.125 mmol, 1.0 equiv), Me_4NCl (13.7 mg, 0.5 equiv) and anhydrous DMSO (0.5 mL). After stirring at 150 °C in a heating block (for 3 to 12 h), the resulting suspension was cooled to room temperature, filtered through a short plug of silica gel (washed with ~5 mL EtOAc) to remove insoluble by-products. To the crude reaction mixture was added 4-fluoroanisole (10 µL, 11.1 mg, 88.3 µmol) as an internal standard. An aliquot was then diluted in deuterated chloroform. Reaction yield/conversion was determined by quantitative ^{1}H and ^{19}F NMR spectroscopy.

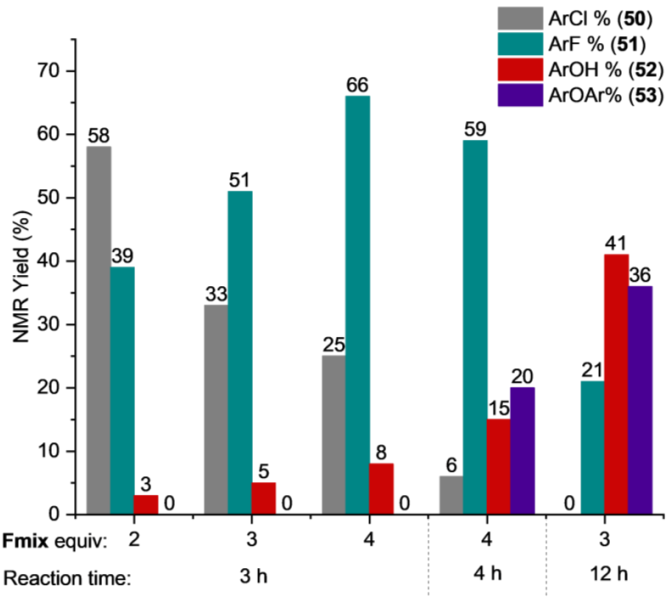

^{19}F qNMR of reaction mixture for reaction using 4 equiv **Fmix** (3 h):

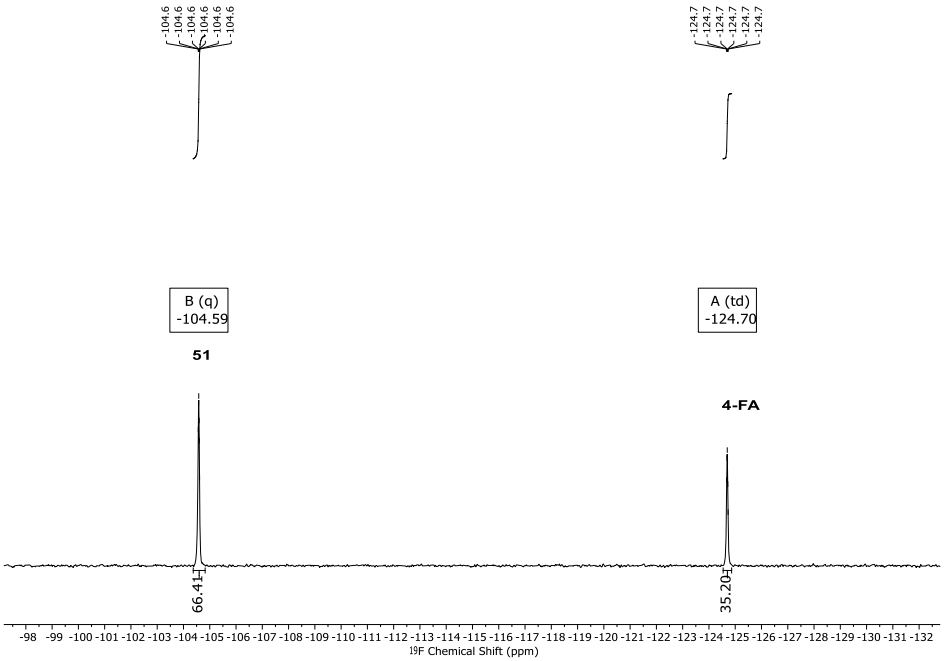

^{1}H qNMR of reaction mixture for reaction using 4 equiv **Fmix** (3 h) - The ArOH (**52**) and ArOAr (**53**) side products were isolated during scale up of this reaction.

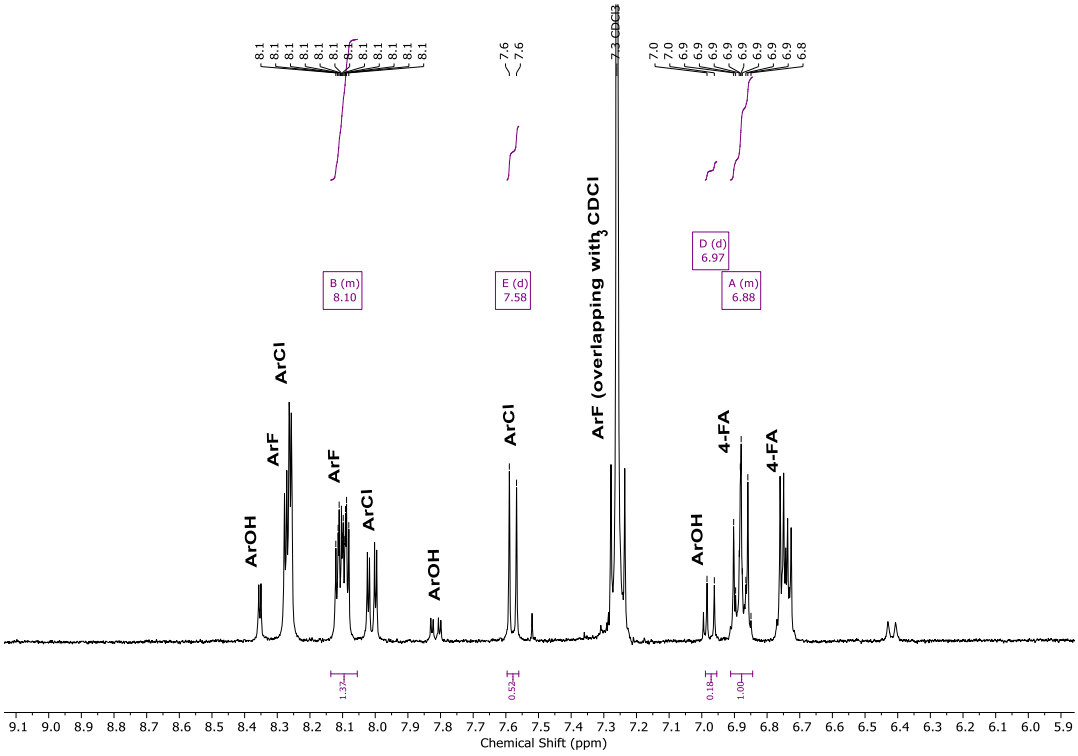

Acyl fluorides

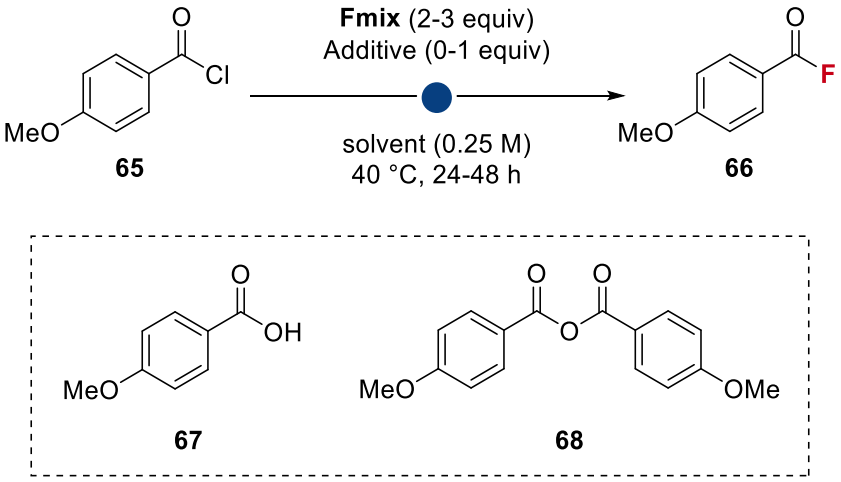

To a glass reaction vessel was added **Fmix** (2-3 equiv, e.g. 2 equiv weighs 128 mg and contains 2 equiv CaF_2 and 5 equiv K_2HPO_4), 4-methoxybenzoyl chloride **65** (0.125 mmol, 1.0 equiv) and anhydrous PhCl or *t*-BuOH (0.5 mL). After stirring at 40 °C in a heating block (24-72 h) the resulting suspension was cooled to room temperature, filtered through a short plug of silica gel (washed with ~5 mL EtOAc) to remove insoluble by-products. To the crude reaction mixture was added 4-fluoroanisole (10 µL, 11.1 mg, 88.3 µmol) as an internal standard. An aliquot was then diluted in deuterated chloroform. Reaction yield/conversion was determined by quantitative ^{1}H and ^{19}F NMR spectroscopy.

Entry	Solvent	**Fmix** equiv	Reaction time (h)	Additive (1 equiv)	**65** (%)	**66** (%)	**67** (%)	**68** (%)
1	*t*-BuOH	2	24	-	0	27	29	37
2	PhCl	2	24	-	82	18	0	0
3	PhCl	2	72	-	0	0	98	0
4	PhCl	2	24	Me_4NCl	55	45	0	0
5	PhCl	2	24	18-crown-6	0	0	0	99
6*	PhCl	-	24	-	3	97	0	0

^{19}F qNMR of reaction mixture for reaction (entry 4)

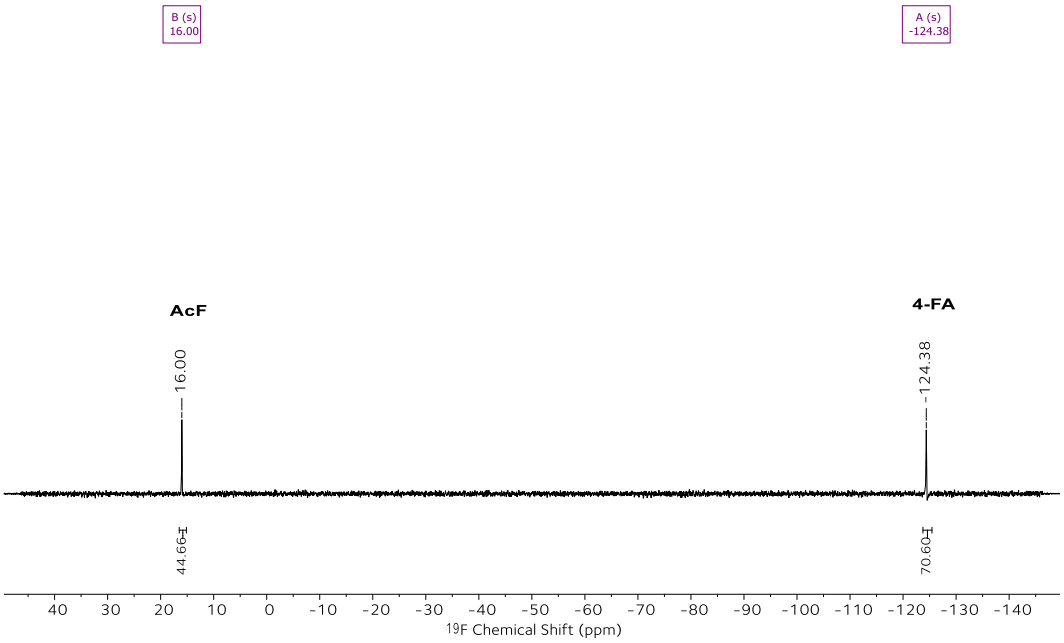

^{1}H qNMR of reaction mixture for reaction (entry 4) - spectra show only acyl fluoride product (**66**) and starting material (**65**). Confirmed by spiking NMR sample with **65**.

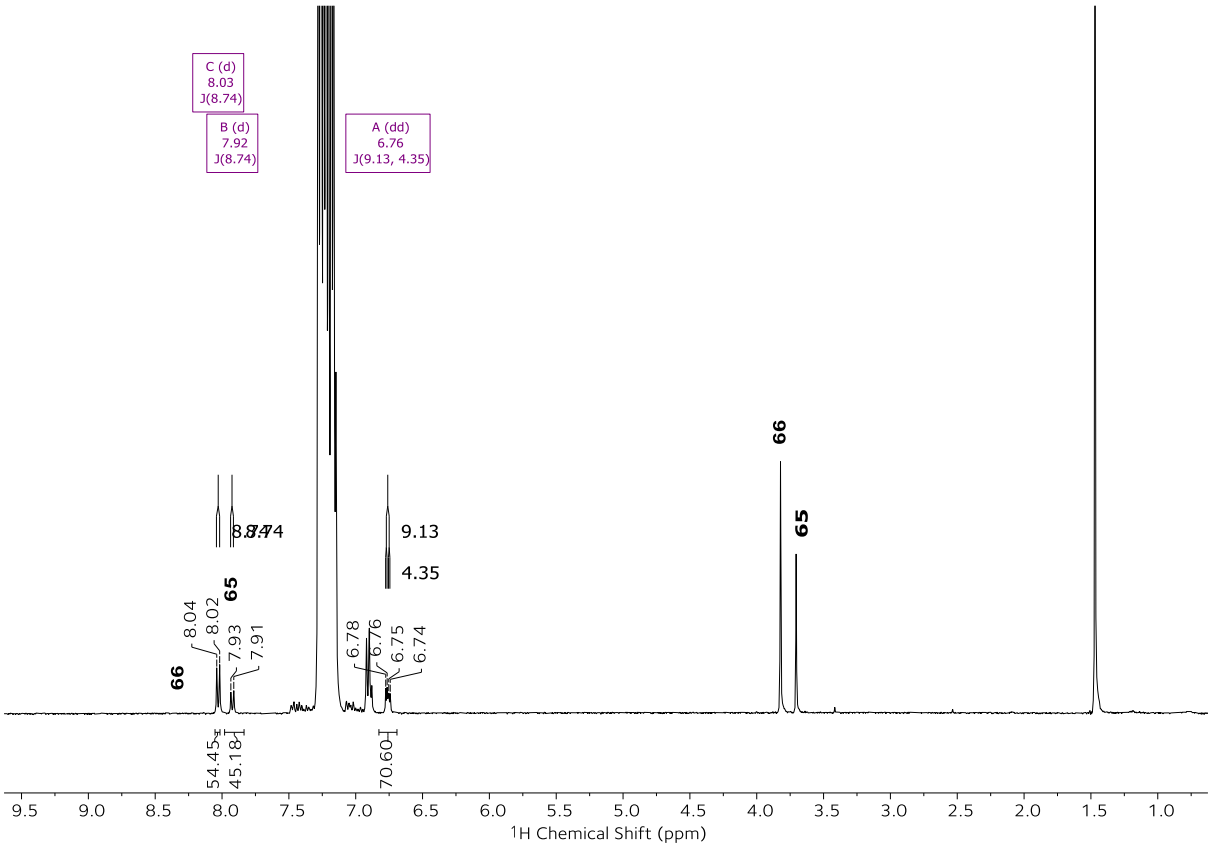

Literature data for 4-methoxy benzoic acid (**67**) and anhydride **68** can be found in refs[5,6] .

4.2.5 S-F bond formation using Fmix

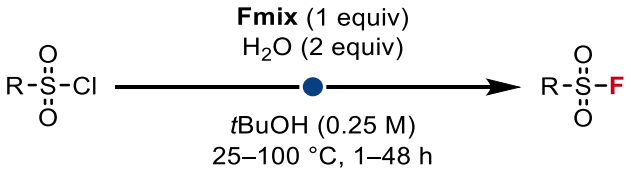

To a glass reaction vessel was added **Fmix** (257 mg, 1.0 equiv relative to CaF_2 and 2.5 equiv relative to K_2HPO_4), the corresponding sulfonyl chloride (0.5 mmol, 1.0 equiv) and anhydrous *tert*-BuOH (2 mL) unless otherwise stated. H_2O (18 µL, 2.0 equiv) was added to the reaction mixture. After stirring at 25 – 100 °C in a heating block, the resulting suspension was cooled to room temperature, filtered through a short plug of silica gel (washed with ~15 mL EtOAc) to remove insoluble by-products and the solvent was removed *in vacuo* to afford the corresponding sulfonyl fluoride. If necessary, the product was purified by flash column chromatography on silica gel.

4.2.6 S-F product characterisation

4-Methylbenzenesulfonyl fluoride (**1**)

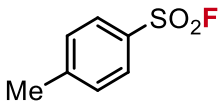

1

Synthesized from 4-methylbenzenesulfonyl chloride (TsCl) (96 mg, 0.50 mmol) following general procedure **GP1** using *t*BuOH and stirring at 100 °C for 5 h to give 4-methylbenzenesulfonyl fluoride (**1**) as a white crystalline solid (75 mg, 0.43 mmol, 86%) without any further purification.

^{1}H NMR (400 MHz, $CDCl_3$) δ 7.89 (d, *J* = 8.4 Hz, 2H), 7.42 (d, *J* = 8.4 Hz, 2H), 2.49 (s, 3H).

^{13}C NMR (101 MHz, $CDCl_3$) δ 147.2, 130.4, 130.2 (d, *J* = 24.3 Hz), 128.5, 22.0.

^{19}F NMR (377 MHz, $CDCl_3$) δ 66.25 (s).

MS (EI, 70 eV) m/z (%) 173.98 ([M]$^{+\cdot}$, 34), 91.04 (64), 65.02 (13), 31.99 (100).

IR (neat) 2927, 1594, 1409, 1214, 755 cm^{-1}

m.p. 40–42 °C (lit. 41–42 °C) [7]

Anal. Calcd. for $C_7H_7FO_2S$: C, 48.27; H, 4.05; S, 18.41. Found: C, 47.95; H, 4.15; S, 19.00.

CAS 455-16-3

Spectroscopic data are in accordance with those in literature [8].

Naphthalene-2-sulfonyl fluoride (**2**)

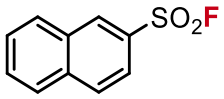

2

Synthesized from naphthalene-2-sulfonyl chloride (113 mg, 0.50 mmol) following general procedure **GP1** using EtCN and stirring at 100 °C for 5 h to give naphthalene-2-sulfonyl fluoride (**2**) as a white solid (103 mg, 0.49 mmol, 98%) without any further purification.

^{1}H NMR (400 MHz, $CDCl_3$) δ 8.62 (s, 1H), 8.10 – 8.06 (m, 1H), 8.07 – 8.01 (m, 1H), 8.00 – 7.96 (m, 1H), 7.96 – 7.91 (m, 1H), 7.79 – 7.73 (m, 1H), 7.73 – 7.67 (m, 1H).

^{13}C NMR (101 MHz, $CDCl_3$) δ 136.1, 131.9, 131.1, 130.5, 130.0, 129.7 (d, J = 24.6 Hz), 129.7, 128.4, 128.3, 122.3.

^{19}F NMR (377 MHz, $CDCl_3$) δ 66.33 (s).

MS (EI, 70 eV) m/z (%) 210.02 ([M]$^{+\cdot}$, 100), 127.04 (49), 115.04 (41), 126.04 (21.09).

IR (neat) 2927, 1401, 1211, 1198, 757 cm^{-1}

m.p. 87–88 °C (lit. 86–88 °C) [7]

Anal. Calcd. for $C_{10}H_7FO_2S$: C, 57.13; H, 3.36; S, 15.25. Found: C, 56.50; H, 3.60; S, 15.85.

CAS 325-12-2

Spectroscopic data are in accordance with those in literature [8].

4-Bromo-2-methylbenzenesulfonyl fluoride (**3**)

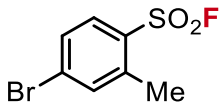

3

Synthesized from 4-bromo-2-methylbenzenesulfonyl chloride (135 mg, 0.50 mmol) following general procedure **GP1** using EtCN and stirring at 100 °C for 5 h to give 4-bromo-2-methylbenzenesulfonyl fluoride (**3**) as a white solid (91 mg, 0.36 mmol, 72%) without any further purification.

^{1}H NMR (400 MHz, $CDCl_3$) δ 7.89 (d, *J* = 8.5 Hz, 1H), 7.60 (d, *J* = 1.6 Hz, 1H), 7.56 (dt, *J* = 8.5, 1.6 Hz, 1H), 2.67 (s, 3H).

^{13}C NMR (101 MHz, $CDCl_3$) δ 140.1, 135.9, 131.6, 131.3, 130.8, 130.1, 20.3.

^{19}F NMR (377 MHz, $CDCl_3$) δ 60.85 (s).

MS (EI, 70 eV) m/z (%) 253.91 (^{81}Br[M]$^{+\cdot}$, 85), 251.91 (^{79}Br[M]$^{+\cdot}$, 84), 169.95 (60), 167.95 (61), 89.03 (100).

IR (neat) 1570, 1581, 1407, 1209, 859, 775, 698, 621 cm^{-1}

m.p. 58–61 °C

Anal. Calcd. for $C_7H_6BrFO_2S$: C, 32.22; H, 2.39; S, 12.67. Found: C, 32.94; H, 2.54; S, 13.33.

CAS 1934405-42-1

5-Bromothiophene-2-sulfonyl fluoride (**4**)

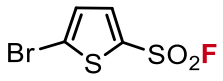

4

To a glass reaction vessel was added 5-bromothiophene-2-sulfonyl chloride (131 mg, 0.50 mmol) and *t*BuOH, followed by **Fmix** (308 mg, 1.2 equiv relative to CaF_2 and 3.0 equiv relative to K_2HPO_4) and H_2O (18 µL, 2.0 equiv). After stirring at 80 °C for 12 h, the resulting suspension was cooled to room temperature, filtered over a short plug of silica gel (washed with ~15 mL $CHCl_3$) to remove insoluble by-products and the solvent was removed under reduced pressure. Purification by flash column chromatography on silica (pentane/ethyl acetate 100:0 to 95:5) gave 5-bromothiophene-2-sulfonyl fluoride (**4**) as a pale-yellow oil (89 mg, 0.36 mmol, 73%).

^{1}H NMR (400 MHz, $CDCl_3$) δ 7.68 (dd, *J* = 4.1, 1.2 Hz, 1H), 7.21 (dd, *J* = 4.1, 0.9 Hz, 1H).

^{13}C NMR (101 MHz, $CDCl_3$) δ 137.3, 132.0 (d, *J* = 31.7 Hz), 131.3, 125.4 (d, *J* = 2.4 Hz).

^{19}F NMR (377 MHz, $CDCl_3$) δ 71.39.

MS (EI, 70 eV) m/z (%) 245.87 (^{81}Br[M]$^{+\cdot}$, 83), 243.87 (^{79}Br[M]$^{+\cdot}$, 78), 148.9 (71), 81.99 (100), 38.04 (25).

IR (neat) 1733, 1465, 1289, 1210, 768 cm^{-1}

CAS 108158-00-5

Spectroscopic data are in accordance with those in literature [9].

[1,1'-Biphenyl]-4-sulfonyl fluoride (**5**)

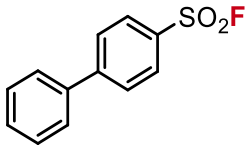

5

Synthesized from [1,1'-biphenyl]-4-sulfonyl chloride (126 mg, 0.50 mmol) following general procedure **GP1** using *t*BuOH and stirring at 100 °C for 5 h. Purification by flash column chromatography on silica (pentane/ethyl acetate 100:0 to 90:10) gave [1,1'-biphenyl]-4-sulfonyl fluoride (**5**) as a white solid (92 mg, 0.39 mmol, 78%) without any further purification.

^{1}H NMR (400 MHz, $CDCl_3$) δ 8.10 – 8.04 (m, 2H), 7.87 – 7.79 (m, 2H), 7.67 – 7.59 (m, 2H), 7.57 – 7.43 (m,3H).

^{13}C NMR (101 MHz, $CDCl_3$) δ 148.8, 138.7, 131.5 (d, *J* = 24.8 Hz), 129.4, 129.3, 129.1, 128.3, 127.6.

^{19}F NMR (377 MHz, $CDCl_3$) δ 66.52 (s).

MS (EI, 70 eV) m/z (%) 236.04 ([M]$^{+\cdot}$, 100), 152.07 (40), 141.07 (28), 151.07 (13).

IR (neat) 1590, 1408, 1212, 1008, 1188, 786, 745 cm^{-1}

m.p. 77–79 °C (lit. 78–79 °C) [10]

Anal. Calcd. for $C_{12}H_9FO_2S$: C, 61.01; H, 3.84; S, 13.57. Found: C, 60.91; H, 4.06; S, 14.09.

CAS 325-04-2

Spectroscopic data are in accordance with those in literature [11].

4-Acetamidobenzenesulfonyl fluoride (**6**)

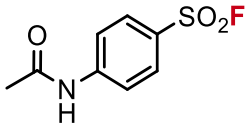

6

Synthesized from 4-acetamidobenzenesulfonyl chloride (117 mg, 0.50 mmol) following general procedure **GP1** using EtCN and stirring at 100 °C for 5 h. Purification by flash column chromatography on silica (pentane/ethyl acetate 100:0 to 80:20) gave 4-acetamidobenzenesulfonyl fluoride (**6**) as a white solid (84 mg, 0.39 mmol, 77%).

^{1}H NMR (400 MHz, CD_3CN) δ 8.83 (br s, 1H), 7.96 (d, *J* = 9.0 Hz, 2H), 7.87 (d, *J* = 9.0 Hz, 2H), 2.12 (s, 3H).

^{13}C NMR (101 MHz, CD_3CN) δ 170.6, 147.2, 130.9, 126.3 (d, *J* = 24.2 Hz), 120.0, 24.6.

^{19}F NMR (377 MHz, CD_3CN) 65.70 (s)

MS (EI, 70 eV) m/z (%) 217.02 ([M]$^{+\cdot}$, 21), 175.00 ([M-COMe]$^{+\cdot}$, 100), 43.03 (38), 108.03 (22).

IR (neat) 3345, 2927, 1690, 1591, 1531, 1401, 1208, 1181, 767 cm^{-1}

m.p. 174–175 °C (lit. 174–175 °C) [12]

CAS 329-20-4

Spectroscopic data are in accordance with those in literature [13].

4-Iodobenzene-1-sulfonyl fluoride (**7**)

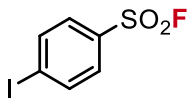

7

Synthesized from 4-iodobenzene-1-sulfonyl chloride (151 mg, 0.50 mmol) following general procedure **GP1** using EtCN and stirring at 100 °C for 5 h to give 4-iodobenzene-1-sulfonyl fluoride (**7**) as a pale-yellow solid (112 mg, 0.39 mmol, 78%) without any further purification.

^{1}H NMR (400 MHz, $CDCl_3$) δ 8.01 (d, *J* = 8.3 Hz, 2H), 7.71 (d, *J* = 8.3 Hz, 2H).

^{13}C NMR (101 MHz, $CDCl_3$) δ 139.2, 132.8 (d, *J* = 25.7 Hz), 129.6, 104.2.

^{19}F NMR (377 MHz, $CDCl_3$) δ 66.25 (s).

MS (EI, 70 eV) m/z (%) 285.88 ([M]$^{+\cdot}$, 100), 218.92 (11), 158.97 (16), 92.01 (20)

IR (neat) 2360, 1568, 1408, 1390, 1211, 774 cm^{-1}

m.p. 84–85 °C (lit. 85 °C) [7]

Anal. Calcd. for $C_6H_4FIO_2S$: C, 25.19; H, 1.41; S, 11.21. Found: C, 24.93; H, 1.46; S, 11.94.

CAS 4241-66-1

Spectroscopic data are in accordance with those in literature [14].

4-Nitrobenzenesulfonyl fluoride (**8**)

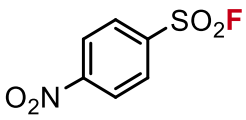

8

Synthesized from 4-nitrobenzenesulfonyl chloride (111 mg, 0.50 mmol) following **GP1** using EtCN and stirring at 100 °C for 1 h to give 4-nitrobenzenesulfonyl fluoride (**8**) as a pale-yellow solid (73 mg, 0.37 mmol, 73%) without any further purification.

^{1}H NMR (400 MHz, $CDCl_3$) δ 8.49 (d, *J* = 8.0 Hz, 2H), 8.25 (d, *J* = 8.0 Hz, 2H).

^{13}C NMR (101 MHz, $CDCl_3$) δ 151.9, 138.5 (d, *J* = 27.0 Hz), 130.2, 125.0.

^{19}F NMR (377 MHz, $CDCl_3$) δ 66.25 (s).

MS (EI, 70 eV) m/z (%) 204.98 ([M]$^{+\cdot}$, 43), 158.97 (28), 92.02 (38).

IR (neat) 2363, 1531, 1417, 1369, 1214, 784 cm^{-1}

m.p. 75–76 °C (lit. 75–76 °C) [14]

Anal. Calcd. for $C_6H_4FNO_4S$: C, 35.13; H, 1.97; N, 6.83; S, 15.63. Found: C, 34.41; H, 1.91; N, 6.24; S, 15.78.

CAS 349-96-2

Spectroscopic data are in accordance with those in literature [14].

Benzyl 4-chloro-5-(fluorosulfonyl)-2-((furan-2-ylmethyl)amino)benzoate (**9**)

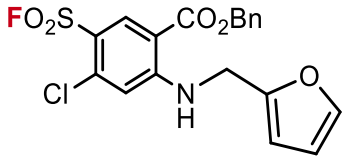

9

To a glass reaction vessel was added **Fmix** (128 mg, 1.0 equiv relative to CaF_2 and 2.5 equiv relative to K_2HPO_4), benzyl 4-chloro-5-(chlorosulfonyl)-2-((furan-2-ylmethyl)amino)benzoate (110 mg, 0.25 mmol) (**S2**), H_2O (9 µL, 2.0 equiv) and anhydrous *t*BuOH (1 mL). After stirring at 80 °C for 5 hours, the resulting suspension was cooled to room temperature, filtered through a short plug of silica gel (washed with ~5 mL EtOAc),

and the solvent was removed *in vacuo*. Purification by flash column chromatography on silica (pentane/ethyl acetate 90:10) gave benzyl 4-chloro-5-(fluorosulfonyl)-2-((furan-2-ylmethyl)amino)benzoate (**9**) as a pale yellow solid (71 mg, 0.17 mmol, 67%).

^{1}H NMR (400 MHz, $CDCl_3$) δ 8.98 – 8.92 (m, 1H), 8.66 (s, 1H), 7.46 – 7.30 (m, 6H), 6.95 (s, 1H), 6.36 (dd, *J* = 3.2, 1.8 Hz, 1H), 6.33 – 6.27 (m, 1H), 5.34 (s, 2H), 4.47 (d, *J* = 5.7 Hz, 2H).

^{13}C NMR (101 MHz, $CDCl_3$) δ 166.5, 154.6, 149.6, 143.0, 139.1, 137.1, 135.3, 128.9, 128.8, 128.4, 116.6 (d, *J* = 26.3 Hz), 114.2, 110.7, 108.6, 108.3, 67.3, 40.4.

^{19}F NMR (377 MHz, $CDCl_3$) δ 61.7 (s).

IR (neat) 3333, 2980, 2361, 1686, 1569, 1418, 1201, 1106, 770, 732 cm^{-1}

m.p. 92–93 °C

HRMS (ESI) m/z calculated for $C_{19}H_{14}{}^{35}ClFNO_5S$ $[M-H]^-$ 422.0271, found 422.0278; $C_{19}H_{14}{}^{37}ClFNO_5S$ $[M-H]^-$ 424.0241, found 424.0272.

Spectroscopic data are in accordance with those in literature [8].

2-Nitrobenzenesulfonyl fluoride (**10**)

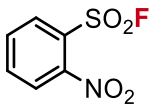

10

Synthesized from 2-nitrobenzenesulfonyl chloride (111 mg, 0.50 mmol) following **GP1** using *t*BuOH and stirring at 100 °C for 5 h to give 2-nitrobenzenesulfonyl fluoride (**10**) as a pale-yellow solid (51 mg, 0.25 mmol, 50%) without any further purification.

^{1}H NMR (400 MHz, $CDCl_3$) δ 8.25 (dd, *J* = 7.9, 1.5 Hz, 1H), 8.05 (d, *J* = 7.9, 1H), 7.97 (td, *J* = 7.8, 1.5 Hz, 1H), 7.93 – 7.84 (m, 1H).

^{13}C NMR (101 MHz, $CDCl_3$) δ 148.3, 136.7, 133.4, 132.0 (d, *J* = 1.6 Hz), 127.2 (d, *J* = 29.1 Hz), 126.0.

^{19}F NMR (377 MHz, $CDCl_3$) δ 65.07 (s).

MS (EI, 70 eV) m/z (%) 204.97 ($[M]^{+\cdot}$, 81), 92.02 (100), 80.02 (57), 64.03 (68).

IR (neat) 2928, 2361, 1594, 1444, 1215, 805, 780 cm^{-1}

m.p. 57–58 °C (lit. 55–57 °C) [14]

Anal. Calcd. for $C_6H_4FNO_4S$: C, 35.13 ; H, 1.97; N, 6.83; S, 15.63. Found: C, 34.82; H, 2.11; N, 6.35; S, 16.13.

CAS 433-98-7

Spectroscopic data are in accordance with those in literature [8].

Benzene-1,2-disulfonyl fluoride (**11**)

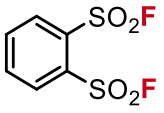

11

Synthesized following **GP1** where 2.2 equivalents of **FImix** (641 mg) was added to benzene-1,2-disulfonyl chloride (138 mg, 0.5 mmol) in anhydrous *t*BuOH and stirring at 100 °C for 5 h to give benzene-1,2-disulfonyl fluoride (**11**) as a white solid (67 mg, 0.28 mmol, 55%) without any further purification.

^{1}H NMR (400 MHz, $CDCl_3$) δ 8.50 – 8.41 (m, 2H), 8.10 – 8.01 (m, 2H).

^{13}C NMR (101 MHz, $CDCl_3$) δ 136.2, 133.7, 132.6 (d, *J* = 29.5 Hz).

^{19}F NMR (377 MHz, $CDCl_3$) δ 65.81 (s).

MS (EI, 70 eV) m/z (%) 241.93 ($[M]^{+\cdot}$, 22), 92.01 (15.19), 64.01 (10), 32.00 (100).

IR (neat) 2981, 2360, 1534, 1411, 1215, 1121, 789 cm^{-1}

m.p. 127–128 °C (lit. 126–128 °C) [14]

Anal. Calcd. for $C_6H_4F_2O_4S_2$: C, 29.75; H, 1.66; S, 26.47. Found: C, 29.63; H, 1.82; S, 27.59.

CAS 115560-96-8

Spectroscopic data are in accordance with those in literature [14].

Hexadecane-1-sulfonyl fluoride (**12**)

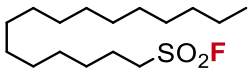

12

Synthesized from 1-hexadecanesulfonyl chloride (163 mg, 0.50 mmol) following general procedure **GP1** using *t*BuOH and stirring at 100 °C for 5 h to give 1-hexadecanesulfonyl fluoride (**12**) as a white solid (116 mg, 0.38 mmol, 75%) without any further purification.

^{1}H NMR (400 MHz, $CDCl_3$) δ 3.39 – 3.30 (m, 2H), 2.00 – 1.88 (m, 2H), 1.51 – 1.45 (m, 2H), 1.35 – 1.26 (m, 24H), 0.88 (t, *J* = 6.2 Hz, 3H).

^{13}C NMR (101 MHz, $CDCl_3$) [overlapping signals] δ 51.0 (d, *J* = 16.0 Hz), 32.1, 29.8, 29.7 (overlapping signals), 29.6, 29.5, 29.3, 28.9, 28.0, 23.5, 22.8, 14.2.

^{19}F NMR (377 MHz, $CDCl_3$) δ 53.23 (t, *J* = 4.2 Hz).

MS (EI, 70 eV) m/z (%) 308.20 ([M]$^{+\cdot}$, 1), 71.07 (70), 57.06 (100).

IR (neat) 2917, 2849, 2361, 1461, 1393, 1209, 1198, 804, 752 cm^{-1}

m.p. 35–36 °C (lit. 36–37 °C) [15]

Anal. Calcd. for $C_{16}H_{33}FO_2S$: C, 62.29; H, 10.78; S, 10.39. Found: C, 63.04; H, 11.31; S, 9.61.

CAS 86855-26-7

Spectroscopic data are in accordance with those in literature [16].

(*E*)-2-Phenylethene-1-sulfonyl fluoride (**13**)

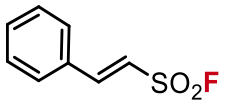

13

Synthesized from (*E*)-2-Phenylethene-1-sulfonyl chloride (101 mg, 0.50 mmol) following general procedure **GP1** using *t*BuOH and stirring at 100 °C for 5 h to give (*E*)-2-phenylethene-1-sulfonyl fluoride (**13**) as a white solid (61 mg, 0.33 mmol, 66%) without any further purification.

^{1}H NMR (400 MHz, $CDCl_3$) δ 7.82 (d, *J* = 15.5, 1H), 7.67 – 7.40 (m, 5H), 6.87 (d, *J* = 15.5, 1H).

^{13}C NMR (101 MHz, $CDCl_3$) δ 149.0 (d, *J* = 2.8 Hz), 132.8, 131.1, 129.5, 129.2, 118.1 (d, *J* = 28.1 Hz).

^{19}F NMR (377 MHz, $CDCl_3$) δ 62.32 (s).

MS (EI, 70 eV) m/z (%) 186.00 ([M]$^{+\cdot}$, 38), 103.04 (19), 102.03 (100), 77.03 (26), 51.02 (12), 32 (78).

IR (neat) 2980, 2924, 2360, 1615, 1395, 1205, 1189, 982, 872, 834, 808 cm^{-1}

m.p. 96–97 °C (lit. 96–97 °C) [17]

Anal. Calcd. for $C_8H_7FO_2S$: C, 51.60; H, 3.79; S, 17.22. Found: C, 51.00; H, 4.11; S, 17.60.

CAS 405-18-5

Spectroscopic data are in accordance with those in literature [18].

Methane sulfonyl fluoride (**14**)

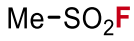

14

Synthesized from methane sulfonyl chloride (57 mg, 0.5 mmol) following **GP1** in a sealed microwave vial using anhydrous *t*BuOH and stirring at 60 °C for 16 h.

^{1}H NMR (400 MHz, $CDCl_3$) 3.23 (d, *J* = 5.1 Hz, 1H).

^{19}F NMR (377 MHz, $CDCl_3$) δ 61.04 (m)

Calculated yield (**14**): 52% (by ^{19}F-NMR using 4-fluoroanisole as internal standard)

CAS 558-25-8

Spectroscopic data are in accordance with those in literature [8].

Cyclopropane sulfonyl fluoride (**15**)

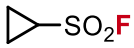

15

Synthesized from cyclopropane sulfonyl chloride (70 mg, 0.5 mmol) following **GP1** in a sealed microwave vial using anhydrous MeCN and stirring at 100 °C for 16 h.

^{1}H NMR (400 MHz, $CDCl_3$) δ 2.61 – 2.50 (m, 1H), 1.41 – 1.24 (m, 4H).

^{19}F NMR (377 MHz, $CDCl_3$) δ 56.93 (s)

Calculated yield (**15**): 83% (by ^{19}F-NMR using 4-fluoroanisole as internal standard)

Spectroscopic data are in accordance with those in literature [8].

Pyridine-3-sulfonyl fluoride (**16**)

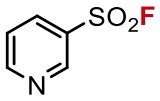

16

To a glass reaction vessel was added pyridine-3-sulfonyl chloride (88 mg, 0.50 mmol) and *t*BuOH (2 mL), followed by **Fmix** (257 mg, 1.0 equiv relative to CaF_2 and 2.5 equiv relative to K_2HPO_4) and H_2O (18 µL, 2.0 equiv). After stirring at 40 °C for 16 h, the resulting suspension was cooled to room temperature, filtered over a short plug of silica gel (washed with ~15 mL $CHCl_3$) to remove insoluble by-products and the solvent was removed *in vacuo*. Pyridine-3-sulfonyl fluoride (**16**) was obtained as a colorless liquid (38 mg, 0.24 mmol, 47%) without any further purification.

^{1}H NMR (400 MHz, $CDCl_3$) δ 9.25 – 9.17 (m, 1H), 8.99 (dd, *J* = 4.9, 1.7 Hz, 1H), 8.30 (ddd, *J* = 8.1, 2.4, 1.7 Hz, 1H), 7.65 – 7.57 (m, 1H).

^{13}C NMR (101 MHz, $CDCl_3$) δ 156.1, 149.1 136.2, 130.3 (d, *J* = 25.7 Hz), 124.3.

^{19}F NMR (377 MHz, $CDCl_3$) δ 68.02 (s).

MS (EI, 70 eV) m/z (%) 160.99 ($[M]^{+\cdot}$, 100), 78.03 ($[C_5H_4N]^{+\cdot}$, 86), 32.00 (43).

IR (neat) 3066, 1573, 1422, 1404, 1210, 1020, 779, 733 cm^{-1}

CAS 1373307-61-9

Spectroscopic data are in accordance with those in literature [19].

Pyridine-2-sulfonyl fluoride (PyFluor) (**17**)

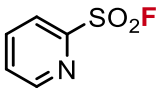

17

Synthesized from pyridine-2-sulfonyl chloride (**S3**) (88 mg, 0.50 mmol) following **GP1** using anhydrous 1,2-dichlorobenzene and stirring at 25 °C for 5 h. Purification by flash column chromatography on silica (pentane/ethyl acetate 95:5 to 85:15) gave pyridine-2-sulfonyl fluoride (**17**) as a colorless liquid (43 mg, 0.27 mmol, 54%).

^{1}H NMR (500 MHz, $CDCl_3$) δ 8.85 (d, *J* = 4.8 Hz, 1H), 8.14 (d, *J* = 7.9 Hz, 1H), 8.06 (tt, *J* = 7.8, 1.5 Hz, 1H), 7.72 (ddd, *J* = 7.7, 4.7, 1.2 Hz, 1H).

^{13}C NMR (126 MHz, $CDCl_3$) δ 151.5 (d, *J* = 30.4 Hz), 151.2, 138.8, 129.3, 124.24 (d, *J* = 2.1 Hz).

^{19}F NMR (377 MHz, $CDCl_3$) δ 55.87.

MS (EI, 70 eV) m/z (%) 160.99 ($[M]^{+\cdot}$, 38), 78.04 ($[C_5H_4N]^{+\cdot}$, 100), 51.04 (30).

IR (neat) 2981, 2359, 1431, 1416, 1220, 802, 776 cm^{-1}

m.p. 30–33 °C (lit. 29–34 °C) [20]

CAS 878376-35-3

Spectroscopic data are in accordance with those in literature [12,20].

N-Tosyl-4-chlorobenzenesulfonimidoyl fluoride (SulfoxFluor) (**18**)

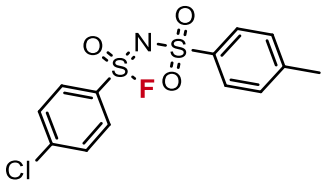

18

Synthesized from *N*-tosyl-4-chlorobenzenesulfonimidoyl chloride (**S4**) (182 mg, 0.50 mmol) following general procedure **GP1** using EtCN and stirring at 100 °C for 5 h. Purification by flash column chromatography on silica (pentane/ethyl acetate 10:1 to 5:1) gave *N*-tosyl-4-chlorobenzenesulfonimidoyl fluoride (**18**) as a colorless oil which solidified upon standing to give a white solid (137 mg, 0.39 mmol, 79%)

^{1}H NMR (400 MHz, $CDCl_3$) δ 7.98 (d, *J* = 8.9 Hz, 2H), 7.93 (d, *J* = 8.4 Hz, 2H), 7.59 (d, *J* = 8.9 Hz, 2H), 7.34 (d, *J* = 8.4 Hz, 2H), 2.44 (s, 3H).

^{13}C NMR (101 MHz, $CDCl_3$) δ 144.7, 143.5, 138.7, 131.5 (d, *J* = 21.8 Hz), 130.3, 129.9, 129.6, 127.2, 21.8.

^{19}F NMR (377 MHz, $CDCl_3$) δ 74.63 (s).

HRMS (ESI) m/z calculated for $C_{13}H_{12}{}^{35}ClFNO_3S_2$ $[M+H]^+$ 347.9926, found 347.9938; $C_{13}H_{12}{}^{37}ClFNO_3S_2$ $[M+H]^+$ 349.9897, found 349.9911.

IR (neat) 2981, 1577, 1398, 1336, 1184, 1164, 1085, 1012, 835, 815, 785, 705 cm^{-1}

m.p. 112–113 °C (lit. 110–112 °C) [21]

CAS 2143892-50-4

Spectroscopic data are in accordance with those in literature [21].

Ethene sulfonyl fluoride (ESF) (**19**)

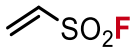

19

Synthesized from ethene sulfonyl chloride (**S5**) (63 mg, 0.5 mmol) following **GP1** in a sealed microwave vial using EtCN and stirring at 25 °C for 48 h.

^{1}H NMR (400 MHz, $CDCl_3$) δ 6.82 (ddd, *J* = 16.6, 9.1, 2.1 Hz, 1H), 6.76 (d, *J* = 16.5 Hz, 1H), 6.47 (dd, *J* = 9.2, 5.2 Hz, 1H).

^{19}F NMR (377 MHz, $CDCl_3$) δ 57.23 (s)

MS (EI, 70 eV) m/z (%) 32.0 (100), 43.02 ($[C_3H_7]^{+\cdot}$,14), 66.95 (12), 109.95 ($[M]^{+\cdot}$, 7).

CAS 677-25-8

Calculated yield (**19**): 72 % (by ^{19}F-NMR using 4-fluoroanisole as internal standard)

Spectroscopic data are in accordance with those in literature [22].

(*E*)-2-((3,7-dimethylocta-2,6-dien-1-yl)thio)ethane-1-sulfonyl fluoride (**20**)

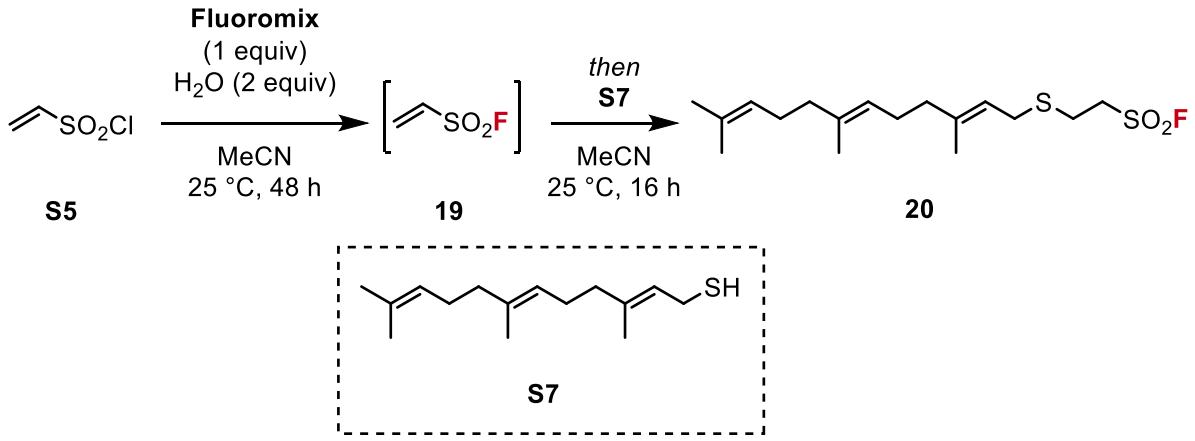

To a microwave vial was added ethene sulfonyl chloride (**S5**) (63 mg, 0.5 mmol), **Fmix** (257 mg, 1.0 equiv relative to CaF_2 and 2.5 equiv relative to K_2HPO_4), H_2O (18 µL, 2.0 equiv) and anhydrous MeCN (2 mL). The vial was sealed and after stirring at 25 °C for 48 h, (*E*)-3,7-dimethylocta-2,6-diene-1-thiol (*trans,trans*-farnesyl mercaptan) (**S7**) (95 mg, 0.40 mmol, 1.1 equiv respect to ESF (**19**)) was added. After stirring at 25 °C for an additional 16 h the resulting suspension was filtered through a short plug of silica gel (washed with ~15 mL EtOAc) to remove insoluble by-products and the solvent was removed *in vacuo*. Purification by flash column chromatography on silica (pentane, 100%) gave (*E*)-2-

((3,7-dimethylocta-2,6-dien-1-yl)thio)ethane-1-sulfonyl fluoride (**20**) as a colorless oil (69 mg, 0.20 mmol, 40% over 2 steps from **S5**).

^{1}H NMR (400 MHz, $CDCl_3$) δ 5.22 (tq, *J* = 7.8, 1.5 Hz, 1H), 5.13 – 5.04 (m, 2H), 3.63 – 3.52 (m, 2H), 3.23 (d, *J* = 7.8 Hz, 2H), 3.00 – 2.87 (m, 2H), 2.19 – 1.92 (m, 8H), 1.68 (br s, 6H), 1.60 (s, 6H).

^{13}C NMR (101 MHz, $CDCl_3$) δ 140.9, 135.8, 131.5, 124.4, 123.6, 119.3, 51.5 (d, *J* = 14.9 Hz), 39.8, 39.7, 29.8, 26.9, 26.5, 25.9, 23.9, 17.8, 16.3, 16.2.

^{19}F NMR (377 MHz, $CDCl_3$) δ 53.55 (t, *J* = 4.7 Hz).

HRMS (APCI) m/z calculated for $C_{17}H_{30}FO_2S_2$ $[M+H]^+$ 349.1666, found 349.1666.

IR (neat) 2926, 1410, 1305, 1232, 1191, 821, 729 cm^{-1}

Spectroscopic data are in accordance with those in literature [23].

4-(2-(1,3-Dioxoisoindolin-2-yl)ethyl)benzenesulfonyl fluoride (**21**)

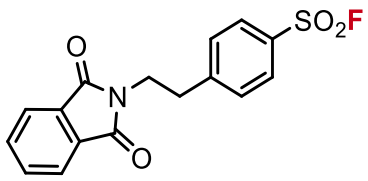

21

Synthesized from 4-(2-(1,3-dioxoisoindolin-2-yl)ethyl)benzenesulfonyl chloride (**S8**) (175 mg, 0.50 mmol) following **GP1** using EtCN and stirring at 100 °C for 5 h to give 4-(2-(1,3-dioxoisoindolin-2-yl)ethyl)benzenesulfonyl fluoride (**21**) as white crystals (84 mg, 0.25 mmol, 50%) without any further purification.

^{1}H NMR (400 MHz, $CDCl_3$) δ 7.98 – 7.88 (m, 2H), 7.86 – 7.78 (m, 2H), 7.77 – 7.68 (m, 2H), 7.55 – 7.47 (m, 2H), 4.02 – 3.93 (m, 2H), 3.14 (dd, *J* = 8.2, 6.8 Hz, 2H).

^{13}C NMR (101 MHz, $CDCl_3$) δ 168.2, 146.9, 134.3, 131.9, 131.5 (d, *J* = 24.6 Hz), 130.3, 128.9, 123.6, 38.4, 34.7.

^{19}F NMR (377 MHz, $CDCl_3$) δ 66.26 (s).

HRMS (ESI) m/z calculated for $C_{16}H_{13}FNO_4S$ $[M+H]^+$ 334.0544, found 334.0560.

IR (neat) 1769, 1713, 1125, 1354, 994, 779, 736 cm^{-1}

m.p. 170–173 °C

Anal. Calcd. for $C_{16}H_{13}FNO_4S$: C, 57.65; H, 3.63; N, 4.20; S, 9.62. Found: C, 56.63; H, 3.92; N, 3.88; S, 9.85.

5-(Dimethylamino)naphthalene-1-sulfonyl fluoride (Dansyl Fluoride) (**22**)

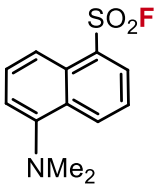

22

Synthesized from dansyl chloride (135 mg, 0.5 mmol) following **GP1** using anhydrous *t*BuOH and stirring at 100 °C for 5 h to give 5-(dimethylamino)naphthalene-1-sulfonyl fluoride (**22**) as a yellow solid (91 mg, 0.36 mmol, 72%) without any further purification.

^{1}H NMR (400 MHz, $CDCl_3$) δ 8.70 (d, *J* = 8.6 Hz, 1H), 8.34 (d, *J* = 7.3 Hz, 1H), 8.18 (dd, *J* = 8.7, 3.4 Hz, 1H), 7.65 (dd, *J* = 8.7, 7.3 Hz, 1H), 7.58 (ddd, *J* = 8.7, 7.4, 1.5 Hz, 1H), 7.25 (d, *J* = 7.6 Hz, 1H), 2.90 (s, 6H).

^{13}C NMR (101 MHz, $CDCl_3$) δ 152.2, 133.4, 131.1 (d, *J* = 2.0 Hz), 130.0 (d, *J* = 7.4 Hz), 129.7, 129.5, 129.3 (d, *J* = 23.0 Hz), 123.1, 118.6, 116.1, 45.6.

^{19}F NMR (377 MHz, $CDCl_3$) δ 62.15 (s).

MS (EI, 70 eV) m/z (%) 253.04 ($[M]^{+\cdot}$, 100), 168.08 (30), 43.98 (16).

IR (neat) 2957, 1570, 1485, 1414, 1236, 1197, 1075, 806, 786 cm^{-1}

m.p. 50–51 °C (lit. 48–50 °C) [24]

Anal. Calcd. for $C_{12}H_{12}FNO_2S$: C, 56.90; H, 4.78; N, 5.53; S, 12.66. Found: C, 57.11; H, 5.26; N, 5.20; S, 12.72.

CAS 34523-28-9

Spectroscopic data are in accordance with those in literature [25].

Benzyl (*S*)-(1-(fluorosulfonyl)-4-methylpentan-2-yl)carbamate (**23**)

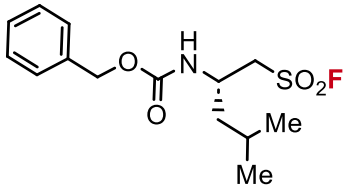

23

(*S*)-*S*-(2-(((Benzyloxy)carbonyl)amino)-4-methylpentyl) ethanethioate (**S10**) (170 mg, 0.55 mmol, 1 equiv) dissolved in MeCN (441 µL) was added to a cooled (0 °C) mixture of *N*-chlorosuccinimide (294 mg, 2.20 mmol), HCl (2 M, 147 µL) and MeCN (735 µL). After stirring for 15 min at 25 °C, the solution was diluted in isopropyl ether (2 mL), washed with brine (2 x 2 mL), dried over $MgSO_4$, filtered and concentrated *in vacuo* to afford crude benzyl (*S*)-(1-(chlorosulfonyl)-4-methylpentan-2-yl)carbamate (167 mg, 0.5 mmol, 91%) which was immediately used without further purification in the next step. To the crude sulfonyl chloride was added **Fmix** (257 mg, 1.0 equiv relative to CaF_2 and 2.5 equiv relative to K_2HPO_4), H_2O (18 µL, 2.0 equiv) and anhydrous *t*BuOH (2 mL). After stirring at 80 °C for 5 h, the resulting suspension was cooled to room temperature, filtered through a short plug of silica gel (washed with ~5 mL EtOAc), and the solvent was removed *in vacuo*. Purification by flash column chromatography on silica (pentane/EtOAc 100:0 to 80:20) gave benzyl (*S*)-(1-(fluorosulfonyl)-4-methylpentan-2-yl)carbamate (**23**) as a white solid (72 mg, 0.23 mmol, 45% respect to benzyl (*S*)-(1-(chlorosulfonyl)-4-methylpentan-2-yl)carbamate).

^{1}H NMR (400 MHz, $CDCl_3$) δ 7.44 – 7.31 (m, 5H), 5.11 (s, 2H), 5.09 (br s, 1H), 4.27 – 4.13 (m, 1H), 3.86 – 3.53 (m, 2H), 1.78 – 1.59 (m, 2H), 1.60 – 1.46 (m, 1H), 0.95 (dd, *J* = 6.5, 2.7 Hz, 6H).

^{13}C NMR (101 MHz, $CDCl_3$) δ 155.6, 136.1, 128.7 (2C), 128.5, 128.2, 67.3, 54.9 (d, *J* = 12.3 Hz), 46.0, 42.0, 29.8, 24.9, 23.0, 21.7.

^{19}F NMR (377 MHz, $CDCl_3$) δ 62.95 (s).

HRMS (ESI) m/z calculated for $C_{14}H_{21}FNO_4S$ $[M+H]^+$ 318.1170, found 318.1182.

IR (neat) 3337, 2958, 2928, 2362, 1539, 1407, 1385, 1273, 1198, 1050, 803, 731 cm^{-1}

m.p. 80–81 °C

CAS 1169199-23-8

Spectroscopic data are in accordance with those in literature [26].

Phenylmethanesulfonyl fluoride (**24**)

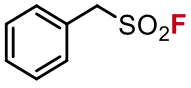

24

Synthesized from phenylmethanesulfonyl chloride (96 mg, 0.50 mmol) following **GP1** using *t*BuOH and stirring at 100 °C for 5 h to give phenylmethanesulfonyl fluoride (**24**) as a white crystalline solid (23 mg, 0.13 mmol, 26%) without any further purification.

^{1}H NMR (400 MHz, $CDCl_3$) δ 7.51 – 7.39 (m, 5H), 4.60 (d, *J* = 3.2 Hz, 2H).

^{13}C NMR (101 MHz, $CDCl_3$) δ 130.8, 130.1, 129.5, 125.6, 56.9 (d, *J* = 17.7 Hz).

^{19}F NMR (377 MHz, $CDCl_3$) δ 51.36 (t, *J* = 3.2 Hz).

MS (EI, 70 eV) m/z (%) 174.00 ([M]$^{+\cdot}$, 18), 91.05 (100), 65.04 (16), 32.00 (47).

IR (neat) 1501, 1395, 1211, 1190, 795, 776 cm^{-1}

m.p. 91–94 °C (lit. 92–93 °C) [12]

Anal. Calcd. for $C_7H_7FO_2S$: C, 48.27; H, 4.05; S, 18.41. Found: C, 47.58; H, 4.29; S, 18.87.

CAS 329-98-6

Spectroscopic data are in accordance with those in literature [12].

Methyl 4-(fluorosulfonyl)benzoate (**25**)

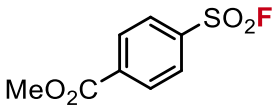

25

Synthesized from methyl 4-(chlorosulfonyl)benzoate (117 mg, 0.50 mmol) following **GP1** using anhydrous *t*BuOH and stirring at 100 °C for 5 h. Purification by flash column chromatography on silica (pentane/CH_2Cl_2 50:50) gave methyl 4-(fluorosulfonyl)benzoate (**25**) as a white solid (55 mg, 0.25 mmol, 50%).

^{1}H NMR (400 MHz, $CDCl_3$) δ 8.32 – 8.21 (m, 2H), 8.13 – 8.04 (m, 2H), 3.98 (s, 3H).

^{13}C NMR (101 MHz, $CDCl_3$) δ 165.03, 136.8 (d, *J* = 25.9 Hz), 136.6, 130.8, 128.6, 53.1.

^{19}F NMR (377 MHz, $CDCl_3$) δ 65.83 (s).

MS (EI, 70 eV) m/z (%) 217.99 ([M]$^{+\cdot}$, 18), 186.97 (100), 92.01 (14), 75.02 (12), 32 (63).

IR (neat) 2970, 2925, 2359, 1728, 1440, 1410, 1279, 1210, 1107, 1093, 782, 760 cm^{-1}

m.p. 85–87 °C (lit. 84–86 °C) [10]

CAS 124397-38-2

Spectroscopic data are in accordance with those in literature [8].

4.2.7 C(sp^3)-F bond formation using Fmix

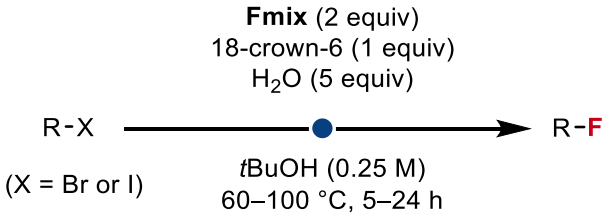

To a glass reaction vessel was added **Fmix** (513 mg, 2.0 equiv relative to CaF_2 and 5.0 equiv relative to K_2HPO_4), the corresponding R–Br (or R–I if stated) (0.5 mmol, 1.0 equiv), 18-crown-6 (132.2 mg, 1.0 equiv) and anhydrous *t*BuOH (2 mL) unless otherwise stated. H_2O (45 µL, 5.0 equiv) was added to the reaction mixture. After stirring at 60 – 100 °C in a heating block, the resulting suspension was cooled to room temperature, filtered through a short plug of silica gel (washed with ~15 mL EtOAc) to remove insoluble by-products and the solvent was removed *in vacuo*. The crude product was purified by flash column chromatography on silica gel to afford the corresponding fluorinated product.

Job Struijs synthesised benzylic fluorides (**30** to **34**) and α-fluoro carbonyls (**37**, **39** and **42**).

4.2.8 C(sp^3)-F product characterisation

2-(Fluoromethyl)naphthalene (**30**)

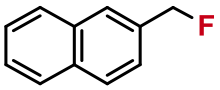

30

Synthesized from 2-(bromomethyl)naphthalene (110.8 mg, 0.50 mmol) following general procedure **GP2** using *t*BuOH and stirring at 100 °C for 15 h. Purification by flash column chromatography on silica (pentane/ethyl acetate 100:0 to 90:10) gave 2-(fluoromethyl)naphthalene (**30**) as a white crystalline solid (61.9 mg, 0.39 mmol, 77%).

^{1}H NMR (400 MHz, $CDCl_3$) δ 7.93 – 7.79 (m, 4H), 7.58 – 7.45 (m, 3H), 5.55 (d, *J* = 48.0 Hz, 2H).

^{13}C NMR (101 MHz, $CDCl_3$) [overlapping signals] δ 133.8 (d, *J* = 16.7 Hz), 133.5 (d, *J* = 2.1 Hz), 133.3, 128.6, 128.2, 127.9, 126.9 (d, *J* = 7.4 Hz), 126.6 (d, *J* = 7.8 Hz), 125.1 (overlapping signals), 84.9 (d, *J* = 166.3 Hz).

^{19}F NMR (377 MHz, $CDCl_3$) δ -206.72 (t, *J* = 48.0 Hz).

HRMS (ESI) m/z calculated for $C_{11}H_9F$ $[M]^+$ 160.06828, found 160.06863.

IR (neat) 2972, 1179, 1018, 964, 946, 827, 748 cm^{-1}

m.p. 51–53 °C (lit. 52–53 °C) [27]

CAS 55831-11-3

Spectroscopic data are in accordance with those in literature [28]

1-(Fluoromethyl)naphthalene (**31**)

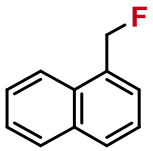

31

Synthesized from 1-(bromomethyl)naphthalene (110.8 mg, 0.50 mmol) following general procedure **GP2** using *t*BuOH and stirring at 100 °C for 15 h. Purification by flash column chromatography on silica (pentane/ethyl acetate 100:0 to 90:10) gave 1-(fluoromethyl)naphthalene (**31**) as a colorless oil (51.5 mg, 0.32 mmol, 64%).

^{1}H NMR (400 MHz, $CDCl_3$) δ 8.09 (d, *J* = 8.7 Hz, 1H), 7.95 – 7.86 (m, 2H), 7.67 – 7.52 (m, 3H), 7.48 (ddd, *J* = 8.2, 6.9, 1.2 Hz, 1H), 5.86 (d, *J* = 47.9 Hz, 2H).

^{13}C NMR (101 MHz, $CDCl_3$) δ 133.8 (d, *J* = 1.7 Hz), 131.9 (d, *J* = 15.3 Hz), 131.5 (d, *J* = 2.1 Hz), 130.0 (d, *J* = 3.5 Hz), 128.8, 126.98 (d, *J* = 8.4 Hz), 126.86 (d, *J* = 1.6 Hz), 126.24, 125.31 (d, *J* = 1.9 Hz), 123.68, 83.47 (d, *J* = 165.7 Hz).

^{19}F NMR (377 MHz, $CDCl_3$) δ -206.15 (t, *J* = 47.9 Hz).

HRMS (ESI) m/z calculated for $C_{11}H_9F$ $[M]^+$ 160.06828, found 160.06840.

IR (neat) 2980, 1513, 1378, 1169, 967, 801, 775 cm^{-1}

CAS 55831-10-2

Spectroscopic data are in accordance with those in literature [29].

1-(Fluoromethyl)-4-nitrobenzene (**32**)

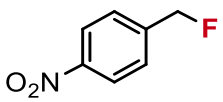

32

Synthesized from 1-(bromomethyl)-4-nitrobenzene (108.0 mg, 0.50 mmol) following general procedure **GP2** using *t*BuOH and stirring at 100 °C for 15 h. Purification by flash

column chromatography on silica (pentane/ethyl acetate 100:0 to 90:10) gave 1-(fluoromethyl)-4-nitrobenzene (**32**) as a yellow solid (55.5 mg, 0.36 mmol, 72%).

^{1}H NMR (400 MHz, $CDCl_3$) δ 8.28 – 8.21 (m, 2H), 7.56 – 7.49 (m, 2H), 5.51 (d, *J* = 47.0 Hz, 2H).

^{13}C NMR (101 MHz, $CDCl_3$) δ 148.02, 143.53 (d, *J* = 17.5 Hz), 127.15 (d, *J* = 7.1 Hz), 123.95, 83.00 (d, *J* = 170.7 Hz).

^{19}F NMR (377 MHz, $CDCl_3$) δ -215.66 (t, *J* = 47.0 Hz).

HRMS (ESI) m/z calculated for $C_7H_6FNO_2$ $[M]^+$ 155.03771, found 155.03720.

IR (neat) 2980, 1606, 1501, 1456, 1349, 1110, 1022, 842, 797, 734 cm^{-1}

m.p. 38–39 °C (lit. 37–38 °C) [30]

CAS 500-11-8

Spectroscopic data are in accordance with those in literature [31].

Methyl 4-(fluoromethyl)benzoate (**33**)

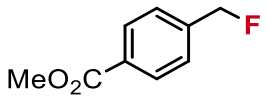

33

Synthesized from methyl 4-(bromomethyl)benzoate (114.5 mg, 0.50 mmol) following general procedure **GP2** using *t*BuOH and stirring at 100 °C for 15 h. Purification by flash column chromatography on silica (pentane/ethyl acetate 100:0 to 90:10) gave methyl 4-(fluoromethyl)benzoate (**33**) as a colorless oil (61.3 mg, 0.36 mmol, 73%).

^{1}H NMR (400 MHz, $CDCl_3$) δ 8.10 – 8.02 (m, 2H), 7.47 – 7.39 (m, 2H), 5.45 (d, *J* = 47.2 Hz, 2H), 3.93 (s, 3H).

^{13}C NMR (101 MHz, $CDCl_3$) δ 166.8, 141.3 (d, *J* = 17.2 Hz), 130.4 (d, *J* = 2.3 Hz), 130.0, 126.7 (d, *J* = 6.6 Hz), 83.8 (d, *J* = 168.5 Hz), 52.4.

^{19}F NMR (377 MHz, $CDCl_3$) δ -212.84 (t, *J* = 47.2 Hz).

HRMS (ESI) m/z calculated for $C_9H_9FO_2[M]^+$ 168.05811, found 168.05773.

IR (neat) 2961, 1724, 1435, 1282, 1109, 956, 758 cm^{-1}

CAS 64299-49-6

Spectroscopic data are in accordance with those in literature [32].

Ethyl 2-fluoro-2-(5,5,8,8-tetramethyl-5,6,7,8-tetrahydronaphthalen-2-yl)acetate (**34**)

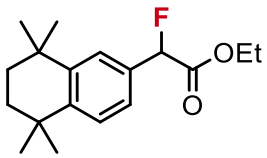

34

Synthesized from ethyl 2-bromo-2-(5,5,8,8-tetramethyl-5,6,7,8-tetrahydronaphthalen-2-yl)acetate (**S13**) following general procedure **GP2** using *t*BuOH and stirring at 100 °C for 18 h. Purification by flash column chromatography on silica (pentane/ethyl acetate 100:0 to 90:10) gave ethyl 2-fluoro-2-(5,5,8,8-tetramethyl-5,6,7,8-tetrahydronaphthalen-2-yl)acetate (**34**) as a colorless oil (61.4 mg, 0.21 mmol, 42%).

^{1}H NMR (400 MHz, $CDCl_3$) δ 7.39 – 7.36 (m, 1H), 7.35 – 7.31 (m, 1H), 7.23 – 7.18 (m, 1H), 5.72 (d, *J* = 48.1 Hz, 1H), 4.35 – 4.17 (m, 2H), 1.69 (s, 4H), 1.31 – 1.25 (m, 15H).

^{13}C NMR (101 MHz, $CDCl_3$) [overlapping signals] δ 169.0 (d, *J* = 27.8 Hz), 146.7 (d, *J* = 2.6 Hz), 145.6, 131.4 (d, *J* = 20.3 Hz), 127.2, 125.3 (d, *J* = 5.9 Hz), 124.0 (d, *J* = 5.5 Hz), 89.7 (d, *J* = 184.7 Hz), 61.8, 35.1, 35.0, 34.5, 34.4, 31.9 (overlapping signals), 14.2.

^{19}F NMR (377 MHz, $CDCl_3$) δ -177.74 (d, *J* = 48.0 Hz).

MS (ESI) m/z calculated for $C_{18}H_{25}FO_2Na$ $[M+Na]^+$ 315.1731, found 315.1744.

IR (neat) 2964, 2935, 1762, 1461, 1194 cm^{-1}

Ethyl 2-fluoro-2-phenylacetate (**35**)

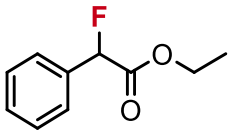

35

Synthesized from ethyl 2-bromo-2-phenylacetate (121.6 mg, 0.5 mmol) following general procedure **GP2** using *t*BuOH and stirring at 100 °C for 18 h. Purification by flash column chromatography on silica (pentane/ethyl acetate 100:0 to 99:1) gave ethyl 2-fluoro-2-phenylacetate (**35**) as a colorless oil (37.0 mg, 0.20 mmol, 41%).

^{1}H NMR (400 MHz, $CDCl_3$) δ 7.60 – 7.45 (m, 2H), 7.45 – 7.38 (m, 3H), 5.77 (d, *J* = 47.8 Hz, 1H), 4.34 – 4.15 (m, 2H), 1.26 (t, *J* = 7.1 Hz, 3H).

^{13}C NMR (101 MHz, $CDCl_3$) δ 168.7 (d, *J* = 27.5 Hz), 134.5 (d, *J* = 20.4 Hz), 129.7 (d, *J* = 2.3 Hz), 128.9, 126.8 (d, *J* = 6.2 Hz), 89.5 (d, *J* = 185.5 Hz), 62.0, 14.2.

^{19}F NMR (377 MHz, $CDCl_3$) δ -179.87 (d, *J* = 47.8 Hz).

MS (EI, 70 eV) m/z (%) 109.04 ($[C_7H_6F]^{+\cdot}$, 100), 83.02 (11), 110.03 (10), 182.05 ($[M]^{+\cdot}$, 8.43).

IR (neat) 2981, 1735, 1372, 1214, 1188, 1056, 1027, 734 cm^{-1}

CAS 643-77-6

Spectroscopic data are in accordance with those in literature [33].

N,N-Diethyl-2-fluoro-2-phenylacetamide (**36**)

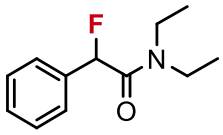

36

Synthesized from 2-bromo-*N,N*-diethyl-2-phenylacetamide (**S14**) (135 mg, 0.5 mmol) following general procedure **GP2** using *t*BuOH and stirring at 100 °C for 24 h. Purification by flash column chromatography on silica (pentane/ethyl acetate 95:5) gave *N,N*-diethyl-2-fluoro-2-phenylacetamide (**36**) as a white solid (82.0 mg, 0.39 mmol, 78%).

^{1}H NMR (400 MHz, $CDCl_3$) δ 7.49 – 7.32 (m, 5H), 6.00 (d, *J* = 49.5 Hz, 1H), 3.40 (qd, *J* = 7.0, 2.7 Hz, 2H), 3.27 – 3.05 (m, 2H), 1.13 (t, *J* = 7.1 Hz, 3H), 0.98 (t, *J* = 7.1 Hz, 3H).

^{13}C NMR (101 MHz, $CDCl_3$) δ 167.0 (d, *J* = 22.2 Hz), 135.0 (d, *J* = 19.9 Hz), 129.5 (d, *J* = 2.7 Hz), 129.0, 127.0 (d, *J* = 5.4 Hz), 90.7 (d, *J* = 182.6 Hz), 41.3 (d, *J* = 3.8 Hz), 40.6, 13.9, 12.7.

^{19}F NMR (377 MHz, $CDCl_3$) δ -172.33 (d, *J* = 49.5 Hz).

HRMS (ESI) m/z calculated for $C_{12}H_{17}FNO$ $[M+H]^+$ 210.1304, found 210.1289.

IR (neat) 1724, 1435, 1279, 1006, 913, 733, cm^{-1}

m.p. 45–47 °C

CAS 41073-08-9

Tert-butyl 2-fluoroacetate (**37**)

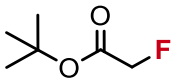

37

Synthesized from tert-butyl 2-bromoacetate (97.5 mg, 0.5 mmol) following general procedure **GP2** in a sealed microwave vial using anhydrous *t*BuOH and stirring at 100 °C for 18 h.

^{1}H NMR (400 MHz, $CDCl_3$) 4.70 (d, *J* = 47.3 Hz, 2H), 1.48 (s, 9H).

^{19}F NMR (377 MHz, $CDCl_3$) δ -227.68 (t, *J* = 46.8 Hz).

(EI, 70 eV) m/z (%) 119.02 ($[C_5H_8FO_2]^{+\cdot}$, 46), 61.00 ($[C_2H_2FO]^{+\cdot}$, 43), 59.04 (75), 57.07 ($[C_4H_9]^{+\cdot}$, 100)

Calculated yield (**37**): 73% (by ^{19}F-NMR using 4-fluoroanisole as internal standard)

CAS 406-74-6

Spectroscopic data are in accordance with those in literature [34].

2-Fluoro-*N,N*-diethylacetamide (**38**)

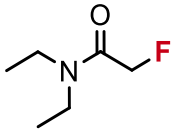

38

Synthesized from 2-bromo-*N,N*-diethylacetamide (97 mg, 0.5 mmol) following general procedure **GP2** using *t*BuOH and stirring at 60 °C for 5 h. Purification by flash column chromatography on silica (diethyl ether, 100%, product visualized using $KMnO_4$ stain) gave 2-fluoro-*N,N*-diethylacetamide (**38**) as a colorless oil (54 mg, 0.41 mmol, 81%).

^{1}H NMR (400 MHz, $CDCl_3$) δ 4.96 (d, *J* = 47.3 Hz, 2H), 3.41 (q, *J* = 7.1 Hz, 2H), 3.33 – 3.20 (m, 2H), 1.26 – 1.11 (m, 6H).

^{13}C NMR (101 MHz, $CDCl_3$) δ 165.9, 79.9 (d, *J* = 179.1 Hz), 41.0 (d, *J* = 4.3 Hz), 40.3, 14.3, 12.8.

^{19}F NMR (377 MHz, $CDCl_3$) δ -224.95 (t, *J* = 47.3 Hz).

HRMS (ESI) m/z calculated for $C_6H_{12}FNO$ $[M]^+$ 133.0897, found 133.1057

IR (neat) 1668, 1472, 1441, 1383, 1364, 1072, 1034 cm^{-1}

CAS 364-92-1

Methyl 2-fluoropropanoate (**39**)

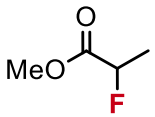

39

Synthesized from methyl 2-bromopropanoate (83.5 mg, 0.5 mmol) following general procedure **GP2** in a sealed microwave vial using anhydrous *t*BuOH and stirring at 100 °C for 18 h.

^{1}H NMR (400 MHz, $CDCl_3$) δ 5.00 (dq, *J* = 48.6, 6.9 Hz, 1H), 3.78 (s, 3H), 1.58 (dd, *J* = 23.7, 6.9 Hz, 3H).

^{19}F NMR (377 MHz, $CDCl_3$) δ -184.55 (dq, *J* = 47.6, 23.7 Hz).

(EI, 70 eV) m/z (%) 106.01 ($[M]^{+\cdot}$, 7), 59.00 (95), 47.03 (100, $[C_2H_4F]^{+\cdot}$,100), 46.02 (25).

Calculated yield (**35**): 53% (by ^{19}F-NMR using 4-fluoroanisole as internal standard)

CAS 2366-56-5

Spectroscopic data are in accordance with those in literature [35].

2-Fluoro-1-phenylpropan-1-one (**40**)

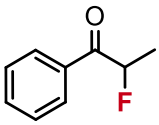

40

Synthesized from 2-bromo-1-phenylpropan-1-one (**S15**) (105 mg, 0.5 mmol) following general procedure **GP2** using *t*BuOH and stirring at 100 °C for 5 h. Purification by preparative TLC (pentane/ethyl acetate 98:2) gave 2-fluoro-1-phenylpropan-1-one (**40**) as a colorless oil (41.8 mg, 0.28 mmol, 55%).

^{1}H NMR (400 MHz, $CDCl_3$) δ 8.03 – 7.93 (m, 2H), 7.65 – 7.56 (m, 1H), 7.55 – 7.44 (m, 2H), 5.71 (dq, *J* = 48.6, 6.8 Hz, 1H), 1.67 (dd, *J* = 24.0, 6.8 Hz, 3H).

^{13}C NMR (101 MHz, $CDCl_3$) δ 197.1 (d, *J* = 19.5 Hz), 134.2, 134.0, 129.1 (d, *J* = 3.7 Hz), 128.9, 90.4 (d, *J* = 180.1 Hz), 18.5 (d, *J* = 22.7 Hz).

^{19}F NMR (377 MHz, $CDCl_3$) δ -181.35 (dq, *J* = 48.4, 24.1 Hz).

MS (EI, 70 eV) m/z (%) 105.01 ($[C_7H_5O]^{+\cdot}$, 100), 77.03 (57), 51.03 (18), 152.03 ($[M]^{+\cdot}$, 4).

IR (neat) 2981, 1700, 1598, 1451, 1233, 1132, 1084, 970, 791, 698 cm^{-1}

CAS 21120-36-5

Spectroscopic data are in accordance with those in literature [36].

2-Fluoro-1-phenylbutan-1-one (**41**)

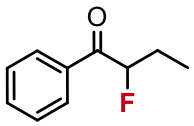

41

Synthesized from 2-bromo-1-phenylbutan-1-one (**S16**) (114 mg, 0.5 mmol) following general procedure **GP2** using *t*BuOH and stirring at 100 °C for 5 h. Purification by flash column chromatography on silica (pentane/ethyl acetate 98:2) gave 2-fluoro-1-phenylbutan-1-one (**41**) as a colorless oil (45 mg, 0.27 mmol, 54%).

^{1}H NMR (400 MHz, $CDCl_3$) δ 7.99 – 7.92 (m, 2H), 7.65 – 7.55 (m, 1H), 7.54 – 7.43 (m, 2H), 5.51 (ddd, *J* = 49.3, 7.6, 4.5 Hz, 1H), 2.19 – 1.87 (m, 2H), 1.09 (t, *J* = 7.4 Hz, 3H).

^{13}C NMR (101 MHz, $CDCl_3$) δ 197.0 (d, *J* = 19.5 Hz), 134.6, 133.9, 129.0 (d, *J* = 3.8 Hz), 128.9, 95.0 (d, *J* = 183.6 Hz), 26.3 (d, *J* = 21.7 Hz), 9.2 (d, *J* = 4.5 Hz).

^{19}F NMR (377 MHz, $CDCl_3$) δ -190.92 (dtq, *J* = 49.3, 28.3, 22.3 Hz).

MS (EI, 70 eV) m/z (%) 105.05 ($[C_7H_5O]^{+\cdot}$, 100), 77.05 (53), 51.04 (16), 166.06 ($[M]^{+\cdot}$, 6).

IR (neat) 2980, 1700, 1598, 1450, 1263, 969, 696 cm^{-1}

CAS 23071-44-5

Spectroscopic data are in accordance with those in literature [37].

16-Fluoro-3β-hydroxy-5-androsten-17-one (**42**)

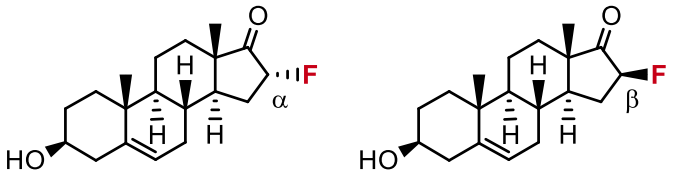

α–**42** β–**42**

Synthesized from 3β-Hydroxy-16α-bromoandrost-5-en-17-one (**S17**) (91.8 mg, 0.25 mmol) following general procedure **GP2** using *t*BuOH and stirring at 100 °C for 24 h. Purification by flash column chromatography on silica (pentane/ethyl acetate 80:20 to 70:30) gave 16-fluoro-3β-hydroxy-5-androsten-17-one (**42**) as a mixture of diastereomers (1.00:2.31, α :β) as a white solid (18.3 mg, 0.06 mmol, 24%).

16α-Fluoro-3β-hydroxy-5-androsten-17-one (minor diastereomer, α-**42**):

^{1}H NMR (400 MHz, $CDCl_3$) δ 5.37 (m, 1H), 5.10 (dd, *J* = 50.6, 7.5 Hz, 1H), 3.52 (m, 1H), 2.38 – 0.98 (overlapping m, 18H), 1.03 (s, 3H), 0.93 (s, 3H).

^{13}C NMR (101 MHz, $CDCl_3$) δ 213.3 (α, d, *J* = 12.3 Hz), 141.2 (α), 120.7 (α), 90.2 (d, *J* = 186.6 Hz), 71.6 (α), 50.1 (α), 48.8 (α), 47.7 (α), 42.3 (α), 37.2 (α), 36.7 (α), 31.6 (α), 31.5 (α), 31.3 (α), 30.6 (α), 30.0 (α, d, *J* = 20.7 Hz), 20.1 (α), 19.6 (α), 13.93 (α).

^{19}F NMR (377 MHz, $CDCl_3$) δ -192.41 (ddd, *J* = 50.6, 30.3, 27.1 Hz).

16β -Fluoro-3β-hydroxy-5-androsten-17-one (major diastereomer, β-**42**):

^{1}H NMR (400 MHz, $CDCl_3$) δ 5.37 (m, 1H), 4.70 (β, dt, *J* = 50.1, 8.4 Hz, 1H), 3.52 (m, 1H), 2.47 (β, ddd, *J* = 13.0, 8.3, 5.2 Hz, 1H), 2.38 – 0.98 (m, 17H), 1.04 (s, 3H), 1.01 (β, s, 3H).

^{13}C NMR (101 MHz, $CDCl_3$) δ 213.4 (d, *J* = 11.8 Hz), 141.3 (β), 120.6 (β), 91.7 (β, d, *J* = 194.2 Hz), 71.6 (β), 50.5 (β), 46.6 (β), 44.8 (β, d, *J* = 6.4 Hz), 42.3 (β), 37.2 (β), 36.9 (β), 31.7 (β), 31.6 (β), 31.0 (β), 30.8 (β), 29.5 (β, d, *J* = 17.7 Hz), 20.2 (β), 19.5 (β), 14.4 (β).

^{19}F NMR (377 MHz, $CDCl_3$) δ -184.97 (β, ddd, *J* = 50.1, 22.1, 2.4 Hz).

HRMS (ESI) m/z calculated for $C_{19}H_{27}FO_2Na$ $[M+Na]^+$ 329.1887, found 329.1896.

IR (neat) 3389, 1756, 1051, 1010, 911, 734 cm^{-1}

Spectroscopic data are in accordance with those in literature [38].

2-Fluoro-1-(4-methoxyphenyl)propan-1-one (**43**)

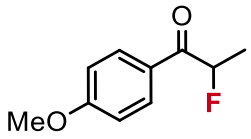

43

Synthesized from 2-bromo-1-(4-methoxyphenyl)propan-1-one (122 mg, 0.5 mmol) following general procedure **GP2** using *t*BuOH and stirring at 100 °C for 5 h. Purification by flash column chromatography on silica (pentane/ethyl acetate 90:10) gave 2-fluoro-1-(4-methoxyphenyl)propan-1-one (**43**) as a viscous yellow oil (77 mg, 0.42 mmol, 85%).

^{1}H NMR (200 MHz, $CDCl_3$) δ 8.06 – 7.90 (m, 2H), 7.03 – 6.87 (m, 2H), 5.66 (dq, *J* = 48.8, 6.8 Hz, 1H), 3.88 (s, 3H), 1.65 (dd, *J* = 24.1, 6.8 Hz, 3H).

^{13}C NMR (101 MHz, $CDCl_3$) δ 195.4 (d, *J* = 19.3 Hz), 164.1, 131.5 (d, *J* = 4.1 Hz), 127.0 (d, *J* = 1.8 Hz), 114.1, 90.4 (d, *J* = 179.8 Hz), 55.6, 18.6 (d, *J* = 22.8 Hz).

^{19}F NMR (377 MHz, $CDCl_3$) δ -180.45 (dq, *J* = 48.4, 24.2 Hz).

HRMS (ESI) m/z calculated for $C_{10}H_{12}FO_2$ $[M+H]^+$ 183.0816, found 183.0851

IR (neat) 2981, 1688, 1600, 1512, 1263, 1241, 1130, 1083, 1029, 843, 734 cm^{-1}

CAS 250277-92-0

Spectroscopic data are in accordance with those in literature [39].

2-Fluoro-1-(isoindolin-2-yl)ethan-1-one (**44**)

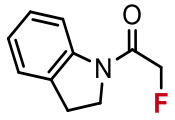

44

Synthesized from 2-bromo-1-(isoindolin-2-yl)ethan-1-one (**S18**) (120 mg, 0.5 mmol) following general procedure **GP2** using *t*BuOH and stirring at 100 °C for 5 h. Purification by flash column chromatography on silica (pentane/ethyl acetate 80:20 to 50:50) gave 2-fluoro-1-(isoindolin-2-yl)ethan-1-one (**44**) as a white solid (82 mg, 0.46 mmol, 91%).

^{1}H NMR (400 MHz, $CDCl_3$) δ 8.21 (d, *J* = 8.1 Hz, 1H), 7.21 (t, *J* = 8.0 Hz, 2H), 7.06 (td, *J* = 7.4, 1.1 Hz, 1H), 4.99 (d, *J* = 46.9 Hz, 2H), 3.99 (t, *J* = 8.4 Hz, 2H), 3.22 (t, *J* = 8.4 Hz, 2H).

^{13}C NMR (101 MHz, $CDCl_3$) δ 164.7 (d, *J* = 19.3 Hz), 142.5, 130.9, 127.8, 124.7, 124.6, 117.3, 80.0 (d, *J* = 180.5 Hz), 46.3 (d, *J* = 4.4 Hz), 28.5.

^{19}F NMR (377 MHz, $CDCl_3$) δ -226.76 (t, *J* = 46.9 Hz).

HRMS (ESI) m/z calculated for $C_{10}H_{11}FNO$ $[M+H]^+$ 180.0819, found 180.0816

IR (neat) 2935, 1672, 1487, 1466, 1428, 1077, 911, 775 cm^{-1}

m.p. 138–140 °C (lit. 139–141 °C) [40].

Spectroscopic data are in accordance with those in literature [40].

2-(4-Fluorobutyl)isoindoline-1,3-dione (**45**)

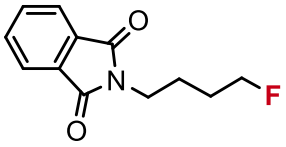

45

Synthesized from 2-(4-bromobutyl)isoindoline-1,3-dione (141 mg, 0.5 mmol) following general procedure **GP2** using *t*BuOH and stirring at 100 °C for 24 h. Purification by flash column chromatography on silica (pentane/ethyl acetate 1:0 to 7:3) gave 2-(4-fluorobutyl)isoindoline-1,3-dione (**45**) as a waxy white solid (58 mg, 0.26 mmol, 52%).

^{1}H NMR (400 MHz, $CDCl_3$) ^{1}H NMR (400 MHz, $CDCl_3$) δ 7.89 – 7.79 (m, 2H), 7.76 – 7.66 (m, 2H), 4.47 (dt, *J* = 47.4, 5.7 Hz, 2H), 3.74 (t, *J* = 6.9 Hz, 2H), 1.92 – 1.63 (m, 4H).

^{13}C NMR (101 MHz, $CDCl_3$) δ 168.5, 134.1, 132.2, 123.4, 83.5 (d, *J* = 165.3 Hz), 37.6, 27.9 (d, *J* = 20.1 Hz), 24.7 (d, *J* = 5.0 Hz).

^{19}F NMR (377 MHz, $CDCl_3$) δ -217.33 – -220.41 (m).

HRMS (ESI) m/z calculated for $C_{12}H_{12}FNO_2$ $[M]^+$ 221.0847, found 221.1003

IR (neat) 2970, 1698, 1443, 1398, 1042, 1024, 869, 717 cm^{-1}

m.p. 57–59 °C

Spectroscopic data are in accordance with those in literature [41].

(3-Fluoropropyl)benzene (**46**)

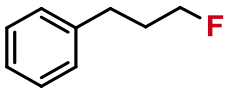

46

Synthesized from (3-iodopropyl)benzene (**S19**) (123 mg, 0.5 mmol) following a modified general procedure **GP2** using **Fmix** (770 mg, 2.5 equiv), 18-crown-6 (198 mg, 1.5 equiv), *t*BuOH (2 mL) and H_2O (5 equiv). The reaction mixture is stirred at 90 °C for 18 h. Purification by flash column chromatography on silica (pentane/ethyl acetate 100:0 to 98:2) gave (3-fluoropropyl)benzene (**46**) as a pale-yellow oil (46 mg, 0.33 mmol, 67%).

^{1}H NMR (400 MHz, $CDCl_3$) δ 7.36 – 7.29 (m, 2H), 7.25 – 7.19 (m, 3H), 4.48 (dt, *J* = 47.2, 6.0 Hz, 2H), 2.77 (t, *J* = 7.6 Hz, 2H), 2.15 – 1.93 (m, 2H).

^{13}C NMR (101 MHz, $CDCl_3$) δ 141.2, 128.6, 128.6, 126.2, 83.3 (d, *J* = 164.7 Hz), 32.2 (d, *J* = 19.8 Hz), 31.5 (d, *J* = 5.4 Hz).

^{19}F NMR (377 MHz, $CDCl_3$) δ -219.97 (tt, *J* = 47.2, 25.3 Hz).

MS (EI, 70 eV) m/z (%) 91.07 ($[C_7H_7]^{+\cdot}$, 100), 138.07 ($[M]^{+\cdot}$, 35), 92.06 (24), 65.04 (14).

IR (neat) 2980, 2360, 1395, 1028 cm^{-1}

CAS 2038-62-2

Spectroscopic data are in accordance with those in literature [42].

(3-Fluoropropoxy)benzene (**47**)

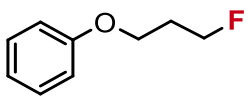

47

Synthesized from (3-bromopropoxy)benzene (108 mg, 0.5 mmol) following a modified general procedure **GP2** using **Fmix** (770 mg, 2.5 equiv), 18-crown-6 (198 mg, 1.5 equiv), *t*BuOH (2 mL) and H_2O (5 equiv). The reaction mixture is stirred at 90 °C for 18 h. Purification by flash column chromatography on silica (pentane/ethyl acetate 100:0 to 96:4) gave (3-fluoropropoxy)benzene (**47**) as a pale-yellow oil (36 mg, 0.24 mmol, 47%).

^{1}H NMR (400 MHz, $CDCl_3$) δ 7.34 – 7.27 (m, 2H), 6.97 (tt, *J* = 7.4, 1.1 Hz, 1H), 6.95 – 6.89 (m, 2H), 4.67 (dt, *J* = 47.1, 5.8 Hz, 2H), 4.11 (t, *J* = 6.1 Hz, 2H), 2.19 (dp, *J* = 25.9, 6.0 Hz, 2H).

^{13}C NMR (101 MHz, $CDCl_3$) δ 158.9, 129.6, 121.0, 114.6, 80.9 (d, *J* = 164.4 Hz), 63.5 (d, *J* = 5.3 Hz), 30.6 (d, *J* = 20.1 Hz).

^{19}F NMR (377 MHz, $CDCl_3$) δ -222.20 (tt, *J* = 47.2, 26.0 Hz).

HRMS (ESI) m/z calculated for $C_9H_{12}FO$ $[M+H]^+$ 155.0867, found 155.0988

IR (neat) 2972, 1601, 1587, 1503, 1474, 1247, 1051, 755 cm^{-1}

CAS 70659-93-7

Spectroscopic data are in accordance with those in literature [43].

(3-Fluoroprop-1-yn-1-yl)benzene (**48**)

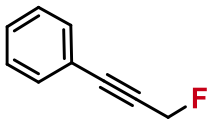

48

Synthesized from (3-bromoprop-1-yn-1-yl)benzene (**S20**) (98 mg, 0.5 mmol) following general procedure **GP2** using *t*BuOH and stirring at 80 °C for 18 h. Purification by flash column chromatography on silica (pentane/ethyl acetate 100:0 to 98:2) gave (3-Fluoroprop-1-yn-1-yl)benzene (**48**) as a colorless oil (49 mg, 0.37 mmol, 73%).

^{1}H NMR (400 MHz, $CDCl_3$) δ 7.52 – 7.45 (m, 2H), 7.39 – 7.31 (m, 3H), 5.19 (d, *J* = 47.6 Hz, 2H).

^{13}C NMR (101 MHz, $CDCl_3$) δ 132.0 (d, *J* = 3.1 Hz), 129.2, 128.5, 121.9 (d, *J* = 4.3 Hz), 89.6 (d, *J* = 12.0 Hz), 82.7 (d, *J* = 21.4 Hz), 71.3 (d, *J* = 165.1 Hz).

^{19}F NMR (377 MHz, $CDCl_3$) δ -213.47 (t, *J* = 47.7 Hz).

MS (EI, 70 eV) m/z (%) 133.08 (100), 134.07 ([M]$^{+\cdot}$, 71), 115.06 (14), 107.03 (10).

IR (neat) 2981, 2361, 1218, 1010, 828 cm^{-1}

Spectroscopic data are in accordance with those in literature [44].

Benzyl (*E*)-4-fluorobut-2-enoate (**49**)

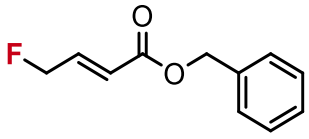

49

Synthesized from benzyl (*E*)-4-bromobut-2-enoate (**S21**) (128 mg, 0.5 mmol) following general procedure **GP2** using *t*BuOH and stirring at 80 °C for 18 h. Purification by flash column chromatography on silica (pentane/ethyl acetate 100:0 to 98:2) gave benzyl (*E*)-4-fluorobut-2-enoate (**49**) as a colorless oil (68 mg, 0.35 mmol, 70%).

^{1}H NMR (400 MHz, $CDCl_3$) δ 7.40 – 7.30 (m, 5H), 7.01 (ddt, *J* = 23.1, 15.8, 3.7 Hz, 1H), 6.23 – 6.12 (m, 1H), 5.21 (s, 2H), 5.06 (ddd, *J* = 46.1, 3.7, 2.1 Hz, 2H).

^{13}C NMR (101 MHz, $CDCl_3$) δ 165.7, 142.2 (d, *J* = 16.0 Hz), 135.9, 128.7, 128.5, 128.4, 121.2 (d, *J* = 11.4 Hz), 81.2 (d, *J* = 171.8 Hz), 66.6.

^{19}F NMR (377 MHz, $CDCl_3$) δ -223.43 (tdd, *J* = 46.2, 23.0, 1.7 Hz).

HRMS (ESI) m/z calculated for $C_{11}H_{12}FO_2$ $[M+H]^+$ 195.0816, found 195.0893

IR (neat) 1725, 1669, 1306, 1277, 1170, 1003, 967, 750 cm^{-1}

4.2.9 C(sp^2)-F bond formation using Fmix

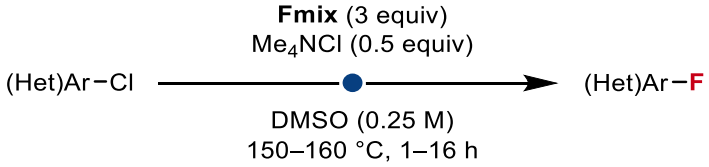

To an oven dried glass reaction vessel was added **Fmix** (770 mg, 3.0 equiv relative to CaF_2 and 7.5 equiv relative to K_2HPO_4), the corresponding (hetero)aryl chloride (0.5 mmol, 1.0 equiv), Me_4NCl (27.4 mg, 0.5 equiv) and anhydrous DMSO (2 mL) unless otherwise stated. After stirring at 150 °C – 160 °C in a heating block, the resulting suspension was cooled to room temperature, filtered through a short plug of silica gel (washed with ~15 mL EtOAc) to remove insoluble by-products. The filtrate was washed with brine (10 mL). The organic extract was collected and the aqueous layer was washed with EtOAc (2 x 5 mL). The combined organic extracts were dried over $MgSO_4$, filtered and concentrated *in vacuo*. The crude product was purified by flash column chromatography on silica gel to afford the corresponding fluorinated product.

4.2.10 C(sp^2)-F product characterisation

2-Chloro-1-fluoro-4-nitrobenzene (**51**)

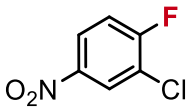

51

Synthesized from 1,2-dichloro-4-nitrobenzene (96.0 mg, 0.5 mmol, 1.0 equiv) following a modified general procedure **GP3** using **Fmix** (1.03 g, 4.0 equiv), Me_4NCl (27.4 mg, 0.25 mmol, 0.5 equiv) and anhydrous DMSO (2 mL). The reaction mixture is stirred at 150 °C for 4 h. Purification by flash column chromatography on silica (pentane/diethyl ether 100:0 to 95:5) gave 2-chloro-1-fluoro-4-nitrobenzene (**51**) as a pale-yellow solid (42.1 mg, 0.24 mmol, 48%).

^{1}H NMR (400 MHz, $CDCl_3$) δ 8.36 (dd, *J* = 6.3, 2.7 Hz, 1H), 8.18 (ddd, *J* = 9.1, 4.1, 2.8 Hz, 1H), 7.32 (dd, *J* = 9.1, 7.9 Hz, 1H).

^{13}C NMR (101 MHz, $CDCl_3$) δ 162.0 (d, *J* = 260.0 Hz), 144.4, 126.8 (d, *J* = 1.7 Hz), 124.2 (d, *J* = 8.9 Hz), 122.6 (d, *J* = 19.7 Hz), 117.3 (d, *J* = 23.4 Hz).

^{19}F NMR (377 MHz, $CDCl_3$) δ -103.90 (m).

MS (EI, 70 eV) m/z (%) 174.96 (^{35}Cl[M]$^{+\cdot}$, 82), 176.96 (^{37}Cl[M]$^{+\cdot}$, 27), 128.96 (100), 92.99 (39), 108.96 (37).

IR (neat) 2360, 1544, 1528, 1354, 1260, 1049, 899, 742 cm^{-1}

m.p. 46–47 °C (lit. 41.5 °C) [45]

CAS 350-30-1

Spectroscopic data are in accordance with those in literature [46].

6-Fluoronicotinonitrile (**54**)

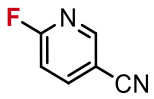

54

Synthesized from 6-chloronicotinonitrile (69.3 mg, 0.5 mmol, 1.0 equiv), following general procedure **GP3** with stirring at 150 °C for 1.5 h. Purification by flash column chromatography on silica (pentane/ethyl acetate 8:2 to 7:3) gave 6-fluoronicotinonitrile (**54**) as a white solid (37.2 mg, 0.30 mmol, 61%).

^{1}H NMR (400 MHz, $CDCl_3$) δ 8.58 (dt, *J* = 2.4, 0.8 Hz, 1H), 8.08 (ddd, *J* = 8.5, 7.1, 2.4 Hz, 1H), 7.10 (ddd, *J* = 8.6, 3.1, 0.7 Hz, 1H).

^{13}C NMR (101 MHz, $CDCl_3$) δ 165.1 (d, *J* = 249.1 Hz), 152.4 (d, *J* = 16.8 Hz), 144.5 (d, *J* = 9.2 Hz), 115.7, 111.0 (d, *J* = 37.9 Hz), 108.2 (d, *J* = 4.9 Hz).

^{19}F NMR (377 MHz, $CDCl_3$) δ -57.34 (d, *J* = 7.4 Hz).

MS (EI, 70 eV) m/z (%) 122.00 ([M]$^{+\cdot}$,100), 94.99 (39), 76.00 (11), 32.00 (10)

IR (neat) 2917, 2240, 1605, 1438, 1265, 1105, 809, 755 cm^{-1}

m.p. 51–52 °C (lit. 52–53 °C) [47]

CAS 3939-12-6

Spectroscopic data are in accordance with those in literature [47].

2-Fluoronicotinonitrile (**55**)

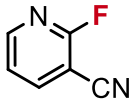

55

Synthesized from 2-chloronicotinonitrile (69.3 mg, 0.5 mmol, 1.0 equiv), following general procedure **GP3** with stirring at 150 °C for 1 h. Purification by flash column chromatography on silica (pentane/ethyl acetate 8:2 to 7:3) gave 2-fluoronicotinonitrile (**55**) as a white solid (35.6 mg, 0.29 mmol, 58%).

^{1}H NMR (400 MHz, $CDCl_3$) δ 8.48 (ddd, *J* = 4.9, 2.0, 1.0 Hz, 1H), 8.16 – 8.08 (m, 1H), 7.37 (ddd, *J* = 7.6, 4.9, 1.6 Hz, 1H).

^{13}C NMR (101 MHz, $CDCl_3$) δ 162.8 (d, *J* = 247.6 Hz), 152.2 (d, *J* = 14.7 Hz), 144.6, 121.7 (d, *J* = 4.8 Hz), 112.7 (d, *J* = 5.8 Hz), 97.5 (d, *J* = 31.5 Hz).

^{19}F NMR (377 MHz, $CDCl_3$) δ -59.95 (d, *J* = 8.5 Hz).

MS (EI, 70 eV) m/z (%) 122.01 ([M]$^{+\cdot}$,100), 94.99 (37), 76.01 (13), 50.02 (7)

IR (neat) 2241, 1594, 1483, 1384, 1278, 1026, 848 cm^{-1}

m.p. 30–31 °C (lit. 30–30.5 °C) [48]

CAS 3939-13-7

Spectroscopic data are in accordance with those in literature [49].

6-Fluoroimidazo[1,2-*b*]pyridazine (**56**)

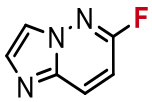

56

Synthesized from 6-chloroimidazo[1,2-*b*]pyridazine (76.8 mg, 0.5 mmol, 1.0 equiv), following general procedure **GP3** with stirring at 150 °C for 9 h. Purification by flash column chromatography on silica (pentane/ethyl acetate 3:7 to 1:9) gave 6-Fluoroimidazo[1,2-*b*]pyridazine (**56**) as a white solid (25.2 mg, 0.18 mmol, 37%).

^{1}H NMR (400 MHz, $CDCl_3$) δ 8.01 (dd, *J* = 9.6, 7.3 Hz, 1H), 7.85 (s, 1H), 7.77 (s, 1H), 6.86 (d, *J* = 9.6 Hz, 1H).

^{13}C NMR (101 MHz, $CDCl_3$) δ 160.4 (d, *J* = 240.5 Hz), 138.2, 134.8 (d, *J* = 3.6 Hz), 129.8 (d, *J* = 11.0 Hz), 117.7, 108.1 (d, *J* = 37.4 Hz).

^{19}F NMR (377 MHz, $CDCl_3$) δ -86.89 (d, *J* = 7.3 Hz).

HRMS (ESI) m/z calculated for $C_6H_5FN_3$ $[M+H]^+$ 138.0462, found 138.1902.

IR (neat) 3088, 2981, 1533, 1371, 1292, 1144, 798 cm^{-1}

m.p. 83–85 °C

CAS 113501-27-2

Spectroscopic data are in accordance with those in literature [50].

3-Fluoro-6-phenylpyridazine (**57**)

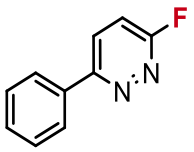

57

Synthesized from 3-chloro-6-phenylpyridazine (95.3 mg, 0.5 mmol, 1.0 equiv), following general procedure **GP3** with stirring at 150 °C for 16 h. Purification by flash column chromatography on silica (pentane/ethyl acetate 9:1 to 6:4) gave 3-fluoro-6-phenylpyridazine (**57**) as a white solid (24.5 mg, 0.14 mmol, 28%).

^{1}H NMR (400 MHz, $CDCl_3$) δ 8.08 – 7.95 (overlapping m, 3H), 7.61 – 7.46 (m, 3H), 7.28 (dd, *J* = 9.2, 2.0 Hz, 1H).

^{13}C NMR (101 MHz, $CDCl_3$) δ 166.19 (d, *J* = 244.4 Hz), 159.37 (d, *J* = 3.2 Hz), 135.34 (d, *J* = 1.8 Hz), 130.39, 129.58 (d, *J* = 7.2 Hz), 129.26, 127.22, 116.15 (d, *J* = 33.4 Hz).

^{19}F NMR (376 MHz, $CDCl_3$) δ -82.15 (d, *J* = 6.9 Hz).

HRMS (ESI) m/z calculated for $C_{10}H_8FN_2$ $[M+H]^+$ 175.0666, found 175.0655.

IR (neat) 2981, 1558, 1451, 1429, 1282, 1109, 855, 779, 741 cm^{-1}

m.p. 127–128 °C (lit. 127–127.6) [50]

CAS 144864-03-9

Spectroscopic data are in accordance with those in literature [50].

7-Chloro-4-fluoroquinoline (**58**)

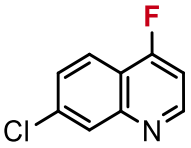

58

Synthesized from 4,7-dichloroquinoline (99.0 mg, 0.5 mmol, 1.0 equiv), following general procedure **GP3** with stirring at 160 °C for 16 h. Purification by flash column chromatography on silica (pentane/ethyl acetate 8:2 to 6:4) gave 7-Chloro-4-fluoroquinoline (**58**) as a white solid (32.0 mg, 0.18 mmol, 35%).

^{1}H NMR (400 MHz, $CDCl_3$) δ 8.87 (dd, *J* = 8.2, 5.2 Hz, 1H), 8.15 (d, *J* = 2.0 Hz, 1H), 8.05 (dd, *J* = 8.9, 1.4 Hz, 1H), 7.57 (dd, *J* = 8.9, 2.1 Hz, 1H), 7.11 (ddd, *J* = 9.6, 5.1, 1.3 Hz, 1H).

^{13}C NMR (101 MHz, $CDCl_3$) δ 165.5 (d, *J* = 269.9 Hz), 152.7 (d, *J* = 8.2 Hz), 150.8 (d, *J* = 4.3 Hz), 137.0, 128.3 (d, *J* = 1.4 Hz), 128.2 (d, *J* = 3.7 Hz), 122.2 (d, *J* = 4.9 Hz), 118.2 (d, *J* = 13.3 Hz), 106.2 (d, *J* = 14.5 Hz).

^{19}F NMR (377 MHz, $CDCl_3$) δ -111.41 (s).

HRMS (ESI) m/z calculated for $C_9H_6{}^{35}ClFN$ $[M+H]^+$ 182.0167, found 182.0176; $C_9H_6{}^{37}ClFN$ $[M+H]^+$ 184.0138, found 184.0139.

IR (neat) 1628, 1423, 1093, 881, 846, 819 cm^{-1}

m.p. 50–52 °C (lit. 50.2–50.7 °C) [50]

CAS 103526-68-7

Spectroscopic data are in accordance with those in literature [50].

4.2.11 Side reactivity of (hetero)aryl fluorides

Electron deficient (hetero)aryl fluorides, such as those prepared in this work, are highly reactive electrophiles that can undergo side reactions to form undesired side products such as phenols and aryl ethers [51,52].

The formation aryl ether 4,4'-oxybis(3-chloro-1-nitrobenzene) **53** was observed in the S_NAr fluorination of 1,2-dichloro-4-nitrobenzene using **Fmix**.

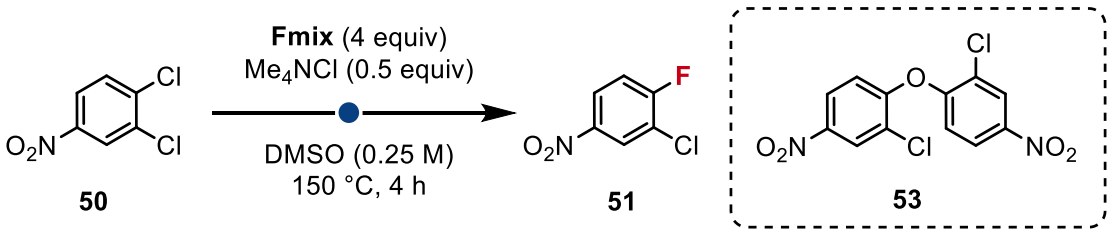

When aryl fluoride **50** was exposed to K_2HPO_4 under identical reaction conditions both **51** and aryl ether **53** were observed in the reaction mixture by ^{1}H NMR. In a control experiment, reacting 1,2-dichloro-4-nitrobenzene with K_2HPO_4 under identical conditions led to starting material recovery only.

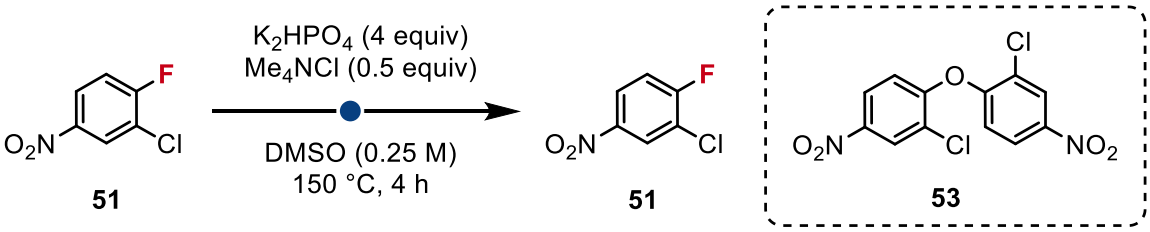

The low to modest yields of the (hetero)aryl fluorides obtained in this work can therefore be attributed to the sensitivity of the products towards phosphate containing species (or derivative thereof) found in **Fmix**.

Side product **53** (CAS 13867-27-1) was isolated during the purification of **51** and characterised by ^{1}H NMR spectroscopy [53].

^{1}H NMR (400 MHz, $CDCl_3$) δ 8.45 (d, *J* = 2.7 Hz, 2H), 8.18 (dd, *J* = 9.0, 2.6 Hz, 2H), 7.04 (d, *J* = 9.0 Hz, 2H).

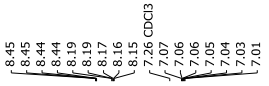

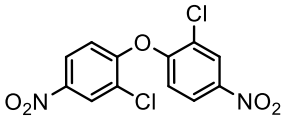

53 ^{1}H NMR

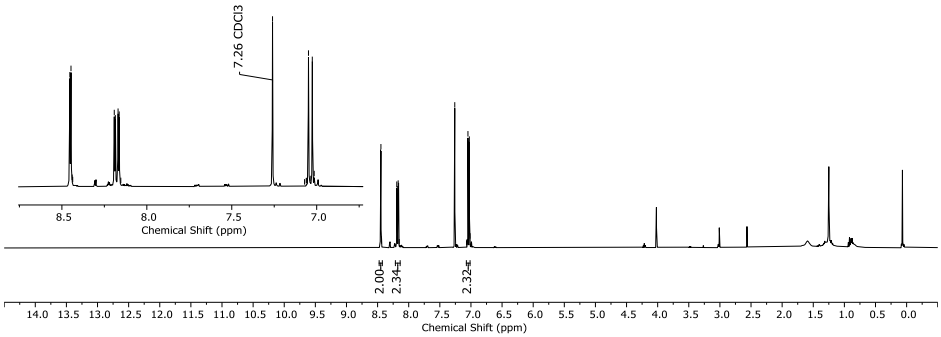

The formation aryl ether 4,4'-oxybis(3-chloro-1-nitrobenzene) **53** was observed in the S_NAr fluorination of 1,2-dichloro-4-nitrobenzene using **Fmix**.

For comparison, the ^1H NMR spectra of isolated **53 (top)** and **52 (bottom)** are provided below:

Phenol 52: ^1H NMR (400 MHz, $CDCl_3$) δ 8.30 (d, *J* = 2.7 Hz, 1H), 8.13 (dd, *J* = 9.0, 1.7 Hz, 1H), 7.13 (d, *J* = 9.0 Hz, 1H).

Aryl ether 53: ^1H NMR (400 MHz, $CDCl_3$) δ 8.45 (d, *J* = 2.7 Hz, 2H), 8.18 (dd, *J* = 9.0, 2.6 Hz, 2H), 7.04 (d, *J* = 9.0 Hz, 2H).

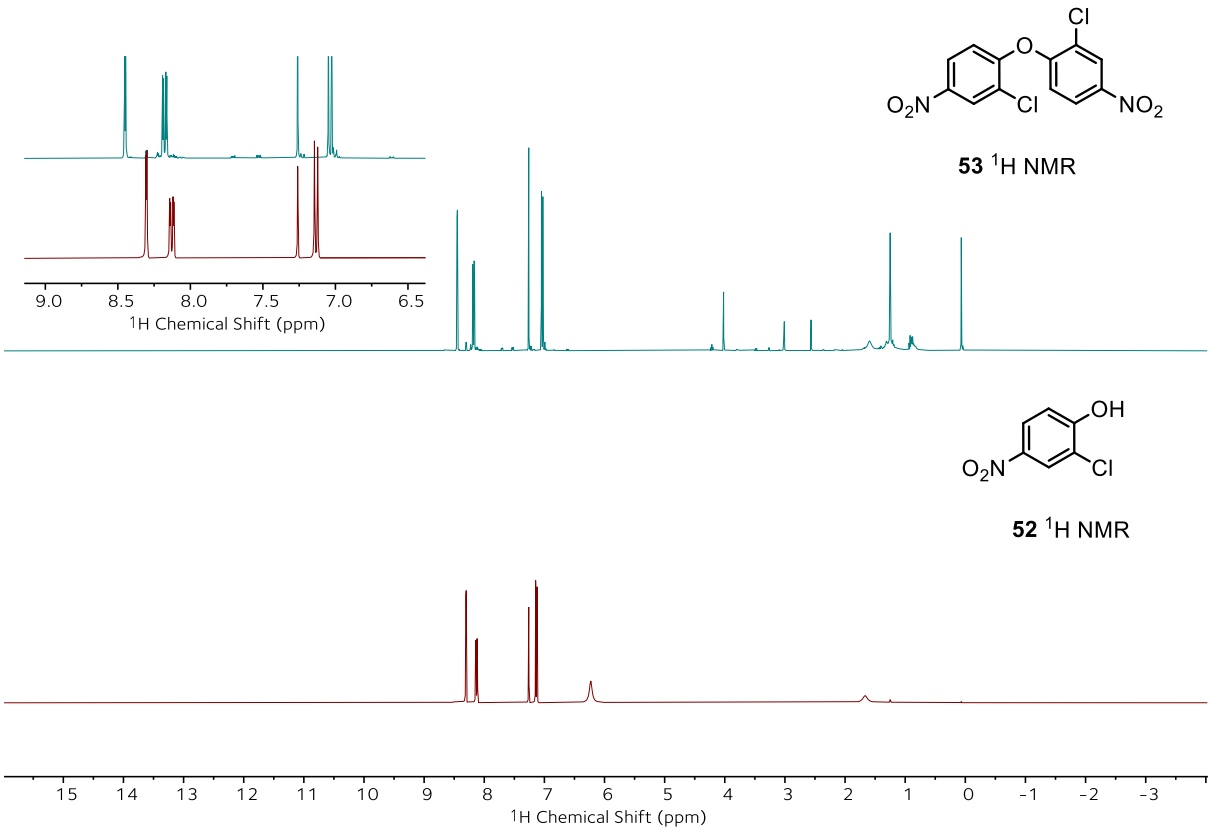

4.2.12 Substrate Synthesis

Job Struijs synthesised substrates **S11-S14** and **S16-S18**.

Benzyl 4-chloro-2-((furan-2-ylmethyl)amino)-5-sulfamoylbenzoate (benzyl furosemide) (**S1**)

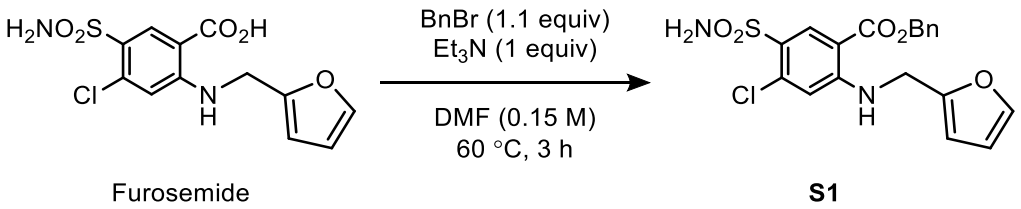

Furosemide **S1**

S1 was synthesized according to a modified literature procedure [8]. Benzyl bromide (196 µL, 1.65 mmol) and Et_3N (207 µL, 1.50 mmol) is added to a solution of furosemide (500 mg, 1.5 mmol) in DMF (10 mL). The mixture was stirred at 60 °C for 3 h. The mixture was quenched with sat. aq. NH_4Cl (10 mL) and diluted with EtOAc (20 mL). The organic extracts are washed with H_2O (15 mL), 1 M NaOH (10 mL), dried over $MgSO_4$, filtered and concentrated *in vacuo*. The crude product was purified by flash column chromatography on silica (pentane/ethyl acetate 90:10 to 60:40) to give benzyl furosemide (**S1**) as a cream coloured solid (485 mg, 1.15 mmol, 76%).

^{1}H NMR (400 MHz, Acetone-d_6) δ 8.68 – 8.60 (m, 1H), 8.58 (s, 1H), 7.55 – 7.52 (m, 1H), 7.52 – 7.47 (m, 2H), 7.45 – 7.33 (m, 3H), 7.12 (s, 1H), 6.52 (br s, 2H), 6.44 – 6.39 (m, 2H), 5.38 (s, 2H), 4.66 (d, J = 5.8 Hz, 2H).

^{13}C NMR (101 MHz, Acetone-d_6) δ 167.7, 153.9, 152.3, 143.6, 138.3, 137.2, 134.4, 129.6, 129.3, 129.3, 128.2, 114.8, 111.4, 108.7, 67.4, 40.6.

HRMS (ESI) m/z calculated for $C_{19}H_{16}{}^{35}ClN_2O_5S$ $[M-H]^-$ 419.0474, found 419.0472; $C_{19}H_{16}{}^{37}ClN_2O_5S$ $[M-H]^-$ 421.0444, found 421.0444

IR (neat) 3378, 2981, 1731, 1596, 1572, 1329, 1258, 1106, 1081, 743 cm^{-1}

m.p. 95–97 °C (lit. 95.3–97.5 °C) [8]

CAS 885051-42-3

Spectroscopic data are in accordance with those in literature [8].

Benzyl 4-chloro-5-(chlorosulfonyl)-2-((furan-2-ylmethyl)amino)benzoate (benzyl furosemide chloride) (**S2**)

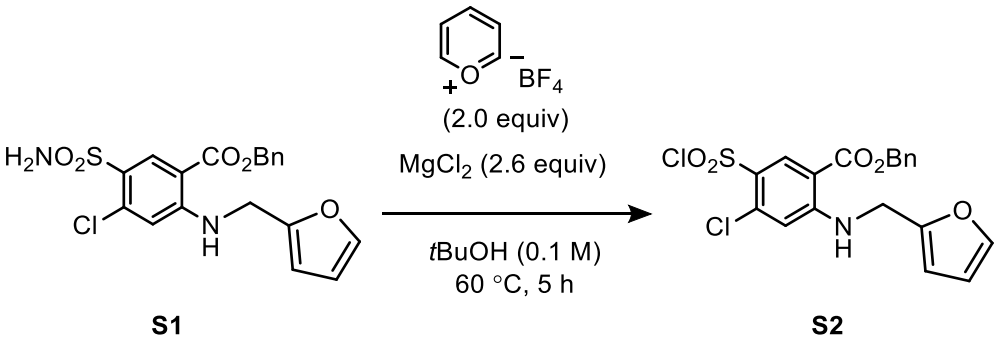

S2 was synthesized according to a literature procedure [54]. A suspension of benzyl furosemide **S1** (300 mg, 0.713 mmol), pyrylium tetrafluoroborate (240 mg, 1.43 mmol) and $MgCl_2$ (173 mg, 1.82 mmol) in *t*BuOH (7 mL) was stirred for 5 min at 25 °C before stirring for 5 h at 60 °C. After 5 h the reaction was cooled, filtered over a short plug of silica gel (washed with ~20 mL EtOAc) and the solvent was removed under reduced pressure. The product was purified by flash column chromatography on silica gel (pentane/EtOAc 8:2) to give benzyl furosemide chloride (**S2**) as a viscous yellow oil (138 mg, 0.313 mmol, 44% yield).

^{1}H NMR (400 MHz, $CDCl_3$) δ 8.97 (br s, 1H), 8.70 (s, 1H), 7.46 – 7.31 (m, 6H), 6.95 (s, 1H), 6.37 (dd, *J* = 3.3, 1.9 Hz, 1H), 6.31 (dd, *J* = 3.3, 0.9 Hz, 1H), 5.34 (s, 2H), 4.48 (d, *J* = 5.6 Hz, 2H).

^{13}C NMR (101 MHz, $CDCl_3$) δ 166.6, 154.4, 149.6, 143.0, 138.8, 135.9, 135.3, 128.9, 128.8, 128.5, 127.4, 114.3, 110.8, 108.4, 108.3, 67.3, 40.4.

HRMS (ESI) m/z calculated for $C_{19}H_{14}{}^{35}Cl_2NO_5S$ $[M-H]^-$ 437.9975, found 437.9983; $C_{19}H_{14}{}^{35}Cl^{37}ClNO_5S$ $[M-H]^-$ 439.9945, found 439.9869; $C_{19}H_{14}{}^{37}Cl_2NO_5S$ $[M-H]^-$ 441.9916, found 441.9808.

IR (neat) 3327, 2980, 1694, 1590, 1374, 1261, 1172, 1096, 787 cm^{-1}

Spectroscopic data are in accordance with those in literature [54].

Pyridine-2-sulfonyl chloride (**S3**)

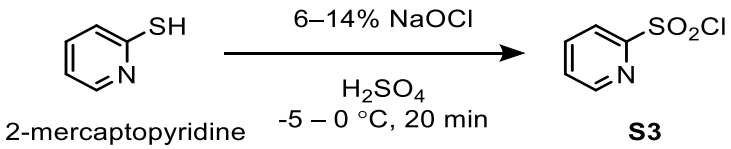

2-mercaptopyridine **S3**

Note: Warning! The addition of sodium hypochlorite solution to 2-mercaptopyridine in sulfuric acid generates Cl_2 gas. The system must not be closed and should be adequately ventilated.

S3 was synthesized according to a literature procedure [20]. A multi-neck flask fitted with an addition funnel and thermometer was charged with 2-mercaptopyridine (200 mg, 1.80 mmol) in sulfuric acid (2.9 mL, 30 equiv) and was cooled to –5 °C while open to atmosphere. Sodium hypochlorite solution (8.6 mL, 6-14% active chlorine, EMPLURA®) was added dropwise over approximately 10 minutes while maintaining the temperature below 0 °C. After complete addition, the mixture was stirred for 20 minutes at 0 °C after which it was diluted with H_2O (10 mL) and extracted twice with EtOAc (10 mL). The combined organic extracts were dried over Na_2SO_4, filtered and concentrated *in vacuo* afford 2-pyridinesulfonyl chloride (**S3**) as a colorless oil (274 mg, 1.54 mmol, 86%). The crude pyridine-2-sulfonyl chloride (**S3**) was immediately used without any further purification.

^{1}H NMR (400 MHz, C_6D_6) δ 7.94 (ddd, *J* = 4.6, 1.8, 0.9 Hz, 1H), 7.33 (dt, *J* = 7.9, 0.9 Hz, 1H), 6.58 (td, *J* = 7.8, 1.8 Hz, 1H), 6.27 (ddd, *J* = 7.7, 4.6, 0.9 Hz, 1H).

^{13}C NMR (126 MHz, C_6D_6) δ 159.5, 150.3, 138.1, 128.4, 121.4.

HRMS (ESI) m/z calculated for $C_5H_5{}^{35}ClNO_2S$ $[M+H]^+$ 177.9724, found 177.9726; $C_5H_5{}^{37}ClNO_2S$ $[M+H]^+$ 179.9695, found 179.9700.

CAS 66715-65-9

Spectroscopic data are in accordance with those in literature [20].

N-Tosyl-4-chlorobenzenesulfonimidoyl chloride (**S4**)

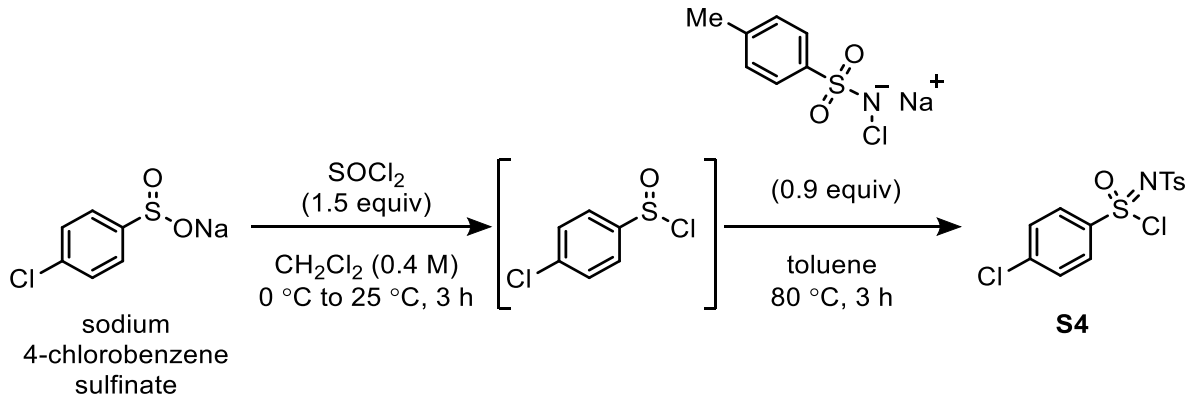

S4 was synthesized according to a modified literature procedure [21]. A multi-neck flask fitted with an SO_2 absorption apparatus was charged with sodium 4-chlorobenzenesulfinate (4.0 g, 20.1 mmol) and anhydrous dichloromethane (50 mL). The reaction mixture was cooled to 0 °C, then thionyl chloride (1.83 mL, 30.2 mmol) slowly (over 5 minutes) with vigorous stirring. After complete addition, the mixture was stirred at 0 °C for 30 minutes, then warmed to 25 °C and stirred at this temperature for 3 h. After removal of the solids through filtration, the solution was concentrated to afford crude 4-chlorobenzenesulfinyl chloride as a pale-yellow oil. The crude 4-chlorobenzenesulfinyl chloride was immediately added to a mixture of anhydrous chloramine T (4.0 g, 17.6 mmol) and anhydrous toluene (25 mL) and stirred at 80 °C for 3 h. After cooling to 25 °C the solids were removed through filtration and washed with toluene. The filtrate was concentrated *in vacuo* to give a crystalline residue. Purification by flash column chromatography on silica (petroleum ether/ethyl acetate 20:1 to 20:3) gave *N*-tosyl-4-chlorobenzenesulfonimidoyl chloride (**S4**) as a white waxy solid (2.52 g, 6.92 mmol, 34%).

^{1}H NMR (400 MHz, $CDCl_3$) δ 7.99 (d, *J* = 8.9 Hz, 2H), 7.95 (d, *J* = 8.4 Hz, 2H), 7.58 (d, *J* = 8.9 Hz, 2H), 7.39 – 7.31 (m, 2H), 2.42 (s, 3H).

^{13}C NMR (101 MHz, $CDCl_3$) δ 144.8, 142.8, 140.8, 138.2, 130.2, 129.8, 128.4, 127.5, 21.7.

HRMS (ESI) m/z calculated for $C_{13}H_{11}{}^{35}Cl_2NO_3S_2$ $[M]^+$ 363.9630, found 363.9650; $C_{13}H_{11}{}^{35}Cl^{37}ClNO_3S_2$ $[M]^+$ 364.9528, found 364.9682; $C_{13}H_{11}{}^{37}Cl_2NO_3S_2$ $[M]^+$ 367.9532, found 367.9583.

IR (neat) 3099, 2980, 2359, 1472, 1397, 1310, 1161, 1112, 1086, 732 cm^{-1}

m.p. 90–91 °C (lit. 90–92 °C) [21]

CAS 2143892-52-6

Spectroscopic data are in accordance with those in literature [21].

Ethene sulfonyl chloride (**S5**)

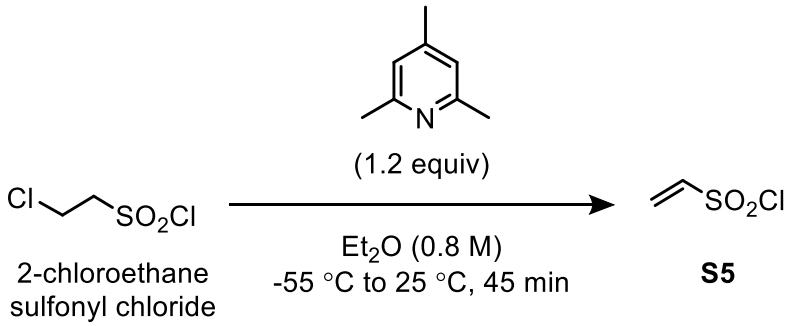

S5 was synthesized according to a literature procedure [55]. To the solution of 2-chloroethane sulfonyl chloride (1.67 mL, 16 mmol) in Et_2O (10 mL) at -55 °C was added a solution of 2,4,6-collidine (2.50 mL, 18.9 mmol) in Et_2O (10 mL). The slurry was stirred for 45 minutes and allowed to warm to 25 °C. After cooling to 0 °C, 1% aq. H_2SO_4 (2 mL) was added with stirring. The organic extracts were separated, washed with H_2O and brine and dried over Na_2SO_4. Solvent was removed *in vacuo* (40 °C/atm. press.) to afford ethene sulfonyl chloride (**S5**) as a pale-yellow oil (1.48 g, 13.4 mmol, 84%). The crude ethene sulfonyl chloride (**S5**) was immediately used without any further purification.

^{1}H NMR (400 MHz, $CDCl_3$) δ 7.01 (dd, *J* = 16.2, 9.5 Hz, 1H), 6.59 – 6.49 (m, 1H), 6.24 (dd, *J* = 9.5, 1.8 Hz, 1H).

^{13}C NMR (101 MHz, $CDCl_3$) δ 140.9, 130.0.

IR (neat) 3117, 3075, 1371, 1166, 1049, 982, 757 cm^{-1}

CAS 6608-47-5

Spectroscopic data are in accordance with those in literature [56].

Trans, trans-farnesyl isothiuronium bromide (**S6**)

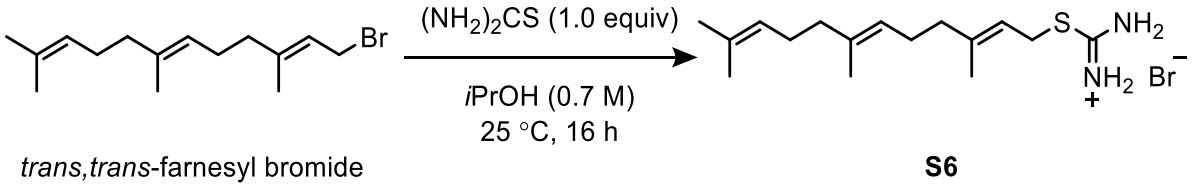

S6 was synthesized according to a literature procedure [23]. To a solution of thiourea (760 mg, 10 mmol) in anhydrous *i*PrOH (15 mL) was added *trans, trans*-farnesyl bromide (2.85 g, 10 mmol). The reaction mixture was stirred at 25 °C for 16 h. Solvent was removed *in vacuo* and the solid residue was washed with hexane (4 x 20 mL). The solid was dried at 40 °C under high vacuum (≤ 0.1 mbar) for 16 h to give crude *trans, trans*-farnesylisothiuronium (**S6**) as a pale brown solid (2.55 g, 7.06 mmol, 71%) which was used directly in the next step without further purification.

^{1}H NMR (400 MHz, MeOD) δ 5.36 – 5.26 (m, 1H), 5.14 – 5.04 (m, 2H), 3.87 (d, *J* = 7.8 Hz, 2H), 2.20 – 1.87 (m, 8H), 1.77 (d, *J* = 1.4 Hz, 3H), 1.67 (d, *J* = 1.4 Hz, 3H), 1.60 (s, 6H).

^{13}C NMR (101 MHz, MeOD) δ 173.1, 145.9, 136.7, 132.2, 125.4, 124.7, 116.2, 40.8, 40.5, 30.5, 27.8, 27.2, 25.9, 17.8, 16.4, 16.1.

HRMS (ESI) m/z calculated for $C_{16}H_{30}{}^{79}BrN_2S$ $[M+H]^+$ 361.1308, found 361.1491.

IR (neat) 3085, 2979, 1649, 1437, 1075, 689 cm^{-1}

m.p. 111–118 °C (lit. 119–120 °C) [23]

Spectroscopic data are in accordance with those in literature [23].

(*E*)-3,7-Dimethylocta-2,6-diene-1-thiol (*trans, trans* farnesyl mercaptan) (**S7**)

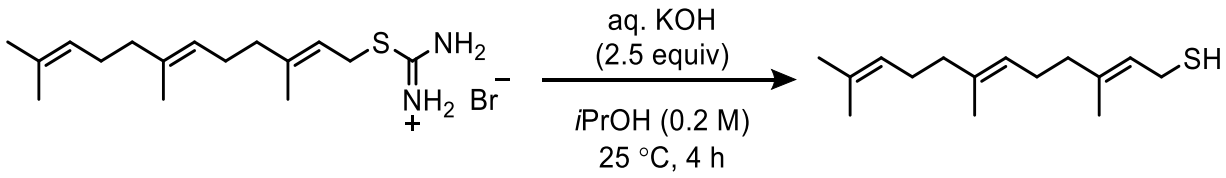

S6 **S7**

S7 was synthesized according to a literature procedure [23]. Under N_2 atmosphere, KOH (854 mg, 15.2 mmol) in H_2O (2 mL) was added to a solution of *trans,trans*-farnesylisothiuronium (**S6**) (2.2 g, 6.09 mmol) in *i*PrOH (30 mL). The mixture was stirred at 25 °C for 4 h. Once complete (monitored by TLC), the reaction was acidified to pH 5 with conc. HCl and extracted with EtOAc (4 x 50 mL). The organic extracts were washed with brine (25 mL), dried over $MgSO_4$, filtered and concentrated *in vacuo* to provide a yellow oil. Purification by flash column chromatography (pentane/ethyl acetate 100:0 to 90:10) gave *trans, trans* farnesyl mercaptan (**S7**) as a pale-yellow oil (749 mg, 3.14 mmol, 52%).

^{1}H NMR (400 MHz, $CDCl_3$) δ 5.39 – 5.29 (m, 1H), 5.14 – 5.04 (m, 2H), 3.16 (t, *J* = 7.4 Hz, 2H), 2.15 – 1.93 (m, 8H), 1.68 (t, *J* = 1.4 Hz, 3H), 1.66 (d, *J* = 1.4 Hz, 3H), 1.60 (d, *J* = 1.4 Hz, 6H), 1.43 – 1.36 (m, 1H).

^{13}C NMR (101 MHz, $CDCl_3$) δ 137.7, 135.5, 131.5, 124.5, 123.9, 123.4, 39.8, 39.5, 26.9, 26.4, 25.9, 22.3, 17.9, 16.2, 15.9.

HRMS (ESI) m/z calculated for $C_{15}H_{26}S$ $[M]^+$ 238.1750, found 238.0822.

IR (neat) 2980, 2928, 2360, 1717, 1654, 1447, 1380, 1155, 741 cm^{-1}

CAS 138077-74-4

Spectroscopic data are in accordance with those in literature [57].

4-(2-(1,3-Dioxoisoindolin-2-yl)ethyl)benzene sulfonyl chloride (**S8**)

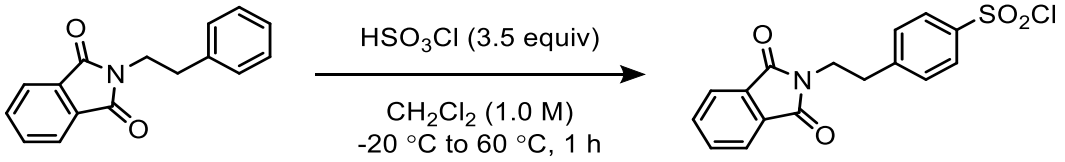

2-phenethylisoindoline-1,3-dione **S8**

S8 was synthesized according to a literature procedure [58] using a glass pressure tube. To a solution of 2-phenethylisoindoline-1,3-dione (1.0 g, 3.98 mmol) in CH_2Cl_2 (3 mL) was added chlorosulfonic acid (0.93 mL, 13.9 mmol) at – 20 °C. The solution was heated to 60 °C and stirred for 1 h. The solution was cooled to 25 °C and poured onto crushed ice. The crude product was purified by flash column chromatography on silica (pentane/ethyl acetate 50:50) to give (**S8**) as a light pink solid (1.22 g, 3.49 mmol, 88%).

^{1}H NMR (400 MHz, DMSO) δ 7.91 – 7.77 (m, 4H), 7.53 – 7.47 (m, 2H), 7.18 – 7.13 (m, 2H), 3.80 (t, *J* = 7.3, 6.7 Hz, 2H), 2.91 (t, *J* = 7.3 Hz, 2H).

^{13}C NMR (101 MHz, DMSO-d_6) δ 167.8, 146.0, 139.0, 134.5, 131.5, 128.1, 125.8, 123.2, 38.8, 33.5.

HRMS (ESI) m/z calculated for $C_{16}H_{13}{}^{35}ClNO_4S$ $[M+H]^+$ 350.0249, found 350.0260; $C_{16}H_{13}{}^{37}ClNO_4S$ $[M+H]^+$ 352.0219, found 352.0820.

IR (neat) 2940, 1769, 1701, 1394, 1354, 1328, 1041, 781 cm^{-1}

m.p. 169–170 °C (lit. 171 °C) [59]

Spectroscopic data are in accordance with those in literature [58].

(*S*)-2-(((Benzyloxy)carbonyl)amino)-4-methylpentyl methanesulfonate (**S9**)

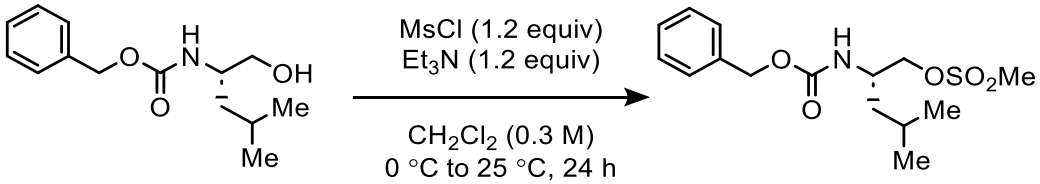

Cbz-L-leucinol **S9**

S9 was synthesized according to a literature procedure [26]. Anhydrous Et_3N (998 µL, 7.16) was added to a solution of Cbz-L-leucinol (1.5 g, 5.97 mmol) in anhydrous CH_2Cl_2 (20 mL). After cooling to 0 °C, MsCl (554 µL, 7.16 mmol) was added dropwise and the reaction was stirred for 24 h at 25 ° C. The solution is then washed with 5 % citric acid (10 mL), H_2O (10 mL) and brine (10 mL). The organic extracts were dried over Na_2SO_4, filtered and concentrated *in vacuo*. The corresponding residue was purified by flash column chromatography (pentane/ethyl acetate 90:10 to 50:50) to give **S9** as a viscous colorless oil (1.54 g, 4.68 mmol, 78%).

^{1}H NMR (400 MHz, $CDCl_3$) δ 7.40 – 7.27 (m, 5H), 5.16 – 5.04 (m, 2H), 4.81 (d, *J* = 8.7 Hz, 1H), 4.28 (dd, *J* = 10.2, 3.8 Hz, 1H), 4.16 (dd, *J* = 10.2, 4.2 Hz, 1H), 4.06 – 3.93 (m, 1H), 2.95 (s, 3H), 1.72 – 1.65 (m, 1H), 1.52 – 1.31 (m, 2H), 0.93 (d, *J* = 6.5 Hz, 6H).

^{13}C NMR (101 MHz, $CDCl_3$) δ 156.0, 136.4, 128.7, 128.4, 128.3, 71.4, 67.1, 48.6, 40.2, 37.4, 24.7, 23.1, 22.1.

HRMS (ESI) m/z calculated for $C_{15}H_{24}NO_5S$ $[M+H]^+$ 330.1370, found 330.1389.

IR (neat) 3385, 2980, 1697, 1529, 1455, 1345, 1183, 989, 820 cm^{-1}

CAS 1374636-02-8

Spectroscopic data are in accordance with those in literature [26].

(*S*)-*S*-(2-(((Benzyloxy)carbonyl)amino)-4-methylpentyl) ethanethioate (**S10**)

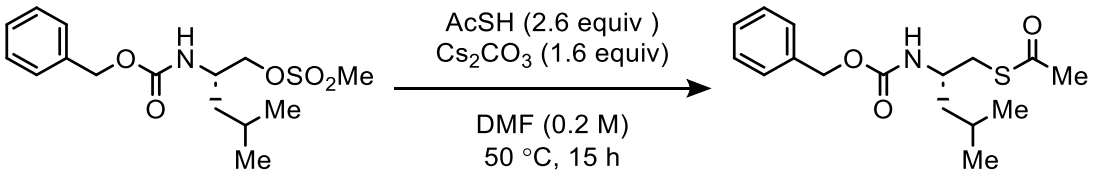

S9 **S10**

S10 was synthesized according to a literature procedure [26]. Under N_2 atmosphere, thioacetic acid (272 µL, 1.18 mmol) was added to a suspension of Cs_2CO_3 (643 mg, 1.97 mmol) in DMF (16 mL). After stirring for 30 min at 25 °C, **S9** (1.0 g, 3.04 mmol) was added in one portion and the mixture was stirred in an aluminium foil covered flask at 50 °C for 16 h. After evaporation of the solvent, the residue was redissolved in ethyl acetate (12 mL), washed with 5% $NaHCO_3$ (8 mL) and H_2O (5 mL). The organic extracts were separated, dried over Na_2SO_4, filtered and concentrated *in vacuo*. The corresponding brown residue was purified by flash column chromatography (pentane/ethyl acetate 100:0 to 90:10) to give **S10** as a waxy brown solid (747 mg, 2.41 mmol, 80%).

^{1}H NMR (400 MHz, $CDCl_3$) δ 7.42 – 7.30 (m, 5H), 5.12 (d, *J* = 12.3 Hz, 1H), 5.06 (d, *J* = 12.3 Hz, 1H), 4.65 (d, *J* = 9.1 Hz, 1H), 3.94 – 3.82 (m, 1H), 3.12 (dd, *J* = 13.9, 4.7 Hz, 1H), 2.99 (dd, *J* = 13.9, 7.2 Hz, 1H), 2.30 (s, 3H), 1.73 – 1.57 (m, 1H), 1.44 – 1.23 (m, 2H), 0.91 (d, *J* = 6.6 Hz, 6H).

^{13}C NMR (101 MHz, $CDCl_3$) δ 195.8, 156.1, 136.7, 128.6, 128.2, 128.2, 66.8, 49.4, 43.7, 34.4, 30.7, 25.0, 23.1, 22.3.

HRMS (ESI) m/z calculated for $C_{16}H_{23}NO_3S$ $[M+H]^+$ 310.1471 found 310.1481.

IR (neat) 3346, 2980, 1689, 1537, 1274, 1253, 1126, 1037, 955 cm^{-1}

m.p. 52–54 °C (lit. 56–58 °C) [60]

CAS 744265-92-7

Spectroscopic data are in accordance with those in literature [26].

Ethyl 2-oxo-2-(5,5,8,8-tetramethyl-5,6,7,8-tetrahydronaphthalen-2-yl)acetate (**S11**)

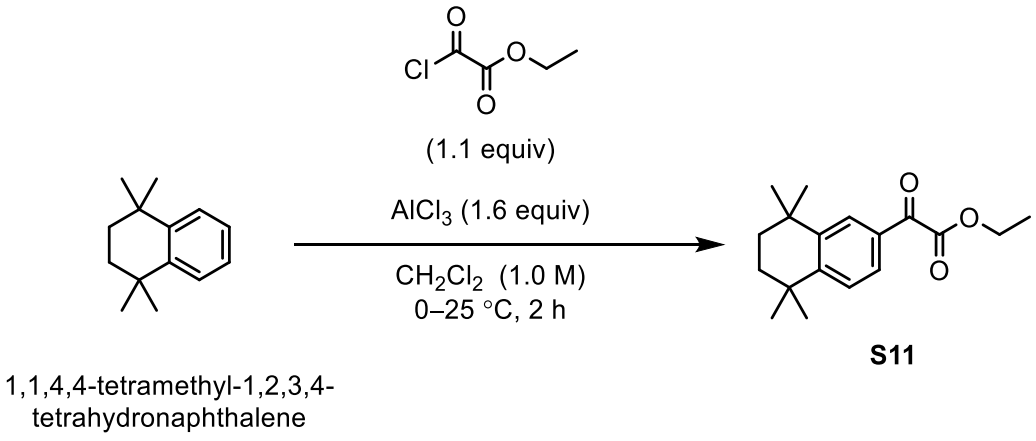

S11 was synthesized according to a literature procedure [61] .To a three-necked flask (equipped with addition funnel, argon inlet adapter and condenser with NaOH trap attached) was added 1,2,3,4-tetrahydro-1,1,4,4-tetramethylnaphthalene (3.0 g, 15.9 mmol), ethyl oxalyl chloride (1.95 mL, 17.5 mmol) and CH_2Cl_2 (17 mL). The reaction mixture was cooled

to 0 °C and $AlCl_3$ (3.4 g, 25.4 mmol) was added portion wise while maintaining the temperature at 0 °C. The reaction mixture was stirred for 15 minutes at 0 °C and then stirred for an additional 2 h at 25 °C. Once complete (monitored by TLC), the reaction mixture was poured into iced water (75 mL). The aqueous layer was extracted with CH_2Cl_2 (3 x 20 mL). The combined organic extracts were washed with saturated $NaHCO_3$ solution (30 mL), brine (30 mL), dried over Na_2SO_4 and concentrated *in vacuo*. Purification by flash chromatography (pentane/ethyl acetate 98:2) afforded ethyl 2-oxo-2-(5,5,8,8-tetramethyl-5,6,7,8-tetrahydronaphthalen-2-yl)acetate (**S11**) as a pale-yellow oil (4.13 g, 14.3 mmol, 90%).

^{1}H NMR (400 MHz, $CDCl_3$) δ 7.98 (d, *J* = 1.9 Hz, 1H), 7.71 (dd, *J* = 8.3, 1.9 Hz, 1H), 7.43 (d, *J* = 8.3 Hz, 1H), 4.44 (q, *J* = 7.2 Hz, 2H), 1.70 (s, 4H), 1.42 (t, *J* = 7.1 Hz, 3H), 1.30 (s, 6H), 1.30 (s, 6H).

^{13}C NMR (101 MHz, $CDCl_3$) [overlapping signals] δ 186.5, 164.4, 153.3, 146.1, 130.1, 128.7, 127.4, 127.3, 62.3, 35.1, 34.8, 34.7, 34.6, 31.8 (overlapping signals), 31.6 (overlapping signals), 14.3.

HRMS (ESI) m/z calculated for $C_{18}H_{24}O_3Na$ $[M+Na]^+$ 311.1618, found 311.1623.

IR (neat) 2970, 2360, 1737, 1684, 1601, 1459, 1205, 1182, 1029 cm^{-1}

Spectroscopic data are in accordance with those in literature [61].

Ethyl 2-hydroxy-2-(5,5,8,8-tetramethyl-5,6,7,8-tetrahydronaphthalen-2-yl)acetate (**S12**)

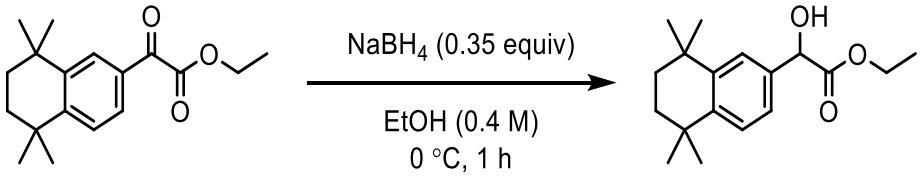

S11 **S12**

S12 was synthesized according to a literature procedure [61]. To a three-necked flask (equipped with addition funnel, argon inlet adapter and temperature probe) was added $NaBH_4$ (0.138 g, 3.64 mmol) and EtOH (12 mL). The reaction mixture was cooled 0 °C and a solution of ethyl 2-oxo-2-(5,5,8,8-tetramethyl-5,6,7,8-tetrahydronaphthalen-2-yl)acetate (**S11**) (3.0 g, 10.4 mmol) in EtOH (28 ml) was added portion wise while maintaining the temperature at 0 °C. The reaction mixture was then stirred for 1 h at 0 °C. Once complete (monitored by TLC), the reaction mixture was quenched with ice-water (50 ml) and acidified to pH 3 using 1 M HCl. The mixture was extracted with EtOAC (30 mL) and the organic extracts were washed with a saturated $NaHCO_3$, brine and dried over Na_2SO_4. Removal of solvent *in vacuo* gave ethyl 2-hydroxy-2-(5,5,8,8-tetramethyl-5,6,7,8-tetrahydronaphthalen-2-yl)acetate (**S12**) as a colorless oil in quantitative yield.

^{1}H NMR (400 MHz, $CDCl_3$) δ 7.34 (d, *J* = 2.0 Hz, 1H), 7.29 (d, *J* = 8.2 Hz, 1H), 7.16 (dd, *J* = 8.2, 2.0 Hz, 1H), 5.12 (br s, 1H), 4.32 – 4.14 (m, 2H), 3.35 (br s, 1H), 1.68 (s, 4H), 1.45 – 1.04 (m, 15H)

^{13}C NMR (101 MHz, $CDCl_3$) [overlapping signals] δ 174.0, 145.2, 145.2, 135.4, 127.0, 124.9, 123.6, 73.0, 62.2, 35.2, 35.1, 34.5, 34.3, 32.0 (overlapping signals), 14.2.

HRMS (ESI) m/z calculated for $C_{18}H_{26}O_3Na$ $[M+Na]^+$ 313.1774, found 313.1787.

IR (neat) 3478, 2961, 1738, 1495, 1460, 1260, 1021, 814 cm^{-1}

Spectroscopic data are in accordance with those in literature [61].

Ethyl 2-bromo-2-(5,5,8,8-tetramethyl-5,6,7,8-tetrahydronaphthalen-2-yl)acetate (**S13**)

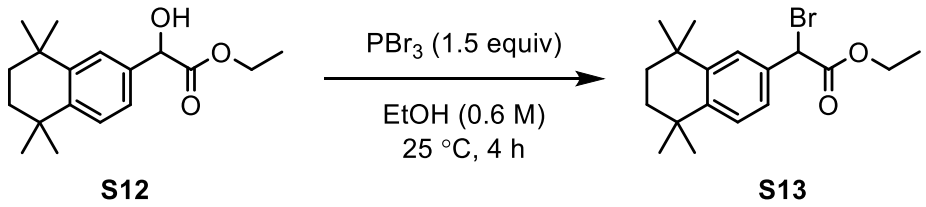

S12 **S13**

S13 was synthesized according to a modified literature procedure [62]. PBr_3 (0.22 ml, 2.30 mmol) was added to a solution of ethyl 2-hydroxy-2-(5,5,8,8-tetramethyl-5,6,7,8-tetrahydronaphthalen-2-yl)acetate (**S12**) (1.00 g, 3.44 mmol) in CH_2Cl_2 (6 mL) at 0 °C. The solution was stirred for 4 h at 25 °C. Once complete (monitored by TLC), the reaction was quenched with H_2O (5 mL). The mixture was extracted with EtOAc (3 x 7 ml) and the combined organic extracts were washed with brine (7 mL) dried over Na_2SO_4 and concentrated *in vacuo*. Purification by flash chromatography (pentane/ethyl acetate 98:2) gave ethyl 2-bromo-2-(5,5,8,8-tetramethyl-5,6,7,8-tetrahydronaphthalen-2-yl)acetate (**S13**) as a colorless oil (0.67 g, 1.90 mmol, 55%).

^{1}H NMR (400 MHz, $CDCl_3$) δ 7.43 (d, *J* = 2.0 Hz, 1H), 7.32 (dd, *J* = 8.3, 2.0 Hz, 1H), 7.28 (d, *J* = 8.2 Hz, 1H), 5.30 (s, 1H), 4.32 – 4.16 (m, 2H), 1.67 (s, 4H), 1.30 (t, *J* = 7.1 Hz, 3H), 1.28 (s, 6H), 1.27 (s, 6H).

^{13}C NMR (101 MHz, $CDCl_3$) δ 168.6, 146.4, 145.5, 132.7, 127.3, 127.1, 125.9, 62.5, 47.4, 35.1, 35.0, 34.5, 34.4, 31.9, 31.9, 31.9, 31.8, 14.1.

HRMS (ESI) m/z calculated for $C_{18}H_{26}{}^{79}BrO_2$ $[M+H]^+$ 353.1111, found 353.1124; $C_{18}H_{26}{}^{81}BrO_2$ $[M+H]^+$ 355.1090, found 355.1097.

IR (neat) 2959, 2926, 2861, 1746, 1140, 1028 cm^{-1}

2-Bromo-*N,N*-diethyl-2-phenylacetamide (**S14**)

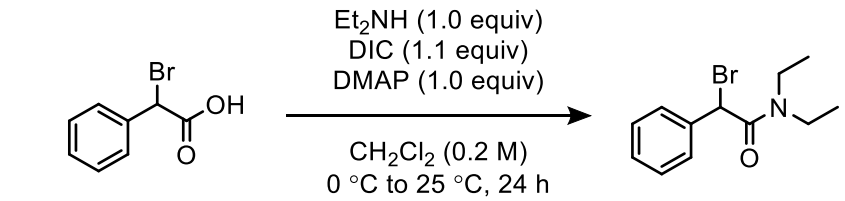

α-bromophenylacetic acid **S14**

S14 was synthesized according to a literature procedure [63]. α-Bromophenylacetic acid (2.15 g, 10.0 mmol), diethyl amine (1.03 mL, 10.0 mmol), and 4-dimethylaminopyridine (122 mg, 1.0 mmol) were dissolved in CH_2Cl_2 (50 ml). The solution was cooled to 0 °C, followed by the addition of *N,N'*-diisopropylcarbodiimide (1.70 ml, 11.0 mmol). The reaction mixture was then allowed to warm to 25 °C and stirred for 24 h. Once complete (monitored by TLC), the reaction mixture was diluted with CH_2Cl_2 (30 ml) and then quenched with H_2O (30 ml). The organic extracts were separated and the aqueous phase was extracted CH_2Cl_2 (2 x 30 ml). The combined organic extracts were dried over Na_2SO_4 and concentrated *in vacuo*. Purification by flash chromatography (pentane/ethyl acetate 90:10 to 80:20) gave 2-bromo-*N,N*-diethyl-2-phenylacetamide (**S14**) as a colorless oil (860 mg, 3.18 mmol, 32%).

^{1}H NMR (400 MHz, $CDCl_3$) δ 7.58 – 7.53 (m, 2H), 7.38 – 7.29 (m, 3H), 5.67 (s, 1H), 3.48 – 3.25 (m, 4H), 1.16 (t, *J* = 7.1 Hz, 3H), 1.13 (t, *J* = 7.1 Hz, 3H).

^{13}C NMR (101 MHz, $CDCl_3$) δ 166.5, 136.9, 129.0, 128.9, 128.9, 46.9, 42.7, 41.5, 14.6, 12.7.

HRMS (ESI) m/z calculated for $C_{12}H_{16}{}^{79}BrNONa$ $[M+Na]^+$ 292.0308, found 292.0318; $C_{12}H_{16}{}^{81}BrNONa$ $[M+Na]^+$ 294.0287, found 294.0295

IR (neat) 2980, 1651, 1484, 1458, 1137, 696 cm^{-1}

CAS 91801-96-6

Spectroscopic data are in accordance with those in literature [63].

2-Bromo-1-phenylpropan-1-one (**S15**)

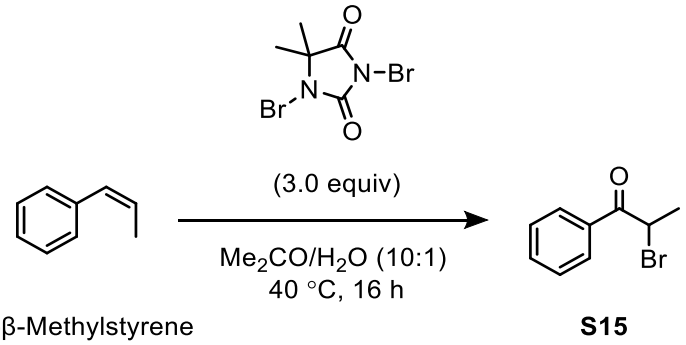

cis-β-Methylstyrene **S15**

S15 was synthesized according to a literature procedure [64]. 1,3-Dibromo-5,5-dimethylhydantoin (3.65 g, 12.8 mmol) was added to a solution of *cis*-β-methyl styrene (550 µL, 4.25 mmol) in acetone (60 mL) and H_2O (6 mL). The reaction mixture was stirred at 80 °C for 1 h then 40 °C for 16 h. Once complete (monitored by TLC), the reaction was quenched with saturated $NaHCO_3$ solution (5 mL) and extracted with EtOAc (20 mL). Organic extracts were washed with brine (20 mL), dried over Na_2SO_4 and concentrated *in vacuo*. Purification by flash chromatography (pentane/ethyl acetate 100:0 to 95:5) gave 2-bromo-1-phenylpropan-1-one (**S15**) as a colorless oil (797 mg, 3.74 mmol, 88%).

^{1}H NMR (400 MHz, $CDCl_3$) δ 8.12 – 7.96 (m, 2H), 7.64 – 7.55 (m, 1H), 7.55 – 7.40 (m, 2H), 5.30 (q, *J* = 6.6 Hz, 1H), 1.91 (d, *J* = 6.6 Hz, 3H).

^{13}C NMR (101 MHz, $CDCl_3$) δ 193.5, 134.2, 133.8, 129.1, 128.9, 41.6, 20.3.

MS (EI, 70 eV) m/z (%) 105.05 ($[C_7H_5O]^{+\cdot}$, 100), 77.05 (44), 51.04 (15), 213.97 (^{81}Br$[M]^{+\cdot}$, 2), 211.98 (^{79}Br$[M]^{+\cdot}$, 2).

IR (neat) 2981, 1689, 1449, 1238, 949, 707 cm^{-1}

CAS 2114-00-3

Spectroscopic data are in accordance with those in literature [64].

2-Bromo-1-phenylbutan-1-one (**S16**)

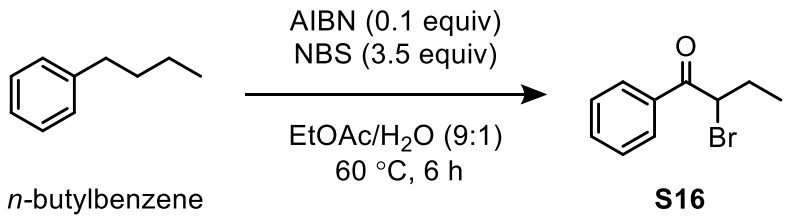

n-butylbenzene **S16**

To a solution of *n*-butylbenzene (1.20 g, 9.0 mmol) in EtOAc/water (9:1, 54 mL) was added *N*-bromosuccinimide (5.61 g, 31.5 mmol) and AIBN (148 mg, 0.9 mmol) at 25 °C. The mixture was heated to 60 °C and stirred for 6 h. Once complete (monitored by TLC), the reaction was cooled to 25 °C and then quenched with saturated $NaHCO_3$ solution (40 ml). The reaction mixture was then extracted using EtOAc (2 x 30 ml). The organic extracts were dried over Na_2SO_4 and concentrated *in vacuo*. Purification by flash chromatography (pentane/ethyl acetate 100:0 to 98:2) gave 2-bromo-1-phenylbutan-1-one (**S16**) as a colorless oil (1.46 g, 6.43 mmol, 72%).

^{1}H NMR (400 MHz, $CDCl_3$) δ 8.06 – 7.98 (m, 2H), 7.63 – 7.56 (m, 1H), 7.53 – 7.45 (m, 2H), 5.07 (dd, *J* = 7.7, 6.3 Hz, 1H), 2.32 – 2.08 (m, 2H), 1.09 (t, *J* = 7.3 Hz, 3H).

^{13}C NMR (101 MHz, $CDCl_3$) δ 193.4, 134.7, 133.8, 129.0, 128.9, 49.2, 27.0, 12.3.

HRMS (ESI) m/z calculated for $C_{10}H_{12}{}^{79}BrO$ $[M+H]^+$ 227.0066, found 227.0055; $C_{10}H_{12}{}^{81}BrO$ $[M+H]^+$ 229.0046, found 229.0047.

IR (neat) 2980, 1687, 1448, 1225, 801, 704 cm^{-1}

CAS 877-35-0

Spectroscopic data are in accordance with those in literature [65].

3β-Hydroxy-16α-bromoandrost-5-en-17-one (**S17**)

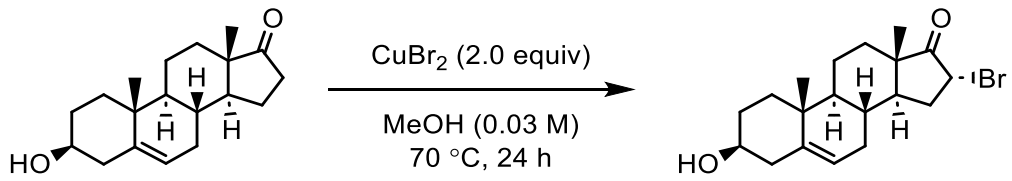

3β-hydroxyandrost-5-en-17-one **S17**

S17 was synthesized according to a modified literature procedure [66]. To a solution of 3β-Hydroxyandrost-5-en-17-one (836 mg, 2.9 mmol) in anhydrous MeOH (100 mL) was added $CuBr_2$ (1.30 g, 5.8 mmol). The suspension was stirred at 70 °C for 24 h. Once complete (monitored by TLC), H_2O (250 mL) was added to the reaction mixture followed by extraction with CH_2Cl_2 (3 x 150 mL). The organic fractions were combined and dried over Na_2SO_4, filtered and concentrated *in vacuo* to give a crude solid. Purification by crystallization from MeOH gave 3β-hydroxy-16α-bromoandrost-5-en-17-one (**S17**) as a white solid (978 mg, 2.66 mmol, 92%).

^{1}H NMR (400 MHz, $CDCl_3$) δ 5.37 (dt, *J* = 5.4, 1.9 Hz, 1H), 4.57 – 4.50 (m, 1H), 3.59 – 3.48 (m, 1H), 2.36 – 2.13 (m, 4H), 2.10 – 1.99 (m, 1H), 1.98 – 1.91 (m, 1H), 1.90 – 1.64 (m, 6H), 1.57 – 1.38 (m, 3H), 1.17 – 1.05 (m, 2H), 1.03 (s, 3H), 0.92 (s, 3H).

^{13}C NMR (101 MHz, $CDCl_3$) δ 213.5, 141.2, 120.8, 71.7, 50.2, 48.4, 47.7, 46.4, 42.3, 37.2, 36.8, 34.3, 32.4, 31.7, 30.9, 30.7, 20.4, 19.6, 14.1.

MS (ESI) m/z calculated for $C_{19}H_{27}{}^{79}BrO_2Na$ $[M+Na]^+$ 389.1087, found 389.1088; $C_{19}H_{27}{}^{81}BrO_2Na$ $[M+Na]^+$ 391.1066, found 391.1072.

IR (neat) 3654, 2970, 1737, 1629, 1267, 1044, 1025 cm^{-1}

m.p. 172-174 °C

Spectroscopic data are in accordance with those in literature [66].

2-Bromo-1-(indolin-1-yl)ethan-1-one (**S18**)

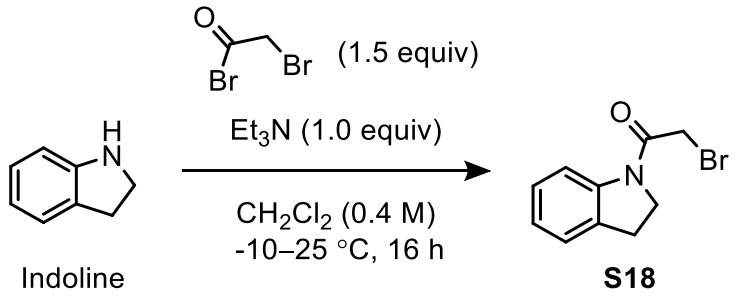

S18 was synthesized according to a literature procedure [67]. Bromoacetyl bromide (2.2 ml, 25.2 mmol) was added to a solution of indoline (2.0 g, 16.8 mmol) and triethylamine (3.53 ml, 25.2 mmol) in anhydrous CH_2Cl_2 (65 ml) at -10 °C. The reaction mixture was warmed to 25 °C and stirred for 16 h. Once complete (monitored by TLC), the reaction mixture was washed with H_2O (20 ml), 1M HCl (20 ml) and saturated Na_2CO_3 solution (20 ml). The organic extracts were dried over Na_2SO_4 and concentrated *in vacuo*. The crude product was purified by dissolving in EtOAc (75 ml) and precipitating by adding hexane (125 ml). The precipitate was filtered and washed with EtOAc (50 mL) and hexane (50 mL). Repeating this procedure on solid obtained by evaporating the solvents from the mother liquor gave 2-bromo-1-(indolin-1-yl)ethan-1-one (**S18**) as an off-white solid (3.99 g, 16.6 mmol, 99%).

^{1}H NMR (400 MHz, $CDCl_3$) δ 8.21 (d, *J* = 8.2 Hz, 1H), 7.25 – 7.17 (m, 2H), 7.07 (t, *J* = 7.5 Hz, 1H), 4.19 (t, *J* = 8.4 Hz, 2H), 3.95 (s, 2H), 3.24 (t, *J* = 8.4 Hz, 2H).

^{13}C NMR (101 MHz, $CDCl_3$) δ 164.3, 142.6, 131.5, 127.8, 124.8, 124.6, 117.5, 48.4, 28.6, 28.3.

HRMS (ESI) m/z calculated for $C_{10}H_{10}{}^{79}BrNONa$ $[M+Na]^+$ 261.9838, found 261.9829; $C_{10}H_{10}{}^{81}BrNONa$ $[M+Na]^+$ 263.9818, found 263.9805.

IR (neat) 1655, 1597, 1479, 1468, 1447, 1406, 1346, 1256, 1135, 1101, 763 cm^{-1}

m.p. 125–126 °C (lit. 124–126 °C) [67]

CAS 73392-01-5

Spectroscopic data are in accordance with those in literature [67].

(3-Iodopropyl)benzene (**S19**)

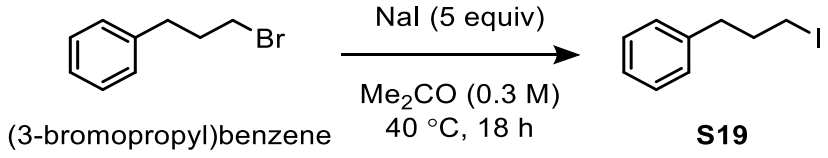

S19 was synthesized according to a modified literature procedure [68]. To a solution of (3-bromopropyl)benzene (398 mg, 2.0 mmol) in acetone (6 mL) was added NaI (1.5 g, 10.0 mmol). The reaction was stirred for 18 h at 40 °C. Once complete (monitored by TLC), the reaction mixture was concentrated *in vacuo* and CH_2Cl_2 (5 mL) was added. The reaction mixture was filtered and the solids were washed with CH_2Cl_2 (2 x 10 mL). The organic extracts were washed with H_2O (5 mL), sodium thiosulfate (5 mL), brine (5 mL), dried over Na_2SO_4 and concentrated *in vacuo* to give (3-iodopropyl)benzene (**S19**) as a yellow oil (490 mg, 1.99 mmol, 99%). The product was directly used in the subsequent step without further purification.

^{1}H NMR (400 MHz, $CDCl_3$) δ 7.35 – 7.26 (m, 2H), 7.25 – 7.17 (m, 3H), 3.18 (t, *J* = 6.8 Hz, 2H), 2.74 (t, *J* = 7.3 Hz, 2H), 2.21 – 2.09 (m, 2H).

^{13}C NMR (101 MHz, $CDCl_3$) δ 140.5, 128.7, 128.6, 126.3, 36.4, 35.0, 6.5.

MS (EI, 70 eV) m/z (%) 91.08 ($[C_7H_7]^{+\cdot}$, 100), 246 (41), 119.07 (20), 65.05 (15).

IR (neat) 2981, 1558, 1541, 1262, 1214, 955, 698 cm^{-1}

CAS 4119-41-9

Spectroscopic data are in accordance with those in literature [68].

(3-Bromoprop-1-yn-1-yl)benzene (**S20**)

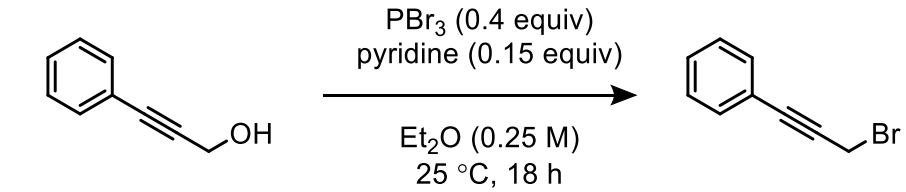

3-Phenyl-2-propyn-1-ol **S20**

S20 was synthesized according to a literature procedure [69]. Phosphorus tribromide (190 µL, 2.0 mmol) was added slowly to a solution of 3-phenyl-2-propyn-1-ol (661 mg, 5.0 mmol) and pyridine (60 µL, 0.75 mmol) in Et_2O (20 mL) at 0 °C. The resulting solution was stirred at 25 °C for 18 h. Once complete (monitored by TLC), the reaction was quenched with saturated $NaHCO_3$ solution (80 ml) and the organic layer was separated. The aqueous phase was extracted with Et_2O (3 x 45 mL) and the combined organic extracts were dried over $MgSO_4$, filtered and concentrated *in vacuo*. Purification by flash chromatography (pentane, 100%) gave (3-bromoprop-1-yn-1-yl)benzene (**S20**) as a colorless oil (492 mg, 2.52 mmol, 51%).

^{1}H NMR (400 MHz, $CDCl_3$) δ 7.55 – 7.43 (m, 2H), 7.41 – 7.27 (m, 3H), 4.18 (s, 2H).

^{13}C NMR (101 MHz, $CDCl_3$) δ 132.0, 129.0, 128.4, 122.2, 86.8, 84.4, 15.4.

HRMS (ESI) m/z calculated for $C_9H_8{}^{79}Br$ $[M+H]^+$ 194.9804, found 195.0881; $C_9H_8{}^{81}Br$ $[M+H]^+$ 196.9783, found 197.0791.

IR (neat) 2981, 1490, 1382, 1272, 1203, 690 cm^{-1}

CAS 1794-48-5

Spectroscopic data are in accordance with those in literature [70].

Benzyl (*E*)-4-bromobut-2-enoate (**S21**)

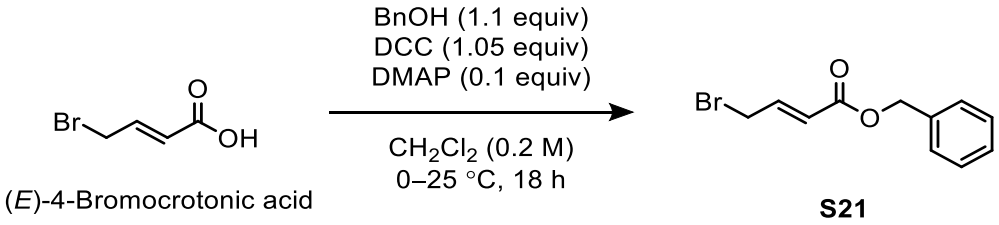

S21 was synthesized according to a literature procedure [71]. (*E*)-4-bromocrotonic acid (1.0 g, 6.10 mmol), benzyl alcohol (690 µL, 6.71 mmol) and 4-dimethylaminopyridine (75 µL, 0.606 mmol) were dissolved in CH_2Cl_2 (30 ml). The solution was cooled to 0 °C, followed by the addition of *N,N'*-dicyclohexylcarbodiimide (1.32 g, 6.41 mmol). The reaction mixture was then allowed to warm to 25 °C and stirred for 18 h. Once complete (monitored by TLC), the reaction mixture was filtered, concentrated *in vacuo* and purified by flash chromatography (petroleum ether: ethyl acetate 98:2) to give benzyl (*E*)-4-bromobut-2-enoate (**S21**) as a white solid (659 mg, 2.58 mmol, 42%).

^{1}H NMR (400 MHz, $CDCl_3$) δ 7.43 – 7.30 (m, 5H), 7.05 (dt, *J* = 15.3, 7.3 Hz, 1H), 6.08 (dt, *J* = 15.3, 1.3 Hz, 1H), 5.20 (s, 2H), 4.00 (dd, *J* = 7.3, 1.3 Hz, 2H).

^{13}C NMR (101 MHz, $CDCl_3$) δ 165.4, 142.4, 135.8, 128.7, 128.5, 128.4, 124.4, 66.7, 29.2.

MS (EI, 70 eV) m/z (%) 91.03 ($[C_7H_7]^{+\cdot}$, 100), 31.99 (36), 157.01 (31), 255.94 (^{81}Br[M]$^{+\cdot}$, 2), 253.92 (^{79}Br[M]$^{+\cdot}$, 2).

IR (neat) 2981, 1719, 1324, 1192, 963, 699 cm^{-1}

m.p. 41–42 °C (lit. 41.8–42.4 °C) [72]

CAS 852402-28-9

Spectroscopic data are in accordance with those in literature [71].

4.2.13 Characterisation of Fmix

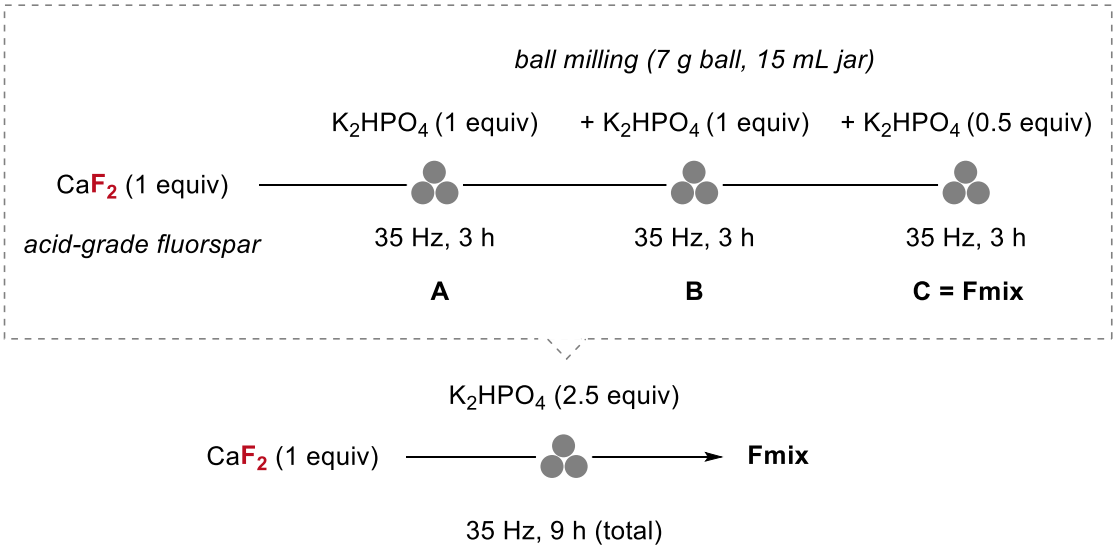

X-ray powder diffraction data of **Fmix** collected at room temperature:

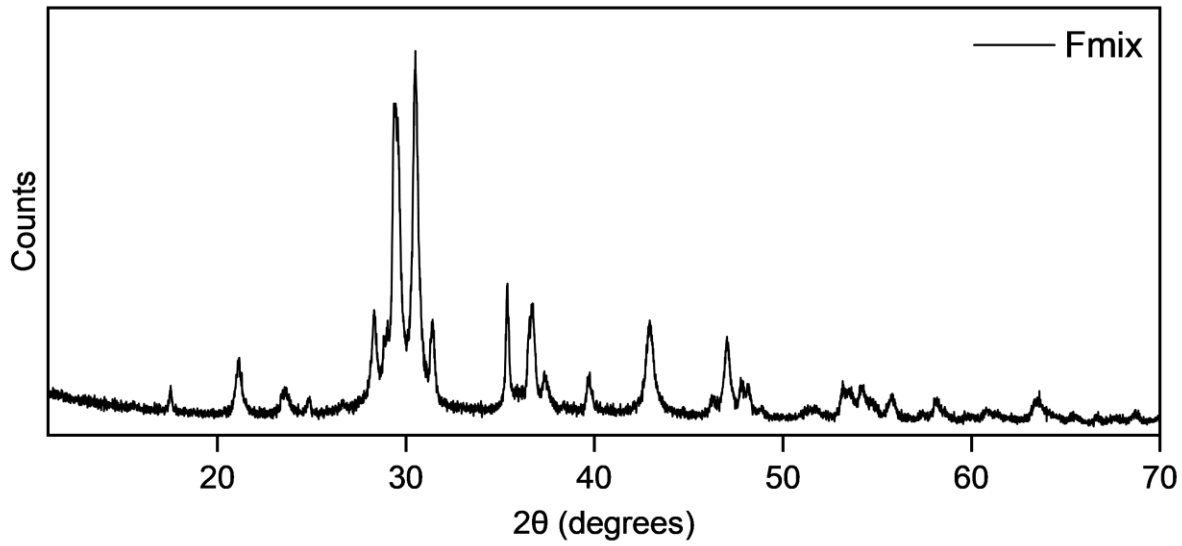

NMR (D_2O) spectroscopy data of **Fmix** collected at room temperature:

To a sample of **Fmix** (20 mg) was added 0.8 mL D_2O. The suspension was transferred to a 1 mL centrifuge tube. Centrifugation with an acceleration time of 120 seconds (13,500 rpm) (included in the overall centrifugation time) at 25 °C followed and the supernatant was analysed by NMR spectroscopy [73].

^{1}H NMR (565 MHz, D_2O) no signals observed.

^{19}F NMR (471 MHz, D_2O) δ -73.82 (d, $^{1}J_{P-F}$ = 864.3 Hz, PO_3F^{2-}), -121.89 (s, aq. F^-).

^{31}P NMR (203 MHz, D_2O) δ 2.67 (s, HPO_4^{2-}), 1.08 (d, $^{1}J_{P-F}$ = 864.3 Hz, PO_3F^{2-}).

Solid-state NMR spectroscopy data of **Fmix** (data acquired by Dr. C. Goult and J. Struijs):

^{19}F NMR (376 MHz, Solid) δ -71.57 (PO_3F^{2-}), -108.08 (F-), -121.20 – -147.83 (m, **X**).

^{31}P NMR (162 MHz, Solid) δ 10.0 – -3.0 (HPO_4^{2-}).

^{19}F DPMAS: D_1 = 67.5 s (T_1 = 1.4-12.8 s), ν_{rot} = 20 kHz (Fmix) (* denotes spinning side bands)

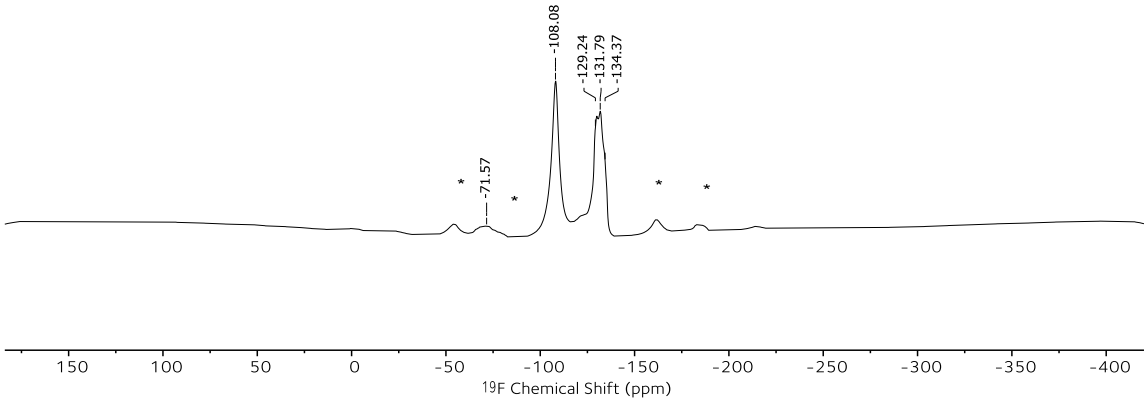

^{31}P DPMAS: D_1 = 47.5 s (T_1 = 9.5 s), ν_{rot} = 10 kHz (Fmix) (* denotes spinning side bands)

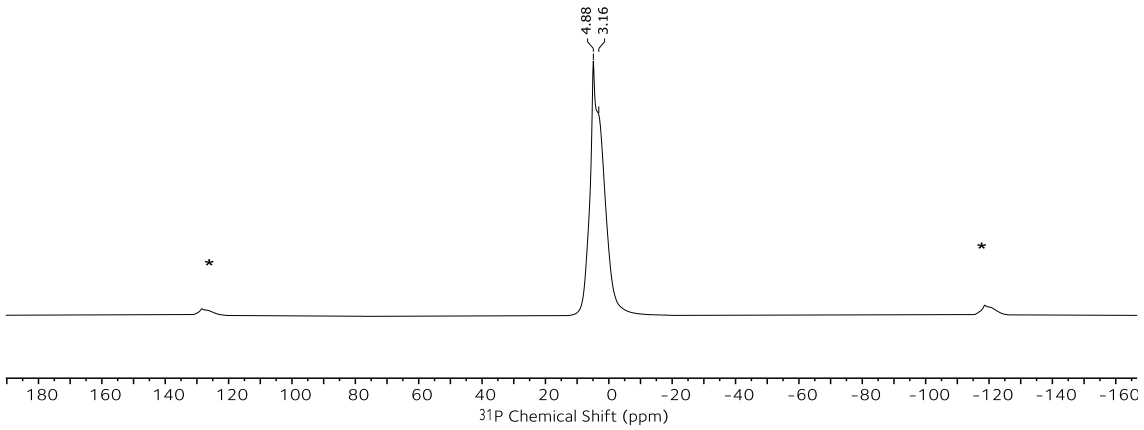

^{1}H DPMAS: D_1 = 120 s (T_1 = 32.1 s), ν_{rot} = 20 kHz (Fmix) (* denotes spinning side bands)

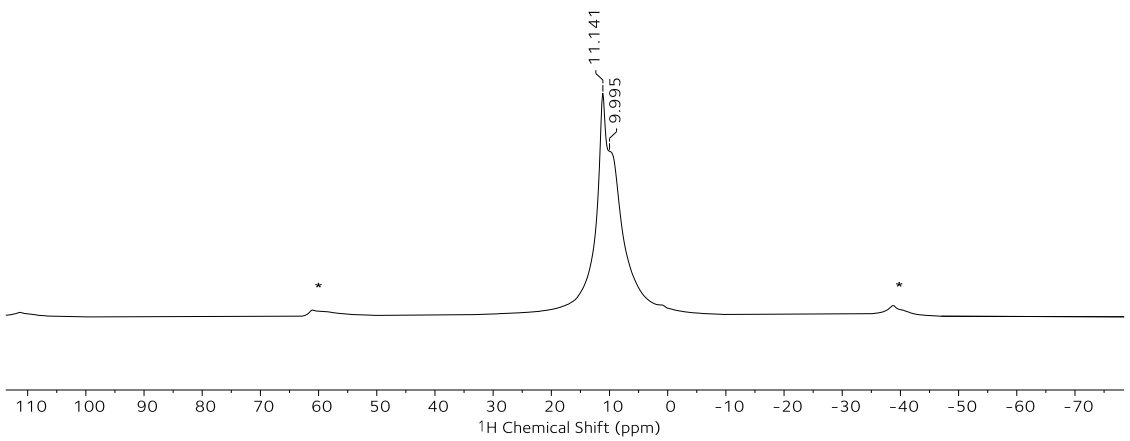

4.2.14 Quantification of fluoride and monofluorophosphate from Fmix by ^{19}F NMR spectroscopy (D_2O)

To a sample of the powder (**A** to **C**) (containing 0.25 mmol CaF_2) and CF_3SO_3Na (5.0 mg, 0.0291 mmol) as internal standard was added D_2O (0.8 mL). The suspension was transferred to a 1 mL centrifuge tube. Centrifugation with an acceleration time of 120 seconds (13.5 rpm) (included in the overall centrifugation time) at 25 °C followed and the supernatant was analysed by quantitative ^{19}F-NMR spectroscopy (T_1 in range 2 to 10 sec and d_1 = 50 sec). Experiments were conducted in triplicate and a mean was calculated with standard error.

Entry	Mixture	Mean F (%)	+/- S.E.	Mean P-F (%)	+/- S.E.
1	Milled Fluorspar (0.25 mmol)	0.1179%	0.1179%	0%	0
2	A	10.4626%	10.4626%	0.69%	0.01%
3	B	15.8773%	15.8773%	1.15%	0.19%
4	C	16.7113%	16.7113%	1.20%	0.005%

Measuring T_1 relaxation times for fluoride and monofluorophosphate

An inversion recovery measurement was made on an AVB 500 in order to determine the T_1 of the ^{19}F nuclei (fluoride, CF_3SO_3Na and monofluorophosphate) present in the solution.

The longitudinal relaxation time constants T_1 were measured via ^{19}F inversion recovery experiments on an AVB 500. T_1 was calculated by non-linear fitting using Dynamic Center 2.8.1. The experiment was acquired with the following parameters.

Fitted function:	f(t) = Io * [1 - a*exp (-t/T1)]
Random error estimation of data:	RMS per spectrum (or trace/plane)
Systematic error estimation of data:	worst case per peak scenario
Fit parameter Error estimation method:	from fit using calculated y uncertainties
Confidence level:	95%
Used peaks:	peaks from Q:/AVB500/2022/data/vggroup/nmr/cp675101908/4/pdata/1/peaklist1D.xml
Used integrals:	peak intensities

Peak name	F2 [ppm]	Io	error	T1 [s]	error	a	error	fitInfo
1	-121.929	3.94e+08	6.582e+04	10.3	0.002729	1.87	0.0001843	Done

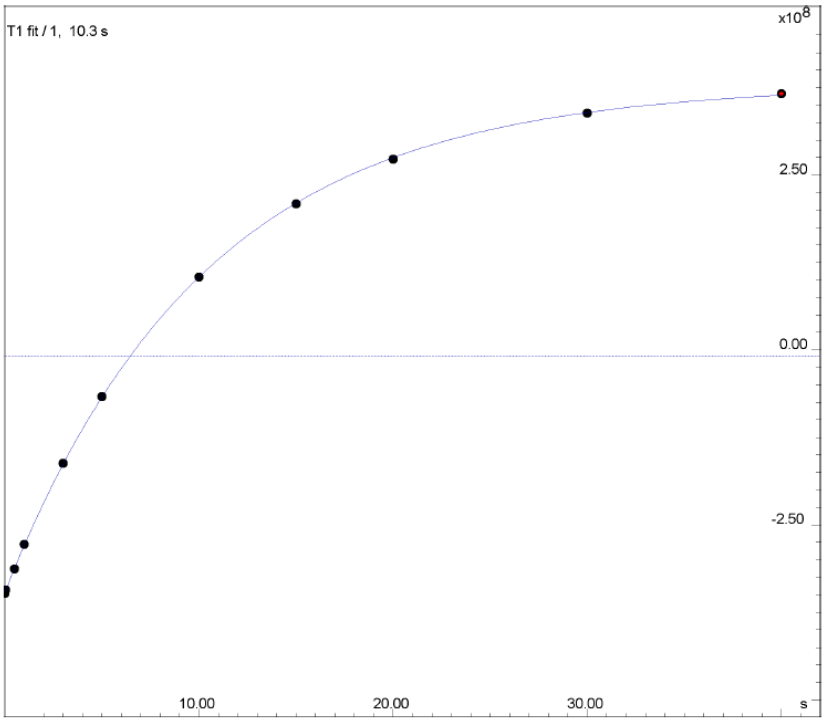

Inversion recovery plot of aq. F^- in the sample, experimental data (dots) and fitted function (line). T_1 = 10.3 s.

Fitted function:	f(t) = Io * [1 - a*exp (-t/T1)]
Random error estimation of data:	RMS per spectrum (or trace/plane)
Systematic error estimation of data:	worst case per peak scenario
Fit parameter Error estimation method:	from fit using calculated y uncertainties
Confidence level:	95%
Used peaks:	peaks from Q:/AVB500/2022/data/vggroup/nmr/cp675101908/3/pdata/1/peaklist1D.xml
Used integrals:	peak intensities

Peak name	F2 [ppm]	T1 [s]	error	fitInfo
1	-72.856	4.53	0.04383	Done
2	-74.692	2.21	0.01803	Done
3	-78.806	4.86	0.001297	Done

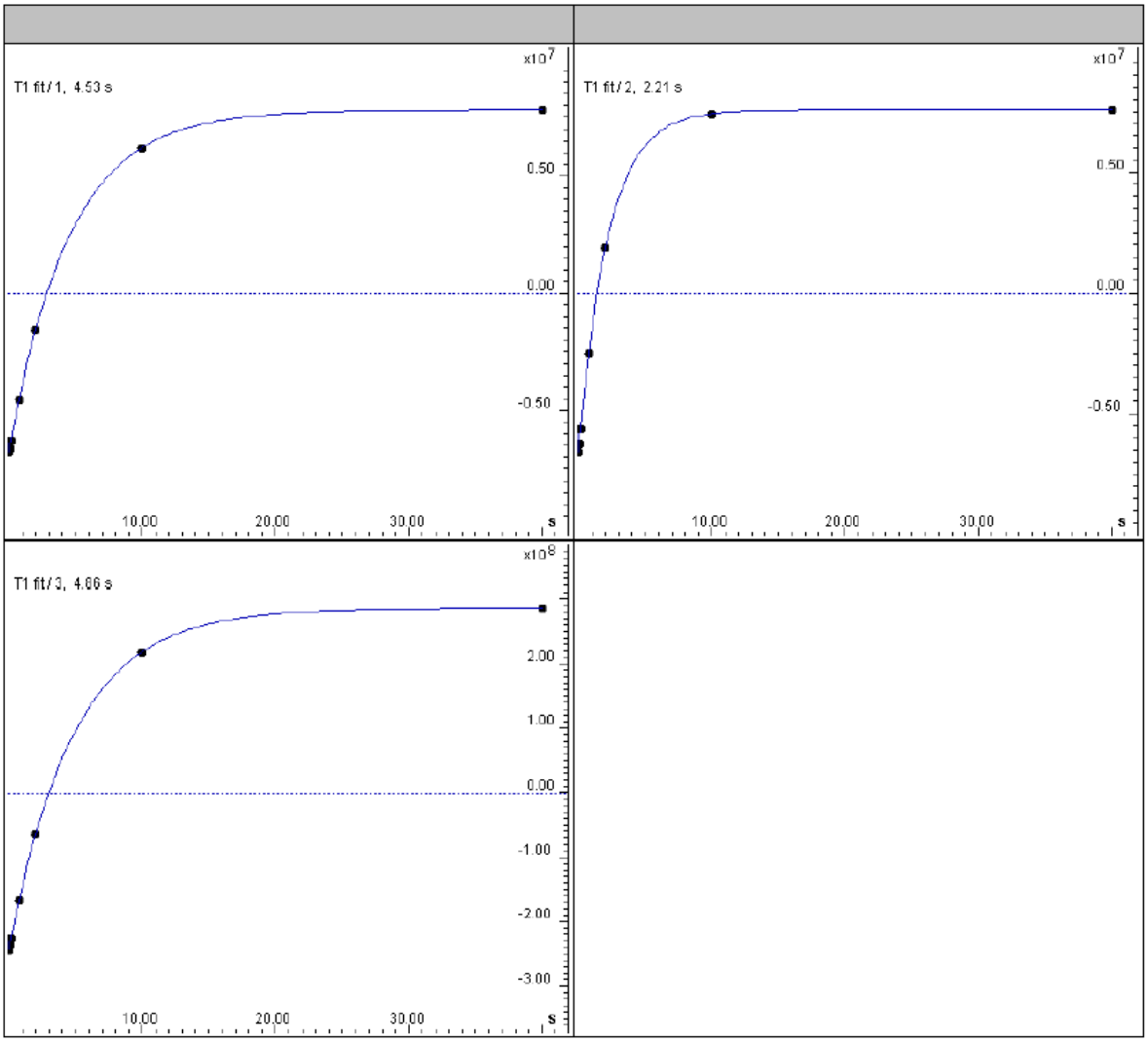

Inversion recovery plot of CF_3SO_3Na and monofluorophosphate in the sample, experimental data (dots) and fitted function (line). T_1 within the range 2 to 5 s.

T_1 of the ^{19}F nuclei (fluoride and monofluorophosphate) present in the solution and the values were found to lie in the range of 2 to 10 seconds. These values allow for reliable integration using a scan delay (d_1) of 50 s.

4.2.15 Characterisation of X

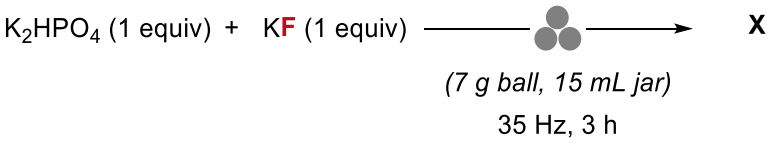

X was prepared by ball milling an equimolar amount of anhydrous KF with anhydrous K_2HPO_4. To a 15 mL stainless steel milling jar was added a stainless steel ball (7 g), anhydrous KF (250 mg, 4.30 mmol) and anhydrous K_2HPO_4 (749 mg, 4.30 mmol) to give approximately 1 g of material for milling. The jar was then closed and securely fitted to the mill which was set for 3 h at the frequency of 35 Hz. Upon completion, the jar was opened and the white powder (**X**) was collected and analysed by PXRD and NMR spectroscopy.

Rietveld refinement was carried out by Prof. M. Hayward.

Observed, calculated and difference plots from the structural refinement of phase **X** against X-ray powder diffraction data collected at room temperature:

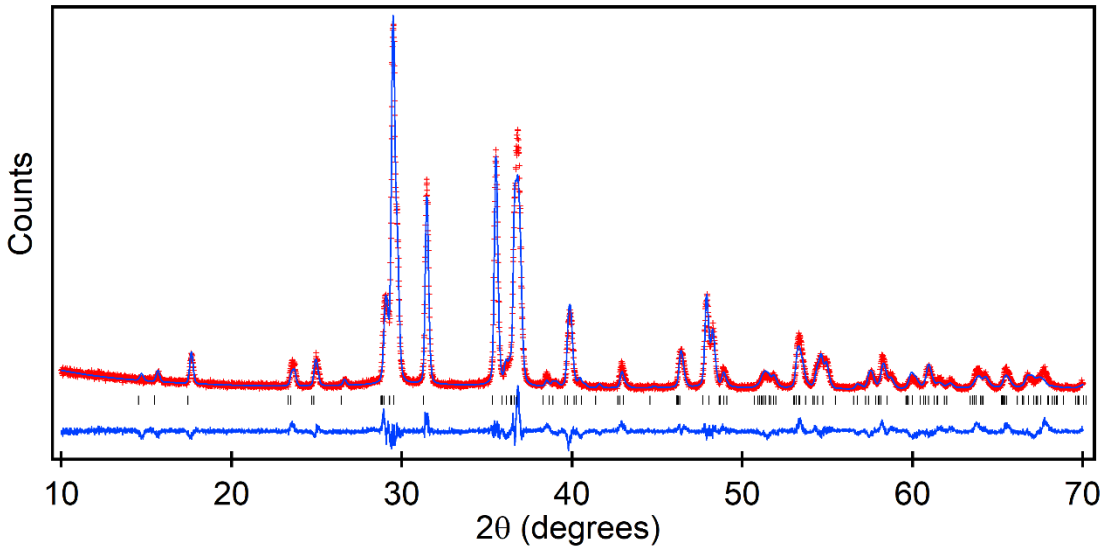

Proposed structure of phase **X** [$K_3(HPO_4)F$:

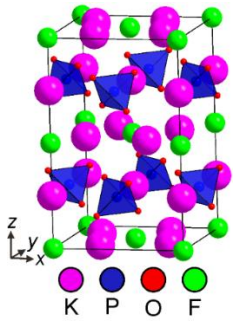

Structural parameters from the refinement of phase **X** against X-ray powder diffraction data collected at room temperature (calculated by Prof. M. Hayward):

Atom	site	*x*	*y*	*z*	B_{iso} (Å^2)
K(1)	4*a*	0	0	¼	0.84(2)
K(2)	4*a*	0.187(1)	0.686(1)	0	0.84(2)
K(3)	4*a*	0.293(1)	0.182(1)	0	0.84(2)
F(1)	4*a*	0	0	0	2.43(2)
P(1)	4*a*	0	½	¼	1.15(3)
O(1)	4*a*	0.157(2)	0.608(1)	0.667(1)	0.32(2)
O(2)	4*a*	0.357(2)	0.888(1)	0.174(1)	0.32(2)
O(3)	4*a*	0.549(2)	0.885(1)	0.358(1)	0.32(2)
O(4)	4*a*	0.346(2)	0.190(1)	0.306(1)	0.32(2)

$K_3(HPO_4)F$

space group: *I*1*c*1 (#9)

a = 7.1684(8) Å, *b* = 7.1989(8) Å, *c* = 11.438(1) Å, β = 90.586(3) °, volume = 590.2(1) Å^3

Radiation: Cu K_{α_1} λ = 1.5406 Å

R_{Bragg} = 6.18, Rp = 9.2%, wRp = 12.8 %

NMR (D_2O) spectroscopy data of **X** collected at room temperature:

To a sample of **X** (20 mg) was added 0.8 mL D_2O. The suspension was transferred to a 1 mL centrifuge tube. Centrifugation with an acceleration time of 120 seconds (13,500 rpm) (included in the overall centrifugation time) at 25 °C followed and the supernatant was analysed by NMR spectroscopy [73].

^{1}H NMR (500 MHz, D_2O) no signals observed

^{19}F NMR (471 MHz, D_2O) δ -121.98 (s, aq. F^-).

^{31}P NMR (203 MHz, D_2O) δ 2.71 (s, HPO_4^{2-}).

Solid-state NMR spectroscopy data of **X** (data acquired by Dr. C. Goult and J. Struijs):

^{1}H NMR (400 MHz, Solid) δ 11.2 (HPO_4^{2-}, X_H), 6.2 (H_2O, X_H).

^{19}F NMR (376 MHz, Solid) δ –128.9 (F^-, X_F), –129.6 (F^-, X_F), –132.1 (F^-, X_F), –134.7 (F^-, X_F), –135.4 (F^-, X_F).

^{31}P NMR (162 MHz, Solid) δ 5.0 (HPO_4^{2-}, X_P).

^{19}F DPMAS: D_1 = 67.5 s (T_1 = 1.4–12.8 s), ν_{rot} = 20 kHz (**X**) (* denotes spinning side bands)

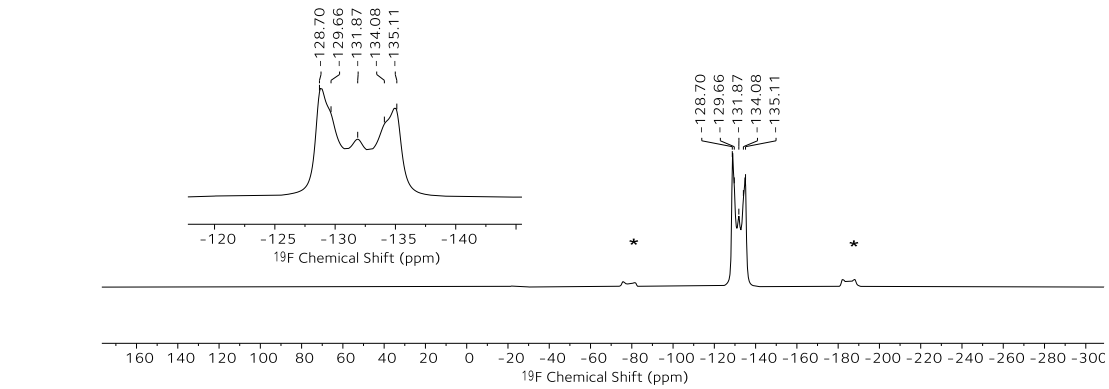

^{31}P {^{1}H} DPMAS: D_1 = 50 s (T_1 = 9.0 s), ν_{rot} = 20 kHz (**X**) (* denotes spinning side bands)

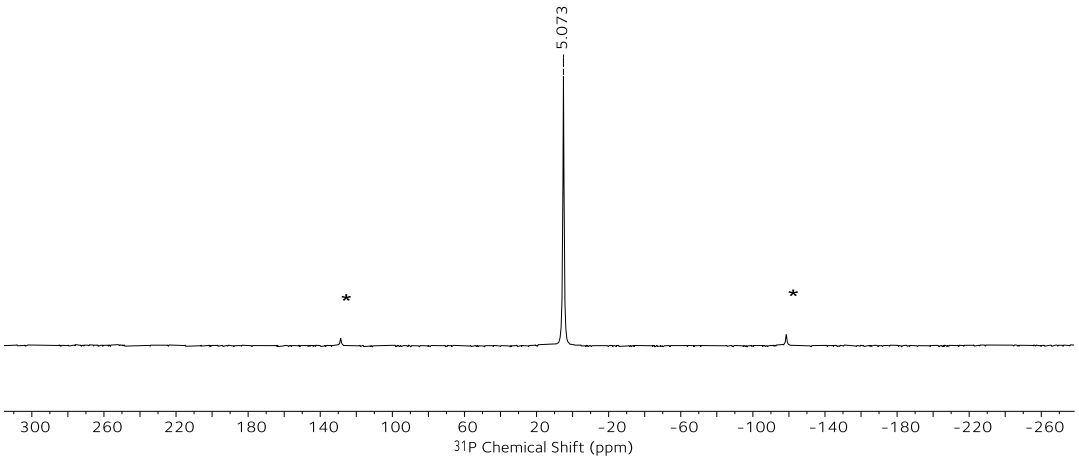

^{1}H ss NMR: D_1 = 20.0 s (T_1 = 27 s), ν_{rot} = 20 kHz (**X**) (* denotes spinning side bands)

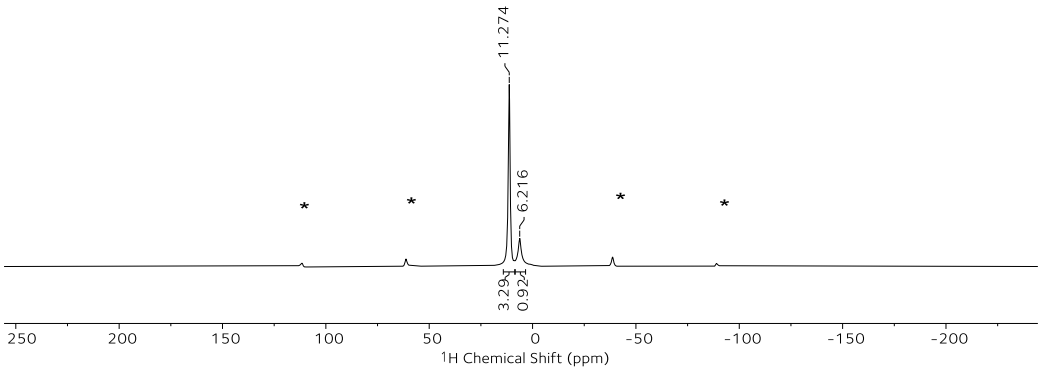

4.2.16 Characterisation of Y

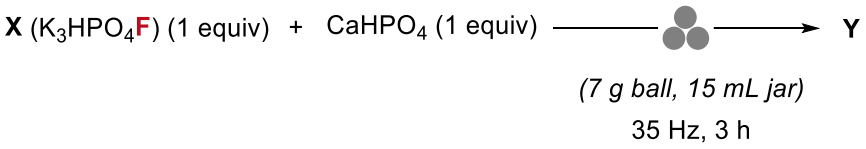

Y was prepared by ball milling **X** with anhydrous $CaHPO_4$. To a clean 15 mL stainless steel milling jar was added **X** (632 mg, prepared from an equimolar amount of KF and anhydrous K_2HPO_4, 2.72 mmol), anhydrous $CaHPO_4$ (370 mg, 2.72 mmol) and a stainless steel ball (7 g). The jar was then closed and securely fitted to the mill which was set for 3 h at the frequency of 35 Hz. Upon completion, the jar was opened and the white powder (**Y**) was collected and analysed by PXRD and NMR spectroscopy.

Rietveld refinement was carried out by Prof. M. Hayward.

Observed, calculated and difference plots from the structural refinement of phase **Y** against X-ray powder diffraction data collected at room temperature:

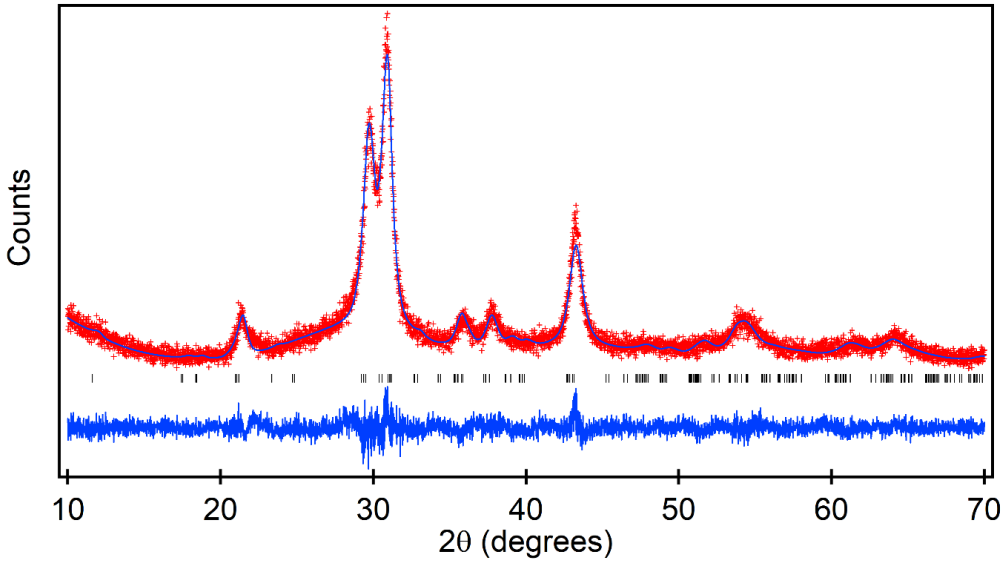

Proposed structure of phase **Y** ($K_{2-x}Ca_y(PO_3F)_a(PO_4)_b$) (crystalline phase):

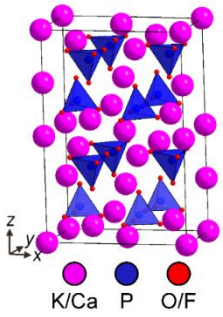

Structural parameters from the refinement of phase **Y** against X-ray powder diffraction data collected at room temperature (calculated by Prof. M. Hayward):

Atom	site	*x*	*y*	*z*	Fraction	B_{iso} (Å^2)
K/Ca(1)	8*f*	0.171(3)	½	0.414(1)	1	3.21(4)
K/Ca(2)	4*e*	0	0	¼	1	3.21(4)
K/Ca(3)	4*a*	0	0	0	0.82(3)	3.21(4)
P(1)	8*f*	0.157(6)	½	0.146(1)	1	3.18(3)
O/F(1)	8*f*	0.150(8)	0.499(10)	0.226(2)	1	3.42(3)
O/F (2)	8*f*	0.083(14)	0.748(18)	0.105(4)	1	3.42(3)
O/F (3)	8*f*	0.069(11)	0.179(16)	0.093(4)	1	3.42(3)
O/F (4)	8*f*	0.322(7)	0.482(27)	0.114(3)	1	3.42(3)

$K_xCa_y(PO_4)_a(PO_3F)_b$

space group: *C* 2/*c* (#15)

a = 10.105(9) Å, *b* = 5.851(3) Å, *c* = 15.155(3) Å, β = 90.155(3) °, volume = 896.2(10) Å^3

Radiation: Cu $K_{\alpha 1}$ λ = 1.5406 Å

R_{Bragg} = 4.25, Rp = 6.1%, wRp = 8.2 %

NMR (D_2O) spectroscopy data of **Y** collected at room temperature:

To a sample of **Y** (20 mg) was added 0.8 mL D_2O. The suspension was transferred to a 1 mL centrifuge tube. Centrifugation with an acceleration time of 120 seconds (13,500 rpm) (included in the overall centrifugation time) at 25 °C followed and the supernatant was analysed by NMR spectroscopy [73].

^{1}H NMR (500 MHz, D_2O) no signals observed

^{19}F NMR (471 MHz, D_2O) δ -73.91 (d, $^1J_{P-F}$ = 864.6 Hz, PO_3F^{2-}), -122.21 (s, aq. F^-)

^{31}P NMR (203 MHz, D_2O) δ 2.34 (s), 1.04 (d, $^1J_{P-F}$ = 864.6 Hz, PO_3F^{2-}).

Solid-state NMR spectroscopy data of the solid prepared from ball milling KF, K_2HPO_4 and $CaHPO_4$ (which contains the crystalline phase of **Y**) was recorded.

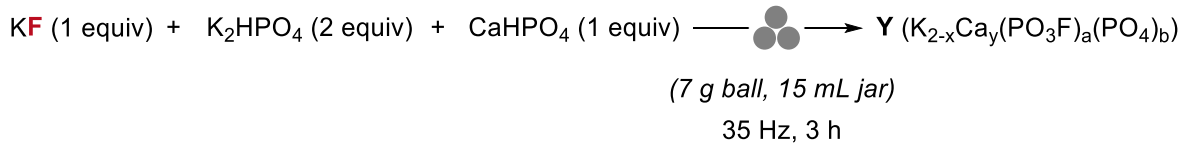

To a clean 15 mL stainless steel milling jar was added KF (116 mg, 2.00 mmol), anhydrous K_2HPO_4 (697 mg, 4.00 mmol) and anhydrous $CaHPO_4$ (272 mg, 2.00 mmol) and a stainless steel ball (7 g). The jar was then closed and securely fitted to the mill which was set for 3 h at the frequency of 35 Hz.

PXRD of resultant solid:

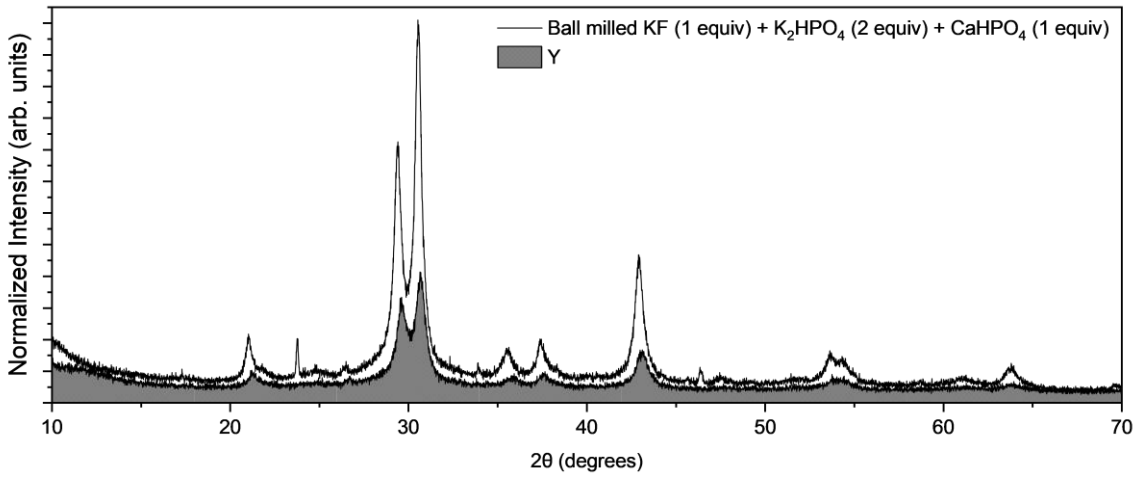

^{19}F Solid-state NMR of resultant solid (data acquired by J. Struijs):

^{19}F NMR (376 MHz, Solid) δ -71.98 (PO_3F^{2-}), -115.52 (F^-), -131.65 (KF).

^{19}F DPMAS: D_1 = 10 s ν_{rot} = 20 kHz (* denotes spinning side bands)

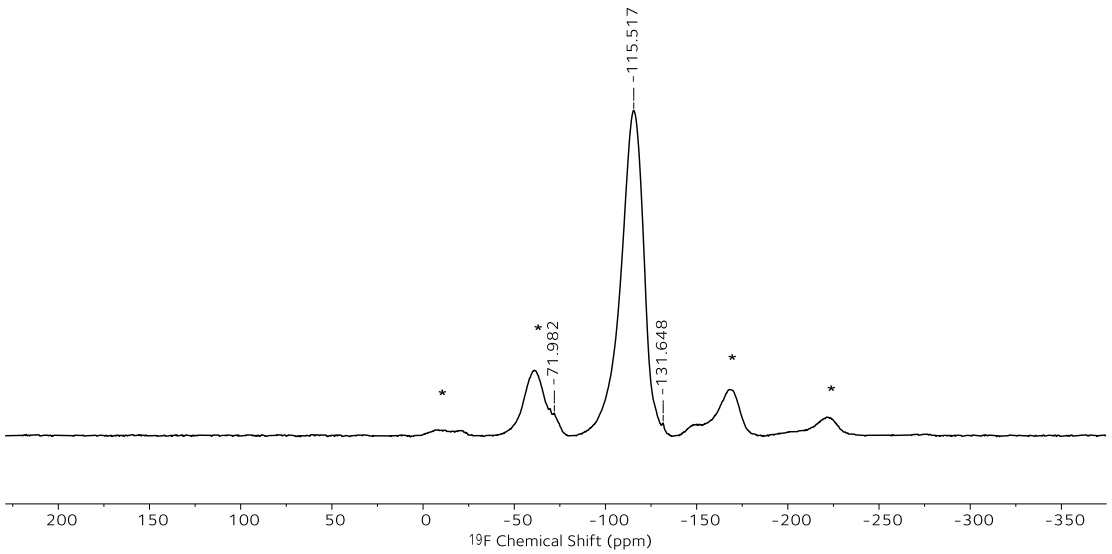

4.2.17 Characterisation of Z

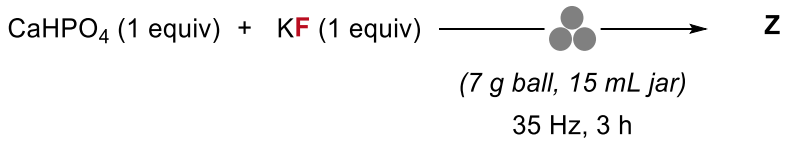

An equimolar amount of anhydrous KF with anhydrous $CaHPO_4$ was ball milled to afford an amorphous phase (**Z**). To a 15 mL stainless steel milling jar was added a stainless steel ball (7 g), anhydrous KF (299 mg, 5.15 mmol) and anhydrous $CaHPO_4$ (700 mg, 5.15 mmol) to give approximately 1 g of material for milling. The jar was then closed and securely fitted to the mill which was set for 3 h at the frequency of 35 Hz.

X-ray powder diffraction data of **Z** collected at room temperature:

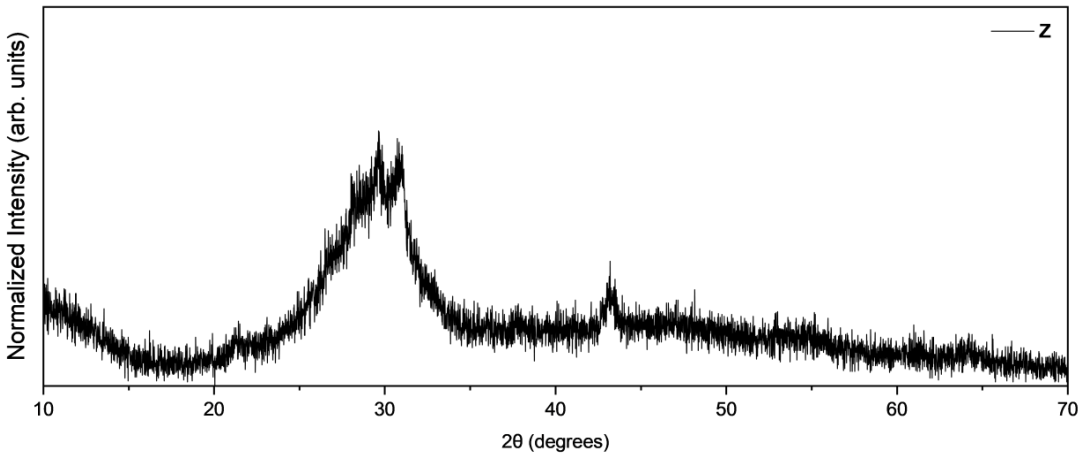

NMR (D_2O) spectroscopy data of **Z** collected at room temperature:

To a sample of $\mathbf{Z_{(KCa)}}$ (20 mg) was added 0.8 mL D_2O. The suspension was transferred to a 1 mL centrifuge tube. Centrifugation with an acceleration time of 120 seconds (13,500 rpm) (included in the overall centrifugation time) at 25 °C followed and the supernatant was analysed by NMR spectroscopy [73].

^{1}H NMR (500 MHz, D_2O) no signals observed

^{19}F NMR (471 MHz, D_2O) δ -73.96 (d, $^1J_{P-F}$ = 866.9 Hz, PO_3F^{2-}), -122.19 (s, aq. F^-).

^{31}P NMR (203 MHz, D_2O) δ 1.73 (s), 1.00 (d, $^1J_{P-F}$ = 866.4 Hz, PO_3F^{2-}).

Solid-state NMR spectroscopy data of **Z** (data acquired by Dr. C. Goult):

^{1}H NMR (400 MHz, Solid) δ 26.24 – -16.75 (m), 6.84 (H_2O)

^{19}F NMR (376 MHz, Solid) δ -103.10 (F^-), -132.08 (KF).

^{31}P NMR (162 MHz, Solid) δ -1.32 (HPO_4^{2-}).

^{19}F DPMAS: D_1 = 10 s ν_{rot} = 20 kHz (**Z**) (* denotes spinning side bands)

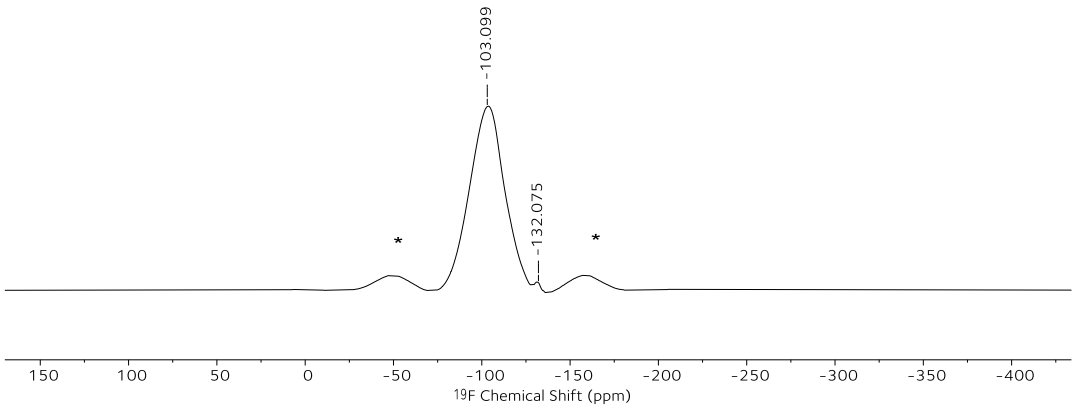

^{31}P DPMAS: D_1 = 2.6 s ν_{rot} = 13 kHz (**Z**) (* denotes spinning side bands)

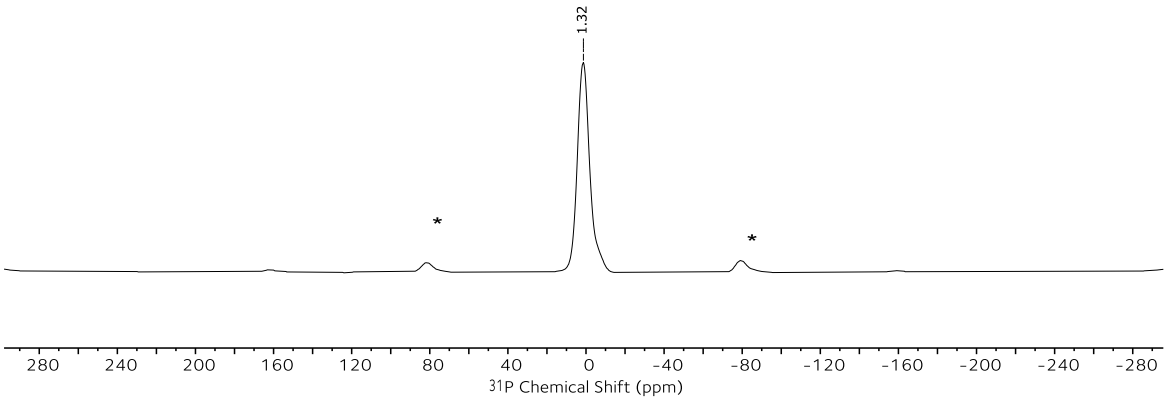

^{1}H DPMAS: D_1 = 5 s ν_{rot} = 20 kHz (**Z**)

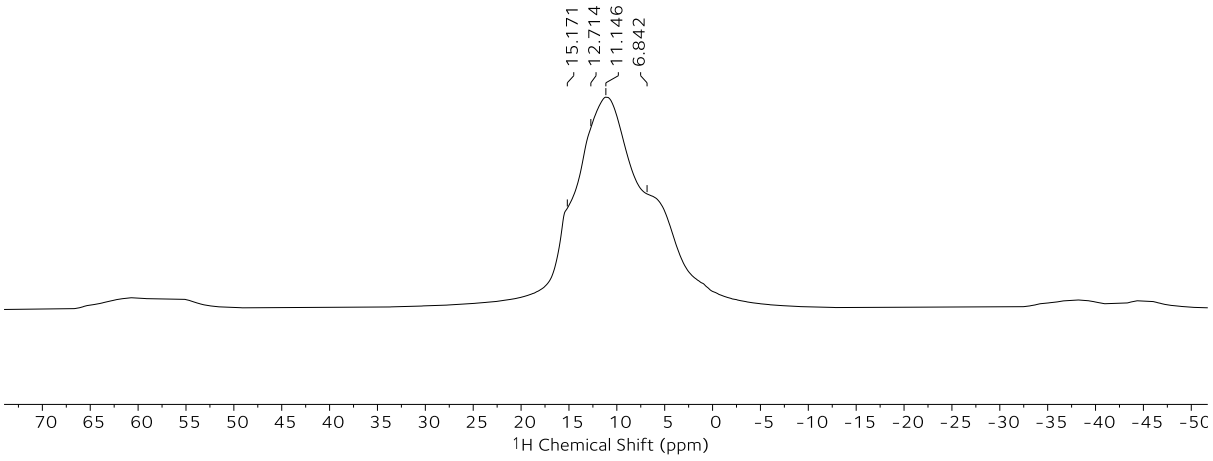

4.2.18 Characterisation of Z'

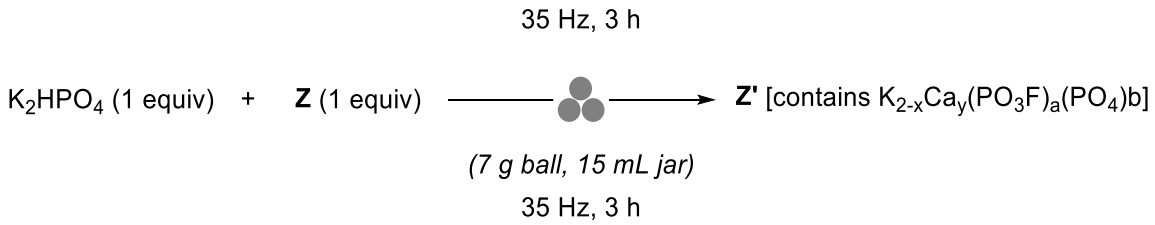

Z' was prepared by ball milling **Z** with anhydrous K_2HPO_4. To a 15 mL stainless steel milling jar was added a stainless steel ball (7 g), **Z** (528 mg, prepared from an equimolar amount of KF and $CaHPO_4$, 2.72 mmol) and anhydrous K_2HPO_4 (474 mg, 2.72 mmol) to give approximately 1 g of material for milling. The jar was then closed and securely fitted to the mill which was set for 3 h at the frequency of 35 Hz.

Rietveld refinement was carried out by Prof. M. Hayward.

Observed, calculated and difference plots from the structural refinement of phase **Z'** against X-ray powder diffraction data collected at room temperature:

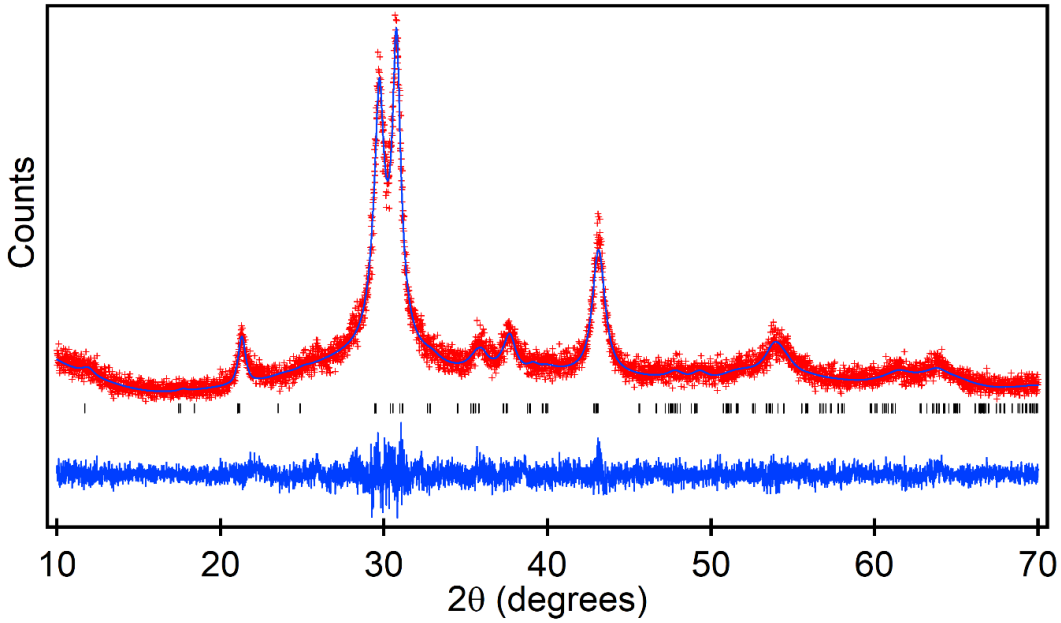

Structural parameters from the refinement of phase **Z'** against X-ray powder diffraction data collected at room temperature (calculated by Prof. M. Hayward):

Atom	site	*x*	*y*	*z*	Fraction	B_{iso} (Å^2)
K/Ca(1)	8*f*	0.177(6)	½	0.419(5)	1	3.71(6)
K/Ca(2)	4*e*	0	0	¼	1	3.71(6)
K/Ca(3)	4*a*	0	0	0	0.78(4)	3.71(6)
P(1)	8*f*	0.157(6)	½	0.160(5)	1	3.36(9)
O/F(1)	8*f*	0.148(12)	0.502(11)	0.224(8)	1	3.31(16)
O/F (2)	8*f*	0.081(12)	0.753(16)	0.109(9)	1	3.31(16)
O/F (3)	8*f*	0.061(14)	0.184(14)	0.098(7)	1	3.31(16)
O/F (4)	8*f*	0.316(10)	0.487(24)	0.116(8)	1	3.31(16)

$K_xCa_y(PO_4)_a(PO_3F)_b$

space group: *C* 2/*c* (#15)

a = 10.107(22) Å, *b* = 5.880(10) Å, *c* = 15.115(28) Å,
β = 90.12(12) °, volume = 898.3(30) Å^3

Radiation: Cu $K_{\alpha 1}$ λ = 1.5406 Å

R_{Bragg} = 1.06, Rp = 8.89%, wRp = 11.7 %

NMR (D_2O) spectroscopy data of **Y** collected at room temperature:

To a sample of **Y** (20 mg) was added 0.8 mL D_2O. The suspension was transferred to a 1 mL centrifuge tube. Centrifugation with an acceleration time of 120 seconds (13,500 rpm) (included in the overall centrifugation time) at 25 °C followed and the supernatant was analysed by NMR spectroscopy.

^{1}H NMR (500 MHz, D_2O) no signals observed

^{19}F NMR (471 MHz, D_2O) δ -73.86 (d, $^1J_{P-F}$ = 865.2 Hz, PO_3F^{2-}), -121.98 (s, aq. F^-).

^{31}P NMR (203 MHz, D_2O) δ 2.38 (s), 1.06 (d, $^1J_{P-F}$ = 865.2 Hz, PO_3F^{2-}).

4.2.19 Reactivity of X, Y, Y', Z, Z' compared to Fmix and KF

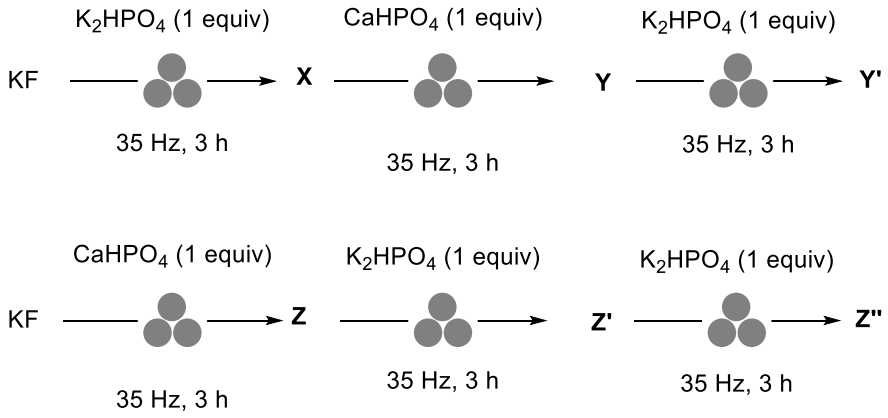

Compounds **X**, **Y**, **Z** and **Z'** were prepared as described above.

Y' was prepared by ball milling **Y** with anhydrous K_2HPO_4. To a 15 mL stainless steel milling jar was added a stainless steel ball (7 g), **Y** (682 mg, prepared from an equimolar amount of KF, K_2HPO_4 and $CaHPO_4$, 1.85 mmol) and K_2HPO_4 (322 mg, 1.85 mmol) to give approximately 1 g of material for milling. The jar was then closed and securely fitted to the mill which was set for 3 h at the frequency of 35 Hz.

Z'' was prepared in an analogous manner, by ball milling **Z'** (682 mg, prepared from an equimolar amount of KF, $CaHPO_4$ and K_2HPO_4, 1.85 mmol) and K_2HPO_4 (322 mg, 1.85 mmol) at 35 Hz for 3 h.

The reactivity of **X**, **Y**, **Y'**, **Z**, **Z'**, **Z''** and KF was tested in the fluorination of 4-toluenesulfonyl chloride in solution and compared to the reactivity of **Fmix**.

To a glass reaction vessel was added 4-toluenesulfonyl chloride (0.125 mmol, 1.0 equiv), the fluorinating reagent (**X**, **Y**, **Y'**, **Z**, **Z'** **Fluoromix** or **KF**) (0.5 equiv or 1.0 equiv respect to fluoride, e.g.)* and anhydrous *t*BuOH (0.25 M). H_2O (4.5 µL, 2 equiv) was added to the reaction mixture. After stirring for 5 h at the 100 °C, the resulting suspension was cooled to room temperature, the crude reaction mixture was passed through a plug of silica eluting with EtOAc, concentrated *in vacuo,* and 4-fluoroanisole (10 µL, 11.1 mg, 88.3 µmol) was added as an internal standard. An aliquot was then diluted in deuterated chloroform. Reaction yield/conversion was determined by quantitative ^{1}H and ^{19}F NMR spectroscopy.

*0.5 equiv of **Fluoromix** contains 0.125 mmol of fluoride. 1.0 equiv of **KF**, $\mathbf{X_{(K)}}$ and $\mathbf{Y_{(KCa)}}$ contains 0.125 mmol of fluoride.

Reactions using KF, **Fmix**, **X** and **Y** were run in triplicate. Reported TsCl and TsF(**1**) % presented in the graph below are an average of 3 runs.

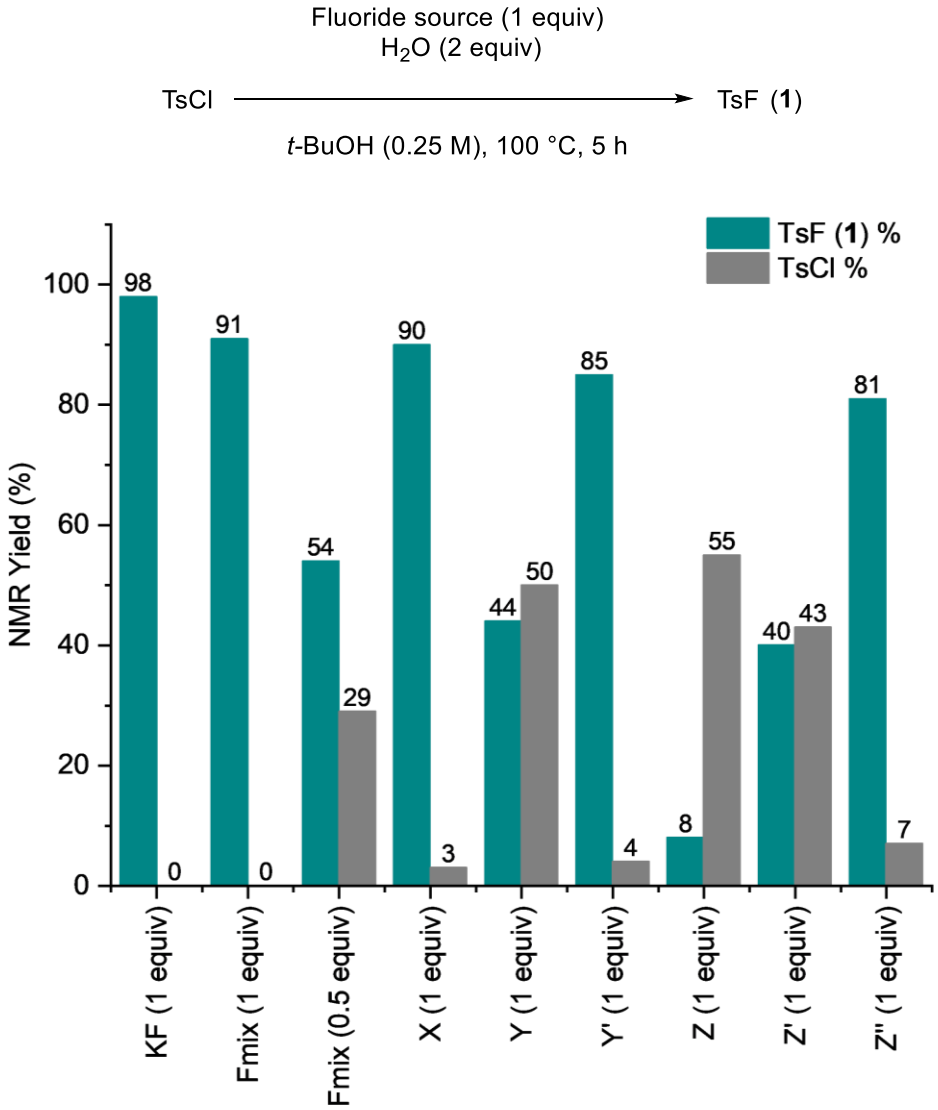

4.2.20 Observation of apatite

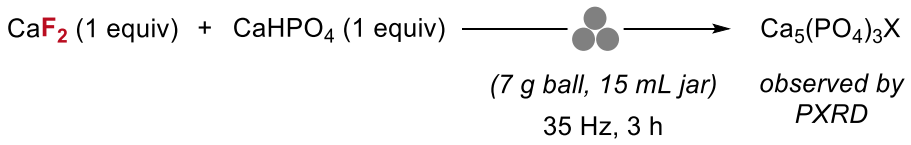

To a 15 mL stainless steel milling jar was added a stainless steel ball (7 g), CaF_2 (363 mg, 4.65 mmol) and anhydrous $CaHPO_4$ (633 mg, 4.65 mmol) to give approximately 1 g of material for milling. The jar was then closed and securely fitted to the mill which was set for 3 h at the frequency of 35 Hz. The resultant powder was insoluble in water and characterised by PXRD. The solid contains an apatite phase [$Ca_5(PO_4)_3X$ where X = F or OH] and CaF_2.

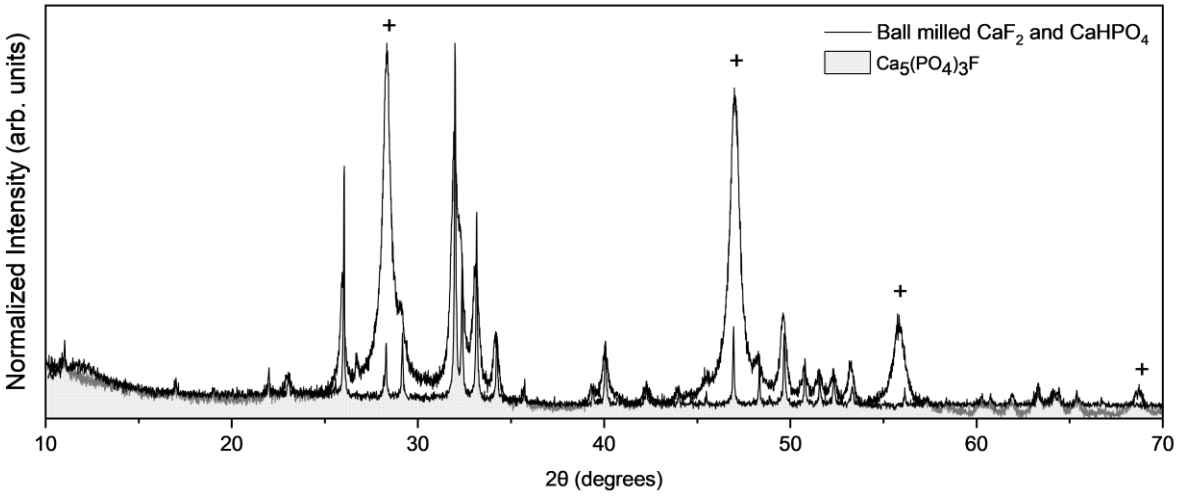

4.2.21 Mechanochemical reaction between KF and $CaHPO_4$

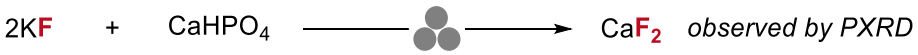

(7 g ball, 15 mL jar)

35 Hz, 3 h

To a 15 mL stainless steel milling jar was added a stainless steel ball (7 g), KF (465 mg, 8.00 mmol) and anhydrous $CaHPO_4$ (544 mg, 4.00 mmol) to give approximately 1 g of material for milling. The jar was then closed and securely fitted to the mill which was set for 3 h at the frequency of 35 Hz. The resultant powder characterised by PXRD. The resultant powder contains CaF_2 and an unidentified crystalline phase.

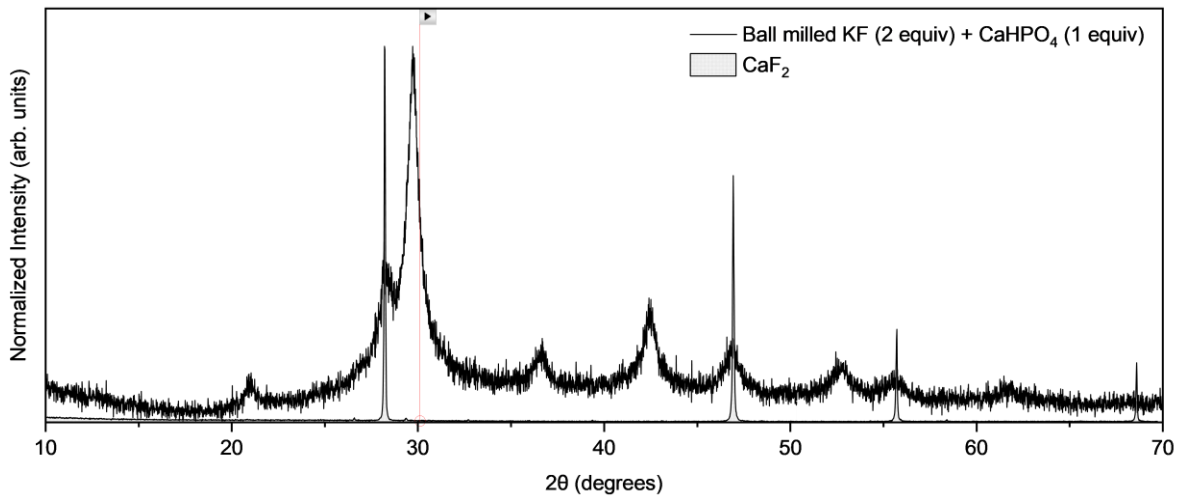

4.2.22 Thermal reaction between CaF_2 and K_2HPO_4

The reaction between CaF_2 and anhydrous K_2HPO_4 was examined by a high-temperature ceramic synthesis method. Acid grade fluorspar (309 mg, 3.96 mmol) and anhydrous K_2HPO_4 (690 mg, 3.96 mmol) were weighed, ground and calcined in air at 200 °C for 1 h (using a ceramic crucible). The white powder was then reground and heated at 500 °C for 1 h. The resultant powder was analysed by PXRD and only Bragg peaks corresponding to CaF_2 (+) and $K_4P_2O_7$ were observed.

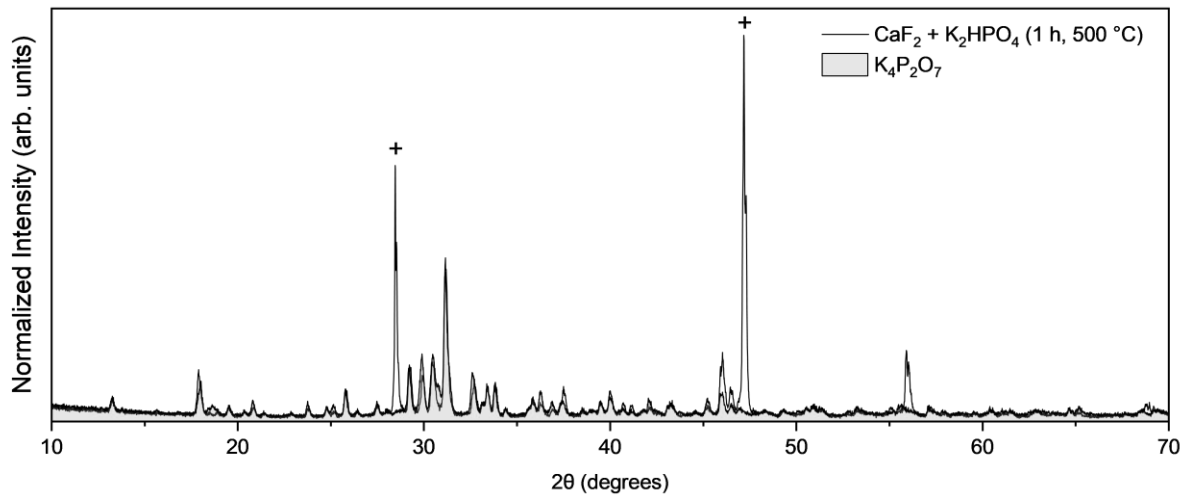

4.2.23 Scale up preparation of Fmix and application

To prepare powder **A** (1:1 ratio of fluorspar:K_2HPO_4), acid grade fluorspar (1.86 g, 23.82 mmol), K_2HPO_4 (4.15 g, 23.82 mmol) and a stainless steel ball (16 g) were added to a 35 mL stainless steel-milling jar to give approximately 6 g of material for milling. The jar was closed and securely fitted to the mill which was set for 3 h at the frequency of 35 Hz. Upon completion, the jar was opened and the white powder **A** was collected.

To prepare powder **B** (1:2 ratio of fluorspar: K_2HPO_4), powder **A** (3.55 g, contains 14.08 mmol acid grade fluorspar and 14.08 mmol K_2HPO_4), K_2HPO_4 (2.45 g, 14.08 mmol) and one stainless steel ball (16 g) were added to a 35 mL stainless steel milling jar to give approximately 6 g of material for milling. The jar was closed and securely fitted to the mill which was set for 3 h at the frequency of 35 Hz. Upon completion, the jar was opened and the white powder **B** was collected.

To prepare powder **C** (**Fmix**) (1:2.5 ratio of fluorspar: K_2HPO_4), powder **B** (4.99 g, contains 11.7 mmol acid grade fluorspar and 23.4 mmol K_2HPO_4), K_2HPO_4 (1.02 g, 5.85 mmol) and a stainless steel ball (6 g) were added to a 35 mL stainless steel milling jar to give approximately 6 g of material for milling. The jar was closed and securely fitted to the mill which was set for 3 h at the frequency of 35 Hz. Upon completion, the jar was opened and 21.45 g of the white powder **C** (**Fmix**) was collected.

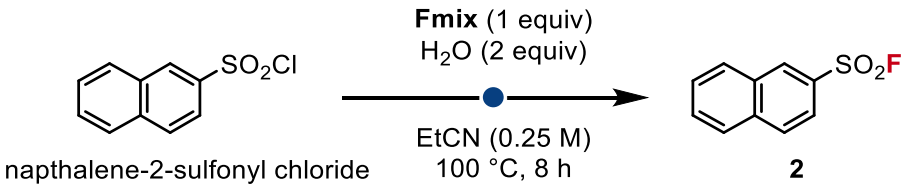

To a 250 mL glass round bottom flask equipped with a 15 g PTFE magnetic stir bar (3.5 cm) was added 11.32 g (1 equiv) of **Fmix** (powder **C**), naphthalene-2-sulfonyl chloride (5 g, 22.05 mmol, 1 equiv) and EtCN (88.2 mL). H_2O (0.8 mL, 44.1 mmol) was then added to the reaction mixture which was stirred at 100 °C. After 8 h, an aliquot (10 µL) of the reaction mixture was analysed by GC-MS which confirmed complete consumption of the starting material. The resulting suspension was cooled to room temperature and filtered over celite (washing with EtOAc). The filtrate was concentrated *in vacuo* to give solely naphthalene-2-sulfonyl fluoride (**2**) as a pale-yellow solid (1.90 g, 9.04 mmol, 41%).

Full characterisation data can be found in Section 4.2.6.

PXRD of scaled up **Fmix:**

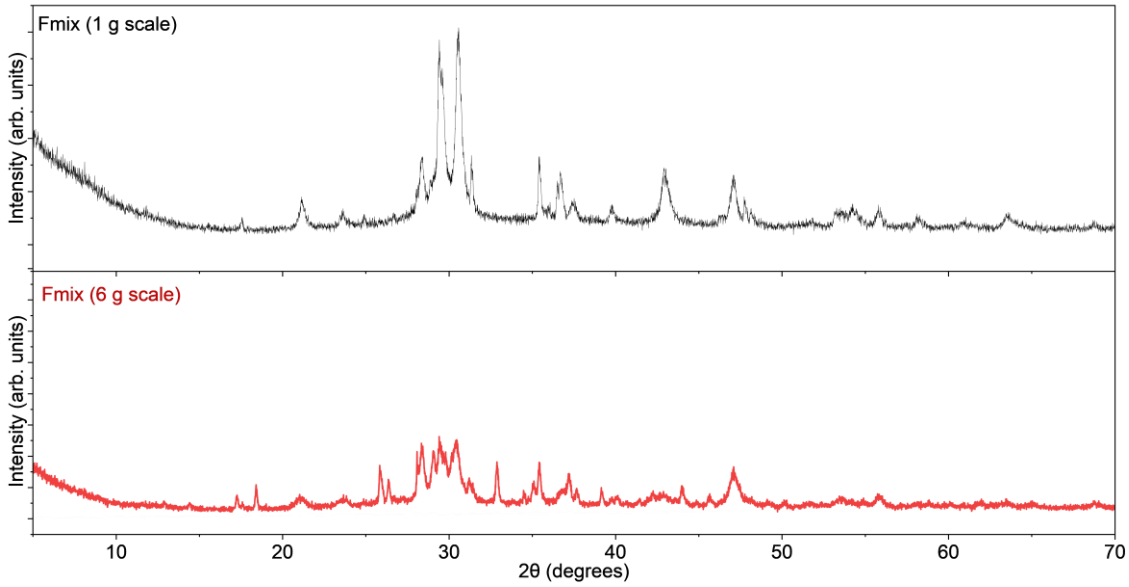

Unlike the Fmix prepared on 1 g scale (15 mL stainless steel jar, 7 g stainless steel ball), unreacted K_2HPO_4 is still present in the Fmix prepared on 6 g (30 mL stainless steel jar, 16 g stainless steel ball).

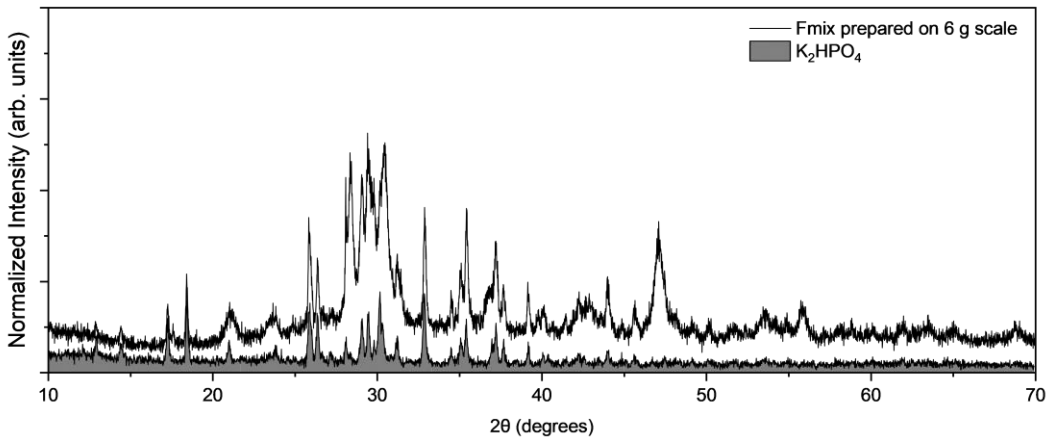

4.2.24 Synthesis of K_2PO_3F and $CaPO_3F{\cdot}2H_2O$

K_2PO_3F was prepared by ball milling an equimolar amount of anhydrous KF with potassium metaphosphate (98% KPO_3, STREM CHEMICALS). To a 15 mL stainless steel milling jar was added a stainless steel ball (7 g), anhydrous KF (332 mg, 5.70 mmol) and KPO_3 (672 mg, 5.70 mmol) to give approximately 1 g of material for milling. The jar was then closed and securely fitted to the mill which was set for 3 h at the frequency of 35 Hz. Upon completion, the jar was opened and the white powder was collected and analysed by PXRD. K_2PO_3F was formed as the sole crystalline product.

$CaPO_3F{\cdot}2H_2O$ was synthesised by a precipitation reaction at 40 °C. A solution of anhydrous calcium chloride (1 M) was added to a sodium monofluorophosphate containing solution (1 M) in a drop-wise manner with stirring at 40 °C. Immediate precipitation is observed. The solid is filtered and washed with water (15 mL), before allowing to dry at room temperature overnight. The resultant powder was collected and analysed by PXRD. $CaPO_3F$ dihydrate was formed as the sole crystalline product.

4.2.25 Synthesis of $KCaF_3$

$KCaF_3$ was prepared by ball milling an equimolar amount of anhydrous KF with calcium fluoride (CaF_2, ≥ 97.0%, Alfa Aesar). To a 15 mL stainless steel milling jar was added a stainless steel ball (7 g), anhydrous KF (586 mg, 7.50 mmol) and CaF_2 (436 mg, 7.50 mmol) to give approximately 1 g of material for milling. The jar was then closed and securely fitted to the mill which was set for 3 h at the frequency of 35 Hz. Upon completion, the jar was opened and the white powder was collected and analysed by PXRD. The resultant solid contained crystalline CaF_2 and $KCaF_3$, no crystalline forms of KF were observed.

Alternatively, **$KCaF_3$** was prepared by a high-temperature ceramic synthesis method. Anhydrous KF (586 mg, 7.50 mmol) and CaF_2 (436 mg, 7.50 mmol) were weighed, ground and calcined in air at 200 °C for 1 h (using a ceramic crucible). The white powder was then reground and heated at 520 °C for 1 h. The white powder was analysed by PXRD and only Bragg peaks corresponding to $KCaF_3$ were observed.

4.3 Low-Temperature Activation of Fluorspar in Water via Brønsted and Lewis Acid Cooperativity

The experimental section for this work has been partially disclosed in the Supplementary Information of: I. Klose, C. Patel, A. Mondal, A. Schwarz, G. Pupo, V. Gouverneur, Fluorspar to fluorochemicals upon low-temperature activation in water. *Nature* (accepted 2024).

HBF_4 synthesis (including optimisation) and all Balz-Schiemann fluorination was conducted by Dr. A. Mondal and experimental data can be found in the supplementary information of the published manuscript on this work.

4.3.1 Brønsted acid evaluation for CaF_2 activation

This work was completed in collaboration with Dr. A. Mondal and Dr. I. Klose.

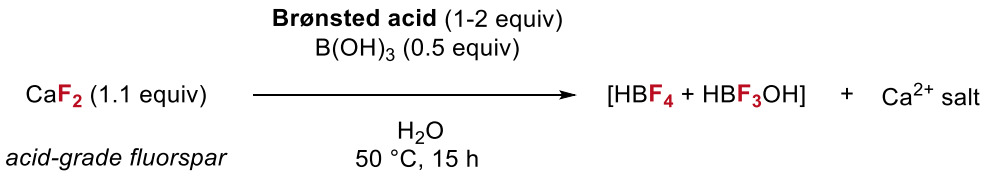

To a 15 mL conical sterile polypropylene (PP) tube was added acid grade fluorspar (344 mg, 4.40 mmol, 1.1 equiv.), $B(OH)_3$ (124 mg, 2.0 mmol, 0.5 equiv), acid activator (8.0 mmol, 2.0 equiv. for 'mono-acids', 4.0 mmol, 1.0 equiv. for 'di- and oligo-acids') and H_2O (1 mL). The tubes were capped. Each reaction was stirred at 50 °C for 15 h. The suspension was allowed to settle and the total amount of HBF_4 and HBF_3OH was assessed by quantitative ^{19}F NMR spectroscopy (D_2O) using sodium triflate (NaOTf) as internal standard.

	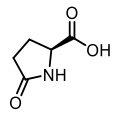	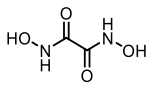	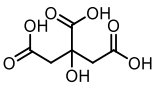	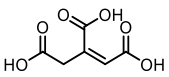	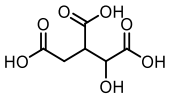
	L-pyroglutamic acid	oxalylhydroxamic acid	citric acid	*cis*-aconitic acid	isocitric acid
$[HBF_4 + HBF_3OH]$	0% + 1%	0%	3% + 1%	0% + 1%	0% + 1%
pK_a	3.5	9.0	3.1, 4.7	3.8, 5.6	3.4, 4.6
	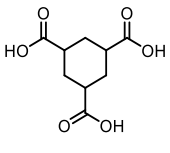	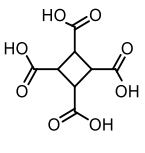	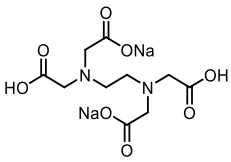	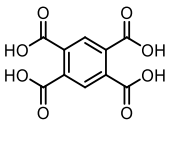	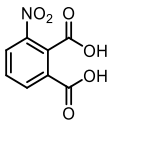
	1,3,5-cyclohexane-tricarboxylic acid	1,2,3,4-cyclobutanetetra-carboxylic acid	disodium ethylenediamine -tetraacetic acid	pyromellitic acid	3-nitrophthalic acid
$[HBF_4 + HBF_3OH]$	0%	2% + 1%	0%	8% + 5%	0% + 1%
pK_a	4.0, 6.0	1.8, 4.4	6.2, 10.2	1.9, 2.9	1.9

	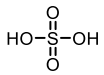	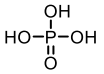
	sulfuric acid	phosphoric acid
$[HBF_4 + HBF_3OH]$	49% + 20%	0% + 4%
pK_a	-2.8, 2	2.1, 7.2

	HO_4Cl	HCl	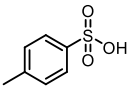		
	perchloric acid	hydrochloric acid	tosic acid	methanesulfonic acid	trifluoroacetic acid
$[HBF_4 + HBF_3OH]$	26% + 13%	40% + 20%	18% + 10%	38% + 27%	0%
pK_a	-15.0	-6.2	-2.8	-1.9	-0.3
	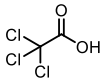				
	trichloroacetic acid	difluoroacetic acid	propiolic acid	lactic acid	pyruvic acid
$[HBF_4 + HBF_3OH]$	8% + 1%	3% + 2%	2% + 0%	2% + 2%	0%
pK_a	0.7	1.3	1.9	2.5	2.5
	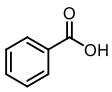	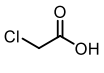	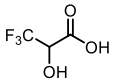	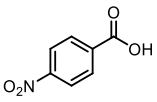	
	benzoic acid	chloroacetic acid	trifluorolactic acid	4-nitrobenzoic acid	2,2-dihydroxyacetic acid
$[HBF_4 + HBF_3OH]$	0%	0%	0%	0%	4% + 2%
pK_a	2.5	2.9	2.9	2.9	3.2
	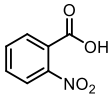	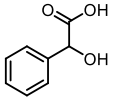	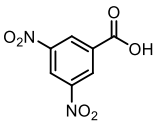		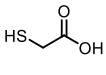
	2-nitrobenzoic acid	mandelic acid	3,5-nitrobenzoic acid	thioacetic acid	mercaptoacetic acid
$[HBF_4 + HBF_3OH]$	0%	3% + 4%	0%	0%	1% + 0%
pK_a	3.2	3.4	3.4	3.4	3.8
		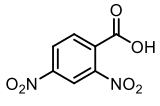	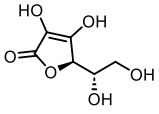	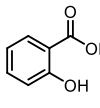	
	formic acid	2,4-nitrobenzoic acid	ascorbic acid	salicyclic acid	acetic acid
$[HBF_4 + HBF_3OH]$	1% + 0%	1% + 0%	1% + 0%	0%	0%
pK_a	3.7	3.9	4.2	4.2	4.7

	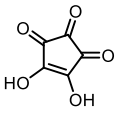	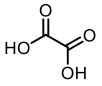	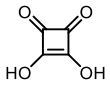	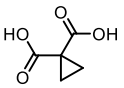	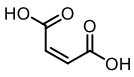
	croconic acid	oxalic acid	squaric acid	cyclopropyl malonic acid	*(Z)*-butenedioic acid
$[HBF_4 + HBF_3OH]$	36% + 11%	76% + 20%	18% + 9%	5 % + 6%	2% + 2%
pK_a	0.8, 2.2	1.3, 4.1	1.5, 3.4	1.8, 4.0	1.9, 6.0
	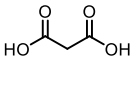	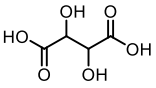	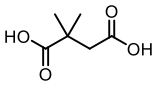	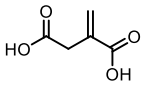	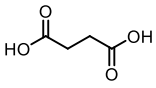
	malonic acid	tartaric acid	2,2-dimethylsuccinic acid	2-methylenesuccinic acid	succinic acid
$[HBF_4 + HBF_3OH]$	1% + 1%	1% + 1%	0%	0%	0%
pK_a	2.9, 5.7	3.0, 4.3	4.1, 5.4	3.8, 5.6	4.2, 5.6
	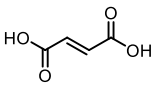	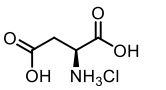	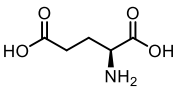	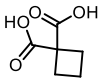	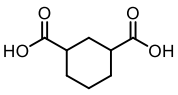
	E-butenedioic acid	L-aspartic acid HCl	L-Aspartic acid	cyclobutane-1,1-dicarboxylic acid	cyclohexane-1,3-dicarboxylic acid
$[HBF_4 + HBF_3OH]$	0%	0% + 1%	0%	0% + 1%	0%
pK_a	3.0, 4.4	2.0, 3.9	4.3, 10.0	3.1, 5.9	4.3, 6.0

^{19}F quantitative NMR (D_2O) of crude reaction mixture of acid grade fluorspar (CaF_2), H_2Ox and $B(OH)_3$ (2.0 mmol). HBF_4 (-150.3 ppm), HBF_3OH (-145.6 ppm) and trace $HOxBF_2$ (-152.4 ppm) produced. 0.13 mmol of NaOTf used as internal standard (-78.9 ppm). ^{19}F NMR Yields of HBF_4 and HBF_3OH are 76% and 20%, respectively.[74]

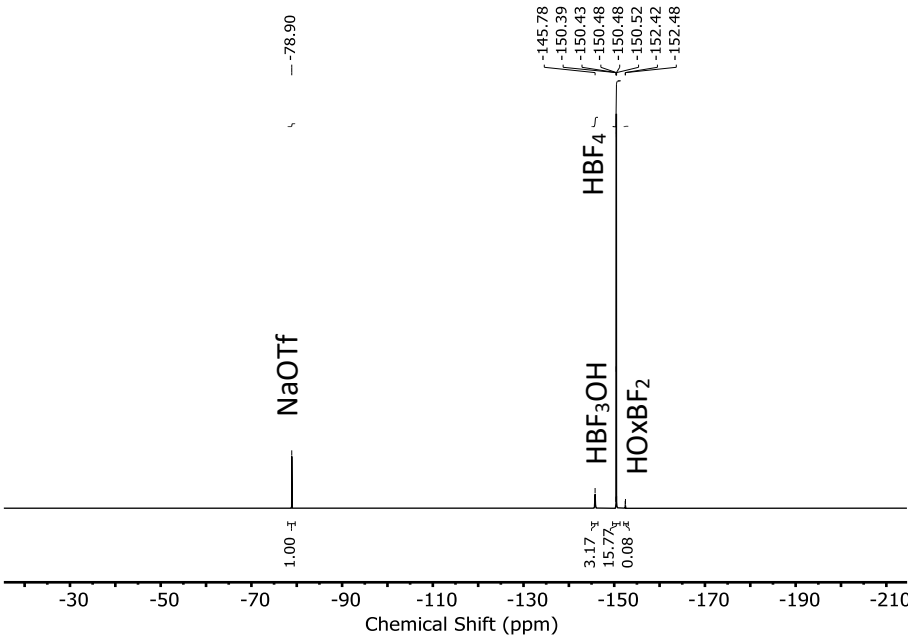

4.3.2 Reaction monitoring and characterisation

CAUTION! HF is a corrosive and toxic substance that will corrode glassware. Safe handling can be conducted with plastic syringes and metal needles, with KOH (aq.) employed to quench excess HF. Always handle HF while wearing gloves and in a fume hood. As a precautionary measure, have calcium gluconate gel nearby and apply immediately and liberally on skin exposed to HF. The following reactions were conducted in polypropylene vessels or directly in Teflon NMR thin wall (5 mm) liners.

HF limit of detection

To evaluate the threshold at which sensitivity limits the capability of NMR to detect HF, a series of experiments were undertaken to determine the limit of detection (LOD) of HF in H_2O:D_2O 90%:10% at (470 MHz, 32 scans, d1 = 50 s). A series of samples were created with concentrations of HF (48% aq. HF) ranging from 0.005 M to 0.5 M. Signals for HF within the range of -152.2 to -159.9 ppm are observed across all concentrations measured.[75] For integration errors < 1%, a signal-to-noise ratio (SNR) ≥150 is acceptable [45]. SNR was calculated from the spectra using an MNova software tool.[76]

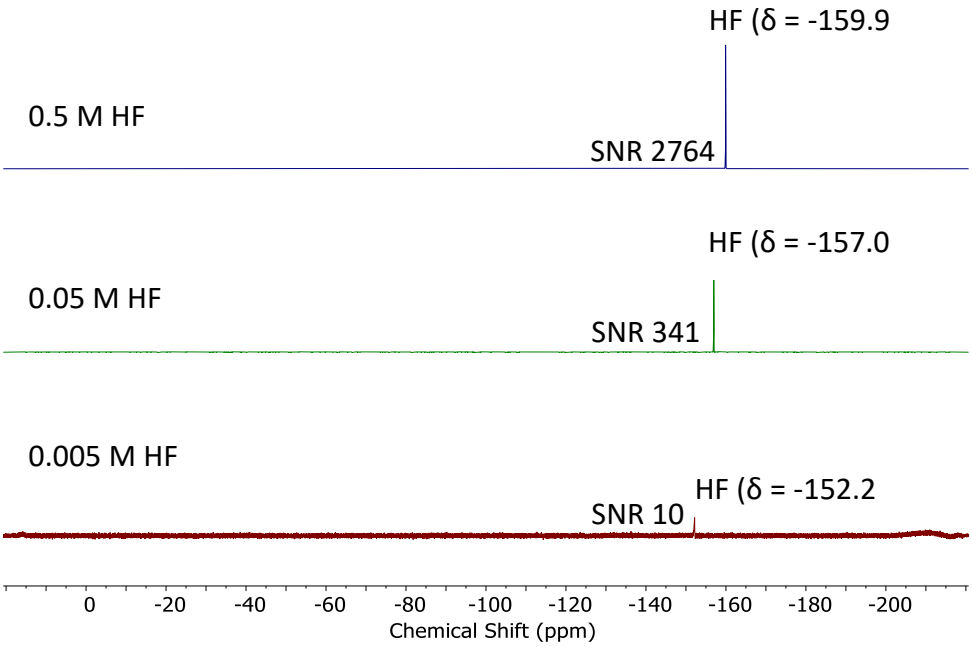

Reaction monitoring in absence of Lewis acid

The reaction between acid grade fluorspar (CaF_2, > 97.0%, Minersa Group) with anhydrous oxalic acid in D_2O was monitored at 50 °C over a period 8 h. Into a Teflon NMR thin wall (5 mm) liner was added acid grade fluorspar (97% CaF_2, 40 mg, 0.5 mmol, 1.1 equiv), anhydrous oxalic acid (41 mg, 0.45 mmol, 1.0 equiv), sodium triflate (10 mg) and D_2O (0.5 mL). The Teflon liner was plugged tightly with a Teflon cap and inserted through a custom-built holder (filled with ice) and then placed an ultrasonic bath filled with water heated to 50 °C. The sample was sonicated and ^{19}F NMR experiments (470 MHz, 64 scans, d1 = 70 s)

were conducted at various time points. At these time points, the Teflon liner was removed from the water bath and placed into an ice bath (0 °C). The suspension was allowed to settle before inserting the Teflon liner into a glass NMR tube. The samples were then analysed by ^{19}F NMR spectroscopy and once completed, heating at 50 °C with sonication was resumed until the next time point.

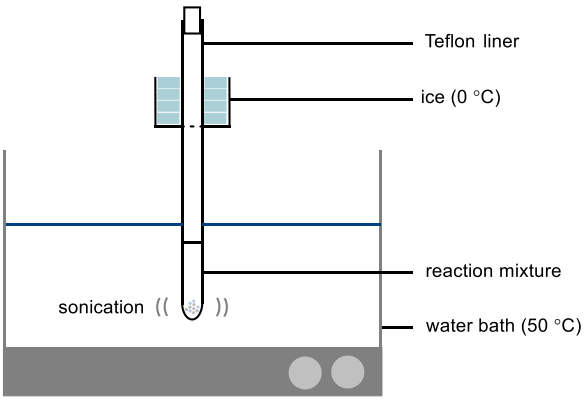

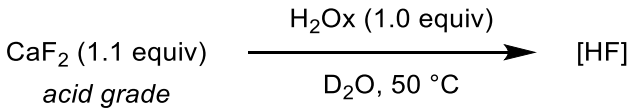

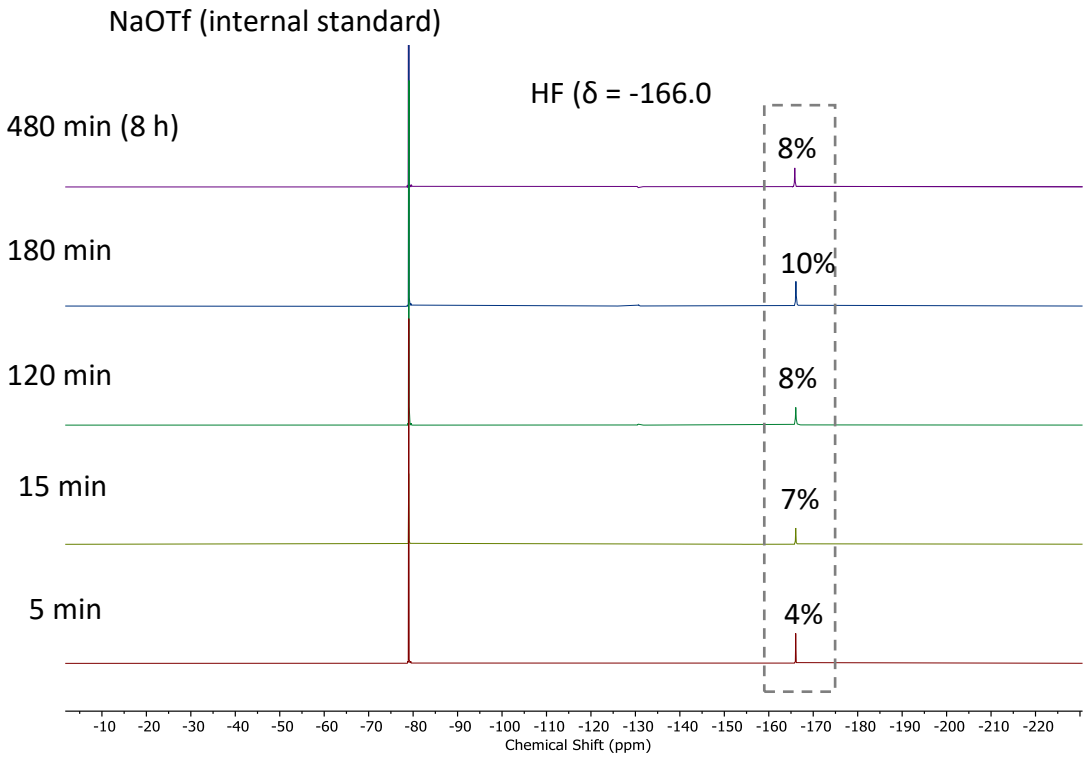

Entry	Time (min)	HF (%)	HF mmol	HF conc. (M)	SNR
1	5	4	0.033	0.07	280
2	15	7	0.066	0.13	178
3	120	8	0.070	0.14	159
4	180	10	0.089	0.18	338
5	480	8	0.075	0.15	219

Reaction monitoring in presence of Lewis acid

Into a Teflon NMR thin wall (5 mm) liner was added acid grade fluorspar (97% CaF_2, 40 mg, 0.5 mmol, 1.1 equiv), anhydrous oxalic acid (41 mg, 0.45 mmol, 1.0 equiv), sodium triflate (10 mg), $B(OH)_3$ (14 mg, 0.23 mmol, 0.5 equiv) or SiO_2 (18 mg, 0.32 mmol, 0.7 equiv) and D_2O (0.5 mL). The Teflon liner was plugged tightly with a Teflon cap and inserted through a custom-built holder (filled with ice) and then placed a water bath heated at 50 °C. The sample was sonicated and ^{19}F NMR experiments (470 MHz, 64 scans, d1 = 70 s) were conducted at various time points. The suspension was allowed to settle before inserting the Teflon liner into a glass NMR tube. The samples were then analysed by ^{19}F NMR spectroscopy and once completed, heating at 50 °C with sonication was resumed until the next time point.

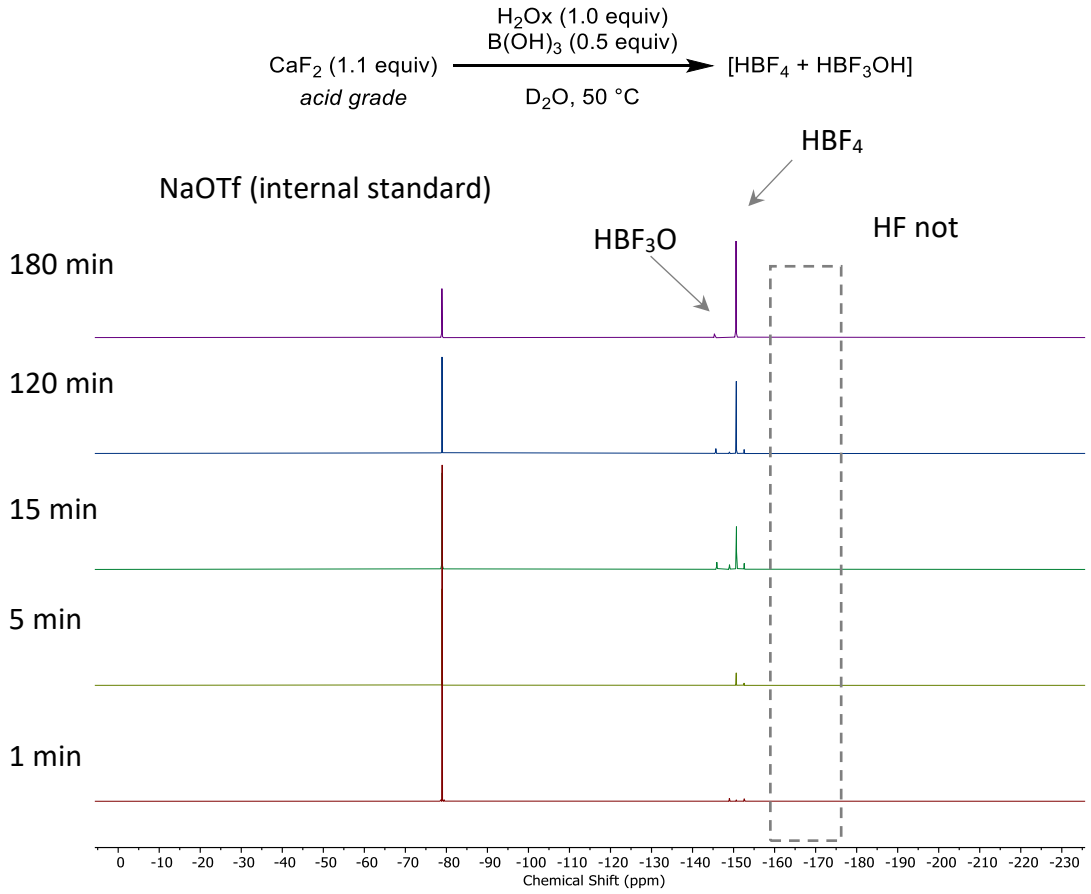

HBF_4 (%) and HBF_3OH (%) quantified over course of reaction between acid grade fluorspar (CaF_2) with H_2Ox and $B(OH)_3$ in D_2O at 50 °C.

Entry	Time (min)	HBF_4 (%)	HBF_3OH (%)
1	1	<1	1
2	5	16	6
3	15	22	10
4	120	44	12
5	180	96	3

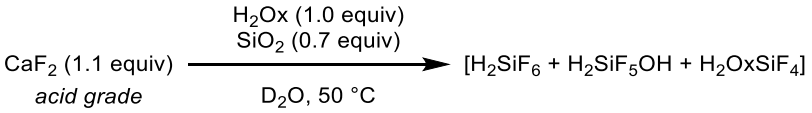

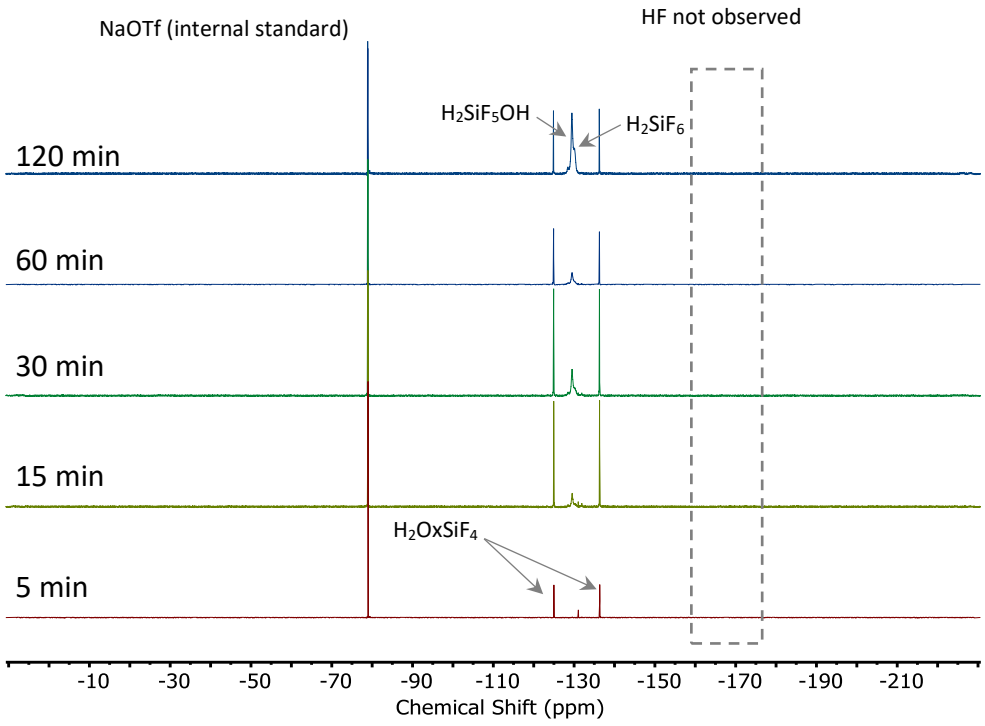

4.3.3 Characterisation of of aqueous boron fluorine products

The reaction between acid grade fluorspar (CaF_2, > 97.0%, Minersa Group) with anhydrous oxalic acid and $B(OH)_3$ in D_2O was monitored at 50 °C. Monitoring of the reaction by ^{19}F NMR enabled the identification of HBF_4, HBF_3OH and $HOxBF_2$ in solution.

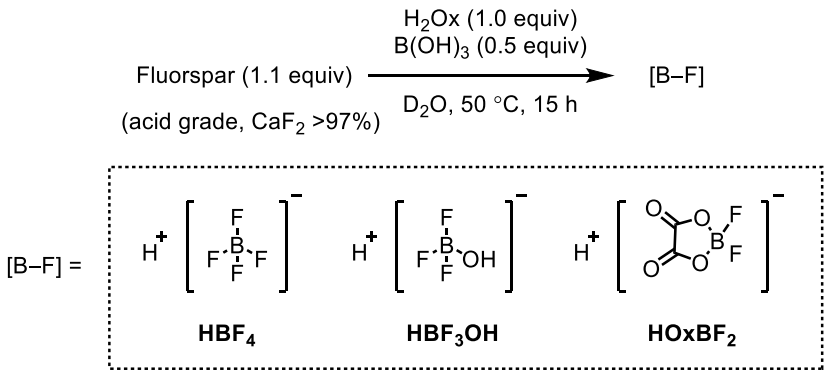

Characterisation of the species was achieved using ^{11}B NMR and ^{19}F NMR analysis. All spectra were collected at 25 °C and can be found in Chapter **3**. Coupling between ^{19}F and ^{11}B leads to a quintet of peaks in the ^{11}B NMR spectrum for the BF_4 ion at -1.46 ppm, which cannot be resolved with the instrument, and a quartet for the HBF_3OH at -0.03 ppm.

HBF_4:

^{19}F NMR (377 MHz, D_2O) δ -150.3 ([^{10}B]HBF_4]), -150.3 ppm ([^{11}B]HBF_4], q, *J*= 1.1 Hz)

^{11}B NMR (128 MHz, D_2O) δ -1.46 (br s).

HBF_3OH:

^{19}F NMR (377 MHz, D_2O) δ -145.26 (overlapping br s and q, *J*= 10.7 Hz)

^{11}B NMR (128 MHz, D_2O) δ -0.03 (q, *J*= 10.7 Hz)

$HOxBF_2$:

^{19}F NMR (377 MHz, D_2O) δ -152.27 ([^{10}B]$HOxBF_2$], br s), -152.34 ([^{11}B]$HOxBF_2$], br s)

^{11}B NMR (D_2O) δ 2.84 (br s)

Data is in accordance with literature values. The peak at -2.84 ppm in the ^{11}B NMR spectrum of the reaction mixture was assigned to a difluoro(oxalato)borate species ($HOxBF_2$).[77]

4.3.4 Characterisation of aqueous silicon fluorine products

The reaction between acid grade fluorspar (CaF_2, > 97.0%, Minersa Group) with anhydrous oxalic acid and SiO_2 in D_2O was monitored at 50 °C by ^{19}F NMR.

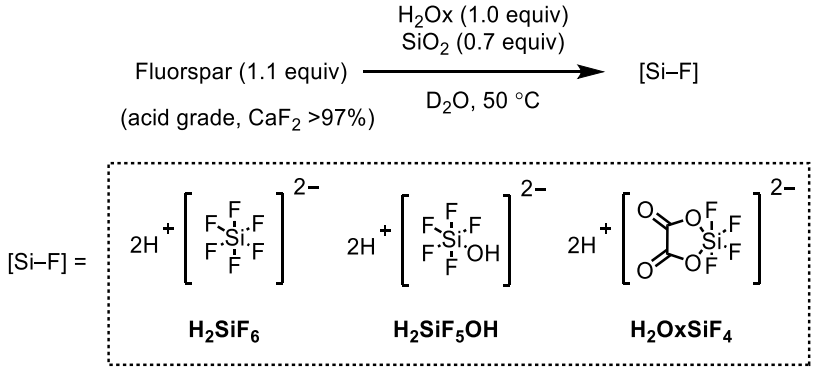

The formation of H_2SiF_6 was observed after 5 min by ^{19}F NMR, in addition to two fluorine resonances (triplets) at -124.9 ppm and -136.2 ppm with J_{F-F} coupling values of 8.9 Hz.[78] These resonances are assigned to the oxalate fluorosilicate species H_2OxSiF_4 [79]. $^{29}Si\{^{19}F\}$ NMR spectra was acquired using a ^{29}Si-^{19}F rINEPT NMR method[80,81]. $^{29}Si\{^{19}F\}$ NMR spectra of the reaction mixture after 5 min displayed 2 signals at -178.2 ppm and -182.8 ppm. The ^{19}F-^{29}Si bond of H_2SiF_6 and H_2OxSiF_4 was confirmed by a ^{19}F-^{29}Si HMBC experiment optimized for a short-range coupling. The ^{19}F to ^{29}Si rINEPT experiment was used to confirm J couplings.

H_2SiF_6:

^{19}F NMR (470 MHz, D_2O) δ -129.6 (br s).

$^{29}Si\{^{19}F\}$ NMR (100 MHz, D_2O) δ -178.2 (s).

H_2OxSiF_4:

^{19}F NMR (470 MHz, D_2O) δ -124.9 ppm (t, J_{F-F} = 8.9 Hz), -136.2 ppm (t, J_{F-F} = 8.9 Hz).

$^{29}Si\{^{19}F\}$ NMR (100 MHz, D_2O) δ -182.8 (s).

H_2SiF_5OH:

^{19}F NMR (470 MHz, D_2O) δ -128.9 (br s)

Peaks corresponding to H_2SiF_6 and H_2SiF_5OH are broad and overlap due to fast fluoride exchange. Basic hydrolysis of the [Si-F] species using KOH (6 equiv) affords an aqueous solution of KF as the sole aqueous fluorine containing species, evidenced by ^{19}F NMR.

All spectra for H_2SiF_6, H_2SiF_5OH and H_2OxSiF_4 can be found in Chapter **3**.

4.3.5 Characterisation of insoluble by-product formed in the reaction of AGF with H_2Ox and Lewis acid in water

Powder X-ray diffraction patterns of insoluble by-product formed in the reaction of acid grade fluorspar (CaF_2) with H_2Ox and $B(OH)_3$ after 15 h at 50 °C (top), $CaOx{\cdot}H_2O$ (middle) and acid grade fluorspar (CaF_2) (bottom). All powder X-ray diffraction patterns recorded at room temperature.

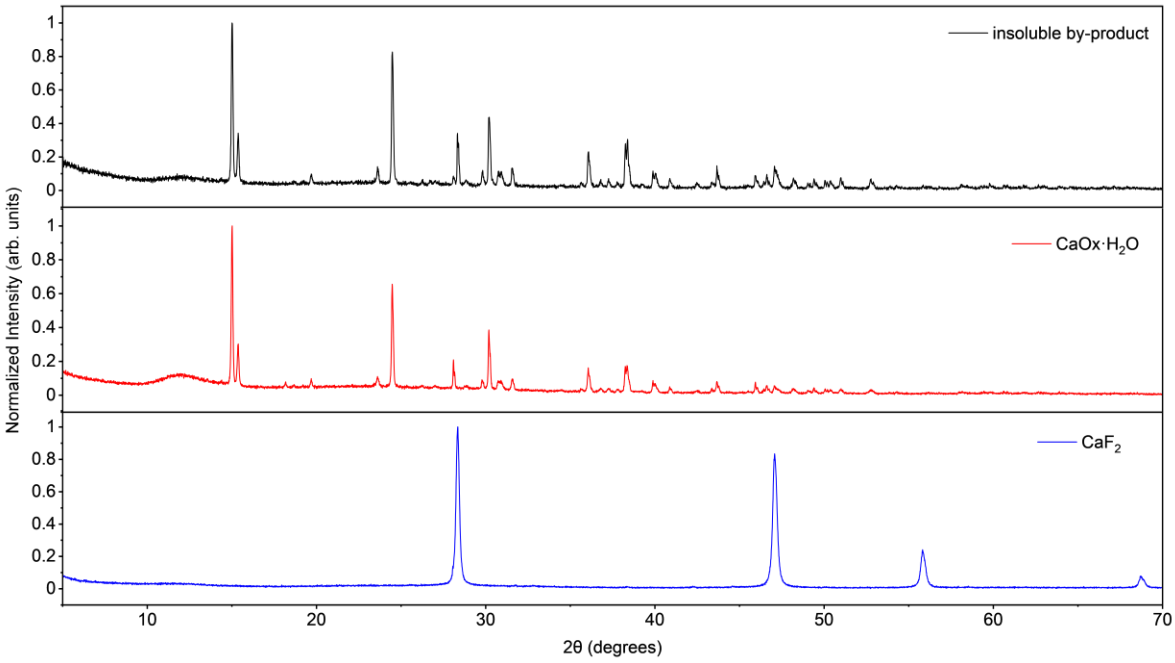

4.3.6 Optimisation of KF preparation from AGF

Activation of acid grade fluorspar (> 97% CaF_2) using anhydrous oxalic acid (H_2Ox) and silica gel (SiO_2) was investigated. Filtration of the suspension followed by basification with KOH affords KF.

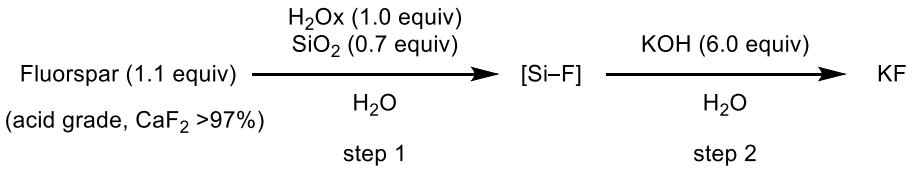

Step 1 - Cooperative activation of fluorspar

Acid grade fluorspar (644.0 mg, 8.0 mmol, 1.1 equiv), silica gel (306.0 mg, 5.1 mmol, 0.7 equiv) and oxalic acid (655 mg, 7.3 mmol, 1.0 equiv) were weighed into a 50 mL conical

sterile polypropylene (PP) centrifuge tube. H_2O (2.5 mL) was added and the mixture was heated with stirring at the indicated temperature for the indicated reaction time. The resulting suspension was cooled to ambient temperature, diluted with H_2O (5 mL) and filtered using a Büchner funnel into a 50 mL PP tube. Filtered solids were washed with H_2O (2.5 mL) to give an aqueous solution (~ 10 mL) containing H_2SiF_6, H_2SiF_5OH and $OxSiF_4$.

Step 2 - Basic hydrolysis of Si–F species

The first step of this reaction affords a theoretical maximum of 2.4 mmol of H_2SiF_6. Accordingly, KOH (85%, 951 mg, 14.4 mmol) was added portion-wise to the aqueous solution (containing H_2SiF_6, H_2SiF_5OH and $OxSiF_4$). The reaction was heated with stirring at the indicated temperature for the indicated reaction time. The resulting suspension was filtered using a fritted glass filter to separate insoluble by-products from the solution and washed with water (2 x 5 mL). The filtrate was concentrated *in vacuo* (50 °C) and dried under high vacuum (< 0.1 mbar). Gentle heating (100 °C) of the flask under vacuum for 5 min followed by drying overnight under high vacuum provided a white solid product.

KF analysis

To assess the quantity of KF in the solid product, a sample of the solid product (14 mg) and NaOTf as an internal standard was dissolved in D_2O. The purity of KF in the solid was assessed by quantitative ^{19}F NMR.[82]

This 2-step procedure was optimized for temperature, reaction time, concentration and equivalents of SiO_2. The KF yield (%) was calculated for each reaction using equation (1).

$$\text{purity of KF} \times \text{mass of solid product} = \text{KF yield (\%)} \quad (1)$$

Reaction Temperature

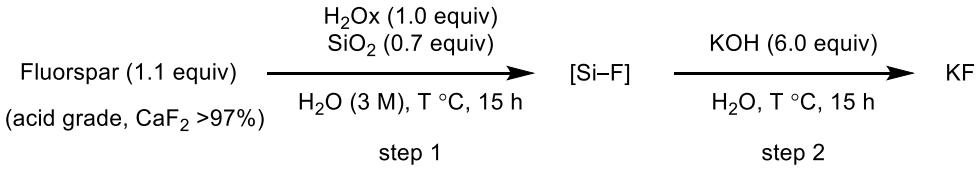

Entry	step 1 T (° C)	step 2 T (° C)	product (KF) mass	KF purity	KF yield
1	25	50	98	24	24
2	25	70	99	33	33
3	50	25	87	46	40
4	50	50	87	81	71
5	50	70	99	87	86
6	70	25	94	28	26
7	70	50	93	77	72
8	70	70	96	76	73

Reaction temperatures of 50 °C for step 1 and 70 °C for step 2 proved to be optimal for KF yield (86%).

Reaction Time

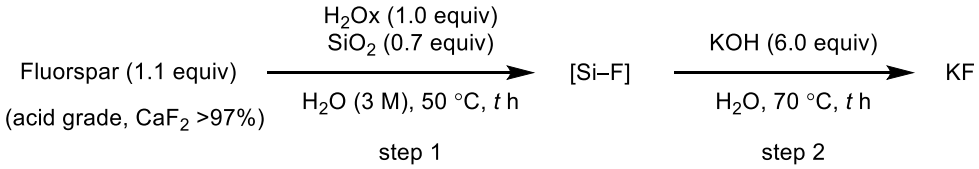

Entry	step 1 time (h)	step 2 time (h)	product (KF) mass	KF purity	KF yield
1	1	1	100	54	54
2	1	15	100	46	45
3	3	1	99	53	52
4	3	15	99	38	38
5	15	1	97	81	80
6	15	3	96	92	89
7	15	15	99	87	86

Reaction times of 15 h for step 1 and 1 h (or above) for step 2 proved to be optimal for KF yield (up to 89%).

Reaction Concentration

The effect of concentration (respect to oxalic acid) in step 1 (activation of acid grade fluorspar using oxalic acid and SiO_2) was studied.

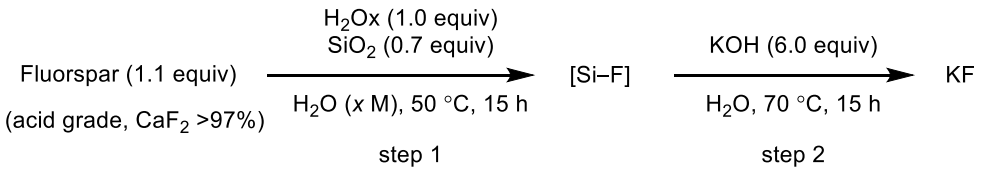

Entry	H_2Ox concentration (M)	Step 1 H_2O volume (mL)	product (KF) mass	KF purity (%)	KF yield (%)
1	0.5	14.5	95	96	91
2	2.0	3.7	92	81	74
3	3.0	2.4	99	87	86
4	4.0	1.8	97	83	80

Oxalic acid concentration of 0.5 M was found be optimal for KF yield (91%). These conditions also ensure complete dissolution of oxalic acid in water.

Equivalents of SiO_2

The effect of reducing SiO_2 equivalents (respect to oxalic acid) in step 1 was studied.

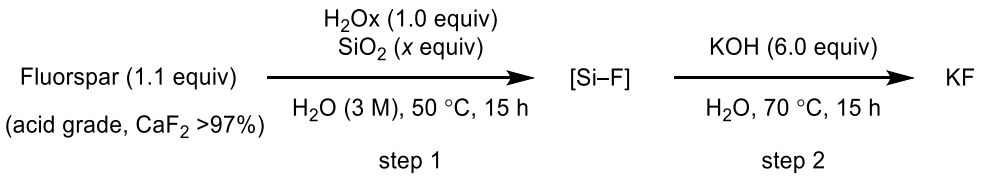

Entry	equivalents of SiO_2	product (KF) mass	KF purity (%)	KF yield (%)
1	0.7	99	87	86
2	0.4	98	84	82
3	0.3	98	97	95

High yields of KF (purity > 97%) were retained when the equivalents of SiO_2 was lowered to 0.3 equivalents. We chose to use 0.4 equivalents of SiO_2 for our final conditions.

Use of oxalic acid dihydrate

Oxalic acid dihydrate is a cheaper alternative to anhydrous oxalic acid. Anhydrous oxalic acid was replaced for oxalic acid dihydrate in step 1.

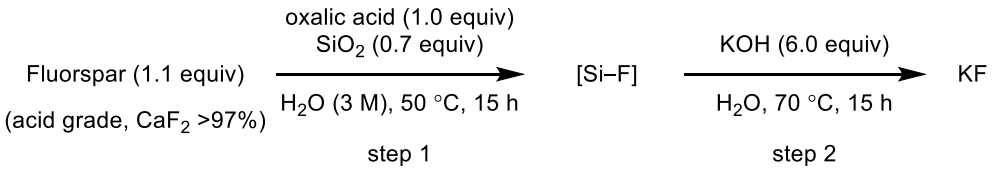

Entry	Oxalic acid	product (KF) mass	KF purity	KF yield
1	anhydrous	99	87	86
2	dihydrate	98	87	85

High KF yield (85%) was retained when anhydrous oxalic acid was replaced for oxalic acid dihydrate in step 1.

4.3.7 Quantification of aqueous silicon fluorine products

Acid grade fluorspar (644.0 mg, 8.0 mmol, 1.1 equiv), silica gel (175.0 mg, 2.9 mmol, 0.4 equiv), H_2O (14.5 mL) and oxalic acid dihydrate (917 mg, 7.3 mmol, 1 equiv) were added into a 50 mL conical sterile polypropylene (PP) centrifuge tube. The reaction mixture was heated with stirring at the 50 °C for 15 h. NaOTf (45 mg, 0.262 mmol) was added as an internal standard to the reaction mixture. The reaction mixture was stirred for 2 minutes and an aliquot of the reaction was analysed by quantitative ^{19}F NMR spectroscopy (D_2O) (32 scans, d1 = 30 s, op1 = 103.5 ppm).

The total amount of [Si-F] species was quantified using the global spectrum deconvolution (GSD) tool available on MestReNova which enables integration of partially overlapping peaks.[76]

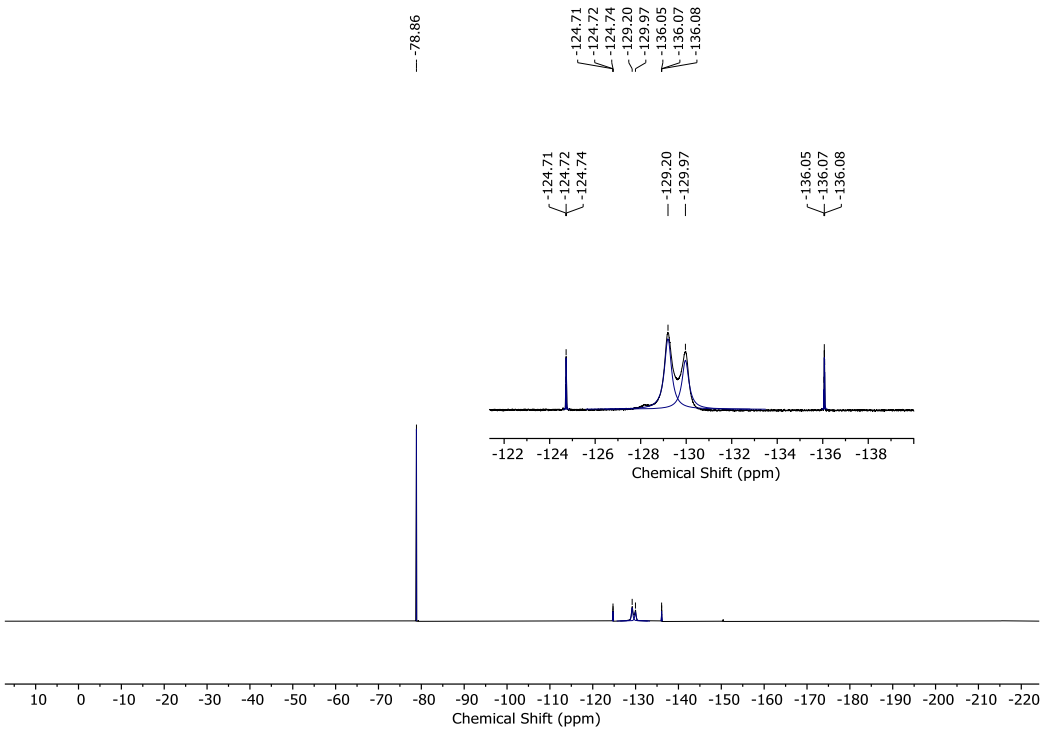

^{19}F NMR (D_2O) spectrum of reaction between acid grade fluorspar (CaF_2), H_2Ox and SiO_2 (15 h, 50 °C). Aqueous species H_2SiF_5OH (br s, -129.2 ppm), H_2SiF_6 (br s, -130.0 ppm) and H_2OxSiF_4 (two triplets at -124.7 ppm and -136.1 ppm with $^2J_{F-F}$ = 8.9 Hz) observed.

	ppm	Intensity	Width	Area
1	-78.86	3737.7	1.18	7717.36
2	-78.87	13.6	1.33	32.71
3	-129.20	260.7	170.66	80429.78
4	-129.97	181.4	166.94	55439.13
5	-136.05	77.3	3.07	393.22
6	-136.07	194.3	3.16	1202.51
7	-136.08	138.0	6.76	1872.93

Global Spectrum Deconvolution (GSD) peak list characterised by chemical shift (ppm), peak intensity, peak width and peak area. Data extracted from the ^{19}F NMR spectrum.

Calculated [Si–F] % values from total peak area values obtained using GSD

Entry	Compound	Total peak area	Normalized area	[Si-F] %
1	NaOTf	7717.36	1	-
2	H_2SiF_6	55439.14	7.18	39
3	$H_2SiF_5(OH)$	80429.78	10.42	56
4	H_2OxSiF_4	3468.66	0.45	2
			Total [Si-F]	97

4.3.8 Preparation and characterisation of K_2SiF_6 prepared from AGF

Treatment of the aqueous solution of H_2SiF_6, H_2SiF_5OH and H_2OxSiF_4 with 2 equivalents of KOH at 25 °C affords K_2SiF_6.

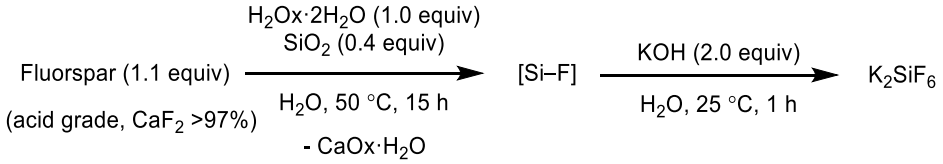

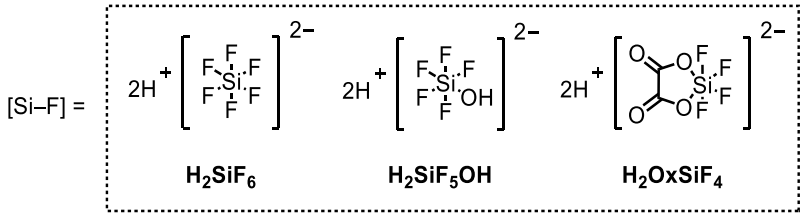

Oxalic acid dihydrate (9.17 g, 72.7 mmol, 1.0 equiv) was dissolved in H_2O (145.6 mL) in a 500 mL PTFE round bottom flask. A mixture of acid grade fluorspar (97% CaF_2, 6.44 g, 80.0 mmol, 1.1 equiv) and silica gel (1.75 g, 29.0 mmol, 0.4 equiv) was added in 3 portions to the solution of oxalic acid dihydrate at 50 °C. The resulting suspension was stirred using a mechanical stirrer at 50 °C. After 15 h, the suspension was cooled to room temperature, and filtered using a Büchner funnel into a 500 mL PTFE round bottom flask. Filtered solids were washed with H_2O (3 x 5 mL) to give a ~160 mL aqueous solution containing H_2SiF_6, H_2SiF_5OH and $OxSiF_4$. The first step of this reaction affords a theoretical maximum of 24 mmol of H_2SiF_6. Accordingly, KOH (85%, 3.17 g, 48 mmol) was added to the filtrate (until pH 7 was reached). The suspension was stirred at 25 °C for 1 h before filtration. The filtered solid was allowed to dry at room temperature and then under high vacuum to give K_2SiF_6 as a white powder (5.08 g, 23 mmol, 96%).

K_2SiF_6 is sparingly soluble in water. The formation of K_2SiF_6 was confirmed by PXRD.

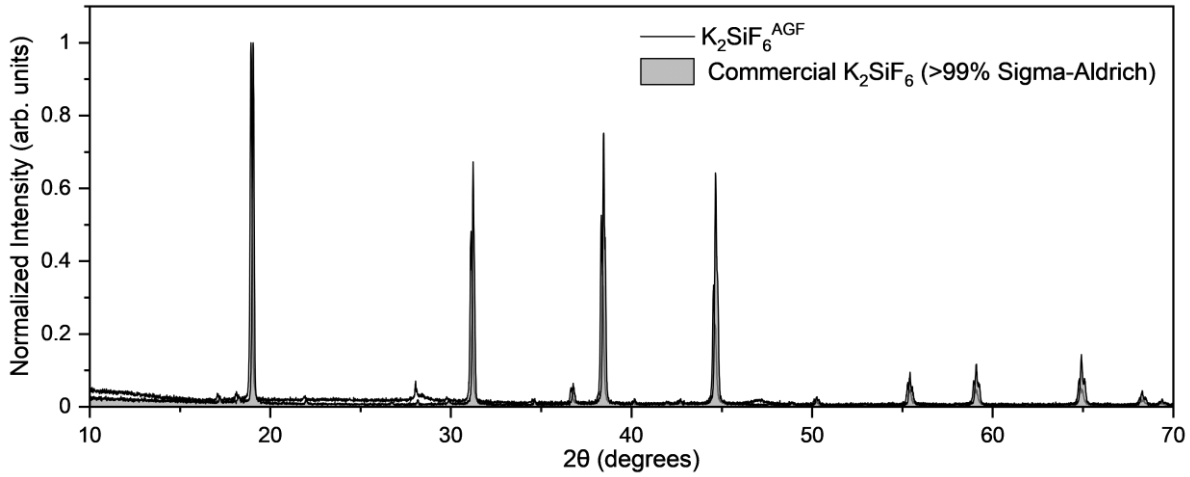

Treatment of the aqueous solution of H_2SiF_6, H_2SiF_5OH and H_2OxSiF_4 with 6 equivalents of KOH at 70 °C affords KF

4.3.9 Preparation and characterisation of KF prepared from AGF

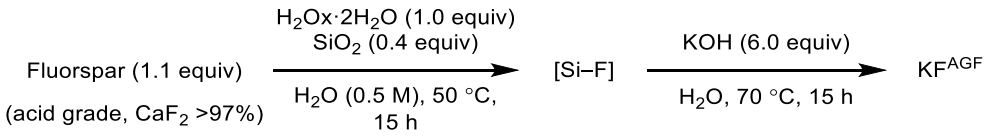

This reaction was performed using 6.44 g of acid grade fluorspar. KF^{AGF} was prepared in a mechanically stirred vessel (500 mL PTFE round bottom flask) using a Teflon stirring shaft (6 mm) with a diamond shaped button (500 mm) purchased from Sigma-Aldrich.

Oxalic acid dihydrate (9.17 g, 72.7 mmol, 1.0 equiv) was dissolved in H_2O (145.6 mL) in a 500 mL PTFE round bottom flask. A mixture of acid grade fluorspar (97% CaF_2, 6.44 g, 80.0 mmol, 1.1 equiv) and silica gel (1.75 g, 29.0 mmol, 0.4 equiv) was added in 3 portions to the solution of oxalic acid dihydrate at 50 °C. The resulting suspension was stirred using a mechanical stirrer at 50 °C. After 15 h, the suspension was cooled to room temperature, and filtered using a Büchner funnel into a 500 mL PTFE round bottom flask. Filtered solids were washed with H_2O (3 x 5 mL) to give a ~ 160 mL aqueous solution containing H_2SiF_6, H_2SiF_5OH and $OxSiF_4$.

The first step of this reaction affords a theoretical maximum of 24 mmol of H_2SiF_6. Accordingly, KOH (85%, 9.50 g, 144 mmol) was added portion-wise to the aqueous solution (containing H_2SiF_6, H_2SiF_5OH and $OxSiF_4$). After the addition is complete, the reaction mixture

was heated with stirring at the 70 °C for 15 h (monitored by ^{19}F NMR spectroscopy). After 15 h a pH of 7 should be reached (acid grade fluorspar derived H_2SiF_6 can be used as a pH regulator). The resulting suspension was allowed to cool to room temperature and the solids were allowed to settle. Filtration using a fritted glass filter followed and insoluble by-products were washed with water (2 x 10 mL). The filtrate was concentrated *in vacuo* (50 °C, 20 mmbar) and dried under high vacuum (< 0.1 mbar). Gentle heating (100 °C) of the flask under vacuum for 5 min followed by drying overnight at room temperature under high vacuum provides acid grade fluorspar derived potassium fluoride (KF^{AGF}) as a white crystalline solid [7.84 g, 136 mmol, 94% (calculated from acid grade fluorspar)].

Purity of KF^{AGF} by quantitative ^{19}F NMR using NaOTf as an internal standard was calculated to be 90%. This gives a total KF^{AGF} yield of 85%. Full purity analysis is given below.

PXRD

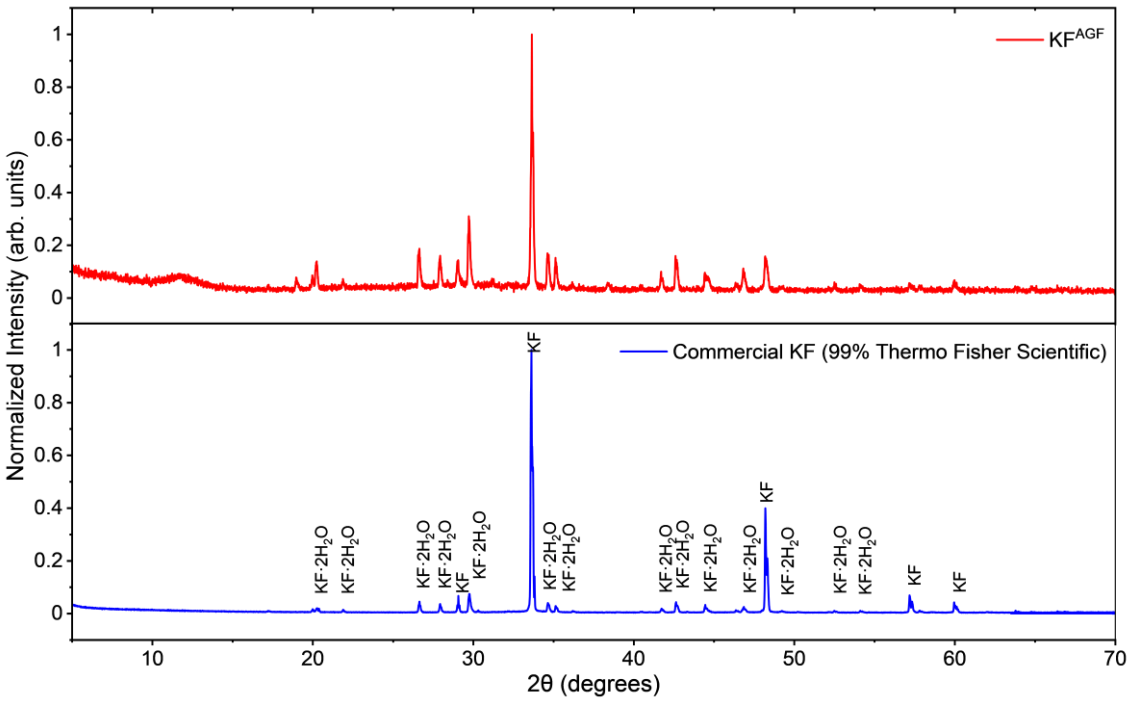

4.3.10 Preparation and characterisation of KF prepared from metspar

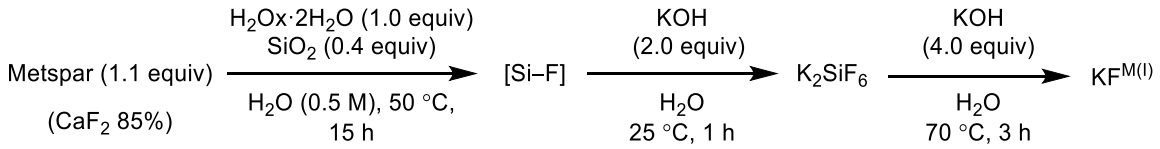

Metspar I sourced from Luoyang Aurora Minechem Co., Ltd. (China) has the following purity profile CaF_2 (85%), SiO_2 (10%), $CaCO_3$ (<5%), S (0.12%), P (0.1%).

Due to the reduced purity of metspar compared to acid grade fluorspar, K_2SiF_6 was first prepared and isolated prior to basic hydrolysis.

Powdered metspar (~ 85% CaF_2, 735 mg, 8.0 mmol, 1.1 equiv), silica gel (175 mg, 2.9 mmol, 0.4 equiv) and oxalic acid dihydrate (917 mg, 7.3 mmol, 1.0 equiv) were weighed into a 50 mL PP tube. H_2O (14.5 mL) was added and the mixture was heated with stirring at 50 °C for 15 h (monitored by ^{19}F NMR spectroscopy). The resulting suspension was cooled to room temperature and filtered with a Büchner funnel into a 50 mL PP conical tube. Filtered solids were washed with H_2O (5 mL) to give an aqueous solution (~ 20 mL) containing H_2SiF_6, H_2SiF_5OH and $OxSiF_4$.

The first step of this reaction affords a theoretical maximum of 2.4 mmol of H_2SiF_6. Accordingly, KOH (85%, 317 mg, 4.8 mmol) was added to the filtrate (until pH 7 was reached). After the addition is complete, the resultant suspension is stirred at 25 °C for 1 h (monitored by ^{19}F NMR spectroscopy) before filtration. The filtered solid was allowed to dry at room temperature overnight to give K_2SiF_6 as a white powder (393 mg, 1.33 mmol, 74%).

To the metspar derived K_2SiF_6 (393 mg, 1.78 mmol) was added a solution of KOH (85%, 471 mg, 7.41 mmol) in water (0.7 mL). The reaction mixture was stirred at 70 °C for 3 h. The resulting suspension was allowed to cool to room temperature and the solids were allowed to settle. Filtration using a fritted glass filter followed and insoluble by-products were washed with water (2 x 5 mL). The filtrate was concentrated *in vacuo* (50 °C, 20 mmbar) and dried under high vacuum (< 0.1 mbar). Gentle heating (100 °C) of the flask under vacuum for 5 min followed by drying overnight under high vacuum at room temperature provides metspar derived potassium fluoride [$KF^{M(I)}$] as a white crystalline solid [458 mg, 7.88 mmol, 74%].

Purity of KF^M by quantitative ^{19}F NMR using NaOTf as an internal standard was calculated to be 98%.

This gives a total $KF^{M(I)}$ yield of 72% (7.73 mmol, calculated from K_2SiF_6), 54% [calculated from metspar I where 1 equivalent CaF_2 (7.27 mmol) theoretically affords 2 equivalents KF (14.54 mmol)].

PXRD

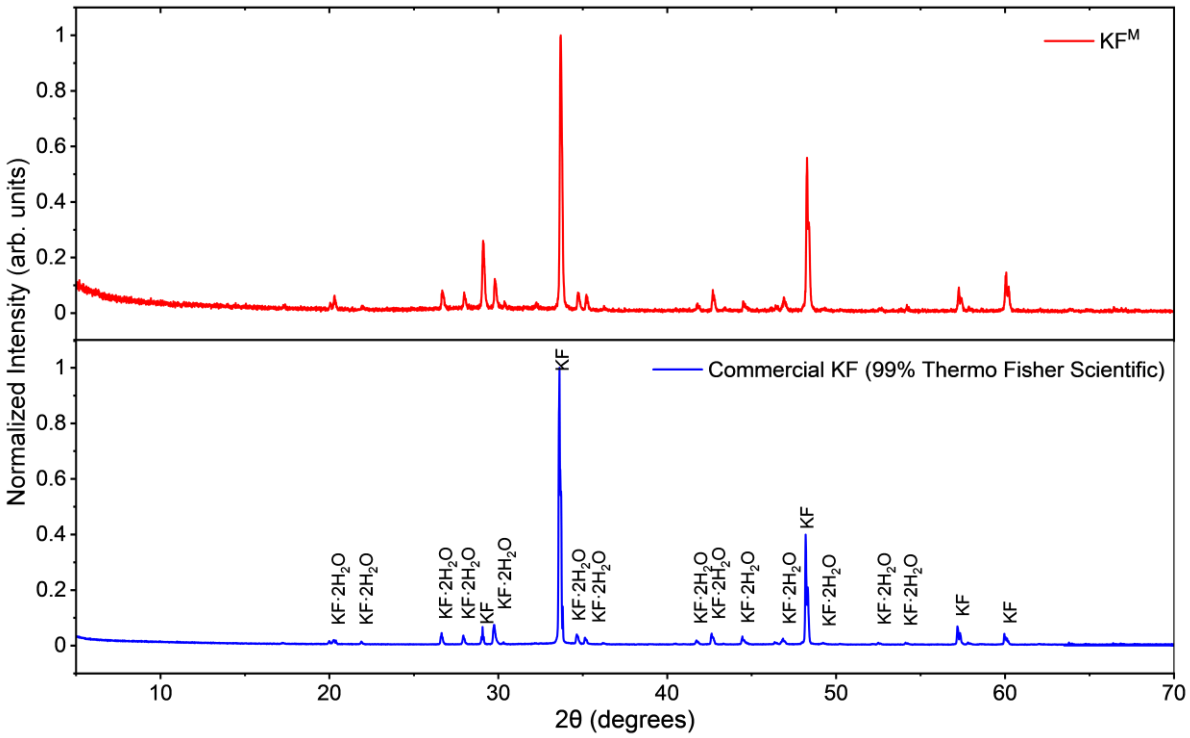

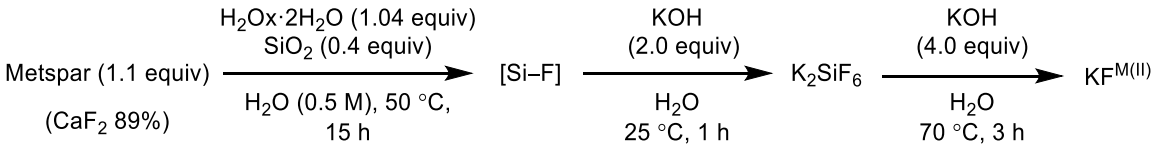

Metspar II was sourced from Mexico (Mexichem Fluor S.A de C.V.) **Metspar^{II}** with the following purity profile: CaF_2 (88.98%), SiO_2 (5.43%), $CaCO_3$ (4.02%), Al_2O_3 (0.41%), Fe_2O_3 (0.24%), S (0.011%), P (0.023%), Pb (<0.001%).

Due to the reduced purity of metspar compared to acid grade fluorspar, K_2SiF_6 was first prepared and isolated prior to basic hydrolysis. Additional 0.04 equiv. of $H_2Ox{\cdot}2H_2O$ was added to the reaction to neutralize 4% $CaCO_3$ found in metspar II.

Powdered metspar (89% CaF_2, 1.40 g, 16.0 mmol, 1.1 equiv), silica gel (350 mg, 5.82 mmol, 0.4 equiv) and oxalic acid dihydrate (1.90 g, 15.1 mmol, 1.04 equiv) were weighed into a 100 mL PTFE round bottom flask. H_2O (29 mL) was added and the mixture was heated with stirring at 50 °C for 15 h (monitored by ^{19}F NMR spectroscopy). The resulting suspension was cooled to room temperature and filtered with a Büchner funnel into a 50 mL PP tube.

Filtered solids were washed with H_2O (5 mL) to give an aqueous solution (~ 35 mL) containing H_2SiF_6, H_2SiF_5OH and $OxSiF_4$.

The first step of this reaction affords a theoretical maximum of 4.8 mmol of H_2SiF_6. Accordingly, KOH (85%, 634 mg, 9.60 mmol) was added to the filtrate (until pH 7 was reached). After the addition is complete, the resultant suspension is stirred at 25 °C for 1 h (monitored by ^{19}F NMR spectroscopy) before filtration. The filtered solid was allowed to dry at room temperature overnight to give K_2SiF_6 as a white powder (873 mg, 3.96 mmol, 83%).

To the metspar derived K_2SiF_6 (873 mg, 3.96 mmol) was added a solution of KOH (85%, 1.05 g, 15.9 mmol) in water (10 mL). The reaction mixture was stirred at 70 °C for 3 h. The resulting suspension was allowed to cool to room temperature and the solids were allowed to settle. Filtration using a fritted glass filter followed and insoluble by-products were washed with water (2 x 5 mL). The filtrate was concentrated *in vacuo* (50 °C, 20 mmbar) and dried under high vacuum (< 0.1 mbar). Gentle heating (100 °C) of the flask under vacuum for 5 min followed by drying overnight under high vacuum at room temperature provides metspar^{II} derived potassium fluoride [$KF^{M(II)}$] as a white crystalline solid [1.18 g, 20.31 mmol, 85%].

Purity of $KF^{M(II)}$ by quantitative ^{19}F NMR using NaOTf as an internal standard was calculated to be 90%.

This gives a total $KF^{M(II)}$ yield of 77% (18.28 mmol, calculated from K_2SiF_6), 63% (calculated from metspar II where 1 equivalent CaF_2 (14.54 mmol) theoretically affords 2 equivalents KF (29.1 mmol)]).

4.3.12 Purity analysis of KF prepared from AGF and metspar

To assess the quantity of KF in the solid product, a sample of the solid product and sodium triflate (>98 %) as an internal standard was dissolved in D_2O. The purity of KF in the solid was assessed by quantitative ^{19}F NMR (16 scans, d_1= 50 s, o1p = 100.5 ppm).

The purity of compound (x), as a percentage of its nominal weight, can be determined using the following formula as described in reference[82]:

$$P_x = (I_x/I_{is}) \times (N_{is}/N_x) \times (M_x/M_{is}) \times (W_{is}/W_x) \times P_{is} \quad (1)$$

where, *I*, *N*, *M*, *W* and *P* are the integrated area (*I*), number of nuclei (*N*), molecular mass (*M*), gravimetric weight (*W*) and purity (*P*) of the compound of interest (x) and the internal standard compound (is), respectively. Because this is a weight-based % purity, it allows you to evaluate the purity even if other components in the sample are invisible by NMR.

Using the following equation (2) a KF yield (%) was determined for KF^{AGF} and $KF^{M(I/II)}$.

purity of KF x mass of solid product = KF yield (%) (2)

KF^{AGF}

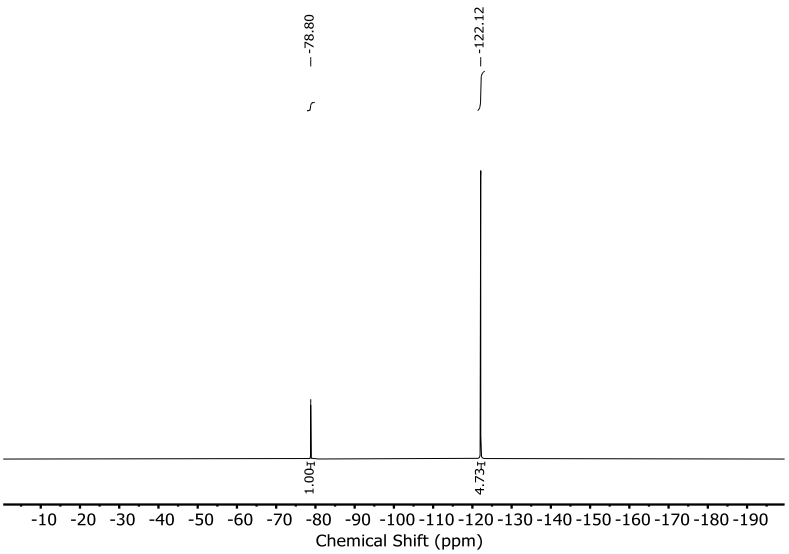

^{19}F qNMR (D_2O) of KF^{AGF} dissolved in D_2O with NaOTf internal standard. KF at -122.12 ppm and NaOTf at -78.80 ppm.

A sample of KF^{AGF} (23.4 mg) and sodium triflate as an NaOTf (4.40 mg) was dissolved in D_2O. The purity of KF in the solid was assessed by quantitative ^{19}F NMR and calculated to be 90%.

^{19}F NMR (377 MHz, D_2O) δ -122.12 (KF, s). No signals were observed by ^{13}C NMR.

$KF^{M(I)}$

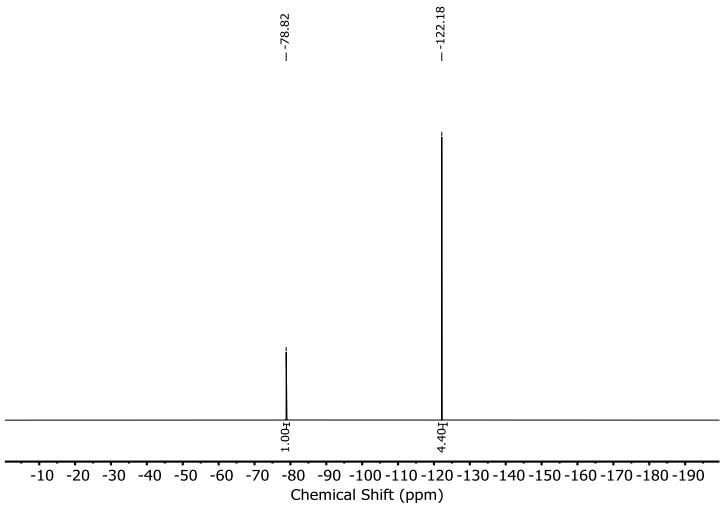

^{19}F qNMR (D_2O) of $KF^{M(I)}$ dissolved in D_2O with NaOTf internal standard. KF at -122.12 ppm and NaOTf at -78.80 ppm.

A sample of $KF^{M(I)}$ (15.5 mg) and sodium triflate as an NaOTf (3.40 mg) was dissolved in D_2O. The purity of $KF^{M(I)}$ in the solid was assessed by quantitative ^{19}F NMR and calculated to be 98%.

^{19}F NMR (377 MHz, D_2O) δ -122.18 (KF, s). No signals were observed by ^{13}C NMR.

$KF^{M(II)}$

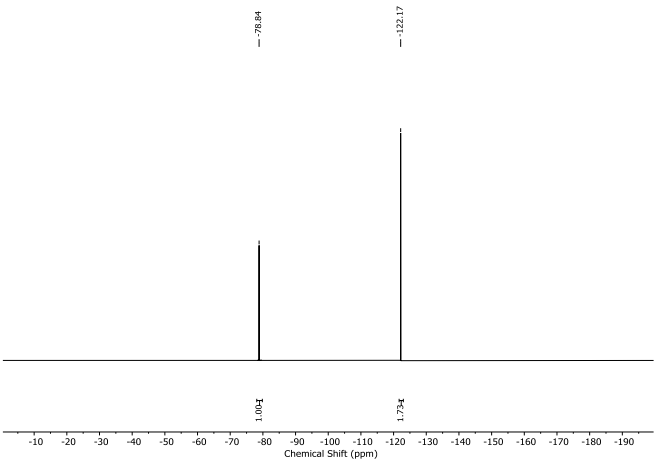

^{19}F qNMR (D_2O) of $KF^{M(II)}$ dissolved in D_2O with NaOTf internal standard. KF at -122.12 ppm and NaOTf at -78.80 ppm.

A sample of $KF^{M(II)}$ (19.4 mg) and sodium triflate as an NaOTf (10.0 mg) was dissolved in D_2O. The purity of $KF^{M(II)}$ in the solid was assessed by quantitative ^{19}F NMR and calculated to be 90%.

^{19}F NMR (377 MHz, D_2O) δ -122.21 (KF, s). No signals were observed by ^{13}C NMR

Inductively Coupled Plasma Optical Emission spectroscopy (ICP-OES) for microanalyses (F, K, Si) of commercial KF samples, KF^{AGF} and $KF^{M(I)}$ was carried out by MEDAC Ltd.

Microanalysis of KF samples

Element	KF (theoretical)	KF Thermo Scientific 99% (metals basis)	KF Sigma Aldrich >99.9% (metals basis)	KF^{AGF}	$KF^{M(I)}$
F (%)	32.70	29.88	31.48	23.76	28.30
K (%)	67.30	61.71	64.70	56.27	62.5
Si (%)	0	n/a	n/a	0.4	0.17

KF exists as anhydrous KF and $KF{\cdot}2H_2O$ [as observed in the PXRD patterns of commercial KF, KF^{AGF} and $KF^{M(I)}$].

Thermogravimetric analysis coupled with mass spectroscopy (TGA-MS) was recorded for KF^{AGF} to identify impurities. The measurement was performed under flowing nitrogen. KF^{AGF} demonstrates a weight loss of 9% within 36 - 130 °C which is attributed to H_2O. This data was collected with assistance from J. Murrell and A. Wang from the group of Prof. M. Hayward.

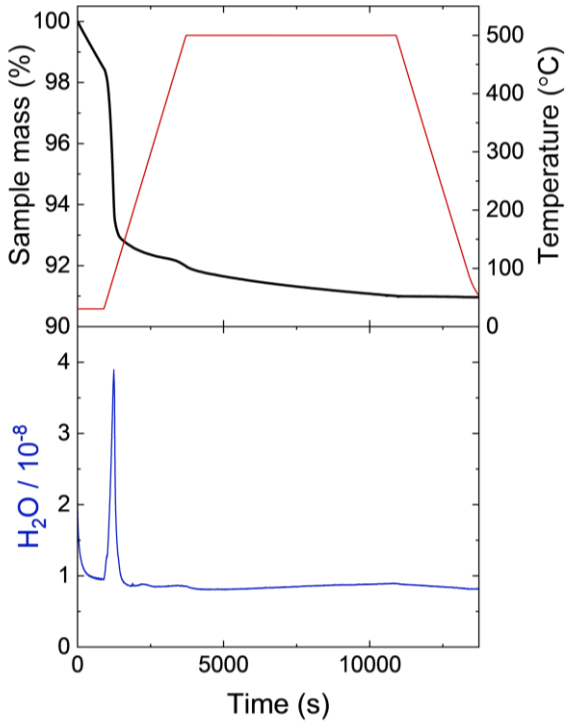

TGA of KF^{AGF} (top graph) with sample mass % (black), temperature (red) and m/e 18 ion trace (bottom graph, blue).

4.3.13 Performance of KF prepared from AGF and metspar

The performance of our KF prepared either using acid grade fluorspar (KF^{AGF}, 90% purity) or metspar ($KF^{M(I)}$, 98% purity) was examined in the fluorination of 2,4-dinitrochlorobenzene and compared against commercial anhydrous KF (KF^{C}, 99% purity, Thermo Scientific Chemicals, CAS 7789-23-3)

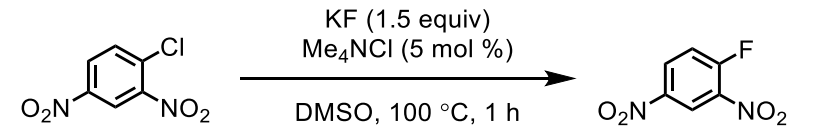

2,4-dinitrochlorobenzene

2,4-dinitrofluorobenzene **(14)**

To an oven dried glass reaction vial was added 2,4-dinitrochlorobenzene (101 mg, 0.5 mmol, 1.0 equiv), KF (22 mg, 0.75 mmol, 1.5 equiv), Me_4NCl (2.7 mg, 0.025 mmol, 0.05 equiv) and anhydrous DMSO (2.5 mL). After stirring at 100 °C for 1 h in a heating block, the resulting suspension was cooled to room temperature. Reaction yield was determined from the crude reaction mixture by quantitative ^{1}H and ^{19}F NMR spectroscopy using 4-fluoroanisole as internal standard.

Entry	KF	source	ArF (%)
1	KF^{C}	commercial	95%
2	KF^{AGF}	this work	90%
3	$KF^{M(I)}$	this work	92%

4.3.14 Preparation of $R_4NF{\cdot}(ROH)_x$ from AGF

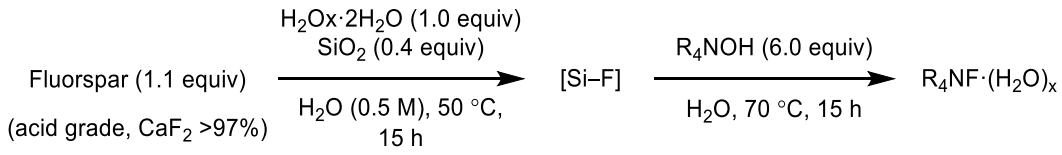

Acid grade fluorspar (644 mg, 8.0 mmol, 1.1 equiv), silica gel (175 mg, 2.9 mmol, 0.4 equiv) and oxalic acid dihydrate (917 mg, 7.3 mmol, 1.0 equiv) were weighed into a 100 mL PTFE round bottom flask. H_2O (14.5 mL) was added and the mixture was heated with stirring at 50 °C for 15 h (monitored by ^{19}F NMR spectroscopy). The resulting suspension was cooled to ambient temperature and filtered with a Büchner funnel into a 50 mL PP tube. Filtered solids were washed with H_2O (5 mL) to give an aqueous solution (~ 20 mL) containing H_2SiF_6, H_2SiF_5OH and $OxSiF_4$.

The first step of this reaction affords a theoretical maximum of 2.4 mmol of H_2SiF_6. Accordingly, Me_4NOH (25 wt. % in H_2O, 5.17 mL, 14.4 mmol) or $^{n}Bu_4NOH$ (40 wt. % in H_2O, 9.44 mL, 14.4 mmol) was added portion wise to the aqueous solution (containing H_2SiF_6, H_2SiF_5OH and $OxSiF_4$). After the addition is complete, the reaction was heated with stirring at 70 °C for 15 h (monitored by ^{19}F NMR spectroscopy). Filtration using a Büchner funnel followed and insoluble by-products were washed with water (2 x 5 mL). The filtrate was concentrated *in vacuo* (50 °C, 20 mmbar) and dried under high vacuum (< 0.1 mbar). Drying overnight under high vacuum at room temperature provides crude tetramethylammonium fluoride (TMAF, Me_4NF) or crude *n*-tetrabutylammonium fluoride (TBAF, nBu_4NF) as hydrates.

$Me_4NF{\cdot}^{t}AmOH$

To the crude tetramethylammonium fluoride (TMAF, Me_4NF) hydrate (1.01 g) was added anhydrous *tert*-amyl alcohol (40 mL) and activated 3Å molecular sieves (powdered, 20 g). The slurry was stirred at 25 °C for 3 h. The slurry was then filtered to remove the solids and

the solids were washed with *tert*-amyl alcohol (3 × 5 mL). The filtrate and alcohol washes were combined and concentrated *in vacuo* (40 °C, 12 mmbar) to yield $Me_4NF\cdot{}^{t}AmOH$ as a white solid (2.3 g, 12.7 mmol, 88%).

^{1}H NMR (400 MHz, $CDCl_3$) δ 3.30 – 3.21 (m, 8H), 1.60 (dq, *J* = 11.9, 8.0 Hz, 8H), 1.40 (dt, *J* = 14.7, 7.4 Hz, 8H), 1.20 (s, 36H), 0.95 (t, *J* = 7.3 Hz, 12H).

^{19}F NMR (376 MHz, $CDCl_3$) δ -120.19 (br s).

^{13}C NMR (101 MHz, $CDCl_3$) δ 68.5, 58.6, 31.2, 24.0, 19.7, 13.6.

Spectroscopic data are in accordance with those in literature [21].

$Bu_4NF\cdot({}^{n}BuOH)_4$

To the crude tetrabutylammonium fluoride (TBAF, $^{n}Bu_4NF$) hydrate (3.86 g) was added anhydrous *tert*-butanol (200 mL) and hexane (50 mL). The slurry was stirred at 90 °C for 30 min. The slurry was then filtered whilst warm and the filtrate was cooled to room temperature before storing at 5 °C overnight. A white crystalline solid precipitated out of the filtrate which was filtered and washed with hexane. The crystalline precipitate was collected and dried under high vacuum for 15 min to give $^{n}Bu_4NF\cdot({}^{t}BuOH)_4$ as a fluffy crystalline solid (5.79 g, 10.4 mmol, 71%).

^{1}H NMR (400 MHz, D_2O) δ 3.10 (s, 12H), 1.42 (q, *J* = 7.5 Hz, 2H), 1.10 (d, *J* = 1.2 Hz, 5H), 0.80 (dd, *J* = 8.2, 6.9 Hz, 2H).

^{19}F NMR (377 MHz, D_2O) δ -122.23 (s).

^{13}C NMR (101 MHz, D_2O) δ 72.1, 55.8 – 54.1 (m), 35.2, 27.1, 7.8.

Spectroscopic data are in accordance with those in literature [22].

Acid grade fluorspar derived $Me_4NF\cdot{}^{t}AmOH$ (A) and $Bu_4NF\cdot({}^{n}BuOH)_4$ (B)

Performance of acid grade fluorspar derived $Me_4NF\cdot{}^tAmOH$

The performance of our acid grade fluorspar derived $Me_4NF\cdot{}^tAmOH$ was examined in the fluorination of 1,4-dinitrobenzene following a modified procedure by Sanford and co-workers.[83]

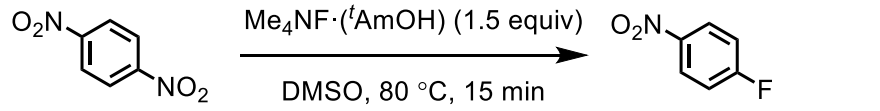

1,4-dinitrobenzene — 4-fluoronitrobenzene (**19**)

To an oven dried glass reaction vial was added 1,4-dinitrobenzene (84 mg, 0.5 mmol, 1.0 equiv), acid grade fluorspar derived $Me_4NF\cdot({}^tAmOH)$ (136 mg, 0.75 mmol, 1.5 equiv) and anhydrous DMSO (2.5 mL). After stirring at 80 °C for 15 minutes in a heating block, the resulting suspension was cooled to room temperature. Reaction yield was determined from the crude reaction mixture by quantitative ^1H and ^{19}F NMR spectroscopy using 4-fluoroanisole as internal standard. Yield of 97% (determined by ^{19}F NMR against 4-fluoroanisole as an internal standard).

4.3.15 Preparation and characterisation of NaF and CsF prepared from AGF

Preparation of NaF from acid grade fluorspar

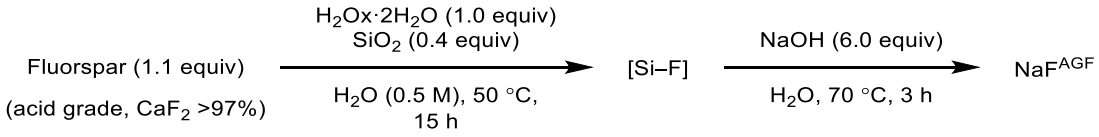

Acid grade fluorspar (644.0 mg, 8.0 mmol, 1.1 equiv), silica gel (306.0 mg, 5.1 mmol, 0.4 equiv) and oxalic acid (951 mg, 7.3 mmol, 1.0 equiv) were weighed into a 50 mL conical sterile polypropylene (PP) centrifuge tube. H_2O (14.5 mL) was added and the mixture was stirred at 50 °C for 15 h.

The resulting suspension was cooled to ambient temperature, diluted with H_2O (5 mL) and filtered using a Büchner funnel into a 50 mL PP tube. Filtered solids were washed with H_2O to give an aqueous solution (~ 20 mL) containing [Si-F] (H_2SiF_6, H_2SiF_5OH and $OxSiF_4$).

The first step of this reaction affords a theoretical maximum of 2.4 mmol of H_2SiF_6. Accordingly, NaOH (98%, 588 mg, 14.4 mmol) was added portion-wise to the aqueous solution (containing H_2SiF_6 and H_2SiF_5OH). The reaction was heated with stirring at the 70 °C for 3 h (monitored by ^{19}F NMR spectroscopy). After 15 h a pH of 7 should be reached (acid grade fluorspar derived H_2SiF_6 can be used as a pH regulator). The resulting suspension was filtered using a fritted glass filter to separate insoluble by-products from the solution and washed with water (2 x 5 mL). The filtrate was concentrated *in vacuo* (50 °C) and dried under high vacuum (< 0.1 mbar). Gentle heating (100 °C) of the flask under vacuum for 5 min followed by drying overnight at room temperature under high vacuum provided NaF^{AGF} as a white solid [541 mg, 12.9 mmol, 90% (calculated from acid grade fluorspar)].

Purity of NaF^{AGF} by quantitative ^{19}F NMR using NaOTf as an internal standard was calculated to be 94%. This gives a total NaF^{AGF} yield of 85%. For full purity analysis provided below.

PXRD

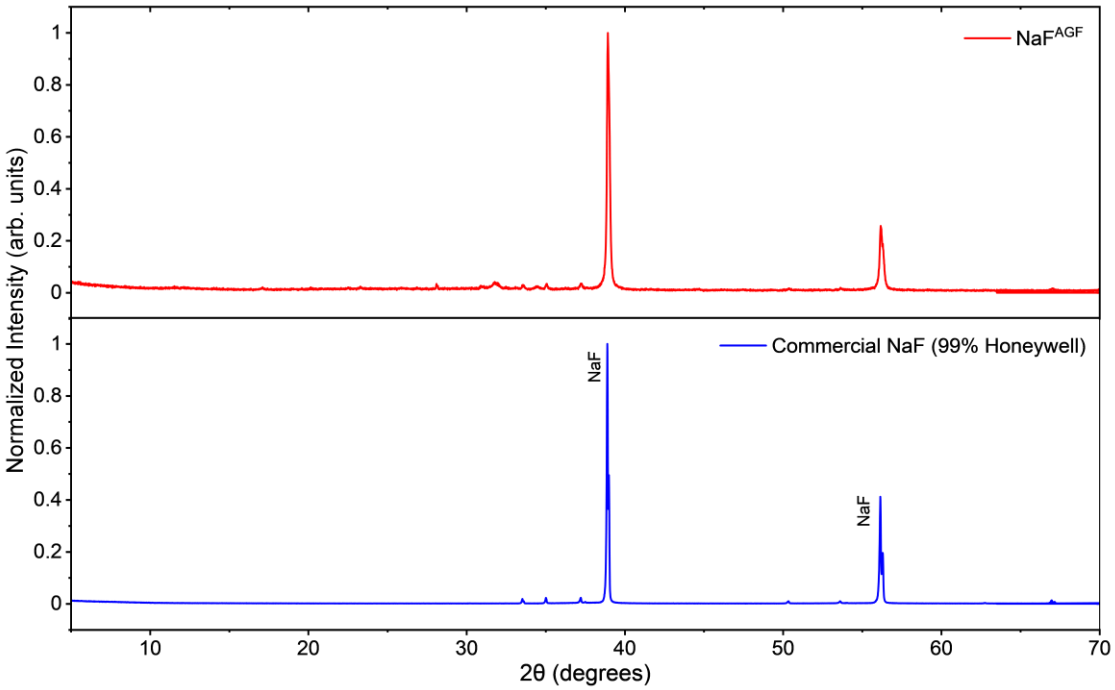

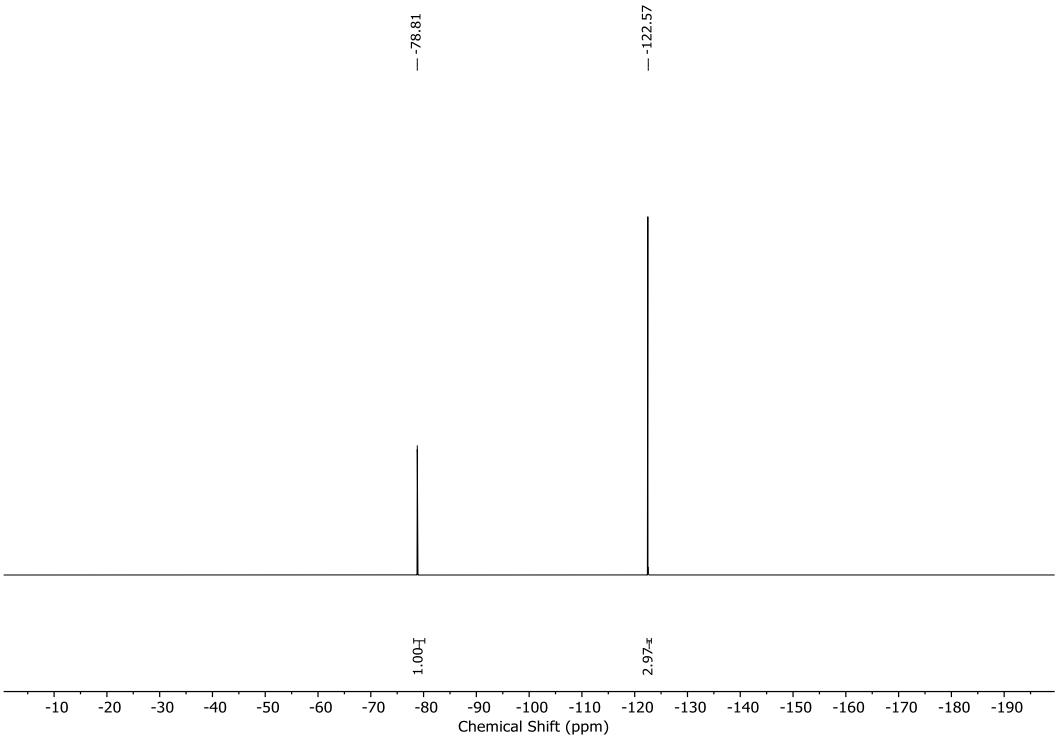

^{19}F qNMR (D_2O) of NaF^{AGF} dissolved in D_2O with NaOTf internal standard. NaF at -122.57 ppm and NaOTf at -78.81 ppm.

A sample of NaF^{AGF} (21.0 mg) and sodium triflate as an NaOTf (9.1 mg) was dissolved in D_2O. The purity of NaF in the solid was assessed by quantitative ^{19}F NMR and calculated to be 94%.

^{19}F NMR (377 MHz, D_2O) δ -121.57 (NaF, s).

Elemental Analysis of NaF^{AGF}

Inductively Coupled Plasma Optical Emission spectroscopy (ICP-OES) for microanalyses of commercial NaF, and NaF^{AGF} was carried out by MEDAC Ltd.

Element	NaF (theoretical)	NaF Honeywell 99%	NaF^{AGF}
F (%)	45.25	46.52	45.23
Na (%)	54.75	52.81	54.63

Preparation of CsF from acid grade fluorspar

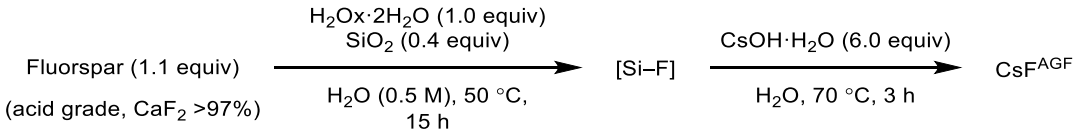

Acid grade fluorspar (644.0 mg, 8.0 mmol, 1.1 equiv), silica gel (306.0 mg, 5.1 mmol, 0.4 equiv) and oxalic acid (951 mg, 7.3 mmol, 1.0 equiv) were weighed into a 50 mL conical sterile polypropylene (PP) centrifuge tube. H_2O (14.5 mL) was added and the mixture was stirred at 50 °C for 15 h.

The resulting suspension was cooled to ambient temperature, diluted with H_2O (5 mL) and filtered using a Büchner funnel into a 50 mL PP tube. Filtered solids were washed with H_2O to give an aqueous solution (~ 20 mL) containing [Si-F] (H_2SiF_6, H_2SiF_5OH and $OxSiF_4$).

The first step of this reaction affords a theoretical maximum of 2.4 mmol of H_2SiF_6. Accordingly, $CsOH{\cdot}H_2O$ (2.42 g, 14.4 mmol) was added portion-wise to the aqueous solution (containing H_2SiF_6 and H_2SiF_5OH). The reaction was heated with stirring at the 70 °C for 3 h (monitored by ^{19}F NMR spectroscopy). After 15 h a pH of 7 should be reached (acid grade fluorspar derived H_2SiF_6 can be used as a pH regulator). The resulting suspension was filtered using a fritted glass filter to separate insoluble by-products from the solution and washed with water (2 x 5 mL). The filtrate was concentrated *in vacuo* (50 °C) and dried under high vacuum (< 0.1 mbar). Gentle heating (100 °C) of the flask under vacuum for 5 min followed by drying overnight at room temperature under high vacuum provided CsF^{AGF} as a white solid [2.04 g, 13.9 mmol, 93% (calculated from acid grade fluorspar)].

Purity of CsF^{AGF} by quantitative ^{19}F NMR using NaOTf as an internal standard was calculated to be 96%. This gives a total CsF^{AGF} yield of 89%. For full purity analysis provided below.

A sample of CsF^{AGF} could not be analysed by PXRD because the sample is highly hygroscopic and deliquesces.

CsF^{AGF}

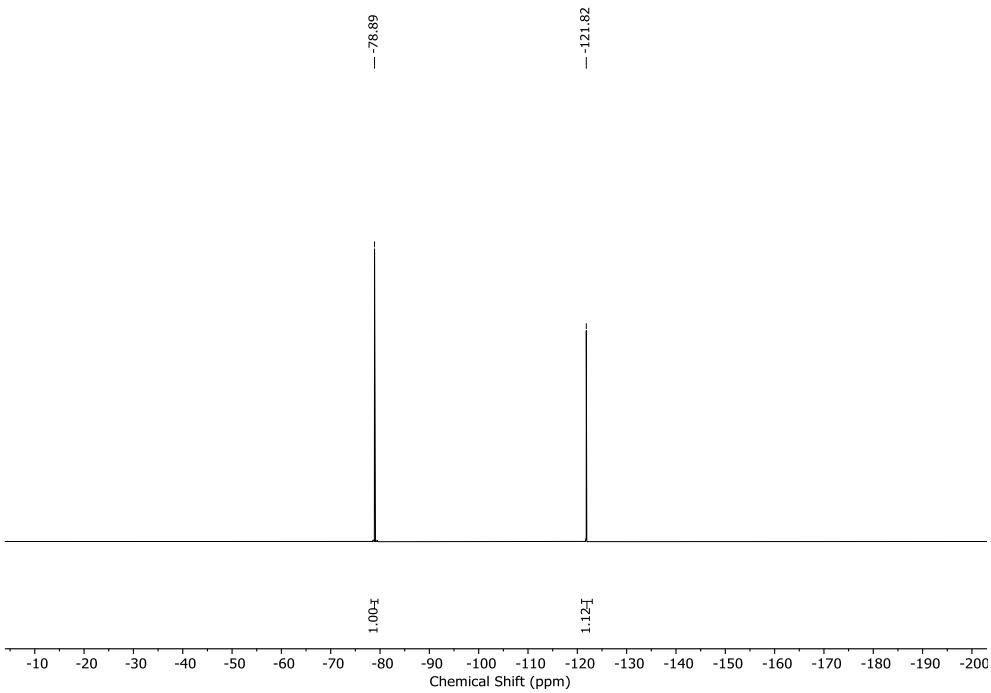

^{19}F qNMR (D_2O) of CsF^{AGF} dissolved in D_2O with NaOTf internal standard. CsF at -121.82 ppm and NaOTf at -78.89 ppm.

A sample of CsF^{AGF} (24.8 mg) and sodium triflate as an NaOTf (8.0 mg) was dissolved in D_2O. The purity of CsF in the solid was assessed by quantitative ^{19}F NMR and calculated to be 96%.

^{19}F NMR (377 MHz, D_2O) δ -121.82 (CsF, s).

Elemental Analysis of CsF^{AGF}

Inductively Coupled Plasma Optical Emission spectroscopy (ICP-OES) for microanalyses of commercial CsF and CsF^{AGF} was carried out by MEDAC Ltd. Cs cannot be detected by ICP-OES.

Element	CsF (theoretical)	CsF Sigma-Aldrich 97%	CsF^{AGF}
F (%)	12.51	12.59	11.47

The performance of CsF^{AGF} was assessed in the fluorination of 2-chloroquinonline:

The performance of our CsF prepared either using acid grade fluorspar (CsF^{AGF}) was examined in the fluorination of 2-chloroquinoline and compared against commercial anhydrous CsF (CsF^{C}, 99% purity, Sigma Aldrich CAS 13400-13-0) following a modified procedure by Schultz and co-workers.[84]

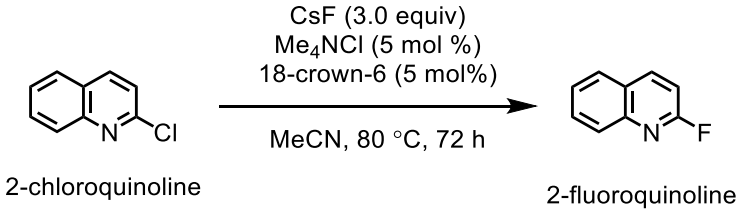

The reactivity of CsF^{AGF} (3 equiv) was tested in the fluorination of 2-chloroquinoline (0.25 mmol, 1 equiv) in the presence of Me_4NCl (5 mol%) and 18-crown-6 (5 mol%) in anh. MeCN at 80 °C for 72 h. Reaction yield was determined from the crude reaction mixture by quantitative ^{1}H and ^{19}F NMR spectroscopy using 4-fluoroanisole as internal standard.

Entry	CsF	source	ArF (%)	ArCl (%)
1	CsF^{C}	commercial	69	31
2	CsF^{AGF}	this work	73	27

4.3.16 Preparation of KF using oxalic acid dihydrate at 25 °C

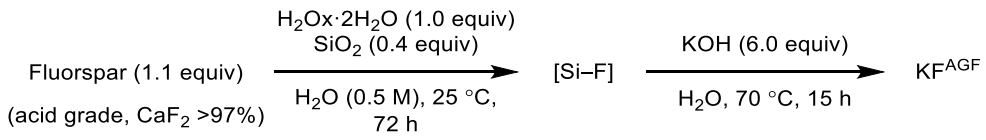

Acid grade fluorspar (644.0 mg, 8.0 mmol, 1.1 equiv), silica gel (306.0 mg, 5.1 mmol, 0.4 equiv) and oxalic acid (951 mg, 7.3 mmol, 1.0 equiv) were weighed into a 50 mL conical sterile polypropylene (PP) centrifuge tube. H_2O (14.5 mL) was added and the mixture was stirred at 25 °C for 72 h.

The resulting suspension was cooled to ambient temperature, diluted with H_2O (5 mL) and filtered using a Büchner funnel into a 50 mL PP tube. Filtered solids were washed with H_2O to give an aqueous solution (~ 20 mL) containing [Si-F] (H_2SiF_6, H_2SiF_5OH and $OxSiF_4$).

The first step of this reaction affords a theoretical maximum of 2.4 mmol of H_2SiF_6. Accordingly, KOH (85%, 951 mg, 14.4 mmol) was added portion-wise to the aqueous solution (containing H_2SiF_6 and H_2SiF_5OH). The reaction was heated with stirring at the 70 °C for 3 h. The resulting suspension was filtered using a fritted glass filter to separate insoluble by-products from the solution and washed with water (2 x 5 mL). The filtrate was concentrated *in vacuo* (50 °C) and dried under high vacuum (< 0.1 mbar). Gentle heating (100 °C) of the flask under vacuum for 5 min followed by drying overnight at room temperature under high vacuum provides acid-grade fluorspar derived potassium fluoride (KF^{AGF}) as a white crystalline solid (798 mg, 13.7 mmol, 95 %).

Purity of KF^{AGF} by quantitative ^{19}F NMR using NaOTf as an internal standard was calculated to be 78%. This gives a total KF^{AGF} yield of 74%. Purity analysis can be seen below.

KF^{AGF} (prepared at 25 °C)

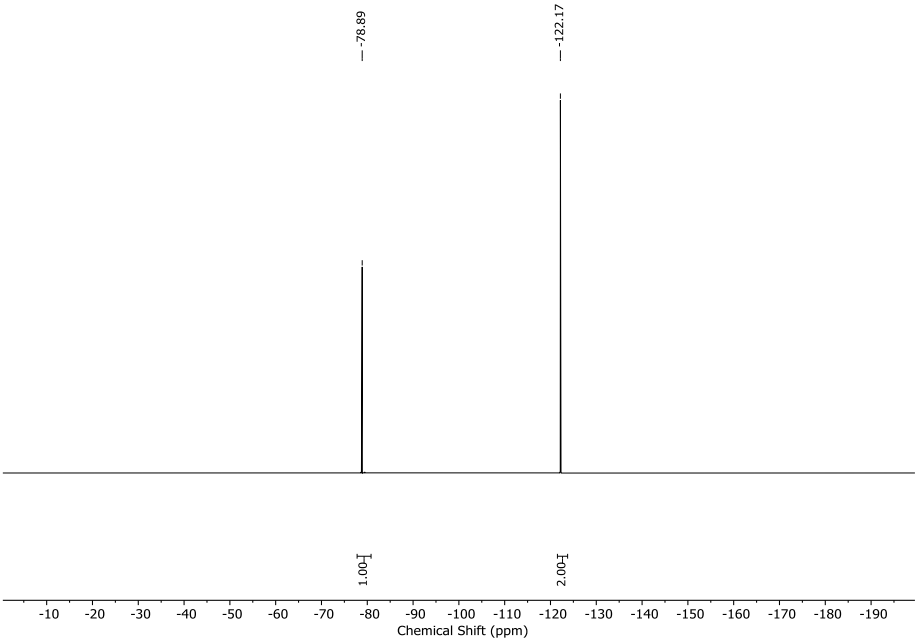

A sample of KF^{AGF} (20.9 mg) and sodium triflate as an NaOTf (8.0 mg) was dissolved in D_2O. The purity of KF in the solid was assessed by quantitative ^{19}F NMR and calculated to be 78%.

^{19}F NMR (377 MHz, D_2O) δ -121.17 (KF, s).

4.3.17 Preparation of KF using sulfuric acid at 50 °C and 25 °C

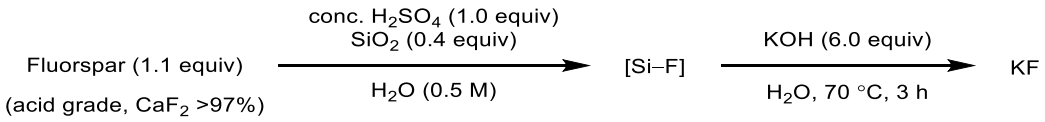

Acid grade fluorspar (644.0 mg, 8.0 mmol, 1.1 equiv), silica gel (306.0 mg, 5.1 mmol, 0.4 equiv) and 95% concentrated sulfuric acid (404 µL, 7.3 mmol, 18 M, 1.0 equiv) were weighed into a 50 mL conical sterile polypropylene (PP) centrifuge tube. H_2O (14.5 mL) was added and the mixture was heated with stirring at either 50 °C or 25 °C for 24 h or 72 h, respectively. The resulting suspension was cooled to ambient temperature, diluted with H_2O (5 mL) and filtered using a Büchner funnel into a 50 mL PP tube. Filtered solids were washed with H_2O to give an aqueous solution (~ 20 mL) containing [Si-F] (H_2SiF_6, and H_2SiF_5OH).

The first step of this reaction affords a theoretical maximum of 2.4 mmol of H_2SiF_6. Accordingly, KOH (85%, 951 mg, 14.4 mmol) was added portion-wise to the aqueous solution (containing H_2SiF_6 and H_2SiF_5OH).

The reaction was heated with stirring at the 70 °C for 3 h. The resulting suspension was filtered using a fritted glass filter to separate insoluble by-products from the solution and washed with water (2 x 5 mL). The filtrate was concentrated *in vacuo* (50 °C) and dried under high vacuum (< 0.1 mbar). Gentle heating (100 °C) of the flask under vacuum for 5 min followed by drying overnight at room temperature under high vacuum provides acid-grade fluorspar derived potassium fluoride (KF^{AGF}) as a white crystalline solid.

KF^{AGF} prepared at 50 °C (24 h) using concentrated H_2SO_4: 817 mg, 14.1 mmol, 98%

Purity of KF^{AGF} by quantitative ^{19}F NMR using NaOTf as an internal standard was calculated to be 46%. This gives a total KF^{AGF} yield of 46%. Purity analysis can be seen below.

KF^{AGF} prepared at 25 °C (72 h) using concentrated H_2SO_4: 830 mg, 14.29 mmol, 99%

Purity of KF^{AGF} by quantitative ^{19}F NMR using NaOTf as an internal standard was calculated to be 36%. This gives a total KF^{AGF} yield of 36%. Purity analysis can be seen below.

Potassium sulfate (K_2SO_4) was identified as a major impurity in the samples of KF prepared at 50 °C (or 25 °C) by PXRD (see below), indicating an incomplete reaction between acid-grade fluorspar, H_2SO_4 and SiO_2.

KF^{AGF} (prepared at 50 °C using H_2SO_4)

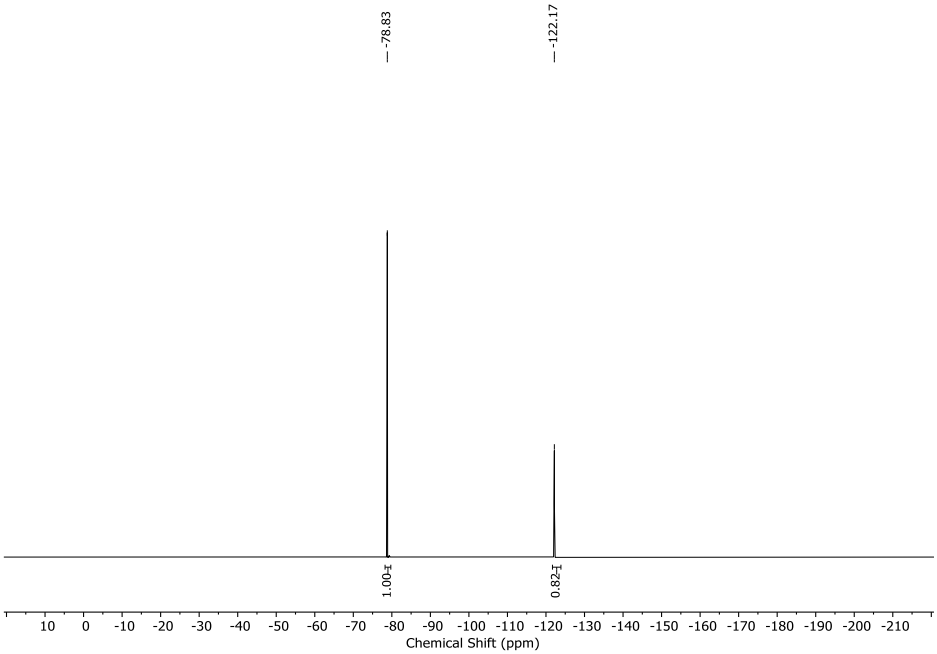

^{19}F qNMR (D_2O) of KF (prepared using H_2SO_4 at 50 °C) dissolved in D_2O with NaOTf internal standard. KF at -122.17 ppm and NaOTf at -78.80 ppm.

A sample of KF^{AGF} (21.3 mg) and sodium triflate as an NaOTf (12.0 mg) was dissolved in D_2O. The purity of KF in the solid was assessed by quantitative ^{19}F NMR and calculated to be 46%.

^{19}F NMR (377 MHz, D_2O) δ -121.17 (KF, s).

PXRD of KF^{AGF} (prepared at 50 °C using H_2SO_4)

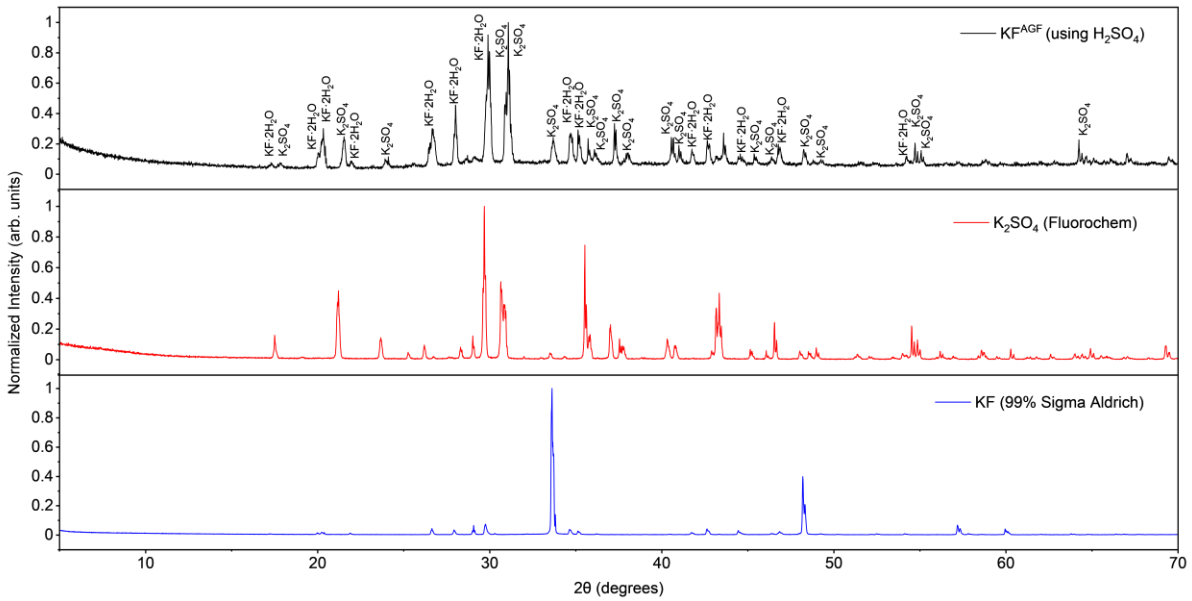

KF^{AGF} (prepared at 25 °C using H_2SO_4)

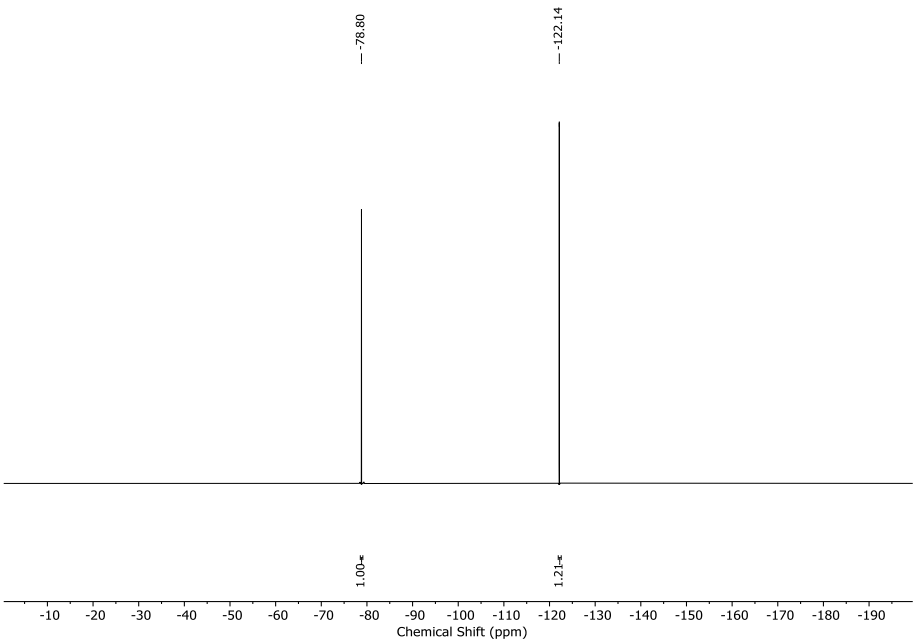

^{19}F qNMR (D_2O) of KF (prepared using H_2SO_4 at 50 °C) dissolved in D_2O with NaOTf internal standard. KF at -122.17 ppm and NaOTf at -78.80 ppm.

A sample of KF^{AGF} (24.1 mg) and sodium triflate as an NaOTf (7.1 mg) was dissolved in D_2O. The purity of KF in the solid was assessed by quantitative ^{19}F NMR and calculated to be 36%.

^{19}F NMR (377 MHz, D_2O) δ -121.14 (KF, s).

PXRD of KF^{AGF} (prepared at 25 °C using H_2SO_4).

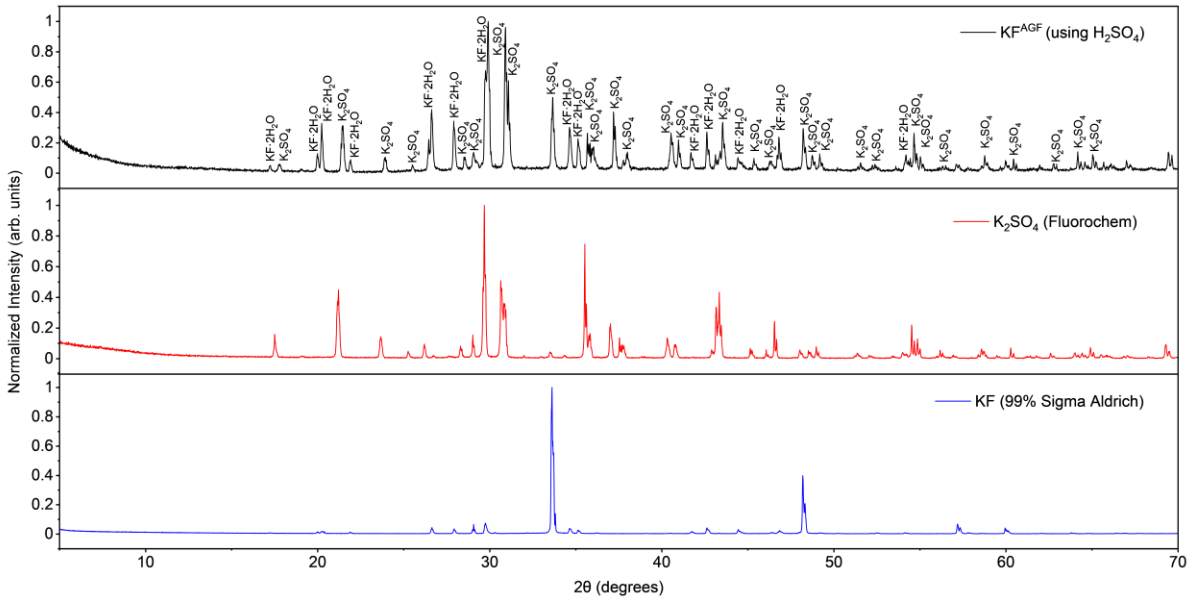

4.3.18 Quantification of [Si-F] species formed (H_2SO_4 as Brønsted acid)

Acid grade fluorspar (644.0 mg, 8.0 mmol, 1.1 equiv), silica gel (306.0 mg, 5.1 mmol, 0.4 equiv) and 95% concentrated sulfuric acid (404 µL, 7.3 mmol, 1.0 equiv) were weighed into a 50 mL conical sterile polypropylene (PP) centrifuge tube. H_2O (14.5 mL) was added and the mixture was heated with stirring at either 25 °C or 50 °C for 15 h. NaOTf (42 mg, 0.269 mmol) was added as an internal standard to the reaction mixture. The reaction mixture was stirred for 2 minutes and an aliquot of the reaction was analysed by quantitative ^{19}F NMR spectroscopy (D_2O) (32 scans, d1 = 30 s, op1 = 103.5 ppm). The total amount of [Si-F] species was quantified using the global spectrum deconvolution (GSD) tool available on MestReNova which enables integration of partially overlapping peaks. This reaction theoretically affords 2.4 mmol of H_2SiF_6 and 2.91 mmol H_2SiF_5OH.

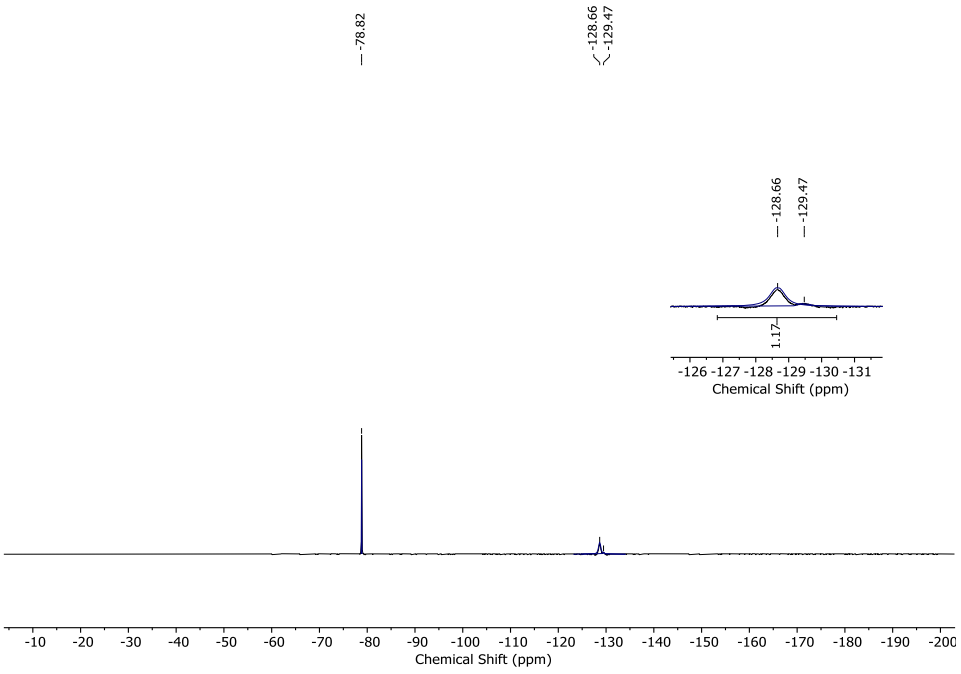

.^{19}F NMR (D_2O) spectrum of reaction between acid grade fluorspar (CaF_2), H_2SO_4 and SiO_2 (24 h, 50 °C). Aqueous species H_2SiF_5OH (br s, -128.66 ppm), H_2SiF_6 (br s, -129.47 ppm) observed. Internal standard NaOTf (s, -78.82).

	ppm	Intensity	Width	Area
1	-78.82	284.7	2.94	2396.78
2	-128.66	35.2	207.84	18796.60
3	-129.47	5.4	175.25	1910.53

Global Spectrum Deconvolution (GSD) peak list characterised by chemical shift (ppm), peak intensity, peak width and peak area.

Calculated [Si-F] % values from total peak area values obtained using GSD:

Entry	Compound	Total peak area	Normalized area	[Si-F] %
1	NaOTf	2396.78	1	-
2	H_2SiF_6	1910.53	0.80	4
3	$H_2SiF_5(OH)$	18796.60	7.84	44
			Total [Si-F]	48

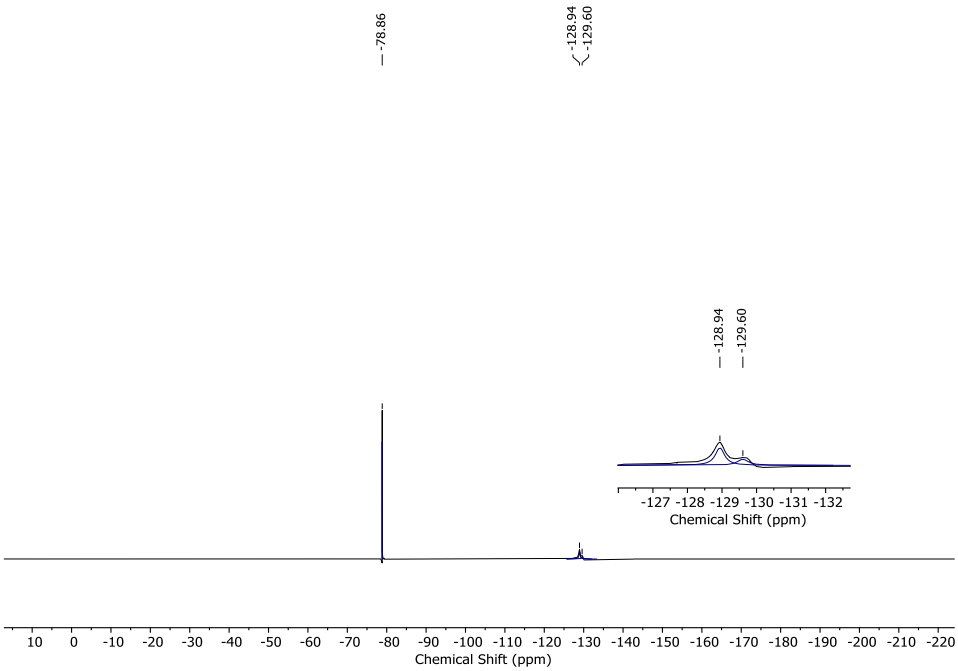

^{19}F NMR (D_2O) spectrum of reaction between acid grade fluorspar (CaF_2), H_2SO_4 and SiO_2 (72 h, 25 °C). Aqueous species H_2SiF_5OH (br s, -128.94 ppm), H_2SiF_6 (br s, -129.60 ppm) observed. Internal standard NaOTf (s, -78.86).

	ppm	Intensity	Width	Area
1	-78.86	3263.2	2.60	15377.56
2	-128.94	200.6	155.19	56397.81
3	-129.60	70.1	186.40	23684.13

Global Spectrum Deconvolution (GSD) peak list characterised by chemical shift (ppm), peak intensity, peak width and peak area.

Calculated [Si-F] % values from total peak area values obtained using GSD:

Entry	Compound	Total peak area	Normalized area	[Si-F] %
1	NaOTf	15377.56	1	-
2	H_2SiF_6	23684.13	1.54	9
3	$H_2SiF_5(OH)$	56397.81	3.67	20
			Total [Si-F]	29

4.3.19 Synthesis of Aryl fluorides by S_NAr Fluorination

General procedure (GP A) using acid grade fluorspar derived KF (KF^{AGF}) or metspar derived KF (KF^{M})

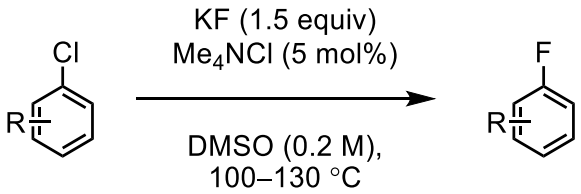

To an oven dried glass reaction vessel was added KF^{AGF} or KF^{M} (1.5 equiv). The KF was dried under high vacuum at 100 °C for at least 1 h. After this time, corresponding chloroarene (1.0 mmol, 1 equiv), Me_4NCl (5.5 mg, 0.05 mmol) and anhydrous DMSO (5 mL) was added to the reaction vessel. The reaction mixture was heated to specified temperature for specified time in a heating block. The resulting suspension was cooled to room temperature, filtered through a short plug of silica gel (washed with ~15 mL EtOAc) to remove insoluble by-products. The filtrate was washed with brine (10 mL). The organic extract was collected and the aqueous layer was washed with EtOAc (2 x 5 mL). The combined organic extracts were dried over anhydrous Na_2SO_4, filtered, and concentrated *in vacuo*. The residue was purified by column chromatography on silica to afford the title compound.

1-Fluoro-2,4-dinitrobenzene (62)

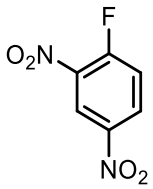

Prepared following **GP A** using 1-chloro-2,4-dinitrobenzene (203 mg, 1.0 mmol) and KF^{AGF} or KF^{M} (87 mg, 1.5 mmol, 1.5 equiv). The reaction is stirred at 70 °C for 1 h. Purification by flash column chromatography on silica using pentane/EtOAc (100:0 to 90:10) gave the title compound as a pale-yellow oil.

Yield using KF^{AGF}: 149 mg, 0.80 mmol, 80%

Yield using KF^{M}: 137 mg, 0.74 mmol, 74%

^{1}H NMR (400 MHz, $CDCl_3$) δ 9.10 – 8.84 (m, 1H), 8.67 – 8.43 (m, 1H), 7.59 – 7.49 (m, 1H).

^{13}C NMR (101 MHz, $CDCl_3$) δ 158.80 (d, *J* = 275.2 Hz), 143.67, 137.18, 130.53 (d, *J* = 10.5 Hz), 122.45, 120.10 (d, *J* = 23.0 Hz).

^{19}F NMR (377 MHz, $CDCl_3$) δ -106.17 (ddd, *J* = 10.1, 6.6, 3.8 Hz).

CAS 350-30-1

Spectroscopic data are in accordance with those in literature.[85]

2-chloro-1-fluoro-4-nitrobenzene (51)

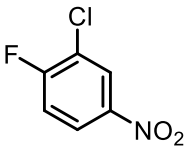

Prepared following **GP A** using 3,4-dichloronitrobenzene (192 mg, 1.0 mmol) and KF^{AGF} (87 mg, 1.5 mmol, 1.5 equiv). The reaction is stirred at 130 °C for 15 h. Purification by flash

column chromatography on silica using pentane/Et_2O (100:0 to 95:5) gave the title compound as a pale-yellow solid.

Yield: 134 mg, 0.76 mmol, 76 %

^{1}H NMR (400 MHz, $CDCl_3$) δ 8.35 (dd, *J* = 9.2, 7.9 Hz, 1H), 8.18 (ddd, *J* = 9.2, 4.1, 2.6 Hz, 1H), 7.32 (dd, *J* = 9.2, 7.9 Hz, 1H).

^{13}C NMR (101 MHz, $CDCl_3$) δ 162.1 (d, *J* = 260.1 Hz), 144.4 (s), 126.9 (d, *J* = 1.6 Hz), 124.2 (d, *J* = 8.9 Hz), 122.7 (d, *J* = 19.6 Hz), 117.3 (d, *J* = 23.4 Hz).

^{19}F NMR (377 MHz, $CDCl_3$) δ -103.98 (m).

CAS 350-30-1

Spectroscopic data are in accordance with those in literature.[86]

2-fluoro-5-nitrobenzonitrile (82)

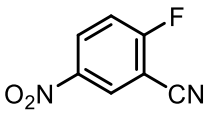

Prepared following **GP A** using 2-chloro-5-nitrobenzonitrile (183 mg, 1.0 mmol) and KF^{AGF} or KF^{M} (87 mg, 1.5 mmol, 1.5 equiv). The reaction is stirred at 100 °C for 6 h. Purification by flash column chromatography on silica using pentane/Et_2O (100:0 to 90:10) gave the title compound as as a pale-yellow solid.

Yield using KF^{AGF}: 157 mg, 0.95 mmol, 95 %

Yield using KF^{M}: 148 mg, 0.89 mmol, 89 %

^{1}H NMR (400 MHz, $CDCl_3$) δ 8.58 (dd, *J* = 5.4, 2.7 Hz, 1H), 8.52 (ddd, *J* = 9.2, 4.4, 2.8 Hz, 1H), 7.45 (dd, *J* = 9.2, 7.7 Hz, 1H).

^{13}C NMR (101 MHz, $CDCl_3$) δ 166.2 (d, *J* = 269.8 Hz), 144.3, 130.6 (d, *J* = 10.3 Hz), 129.7 (d, *J* = 2.1 Hz), 118.0 (d, *J* = 21.9 Hz), 111.8, 103.2 (d, *J* = 17.8 Hz).

^{19}F NMR (377 MHz, $CDCl_3$) δ -95.78 (dt, *J* = 7.7, 4.4 Hz).

CAS 17417-09-3

Spectroscopic data are in accordance with those in literature.[46]

3-chloro-4-fluorobenzonitrile (83)

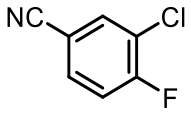

Prepared following **GP A** using 3,4-dichlorobenzonitrile (172 mg, 1.0 mmol) and KF[AGF] (87 mg, 1.5 mmol, 1.5 equiv). The reaction is stirred at 130 °C for 48 h. Purification by flash column chromatography on silica using pentane/Et_2O (100:0 to 90:10) gave the title compound as as a white solid

Yield: 105 mg, 0.68 mmol, 68%

^{1}H NMR (400 MHz, $CDCl_3$) δ 7.74 (dd, *J* = 6.7, 2.1 Hz, 1H), 7.58 (ddd, *J* = 8.5, 4.4, 2.1 Hz, 1H), 7.27 (m, 1H).

^{13}C NMR (101 MHz, $CDCl_3$) δ 161.0 (d, *J* = 259.0 Hz), 134.8, 132.7 (d, *J* = 8.4 Hz), 123.0 (d, *J* = 18.8 Hz), 118.0 (d, *J* = 22.5 Hz), 117.0, 109.7 (d, *J* = 4.4 Hz).

^{19}F NMR (376 MHz, $CDCl_3$) δ -104.73 (ddd, *J* = 8.5, 6.7, 4.4 Hz).

CAS 117482-84-5

Spectroscopic data are in accordance with those in literature.[87]

S_NAr reactions using acid grade fluorspar derived $Me_4NF\cdot{}^t$AmOH:

General procedure (GP B) for fluorodenitration using acid grade fluorspar derived Me_4NF

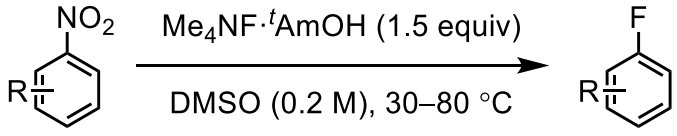

To an oven dried glass reaction vessel containing acid grade fluorspar derived $Me_4NF\cdot{}^t$AmOH (1.5 or 2.5 equiv) was added the corresponding nitroarene (1.0 mmol, 1.0 equiv) and anhydrous DMSO (5 mL). The reaction mixture was heated to specified temperature for specified time in a heating block. The resulting suspension was cooled to room temperature,

filtered through a short plug of silica gel (washed with ~15 mL EtOAc) to remove insoluble by-products. The filtrate was washed with brine (10 mL). The organic extract was collected and the aqueous layer was washed with EtOAc (2 x 5 mL). The combined organic extracts were dried over anhydrous Na_2SO_4, filtered, and concentrated *in vacuo*. The residue was purified by column chromatography on silica to afford the title compound.

2,6-difluorobenzonitrile (84)

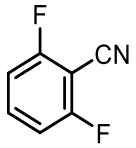

Prepared following **GP B** using 2,6-dinitrobenzonitrile (193 mg, 1.0 mmol) and $Me_4NF{\cdot}^tAmOH$ (544 mg, 3.0 mmol, 3.0 equiv). The reaction is stirred at 30 °C for 15 h. Purification by flash column chromatography on silica using pentane/Et_2O (100:0 to 98:2) gave the title compound as a white solid.

Yield: 117 mg, 0.84 mmol, 84%

^{1}H NMR (400 MHz, $CDCl_3$) δ 7.62 (tt, *J* = 8.5, 6.3 Hz, 1H), 7.11 – 7.02 (m, 2H).

^{13}C NMR (101 MHz, $CDCl_3$) δ 163.3 (dd, *J* = 261.6, 4.2 Hz), 135.8 (t, *J* = 10.1 Hz), 112.3 (dd, *J* = 19.4, 3.7 Hz), 109.2, 92.5 (t, *J* = 19.1 Hz).

^{19}F NMR (377 MHz, $CDCl_3$) δ -101.87 – -105.36 (m).

CAS 1897-52-5

Spectroscopic data are in accordance with those in literature.[88]

4-fluoronitrobenzene (59)

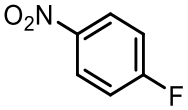

Prepared following **GP B** using 1,4-dinitrobenzene (168 mg, 1.0 mmol) and $Me_4NF{\cdot}^tAmOH$ (272 mg, 1.5 mmol, 1.5 equiv). The reaction is stirred at 80 °C for 15 min. Purification by

flash column chromatography on silica using pentane/EtOAc (100:0 to 90:10) gave the title compound as a yellow oil.

Yield: 124 mg, 0.88 mmol, 88%

^{1}H NMR (400 MHz, $CDCl_3$) δ 8.32 – 8.23 (m, 2H), 7.25 – 7.16 (m, 2H).

^{13}C NMR (101 MHz, $CDCl_3$) δ 166.4 (d, *J* = 258.0 Hz), -144.5, 126.5 (d, *J* = 10.0 Hz), 116.6 (d, *J* = 23.7 Hz).

^{19}F NMR (377 MHz, $CDCl_3$) δ -101.35 – -103.81 (m).

CAS 350-46-9

Spectroscopic data are in accordance with those in literature.[89]

2-fluorobenzonitrile (85)

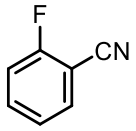

Prepared following **GP B** using 2-nitrobenzonitrile (148 mg, 1.0 mmol) and $Me_4NF\cdot{}^tAmOH$ (272 mg, 1.5 mmol, 1.5 equiv). The reaction is stirred at 80 °C for 18 h. Purification by flash column chromatography on silica using pentane/Et_2O (100:0 to 95:5) gave the title compound as a colorless oil.

Yield: 88 mg, 0.73 mmol, 73%

^{1}H NMR (400 MHz, $CDCl_3$) δ 7.68 – 7.57 (m, 2H), 7.30 – 7.25 (m, 1H), 7.25 – 7.19 (m, 1H).

^{13}C NMR (101 MHz, $CDCl_3$) δ 163.2 (d, *J* = 259.0 Hz), 135.2 (d, *J* = 8.3 Hz), 133.6, 125.0 (d, *J* = 3.8 Hz), 116.59 (d, *J* = 19.4 Hz), 114.1, 101.6 (d, *J* = 15.4 Hz).

^{19}F NMR (377 MHz, $CDCl_3$) δ -106.30 (m).

CAS 394-47-8

Spectroscopic data are in accordance with those in literature.[90]

4.4 References

1. Brouwer, D. H. & Horvath, M. Minimizing the effects of RF inhomogeneity and phase transients allows resolution of two peaks in the (1)H CRAMPS NMR spectrum of adamantane. *Solid State Nucl. Magn. Reson.* **71**, 30–40 (2015).
2. Griffin, J. M., Yates, J. R., Berry, A. J., Wimperis, S. & Ashbrook, S. E. High-resolution ^{19}F MAS NMR spectroscopy: structural disorder and unusual J couplings in a fluorinated hydroxy-silicate. *J. Am. Chem. Soc.* **132**, 15651–15660 (2010).
3. DeVience, S. J., Walsworth, R. L. & Rosen, M. S. NMR of 31P nuclear spin singlet states in organic diphosphates. *J Magn Reson* **333**, 107101 (2021).
4. Wernik, M., Poechlauer, P., Schmoelzer, C., Dallinger, D. & Kappe, C. O. Design and Optimization of a Continuous Stirred Tank Reactor Cascade for Membrane-Based Diazomethane Production: Synthesis of α-Chloroketones. *Org. Process Res. Dev.* **23**, 1359–1368 (2019).
5. R, U. *et al.* Heterogeneous vanadium-catalyzed oxidative cleavage of olefins for sustainable synthesis of carboxylic acids. *Chem. Commun.* **57**, (2021).
6. Bie, F., Liu, X., Szostak, M. & Liu, C. Decarbonylative Alkynylation of Aryl Anhydrides via Palladium Catalysis. *J. Org. Chem.* **88**, 4442–4451 (2023).
7. Bare, G. A. L. Synthesis of Sulfonyl Fluorides Using Direct Chloride/Fluoride Exchange in Potassium Fluoride and Water/Acetone. *J. Org. Chem.* **88**, 4761–4764 (2023).
8. Pérez-Palau, M. & Cornella, J. Synthesis of Sulfonyl Fluorides from Sulfonamides. *Eur. J. Org. Chem.* **2020**, 2497–2500 (2020).
9. Cherepakha, A. Yu. *et al.* Hetaryl Bromides Bearing the SO_2F Group – Versatile Substrates for Palladium-Catalyzed C–C Coupling Reactions. *Eur. J. Org. Chem.* **2018**, 6682–6692 (2018).
10. Tribby, A. L., Rodríguez, I., Shariffudin, S. & Ball, N. D. Pd-Catalyzed Conversion of Aryl Iodides to Sulfonyl Fluorides Using SO2 Surrogate DABSO and Selectfluor. *J. Org. Chem.* **82**, 2294–2299 (2017).
11. Wang, L. & Cornella, J. A Unified Strategy for Arylsulfur(VI) Fluorides from Aryl Halides: Access to Ar-SOF_3 Compounds. *Angew. Chem. Int. Ed.* **59**, 23510–23515 (2020).
12. Laudadio, G. *et al.* Sulfonyl Fluoride Synthesis through Electrochemical Oxidative Coupling of Thiols and Potassium Fluoride. *J. Am. Chem. Soc.* **141**, 11832–11836 (2019).

13. Liu, Y. *et al.* Arenesulfonyl Fluoride Synthesis via Copper-Catalyzed Fluorosulfonylation of Arenediazonium Salts. *Org. Lett.* **22**, 2281–2286 (2020).
14. Dong, J., Krasnova, L., Finn, M. G. & Sharpless, K. B. Sulfur(VI) Fluoride Exchange (SuFEx): Another Good Reaction for Click Chemistry. *Angewandte Chemie International Edition* **53**, 9430–9448 (2014).
15. Zhang, X., Fang, W.-Y., Lekkala, R., Tang, W. & Qin, H.-L. An Easy, General and Practical Method for the Construction of Alkyl Sulfonyl Fluorides. *Adv. Synth. Catal.* **362**, 3358–3363 (2020).
16. Xu, R., Xu, T., Yang, M., Cao, T. & Liao, S. A rapid access to aliphatic sulfonyl fluorides. *Nat Commun* **10**, 3752 (2019).
17. Tryniszewski, M., Basiak, D. & Barbasiewicz, M. Olefination with Sulfonyl Halides and Esters: Synthesis of Unsaturated Sulfonyl Fluorides. *Org. Lett.* **24**, 4270–4274 (2022).
18. Nie, X. *et al.* Radical Fluorosulfonylation: Accessing Alkenyl Sulfonyl Fluorides from Alkenes. *Angew. Chem. Int. Ed.* **60**, 3956–3960 (2021).
19. Song, X. *et al.* Synthesis of aryl sulfonyl fluorides from aryl sulfonyl chlorides using sulfuryl fluoride (SO_2F_2) as fluoride provider. *Tetrahedron* **108**, 132657 (2022).
20. Nielsen, M. K., Ugaz, C. R., Li, W. & Doyle, A. G. PyFluor: A Low-Cost, Stable, and Selective Deoxyfluorination Reagent. *J. Am. Chem. Soc.* **137**, 9571–9574 (2015).
21. Guo, J. *et al.* Rapid Deoxyfluorination of Alcohols with *N* -Tosyl-4-chlorobenzenesulfonimidoyl Fluoride (SulfoxFluor) at Room Temperature. *Chem. Eur. J.* **25**, 7259–7264 (2019).
22. Zheng, Q., Dong, J. & Sharpless, K. B. Ethenesulfonyl Fluoride (ESF): An On-Water Procedure for the Kilogram-Scale Preparation. *J. Org. Chem.* **81**, 11360–11362 (2016).
23. Aguilar, B., Amissah, F., Duverna, R. & Lamango, N. S. Polyisoprenylation Potentiates the Inhibition of Polyisoprenylated Methylated Protein Methyl Esterase and the Cell Degenerative Effects of Sulfonyl Fluorides. *Curr Cancer Drug Targets* **11**, 752–762 (2011).
24. Bianchi, T. A. & Cate, L. A. Phase transfer catalysis. Preparation of aliphatic and aromatic sulfonyl fluorides. *J. Org. Chem.* **42**, 2031–2032 (1977).
25. Passia, M. T. *et al.* Acid-Mediated Imidazole-to-Fluorine Exchange for the Synthesis of Sulfonyl and Sulfonimidoyl Fluorides. *Org. Lett.* **24**, 8802–8805 (2022).

26. Dubiella, C. *et al.* Selective Inhibition of the Immunoproteasome by Ligand-Induced Crosslinking of the Active Site. *Angew. Chem. Int. Ed.* **53**, 11969–11973 (2014).
27. Stavber, S. & Zupan, M. Mild fluorofunctionalization of side chains in alkyl substituted aromatics by cesium fluoroxysulfate. *J. Org. Chem.* **56**, 7347–7350 (1991).
28. Sood, D. E. *et al.* Deoxyfluorination with CuF_2 : Enabled by Using a Lewis Base Activating Group. *Angew Chem Int Ed Engl* **59**, 8460–8463 (2020).
29. Boldrini, C. & Harutyunyan, S. R. Pd-catalyzed allylative dearomatisation using Grignard reagents. *Chem. Commun.* **57**, 11807–11810 (2021).
30. Zhao, M., Li, M. & Lu, W. Visible-Light-Driven Oxidative Mono- and Dibromination of Benzylic- sp3 C–H Bonds with Potassium Bromide/Oxone at Room Temperature. *Synthesis* **50**, 4933–4939 (2018).
31. Alič, B., Petrovčič, J., Jelen, J., Tavčar, G. & Iskra, J. Renewable Reagent for Nucleophilic Fluorination. *J. Org. Chem.* **87**, 5987–5993 (2022).
32. Hu, J., Gao, B., Li, L., Ni, C. & Hu, J. Palladium-Catalyzed Monofluoromethylation of Arylboronic Esters with Fluoromethyl Iodide. *Org. Lett.* **17**, 3086–3089 (2015).
33. Sandoval, B. A., Meichan, A. J. & Hyster, T. K. Enantioselective Hydrogen Atom Transfer: Discovery of Catalytic Promiscuity in Flavin-Dependent 'Ene'-Reductases. *J. Am. Chem. Soc.* **139**, 11313–11316 (2017).
34. Welch, J. T. & Lin, J. Fluoroolefin containing dipeptide isosteres as inhibitors of dipeptidyl peptidase IV(CD26). *Tetrahedron* **52**, 291–304 (1996).
35. Tormena, C. F., Freitas, M. P., Rittner, R. & Abraham, R. J. Conformational behaviour of methyl 2-fluoroesters through theoretical calculations, NMR and IR spectroscopy. *Phys. Chem. Chem. Phys.* **6**, 1152–1156 (2004).
36. Dobson, L. S. & Pattison, G. Rh-Catalyzed arylation of fluorinated ketones with arylboronic acids. *Chem. Commun.* **52**, 11116–11119 (2016).
37. Kitamura, T., Muta, K. & Muta, K. Hypervalent Iodine-Promoted α-Fluorination of Acetophenone Derivatives with a Triethylamine·HF Complex. *J. Org. Chem.* **79**, 5842–5846 (2014).
38. Alevizopoulos, K., Calogeropoulou, T. & Stournaras, C. Compounds and methods for treating neoplasia. (2012).
39. Stadler, D. *et al.* Chiral Benzylic Carbocations: Low-Temperature NMR Studies and Theoretical Calculations. *J. Org. Chem.* **74**, 312–318 (2009).

40. Chen, X. *et al.* Stereoselective Mannich Reaction of N-(tert-Butylsulfinyl)imines with 3-Fluorooxindoles and Fluoroacetamides. *Adv. Synth. Catal.* **359**, 3057–3062 (2017).
41. Lee, C., Lai, J., Epifanov, M., Wang, C. X. & Sammis, G. M. Efficient protocol for the SO_2F_2-mediated deoxyfluorination of aliphatic alcohols. *Journal of Fluorine Chemistry* **251**, 109888 (2021).
42. Lovett, G. H., Chen, S., Xue, X.-S., Houk, K. N. & MacMillan, D. W. C. Open-Shell Fluorination of Alkyl Bromides: Unexpected Selectivity in a Silyl Radical-Mediated Chain Process. *J. Am. Chem. Soc.* **141**, 20031–20036 (2019).
43. Iwasaki, T., Min, X., Fukuoka, A., Kuniyasu, H. & Kambe, N. Nickel-Catalyzed Dimerization and Alkylarylation of 1,3-Dienes with Alkyl Fluorides and Aryl Grignard Reagents. *Angew. Chem. Int. Ed.* **55**, 5550–5554 (2016).
44. Li, W., Lu, Z., Hammond, G. B. & Xu, B. Unbalanced-Ion-Pair-Catalyzed Nucleophilic Fluorination Using Potassium Fluoride. *Org. Lett.* **23**, 9640–9644 (2021).
45. Ingold, C. K. & Vass, C. C. N. LVII.—The nature of the alternating effect in carbon chains. Part XXIII. Anomalous orientation by halogens, and its bearing on the problem of the ortho–para ratio, in aromatic substitution. *J. Chem. Soc. (Resumed)* 417–425 (1928).
46. Lacour, M.-A., Zablocka, M., Duhayon, C., Majoral, J.-P. & Taillefer, M. Efficient Phosphorus Catalysts for the Halogen-Exchange (Halex) Reaction. *Adv. Synth. Catal.* **350**, 2677–2682 (2008).
47. Johansen, M. B. & Lindhardt, A. T. Nucleophilic fluorination facilitated by a CsF–CaF2 packed bed reactor in continuous flow. *Chem. Commun.* **54**, 825–828 (2018).
48. Finger, G. C., Dickerson, D. R., Adl, T. & Hodgins, T. Fluorocyano-benzenes and -pyridines. *Chem. Commun. (London)* 430–431 (1965).
49. Roger, J. *et al.* Diastereoselective Synthesis of Dialkylated Bis(phosphino)ferrocenes: Their Use in Promoting Silver-Mediated Nucleophilic Fluorination of Chloroquinolines. *Eur. J. Inorg. Chem.* **2017**, 330–339 (2017).
50. Morales-Colón, M. T. *et al.* Tetramethylammonium Fluoride Alcohol Adducts for SNAr Fluorination. *Org. Lett.* **23**, 4493–4498 (2021).
51. Adams, D. J. & Clark, J. H. Nucleophilic routes to selectively fluorinated aromatics. *Chem. Soc. Rev.* **28**, 225–231 (1999).
52. Vlasov, V. M. Fluoride ion as a nucleophile and a leaving group in aromatic nucleophilic substitution reactions. *J. Fluor. Chem.* **61**, 193–216 (1993).

53. Singh, K. *et al.* Metal- and Phenol-Free Synthesis of Biaryl Ethers: Access to Dibenzobistriazolo-1,4,7-oxadiazonines and Vancomycin-Like Glyco-Macrocycles as Antibacterial Agents. *J. Org. Chem.* **83**, 14882–14893 (2018).
54. Gómez-Palomino, A. & Cornella, J. Selective Late-Stage Sulfonyl Chloride Formation from Sulfonamides Enabled by Pyry-BF_4. *Angew. Chem. Int. Ed.* **58**, 18235–18239 (2019).
55. Moriarty, R. M. & Tyagi, S. Metal-Free Intramolecular Aziridination of Alkenes Using Hypervalent Iodine Based Sulfonyliminoiodanes. *Org. Lett.* **12**, 364–366 (2010).
56. Yu, C., Lv, Z., Xu, S. & Zhang, J. A convenient synthesis of (*E*)-conjugated polyene sulfonyl derivatives with excellent stereospecificity. *Tetrahedron Lett.* **59**, 3234–3237 (2018).
57. Galaka, T. *et al.* Antiparasitic Activity of Sulfur- and Fluorine-Containing Bisphosphonates against Trypanosomatids and Apicomplexan Parasites. *Molecules* **22**, 82 (2017).
58. Fulp, J. *et al.* Structural Insights of Benzenesulfonamide Analogues as NLRP3 Inflammasome Inhibitors: Design, Synthesis, and Biological Characterization. *J. Med. Chem.* **61**, 5412–5423 (2018).
59. Eberhard, K. D.-C. D., Gerhart, G. D.-C. D., Uwe, H. D.-C. D. & Wolfgang, G. D.-C. D. Neue Sulfonamide und Verfahren zu ihrer Herstellung. (1970).
60. Magar, P. *et al.* Novel Sulfonamide-Based Carbamates as Selective Inhibitors of BChE. *Int. J. Mol. Sci.* **22**, 9447 (2021).
61. Patel, R. N., Chu, L., Chidambaram, R., Zhu, J. & Kant, J. Enantioselective microbial reduction of 2-oxo-2-(1′,2′,3′,4′-tetrahydro-1′,1′,4′,4′-tetramethyl-6′-naphthalenyl)acetic acid and its ethyl ester. *Tetrahedron: Asymmetry* **13**, 349–355 (2002).
62. Ianni, A. & Waldvogel, S. R. Reliable and Versatile Synthesis of 2-Aryl-Substituted Cinnamic Acid Esters. *Synthesis* **2006**, 2103–2112 (2006).
63. Lai, P.-S., Dubland, J. A., Sarwar, M. G., Chudzinski, M. G. & Taylor, M. S. Carbon–carbon bond-forming reactions of α-carbonyl carbocations: exploration of a reversed-polarity equivalent of enolate chemistry. *Tetrahedron* **67**, 7586–7592 (2011).
64. Xu, S., Wu, P. & Zhang, W. 1,3-Dibromo-5,5-dimethylhydantoin (DBH) mediated one-pot syntheses of α-bromo/amino ketones from alkenes in water. *Org. Biomol. Chem.* **14**, 11389–11395 (2016).

65. Lundin, P. M., Esquivias, J. & Fu, G. C. Catalytic Asymmetric Cross-Couplings of Racemic α-Bromoketones with Arylzinc Reagents. *Angew. Chem. Int. Ed. Engl.* **48**, 154–156 (2009).
66. Shi, B., Wu, H., Yu, B. & Wu, J. 23-Oxa-Analogues of OSW-1: Efficient Synthesis and Extremely Potent Antitumor Activity. *Angew. Chem. Int. Ed.* **43**, 4324–4327 (2004).
67. Szcześniak, P., Pieczykolan, M. & Stecko, S. The Synthesis of α,α-Disubstituted α-Amino Acids via Ichikawa Rearrangement. *J. Org. Chem.* **81**, 1057–1074 (2016).
68. Li, S. *et al.* Transition Metal Free Stannylation of Alkyl Halides: The Rapid Synthesis of Alkyltrimethylstannanes. *J. Org. Chem.* **87**, 4291–4297 (2022).
69. Xu, N., Kong, Z., Wang, J. Z., Lovinger, G. J. & Morken, J. P. Copper-Catalyzed Coupling of Alkyl Vicinal Bis(boronic Esters) to an Array of Electrophiles. *J. Am. Chem. Soc.* **144**, 17815–17823 (2022).
70. Kleinbeck, F. & Toste, F. D. Gold(I)-Catalyzed Enantioselective Ring Expansion of Allenylcyclopropanols. *J. Am. Chem. Soc.* **131**, 9178–9179 (2009).
71. Gammack Yamagata, A. D. *et al.* Enantioselective Desymmetrization of Prochiral Cyclohexanones by Organocatalytic Intramolecular Michael Additions to α,β-Unsaturated Esters. *Angew. Chem. Int. Ed.* **54**, 4899–4903 (2015).
72. Sun, G. *et al.* Syntheses, Structures, and Enzymic Evaluations of Conformationally Constrained, Analog Inhibitors of Carnitine Acetyltransferase: (2R,6R)-, (2S,6S)-, (2R,6S)-, and (2S,6R)-6-(Carboxylatomethyl)-2-(hydroxymethyl)-2,4,4-trimethylmorpholinium. *J. Org. Chem.* **60**, 6688–6695 (1995).
73. Zhai, F., Xin, T., Geeson, M. B. & Cummins, C. C. Sustainable Production of Reduced Phosphorus Compounds: Mechanochemical Hydride Phosphorylation Using Condensed Phosphates as a Route to Phosphite. *ACS Cent. Sci.* **8**, 332–339 (2022).
74. Ochoa, G., Pilgrim, C. D., Kerr, J., Augustine, M. P. & Casey, W. H. Aqueous geochemistry at gigapascal pressures: NMR spectroscopy of fluoroborate solutions. *Geochim. Cosmochim. Acta* **244**, 173–181 (2019).
75. Guendouzi, M. E., Faridi, J. & Khamar, L. Chemical speciation of aqueous hydrogen fluoride at various temperatures from 298.15 K to 353.15 K. *Fluid Phase Equilibria* **499**, 112244 (2019).
76. MestreNova Manual https://mnova.pl/files/download/MestReNova-12-0-0_Manual.pdf (2017).

77. Xu, Z. *et al.* Enhanced Performance of a Lithium–Sulfur Battery Using a Carbonate-Based Electrolyte. *Angew. Chem. Int. Ed.* **55**, 10372–10375 (2016).
78. Finney, W. F., Wilson, E., Callender, A., Morris, M. D. & Beck, L. W. Reexamination of Hexafluorosilicate Hydrolysis by ^{19}F NMR and pH Measurement. *Environ. Sci. Technol.* **40**, 2572–2577 (2006).
79. W. Dean, P. A. & F. Evans, D. Spectroscopic studies of inorganic fluoro-complexes. Part III. Fluorine-19 nuclear magnetic resonance studies of silicon(IV), germanium(IV), and titanium(IV) fluoro-complexes. *J. Chem. Soc. A* **0**, 2569–2574 (1970).
80. Burum, D. P. & Ernst, R. R. Net polarization transfer via a *J*-ordered state for signal enhancement of low-sensitivity nuclei. *J. Magn. Reson.* **39**, 163–168 (1980).
81. Morris, G. A. & Freeman, R. Enhancement of nuclear magnetic resonance signals by polarization transfer. *J. Am. Chem. Soc.* **101**, 760–762 (1979).
82. Malz, F. & Jancke, H. Validation of quantitative NMR. *J. Pharm. Biomed. Anal.* **38**, 813–823 (2005).
83. Kim, D. W. *et al.* Facile Nucleophilic Fluorination Reactions Using *tert*-Alcohols as a Reaction Medium: Significantly Enhanced Reactivity of Alkali Metal Fluorides and Improved Selectivity. *J. Org. Chem.* **73**, 957–962 (2008).
84. Hong, C. M., Whittaker, A. M. & Schultz, D. M. Nucleophilic Fluorination of Heteroaryl Chlorides and Aryl Triflates Enabled by Cooperative Catalysis. *J. Org. Chem.* **86**, 3999–4006 (2021).
85. Ponticello, G. S., Engelhardt, E. L., Freedman, M. B. & Baldwin, J. J. Synthesis of 2-chloro-5-hydroxynicotinonitrile: The required intermediate in the total synthesis of a hydroxylated metabolite of (S)-2-(3-t-butylamino-2-hydroxypropoxy)-3-cyanopyridine. *J. Heterocycl. Chem.* **17**, 445–448 (1980).
86. Ung, G. & Bertrand, G. C-F Bond Activation with an Apparently Benign Ethynyl Dithiocarbamate, and Subsequent Fluoride Transfer Reactions. *Chem. Eur. J.* **18**, 12955–12957 (2012).
87. Cohen, D. T. & Buchwald, S. L. Mild Palladium-Catalyzed Cyanation of (Hetero)aryl Halides and Triflates in Aqueous Media. *Org. Lett.* **17**, 202–205 (2015).
88. Cismesia, M. A., Ryan, S. J., Bland, D. C. & Sanford, M. S. Multiple Approaches to the In Situ Generation of Anhydrous Tetraalkylammonium Fluoride Salts for S_NAr Fluorination Reactions. *J. Org. Chem.* **82**, 5020–5026 (2017).

89. Sun, H. & DiMagno, S. G. Room-Temperature Nucleophilic Aromatic Fluorination: Experimental and Theoretical Studies. *Angew. Chem. Int. Ed.* **45**, 2720–2725 (2006).
90. Jelen, J. & Tavčar, G. Deoxyfluorination of Electron-Deficient Phenols. *Org. Lett.* **25**, 3649–3653 (2023).